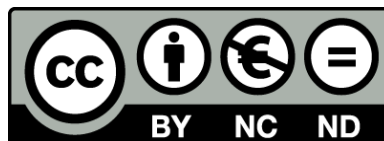




UNIVERSITAT DE  
BARCELONA

**Utilidad de la Cardiorresonancia en la Evaluación  
de la Presencia y Evolución del Sustrato  
Arritmogénico, Estratificación de Riesgo y Tratamiento  
de las Arritmias Ventriculares  
Post-Infarto Crónico de Miocardio**

Beatriz Jáuregui Garrido



Aquesta tesi doctoral està subjecta a la llicència **Reconeixement- NoComercial – SenseObraDerivada 4.0. Espanya de Creative Commons.**

Esta tesis doctoral está sujeta a la licencia **Reconocimiento - NoComercial – SinObraDerivada 4.0. España de Creative Commons.**

This doctoral thesis is licensed under the **Creative Commons Attribution-NonCommercial-NoDerivs 4.0. Spain License.**

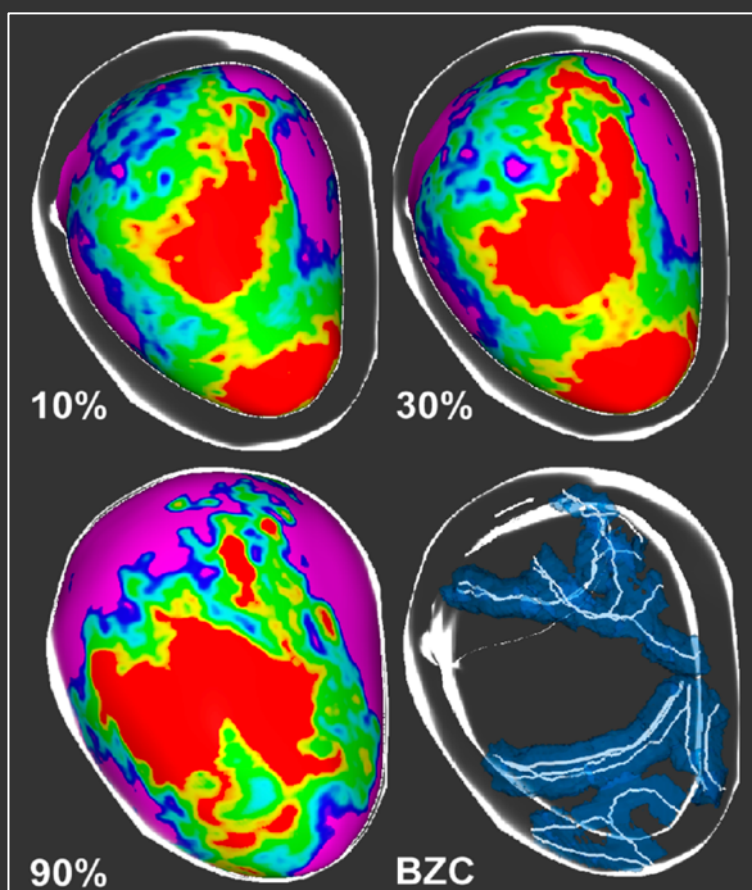


# UTILIDAD DE LA CARDIORRESONANCIA EN LA EVALUACIÓN DE LA PRESENCIA Y EVOLUCIÓN DEL SUSTRATO ARRITMOGÉNICO, ESTRATIFICACIÓN DE RIESGO Y TRATAMIENTO DE LAS ARRITMIAS VENTRICULARES POST-INFARTO CRÓNICO DE MIOCARDIO

MEMORIA DE TESIS DOCTORAL PRESENTADA POR

**BEATRIZ JÁUREGUI GARRIDO**

PARA OPTAR AL GRADO DE DOCTORA EN MEDICINA POR LA UNIVERSITAT DE BARCELONA



## DIRECTORES:

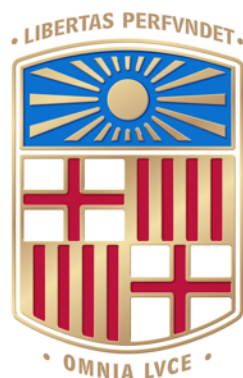
ANTONIO BERRUEZO SÁNCHEZ<sup>1</sup>

JOSÉ TOMÁS ORTIZ PÉREZ<sup>2</sup>

<sup>1</sup>INSTITUTO DEL CORAZÓN, CENTRO MÉDICO TEKNON, BARCELONA

<sup>2</sup>HOSPITAL CLÍNIC DE BARCELONA, UNIVERSITAT DE BARCELONA

**TESIS DOCTORAL**  
UNIVERSITAT DE BARCELONA, 2021



**UTILIDAD DE LA CARDIORRESONANCIA EN LA  
EVALUACIÓN DE LA PRESENCIA Y EVOLUCIÓN DEL  
SUSTRATO ARRITMOGÉNICO, ESTRATIFICACIÓN DE  
RIESGO Y TRATAMIENTO DE LAS ARRITMIAS  
VENTRICULARES POST-INFARTO CRÓNICO DE MIOCARDIO**

**Autor:**

**BEATRIZ JÁUREGUI GARRIDO**

**Directores:**

**ANTONIO BERRUEZO SÁNCHEZ**

**JOSÉ TOMÁS ORTIZ PÉREZ**

PROGRAMA DE DOCTORADO DE MEDICINA E INVESTIGACIÓN TRASLACIONAL. FACULTAD DE MEDICINA Y  
CIENCIAS DE LA SALUD. UNIVERSITAT DE BARCELONA. NOVIEMBRE 2021.



**Informe director/s /tutor sobre l'autorització del dipòsit de la tesi**

Dr./a. Antonio Berruezo Sánchez, com a co-director de la tesi doctoral titulada “Utilidad de la Cardiorresonancia en la Evaluación de la Presencia y Evolución del Sustrato Arritmogénico, Estratificación de Riesgo y Tratamiento de las Arritmias Ventriculares Post-Infarto Crónico de Miocardio ” i, d'acord amb el que s'estableix a l'article 35 Normativa reguladora del Doctorat a la Universitat de Barcelona, emeto el següent:

**INFORME**

*(Informe detallat i motivat sobre el contingut de la tesi i sobre l'autorització de dipòsit de la tesi que s'ha demanat)*

La doctoranda Beatriz Jáuregui presentarà aquesta tesi doctoral en format por articles científics. Aquest treball, que versa sobre molts aspectes rellevants des del punt de vista de l'electrofisiologia cardíaca relatiu a la utilitat de la cardioresonància en pacients amb cardiopatia isquèmica en fase crònica, ens aporta informació rellevant per al diagnòstic i l'evolució del potencial substrat arritmogènic d'arrítmies ventricular, i per la predicció de les mateixes i el seu tractament. La Tesi està linealment estructurada d'acord amb els resultats dels 5 articles que la componen titulats: 1) Follow-up after myocardial infarction to explore the stability of arrhythmogenic substrate- the Footprint Study-; 2) Monocyte subsets are differently associated with infarct size, left ventricular function, and the formation of a potentially arrhythmogenic scar in patients with acute myocardial infarction; 3) arrhythmogenic substrate detection in chronic ischaemic patients undergoing ventricular tachycardia ablation using multidetector cardiac computed tomography compared evaluation with cardiac magnetic resonance; 4) Cardiovascular Magnetic Resonance determinants of ventricular arrhythmic events after myocardial infarction; 5) Cardiac Magnetic Resonance-guided ventricular tachycardia substrate ablation.

Com a director de la doctoranda Beatriz Jáuregui desitjo deixar constància que he supervisat tot el procés d'elaboració d'aquesta tesi, des de la metodologia, recollida de dades, l'anàlisi dels mateixos i les conclusions derivades, havent-se realitzat amb una metodologia científica i ètica irreprotxable. Les troballes de la recerca de la doctoranda ens proporcionen una informació molt valuosa, necessària i pràctica, d'immèdiata aplicació a la pràctica clínica. Al mateix temps suposa un avanç significatiu en la medicina de precisió del tractament de les arrítmies ventriculars, que combina l'ús de tècniques d'imatge cardíaca mitjançant ressonància cardíaca d'alta resolució i un postprocessament d'imatge avançat utilitzant tecnologia d'avantguarda.

Per tant, confirmo que aquest treball compleix amb tots els requisits exigibles per a una tesi doctoral de màxim nivell i subscriu els resultats d'aquesta, i autoritzo a Beatriz Jáuregui perquè presenti aquesta tesi en la Universitat de Barcelona per a optar al grau de Doctor en Medicina.

Atentament,

Dr. Antonio Berruezo Sánchez



Barcelona, 4 d'/de novembre de 2021.

(signat)

Dr./a **Antonio Berruezo Sánchez**

*Un cop s'hagi emplenat l'informe, s'ha d'adjuntar i s'ha de fer arribar al doctorand o al president de la Comissió Acadèmica del programa de doctorat responsable de la tesi.*



**Informe director/s /tutor sobre l'autorització del dipòsit de la tesi**

Dr./a. José Tomás Ortiz Pérez, com a director/tutor de la tesi doctoral titulada “Utilidad de la Cardiorresonancia en la Evaluación de la Presencia y Evolución del Sustrato Arritmogénico, Estratificación de Riesgo y Tratamiento de las Arritmias Ventriculares Post-Infarto Crónico de Miocardio ” i, d'acord amb el que s'estableix a l'article 35 Normativa reguladora del Doctorat a la Universitat de Barcelona, emeto el següent:

**INFORME**

*(Informe detallat i motivat sobre el contingut de la tesi i sobre l'autorització de dipòsit de la tesi que s'ha demanat)*

La doctoranda Beatriz Jáuregui presentarà aquesta tesi doctoral en format per articles científics. Aquest treball, que versa sobre molts aspectes rellevants des del punt de vista de l'electrofisiologia cardíaca relatius a la utilitat de la cardiorresonància en pacients amb cardiopatia isquèmica en fase crònica, ens aporta informació rellevant per al diagnòstic i l'evolució del potencial substrat arritmogènic d'arrítmies ventricular, i per la predicció de les mateixes i el seu tractament. La Tesi està linealment estructurada d'acord amb els resultats dels 5 articles que la componen titulats: 1) Follow-up after myocardial infarction to explore the stability of arrhythmogenic substrate- the Footprint Study-; 2) Monocyte subsets are differently associated with infarct size, left ventricular function, and the formation of a potentially arrhythmogenic scar in patients with acute myocardial infarction; 3) arrhythmogenic substrate detection in chronic ischaemic patients undergoing ventricular tachycardia ablation using multidetector cardiac computed tomography compared evaluation with cardiac magnetic resonance; 4) Cardiovascular Magnetic Resonance determinants of ventricular arrhythmic events after myocardial infarction; 5) Cardiac Magnetic Resonance-guided ventricular tachycardia substrate ablation.

Com a director de la doctoranda Beatriz Jáuregui desitjo deixar constància que he supervisat tot el procés d'elaboració d'aquesta tesi, des de la metodologia, recollida de dades, l'anàlisi dels mateixos i les conclusions derivades, havent-se realitzat amb una metodologia científica i ètica irreprotxable. Les troballes de la recerca de la doctoranda ens proporcionen una informació molt valuosa, necessària i pràctica, d'immediata aplicació a la pràctica clínica. Al mateix temps suposa un avanç significatiu en la medicina de precisió del tractament de les arrítmies ventriculars, que combina l'ús de tècniques d'imatge cardíaca mitjançant ressonància cardíaca d'alta resolució i un postprocessament d'imatge avançat utilitzant tecnologia d'avantguarda.

Per tant, confirmo que aquest treball compleix amb tots els requisits exigibles per a una tesi doctoral de màxim nivell i subscriu els resultats d'aquesta, i autoritzo a Beatriz Jáuregui perquè presenti aquesta tesi en la Universitat de Barcelona per a optar al grau de Doctor en Medicina.

Atentament,

Dr. José Tomás Ortiz Pérez



UNIVERSITAT DE  
BARCELONA

Facultat de Medicina i Ciències de la Salut – Campus Clínic

Barcelona, 4 d'/de novembre de 2021.

(signat)

Dr./a **José Tomás Ortiz Pérez**

*Un cop s'hagi emplenat l'informe, s'ha d'adjuntar i s'ha de fer arribar al doctorand o al president de la Comissió Acadèmica del programa de doctorat responsable de la tesi.*

# AGRADECIMIENTOS

A mis Directores de Tesis, Pepe y Antonio, por haber sido la mentoría, ayuda y guía imprescindibles en la consecución de este trabajo, tan importante para mí.

A todos mis maestros en Cardiología y otros servicios, algunos de ellos ya jubilados, y a mis compañeros-amigos durante mi formación MIR en el Hospital Universitario Virgen del Rocío de Sevilla (2011-2016). Sin esta base fundamental, que tanto me enseñó de Medicina, pero sobre todo de la vida, nada de lo que ha venido después hubiera sido posible.

A todos mis maestros en Electrofisiología Cardíaca, del Hospital Universitario Virgen del Rocío de Sevilla, Hospital Clínic de Barcelona y Centro Médico Teknon de Barcelona: Alonso Pedrote, Eduardo Arana, Manolo Frutos, Antonio Berruezo. Gracias por enseñarme y ayudar a superarme cada día.

A todos los becarios (*fellows*), ya adjuntos, que me precedieron y con los que tuve la suerte de coincidir; fueron mi ejemplo a seguir (Manolo Durán, Federico Gómez, Juan Acosta, José Luis Martos, Álvaro Arce). Gracias a mis co-*fellows* y compañeros en el Clínic (Markus, David, Diego, y muchos más), y a esas enfermeras sin las cuales empezar una vida tan distinta y lejana a la que había conocido antes de llegar a Barcelona hubiera sido tan duro.

Finalmente, gracias a mi familia y en particular a mis padres, por ser mi mayor referente y mis mejores maestros; mi apoyo incondicional, el refugio en la adversidad. El impulso tomado desde una plataforma tan sólida como la que me habéis regalado ha hecho más fácil el salto hasta aquí. Os quiero.





# ÍNDICE GENERAL

<b>1. ÍNDICE DE TABLAS Y FIGURAS .....</b>	<b>15</b>
<b>2. ÍNDICE DE ABREVIATURAS .....</b>	<b>21</b>
<b>3. ARTÍCULOS DE LA TESIS .....</b>	<b>25</b>
<b>4. INTRODUCCIÓN .....</b>	<b>29</b>
a. Arritmias Ventriculares: Definición general y tipos.....	29
○ <i>a.1 Según su morfología .....</i>	<i>29</i>
○ <i>a.2 Según su mecanismo .....</i>	<i>32</i>
○ <i>a.3 Según el sustrato subyacente .....</i>	<i>33</i>
b. Cardiopatía Isquémica: Definición general, epidemiología, patogénesis, evolución y pronóstico .....	36
○ <i>b.1 Definición general y Epidemiología .....</i>	<i>36</i>
○ <i>b.2 Patogénesis de la Cardiopatía Isquémica .....</i>	<i>38</i>
○ <i>b.3 Evolución y Pronóstico de la Cardiopatía Isquémica .....</i>	<i>41</i>
▪ <i>b.3.1 Insuficiencia Cardíaca.....</i>	<i>42</i>
▪ <i>b.3.2 Muerte Súbita y Arritmias Ventriculares.....</i>	<i>45</i>
c. Fisiopatología de las Arritmias Ventriculares: Implicaciones en la Cardiopatía Isquémica .....	53
○ <i>c.1 Trastornos de la formación del impulso.....</i>	<i>53</i>
▪ <i>c.1.1 Trastornos del automatismo .....</i>	<i>55</i>

▪	c.1.2 Actividad desencadenada.....	58
○	c.2 Trastornos de la propagación del impulso: Reentrada.....	60
d.	Estratificación “clásica” del riesgo de Arritmias Ventriculares y Muerte Súbita ...	64
○	d.1 Fracción de eyección del ventrículo izquierdo (FEVI).....	65
○	d.2 Detección de isquemia miocárdica residual.....	69
○	d.3 Detección de potenciales triggers: EV y TVNS .....	69
○	d.4 Estudio electrofisiológico (EEF).....	70
○	d.5 Modelos clínicos multivariable .....	72
○	d.6 ECG de señales promediadas .....	73
○	d.7 Alternancia de la onda T en el ECG .....	74
○	d.8 Marcadores funcionales del sistema nervioso autónomo .....	74
e.	Papel actual de la Resonancia Magnética Cardíaca en la estratificación del riesgo de Arritmias Ventriculares y Muerte Súbita.....	75
f.	Aspectos técnicos relevantes de la Resonancia Magnética .....	80
○	f.1 Física relativa a la Resonancia Magnética .....	80
○	f.2 Secuencias de adquisición en Resonancia Magnética .....	84
○	f.3 Agentes de contraste paramagnético .....	85
○	f.4 Caracterización y cuantificación de la cicatriz miocárdica mediante Resonancia Magnética .....	86
○	f.5 Identificación del sustrato arritmogénico mediante Resonancia Magnética .....	90
g.	Tratamiento de las Arritmias Ventriculares en Cardiopatía Isquémica .....	95
○	g.1 Prevención secundaria de Arritmias Ventriculares .....	95
○	g.2 Tratamiento farmacológico de las Arritmias Ventriculares.....	96
○	g.3 Cirugía antiarrítmica de las Arritmias Ventriculares.....	97
○	g.4 Ablación con catéter de las Arritmias Ventriculares.....	98

▪	g.4.1 Mapa de activación .....	99
▪	g.4.2 Mapa de encarrilamiento (entrainment) .....	100
▪	g.4.3 Mapa de topoestimulación (pacemapping) .....	103
▪	g.4.4 Mapa (y ablación) de sustrato .....	104
h.	Papel de la Resonancia Magnética Cardíaca en la ablación de Arritmias Ventriculares en Cardiopatía Isquémica .....	111
o	h.1 Selección de la vía de abordaje para la ablación .....	111
o	h.2 Integración de la RM-RTG durante la ablación.....	113
i.	Papel de la Tomografía Computarizada en la identificación del sustrato y la ablación de Arritmias Ventriculares en Cardiopatía Isquémica .....	115
<b>5.</b>	<b>HIPÓTESIS DE TRABAJO Y OBJETIVOS .....</b>	<b>119</b>
a.	<b>Hipótesis de trabajo .....</b>	<b>119</b>
b.	<b>Objetivos de la Tesis .....</b>	<b>123</b>
<b>6.</b>	<b>PUBLICACIONES .....</b>	
a.	<b>Subproyecto 1:</b> Utilidad de la cardiorresonancia en la evaluación de la presencia y evolución del sustrato arritmogénico en el post-infarto crónico de miocardio .....	129
o	Artículo 1: <i>Follow-up after Myocardial Infarction to Explore the Stability of Arrhythmogenic Substrate – The FOOTPRINT Study</i> .....	129
o	Artículo 2: <i>Monocyte Subsets are Differently Associated with Infarct Size, Left Ventricular Function, and the Formation of a Potentially Arrhythmogenic Scar in Patients with Acute Myocardial Infarction</i> .....	173

o	Artículo 3: <i>Arrhythmogenic Substrate Detection in Chronic Ischaemic Patients undergoing Ventricular Tachycardia Ablation using Multidetector Cardiac Computed Tomography: Compared Evaluation with Cardiac Magnetic Resonance</i> .....	213
b.	<b>Subproyecto 2:</b> Utilidad de la cardiopresonancia en la estratificación del riesgo arrítmico en el post-infarto crónico de miocardio .....	251
o	Artículo 4: <i>Cardiovascular Magnetic Resonance Determinants of Ventricular Arrhythmic Events after Myocardial Infarction</i> .....	251
c.	<b>Subproyecto 3:</b> Utilidad de la cardiopresonancia en el tratamiento de las arritmias ventriculares en el post-infarto crónico de miocardio.....	303
o	Artículo 5: <i>Cardiac Magnetic Resonance-guided Ventricular Tachycardia Substrate Ablation</i> .....	303
<b>7.</b>	<b>DISCUSIÓN</b> .....	<b>355</b>
a.	Hallazgos principales de la Tesis.....	355
b.	Utilidad de la Resonancia Magnética en la Evaluación de la Presencia y Evolución del Sustrato Arritmogénico.....	357
o	<i>b.1 Cambios histológicos tras la isquemia y formación de la cicatriz post-IAM</i> .....	358
o	<i>b.2 Papel de la Resonancia Magnética en la evaluación de los cambios histológicos post-IAM e implicaciones clínicas</i> .....	363
o	<i>b.3 Evaluación del sustrato arritmogénico mediante otras técnicas de imagen: Comparación de la Tomografía Computarizada frente a la Resonancia Magnética</i> .....	373

c. Utilidad de la Resonancia Magnética en la Estratificación del Riesgo Arrítmico en Cardiopatía Isquémica.....	382
d. Utilidad de la Resonancia Magnética para guiar los Procedimientos de Ablación de Sustrato de Taquicardias Ventriculares .....	391
<b>8. CONCLUSIONES .....</b>	<b>403</b>
<b>9. BIBLIOGRAFÍA .....</b>	<b>409</b>
<b>10. ANEXOS .....</b>	<b>465</b>
a. Anexo I: Hojas de recogida de datos .....	465
b. Anexo II: Aprobación de los Comités de Ética de Investigación Clínica .....	471
c. Anexo III: Publicaciones adicionales al Doctorado.....	477
o <i>Artículos científicos</i> .....	477
o <i>Capítulos de libro</i> .....	482
o <i>Otros materiales o colaboraciones</i> .....	483
d. Anexo IV: Premios y Becas otorgados relacionados con la Tesis.....	485
<b>11. DECLARACIÓN DE CÓDIGO ÉTICO Y BUENAS PRÁCTICAS .....</b>	<b>489</b>



# 1. ÍNDICE DE TABLAS Y FIGURAS

Se recoge aquí el listado de tablas y figuras empleadas en los apartados de Introducción y Discusión de la Tesis. El resto de tablas y figuras se encuentran en cada uno de los artículos de los que la Tesis es compilación.

## TABLAS:

1. Tabla 1: Relación entre la FEVI y el riesgo de mortalidad total y MSC. ....	67
2. Tabla 2: Principales ensayos clínicos aleatorizados sobre el implante de DAI en prevención primaria en CI.....	69
3. Tabla 3: Estudios evaluando el valor predictor de la RM-RTG en la predicción de eventos arrítmicos .....	78
4. Tabla 4: Identificación de los distintos componentes de un circuito de reentrada mediante maniobras de encarrilamiento.....	103
5. Tabla 5: Principales ensayos clínicos aleatorizados comparando la ablación de sustrato de AV en CI vs. tratamiento convencional. ....	109

## FIGURAS:

1. Morfología de las arritmias ventriculares .....	32
2. Mecanismos de remodelado ventricular patológico .....	41



3. Supervivencia en miocardiopatía dilatada en función de su etiología .....	46
4. Fisiopatología de las taquiarritmias causantes de muerte súbita cardiaca en cardiopatía isquémica .....	49
5. Corrientes de membrana que generan el potencial de acción .....	56
6. Morfología del potencial de acción cardiaco.....	57
7. Mecanismos de aumento de automatismo normal .....	58
8. Actividad desencadenada .....	59
9. Circuitos de reentrada.....	63
10. Modelo anatómico esquemático de reentrada.....	63
11. Fases de la resonancia magnética .....	83
12. Modelo esquemático de cicatriz y canal de tejido heterogéneo .....	91
13. Caracterización de la cicatriz con RM .....	92
14. Caracterización del sustrato arritmogénico con EAM frente a RM.....	94
15. Electrogramas identificables por EAM en un BZC de RM .....	95
16. Potenciales medio-diastólicos del istmo crítico en una TV por reentrada .....	101
17. Modelo esquemático de los componentes de un circuito de reentrada .....	103
18. Correlación de la morfología de TV clínica por pacemap en la entrada de un BZC..	105
19. Rangos de voltaje bipolar para los distintos componentes de la cicatriz miocárdica	106
20. Estrategias para ablación de sustrato.....	108
21. Predictores de recurrencia de AV tras ablación de sustrato .....	111
22. Diferencias en supervivencia libre de AV tras ablación de sustrato ( <i>scar dechanneling</i> ) en función de la cardiopatía de base .....	111
23. Evolución de la fibrosis macroscópica en la miocardiopatía no isquémica .....	359

24. Eventos moleculares y celulares clave que intervienen en la formación de la cicatriz post-IAM .....	361
25. Caracterización de la cicatriz mediante análisis automático de las intensidades de señal de píxeles .....	367
26. Identificación automática del volumen y la masa de BZC .....	368
27. Evolución de la distribución y masa de BZC después de un IAM.....	369
28. Remodelado del VI y de la cicatriz tras un IAM .....	370
29. Fibrosis, edema y respuesta monocitaria tras el IAM.....	372
30. Comparación de las áreas adelgazamiento de la pared miocárdica por TAC y zonas de bajo voltaje en el EAM.....	376
31. Mapa de canales de TAC frente a la EAM y mapa de activación de una TV .....	377
32. Correlación entre el área de sustrato estructural identificado por imagen (RM y TAC) y por mapeo de voltaje (EAM).....	378
33. Comparación entre RM y TAC en la identificación de canales .....	380
34. Comparación entre RM y TAC en la identificación de entradas de canales .....	380
35. Utilidad de la TAC en la identificación de estructuras cardiacas relevantes.....	382
36. Integración multimodal de imágenes cardiacas para la planificación de procedimientos de ablación de sustrato de TV.....	383
37. Utilidad de distintas secuencias de RM en la identificación del sustrato arritmogénico .....	385
38. Esquema de la distribución de la masa de BZC.....	388
39. Comparación entre cicatriz arritmogénica vs. no arritmogénica por RM.....	390

40. Supervivencia libre de TV tras ablación de sustrato endocárdica o endo-epicárdica en función del grado de transmuralidad del sustrato .....	394
41. Ablación de sustrato ayudada por RM .....	395
42. Ablación de TV clínica guiada por RM .....	398
43. Detalle esquemático de ablación de TV clínica guiada por RM .....	399
44. Ablación de TV guiada por RM en paciente con TVMS espontánea.....	400





## 2. ÍNDICE DE ABREVIATURAS

AHA: *American Heart Association*

AUC: *Area under the (ROC) curve*

AV: Arritmias ventriculares

BZ: *Border zone*

BZC: *Border zone channels*

CE: *Conformité Européenne* (de la Unión Europea)

CI: Cardiopatía isquémica

DAI: Desfibrilador automático implantable

EAC: Enfermedad arterial coronaria

EAM: *Electroanatomical map*

ECG: Electrocardiograma

EEF: Estudio electrofisiológico

EGM: Electrograma

EV: Extrasistolia ventricular

FDA: *Food and Drug Administration* (de Estados Unidos)

FEVI: Fracción de eyección del ventrículo izquierdo

FV: Fibrilación ventricular

HTC: *Heterogeneous tissue channels*

IAM: Infarto agudo de miocardio

IC: Insuficiencia cardiaca

IM: Infarto de miocardio

LAVA: *Local Abnormal Ventricular Activities*

LP: *Late potentials*

MSC: Muerte súbita cardiaca

NYHA : *New York Heart Association*

PP: Post-potenciales

PPI: *Post-pacing interval*

PPP: Post-potenciales precoces

PPT: Post-potenciales tardíos

PSI : Pixel signal intensity

RM: Resonancia magnética

ROC (curve): *Receiver operating characteristic (curve)*

RS: Ritmo sinusal

RTG: Realce tardío de gadolinio

RVA: Ritmo ventricular acelerado

SCA: Síndrome coronario agudo

SNA: Sistema nervioso autónomo

TAC: Tomografía axial computarizada

TCL: *Tachycardia cycle length*

TRC: Terapia de resincronización cardiaca

TV: Taquicardia ventricular

TVM: Taquicardia ventricular monomórfica

TVMS: Taquicardia ventricular monomórfica sostenida

TVNS: Taquicardia ventricular no sostenida

TVP: Taquicardia ventricular polimórfica

VD: Ventrículo derecho

VI: Ventrículo izquierdo





# 3. ARTÍCULOS DE LA TESIS

La presente Tesis se presenta en formato de compendio de artículos. Consta de 3 objetivos, que se corresponden con sendos subproyectos, y 5 artículos, clasificados de la siguiente manera:

1. **Objetivo/subproyecto 1:** Utilidad de la cardi resonancia en la evaluación de la presencia y evolución del sustrato arritmogénico en el infarto crónico de miocardio:
  - Artículo 1: **Jáuregui B**, Soto-Iglesias S, Penela S, Acosta J, Fernández-Armenta J, Linhart M, Terés S, Syrovnev V, Zaraket F, Hervàs V, Prat-González S, Perea RJ, Morales-Ruiz M, Jiménez W, Lasalvia L, Bosch X, Ortiz-Pérez JT, Berruezo A. Follow-Up After Myocardial Infarction to Explore the Stability of Arrhythmogenic Substrate. JACC Clin Electrophysiol 2020;6:207-218. *FACTOR DE IMPACTO (2020): 6.375. ÁREA DE CONOCIMIENTO: Cardiology and Cardiovascular Medicine. CUARTIL: Q1.*
  - Artículo 2: Bosch X, **Jáuregui B**, Villamor N, Morales-Ruiz M, Ortiz-Pérez JT, Borràs R, Penela D, Soto-Iglesias D, Perea RJ, Doltra A, Prat-González S, Jiménez W, Mira Á, Lasalvia L, Berruezo A. Monocyte Subsets Are Differently Associated with Infarct Size, Left Ventricular Function, and the Formation of a Potentially Arrhythmogenic Scar in Patients with Acute Myocardial Infarction. J Cardiovasc Transl Res 2020;13:722-730. *FACTOR DE IMPACTO (2020):*

4.132. *ÁREA DE CONOCIMIENTO: Cardiology and Cardiovascular Medicine.*  
*CUARTIL: Q1.*

- Artículo 3: **Jáuregui B**, Soto-Iglesias D, Zucchelli G, Penela D, Ordóñez A, Terés C, Chauca A, Acosta J, Fernández-Armenta J, Linhart M, Perea RJ, Dolta A, Ortiz-Pérez JT, Bosch X, Berruezo A. Arrhythmogenic Substrate Detection in Ischemic Patients Undergoing Ventricular Tachycardia Ablation using Multi-Detector Computed Tomography. Compared Evaluation with Cardiac Magnetic Resonance. *Europace* 2021;23:82-90. *FACTOR DE IMPACTO (2020): 5.214. ÁREA DE CONOCIMIENTO: Cardiology and Cardiovascular Medicine. CUARTIL: Q1.*

2. **Objetivo/subproyecto 2:** Utilidad de la cardiorresonancia en la estratificación del riesgo de arritmias ventriculares en el infarto crónico de miocardio:

- Artículo 4: **Jáuregui B**, Soto-Iglesias D, Penela D, Acosta J, Fernández-Armenta J, Linhart M, Prat-González S, Perea RJ, Mont L, Bosch L, Ortiz-Pérez JT, Berruezo A. Cardiovascular Magnetic Resonance Determinants of Ventricular Arrhythmic Events After Myocardial Infarction. *Europace* 2021;euab275 [Online Ahead of Print]. *FACTOR DE IMPACTO (2020): 5.214. ÁREA DE CONOCIMIENTO: Cardiology and Cardiovascular Medicine. CUARTIL: Q1.*

3. **Objetivo/subproyecto 3:** Utilidad de la cardiorresonancia en el tratamiento de las arritmias ventriculares en el infarto crónico de miocardio:

- Artículo 5: Soto-Iglesias D, Penela D, **Jáuregui B**, Acosta J, Fernández-Armenta J, Linhart M, Zucchelli G, Syrovnev V, Zaraket F, Terés C, Perea RJ, Prat-González S, Doltra A, Ortiz-Pérez JT, Bosch X, Cámara Ó, Berruezo A. Cardiac Magnetic Resonance–Guided Ventricular Tachycardia Substrate Ablation. JACC Clin Electrophysiol 2020;6:436–447. *FACTOR DE IMPACTO (2020): 6.375. ÁREA DE CONOCIMIENTO: Cardiology and Cardiovascular Medicine. CUARTIL: Q1.*



# 4. INTRODUCCIÓN

## a. Arritmias Ventriculares: Definición general y tipos:

La taquicardia ventricular (TV) se define como la aparición de tres o más latidos consecutivos con origen en el tejido miocárdico situado por debajo del haz de His, a una velocidad superior a 100 latidos por minuto.

Se han desarrollado numerosos esquemas de clasificación para ayudar en el diagnóstico y tratamiento de las TV. Éstos incluyen la clasificación según la morfología de la taquicardia, según su mecanismo, o de acuerdo a la presencia de cardiopatía subyacente. (1)

### a.1 Clasificación de las TV según su morfología:

Gran parte de la terminología estándar utilizada para describir las TV se basa en criterios morfológicos (Figura 1)(2):

- La TV monomórfica (en adelante, TVM) se describe como aquella con una morfología QRS estable durante toda la taquicardia. Los pacientes pueden presentar una sola TVM o múltiples, estables, visibles en diferentes momentos. Una TV monomórfica sostenida (en adelante, TVMS) dura más de 30 segundos o requiere cardioversión debido a compromiso hemodinámico. Por el contrario, la TV no sostenida (TVNS) dura menos de 30 segundos.

- La TV polimórfica (en adelante, TVP) se refiere a aquella TV con una morfología del QRS cambiante de forma continua, sin ninguna morfología del QRS claramente dominante.
  - La "Torsade de Pointes" es un tipo particular de TVP que aparece en el contexto de un intervalo QT previamente prolongado y que se asocia con una "torsión de picos" (QRS) alrededor de la línea de base isoeleétrica.
- La TV pleomórfica se refiere a la presencia de más de una morfología del QRS durante la taquicardia; sin embargo, no hay un cambio continuo en la morfología, como se observa en la TVP.
  - La TV bidireccional constituye un tipo especial de TV pleomórfica, y se refiere a la alternancia, latido a latido, en el QRS, con un patrón de repetición. Suele verse en el escenario de la toxicidad por digoxina o la TV polimórfica catecolaminérgica.
- El aleteo o "flúter" ventricular se refiere a una TV extremadamente rápida con una configuración del QRS sinusoidal.
- La fibrilación ventricular (FV) es un ritmo ventricular rápido, muy irregular, con amplia variabilidad en la amplitud del QRS, la morfología y la longitud del ciclo. (1,3-5)

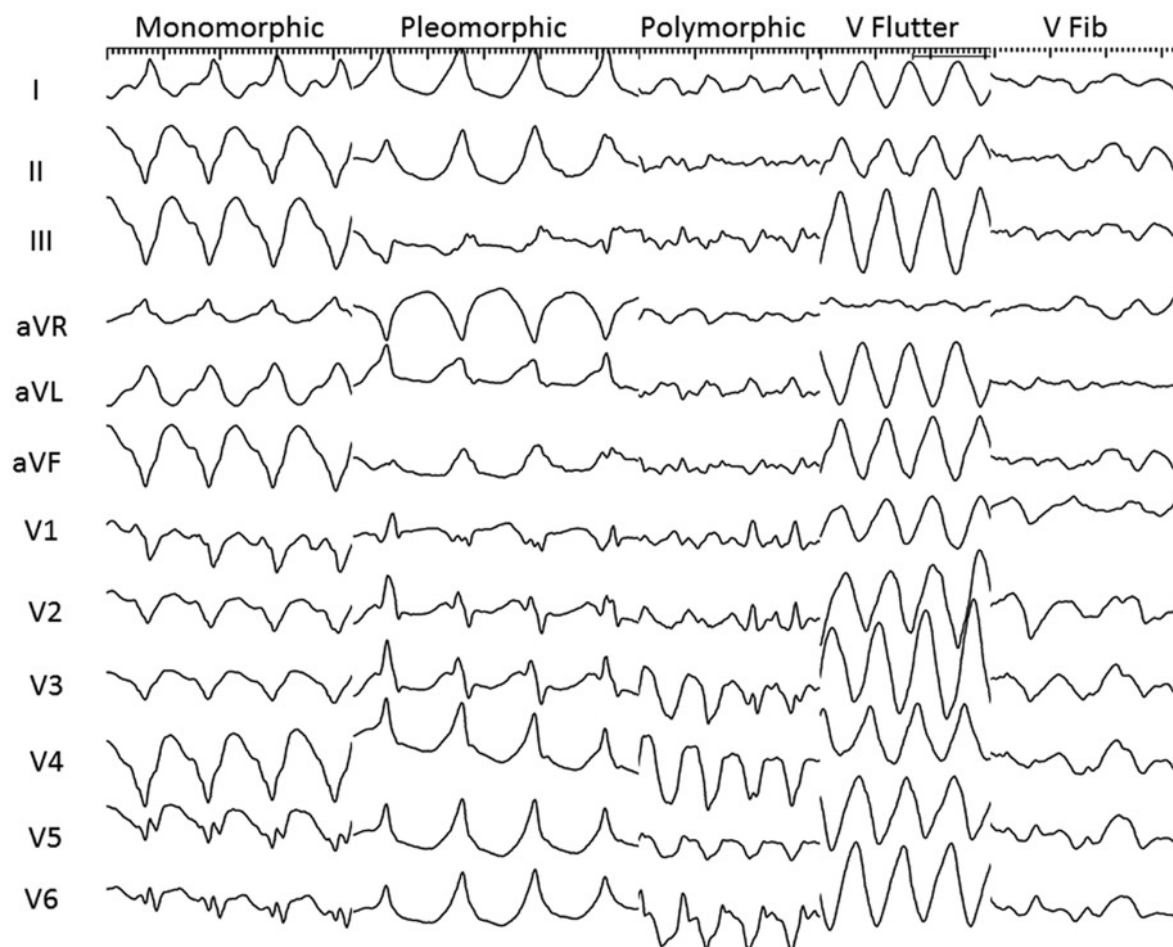


Figura 1. Distintas morfologías de arritmias ventriculares. Los ECG de 12 derivaciones para los tipos más comunes se muestran, de izquierda a derecha, desde las formas más organizadas hasta las que menos. De Verma et al. (2)

Por otro lado, atendiendo a la morfología de las TV, éstas pueden clasificarse según el patrón del QRS en la derivación V1, la transición precordial y el eje en las derivaciones inferiores: (2)

- Las TV con “patrón de bloqueo de rama izquierda” presentan una polaridad QRS predominantemente negativa en la porción terminal de la derivación V1. Estas TV se originan normalmente en el ventrículo derecho (VD) o zona septal del ventrículo izquierdo (VI).



- Las TV con “patrón de bloqueo de rama derecha”, por el contrario, presentan una polaridad QRS predominantemente positiva en la porción terminal de la derivación V1. Estas TV generalmente se originan en el VI.
- Finalmente, la concordancia positiva (QRS predominantemente positivos) en derivaciones precordiales (V1 a V6) indica un origen más basal, mientras que un origen apical da como resultado una concordancia negativa en precordiales. Las TV son de origen inferior (eje superior) cuando el QRS es predominantemente negativo en dos de las tres derivaciones inferiores del ECG (II, III, aVF), mientras las de eje inferior se originan más anteriormente.

### **a.2 Clasificación de las TV según su mecanismo:**

Los mecanismos subyacentes a las TV son los mismos que para otros tipos arritmias: incremento del automatismo, actividad desencadenada o reentrada. Las TV focales se originan en un solo punto y se irradian hacia el resto del miocardio ventricular. Si una TV es de origen focal, el mecanismo es generalmente por automatismo, actividad desencadenada o microrreentrada. Las TV relacionadas con la presencia de cicatriz miocárdica, y que van a ocupar el objeto de la presente Tesis, generalmente implican la propagación eléctrica a través de un gran circuito reentrante dentro de dicha cicatriz. A esto se le denomina TV macrorreentrante, y constituye el origen o mecanismo de la mayor parte de las TV en pacientes con cardiopatía estructural conocida. (5,6)

Los mecanismos responsables de la aparición de arritmias ventriculares (AV) en la cardiopatía isquémica (CI) serán objeto de un apartado específico (“c. Etiopatogénesis de las Arritmias Ventriculares: Implicaciones en la Cardiopatía Isquémica”). De su comprensión se deriva la correlación histológica con los hallazgos de la resonancia magnética (RM), que, tal y como indica el título de la presente Tesis, permite la evaluación de la presencia y evolución del sustrato arritmogénico, estratificación de riesgo y tratamiento de las AV en la CI crónica.

### **a.3 Clasificación de las TV según el sustrato subyacente:**

Según la presencia o no de un sustrato anatómico subyacente, las TV pueden clasificarse (2) en dos grandes grupos: 1) aquellas asociadas a la presencia de cardiopatía estructural (o, lo que sería sinónimo, a la presencia de fibrosis en el miocardio), frente a 2) aquellas no asociadas a cardiopatía, que definiremos como “idiopáticas”:

- TV asociadas a cardiopatía estructural: La mayoría de TVMS en el contexto de cardiopatía estructural se deben a un mecanismo de reentrada que afecta a una región donde existe una cicatriz miocárdica. La etiología más común de las TV macrorreentrantes en este contexto es la presencia de infarto de miocardio previo, es decir, la CI crónica. (1,4) Otras etiologías, relacionadas con la presencia de sustrato que permite la reentrada, incluyen el grupo de las miocardiopatías no isquémicas, trastornos infiltrativos del miocardio, la miocardiopatía arritmogénica o el antecedente de cirugía cardíaca previa. Una excepción notable sería la TV por

reentrada rama-rama (utilizando para la reentrada en lugar de cicatriz miocárdica las ramas derecha e izquierda del haz de His), que puede observarse en la miocardiopatía dilatada no isquémica. (4,7)

- TV no asociadas a cardiopatía estructural (“idiopáticas”): Aproximadamente un 10% de los pacientes que presentan TV no tienen una cardiopatía estructural obvia. En estos casos, rara vez se comportan como arritmias “malignas”. Las TV idiopáticas deben distinguirse de aquéllas que se encuadrarían en el contexto de síndromes arrítmicos hereditarios, ya que la mayoría de las pruebas estructurales y funcionales en ese grupo de patologías también son normales. También debe tenerse en cuenta que las TV idiopáticas pueden aparecer en pacientes con cardiopatía estructural (es decir, TV con un mecanismo no relacionado con la cicatriz miocárdica), por lo que este diagnóstico no debe descartarse en presencia de cardiopatía. Aunque existen diversas maneras de clasificar a las TV idiopáticas, aquí las reuniremos en dos grandes grupos:
  - TV sensibles a adenosina: La mayoría, aproximadamente el 90%, de las TV idiopáticas se clasifican como sensibles a adenosina. Son de origen focal, inducidas por catecolaminas, y son el resultado de post-potenciales tardíos y actividad desencadenada mediada por el monofosfato de adenosina cíclico (cAMP). (8,9) Existen dos formas, la más común de las cuales es la TV monomórfica repetitiva. La terminación de la TV depende del bloqueo directo de los receptores de dihidropiridina con antagonistas de los canales de calcio o maniobras para reducir los niveles de cAMP. Estos incluyen la

utilización de betabloqueantes, maniobras vagales, activación del receptor muscarínico M2 o del receptor de adenosina A1. (1,10)

Las TV sensibles a la adenosina generalmente se originan en los tractos de salida ventriculares. La mayoría, 60 a 80%, se originan en el tracto de salida del ventrículo derecho (TSVD), aunque a menudo se observan desde el tracto de salida del ventrículo izquierdo (TSVI) y las cúspides aórticas. Otros sitios del VI incluyen la continuidad mitro-aórtica, el anillo mitral y orígenes epicárdicos cerca de la gran vena cardíaca o interventricular anterior. Otras localizaciones infrecuentes de TV idiopáticas incluyen las extensiones musculares por encima de la válvula pulmonar, el anillo tricuspideo y los músculos papilares derecho e izquierdo. (11,12)

- TV sensibles a verapamilo: Se conocen también como TV fasciculares y se originan por un mecanismo de reentrada. Representan aproximadamente el 10% de las TV idiopáticas y constituyen la forma más común de TV del VI idiopática. (9) Existe cierta controversia en cuanto a la naturaleza exacta del circuito de reentrada; sin embargo, parece que el fascículo posterior izquierdo junto con tejido de Purkinje anormal, de conducción lenta, proporciona el sustrato para la reentrada y la TV. La adenosina no tiene ningún efecto sobre este tipo de ritmo.

## **b. Cardiopatía Isquémica: Definición general, epidemiología, patogénesis, evolución y pronóstico:**

### **b.1 Definición General y Epidemiología de la Cardiopatía Isquémica:**

En 1970, Burch et al. (13) utilizaron por primera vez el término "cardiopatía isquémica" (en adelante, CI) para describir la patología en la que la presencia de enfermedad arterial coronaria (EAC) crónica (estable) produce disfunción miocárdica grave, con manifestaciones clínicas a menudo indistinguibles de las de una miocardiopatía dilatada primaria. Los síntomas de insuficiencia cardíaca (IC) causados por la existencia de disfunción e hibernación del miocardio isquémico, fibrosis miocárdica difusa, o infartos de miocardio (IM) múltiples, apareciendo estos factores solos o en combinación, son los que dominan el cuadro clínico de la EAC. En algunos pacientes con EAC crónica, la angina de pecho puede aparecer puntualmente, pero más tarde este síntoma disminuye o incluso desaparece a medida que la IC se vuelve más prominente. (14) Durante el diagnóstico de la CI, es importante reconocer la presencia de miocardio hibernado, que resultaría de la presencia de isquemia reversible y es causa de disfunción ventricular, (15) potencialmente corregible mediante revascularización coronaria. (16)

En adelante, cuando nos refiramos a CI, se dará como sobreentendida la ausencia de miocardio hibernado, incluyendo sólo a aquellos pacientes con EAC estable, revascularizada en la medida que haya sido posible, o sin revascularizar en casos con IM evolucionados y territorio dependiente de la coronaria culpable no viable, pero en cualquier caso siempre y cuando encontremos presencia de miocardio necrótico y cicatrizado. (17)

A nivel mundial, la CI afecta a alrededor de 126 millones de personas (1.655 por 100.000), lo que representa aproximadamente el 1,72% del total de la población mundial. Entre 1990 y 2017, 9 millones de muertes fueron causadas por CI en todo el mundo. (18) Los hombres se vieron afectados con más frecuencia que las mujeres, y la incidencia generalmente comenzó a partir de la cuarta década de la vida, aumentando progresivamente con la edad. La prevalencia mundial de CI, además, está aumentando en los últimos años; se estima que la tasa de prevalencia actual de 1.655 por 100.000 habitantes supere los 1.845 por 100.000 para el año 2030. (18) Por regiones, los países de Europa del Este tienen actualmente la prevalencia más alta. (18) En resumen, la CI constituye la principal causa de muerte y discapacidad en todo el mundo.

Por otra parte, la CI sigue siendo la causa predominante de IC en los países desarrollados, y representa hasta el 60% de todos los casos de miocardiopatía. (19) Esto se debe en parte al éxito de las intervenciones de reperfusión precoz en el IM, (20) donde el grado variable de recuperación del miocardio expone a los pacientes a un riesgo igualmente variable de disfunción miocárdica progresiva. Los pacientes con IC por EAC presentan un peor

pronóstico en comparación con los pacientes con miocardiopatía idiopática después de ajustar por variables clínicas basales. (21) Estos hallazgos subrayan la necesidad de un diagnóstico precoz e implementación de terapias adecuadas, en particular relacionadas con la revascularización miocárdica.

### **b.2 Patogénesis de la Cardiopatía Isquémica:**

La patogénesis de la CI está determinada predominantemente por la presencia de isquemia o necrosis y el remodelado o dilatación ventricular. La CI puede ser el resultado de un IM grande y único o de múltiples IM más pequeños. (22) Estos eventos isquémicos van seguidos de una disfunción y dilatación progresivas del VI ("remodelado"), que puede desarrollarse de forma aguda (ej. en casos de un único IM de grandes dimensiones y que afecte a un alto porcentaje de la masa ventricular izquierda), o progresivamente, a lo largo de años. (23) Múltiples eventos moleculares participan en la dilatación progresiva del VI, incluyendo la muerte o apoptosis de los miocitos necróticos, la fibrosis de reemplazo, la inflamación crónica, fenómenos de autofagia, la disfunción mitocondrial y un metabolismo alterado. (24) La remodelación extensa del VI no ocurre en la misma medida en todos los pacientes con IM previo: los IM que afectan a la pared anterior y, sobre todo, cuando son de gran tamaño, son especialmente propensos a este remodelado adverso. Además, en algunos pacientes con CI, la dilatación y disfunción del VI constituye la presentación clínica inicial (IM previo "silente" o inadvertido por el paciente).

El remodelado adverso del VI (Figura 2) se refiere a cambios en su tamaño, forma y función después de una lesión (en nuestro caso, un IM previo). (25) Estos cambios son inicialmente compensatorios, pero posteriormente desadaptativos. La remodelación cardíaca que ocurre unos días después del IM comprende un adelgazamiento radial y un aumento circunferencial de la región del IM. Esto modifica la forma del ventrículo de cónica (normal) a esférica, lo que aumenta la tensión de la pared y perpetúa aún más la isquemia subendocárdica. (26) Estos efectos pueden exacerbar aún más la remodelación posterior, que se asocia con dilatación e hipertrofia compensadora transmural, se extiende más allá de la zona infartada e involucra a todo el ventrículo, alterando la mecánica ventricular general y reduciendo la eficiencia mecánica. En última instancia, la tensión de la pared aumenta, y una mayor dilatación puede provocar incluso una insuficiencia mitral funcional, que no hace sino contribuir al empeoramiento de la IC.

La remodelación precede a los síntomas de IC, pero es progresiva a medida que aparecen los síntomas. (27) Los cambios geométricos van acompañados de alteraciones estructurales y activación neurohormonal, que transforman los mecanismos compensatorios iniciales en cambios desadaptativos que perpetúan los síntomas de IC. (28)



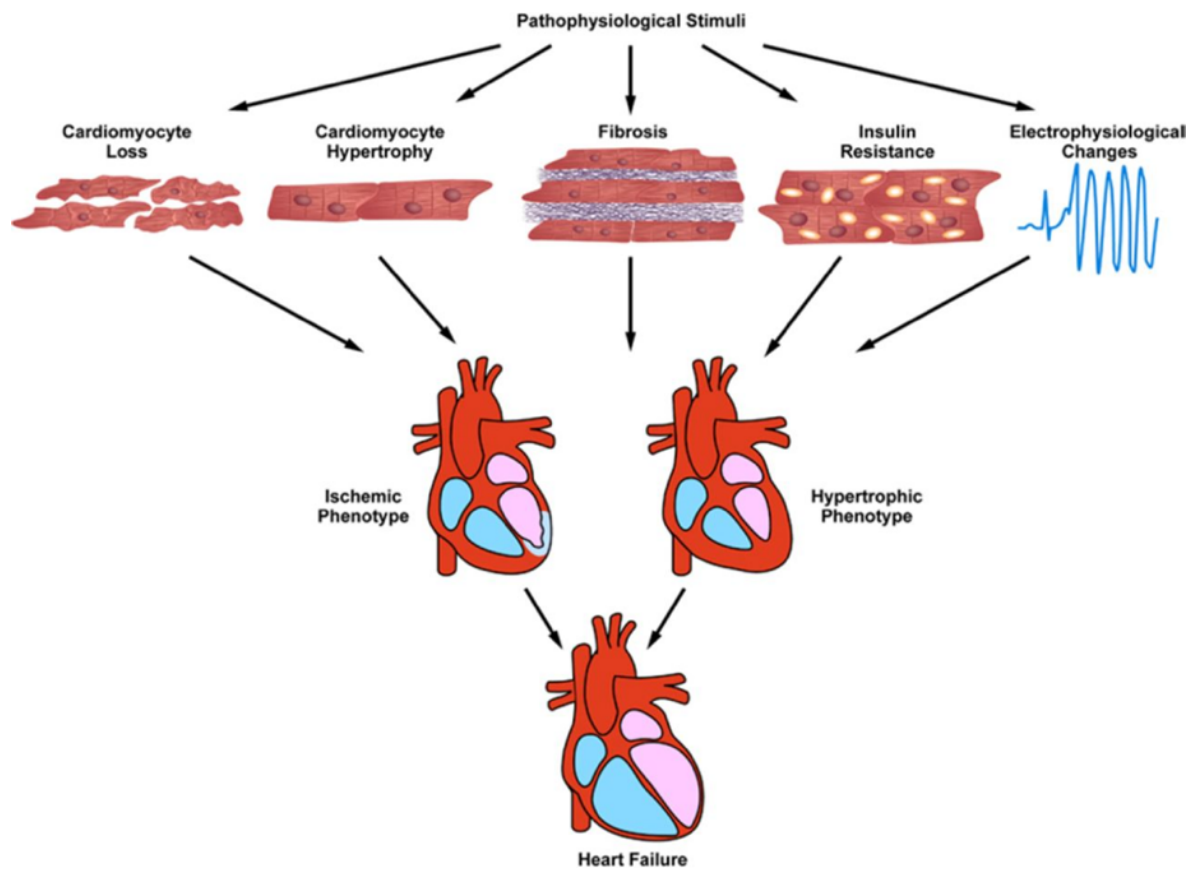


Figura 2: Mecanismos de remodelado ventricular patológico. De Burchfield et al. (25)

### **b.3 Evolución y Pronóstico de la Cardiopatía Isquémica:**

La evolución clínica y el pronóstico de la CI van a venir determinadas por la aparición de eventos adversos que podremos encuadrar en dos grandes grupos desde el punto de vista fisiopatológico: i) la IC y ii) la aparición de AV relacionadas con la muerte súbita cardiaca (MSC).

La IC constituye un síndrome clínico, vía final común de diversas cardiopatías (incluida la CI), que como tal implica la aparición de signos y síntomas debidos a fallo de órgano, esto es, a una incapacidad más o menos severa para llevar a cabo el bombeo efectivo de sangre al organismo. Este “fallo de bomba” se relaciona directamente con ingresos hospitalarios repetidos por descompensación clínica, fallo de otros órganos por hipoperfusión e isquemia (ej. insuficiencia renal) y el empeoramiento progresivo de la capacidad funcional del sujeto. En última instancia, puede aparecer una insuficiencia cardiaca terminal, con ausencia de respuesta al tratamiento farmacológico intensivo, o llegando a requerir soporte circulatorio mecánico o trasplante cardiaco. Finalmente, estos sujetos pueden sufrir muerte por IC refractaria a todas las medidas terapéuticas. Desde el punto de vista electrofisiológico, el final de la vida en esta situación se produce habitualmente por asistolia (ausencia de ritmo cardiaco y parada cardiaca secundaria) o de disociación electromecánica (parada cardiaca en presencia de ritmo residual), aunque también es frecuente encontrar bloqueos de conducción y fibrilación ventricular, que no serían la causa de, sino que acompañarían al proceso de la muerte (“arritmias del final de la vida”). Normalmente, la muerte en estos pacientes suele ser predecible, a menudo precedida por un proceso más o menos prolongado en el tiempo de deterioro clínico progresivo.

Por el contrario, la aparición de AV (TV/FV) constituye una complicación temible en cualquier cardiopatía, incluida la CI; de un lado, por su impredecibilidad, y de otro porque sus consecuencias son potencialmente funestas, al relacionarse directamente con la aparición de MSC. Aunque los mecanismos electrofisiológicos concretos que intervienen en la aparición de estas arritmias en la CI serán discutidos más adelante en profundidad, resulta imprescindible reconocer este tipo de complicación como relacionada, aunque no dependiente de forma lineal con la IC. Así, las AV son causa de MSC, prematura, incluso en pacientes sin síntomas de IC y con una buena calidad de vida previa. En este sentido, uno de los aspectos a mejorar en la Cardiología actual es precisamente mejorar la estratificación del riesgo de AV y MSC en los pacientes con cardiopatía, incluida la CI, y es alrededor de esta cuestión concreta sobre la que se han desarrollado los distintos objetivos planteados en la presente Tesis.

### **b.3.1 Insuficiencia Cardíaca en la Cardiopatía Isquémica:**

A pesar de los notables avances en el tratamiento de la EAC y el IAM durante las últimas décadas, la CI sigue siendo la causa más común de IC. (29,30) De acuerdo con la secuencia temporal entre la aparición del IAM y el desarrollo de IC, se pueden identificar tres presentaciones clínicas que difieren en fisiopatología, características clínicas y resultados: (i) IC aguda, en el momento de la presentación del IAM, (ii) IC durante la hospitalización por IAM y (iii) inicio de la IC después del alta de la hospitalización índice.

Dado que el objeto de la presente Tesis es lo que venimos a denominar "CI crónica", nos centraremos en la aparición de IC tras el alta de la hospitalización índice. Esta IC, que se desarrolla habitualmente a largo plazo desde el evento coronario inicial, se produce a consecuencia de la apoptosis de cardiomiocitos y la formación de cicatrices en el miocardio, eventos que desencadenan una activación neurohumoral crónica (eje renina-angiotensina-aldosterona y sobrerregulación del sistema nervioso simpático) y remodelación ventricular. La remodelación del VI es más pronunciada en hombres, pacientes con IAM de mayor tamaño y reperfusión tardía o fallida del lecho epicárdico o microvascular. (31) El desarrollo de IC es relativamente frecuente en pacientes con CI. Se diagnostica en aproximadamente el 13% de los pacientes a los 30 días del alta hospitalaria, y en el 20-30% al año tras el alta por IAM. (32,33) La incidencia de IC después del alta tras el IAM es más alta en los primeros meses, para disminuir y permanecer estable posteriormente, con una tasa de incidencia del 1.3-2.2% por año. (33)

El desarrollo de IC después de un IAM tiene un impacto significativo en el pronóstico clínico. (34) Entre los sujetos con antecedentes de IAM, el desarrollo de IC aumenta tres veces el riesgo de mortalidad total y cuatro veces la mortalidad cardiovascular. El momento del desarrollo de la IC también tiene un impacto en los eventos adversos. La IC que se desarrolla más de 3 días después del IAM se asocia con un 43% más de riesgo de mortalidad total en comparación con los pacientes con IC que se desarrolla en los primeros 3 días después del IAM. (34) Las estimaciones más recientes de supervivencia a 5 años ajustadas por edad y sexo en 2001 a 2010 frente a 1990 a 2000 fueron del 82% (intervalo de confianza al 95%: 80%-84%) y del 81% (79%-83%) entre los sujetos sin IC, en

comparación con el 61% (57%-64%) y el 54% (51%-57%) entre los pacientes con IC, respectivamente ( $p = 0,05$  para la heterogeneidad en las tendencias). (34)

En conclusión, La IC que se desarrolla después de un IAM constituye un factor de riesgo importante para mortalidad por todas las causas, tanto cardiovasculares como no cardiovasculares. (35) La mayoría de las muertes después de un IAM siguen ocurriendo en pacientes que desarrollan IC, (35) pero es previsible que la mortalidad global, que ya viene disminuyendo en las últimas décadas, (34,35) continúe haciéndolo a expensas de la aparición de nuevas alternativas terapéuticas, más allá de los betabloqueantes, (36) los inhibidores de la enzima convertidora de angiotensina (IECAs), (37) antagonistas de los receptores de aldosterona 2 (ARA-II), y los antialdosterónicos (38): los nuevos inhibidores de la neprilina (sacubitrilo) (39) e inhibidores del co-transportador de sodio-glucosa 2 (iSGLT2). (40)

En la **figura 3** se muestra la supervivencia global de los pacientes con IC secundaria a CI, de forma comparada a otras etiologías causantes de IC:

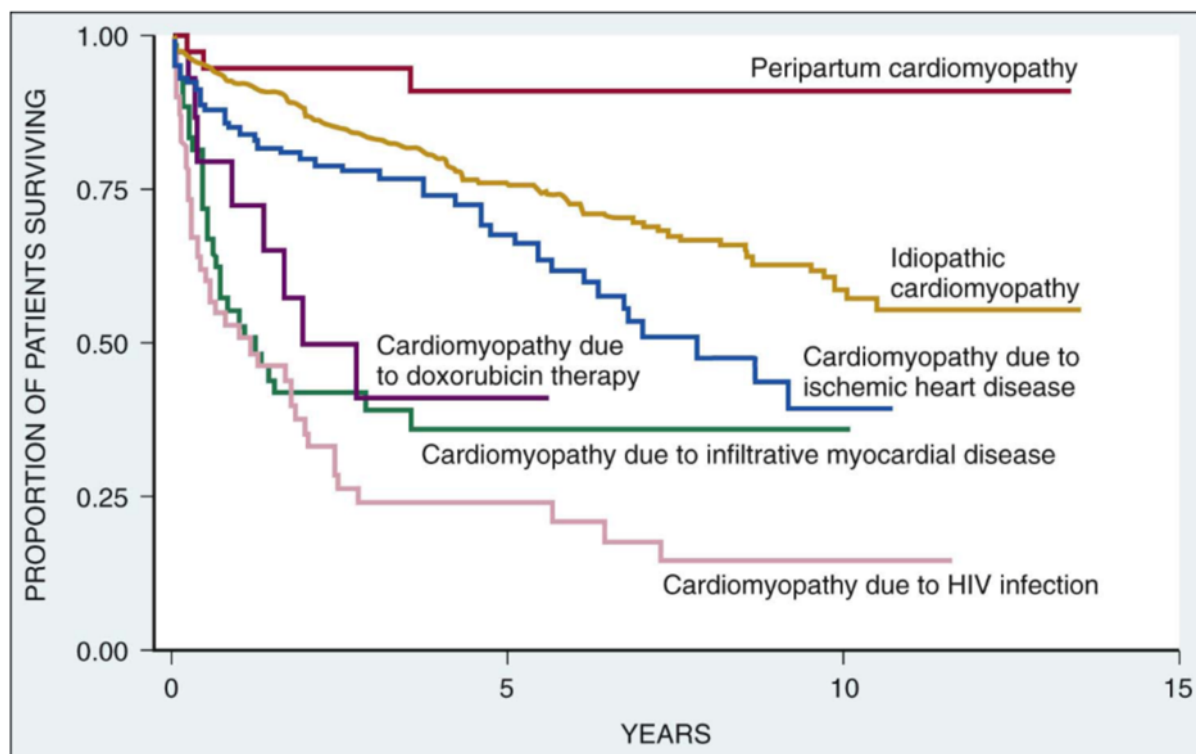


Figura 3. Supervivencia variable en pacientes con miocardiopatía dilatada en función de su etiología. De Felker et al. (35)

### b.3.2 Muerte Súbita y Arritmias Ventriculares en la Cardiopatía Isquémica:

Como ya se comentó al principio del apartado de “Evolución y Pronóstico de la Cardiopatía Isquémica”, las AV son causa de muerte prematura, incluso en pacientes sin síntomas de IC y con una buena calidad de vida previa. Esta característica diferencial sitúa el problema de las AV como uno de los mayores retos de la Cardiología actual en cuanto a su prevención.

La definición aceptada de MSC es la “muerte que ocurre dentro en la primera hora tras la aparición de los síntomas en los casos presenciados, y en las primeras 24 horas de haber sido visto con vida por última vez cuando no hay testigos”. (41,42) Es difícil estimar la incidencia mundial de MSC porque las cifras varían en función de la prevalencia de

cardiopatía coronaria en diferentes países. (43) Las estimaciones del número anual de MSC en los Estados Unidos (EEUU) se basan en gran medida en análisis retrospectivos de certificados de defunción, (44) actualizaciones estadísticas de la American Heart Association (AHA) basadas en datos del Centro Nacional de Estadísticas de Salud de EEUU, (45) y extrapolaciones nacionales de distintos registros. (46,47) Las estadísticas extraídas a partir de certificados de defunción procedentes de estos registros varían desde menos de 250.000 MSC al año cuando la definición etiológica se limita a la presencia de CI, hasta más de 460.000 MSC por año cuando se incluyen todas las causas de MSC. (44,45) Este amplio rango de cifras, así como las diferencias regionales reportadas en cuanto a la incidencia de MSC y los resultados tras una parada cardíaca ya sugieren la necesidad de realizar estudios prospectivos bien diseñados. (48) No obstante, las estimaciones más citadas de MSC permanecen en el rango de 300.000 a 350.000 MSC al año, (49) que corresponden a entre 1 y 2 MSC por cada 1000 personas en la población general.

Teniendo en mente las cifras globales de incidencia de MSC previamente comentadas, se estima que la presencia de EAC y sus consecuencias representan la causa de, al menos, el 80% de las MSC en los países occidentales (unas 240.000 - 280.000 MSC al año), (50) constituyendo las miocardiopatías no isquémicas, que no serán objeto de la presente Tesis, otro 10 a 15%. La EAC también es la causa más común de MSC en muchas áreas del mundo en las que la prevalencia de aterosclerosis es menor que en los países desarrollados. (41)

De entre todas las MSC relacionadas con la presencia de EAC, una proporción sustancial (10-80%) presenta en las autopsias rotura de placa intracoronaria, formación de trombos o

ambos hallazgos, que son indicativos de un síndrome coronario agudo (SCA) relacionado con la muerte. (50-52) Alrededor del 30% tienen una cicatriz miocárdica por un IAM antiguo ("CI crónica"), lo que supone un sustrato arritmogénico para la aparición de TV por reentrada, que estaría directamente relacionada con la muerte en estos casos. (52) En este sentido, cuando consideramos las MSC relacionadas con la presencia de EAC, debemos tener en cuenta que el mecanismo fisiopatológico y el pronóstico de la parada cardíaca y la MSC resultantes van a diferir en función del momento temporal respecto al evento coronario "índice".

Así, los SCA pueden estar relacionados con la parada cardíaca y MSC por causas no arrítmicas (ej. rotura cardíaca) (53) pero también arrítmicas, relacionadas con la génesis de fibrilación ventricular por isquemia aguda (véase capítulo 2c: "Epidemiología comparada de las Arritmias Ventriculares en la Cardiopatía Isquémica"). En cambio, la MSC que aparece a más largo plazo una vez superada la fase del SCA inicial (que no siempre es clínicamente patente, como ya se ha discutido previamente) se relaciona con los procesos de cicatrización miocárdica, el remodelado de la escara y del VI, que implican el desarrollo de un sustrato arritmogénico capaz de provocar la aparición de AV por reentrada, causa de MSC arrítmica en esta población (figura 4). (54)



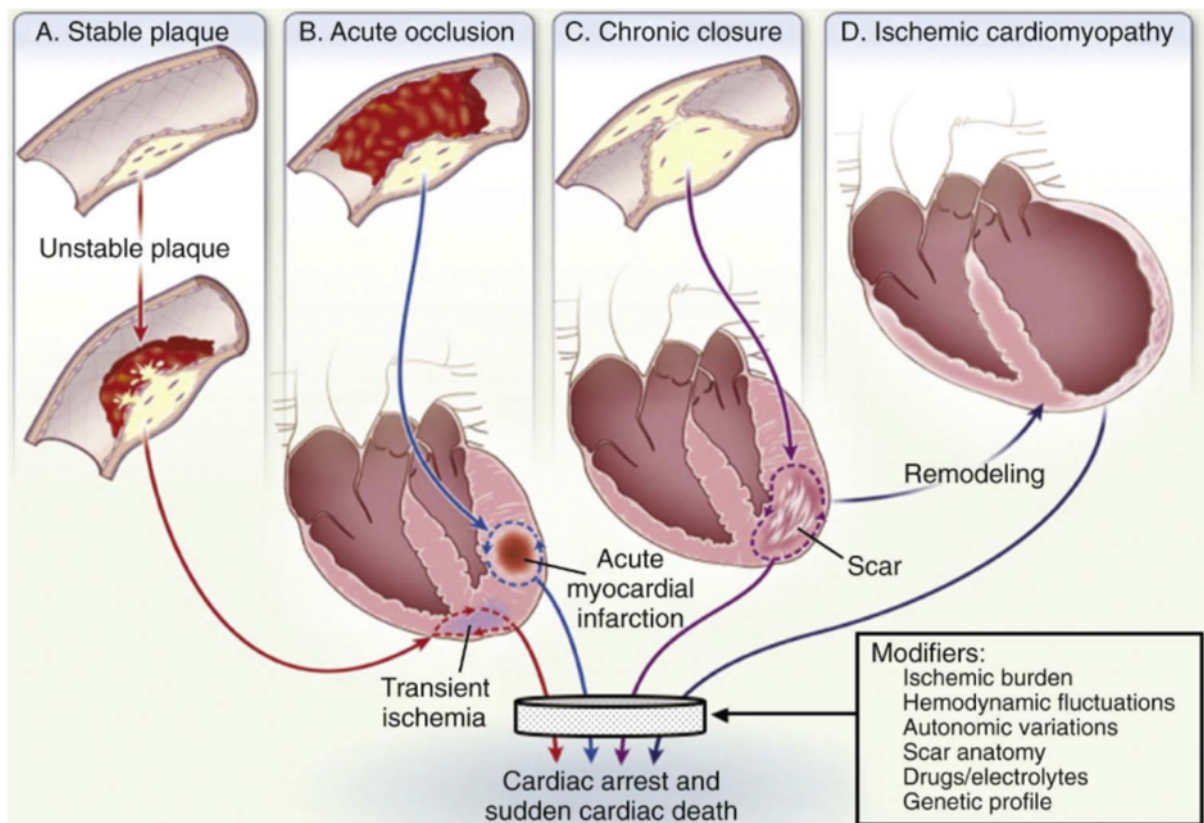


Figura 4. Fisiopatología de las taquiarritmias causantes de MSC en la EAC. De Bonny et al. (54)

El riesgo de MSC es más alto en los primeros 30 días después de un IAM y disminuye gradualmente con el tiempo. (42,55,56) Entre los supervivientes de un IAM con disfunción sistólica del VI o IC, se ha informado que el riesgo de MSC es de aprox. un 1,4% en los primeros 30 días, pero se reduce a aprox. un 0,14% por mes después de 2 años. (55) Esta reducción del riesgo puede deberse a la aplicación de medidas de prevención secundaria, aunque también a la muerte prematura de algunos pacientes, o a ambos factores. Aún así, la MSC es la responsable de entre un tercio y la mitad del total de muertes post-IAM (44,57,58) y por tanto constituye un problema de Salud Pública de primer orden. Por otro lado, la enseñanza "clásica" en la Cardiología actual es que la aparición de AV en las primeras 12-24 h después del IAM no predicen la MSC, aunque este "dogma" está siendo

cuestionado. (59) Las guías de práctica clínica actuales recomiendan evaluar la fracción de eyección del VI (FEVI) unas 6 semanas después del IAM para determinar la indicación de implante de desfibrilador automático implantable (en adelante, DAI) en prevención primaria de la MSC arrítmica. (60-62) Sin embargo, existen algunos trabajos que han relacionado la inducibilidad de TV tras un IAM, mediante un protocolo de estimulación programada ventricular durante la realización de un estudio electrofisiológico, con un alto riesgo de MSC, identificando a pacientes que probablemente se beneficiarían de la implantación de un DAI de manera precoz. (63)

Por otra parte, la incidencia de MSC global después de un IAM ha disminuido a lo largo de los años, en paralelo con la disminución de la mortalidad por CI. (64) En un estudio antiguo, llevado a cabo en la década de los años 80 del s. XX, aproximadamente el 10% de los supervivientes de IAM murieron repentinamente tras un período de seguimiento de 4 años. (65) Esta tasa ya disminuyó, en estudios realizados en la primera década del s. XXI, (58,66) a menos del 1% por año entre los pacientes que recibían tratamiento médico óptimo y revascularización. Esta incidencia de MSC es de esperar que continúe disminuyendo aún más con la reciente aparición de los nuevos tratamientos farmacológicos, ya comentados, en prevención secundaria de IC, como la asociación sacubitrilo-valsartán (67) o los inhibidores del co-transportador de sodio-glucosa 2 (iSGLT2), (68) que influyen directamente en los procesos que intervienen en el remodelado ventricular, probablemente por sus efectos sobre el metabolismo del miocardio, la fibrosis y la función vascular. (39,69-71)

Cuando hablamos de MSC en CI crónica, debemos considerar un concepto que se ha venido denominando “perfil de riesgo dinámico”, y que se relaciona con los cambios en la presencia y peso de distintos marcadores de riesgo a lo largo del tiempo tras un IAM. Entre éstos, se incluyen el remodelado del VI, los cambios en las propiedades anatómicas y electrofisiológicas de la cicatriz miocárdica (escara) y la progresión de la propia EAC. (72) De hecho, el riesgo de MSC más allá de los primeros 30 días después de un IAM aumenta notablemente por la presencia de IC concomitante o de eventos isquémicos recurrentes, que pueden ocurrir con cierta frecuencia durante el seguimiento. (64,66,73,74) Entre los participantes del ensayo clínico MADIT-II, (60) uno de los estudios clásicos que sustentan la indicación actual de implante de DAI en prevención primaria para pacientes con CI y FEVI severamente reducida, la IC y la isquemia recurrente se asociaron con un riesgo 1,5 y 2,5 veces mayor de descargas apropiadas por TV y FV, respectivamente. Estos hallazgos subrayan la importancia de la vigilancia continua y probablemente de la necesidad de re-estratificación del riesgo de MSC en pacientes con CI crónica.

Merece la pena recordar en este punto, y directamente en relación con el apartado anterior sobre el pronóstico de la IC en CI, que la disfunción sistólica grave del VI también es un marcador de riesgo elevado de MSC. (75) En las guías de práctica clínica actuales, (3,62) la presencia de FEVI < 35% en CI crónica es el criterio que determina el implante de DAI en prevención primaria de MSC. (60,61) Sin embargo, tan sólo un 20-30% de los pacientes con DAI en prevención primaria, en ensayos clínicos aleatorizados, reciben descargas apropiadas del mismo tras 4 años de seguimiento, lo que reduce el valor predictivo positivo de la FEVI como marcador de riesgo de MSC. (60,61) Además, aproximadamente el 65%

de los pacientes que sufren MSC tienen una función sistólica del VI normal o sólo ligeramente deprimida (es decir, una FEVI de entre el 35 y el 50%). (76-78)

Por lo tanto, la disfunción grave del VI por sí sola no es un marcador suficientemente específico para la MSC, pero podría ser útil cuando se usa con otros predictores o como parte de una puntuación de riesgo multivariable incluyendo diversos parámetros clínicos, como la edad, la clase funcional según la clasificación de la NYHA (*New York Heart Association*), la función renal, la anchura del QRS, la coexistencia de fibrilación auricular, la inducibilidad para TV, la hipertrofia del miocardio, la variabilidad de la frecuencia cardiaca, etc. (79-82) Sin embargo, estos algoritmos de puntuación todavía no han sido validados en series grandes prospectivas. Además, estos marcadores son poco específicos a la hora de discriminar el riesgo de MSC frente al riesgo de muerte no súbita. (79,80,83,84)

Por último, debemos considerar que la "muerte arrítmica" constituye el modelo de MSC, y aquí es donde se relacionan la MSC y las AV. La FV es el paradigma de AV que conduce a una MSC arrítmica, que finalmente evolucionaría a asistolia. Las TV pueden degenerar en FV, rápidamente en el caso de las polimórficas; por desorganización primaria del ritmo, o inestabilidad hemodinámica e isquemia global secundaria en el caso de las TV monomórficas.

En el caso de la CI aguda, es decir, durante un SCA, las concentraciones heterogéneas de potasio y variaciones de pH en el tejido isquémico, junto con el aumento del calcio intracelular en las células dañadas, conducen a alteraciones del potencial de acción (ver

apartado "c. *Fisiopatología de las Arritmias Ventriculares: Implicaciones en la Cardiopatía Isquémica*") y provocan la aparición de reentrada funcional debido a una distribución espacial heterogénea de los períodos refractarios en el tejido, ubicándose habitualmente los *triggers* iniciales en la red subendocárdica de Purkinje. (85,86) El frente de onda de la TV inicial debe dividirse en múltiples ondas para evolucionar a FV, un mecanismo aún no completamente comprendido.

En los pacientes con CI crónica, que son el objeto de la presente Tesis, las AV que provocan MSC son mayoritariamente TV por reentrada anatómica/funcional en relación a las zonas de fibrosis de la cicatriz post-IAM. (1) Además, en estas condiciones se pueden encontrar diferentes desencadenantes para la aparición de AV: alteraciones neurohormonales, factores mecánicos (p. ej. estiramiento del miocardio en condiciones de sobrecarga de volumen/presión, como la IC descompensada), y alteraciones iónicas (relacionadas con la enfermedad o inducidas por el tratamiento médico). (87,88)

### **c. Fisiopatología de las Arritmias Ventriculares: Implicaciones en la Cardiopatía Isquémica**

Los mecanismos generales responsables de las arritmias cardíacas pueden dividirse en: i) trastornos de la formación de los impulsos, ii) trastornos de la conducción de impulsos o iii) una combinación de ambos. Prácticamente todos estos mecanismos pueden ocurrir en el contexto de la CI, si bien en el caso concreto de la CI crónica, es decir, en pacientes con EAC estable pero presencia de cicatriz miocárdica por IM antiguo, el mecanismo de reentrada es el responsable de la inmensa mayoría de AV.

A continuación, se detallan los mecanismos fisiopatológicos subyacentes a la aparición de AV, haciendo particular énfasis en el mecanismo de reentrada por sus implicaciones en la CI crónica.

#### **c.1 Trastornos de la formación de los impulsos**

Este tipo de trastornos pueden referirse a alteraciones del automatismo celular (aumento del automatismo normal en células especializadas del sistema de conducción cardíaco, o la aparición de automatismo anormal en células que a priori no deberían presentar actividad "automática"), o bien a la aparición de actividad desencadenada por post-potenciales anormales.

Antes de ahondar en los mecanismos de alteración de la formación de los impulsos, resulta necesario comprender cómo se originan éstos, en condiciones normales. El potencial de acción cardíaco normal se divide en 5 fases (figura 5): (89)

- La fase 4, o "potencial de reposo", es estable a  $\approx -90$  mV en las células del miocardio que funcionan normalmente.
- La fase 0 es la fase de "despolarización rápida". El potencial de membrana cambia a un rango de voltaje positivo. Esta fase es fundamental para la rápida propagación del impulso cardíaco (velocidad de conducción,  $\theta = 1$  m/s).
- La fase 1 es la fase de "repolarización rápida". Esta fase establece el potencial para la siguiente fase del potencial de acción.
- La fase 2, la "fase de meseta", es la fase más larga. Es única entre las células excitables y marca la fase de entrada de calcio en la célula.
- La fase 3 es la fase de "repolarización final" que restaura el potencial de membrana a su valor de reposo.

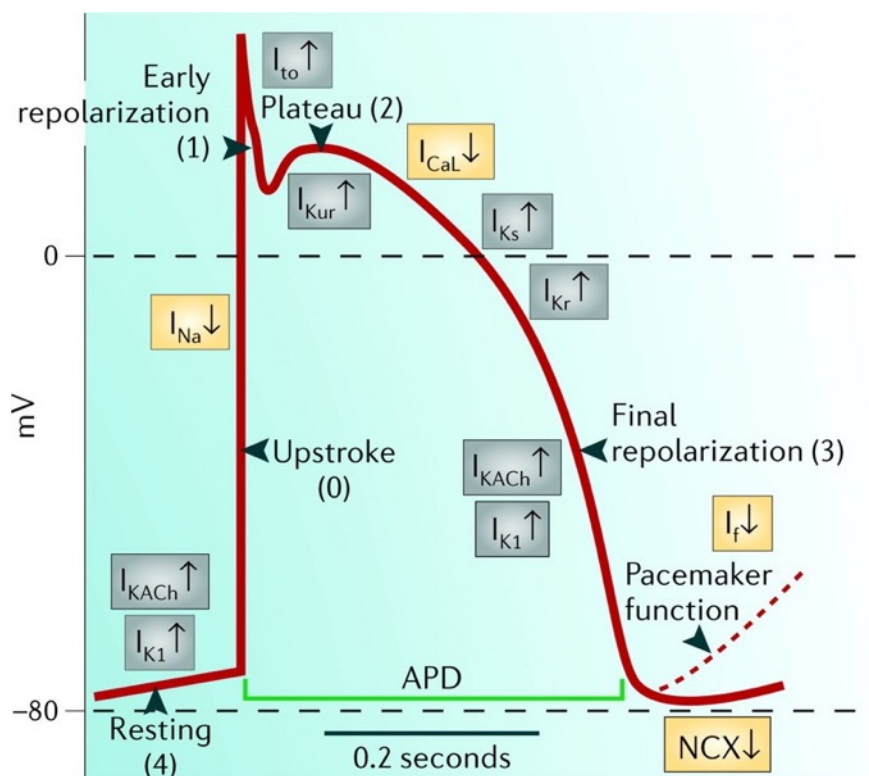


Figura 5. Corrientes de membrana que generan un potencial de acción normal en el miocardio. El potencial de reposo (4), la despolarización rápida (0), repolarización rápida (1), meseta (2) y repolarización final (3) son las 5 fases del potencial de acción. La disminución del potencial al final de la fase 3 en las “células marcapasos”, como el nodo sinusal, se muestra como una línea discontinua. Las corrientes de entrada,  $I_{Na}$ ,  $I_{Ca}$  e  $I_f$ , se muestran en cuadros amarillos; el intercambiador de sodio-calcio ( $NCX$ ) también se muestra en amarillo, aunque es electrogénico y puede generar corriente hacia adentro o hacia afuera. Las corrientes de salida  $I_{KACH}$ ,  $I_{K1}$ ,  $I_{to}$ ,  $I_{Kur}$ ,  $I_{Kr}$  e  $I_K$  se muestran en cuadros grises. La duración del potencial de acción (APD) es de aproximadamente 200 ms. De Nattel et al. (90)

### c.1.1 Aumento del automatismo normal y automatismo anormal

Algunas células cardíacas especializadas, como las células del nodo sinusal o sinoauricular (NSA), el nodo auriculoventricular (NAV) y el sistema His-Purkinje, así como algunas células en ambas aurículas, (91) poseen automatismo, o la capacidad de ser “células marcapasos”. Sus potenciales de acción son significativamente diferentes de los del miocardiocito. El potencial de membrana al inicio de la fase 4 está más despolarizado (-50 a -65 mV), sufren una despolarización diastólica lenta y gradualmente se fusionan en la fase 0. La tasa de despolarización en la fase 0 es mucho más lenta que en las células del miocardio, y da como resultado una propagación lenta del impulso cardíaco en las regiones nodales ( $\theta = 0,1$  a



0,2 m/s). (89) La morfología comparada entre el potencial de acción de las "células marcapasos" y las células del miocardio se muestra en la figura 6:

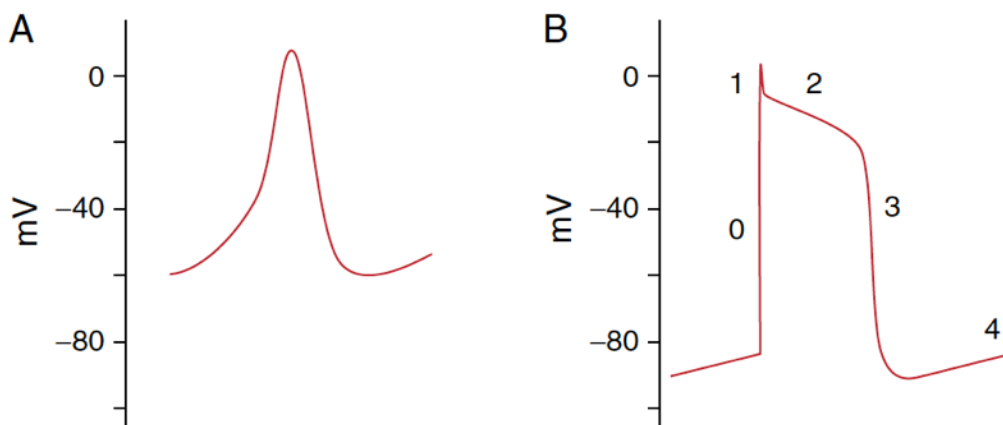


Figura 6. Morfología del potencial de acción cardíaco. A: potencial de acción en el nodo sinusal. B: potencial de acción en las células del miocardio. De Gaztañaga et al. (92)

La actividad marcapasos está controlada por el sistema nervioso autónomo y puede ser modulada (figura 7) por una variedad de factores sistémicos, que incluyen anomalías metabólicas y sustancias endógenas o farmacológicas. La actividad parasimpática reduce la tasa de descarga (es decir, el automatismo) de las células marcapasos. Por el contrario, el sistema nervioso simpático aumenta la frecuencia de dicho automatismo. Las anomalías metabólicas como la hipoxia y la hipopotasemia pueden conducir a un aumento del automatismo normal, como resultado de la inhibición de la bomba de  $\text{Na}^+/\text{K}^+$ .

En el caso concreto de la CI, podremos ver ritmos ventriculares acelerados (RVAs) por un aumento del automatismo en las ramas del haz o los fascículos del sistema de Purkinje, habitualmente durante la reperfusión tras un IAM. La incidencia de RVA varía desde el 8% hasta el 46%. Se ha comprobado que su aparición en este contexto suele ser indicativa de una reperfusión subóptima. (93)

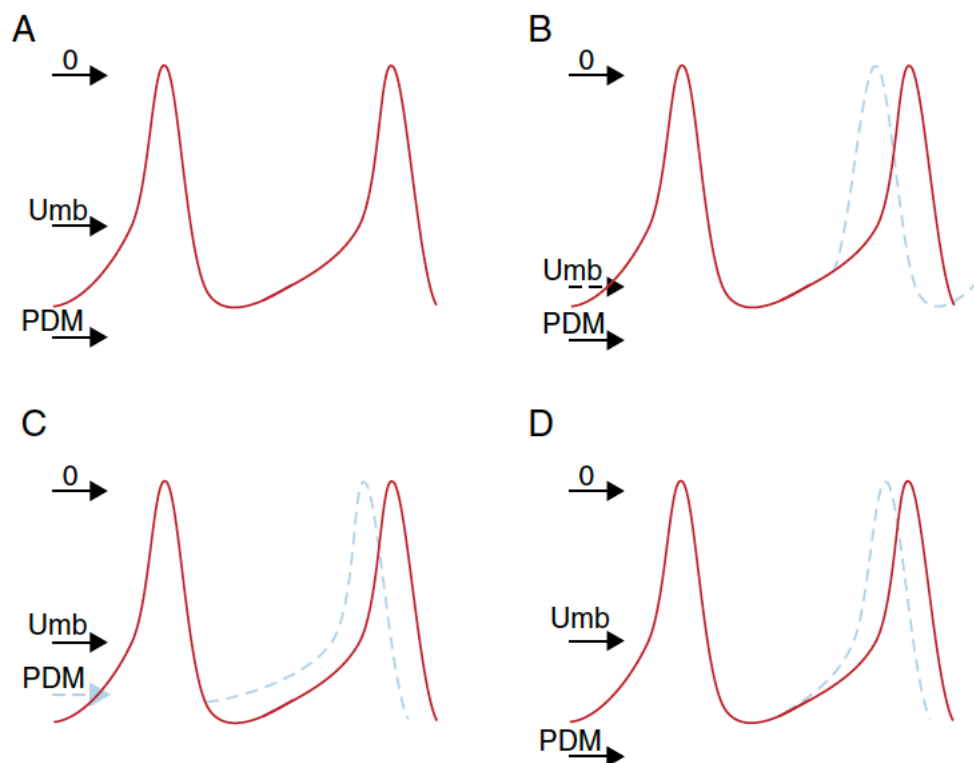


Figura 7. Mecanismos de aumento de automatismo normal. A: normal. B: aumento del umbral de voltaje. C: disminución del potencial diastólico de membrana (PDM). D: aumento de la pendiente de la despolarización de fase 4. PDM: potencial diastólico de membrana; Umb: umbral. De Gaztañaga et al. (92)

Por otro lado, las células sin función de marcapasos del miocardio auricular y ventricular, que en el corazón normal normalmente no muestran automatismo, pueden presentar en determinadas circunstancias propiedades de automaticidad. Esto puede suceder en condiciones que disminuyen el potencial diastólico máximo hacia el potencial umbral, p. ej. en presencia de potasio extracelular elevado, pH intracelular bajo y exceso de catecolaminas. La tasa intrínseca de un foco anormal automático depende del potencial de membrana; cuanto más positivo sea el potencial de membrana, más rápida será la velocidad automática. (94)

En el caso de la CI, podremos observar ritmos idioventriculares acelerados (RIVAs) y TV por automatismo anormal en el miocardio, también en el contexto de la reperfusión aguda durante un IAM.

### c.1.2 Actividad desencadenada

La actividad desencadenada se define por la iniciación del impulso provocada por la aparición de post-potenciales (PP) (oscilaciones del potencial de membrana que ocurren durante o inmediatamente después de un potencial de acción precedente). (95,96) Los PP ocurren sólo en presencia de un potencial de acción previo (el *trigger*) y, cuando alcanzan el umbral potencial, permiten la generación de un nuevo potencial de acción. Ésta puede ser la fuente a su vez de una nueva actividad desencadenada, generando arritmias auto-sostenidas. En función de su relación temporal, se describen dos tipos de PP: los PP precoces (PPP), que ocurren durante las fases 2 o 3 del potencial de acción, y los PP tardíos (PPT), que ocurren tras la finalización de la fase de repolarización (Fig.6).

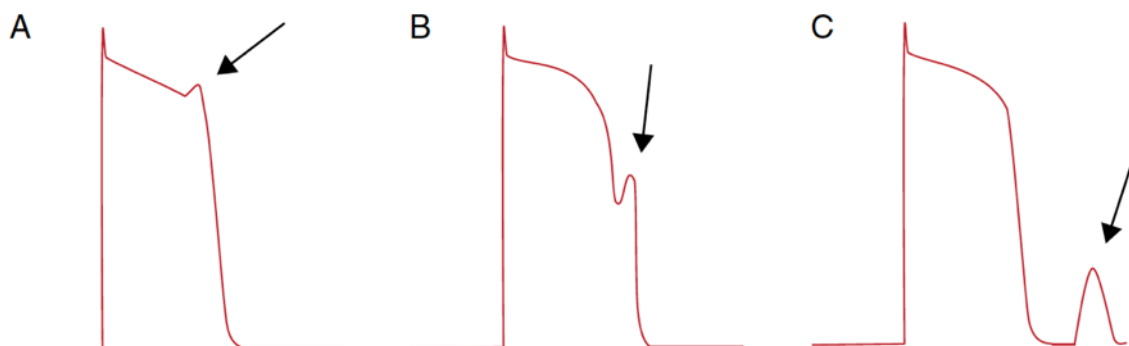


Figura 8. Actividad desencadenada. A: Post-potencial precoz en fase 2. B: Post-potencial precoz en fase 3. C: Post-potencial tardío. De Gaztañaga et al. (92)

Una condición fundamental que subyace al desarrollo de los PPP es la prolongación del potencial de acción, que se manifiesta en el electrocardiograma (ECG) de superficie como prolongación del intervalo QT. Durante la fase de meseta (fase 2), pequeños cambios en las corrientes iónicas de despolarización y repolarización pueden causar notables variaciones en la duración y morfología del potencial de acción. Existe una amplia variedad de situaciones que pueden facilitar las condiciones necesarias para que se produzcan PPP, como p.ej. la bradicardia (que prolonga la duración del potencial de acción), (97) la hipopotasemia, la hipoxia y acidosis, y una amplia variedad de fármacos. (92) En el contexto de la CI, debemos tener en cuenta que la isquemia aguda incrementa la duración del intervalo QT, aumentando la heterogeneidad de la repolarización (98) y facilitando la aparición de PPP. Los PPP son el mecanismo subyacente a las TV polimórficas (TVP) que también podemos encontrar en el contexto de isquemia aguda durante un IAM. (85)

En el caso de los PPT, un factor crítico para su desarrollo es la duración del potencial de acción; a mayor duración, mayor concentración de  $\text{Ca}^{2+}$  intracelular, que facilita su aparición. En el contexto de la CI, podremos observar las siguientes arritmias mediadas por la aparición de PPT: RVAs en el contexto agudo del IAM, por isquemia/reperfusión, y algunas formas de TV repetitiva. (85)

## c.2 Trastornos de la conducción de los impulsos

Dentro de este grupo de trastornos eléctricos a nivel cardiaco, encontraremos los bloqueos de la conducción, que se salen de la temática de la presente Tesis, y los mecanismos de reentrada. Es en este último punto donde centraremos toda nuestra atención en lo sucesivo, pues es el mecanismo implicado en la inmensa mayoría (> 95%) (1) de AV sostenidas (TVMS) que aparecen en los pacientes con CI crónica. La primera descripción de este fenómeno se la debemos a un trabajo clásico de De Bakker et al. (99) En los pacientes con MSC y ECG disponible, el primer detectable es, en la inmensa mayoría de casos, TV o FV. Una TV monomórfica prolongada (que presumiblemente será por reentrada en pacientes con CI) es el principal factor de riesgo para la degeneración en FV, facilitada por la isquemia, la producción de radicales libres y la liberación de calcio intracelular. (100)

La reentrada se produce cuando el frente de onda (dirección del impulso) se propaga repetidamente a lo largo de un circuito de rotación cerrado y lo suficientemente amplio como para permitir que el tejido se encuentre siempre en un estado excitable cuando vuelve a llegar a él dicho frente de onda. Para que se produzca la reentrada, son necesarias dos condiciones *sine qua non*: i) presencia de bloqueo unidireccional de la conducción, y ii) una longitud de ciclo del circuito (que depende del tamaño del circuito y de la velocidad de propagación del frente de onda) de una duración superior a la de cualquiera de los periodos refractarios existentes en el tejido que forma parte de dicho circuito; de esta manera, el tejido adyacente al extremo del frente de onda siempre se encontrará en condiciones de re-excitabilidad (figura 9).

Las TV por reentrada en pacientes con CI crónica (es decir, en presencia de una cicatriz miocárdica por IAM antiguo) tienen su origen principalmente en los haces de miocardio supervivientes que se encuentran en el interior de la cicatriz, separados por tejido conjuntivo y fibrosis, y en presencia de alteraciones del acoplamiento intercelular (conducción enlentecida) (figuras 9 y 10). (1,101) En adelante, definiremos la presencia de "sustrato arritmogénico" anatómico en la CI como la presencia de una cicatriz post-IM heterogénea, con presencia de haces de miocardio viable dentro de las zonas de fibrosis más densa que posibilitan la aparición de TV por reentrada. Las TVMS se producirán, previa presencia del sustrato arritmogénico adecuado, en presencia de determinados desencadenantes, como aumento del tono simpático, desequilibrios electrolíticos, isquemia persistente o descompensación aguda de IC. (1)

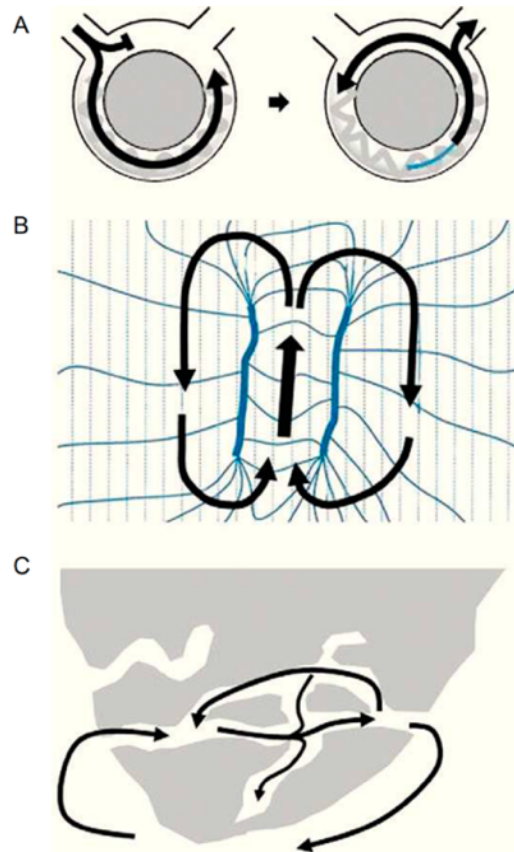


Figura 9. A: Circuito de reentrada que se inicia con un bloqueo unidireccional. B: Circuito de reentrada “en forma de 8” en el que la reentrada se establece a causa de la dispersión de la refractariedad durante la taquicardia. C: Circuito de reentrada anatómica, creado por franjas de miocardio viable en el interior de la cicatriz, con posibilidad de formación de múltiples circuitos de reentrada. De Benito et al. (101,102)

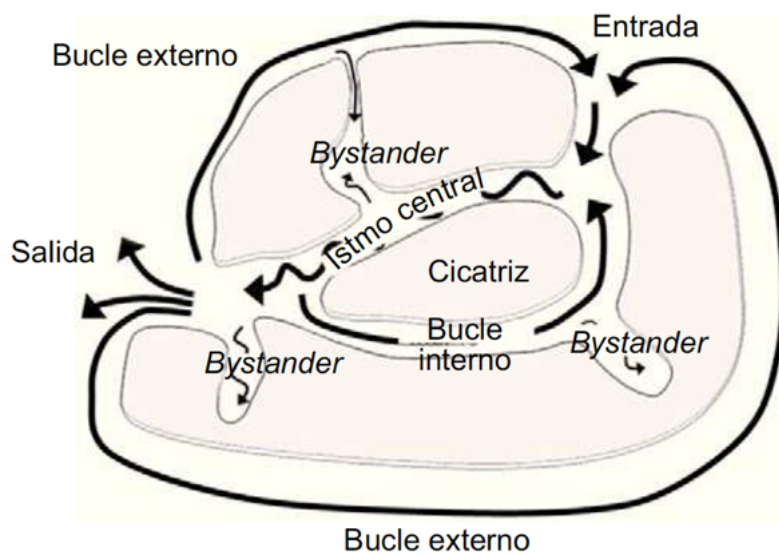


Figura 10. Modelo anatómico esquemático para explicar el mecanismo de formación de TV por reentrada tras un IAM. De Benito et al. (102)

Desde la descripción de los primeros estudios electrofisiológicos (EEF), se han descrito una serie de maniobras de estimulación para demostrar de manera sencilla los diferentes mecanismos de arritmia. Con el apoyo de los resultados obtenidos en modelos experimentales, sabemos que las TV post-IAM tienen su origen en las franjas de miocardio viable del interior de la cicatriz, y que la reentrada es el mecanismo que explica > 95% de los casos. (1) Los registros EEF intracardiacos de las zonas correspondientes a las cicatrices, durante ritmo sinusal (RS), muestran potenciales de bajo voltaje, fraccionados y con componentes retrasados, que corresponden a la actividad de los miocitos supervivientes, con una conducción anormalmente lenta y fraccionada. (1,99,103-108)



#### d. Estratificación “clásica” del riesgo de Arritmias Ventriculares y Muerte Súbita

Como ya se comentó previamente, la MSC continúa representando de un tercio a la mitad del total de muertes en pacientes con CI. (44,57,58) La supervivencia de los pacientes que experimentan una parada cardíaca extrahospitalaria es muy escasa (< 20% en la mayoría de las series), incluso a pesar de la mejoría en formación sobre reanimación cardiopulmonar y el uso de desfibriladores externos automáticos. (109) Por lo tanto, resulta fundamental, y todavía un reto, poder identificar de forma prospectiva a los pacientes que han sufrido un IAM con mayor riesgo de MSC. También debemos de tener en cuenta, como ya se ha explicado en detalle, que el perfil de riesgo de MSC post-IAM es dinámico; así, aproximadamente la mitad de las MSC que ocurren en el primer mes post-IAM se deben a causas no arrítmicas (ej. rotura cardíaca), como también se ha comentado anteriormente. (53)

Se han desarrollado varias pruebas o tests que pretenden estratificar el riesgo de MSC, atendiendo a los mecanismos que subyacen a dicha MSC. Existen pruebas que evalúan la FEVI o la isquemia miocárdica residual; también existen otros tests que identifican posibles desencadenantes de TV o FV, como la presencia de EV y TVNS; pruebas que detectan el sustrato eléctrico real responsable de la génesis de las taquiarritmias ventriculares, como el EEF, el ECG de señales promediadas (SAECG) y la detección de ondas T alternantes (TWA) en el ECG; y pruebas que reflejan la función anormal del sistema nervioso autónomo, incluida la variabilidad de la frecuencia cardíaca (HRV), la sensibilidad barorrefleja (BRS) y la turbulencia de la frecuencia cardíaca (HRT). Influyendo en la actividad de todas estas

variables está la FEVI, que no se relaciona directamente con ningún sustrato arrítmico específico.

Aunque la evidencia disponible referida a cada uno de los tests mencionados se abordará por separado en los siguientes apartados, podríamos resumir la situación de la estratificación actual de riesgo arrítmico en pacientes con cardiopatía estructural (y la CI es el paradigma) con los resultados de un metaanálisis que comparó la precisión predictiva para aparición de eventos arrítmicos mayores de cinco pruebas diferentes: SAECG, HRV, ECG ambulatorio, FEVI y EEF. Las sensibilidades de las pruebas oscilaron del 42,8% al 62,4% y las especificidades del 77,4% al 85,8%, sin que ninguna prueba fuera satisfactoria por sí sola para predecir el riesgo de MSC. (110)

#### **d.1 Fracción de eyección del ventrículo izquierdo (FEVI)**

Múltiples estudios prospectivos han establecido una relación clara entre la mortalidad total y la presencia de FEVI reducida, evaluada mediante ecocardiografía. (111) La mortalidad aumenta cuando la FEVI disminuye  $< 50\%$ , (112) pero tanto la mortalidad total como el riesgo de MSC permanecen bajos hasta que la FEVI desciende a  $\leq 40\%$ . (113) Los pacientes con FEVI  $< 40\%$  muestran un aumento progresivo del riesgo de mortalidad a medida que la FEVI sigue disminuyendo. Debido a la mejora en las terapias de reperfusión, existen relativamente pocos pacientes con FEVI muy baja tras el IAM. (114-116)

Sin embargo, no hay evidencia de la relación causa-efecto entre una FEVI anormal y la ocurrencia de MSC. De hecho, aunque el riesgo absoluto de MSC es mayor en pacientes con FEVI más baja, el número de MSC es mayor en pacientes cuya FEVI es superior. (117) Además, los valores actuales de FEVI que se utilizan para definir las poblaciones de alto riesgo (habitualmente, < 35%) presentan poca sensibilidad, y no identifican hasta, al menos, el 50% de los pacientes con riesgo de MSC (tabla 1). (118)

Punto de corte	% con FEVI < punto de corte	Sensibilidad (MSC o EA) (%)	RR de MSC y/o EA	RR de muerte no súbita o cardiovascular	Ref.
40	34	72	4.6	3.7	Mukharji et al. (73)
40	26	46	2.5	3.7	Farrell et al. (119)
40	26	71	4.8	5.2	Richards et al. (120)
35	25	35	1.6	4.9	Bourke et al. (121)
35	16	41	3.8	5.0	Hohnloser et al. (122)
30 <sup>a</sup>	50	59	1.7	1.5	Buxton et al. (123) <sup>a</sup>
40	23	45	2.9	4.4	Huikuri et al. (58)
30	5	50	22.3	17.9	Bauer et al. (124)
40 <sup>b</sup>	35	50	1.9 (HR)	1.8 (HR)	Exner et al. (125) <sup>b</sup>
30	5	22	5.3	15.6	Bauer et al. (126)
35	11	33	4.5 (HR)	7.2 (HR)	Mäkikallio et al. (127)
<sup>a</sup> El estudio sólo reclutó pacientes con FEVI ≤ 40%. <sup>b</sup> El estudio sólo reclutó pacientes con FEVI < 50%.					

Tabla 1. Relación entre la FEVI y el riesgo de mortalidad total y MSC. De Waks et al. (118)  
(EA: Eventos adversos. RR: Riesgo relativo. HR: Hazard ratio. Ref.: Referencia)

Los principales ensayos clínicos en los que se basa la evidencia actual para la elección de la FEVI como criterio para implante de DAI en prevención primaria en CI se recogen en la tabla 2. Aunque en las guías de práctica clínica (3,62) la presencia de FEVI < 35% (pasados al menos 40 días después del IAM, según los resultados del estudio DINAMIT) (128) (tabla 2) es el criterio que determina actualmente el implante, (60,61) ésta no ha demostrado ser un parámetro sensible ni específico para la predicción de MSC en CI. (58,73,127,119-126)

Sin embargo, se sigue utilizando porque fue el principal criterio de inclusión en los ensayos clínicos pivotaes sobre la utilidad del DAI en prevención de MSC (tabla 2). Como contrapunto, en el reciente estudio PRESERVE EF (*Post Myocardial Infarction Risk Stratification for Sudden Cardiac Death in Patients With Preserved Ejection Fraction*) (129) se encontró que 9 de 575 pacientes (1,6%) con CI y FEVI  $\geq$  40% (media 50,8%) tuvieron terapias apropiadas de DAI por aparición de AV sostenidas tras un seguimiento clínico medio de 32 meses. A estos pacientes, que no tenían indicación estándar para implante de DAI en prevención primaria, se les había indicado el DAI por tener algún factor de riesgo adicional (véanse los subapartados d.2 a d.8) y un EEF de inducibilidad positivo.

<b>Estudio</b>	<b>Año</b>	<b>Criterios de inclusión</b>	<b>Pacientes incluidos</b>	<b>Grupo control</b>	<b>Endpoint primario</b>	<b>Resultados</b>
<b>MADIT I</b> (130)	1996	IAM previo, FEVI $\leq$ 35%, TVNS, TV inducible en EEF, clase NYHA I-III	196	Tratamiento convencional	Mortalidad por todas las causas	54% RRR con el DAI (p = 0,009); 23% RR absoluto
<b>CABG-PATCH</b> (131)	1997	FEVI < 35%, cirugía de revascularización coronaria electiva, SAECG anormal	900	Tratamiento convencional	Mortalidad por todas las causas	Sin diferencias entre ambos brazos
<b>MUSTT</b> (132)	2000	IAM previo, FEVI $\leq$ 40%, TVNS, TV inducible en EEF	704	Tratamiento antiarrítmico guiado por el EEF o convencional	Parada cardíaca o muerte de causa arrítmica	60% RRR con el DAI (p < 0,001); 31% RR absoluto
<b>MADIT II</b> (60)	2002	IAM previo ( $\leq$ 1 mes), FEVI $\leq$ 30%, clase NYHA I-III	1232	Tratamiento convencional	Mortalidad por todas las causas	31% RRR con el DAI (p = 0,016); 6% RR absoluto
<b>DINAMIT</b> (128)	2004	IAM reciente (6-40 días), FEVI $\leq$ 35%, variabilidad de FC anormal o FC media elevada en Holter de 24 h, clase NYHA I-III	674	Tratamiento convencional	Mortalidad por todas las causas	Sin diferencias, pero 58% RRR con el DAI para aparición de AV (p = 0,009)
<b>SCD-HeFT</b> (61)*	2005	CI y miocardiopatía no isquémica con FEVI $\leq$ 35%, clase NYHA II-III	2521	Tratamiento convencional $\pm$ amiodarona	Mortalidad por todas las causas	23% RRR con el DAI (p = 0,007); 7% RR absoluto

Tabla 2. Principales ensayos clínicos aleatorizados sobre el implante de DAI en prevención primaria en CI. \*El estudio SCD-HeFT incluyó no sólo pacientes con CI, sino también con miocardiopatía no isquémica. (FC: frecuencia cardíaca; RR: reducción de riesgo; RRR: reducción de riesgo relativo. Resto de abreviaturas como en el texto.)

## d.2 Detección de isquemia miocárdica residual

La importancia de la isquemia después del IAM como contribuyente a la mortalidad total se conoce desde hace mucho tiempo; de hecho, la realización de prueba de esfuerzo para detectar isquemia residual es una parte estándar de la evaluación posterior al IAM. Sin embargo, aunque la asociación entre la isquemia y la MSC post-IAM tiene sentido fisiológico, la contribución real de la isquemia a la MSC es menos clara, ya que la mayoría de los ensayos aleatorizados grandes sobre implante de DAI requerían que los pacientes se sometieran a evaluación y tratamiento adecuado para la isquemia antes de su reclutamiento. Aún así, la presencia de isquemia reversible se ha relacionado con la aparición de EV espontánea y TVNS detectables en Holter ECG de 24 horas. (133) La isquemia detectada por ecocardiografía de estrés también se asocia con un mayor riesgo de TV/FV en pacientes tratados con DAI. (134) Por otra parte, a partir de datos de autopsias se demuestra una prevalencia significativamente mayor de hallazgos coronarios agudos en pacientes con EAC e IC que mueren súbitamente respecto a aquéllos que fallecen de manera no súbita. (135)

## d.3 Detección de potenciales *triggers*: EV y TVNS

Múltiples estudios han demostrado una asociación entre EV frecuente y la TVNS detectadas en Holter y la mortalidad global. (136) Actualmente, las TVNS se encuentran en el 6-10% de los pacientes con historia de IAM. (122,137,138) Sin embargo, el hallazgo de EV/TVNS adolece de falta de sensibilidad: no identifican hasta un 40% de las MSC que ocurren a posteriori. Otra importante limitación es la ausencia de evidencia mecanística que vincule

este tipo de arritmias (que suelen tener un origen focal) con la aparición de TV sostenidas o FV en la mayoría de los pacientes. La presencia de TVNS está estrechamente relacionada con la función del VI, siendo su prevalencia mayor en pacientes con FEVI más baja, que por otra parte están sujetos a un mayor riesgo de mortalidad por IC. (138) En resumen, la monitorización Holter para la detección de EV y TVNS no es una prueba de estratificación de riesgo de MSC útil.

#### **d.4 Estudio electrofisiológico (EEF)**

La capacidad de iniciar de forma reproducible una arritmia mediante estimulación eléctrica programada durante un EEF es considerado un sello distintivo de mecanismo reentrante, (139) siendo descrito este hecho por primera vez por Wellens et al. en 1972. (104) La inducción de una taquicardia monomórfica sostenida hemodinámicamente tolerada (particularmente con una longitud de ciclo  $\geq 240$  ms) sólo ocurre en pacientes con TV espontánea, paro cardíaco o en presencia de un sustrato conocido por ser arritmogénico. (1) El EEF de inducción se basa en la estimulación ventricular desde el ápex y/o tracto de salida del ventrículo derecho; aunque existen diferentes protocolos, los más extendidos se basan en la estimulación con trenes de 8-10 estímulos con hasta 2-3 extraestímulos (140) (la adición de más extraestímulos facilita la inducción de cualquier tipo de AV, pero la prueba perdería especificidad). (1) Existen varios estudios prospectivos clásicos que demostraron la existencia de un posible vínculo entre la inducibilidad, durante la realización de un EEF, de TV monomórfica sostenida (TVMS) y la incidencia de MSC. (110,141-145)

Con estos antecedentes, se llevó a cabo a finales de los años 90 el clásico estudio MUSTT (146) para evaluar la utilidad clínica de la terapia antiarrítmica (tanto farmacológica como con DAI) guiada por el EEF para reducir el riesgo de MSC y la mortalidad total. El estudio MUSTT estableció que la inducibilidad para TV sostenida en pacientes con CI y FEVI  $\leq$  40% se asoció con un riesgo significativamente mayor de muerte por causa arrítmica y paro cardíaco (18% vs. 12% en pacientes sin TV inducible a los 2 años de seguimiento; 32% vs. 24% a los 5 años,  $p < 0,001$  en ambos casos). Sin embargo, el riesgo de MSC a 2 años en pacientes sin TV sostenida inducible era todavía del 12%. (132) En un estudio mucho más reciente, y con un mayor porcentaje de pacientes recibiendo tratamiento óptimo con betabloqueantes e IECA respecto al MUSTT, se encontró que el valor predictivo negativo del EEF era significativamente mayor (96%). (147)

No obstante, el EEF puede tener sus limitaciones. En un subestudio del ensayo MADIT-II, (148) en los pacientes con FEVI  $\leq$  30%, la inducibilidad para TV predijo la aparición de TV clínica, pero no de FV. Esto podría explicarse por el hecho de que los pacientes con FEVI muy deprimida tienen una mayor prevalencia de IC, que a su vez puede ser causa de FV y MSC por mecanismos distintos a la TV monomórfica (arritmias de los estadios finales de la IC, como se comentó previamente). Por tanto, cabría esperar una mayor utilidad predictiva del EEF para MSC de causa arrítmica en pacientes con FE  $>$  30%. Aún así, un EEF negativo podría ayudar a identificar a los pacientes con bajo riesgo de MSC, para los que no se espera un beneficio clínico significativo con el implante de DAI. (149) En pacientes con FEVI  $\leq$  30%, sin TV inducible pero en presencia de otros factores de riesgo, el estudio MUSTT



(132,146) demostró una incidencia residual de MSC no despreciable. Por lo tanto, el EEF no puede usarse como la única prueba para la estratificación del riesgo.

#### d.5 Modelos clínicos multivariable

En el clásico ensayo MADIT-II, (60) los investigadores realizaron un análisis multivariable que identificó 5 factores clínicos que influían sobre el beneficio, en términos de supervivencia, del implante de DAI en prevención primaria: clase funcional NYHA > 2, la presencia concomitante de fibrilación auricular, duración del QRS > 120 ms, edad > 70 años, y la presencia de BUN (*blood urea nitrogen*) > 26 o < 50 mg/dl. Los pacientes sin ningún factor de riesgo, o bien con  $\geq 3$  factores de riesgo, no obtuvieron ningún beneficio de supervivencia con el DAI porque su mortalidad fue demasiado baja o demasiado alta, respectivamente. Por el contrario, la supervivencia en pacientes con 1-2 factores de riesgo mejoró con el DAI. (81) En la misma línea, en el estudio MUSTT se demostró que, en los pacientes con FEVI  $\leq 30\%$  como único factor de riesgo, el riesgo de MSC a dos años era sólo del 2-3%, mientras que la mortalidad total prevista era superior, del 5-6%. (79) Ese riesgo de mortalidad podía ser similar también para pacientes con FEVI mayores, en presencia de factores de riesgo adicionales. Otros modelos clínicos similares han arrojado conclusiones parecidas a las comentadas. (82,150,151)

La conclusión que puede extraerse de la utilización de modelos clínicos para estratificar el riesgo de AV y MSC es que, salvo el criterio de inducibilidad para TV en el EEF del modelo derivado del estudio MUSTT, (79) ninguna de las variables empleadas refleja los posibles

mecanismos o susceptibilidad para tener arritmias. Más bien, identifican comorbilidades potenciales que compiten con la MSC por la mortalidad total. Por lo tanto, sólo pueden ayudar a identificar a pacientes en los que es poco probable que obtengan un beneficio de supervivencia del DAI (que son precisamente los que clásicamente tendrían indicación, por tener FEVI bajas), pero no pueden identificar a los pacientes específicamente en riesgo alto de presentar arritmias potencialmente letales. Tampoco han sido validados prospectivamente en estudios clínicos dirigidos, por lo que su utilidad resulta muy limitada.

#### d.6 ECG de señales promediadas

El ECG de señales promediadas (*signal-averaged ECG*, SAECG) es una técnica no invasiva que permite la detección de áreas de miocardio anormal que presenta conducción enlentecida ("potenciales tardíos"), un fenómeno necesario para la aparición de TV por reentrada. La promediación y el filtrado de señales eliminan el ruido de fondo, de manera que las señales de baja amplitud, en el rango de microvoltios ( $\mu\text{V}$ ) y que normalmente se pierden en el ruido de un ECG estándar, pueden detectarse. (152) En el estudio MUSTT, (153) por ejemplo, se encontró que en pacientes con SAECG anormal, el riesgo de muerte no súbita excedía el de MSC, y por lo tanto la técnica de SAECG parece poco específica para la predicción de MSC. (110)

### d.7 Alternancia de la onda T

La alternancia de la onda T (*T wave alternans*, TWA) describe alteraciones en la amplitud de la onda T en latidos alternos, que reflejan anomalías en la señalización del calcio intracelular que resultan en heterogeneidad, latido a latido, en la duración del potencial de acción cardíaco y la morfología de la onda T. (154-156) Los estudios SCD-HeFT, (157) MASTER (158) y ABCD (159) encontraron que la presencia de TWA no tenía utilidad para predecir eventos arrítmicos en pacientes con FEVI  $\leq 40\%$ . En pacientes con FEVI  $> 40\%$ , la presencia de TWA se ha asociado con un *hazard ratio* ajustado para eventos arrítmicos de 19,7 (9% de eventos en pacientes con TWA positivo vs.  $< 1\%$  en pacientes con TWA negativo). Además del hecho de que el papel de la TWA no esté claro en pacientes con FEVI significativamente reducida, otras limitaciones incluyen el hecho de que la TWA no pueda medirse en presencia de fibrilación auricular o EV frecuentes.

### d.8 Marcadores funcionales del sistema nervioso autónomo

Tradicionalmente, se ha pensado que el sistema nervioso autónomo (SNA) puede modular la interacción entre diversos factores desencadenantes para la aparición de taquiarritmias ventriculares y MSC y el sustrato electrofisiológico subyacente. Como marcadores funcionales del SNA, se han evaluado la variabilidad y turbulencia de la frecuencia cardíaca, la sensibilidad barorrefleja, e incluso técnicas de imagen con radionúclidos para identificar zonas de miocardio denervado. El resumen es que ninguna de estas técnicas ha demostrado con suficiente fiabilidad predecir el riesgo de AV y MSC post-IAM. (160)

## e. Papel actual de la Resonancia Magnética Cardíaca en la estratificación del riesgo de Arritmias Ventriculares y Muerte Súbita

Como ya se ha comentado previamente, la FEVI no resulta un óptimo marcador de riesgo de AV y MSC, ni en CI ni en miocardiopatías no isquémicas, (60,61,76-78) y sin embargo continúa siendo el criterio por que se basan las guías de práctica clínica de la Cardiología actual (3,62) para determinar la indicación de implante de DAI en prevención primaria de MSC (para pacientes con FEVI < 35%). (60,61)

En este sentido, resulta notorio que la RM cardíaca ni siquiera aparezca en la sección correspondiente a CI de las últimas guías. (3,62) Aunque sólo fuera por la evaluación de la FEVI, la RM es más precisa y reproducible que la ecocardiografía para calcular este parámetro. (161) La caracterización del miocardio por RM mediante la utilización de secuencias de realce tardío de gadolinio (RTG) ha permitido responder preguntas clínicamente relevantes que actualmente no son evaluables sólo con la FEVI o con el uso de otras modalidades de imagen no invasiva. De hecho, el papel diagnóstico y pronóstico de la RM en CI y las AV ha sido ya reconocido en varios artículos y documentos de consenso más recientes. (5,162,163)

Existen numerosos estudios que ya han demostrado un vínculo entre la presencia de fibrosis evaluada con RM y la aparición de AV en pacientes con CI. En un metaanálisis reciente de Disertori et al. (164) incluyendo a 2.850 pacientes de 19 estudios diferentes (tabla 2), se observaron 423 eventos arrítmicos durante una mediana de 2,8 años de

seguimiento. Los autores definieron un criterio de valoración de evento arrítmico compuesto que incluía MSC, MSC abortada, TV, FV y terapia apropiada de DAI. Utilizando este criterio de valoración, el metaanálisis de los autores encontró que los pacientes sin RTG tenían una tasa de eventos anual del 1,7%, en comparación con la tasa de eventos del 8,6% al año en pacientes con RTG. (164) Interesante resulta el hecho de que, en la práctica totalidad de los estudios que incluyeron pacientes con CI, el 100% de aquéllos con el evento arrítmico de estudio tenía fibrosis macroscópica en la RM-RTG (tabla 2). (164)

Aunque todos los estudios incluidos en la tabla 3 han mostrado que la extensión y heterogeneidad de la cicatriz miocárdica es un predictor de AV y mortalidad, continúa siendo una incógnita si la RM podría facilitar la toma de decisiones clínicas en relación a la estratificación de riesgo arrítmico, más allá de la utilización de la FEVI. En este sentido, un trabajo previo de Klem et al. (165), incluido en el metaanálisis previamente mencionado (164) y basado en una cohorte de pacientes isquémicos con un amplio rango de valores de FEVI, analizó el riesgo de eventos arrítmicos: los pacientes con FEVI > 30% y fibrosis > 5% de la masa miocárdica total tenían un riesgo de AV mayor al de aquellos pacientes con FEVI > 30% y cicatriz pequeña (< 5%), pero similar al de pacientes con FEVI < 30%. De manera análoga, aquellos pacientes con FEVI < 30% y fibrosis < 5% presentaban un riesgo de eventos arrítmicos similar al de los pacientes con FEVI > 30%.

<b>Autores (Ref.)</b>	<b>Año</b>	<b>Pacientes (n)</b>	<b>Seguimiento (meses)</b>	<b>Evento arrítmico</b>	<b>% de prevalencia de RTG</b>
<b>Estudios incluyendo pacientes con CI</b>					
Roes et al. (166)	2009	91	9 (2-20)	Terapia de DAI	100
Boyé et al. (167)	2011	52	41 ± 11	Terapia de DAI o muerte cardiaca	100
De Haan et al. (168)	2011	55	24 (11-36)	Terapia de DAI o TV	100
Alexandre et al. (169)	2013	66	42 (22-52)	Terapia de DAI	100
Demirel et al. (170)	2014	94	65 (54-79)	Terapia de DAI o TV	100
<b>Estudios incluyendo pacientes con miocardiopatías no isquémicas</b>					
Assomull et al. (171)	2006	101	22 ± 12	MSC o TV	35
Iles et al. (172)	2011	61	19 (13-29)	Terapia de DAI	51
Leyva et al. (173)	2012	97	35*	MSC	26
Gulati et al. (174)	2013	472	64*	Terapia de DAI, MSC o MSC abortada	30
Neilan et al. (175)	2013	162	29 ± 18	Terapia de DAI o MSC	50
Muller et al. (176)	2013	185	21*	Terapia de DAI o MSC abortada	51
Perazzolo-Marra et al. (177)	2014	137	36*	Terapia de DAI, MSC o TV/FV	56
Masci et al. (178)	2014	228	23 (13-37)	Terapia de DAI, MSC o MSC abortada	27
<b>Estudios incluyendo pacientes con CI y miocardiopatías no isquémicas (CI/no CI)</b>					
Fernández-Armenta et al. (179)	2012	78 (41/37)	25 (15-34)	Terapia de DAI	69
Gao et al. (180)	2012	124 (59/65)	21 ± 9	Terapia de DAI, MSC o MSC abortada	100/71
Klem et al. (165)	2012	137 (73/64)	24 (20-29)	Terapia de DAI o MSC	96/58
Wu et al. (181)	2012	235 (137/98)	43*	Terapia de DAI	73
Mordi et al. (182)	2014	157 (61/96)	31*	Terapia de DAI	100/25
Almehmadi et al. (183)	2014	318 (149/169)	16*	Terapia de DAI o MSC	78

Tabla 3. Estudios evaluando el valor predictor de la RM-RTG en la predicción de eventos arrítmicos. De Disertori et al. (164)  
(\*Valor mediana, sin rango intercuartílico.)

La capacidad de la RM-RTG para detectar fibrosis miocárdica está respaldada por estudios de correlación histológica. (174,184) Como ya se ha discutido previamente, la presencia de conducción eléctrica lenta y heterogénea asociada a la fibrosis puede favorecer la reentrada, aumentando la vulnerabilidad a la aparición de TV/FV. (87,185-187) En la zona gris, tejido heterogéneo o *border zone* (BZ) coexisten áreas con diferentes niveles de fibrosis, resultando en miocardio tanto viable como no viable, que puede ser identificado con RM. (185) Además, los canales de tejido heterogéneo (*heterogeneous tissue channels*, HTC) o de *border zone* (BZC) detectados por RM se correlacionan con los canales de conducción lenta identificables mediante mapas de voltaje endocárdico en los EEF, (188-191) y con los istmos de los circuitos de reentrada. (192) Los HTC/BZC los definiremos, por tanto y de aquí en adelante, como *"corredores de tejido miocárdico viable, heterogéneo, que conectan dos áreas de miocardio sano, y están rodeados por tejido no conductor (fibrosis densa), o bien una zona de fibrosis densa y un obstáculo anatómico inexcitable (p.ej. los anillos valvulares)"*.

Mucho más recientemente, en el estudio CMR-SCD (*Cardiovascular Magnetic Resonance for the prediction of Sudden Cardiac Death*), (193) la presencia de fibrosis miocárdica y la masa de tejido heterogéneo (lo que hemos venido a denominar BZ), analizados ambos mediante RM-RTG, se evaluó en relación con la aparición de MSC y el evento compuesto de MSC o AV. De 947 pacientes analizados de manera retrospectiva, hubo 29 casos de MSC (2,96%) y 80 de MSC o AV (8,17%) tras una mediana de seguimiento de 5,82 años. La presencia visual de fibrosis miocárdica o de tejido heterogéneo en la RM se asociaron fuertemente con la aparición de MSC y del evento compuesto MSC o AV. En un análisis de

riesgos competitivos, por el contrario, las asociaciones entre una FEVI < 35% y la aparición de MSC, o bien del compuesto MSC o AV, fueron mucho más débiles. (193) Además, todos los pacientes que tuvieron eventos (MSC o AV) tenían fibrosis visible en la RM. Para más inri, el punto de corte de FEVI < 35% se asoció muy débilmente tanto con la aparición de MSC (área bajo la curva de la curva ROC 0,68) como con el compuesto de MSC y AV (área bajo la curva de 0,75).

Además de la correlación histológica y "funcional" (mediante mapas de voltaje en los EEF), recientemente se ha demostrado, mediante modelos informáticos de simulación a partir de imágenes de RM-RTG de IAM en cerdos, (194) que se puede predecir con precisión la morfología de las TV potencialmente inducibles y la ubicación del circuito responsable en cada caso, lo que sugiere que los métodos actuales para el análisis de la BZ podrían ser eventualmente complementados con herramientas aún más sofisticadas (modelos informáticos, *machine learning*...) para identificar los circuitos de reentrada a través de los hallazgos de la RM.

A pesar de que existe una creciente evidencia científica a favor de la relación entre los hallazgos de la RM-RTG y la aparición de AV/MS, particularmente en CI pero también en otras miocardiopatías, todavía hacen falta estudios adicionales, estandarización de los métodos de adquisición de las imágenes y análisis del rendimiento diagnóstico de cada uno de los parámetros evaluables mediante esta técnica, así como búsqueda de herramientas de post-procesado de las imágenes de RM que permitan obtener análisis fiables y reproducibles.



## f. Aspectos técnicos relevantes de la Resonancia Magnética Cardíaca

Una vez introducido el papel actual de la RM en la estratificación de riesgo arrítmico, y antes de abordar la utilidad de esta técnica en el tratamiento de las AV asociadas a la presencia de cicatriz en el miocardio, realizaremos en este apartado un repaso de los principios físicos relativos a las imágenes de RM, la utilización de distintos tipos de secuencia y contrastes paramagnéticos para la obtención de datos adicionales sobre la composición y estructura del miocardio, y finalmente el uso de herramientas de post-procesado de las imágenes “crudas” de RM para su utilización clínica. Es importante conocer todos estos aspectos, a fin de comprender mejor el contenido y la discusión de los artículos incluidos en la presente Tesis.

### f.1 Física relativa a la Resonancia Magnética

Los primeros trabajos que describieron la utilidad de la RM como técnica diagnóstica fueron publicados en la década de los años 40 del s. XX. (195,196) Los átomos que componen nuestro organismo (y toda la materia) están compuestos por electrones que rodean al núcleo, a su vez compuesto por protones y neutrones. El protón, partícula subatómica, tiene una carga eléctrica positiva y gira continuamente sobre sí mismo, lo que denominamos espín (*spin*). Al rotar, la carga positiva gira igualmente, generando una corriente eléctrica que va acompañada de un pequeño campo magnético; de esta manera, los protones funcionan como “pequeños imanes”. (197)

Cuando un paciente es introducido dentro de un campo magnético potente, los protones de sus átomos se alinean con ese campo externo, presentando, además del movimiento de espín, un movimiento de precesión (como una peonza) alrededor del eje mayor del campo magnético externo. Los protones tendrán un movimiento giroscópico alrededor del eje mayor del campo magnético del escáner a una frecuencia determinada, que llamaremos frecuencia de precesión, de resonancia o de Larmor, y que depende de la potencia del campo externo y de las propiedades de cada núcleo. La mayoría de los protones se alinearán en la dirección de ese campo, por lo que el efecto neto será la generación de un campo magnético intrínseco con la misma dirección que la del campo externo (magnetización longitudinal). (197)

Esta magnetización longitudinal no es medible al encontrarse alineada con el campo externo, por lo que es necesario introducir una "perturbación" que modifique la orientación del campo intrínseco y nos permita evaluar la composición protónica de los distintos tejidos. Esta perturbación se consigue mediante la introducción de ráfagas de pulsos de radiofrecuencia (RF) a la misma frecuencia que la de Larmor, lo cual permite cambiar la dirección del campo magnético de los protones al transmitirles energía. Un pulso "de excitación" permitirá inclinar la magnetización longitudinal a un plano transversal (90°, magnetización transversal), y un pulso "de inversión" invertirá completamente el sentido de la magnetización (180°). (197)

Al aplicar un pulso de excitación de RF, se provoca una transferencia de energía ("resonancia"): primero, los protones absorben energía y pasan de un estado de reposo a

un estado de excitación (paso de magnetización longitudinal a transversal); al cesar el pulso de RF, los protones regresan a la situación de reposo, liberando la energía previamente absorbida (figura 11). Por ello, los equipos de RM disponen de una bobina transmisora de RF y de bobinas receptoras, que son combinaciones de bucles de alambre (actualmente hasta 128) colocados alrededor del pecho del paciente, cerca del corazón, y que permiten detectar esa transmisión de energía tras el cese de los pulsos de excitación.

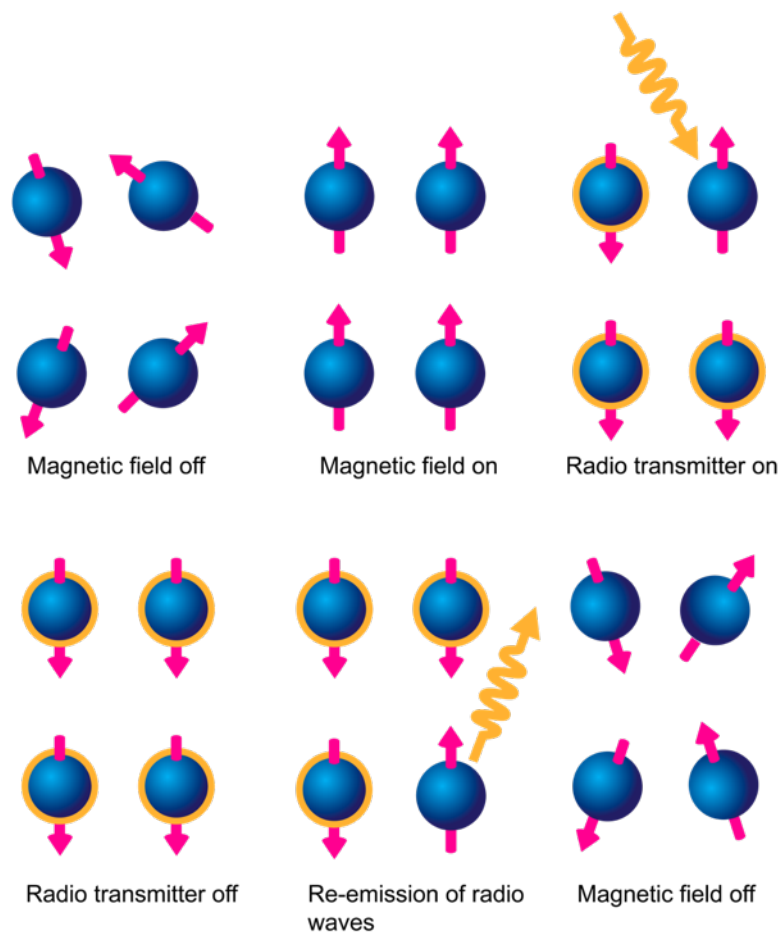


*Figura 11. Fases de la resonancia magnética. Magnetización longitudinal al someter a los protones a un campo magnético externo; aplicación de pulso de RF (en la imagen, pulso de inversión) que modifica el eje de precesión de los protones; finalmente, emisión de energía en forma de RF tras el cese del pulso aplicado, y vuelta al estado de reposo tras eliminar el campo magnético externo. (198)*

Por otra parte, el tiempo que tarda un tejido (sus protones) en recuperar la situación de reposo se conoce como "tiempo de relajación". En la obtención de imágenes de RM se

evalúan dos medidas de tiempo asociadas: a) el tiempo de relajación longitudinal (tiempo T1) o relajación *spin*-medio, y b) el tiempo de relajación transversal (tiempo T2) o *spin-spin*. El T1 es el tiempo que tarda un tejido en recuperar la posición de equilibrio tras cesar un pulso de excitación; p. ej., la grasa tiene un T1 muy corto (señal hiperintensa) y el agua/líquido muy largo (señal hipointensa). La presencia de sustancias paramagnéticas, como los quelatos de gadolinio, acortan el T1 (aumentan la velocidad de relajación longitudinal). (197)

Cuando se produce la magnetización longitudinal, al cabo de un tiempo aparecen distorsiones en el campo magnético, debidas a inhomogeneidades en el imán que crea el campo o a interacciones espín-espín. Los espines experimentan campos magnéticos locales que resultan de la combinación del campo magnético aplicado y de los campos magnéticos de los espines vecinos. Esto provoca la aparición de no una única frecuencia de Larmor, sino de "distribuciones de frecuencias" de Larmor, y por tanto el desfase de los espines. El T2 se refiere al tiempo que tarda un tejido en perder esa "coherencia de fase", y depende de su composición: el agua/líquido tiene un T2 muy largo (señal hiperintensa), mientras que otros, como el aire/gas o los tejidos calcificados tienen un T2 muy corto (señal hipointensa). (199)

El hidrógeno ( $^1\text{H}$ ) es el núcleo más comúnmente observado en la RM debido a que tiene la mayor sensibilidad nuclear a la RM, presenta una abundancia natural del 99,98% y aproximadamente el 10% del peso corporal magro es hidrógeno. Este elemento se encuentra en el organismo en forma de agua, como hidratos de carbono o en la grasa,

presentando estos últimos diferentes frecuencias de resonancia y tiempos de relajación en función de su estructura química. Por tanto, en los tejidos biológicos encontraremos una amplia gama de valores de tiempos de relajación, que es lo que genera el contraste en las imágenes de RM. La detección de diversas patologías puede establecerse en función de los cambios en las características de relajación magnética de los tejidos afectados. (199)

Para generar las imágenes, los sistemas de RM disponen de tres bobinas, que permiten generar gradientes a lo largo de cualquiera de los tres ejes ortogonales ( $x, y, z$ ). Existen tres técnicas principales de discriminación espacial (200,201) basadas en el uso de campos de gradiente: excitación selectiva para definir el corte de imagen; y codificaciones de frecuencia y de fase para codificar la información espacial en los dos ejes en el plano del segmento excitado. Matemáticamente, la transformación de Fourier bidimensional se puede utilizar para transformar los datos de frecuencia en una imagen de RM.

## **f.2 Secuencias de adquisición en Resonancia Magnética**

Una secuencia de resonancia magnética es una combinación particular de pulsos de RF y de gradiente que crean una imagen de RM con un contraste específico de tejido. El contraste cambia con el tiempo entre la excitación de RF y la lectura de la señal de RM (tiempo de eco, TE), el tiempo entre las excitaciones de RF (tiempo de repetición, TR) y los tipos y combinaciones de pulsos de RF y de gradiente. (202)

Las secuencias de eco de espín rápido (*fast spin echo*, FSE) pueden proporcionar imágenes ponderadas en T2 de alta resolución. Las secuencias FSE combinadas con “doble inversión-recuperación” pueden producir imágenes ponderadas en T2 de “sangre negra”, que se han utilizado para identificar regiones edematosas en el IAM.

Las secuencias de eco de gradiente (*gradient echo*, GRE), como el disparo rápido de ángulo bajo o la secuencia de estado estacionario de precesión libre (*steady state free precession*, SSFP) permiten TR muy cortos y, por lo tanto, se pueden utilizar para obtener imágenes cinematográficas del corazón latiendo y otras aplicaciones dinámicas (perfusión, angiografía). Las secuencias de GRE combinadas con una preparación de inversión-recuperación producen imágenes ponderadas en T1 que se pueden utilizar para la detección de cicatrices isquémicas con RTG. (203-206) Existen múltiples tipos de secuencias de RM específicas para diversas aplicaciones clínicas, que escapan al objetivo de la presente Tesis. (199)

### **f.3 Agentes de contraste paramagnético**

Los agentes de contraste paramagnético basados en el gadolinio se utilizan de forma rutinaria en varias aplicaciones de la RM, permitiendo mejorar la sensibilidad y especificidad de la prueba. Como ya se ha discutido previamente, el gadolinio acelera el T1 (relajación longitudinal), aumentando la señal de las imágenes potenciadas en T1. La angiografía por resonancia magnética visualiza la luz del vaso después de la inyección intravenosa de agentes de contraste. (207) La cicatriz post-IAM se puede detectar mediante

la adquisición de imágenes unos 10-20 min después de la inyección de contrastes a base de gadolinio, que se acumulan en las regiones con cicatriz. (205) Las imágenes de perfusión miocárdica consisten en una secuencia de imágenes consecutivas que muestra el lavado del agente de contraste con la sangre durante su primer paso a través del miocardio. (208) El gadolinio es un compuesto tóxico, por lo que se administra unido a quelantes que impiden su paso a través de las membranas plasmáticas. La incidencia de fibrosis sistémica nefrogénica, (209) una posible complicación asociada a la administración de contrastes de gadolinio en pacientes con insuficiencia renal, es actualmente muy baja, en parte gracias a la vigilancia exhaustiva y la no administración del compuesto en pacientes con insuficiencia renal muy avanzada. (210) Esto, en sí mismo, constituye una limitación para la utilización de RM-RTG, aunque, aún así, los quelantes de gadolinio son mucho menos nefrotóxicos que los contrastes yodados que, por ejemplo, se utilizan en la TAC. (211)

#### **f.4 Caracterización y cuantificación de la cicatriz miocárdica mediante Resonancia Magnética**

La capacidad de la RM-RTG para distinguir el miocardio normal del miocardio con cicatrices se basa en el uso de gadolinio como agente de contraste para resaltar las áreas de fibrosis. El miocardio normal y la cicatriz tienen diferentes velocidades de eliminación de gadolinio; así, mientras que en el miocardio sano la permanencia del gadolinio se limita a algunos minutos, en zonas cicatriciales el lavado se produce más lentamente. Seleccionar el momento correcto para realizar una adquisición tardía post-contraste es fundamental para resaltar sólo las áreas de fibrosis (con contraste), diferenciándolas del miocardio normal,

que aparece en negro. Como ya se ha comentado, varios estudios han demostrado la correlación entre la presencia de RTG y la fibrosis crónica. (206,212)

La resolución espacial en el plano de imagen habitual de la RM-RTG es de  $1,4 \times 1,4$  mm. La correcta adquisición de las imágenes cardíacas se ve obstaculizada por los cambios de posición del corazón durante la respiración y las diferentes fases del ciclo cardíaco. Para superar esta limitación, el abordaje estándar consiste en adquirir múltiples imágenes durante apneas consecutivas y utilizando una sincronización electrocardiográfica, obteniendo así múltiples planos (2D) de eje corto a lo largo del eje largo del VI. Este enfoque da como resultado una resolución óptima en cada plano de eje corto, pero generalmente con una distancia de separación entre cortes. Por otro lado, la reconstrucción de la cicatriz puede ser difícil debido a la existencia de artefactos de volumen parcial (*partial volume*) y posibles desplazamientos entre cortes.

Para controlar las limitaciones anteriores, los protocolos de adquisición 3D han supuesto un gran avance. Este enfoque se basa en la adquisición de imágenes de respiración libre (sin apneas) utilizando una secuencia de inversión-recuperación sincronizada con un navegador respiratorio, que básicamente consiste en obtener una imagen rápida de la posición del diafragma en cada latido cardíaco. Sólo las adquisiciones realizadas en una cierta posición del diafragma que seleccionamos manualmente son aceptadas para la reconstrucción. Este método permite reconstrucciones en 3D sin artefactos de desplazamiento entre cortes, que además tienen un grosor mucho menor y por tanto, permiten minimizar los efectos de volumen parcial. Andreu et al. describieron una



comparación directa de la precisión entre las adquisiciones estándar 2D y las nuevas 3D para identificar y caracterizar el miocardio cicatrizado y el sustrato arritmogénico; (190) después de un post-procesamiento automático de imágenes, la caracterización del sustrato arritmogénico fue superior con la técnica 3D debido a una mayor resolución espacial en comparación con las secuencias 2D convencionales.

La información derivada de la RM-RTG puede ser cualitativa (presencia o ausencia visual de fibrosis) o cuantitativa. Dentro de los métodos de cuantificación de la fibrosis, clásicamente se han venido utilizando técnicas semicuantitativas, evaluando el número de segmentos (de la AHA, *American Heart Association*) afectados por la fibrosis o el grado de transmuralidad (en % referido al grosor parietal total) de la cicatriz. (171,213) Las técnicas cuantitativas "puras" se basan en el hecho de que es posible definir la zona correspondiente a cicatriz como aquella que presenta una intensidad de señal (*pixel signal intensity*, PSI) determinada por encima de la del miocardio normal. En todas las técnicas cuantitativas, el cálculo del volumen/masa de cicatriz se establece asumiendo una densidad para el miocardio de 1,05 g/ml. (214) Igualmente, se puede calcular el volumen/masa relativos de la cicatriz respecto al total del volumen/masa de miocardio. Para la identificación de la cicatriz, algunos documentos de consenso han establecido el punto de corte de  $> 2$  desviaciones estándar (DE) de PSI respecto al miocardio sano. (215) Yan et al. (216) definieron la "zona peri-infarto" (equivalente a BZ) como aquella con una PSI entre 2 y 3 DE superior a la del miocardio sano. Sin embargo, también se utilizan otras técnicas: 3, 4, 5 o 6 DE; cuantificación manual trazando regiones de interés (ROI) alrededor de la cicatriz; y la técnica de "*full width at half maximum*" (FWHM), que utiliza la mitad de la señal máxima dentro de la cicatriz como

umbral. Esta última técnica, sin embargo, presenta problemas de exactitud al asumir siempre que el *core* de la cicatriz es necesariamente “muy brillante”; sin embargo, esta asunción no tiene por qué cumplirse en cicatrices muy heterogéneas, poco densas. (217)

Finalmente, sabemos que la resolución espacial de las imágenes de RTG afecta a la clasificación de los diferentes componentes de la cicatriz miocárdica. Al degradar la resolución espacial se produce un aumento significativo del tejido con viabilidad intermedia clasificado como BZ, sin que existan cambios importantes en el cómputo total del área de infarto. (218)

Recientemente, estudios animales con correlación histológica (219) han reportado una mejor precisión diagnóstica cuando se utiliza un algoritmo basado en la intensidad máxima de píxeles (*maximum signal intensity*, MSI), que define distintos umbrales de PSI para diferenciar los diferentes componentes de la cicatriz: cicatriz densa (*core*) y cicatriz heterogénea (*border zone*, BZ). Schmidt et al. (185) definieron la zona peri-infarto como aquella con PSI superior a la MSI registrada en una ROI en el miocardio sano, pero menor al 50% de la MSI registrada en la cicatriz densa. Para Roes et al., (166) la BZ correspondía con la zona con una  $PSI \geq 35\%$  y  $< 50\%$  de la MSI en la zona de cicatriz densa. No hubo diferencias significativas en la extensión de la cicatriz total entre los métodos de Yan, Schmidt y Roes; sin embargo, se ha reportado cierta variabilidad en la extensión de la detección de *core* vs. zona peri-infarto (BZ) en función del método empleado. (168)

Finalmente, en un trabajo de Andreu et al. (220) se estudiaron diferentes puntos de corte basados en la MSI, describiendo que la mejor correlación con el sustrato arritmogénico

identificable mediante EAM se encontró utilizando un valor de corte del 60% del MSI para diferenciar el core y la BZ, y del 40% para la diferenciación BZ vs. miocardio sano. Este último criterio será el utilizado para la cuantificación y caracterización de los distintos componentes de la cicatriz en los distintos artículos que componen la presente Tesis.

### f.5 Identificación del sustrato arritmogénico mediante Resonancia Magnética

Las fibras de tejido miocárdico superviviente pueden atravesar la densa cicatriz formando canales tortuosos, con propiedades de conducción lenta que soportan la reentrada, (103) al presentar áreas con bloqueo de conducción fijo o funcional (figura 12). Estos haces miocárdicos supervivientes (HTC), generalmente separados por tabiques de colágeno, (221) muestran grados intermedios de fibrosis. Esta característica los hace identificables al mostrar un aspecto heterogéneo en la RM-RTG (figura 13). (222)

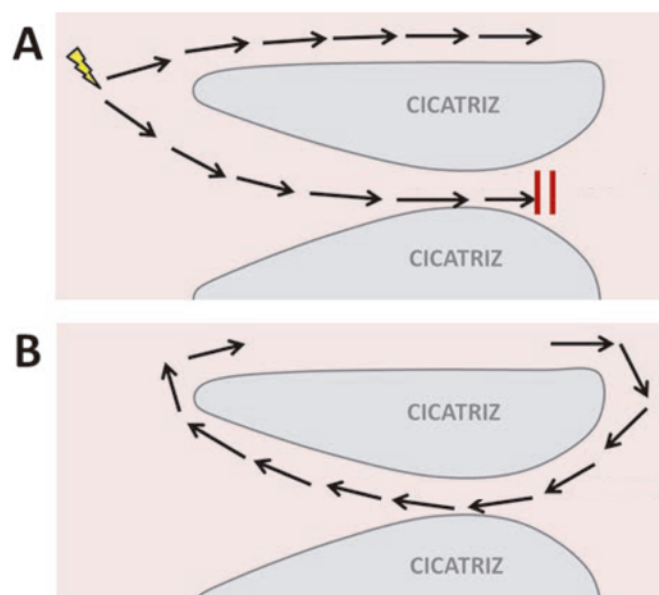


Figura 12. Modelo esquemático de cicatriz con un HTC que transcorre entre dos zonas de cicatriz densa. A) Un impulso eléctrico atraviesa el miocardio y la zona de cicatriz; en la zona del HTC sufre un bloqueo unidireccional (líneas rojas), B) permitiendo que el impulso previo, al rodear la zona de cicatriz, se transmita en sentido inverso, originando la reentrada. De Franco et al. (223)

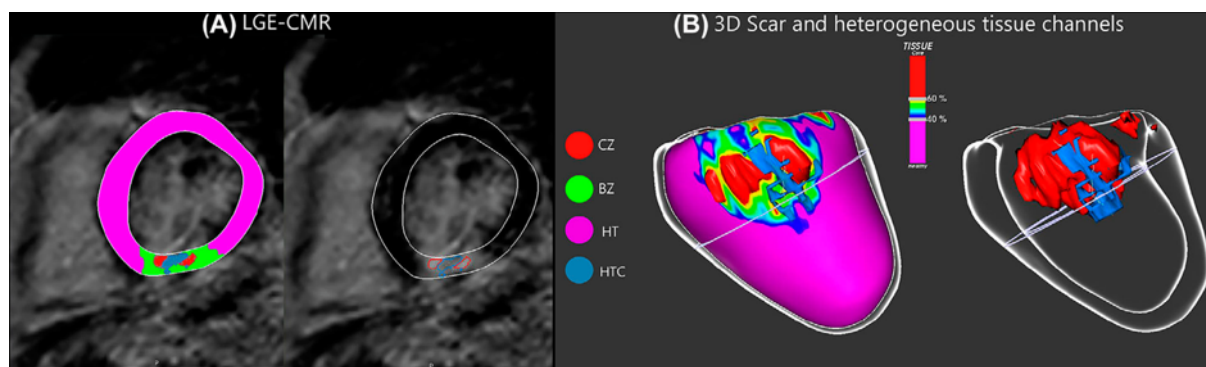


Figura 13. Caracterización de la cicatriz en un paciente isquémico con IAM inferior. (A) Vista de eje corto de la RM-RTG que muestra una cicatriz inferior heterogénea. El miocardio sano se representa en púrpura; el área de BZ está representada en verde; la cicatriz densa [core zone (CZ)] está representada en rojo. Un HTC detectado automáticamente cruzando la cicatriz perpendicular al anillo mitral se representa en azul. (B) La reconstrucción 3D del VI utilizando la información de PSI. La reconstrucción 3D facilita la visualización de la arquitectura de la cicatriz, la relación entre los diferentes componentes de la cicatriz, así como el curso de los canales. De Berruezo et al. (224)

Como consecuencia de la dificultad obvia para obtener comparaciones directas de la histología humana con los hallazgos de la RM, la mayoría de los estudios al respecto han validado la precisión para detectar sustratos arritmogénicos de las imágenes de RM comparándolas con datos electrofisiológicos. Varios estudios han encontrado que el istmo crítico de las TV reentrantes en pacientes con cardiopatía estructural se localiza en áreas de apariencia heterogénea (BZ) en la RM. (225) Pérez-David et al. (188) evaluaron la capacidad de la RM-RTG para identificar HTC dentro de la cicatriz en 18 pacientes postinfarto con TV monomórfica, considerando los canales de conducción identificados por el mapeo del EAM como el *gold standard*. Descubrieron que todos los HTC identificados en la RM correspondían en ubicación y orientación a canales de voltaje (entre 0.5 y 1.5 mV) similares en el EAM. Sin embargo, no sólo los canales de voltaje, sino también los canales de conducción lenta identificables en el EAM pueden identificarse de forma no invasiva con la RM (figura 14). (188-191) En un trabajo de Fernández-Armenta et al., (191) los HTC

definidos por RM identificaron el 74% de los istmos críticos de las TV clínicas y el 50% de todos los canales de conducción lenta identificados en los EAM (figura 15).

Los HTC (o BZC) pueden identificarse en la RM antes de los procedimientos de ablación (tratamiento invasivo de las AV) y luego importarse a los sistemas de navegación empleados durante este tipo de procedimientos (ver apartado siguiente). Debido al escaso grosor de la pared del ventrículo derecho, habitualmente la identificación de HTC por RM se limita al VI. No obstante, aunque los nuevos métodos de adquisición de respiración libre pueden proporcionar una resolución espacial isotrópica de casi 1 mm<sup>3</sup>, podría ser insuficiente para detectar haces muy pequeños de miocitos supervivientes (han sido descritos incluso de < 200 μm) (103) que potencialmente pudieran mantener la reentrada.

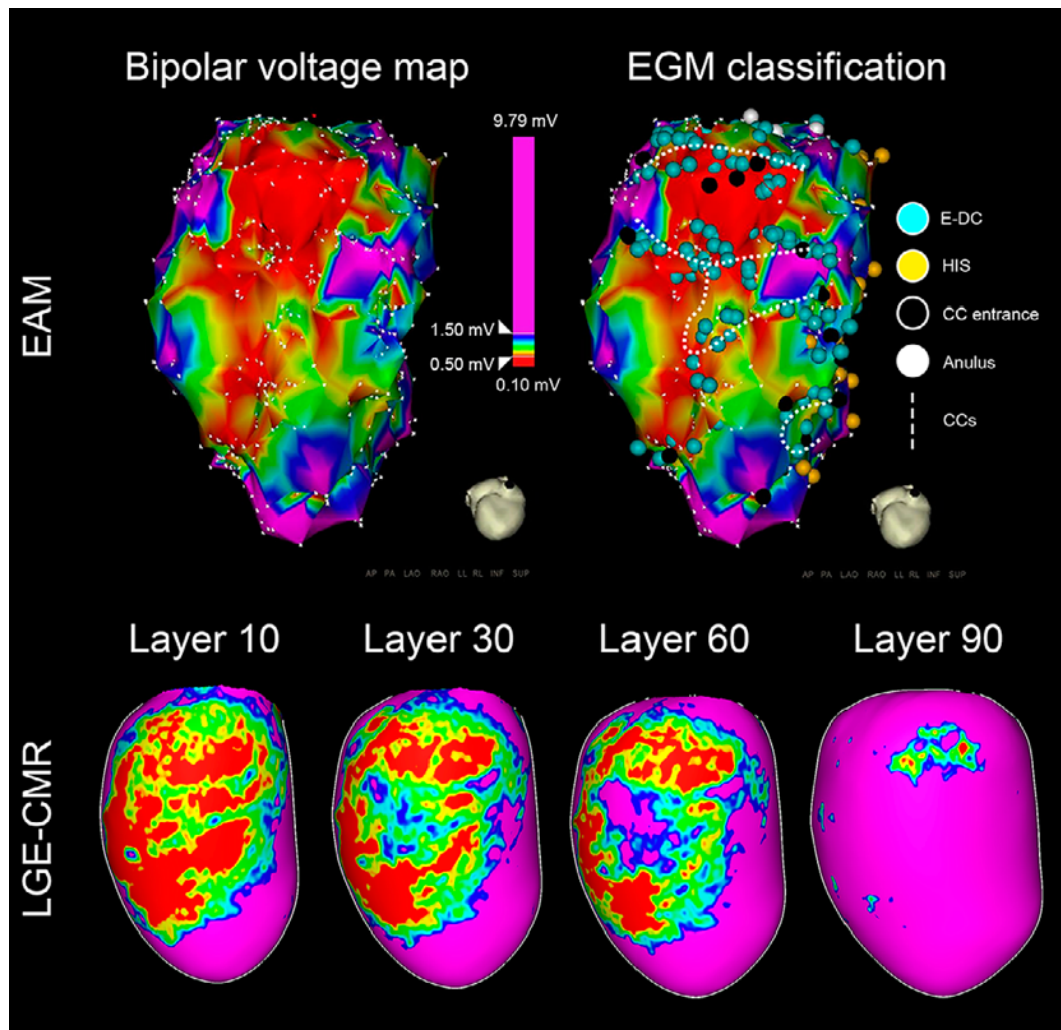


Figura 14. Comparación de la caracterización del sustrato arritmogénico con el mapa electroanatómico (EAM) y los mapas de PSI derivados de la RM-RTG en un paciente con un IAM inferior antiguo. En la parte superior e izquierda, vista posterior del mapa de voltaje usando el valor de corte estándar para el core (0.5 mV) y BZ (1.5 mV), que muestra una cicatriz inferior que involucra los segmentos basal y medioventricular. Arriba y a la derecha, caracterización de los electrogramas locales (EGM): los puntos azules representan EGM con componentes retardados; los puntos negros representan EGM con características de entrada de canal de conducción lenta (CC); los puntos amarillos representan EGM con características de sistema intrínseco de conducción (His-Purkinje). Se representan 3 CC sobre la reconstrucción (líneas de puntos blancos), un canal submitral y dos canales que cruzan la cicatriz de forma paralela al anillo mitral. En la parte inferior de la figura, mapa de PSI previo al procedimiento al 10%, 30%, 60% y 90% del grosor de la pared del ventrículo izquierdo en el mismo paciente. Nótese que los mismos 3 CC se pueden identificar fácilmente en la capa endocárdica al 10%. De Berruezo et al. (224)

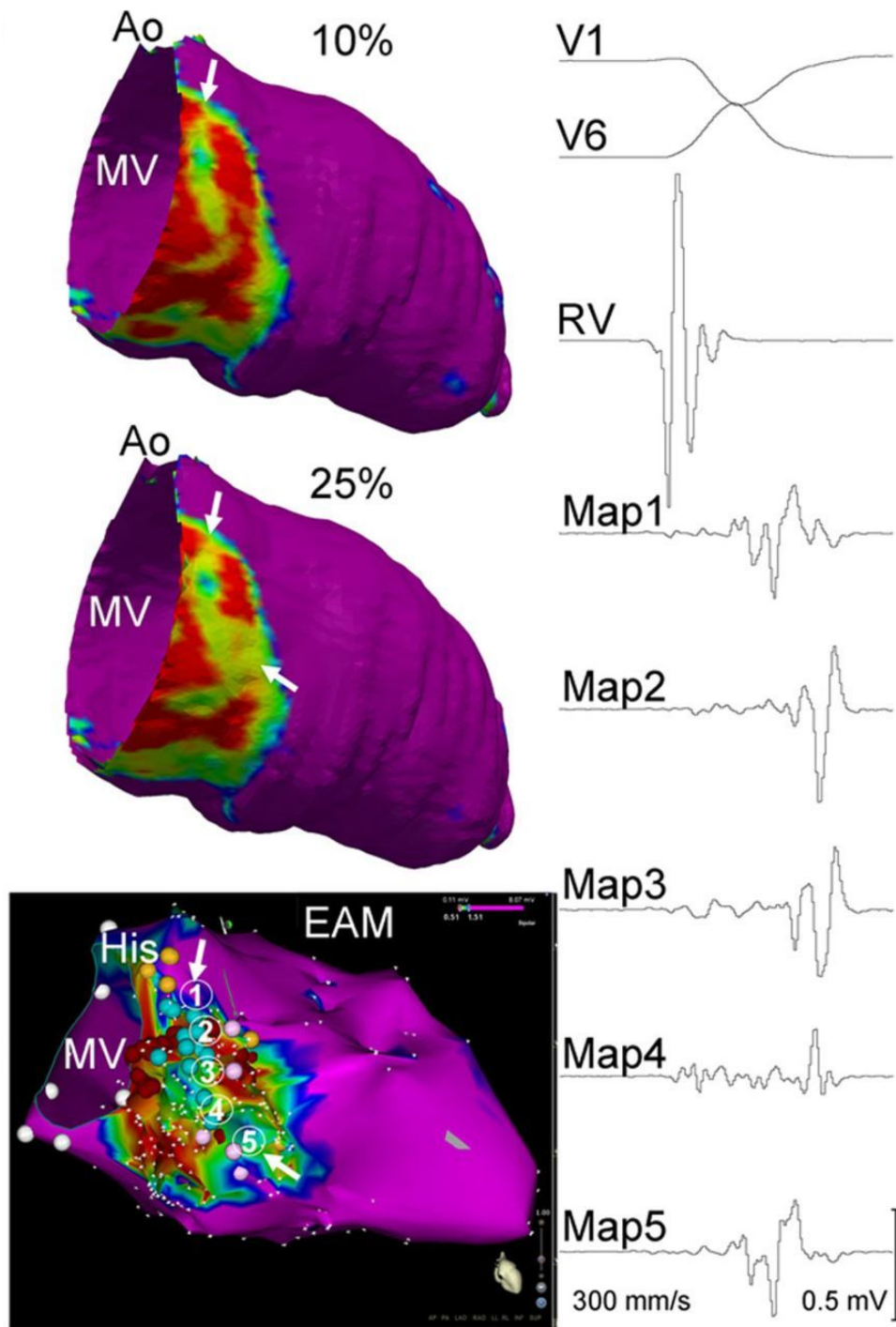


Figura 15. IAM septobasal. Mapas de PSI obtenidos a partir de RM-RTG correspondientes a dos capas subendocárdicas codificadas por colores (se muestran las capas del 10% y 25% del grosor de la pared del miocardio). Se sugiere un BZC en la capa del 10%, que se puede identificar completamente en la del 25% (flechas blancas). El EAM se muestra en la parte inferior; se identifica un canal de conducción lenta (flechas blancas). Los EGM en el canal de conducción lenta (electrogramas 1–5) se muestran a la derecha. Los componentes retardados aislados de estos electrogramas tienen una activación secuencial desde la entrada del canal (número 1 y número 5, flechas blancas) hasta su parte interna durante el ritmo sinusal. Ao indica válvula aórtica; His, His y rama izquierda del mismo; MV, válvula mitral; y RV, ventrículo derecho. De Fernández-Armenta et al. (191)

## g. Tratamiento de las Arritmias Ventriculares en la Cardiopatía Isquémica

En los pacientes con CI y, en general, cualquier otro tipo de cardiopatía estructural con presencia de cicatrices en el miocardio que presentan AV clínicas, caben varios tipos de actuaciones terapéuticas: prevención secundaria, tratamiento farmacológico y tratamiento invasivo mediante cirugía antiarrítmica o ablación percutánea. Abordaremos en este apartado un resumen de todas las estrategias, haciendo énfasis en la ablación, y particularmente en el rol que tiene la RM en este tipo de procedimientos.

### g.1 Prevención secundaria de las Arritmias Ventriculares

Se han realizado tres ensayos [*Antiarrhythmic drugs Versus Implantable Defibrillator (AVID)*, (226) *Canadian Implantable Defibrillator Study (CIDS)*, (227) y *Cardiac Arrest Study Hamburg (CASH)* (228)] en pacientes que habían sufrido un paro cardíaco o AV potencialmente mortal (AV hemodinámicamente inestable o sincopal) en el que se comparó el tratamiento con DAI frente a la terapia con fármacos antiarrítmicos, predominantemente amiodarona. Los resultados de los tres ensayos fueron consistentes, aunque sólo uno (el CIDS) mostró una reducción estadísticamente significativa en la tasa de mortalidad total con el uso del DAI; en el AVID y el CASH, el DAI redujo las tasas de mortalidad arrítmica. Un metaanálisis de los tres ensayos (229) demostró que la terapia con DAI se asoció con una reducción del 50% en la mortalidad por arritmias y del 28% en la reducción en la mortalidad total. No existe evidencia más reciente que sugiera que las recomendaciones anteriores deban cambiarse sustancialmente, por lo que está universalmente aceptada la obligatoriedad



(salvo expectativa de vida < 1 año o negativa expresa del paciente) de implantar un DAI en prevención secundaria para pacientes con AV clínicas asociadas a cardiopatía estructural.

## **g.2 Tratamiento farmacológico de las Arritmias Ventriculares**

Cuando hablamos de tratamiento farmacológico de las AV, debemos distinguir entre la fase aguda ("momento que el paciente presenta la AV") y la fase "crónica", cuando planteamos iniciar un tratamiento con fármacos para prevenir nuevos episodios de AV.

En fase aguda, si la AV es mal tolerada clínica o hemodinámicamente, la cardioversión eléctrica (CVE) es el tratamiento urgente de elección. Sin embargo, en casos de estabilidad hemodinámica, las guías de práctica clínica (3,62) recomiendan indistintamente (con un grado de recomendación IIa) la utilización de procainamida o amiodarona. El ensayo aleatorizado español PROCAMIO (230) fue el primero en comparar ambos fármacos "en vida real". Este trabajo demuestra que la procainamida es más eficaz que la amiodarona para cardiovertir las TV sostenidas, con un 67% de éxito a los  $14 \pm 10$  min de iniciada la perfusión, y que presenta un mejor perfil de seguridad que la amiodarona, por lo que a priori podría ser el fármaco de primera elección en casos con TVMS y buena tolerancia hemodinámica. (230,231)

El papel de los fármacos antiarrítmicos en la prevención de nuevos episodios de AV y MSC en pacientes con CI y FEVI preservada es limitado. La mayoría de los datos provienen del estudio CAST, (232) que mostró que los fármacos bloqueadores de los canales de sodio

(antiarrítmicos de clase IA y IC según la clasificación de Vaughan-Williams (233)) aumentan la mortalidad tras un IAM. Los fármacos de clase II (betabloqueantes) tienen un papel establecido en la reducción de la mortalidad en pacientes con CI y FEVI reducida, pero su efecto sobre la MSC no está probado. Por último, no se ha demostrado que la amiodarona, antiarrítmico de clase III, reduzca la MSC en pacientes con CI y FEVI preservada. Sin embargo, puede tener un papel en el alivio de los síntomas y la reducción de episodios arrítmicos en este grupo de pacientes. Para arritmias sintomáticas pero no potencialmente letales (EV o TVNS), la amiodarona es el fármaco de elección, ya que puede suprimir las arritmias sin empeorar el pronóstico, según los estudios CAMIAT y EMIAT. (57,234)

### g.3 Cirugía antiarrítmica de las Arritmias Ventriculares

Este tipo de tratamiento, con la aparición de las técnicas de ablación con catéter se ha convertido a día de hoy en una opción terapéutica absolutamente excepcional. Las zonas de miocardio muy fibróticas, por la presencia de grandes cicatrices (p. ej. IAM no revascularizado), provocan la aparición de aneurismas; la aneurismectomía del VI se describió por primera vez en 1955 por el cirujano Charles Bailey, de Philadelphia (EEUU), como una opción de tratamiento para las AV que dependían de la zona aneurismática. A finales de los años 70, se describió la resección subendocárdica para el manejo de AV por primera vez, por Josephson et al., lo que se conoció como el "*Pennsylvania peel*". (235) Esta técnica pretendía ampliar los márgenes de la aneurismectomía varios cm, "limando" parcialmente el subendocardio de estos márgenes. Lo interesante de esta técnica es que

se basó en el hallazgo, durante la realización de mapas de activación de las TV, de que los "exit sites" de las TV se podían localizar en esta "border zone" alrededor de los aneurismas.

A pesar de todo ello, la morbimortalidad quirúrgica descrita por los grupos que realizaban este tipo de procedimientos era alta, por lo que esta técnica sólo se ha venido realizando en centros con amplia experiencia quirúrgica. (235-241) La mayoría de las técnicas quirúrgicas se han convertido en la base actual de las técnicas de ablación con catéter por lo que, como ya se ha dicho, la cirugía hoy en día constituye una opción terapéutica raramente empleada.

#### **g.4 Ablación con catéter de las Arritmias Ventriculares**

La ablación exitosa de TV con catéter se reportó inicialmente en 1983 (242) mediante la aplicación de choques de corriente continua con un catéter situado en el "exit site" de la TV. El uso de la ablación ha aumentado progresivamente, sobre todo a partir del desarrollo de la ablación por RF a partir de la década de los años 90. (243) La RF, a diferencia de la corriente continua, aplica pulsos de corriente alterna (de 300 a 750 kHz), causando el calentamiento resistivo del tejido en contacto con el catéter y permitiendo realizar la ablación de forma controlada y directa, evitando los riesgos de la corriente continua. Actualmente, la ablación con catéter se considera el tratamiento de elección para prevenir recurrencias de AV cuando los fármacos antiarrítmicos son ineficaces o tienen efectos secundarios inaceptables. (5) La aparición de los modernos sistemas de navegación electroanatómica (a finales de los años 90), (244) ha facilitado los procedimientos, al ofrecer

la posibilidad de visualizar en vivo la anatomía y la posición exacta de los catéteres, permitiendo además la obtención de mapas tridimensionales con diversos tipos de información disponible de manera simultánea.

La ablación de las TV (y nos referiremos aquí sólo a las TV con un mecanismo reentrante) requiere de la realización de diversas maniobras electrofisiológicas para discernir los componentes del circuito de reentrada responsable. Estas técnicas son: i) mapa de activación, ii) mapa de encarrilamiento, iii) mapa de topoestimulación ("*pacemapping*") y iv) mapa de sustrato.

#### **g.4.1 Mapa de activación**

El mapa de activación se puede utilizar para describir la secuencia de activación miocárdica e identificar los sitios de istmo crítico para la TV reentrante cuando ésta es bien tolerada hemodinámicamente. Los electrogramas (EGM) locales se registran en diferentes localizaciones de los ventrículos y el tiempo de activación se compara con una referencia, generalmente el inicio del complejo QRS durante AV. Los sistemas de mapeo electroanatómico (EAM) anotan los tiempos de activación de diferentes sitios con códigos de colores que resaltan la región con la activación más temprana. Los EGM registrados justo antes del complejo QRS en circuitos de macro-reentrada sugieren *exit sites*, donde el circuito de reentrada interactúa o contacta con la primera zona de activación miocárdica (lo que ya se vino observando en el "*Pennsylvania peel*" quirúrgico (235)). El istmo crítico en las TV por reentrada relacionada con cicatriz exhibe EGM diastólicos fraccionados de baja amplitud (figura 16), consistente con zonas de conducción lenta dentro de la cicatriz, una

característica que puede ser compartida por otros HTC dentro de la cicatriz que no formen parte del istmo crítico (o sea, que sean *by-standers*). Por eso, el mapeo de activación debe combinarse con maniobras de encarrilamiento (*entrainment*).

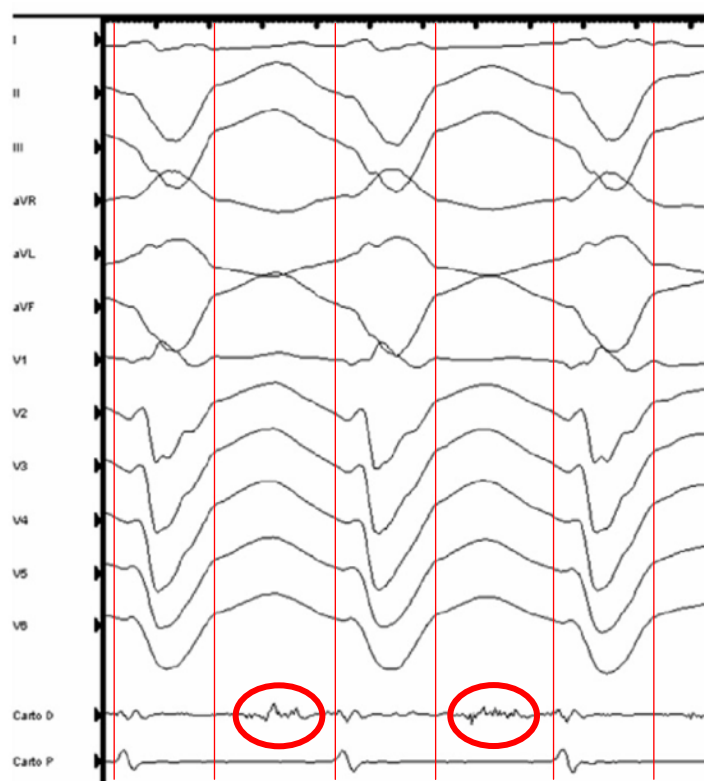


Figura 16. Potenciales medio-diastólicos (círculos rojos) correspondientes a la zona de istmo crítico de una TV por reentrada en relación a una cicatriz miocárdica. Las líneas verticales rojas delimitan el principio y final del QRS. Modificada de Guandalini et al. (245)

#### g.4.2 Mapa de encarrilamiento (*entrainment*)

El encarrilamiento consiste en la aceleración de una taquicardia a la longitud de ciclo o frecuencia del tren de impulsos con que se estimula. Los impulsos penetran en el circuito, propagándose en dos sentidos posibles: el sentido del circuito de la arritmia (sentido ortodrómico, adelanta el siguiente latido de la taquicardia), y el sentido contrario (antidrómico), colisionando con el frente ortodrómico. El último estímulo del tren tarda un tiempo en alcanzar el circuito, rodearlo y volver hasta la posición del electrodo que

estimula; es lo que denominamos intervalo post-estimulación (*post-pacing interval*, PPI). Este PPI es directamente proporcional a la distancia a la que se encuentra el lugar de origen del estímulo (el electrodo) del circuito de reentrada. La diferencia entre el PPI y la longitud de ciclo (TCL, tiempo que tarda un impulso en dar una vuelta al circuito) es el ciclo de retorno, que corresponde justamente al tiempo que tarda nuestro estímulo en llegar y volver al/del circuito. De este modo, si el ciclo de retorno es 0, estaríamos estimulando desde un punto perteneciente al circuito.

Los componentes críticos de un circuito de reentrada (figura 17) son la propia entrada al circuito (*entrance*), el istmo de conducción lenta y la salida (*exit site*); son absolutamente necesarios para mantener la reentrada y tienden a estar anatómicamente delimitados, por lo que la ablación en estos sitios tiene una alta probabilidad de terminación de la arritmia. Estos componentes, así como los "no críticos" (circuito externo o *outer loop*, y circuitos activados de forma pasiva como los *inner loops* o *by-standers*), pueden identificarse mediante maniobras de encarrilamiento, atendiendo a los criterios de PPI y ciclos de retorno recogidos en la tabla 3. (246) Además de estos criterios, se utilizan el grado de fusión y el tiempo transcurrido desde el estímulo hasta el QRS estimulado (S-QRS). La fusión se refiere a la obtención de una morfología de QRS estimulado intermedia entre el QRS de la TV y la que correspondería a un QRS estimulado puro. Cuando se estimula desde sitios anatómicamente "protegidos" (p.ej. el istmo) del circuito, la fusión está "oculta", porque el estímulo sale por el mismo sitio (*exit site*) que la taquicardia, y el QRS estimulado será idéntico al de la taquicardia (tabla 4). (246)

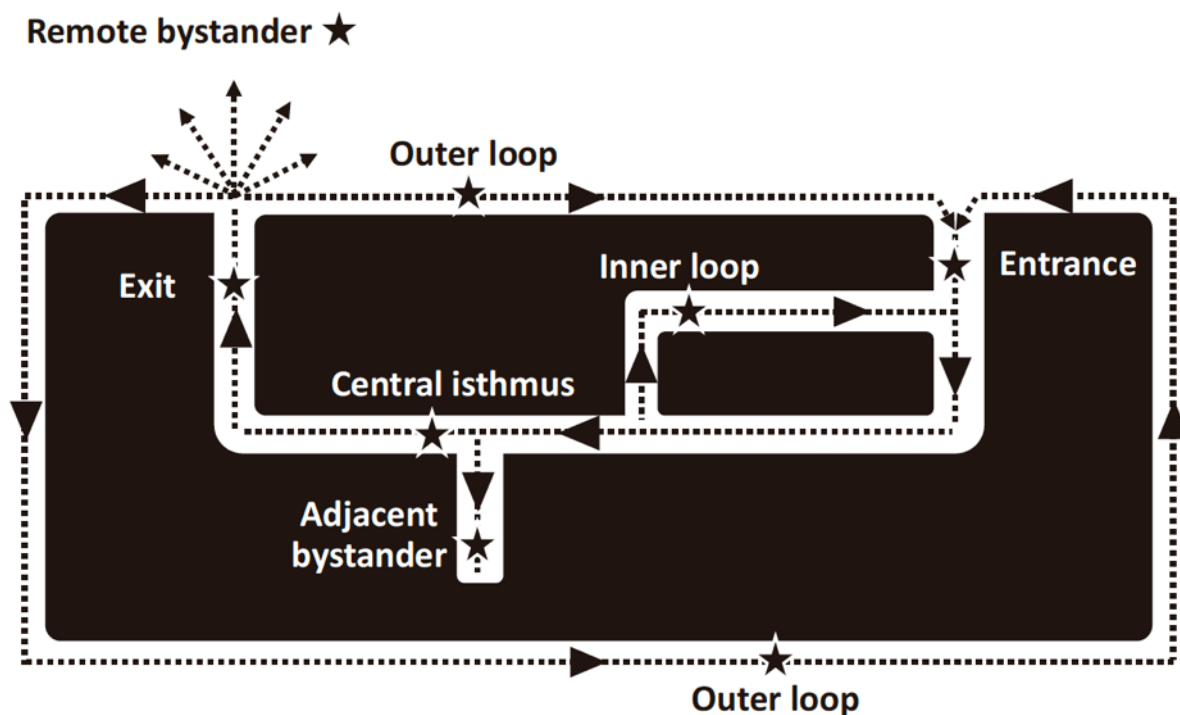


Figura 17. Modelo esquemático de los componentes de un circuito de reentrada. Ver texto para detalles. De Guandalini et al. (245)

Sitio del circuito	Fusión	Encarrilamiento	S-QRS/TCL
Salida	Oculto	$PPI = TCL (\pm 30 \text{ ms})$	< 30%
Istmo central	Oculto	$PPI = TCL (\pm 30 \text{ ms})$	30 - 50%
Entrada	Oculto	$PPI = TCL (\pm 30 \text{ ms})$	50 - 70%
Inner loop	Oculto	$PPI = TCL (\pm 30 \text{ ms})$	> 70%
By-stander adyacente	Oculto	$PPI > TCL$	Variable
Outer loop	Manifiesta	$PPI = TCL (\pm 30 \text{ ms})$	< 30%
By-stander remoto	Manifiesta	$PPI > TCL$	< 30%

Tabla 4. Identificación de los distintos componentes de un circuito de reentrada (figura 16) mediante maniobras de encarrilamiento. De Stevenson et al. (246)

Finalmente, la utilización de las maniobras de encarrilamiento queda limitada (247) al grado de tolerancia hemodinámica de la taquicardia. Además, muchos circuitos de reentrada

tienen una estructura tridimensional, localizándose los componentes críticos del circuito en zonas profundas de la pared miocárdica, no accesibles al catéter mediante mapeo endocárdico o epicárdico. (248,249)

#### **g.4.3 Mapa de topoeestimulación (*pacemapping*)**

Cuando una TV por reentrada es mal tolerada hemodinámicamente, la utilización de esta técnica permite identificar, al realizar una comparación entre la morfología del QRS de la TV y el QRS estimulado, el *exit site* del circuito. En dicho punto, ambas morfologías van a ser coincidentes (cercanas al 100% de correlación). Por el contrario, la estimulación desde miocardio cercano al sitio de entrada al circuito, siendo un punto crítico del mismo, obtiene una morfología de QRS que es completamente opuesta a la de la TV. (250) Tal es así, que en un elegante trabajo de De Chillou et al. (251) se utilizó el criterio de transición abrupta de una morfología de QRS idéntica a la de la TV a una completamente diferente para identificar el lugar del istmo crítico del circuito. En el istmo, por tanto, se pueden obtener morfologías cambiantes, en función de la dirección de propagación del impulso estimulado. (252)

Aunque históricamente, la evaluación del grado de correlación se realizaba de forma cualitativa (p.ej. número de derivaciones concordantes), posteriormente se describieron algoritmos que permitían la cuantificación del grado de correlación, (253,254) y que actualmente van incorporados en el software de los sistemas de navegación electroanatómica. En la **figura 18** se muestra un ejemplo de óptima correlación con el QRS de la TV clínica por *pacemap* (94,2%) al estimular desde el catéter de ablación, posicionado





reentrada exhiben propiedades electrofisiológicas distintas al tejido normal durante el ritmo sinusal, como la presencia de activación lenta o retrasada, que se puede mapear y anotar para la ablación posterior.

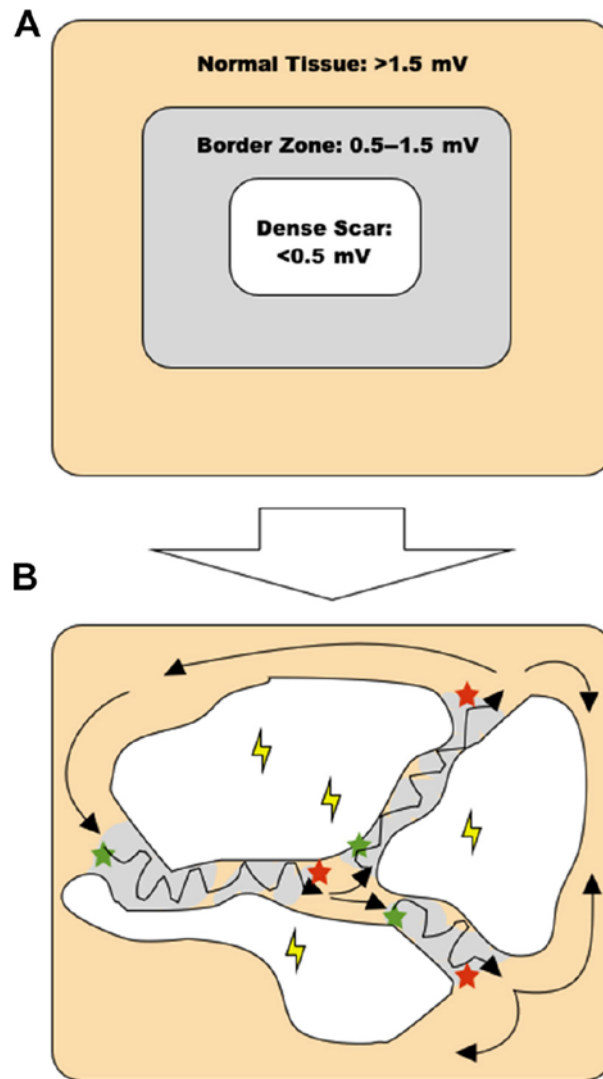


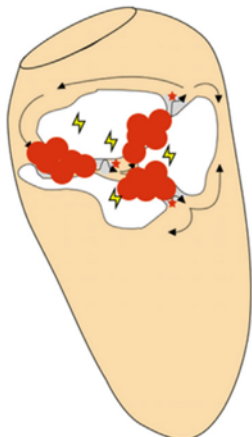
Figura 19. A) Definiciones de voltaje tisular. Desde endocardio, el voltaje normal se define como  $> 1.5$  mV, mientras que el core es  $< 0.5$  mV y BZ es de 0.5 mV a 1.5 mV (EGM bipolares registrados con catéteres con un electrodo en la punta de 4 mm, espacio entre electrodos de 1 mm y filtrado a 10–400 Hz). B) Esquema de los circuitos relacionados con la cicatriz: entrada (estrella verde), istmo (zona gris) y salida (estrella roja). De Briceño et al. (256)

La primera descripción sobre ablación de sustrato la estableció el grupo de Marchlinski, (255) realizando líneas de ablación dentro de la cicatriz en función de los hallazgos del *pacemapping*. Posteriormente, se han descrito varias técnicas de ablación de sustrato,

como la ablación de potenciales tardíos (*late potentials*, LP), (257,258) ablación de EGM anormales (*local abnormal ventricular activities*, LAVA), (259) homogeneización de la cicatriz, (260) aislamiento del *core*, (261) o descanalización de la cicatriz (*scar dechanneling*, SD) (figura 20). (262-264) Independientemente de la técnica empleada, el objetivo *gold standard* de la ablación es la consecución de no inducibilidad para AV sostenidas al terminar el procedimiento. En el ensayo clínico aleatorizado VISTA, de pacientes con CI y TV estable, la ablación del sustrato redujo las recurrencias de TV (15,5% vs. 48,3% al año) en comparación con la ablación convencional, lo que respalda aún más la estrategia de ablacionar todo el sustrato. (265) En un metaanálisis reciente, se demostró que el mapeo de sustrato y la ablación disminuyen el *endpoint* combinado de AV recurrentes y mortalidad total a largo plazo. (266) Por otra parte, se han descrito tasas de descompensación hemodinámica (asociada a aumento de mortalidad) de hasta el 11% cuando se realiza la ablación de forma convencional (es decir, mapeando y ablacionando todas y cada una de las TV inducibles en el paciente). (267)

Los resultados de los 5 ensayos clínicos aleatorizados clásicos (SMASH-VT, VTACH, CALYPSO, VANISH y SMS) (268-272) en los que se basan las indicaciones para ablación de sustrato en CI en la actualidad se recogen en la tabla 5. Sin embargo, se debe destacar la dificultad que tuvieron estos ensayos para el reclutamiento de pacientes; continúan siendo necesarios estudios adicionales con mayor poder estadístico.

**A Scar Dechanneling**



*Identification of a corridor of consecutive EGMs with delayed components (conducting channels), and subsequent ablation of the entrance regions.*

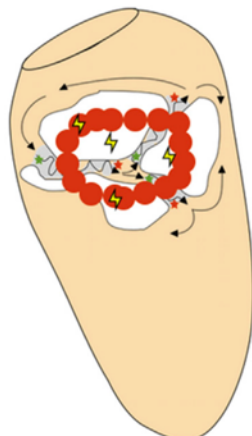
**B Late Potentials and Local Abnormal Ventricular Activities**



*LPs: Ablation of any low voltage EGM (<1.5 mV) with a single component or multiple continuous delayed components, recorded after the surface QRS.*

*LAVA: Ablation of sharp high-frequency ventricular potentials occurring anytime from the ventricular EGM (before-VT; during/after-NSR)*

**C Core Isolation**



*Isolation of the area that incorporates critical VT circuit elements.*

**D Homogenization**



*Ablation lesions aimed to cover the entire scar (homogenization of the scar) targeting all abnormal electrograms.*

Figura 20. Distintas estrategias para la ablación de sustrato. A) Scar dechanneling; B) ablación de potenciales tardíos y LAVAs; C) aislamiento del core; D) homogeneización de la cicatriz. De Briceño et al. (256)

Estudio	Año	Criterios de inclusión	N° pacientes	Brazos del estudio	Hallazgos	Comentarios
Substrate Mapping and Ablation in Sinus Rhythm to Halt Ventricular Tachycardia ( <b>SMASH-VT</b> ) (268)	2007	IAM previo, primera AV o terapia apropiada de DAI, sin FAA previo.	128	Ablación de sustrato endocárdico vs. tratamiento médico estándar.	- La ablación disminuyó la probabilidad de TV que requiriera terapias de DAI (67% vs. 88%; p = 0,007). - Sin diferencias en mortalidad.	Se excluyeron pacientes con FAA.
Ventricular Tachycardia Ablation in Coronary Heart Disease ( <b>VTACH</b> ) (269)	2010	IAM previo, FEVI < 50% y TV estable, candidatos a DAI en prevención secundaria.	107	Ablación de sustrato y DAI vs. DAI sólo. Ambos grupos podían recibir FAA.	- Menor recurrencia de TV con la ablación (29% vs. 47%; p = 0,044) - Sin diferencias en mortalidad.	Hubo una recurrencia > 50% en el brazo ablación a 2 años.
Catheter Ablation for Ventricular Tachycardia in Patients with Implantable Cardioverter Defibrillator ( <b>CALYPSO</b> ) (270)	2015	CI, sin contraindicación para FAA, con $\geq 1$ choque de DAI o $\geq 3$ ATPs apropiadas.	27	Ablación vs. FAA (1ª línea: amiodarona, sotalol; 2ª línea: mexiletina, ranolazina, dofetilide)	- Menor riesgo de recurrencias con FAA (43% vs. 62%). - Tiempo mediana a recurrencia más largo en el brazo ablación (75 vs. 45 días)	Pocos pacientes. Sin poder estadístico suficiente.
Ventricular Tachycardia Ablation versus Escalated Antiarrhythmic Drug Therapy in Ischemic Heart Disease ( <b>VANISH</b> ) (271)	2016	IAM previo, DAI y TV recurrente a pesar de FAA.	259	Ablación vs. escalamiento de FAA (amiodarona, mexiletina)	- Menor aparición de evento compuesto (mortalidad total, tormenta arritmica o terapia apropiada de DAI a los 30 días) en el brazo ablación (59,1% vs. 68,5%; p = 0,04) - Más eventos adversos en el brazo de FAA.	
Substrate Modification Study ( <b>SMS</b> ) (272)	2017	CI, FEVI < 40% y TV inestable espontánea o inducida en EEF tras parada cardiaca o síncope.	111	Ablación de sustrato y DAI vs. DAI sólo.	- Supervivencia libre de AV similar en ablación vs. grupo sólo DAI (49% vs. 52,4%; p = 0,84). - Menor n° de episodios de TV en el grupo ablación (2,8 vs. 8,1; p = 0,015) incluyendo los que requirieron terapia de DAI.	

Tabla 5. Principales ensayos clínicos aleatorizados comparando la ablación de sustrato de AV en CI vs. tratamiento convencional. FAA: Fármacos antiarrítmicos. Tabla modificada de Titz et al. (273)

En un estudio prospectivo multicéntrico reciente, (274) Fernández-Armenta et al. analizaron los resultados clínicos de la ablación de sustrato mediante la técnica de *scar dechanneling* en 402 pacientes, con una mediana de seguimiento de 2 años (P<sub>25</sub>-P<sub>75</sub> 7-39 meses). El 65,8% de los pacientes eran isquémicos. La supervivencia acumulada libre de AV al finalizar el seguimiento fue del 72,2% (figura 21, encontrándose más de la mitad de los pacientes (55%) sin tomar tratamiento antiarrítmico alguno. Hubo una ligera tendencia a una peor supervivencia en pacientes no isquémicos respecto a los isquémicos (figura 22). (274)

Cuando se realizan técnicas de ablación de sustrato, independientemente de la técnica elegida, es importante la evaluación del sustrato "funcional", esto es, identificar zonas con posible conducción enlentecida oculta en ritmo sinusal (es decir, "corredores" potenciales de circuitos de reentrada no visibles ni por mapas de voltaje ni por las características de los EGM, que pueden estar falsamente enmascarados por la señal del miocardio sano circundante). Existen varias técnicas descritas al respecto, que han demostrado mejorar los resultados de la ablación de sustrato. (275-280)

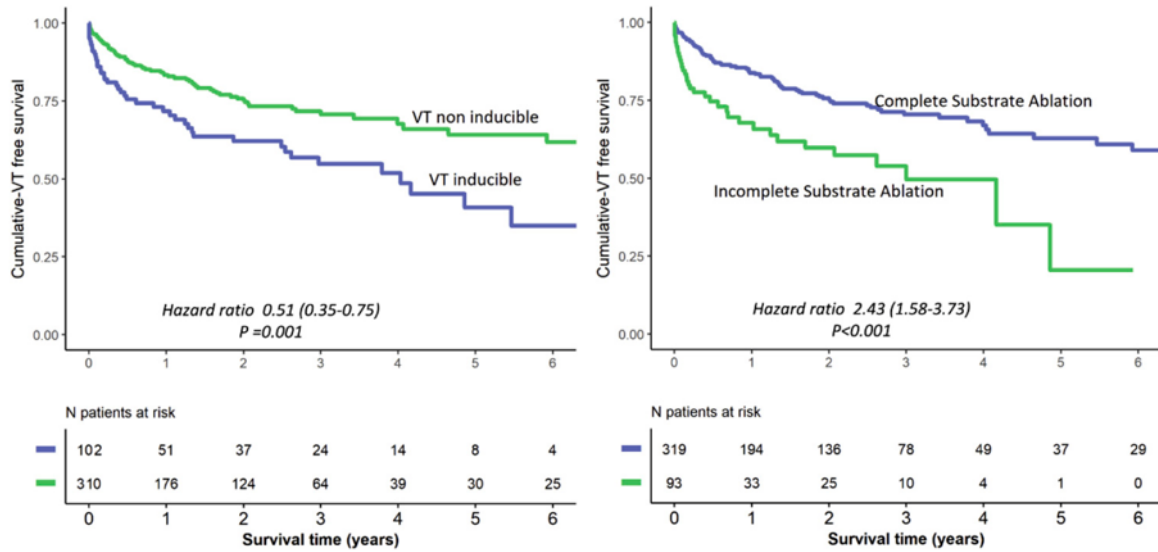


Figura 21. Predictores de recurrencia de AV tras ablación de sustrato asociado a cicatriz miocárdica. La persistencia de inducibilidad para TV con estimulación programada o la no consecución de una ablación completa del área con EGM anormales tiene relación directa con una mayor tasa de recurrencias. De Fernández-Armenta et al. (274)

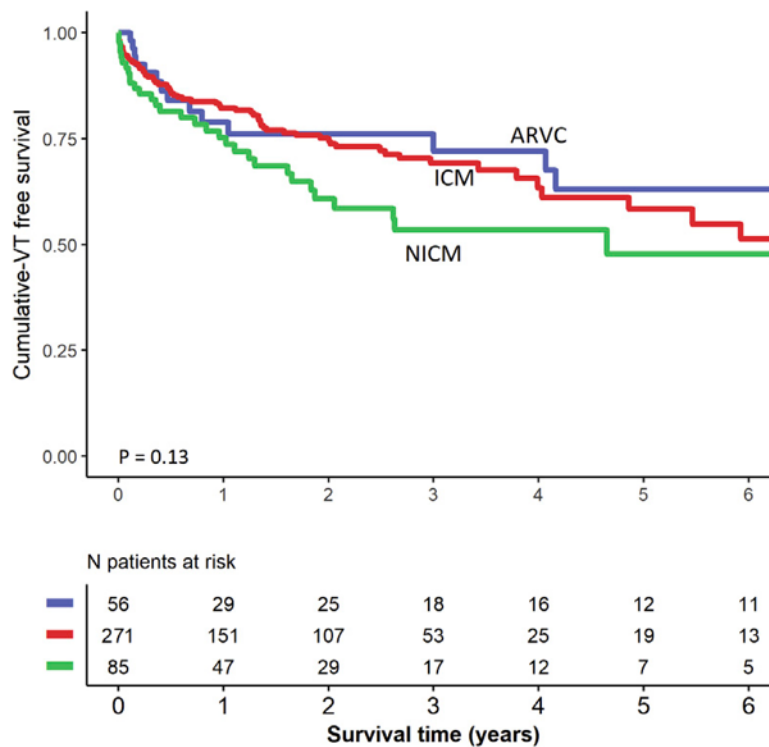


Figura 22. Diferencias en supervivencia libre de AV tras ablación de sustrato (mediante la técnica de scar dechanneling) en función de la cardiopatía de base. ARVC: arrhythmogenic right ventricular cardiomyopathy; ICM: ischemic cardiomyopathy; NICM: non-ischemic cardiomyopathy. De Fernández-Armenta et al. (274)

## **h. Papel de la Resonancia Magnética Cardíaca en la ablación de Arritmias Ventriculares en Cardiopatía Isquémica**

Todo lo que se ha comentado en el apartado anterior respecto a las técnicas de mapeo y ablación, ya sea convencional o de sustrato, resulta aplicable cuando las imágenes de RM están disponibles durante los procedimientos. El hecho de disponer *in situ* de un mapa del sustrato derivado de las imágenes de PSI puede permitir la identificación rápida y fiable de los componentes del circuito de reentrada, si atendemos a la correlación demostrada entre la RM y los hallazgos histológicos, o entre ésta y los hallazgos de los EAM, como ya se ha venido comentando previamente en anteriores apartados de la Tesis.

La utilidad de la RM, además de ayudar en la identificación de las dianas o *targets* de ablación, va aún más allá, al permitir evaluar la localización o el grado de transmuralidad del sustrato, ayudando de esta manera en la toma de decisiones respecto al mejor abordaje para realizar la ablación (acceso endocárdico, epicárdico, o combinado endo-epicárdico). Comentaremos estos aspectos en los siguientes apartados.

### **h.1 Selección de la vía de abordaje para la ablación**

Clásicamente, la decisión acerca de la vía de abordaje a realizar durante la ablación (endocárdica, epicárdica o endo-epicárdica) se ha tomado teniendo en cuenta la morfología del ECG de la TV, la ubicación del sustrato más probable en función de la



cardiopatía subyacente o el éxito o ausencia de él tras una ablación endocárdica previa. (281) Disponer de las imágenes de RM-RTG previamente al procedimiento tiene la utilidad potencial de identificar la ubicación de la fibrosis y, de esta manera, ayudar a una mejor planificación del procedimiento. (189) En un estudio de Andreu et al. (189) realizado en 80 pacientes con TV asociada a cardiopatía estructural, el RTG estaba presente en el 96% de los puntos de ablación exitosa de la TV clínica. Además, la presencia de RTG subepicárdico mostró un 85% de sensibilidad y un 100% de especificidad para predecir un origen epicárdico de la TV.

El acceso epicárdico durante los procedimientos de ablación implica realizar una punción subxifoidea para acceder al espacio pericárdico. En pacientes con CI, la realización de un abordaje combinado endo-epicárdico se ha relacionado con una menor tasa de recurrencia arrítmica durante el seguimiento, ya sea como estrategia de primera línea o después de una ablación endocárdica previamente fallida. (260,282) Sin embargo, cuando se realiza el abordaje endo-epicárdico de manera sistemática, (260) o bien atendiendo meramente al fracaso previo del abordaje endocárdico, (282) la realidad es que una significativa proporción de pacientes no van a presentar sustrato epicárdico ablacionable, por lo que en algunos casos se habrá realizado una técnica no exenta de riesgos (p. ej. perforación cardíaca) y con escasa rentabilidad terapéutica. En este sentido, seleccionar los mejores candidatos para un abordaje endo-epicárdico de primera línea basado en imágenes de RM pre-procedimiento ha demostrado ser mucho más eficiente. (283)

## h.2 Integración de la RM-RTG durante la ablación

La integración de las imágenes de PSI derivadas del RTG en RM permite representar la cicatriz (el sustrato) desde el comienzo del procedimiento, lo que ayuda a enfocar el mapeo con el catéter (EAM) en esta área. Además, la forma, los límites y el tamaño de la cicatriz no se alteran en el RTG como ocurre en los EAM, en éstos debido al efecto de campo lejano del tejido sano circundante, que enmascara en algunos casos los EGM locales patológicos, como ya ha sido discutido previamente. Esto resultaría de especial interés en cicatrices pequeñas, subendocárdicas, heterogéneas. Por otra parte, la integración de la información de PSI permite identificar la presencia de HTC (o BZC), su anchura y profundidad (grado de transmuralidad), y localizar las entradas de los mismos (figura 13).

A pesar de estas ventajas teóricas, no existen estudios aleatorizados previos diseñados para probar los beneficios adicionales reales de este enfoque en comparación con el uso del EAM sólo. Sin embargo, existe evidencia creciente sobre los beneficios de su utilización. Investigadores de Burdeos (Francia) analizaron retrospectivamente la supervivencia libre de TV en una serie consecutiva de 125 pacientes con CI sometidos a ablación de TV, (284) encontrando que el uso de la integración de la RM se asoció de forma independiente con una menor tasa de recurrencias. Otro análisis prospectivo reciente de 24 pacientes con TV asociada a cicatriz mostró que enfocar el EAM en las áreas con RTG se asoció significativamente con menores recurrencias. (285) En un trabajo reciente de Andreu et al. (286) se evaluaron los beneficios de la integración de la RM en una población consecutiva de 159 pacientes sometidos a ablación de TV mediante la técnica de *scar dechanneling*. En este trabajo, la ayuda al procedimiento con integración de la RM se asoció con una menor

necesidad de administración de RF, mayores tasas de no inducibilidad después de la ablación del sustrato y una mayor supervivencia libre de recurrencia de TV. Sin embargo, la elección de los *targets* de ablación (en el caso del *scar dechanneling*, las entradas de canales de conducción lenta) continuó seleccionándose de la manera clásica, esto es, guiada por las características de los EGM registrados por el catéter (el EAM).

En vista de toda esta evidencia, la declaración de consenso de expertos publicada recientemente sobre la ablación con catéter de las AV (5) incluye dos nuevas indicaciones con respecto al uso de la RM: i) la recomendación de realizar una RM-RTG previa al procedimiento en pacientes isquémicos y no isquémicos sometidos a ablación de TV para reducir las recurrencias; y ii) utilizar la información de la RM previa al procedimiento para su planificación. Ambas indicaciones tienen hoy en día una recomendación de clase IIa.

## i. Papel de la Tomografía Computarizada en la identificación del sustrato y la ablación de Arritmias Ventriculares en Cardiopatía Isquémica

Tradicionalmente, la RM-RTG ha estado contraindicada en los portadores de marcapasos o DAI por razones de seguridad. Sin embargo, estudios recientes han demostrado que la RM es segura en estos pacientes. (287,288) Aún así, los artefactos debidos a la presencia de estos dispositivos pueden comprometer la calidad de las imágenes, especialmente en la pared anterior del VI. No obstante, existen secuencias de banda ancha (*wideband*) que han permitido reducir estos artefactos. (289,290)

Frente a la RM, existen varios grupos de investigación que han analizado el posible papel de la tomografía axial computarizada (TAC) para la identificación y análisis del sustrato arritmogénico. La TAC es, habitualmente y en comparación con la RM, una técnica más barata, accesible, rápida y no susceptible a los artefactos de los dispositivos de estimulación. Aunque tiene una mejor resolución espacial que la RM (unos 0.5 mm, lo cual le permite ser la técnica ideal para la delimitación del trayecto de las coronarias, el seno coronario, el nervio frénico y otras estructuras relevantes), (291-293) su relación contraste/ruido es peor. La TAC es una técnica de bajo contraste en los tejidos blandos porque presentan coeficientes de atenuación muy similares. Por eso, la capacidad de la TAC para discriminar miocardio sano de cicatriz es menor que la de la RM.

A pesar de ello, se han descrito dos métodos principales para la caracterización de la cicatriz por TAC: i) áreas de realce tardío de yodo; (294) y ii) áreas de adelgazamiento de la pared ventricular. (295) El realce tardío en la TAC se basa en el hecho de que la cinética de los contrastes yodados (los empleados en la TAC) es similar a la de los basados en el gadolinio, (296) de tal manera que la información mostrada sería parecida a la obtenida con RM-RTG. (297)

En pacientes con CI, la TAC ha mostrado una buena correlación con los EAM de la cicatriz, sobre todo en aquellos pacientes con cicatrices transmurales, pero la correlación es más débil en casos de cicatrices no transmurales o miocardiopatías no isquémicas. (298) Los HTC que transcurren dentro de la cicatriz pueden identificarse mediante la TAC, ya que permite detectar diferencias de grosor parietal local en la zona fibrótica. Las áreas de adelgazamiento detectadas por la TAC se correlacionan con las zonas de bajo voltaje ( $< 1,5$  mV) y con la distribución de LAVA en los EAM. (295,299) Además, se ha descrito una buena correlación entre estos canales de la TAC, definidos como "crestas miocárdicas" (*ridges*), y los istmos de los circuitos de TV. (300)





# 5. HIPÓTESIS DE TRABAJO Y OBJETIVOS

## HIPÓTESIS DE TRABAJO

Esta Tesis, como su título indica, pretende evaluar la utilidad de la RM cardiaca, como técnica de imagen no invasiva, accesible e inocua, para identificar y caracterizar el sustrato arritmogénico en pacientes con CI crónica, de manera que esta técnica sea útil y aplicable al paciente en distintos momentos evolutivos desde el punto de vista arritmico (prevención primaria vs. secundaria) tras el evento isquémico agudo. Así, la Tesis desarrolla a las distintas utilidades que podemos aprovechar de la RM en pacientes con CI, y que serán el contenido de las correspondientes hipótesis y objetivos: i) evaluación de la presencia y evolución temporal del sustrato arritmogénico; ii) utilidad para la estratificación del riesgo arritmogénico; y iii) utilidad en el tratamiento de las AV asociadas a la cicatriz post-IAM.

La utilidad de la RM para caracterizar el remodelado de la cicatriz post-IAM a largo plazo tras un evento isquémico agudo es un aspecto que no ha sido explorado en la literatura, más allá de algún reporte en modelos experimentales animales, o en ser humano a corto plazo (meses) tras el IAM. El remodelado adverso del miocardio remoto a la cicatriz constituye un aspecto fisiopatológico que sí ha sido más ampliamente evaluado, y que tiene



relación con el deterioro progresivo de la función sistólica del VI y aparición de IC. Por el contrario, el remodelado intrínseco en la zona de la cicatriz resulta un proceso desconocido en la clínica. La primera hipótesis de la Tesis plantea que la cicatriz post-IAM sufre un proceso de remodelado intrínseco a largo plazo, y que ese remodelado es evaluable mediante RM. Planteamos, además, que ese proceso de remodelado podría tener consecuencias relevantes en el desarrollo de un potencial sustrato arritmogénico, y que podría explicar por qué muchos pacientes presentan AV años después del evento isquémico agudo.

Por otra parte, los cambios histológicos que ocurren en la cicatriz tras un IAM, y que pueden ser evaluados mediante RM seriadas, dependen de una respuesta inflamatoria local, mediada por diversas citocinas y células del sistema inmunológico, entre las que se encuentran los monocitos. En este sentido, del equilibrio entre las respuestas pro-inflamatoria y anti-inflamatoria va a depender el daño y reparación tisulares que ocurren a nivel local, lo cual estaría en íntima relación con la cantidad y distribución final de "tejido salvado" dentro de la cicatriz. Este resultado podría tener relación con distintos patrones de cicatrización, y con el desarrollo o no de un sustrato arritmogénico "crítico" para generar AV. Planteamos, como segunda hipótesis de la Tesis, que la distribución de las distintas subpoblaciones monocitarias que aparecen tras un IAM podrían influir en las características observables de la cicatriz, medidas por RM.

Por otro lado, en esta Tesis se plantea realizar un estudio comparado entre la RM y otra técnica de imagen ampliamente utilizada en la clínica y por otros grupos de investigación

en Electrofisiología, la tomografía axial computarizada (TAC). Esta técnica permite evaluar diferencias locales de grosor miocárdico dentro del área de adelgazamiento correspondiente a la cicatriz, y permite identificar “canales” de engrosamiento tisular, que serían el equivalente a los corredores o canales de tejido viable/heterogéneo que podemos ver con la RM, y por tanto corresponden con lo que definiríamos como sustrato arritmogénico. La tercera hipótesis de la Tesis plantea la superioridad de la RM respecto a la TAC a la hora de identificar el sustrato arritmogénico de la cicatriz.

Actualmente, la estratificación de riesgo de arritmias ventriculares en pacientes con cardiopatía isquémica crónica se basa en la evaluación de la función sistólica del VI, cuantificada como FEVI. De esta manera, aquellos pacientes con una FEVI < 35% se consideran de alto riesgo y reciben implante de un DAI en prevención primaria, mientras que aquéllos con una FEVI  $\geq$  35% no lo reciben, a pesar de que este último grupo de pacientes es el más frecuente en práctica clínica, y el que engloba, en términos absolutos, el mayor número de eventos arrítmicos durante el seguimiento. La RM podría ser útil para identificar a aquellos pacientes con cardiopatía isquémica crónica que van a desarrollar AV, atendiendo a las características diferenciales de la cicatriz miocárdica que podemos evaluar con la técnica, y de forma independiente a la FEVI. En este sentido, nuestra cuarta hipótesis de la Tesis plantea que la cantidad de cicatriz, y particularmente la cantidad de tejido heterogéneo o *border zone* (BZ) y su distribución en forma de canales o corredores de miocardio viable, son parámetros que permiten estratificar mucho mejor que la FEVI el riesgo arrítmico.

Finalmente, la ablación de sustrato de TV constituye un tratamiento eficaz para pacientes con episodios recurrentes de TV en relación a la presencia de cicatriz miocárdica, como es la cicatriz post-IAM. Sin embargo, las tasas de recurrencia post-ablación, en series modernas, continúan siendo altas, y los procedimientos requieren de una alta cualificación y experiencia por parte de los operadores. Además, este tipo de intervenciones pueden llegar a requerir mucho tiempo en quirófano (habitualmente, horas), incrementando potencialmente el riesgo de complicaciones. Estudios recientes han demostrado que ayudar la ablación mediante la integración de mapas PSI, obtenidos a partir de las imágenes de RM-RTG, resulta en procedimientos más eficientes y consigue mejorar la supervivencia libre de recurrencia de TV. La quinta y última hipótesis de la Tesis plantea que realizar la ablación de sustrato de TV guiada exclusivamente por los mapas PSI obtenidos a partir de las imágenes de RM-RTG es viable y beneficiosa en términos de resultados clínicos post-intervención.

## OBJETIVOS DE LA TESIS

### Objetivos generales:

- Evaluar la presencia de cicatriz miocárdica, caracterizar los componentes de la misma y analizar sus modificaciones a lo largo del tiempo mediante realización de RM seriadas tras un IAM con elevación de ST.
- Evaluar la presencia de potencial sustrato arritmogénico (HTCs en la RM) y su evolución en cada uno de los momentos temporales evaluados tras el IAM.
- Investigar el papel de los monocitos circulantes en sangre periférica (células del sistema inmune implicadas en procesos de inflamación/reparación tisular) y sus distintas subpoblaciones: clásicos o CLM (CD14<sup>++</sup> CD16<sup>-</sup>), intermedios o INTM (CD14<sup>++</sup> CD16<sup>+</sup>) y no clásicos o no-CLM (CD14<sup>+</sup> CD16<sup>++</sup>), en la formación de la cicatriz después de un IAM, evaluada ésta con RM.
- Evaluar el valor predictivo clínico de las diferentes subpoblaciones monocitarias y otros biomarcadores evaluados, en paralelo con el valor predictivo de la RM, así como el valor incremental de la utilización conjunta de biomarcadores y RM.
- Investigar el rendimiento general de la tomografía axial computarizada (TAC) para identificar la presencia de sustrato arritmogénico en pacientes con infarto crónico de miocardio, comparado con el rendimiento de la RM, considerada la técnica de imagen *gold standard*.
- Investigar la utilidad de la RM para identificar a aquellos pacientes post-infarto de miocardio (crónico) en riesgo de presentar AV malignas.

- Evaluar la viabilidad y el beneficio potencial de realizar los procedimientos de ablación de sustrato de TV guiando la ablación exclusivamente mediante los mapas de intensidad de señales de píxeles (PSI) derivados de la RM-RTG.

### Objetivos específicos:

- Validar la utilidad general de la RM, tanto de 1.5 como de 3 Tesla, y un protocolo de adquisición de imágenes en la identificación, medición y evaluación de la fibrosis miocárdica, así como de la distribución cualitativa y cuantitativa de sus distintos componentes.
- Evaluar la utilidad de una adquisición de viabilidad 3D con RM de 3 Tesla en la obtención de imágenes de alta calidad para ser post-procesadas con el software ADAS3D. El objetivo de este post-procesamiento será:
  - Cuantificar la cicatriz.
  - Caracterizar la cicatriz dividiéndola en sus componentes: cicatriz densa ("core") y cicatriz heterogénea ("border zone").
  - Identificar potenciales canales de conducción lenta, equivalentes a HTC's dentro de la cicatriz, mediante reconstrucciones 3D de las imágenes de RM post-procesadas con hasta 10 cortes, desde el endocardio hasta el epicardio.
  - Establecer la posible relación entre las diferentes características de la cicatriz y los eventos clínicos, e identificar potenciales diferencias entre cicatrices arritmogénicas y no arritmogénicas.
  - Disponer de un banco de imágenes de RM post-procesadas en pacientes post-IAM para utilizar en caso de aparición de eventos arrítmicos. Estas

imágenes, incluso, se podrían importar al sistema de navegación utilizado en caso de precisar realizar un tratamiento invasivo (ablación) de las AV.

- Evaluar la utilidad de una adquisición TAC en la obtención de imágenes de alta calidad para ser post-procesadas con el software ADAS3D. El objetivo de este post-procesamiento será:
  - Cuantificar la cicatriz, evaluada como el área con un adelgazamiento mural del miocardio < 5 mm.
  - Caracterizar la cicatriz identificando zonas de engrosamiento local del miocardio con forma de canales o corredores ("*ridges*").
  - Establecer una posible relación entre los *ridges* de miocardio identificados y los canales de tejido heterogéneo identificados por RM-RTG.
  - Disponer de un banco de imágenes de TAC post-procesadas en pacientes post-IAM.
- Evaluar la utilidad del post-procesado de las imágenes de TAC para guiar procedimientos de ablación de sustrato, tras su importación a un sistema de navegación electroanatómica, en comparación con la utilidad de la RM.
- Describir la utilidad predictora para AV de la masa de BZC, nuevo parámetro cuantificable de la cicatriz mediante RM-RTG.
- Evaluar las diferencias en la capacidad predictora de eventos entre distintos parámetros evaluables por RM para la cicatriz: masa total de cicatriz, masa de border zone, masa de core, y masa de canales de border zone.
- Evaluar la capacidad predictiva para eventos arrítmicos de la RM respecto al *gold standard*, que es la FEVI.

- Evaluar el valor predictivo incremental de la utilización de la RM junto a la FEVI para la estratificación del riesgo de presentar AV post-IAM.
- Evaluar la seguridad de los procedimientos de ablación de sustrato de TV mediante una técnica guiada exclusivamente por imagen (RM-RTG).
- Evaluar la eficacia aguda de los procedimientos de ablación de sustrato de TV guiados exclusivamente por RM-RTG, en términos de inducibilidad post-ablación y eliminación completa del sustrato (es decir, eliminación de todos los electrogramas anormales de la cicatriz) empleando la técnica de *scar dechanneling* adaptada al uso exclusivo de RM-RTG.
- Evaluar la eficiencia de los procedimientos de ablación de sustrato de TV guiados exclusivamente por RM-RTG, en términos de tiempo total de procedimiento, tiempo de fluoroscopia y tiempo de RF aplicada.
- Evaluar la eficacia clínica de los procedimientos de ablación de sustrato de TV guiados exclusivamente por RM-RTG, en términos de recurrencias de TVMS o terapias apropiadas de DAI al año de seguimiento.







# 6. PUBLICACIONES

## SUBPROYECTO 1. UTILIDAD DE LA CARDIORRESONANCIA EN LA EVALUACIÓN DE LA PRESENCIA Y EVOLUCIÓN DEL SUSTRATO ARRITMOGÉNICO EN EL POST-INFARTO CRÓNICO DE MIOCARDIO.

### Artículo 1: Follow-Up After Myocardial Infarction to Explore de Stability of Arrhythmogenic Substrate – The FOOTPRINT Study

**Jáuregui B**, Soto-Iglesias S, Penela S, Acosta J, Fernández-Armenta J, Linhart M, Terés S, Syrovnev V, Zaraket F, Hervàs V, Prat-González S, Perea RJ, Morales-Ruiz M, Jiménez W, Lasalvia L, Bosch X, Ortiz-Pérez JT, Berruezo A. Follow-Up After Myocardial Infarction to Explore the Stability of Arrhythmogenic Substrate. *JACC Clin Electrophysiol* 2020;6:207-218. *FACTOR DE IMPACTO (2020): 6.375. ÁREA DE CONOCIMIENTO: Cardiology and Cardiovascular Medicine. CUARTIL: Q1.*

Los objetivos generales del estudio son:

- Evaluar la presencia de cicatriz miocárdica, caracterizar los componentes de la misma y analizar sus modificaciones a lo largo del tiempo mediante realización de RM seriadas tras un IAM con elevación del ST.

- Evaluar la presencia de potencial sustrato arritmogénico (HTC en la RM) en cada uno de los momentos temporales evaluados tras el IAM.

## RESUMEN ESTRUCTURADO

**Objetivos:** Nuestro objetivo es caracterizar el proceso de remodelación de la cicatriz a largo plazo después de un infarto agudo de miocardio (IAM) y el sustrato arritmogénico relacionado con la cicatriz subyacente utilizando resonancia magnética cardíaca con realce tardío de gadolinio (RM-RTG) seriada.

**Antecedentes:** Poco se sabe sobre el curso de tiempo necesario para completar el proceso de cicatrización de la cicatriz después del IAM, que puede evaluarse mediante técnicas de imagen cardíaca no invasivas, como la RM-RTG.

**Métodos:** Se incluyeron de forma consecutiva 56 pacientes con IAM con elevación del ST (IAMCEST) revascularizado. Se realizaron RM-RTG de 3-Tesla a los 7 días (7d), 6 meses (6m) y 4 años (4y) después del IAMCEST. El miocardio se segmentó en 10 capas desde el endo- hasta el epicardio, caracterizando el core, la border zone (BZ) y los canales de BZ (BZC) utilizando un software de post-procesamiento dedicado.

**Resultados:** La edad media fue de  $57 \pm 11$  años, 77% hombres. La fracción de eyección del ventrículo izquierdo (FEVI) mejoró a los 6m del 47% al 51% ( $p < 0,001$ ), permaneciendo estable a los 4y (53%,  $p = 0,21$ ). La masa cicatricial total disminuyó de  $20,3 \pm 14,6$  g a  $15,3 \pm 13,3$  g (6m) y  $12,7 \pm 11,7$  g (4y) ( $p < 0,001$ ). 30/56 (53%) pacientes mostraron una media de  $1,5 \pm 1,3$  CBZ/paciente a los 7 días, disminuyendo a  $1,2 \pm 1,3$  (6m) y  $0,8 \pm 1,0$  (4y) ( $p < 0,01$ ). Solo el 42% de los CBZ iniciales permanecieron presentes después de 4 años. No hubo eventos arrítmicos tras un seguimiento medio de  $62,5 \pm 7,4$  meses.

**Conclusiones:** El post-procesamiento de los datos de la RM permite realizar una evaluación dinámica de las características cuantitativas y cualitativas de las cicatrices post-IAM. El tamaño de la cicatriz y el número de BZC disminuyen de manera constante 4 años después

del IAM. La distribución de BZC se modifica significativamente durante este período de tiempo. Estos parámetros dinámicos pueden evaluarse de manera fiable con RM y su evaluación puede tener valor pronóstico.

## VENTRICULAR ARRHYTHMIAS

# Follow-Up After Myocardial Infarction to Explore the Stability of Arrhythmogenic Substrate



## The Footprint Study

Beatriz Jáuregui, MD, MSc,<sup>a,b</sup> David Soto-Iglesias, MSc, PhD,<sup>a,b</sup> Diego Penela, MD, PhD,<sup>c</sup> Juan Acosta, MD, PhD,<sup>d</sup> Juan Fernández-Armenta, MD, PhD,<sup>e</sup> Markus Linhart, MD,<sup>b</sup> Cheryl Terés, MD,<sup>a</sup> Vladimir Syrovnev, MD,<sup>b</sup> Fatima Zaraket, MD,<sup>b</sup> Vanessa Hervás, RN,<sup>b</sup> Susana Prat-González, MD, PhD,<sup>b</sup> Rosario J. Perea, MD, PhD,<sup>b</sup> Manuel Morales-Ruiz, MD, PhD,<sup>b</sup> Wladimiro Jiménez, MD, PhD,<sup>b</sup> Luis Lasalvia, MD, MIB,<sup>f</sup> Xavier Bosch, MD, PhD,<sup>b</sup> José T. Ortiz-Pérez, MD, PhD,<sup>b</sup> Antonio Berrueto, MD, PhD<sup>a</sup>

### ABSTRACT

**OBJECTIVES** This study aimed to characterize the long-term scar remodeling process after an acute myocardial infarction (AMI) and the underlying scar-related arrhythmogenic substrate using serial late gadolinium enhancement cardiac magnetic resonance (LGE-CMR).

**BACKGROUND** Little is known about the time course needed for completion of the scar healing process after an AMI, which can be assessed by noninvasive cardiac imaging techniques such as LGE-CMR.

**METHODS** Fifty-six patients with revascularized ST-segment elevation AMI (STEMI) were consecutively included. LGE-CMR (3-T) was obtained at 7 days, 6 months, and 4 years after STEMI. The myocardium was segmented into 10 layers from the endocardium to epicardium, characterizing the core, border zone (BZ), and BZ channels (BZCs) using a dedicated post-processing software.

**RESULTS** Mean age of the patients was  $57 \pm 11$  years; 77% were men. Left ventricular ejection fraction improved at 6 months from 47% to 51% ( $p < 0.001$ ) and remained stable at 4 years (53%;  $p = 0.21$ ). Total scar mass decreased from  $20.3 \pm 14.6$  g to  $15.3 \pm 13.3$  g (6 months) and to  $12.7 \pm 11.7$  g (4 years) ( $p < 0.001$ ). Thirty of 56 (53%) patients showed a mean of  $1.5 \pm 1.3$  BZCs/patient at 7 days, decreasing to  $1.2 \pm 1.3$  (6 months) and  $0.8 \pm 1.0$  (4 years) ( $p < 0.01$ ). Only 42% of the initial BZCs remained present after 4 years. There were no arrhythmic events after a mean follow-up of  $62.5 \pm 7.4$  months.

**CONCLUSIONS** CMR data post-processing permitted a dynamic assessment of quantitative and qualitative post-AMI scar characteristics. Scar size and number of BZCs steadily decreased 4 years after AMI. BZC distribution was significantly modified during this time. These dynamic parameters could be reliably assessed with CMR; their evaluation might be of prognostic value. (J Am Coll Cardiol EP 2020;6:207-18) © 2020 by the American College of Cardiology Foundation.

From the <sup>a</sup>Heart Institute, Teknon Medical Center, Barcelona, Spain; <sup>b</sup>Hospital Clínic, University of Barcelona, Barcelona, Spain; <sup>c</sup>Ospedale Guglielmo da Saliceto, Piacenza, Italy; <sup>d</sup>Hospital Universitario Virgen del Rocío, Sevilla, Spain; <sup>e</sup>Hospital Universitario Puerta del Mar, Cádiz, Spain; and the <sup>f</sup>Siemens Healthineers, Tarrytown, New York, USA. This work was supported by Agencia de Gestió d'Ajuts Universitaris i de Recerca (AGAUR), Generalitat de Catalunya (grant number 2014-SGR-471); Instituto de Salud Carlos III (ISCIII), Centro de Investigación Biomédica en Red: FIS-CIBER16 (grant number CB16/11/00354); Fondo de Investigación Sanitaria (FIS) (grant numbers PI14/00759, PI17/01968); and Ministerio de Economía y Competitividad, RETOS (grant numbers RTC-2015-3515-1, RTC-2016-5445-1). This study was partially supported by Siemens Healthineers. Dr. Lasalvia is a stockholder of Siemens Healthineers. Dr. Berrueto is a stockholder in Galgo Medical SL; and has received financial support from Siemens Healthineers. All other authors have reported that they have no relationships relevant to the contents of this paper to disclose.

ISSN 2405-500X/\$36.00

<https://doi.org/10.1016/j.jacep.2019.10.002>

**ABBREVIATIONS  
AND ACRONYMS**

AMI = acute myocardial infarction  
 BZ = border zone  
 BZC = border zone channel  
 CI = confidence interval  
 ICC = intraclass coefficient  
 LGE-CMR = late gadolinium enhancement cardiac magnetic resonance  
 LV = left ventricular  
 LVEF = left ventricular ejection fraction  
 n-RP = no-reflow phenomenon  
 SCD = sudden cardiac death  
 STEMI = ST-segment elevation myocardial infarction  
 VA = ventricular arrhythmias  
 VT = ventricular tachycardia

Many clinical and experimental studies have been conducted in the field of myocardial remodeling after an acute myocardial infarction (AMI). However, myocardial remodeling usually refers exclusively to the maladaptive changes that affect the remote myocardium and cause progressive heart failure, which, in contrast, appear not to be completely dependent on initial MI size (1). Regarding infarcted myocardium, the histopathophysiology of scar healing has been well described (2) and can be assessed by noninvasive cardiac imaging techniques, such as late gadolinium enhancement cardiac magnetic resonance (LGE-CMR). However, little is known about the time needed for scar healing completion in a human population (3).

SEE PAGE 219

Deeper characterization of the scar size and its components (border zone [BZ] and core zone) can be performed in the acute phase of ST-segment elevation myocardial infarction (STEMI) using LGE-CMR (4) and can help to stratify the risk of future arrhythmic events (5-7). Ventricular arrhythmias (VAs) are responsible for a continuous high global incidence of sudden cardiac death (SCD) among the ischemic population, regardless of left ventricular ejection fraction (LVEF) (8-10). Border zone channels (BZCs) within the scar, identified with LGE-CMR, act as ventricular tachycardia (VT) isthmuses (11) and correlate well with the slow conducting channels recognized in electroanatomic maps during VT substrate ablation procedures (12), and thus, constitute the arrhythmogenic substrate of the scar.

In the present study, we sought to characterize the long-term remodeling process of post-AMI scar and its components using LGE-CMR and to describe the potential changes of the subjacent arrhythmogenic substrate.

**METHODS**

**PATIENT SAMPLE.** We report the results of a pre-defined endpoint of a prospective observational study (4). Consecutive patients admitted to our

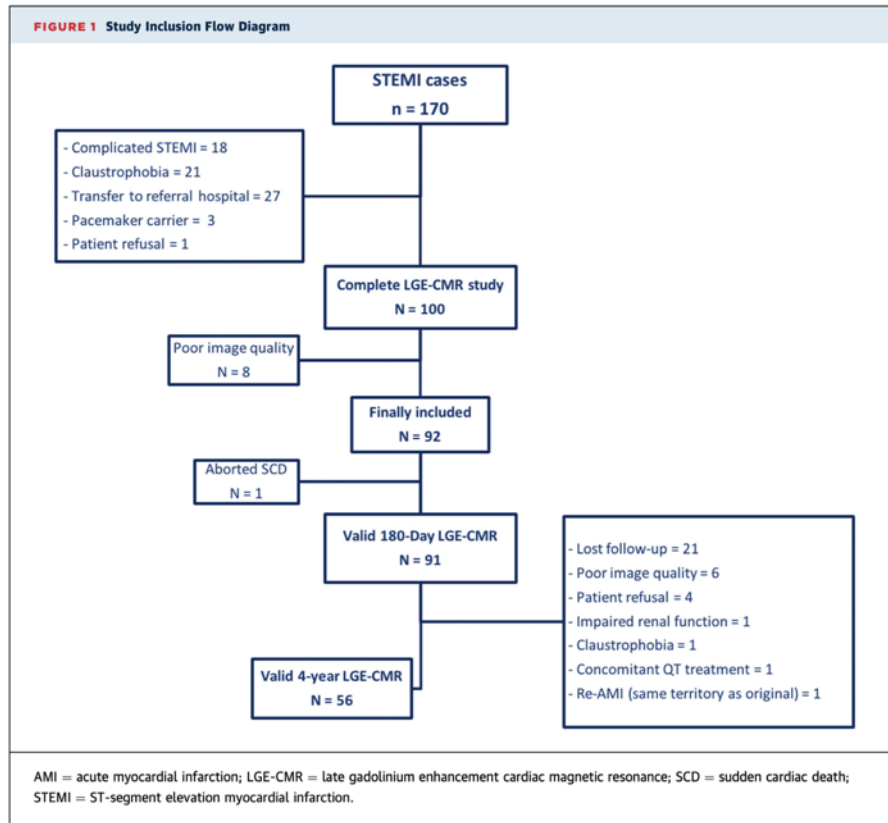
institution with a first STEMI, who had percutaneous revascularization was performed within the first 12 h from symptom onset, were included from September 2012 to June 2014. Patients who had  $\geq 1$  of the following criteria were excluded: STEMI  $>12$  h from symptom onset; history of MI; history of structural heart disease; age younger than 18 years; life expectancy  $<1$  year due to noncardiac pathology; classic contraindication for CMR; or clinical contraindication to perform the study within the first week (i.e., persistent Killip III to IV score, persistent hemodynamic instability, invasive ventilation, or intra-aortic balloon pump/left ventricular [LV] assist device). Patients who were transferred to another institution within 7 days after admission were also excluded. LGE-CMR was performed at  $7 \pm 2$  days, 6 months, and 4 years post-STEMI in all patients. The study complied with the Declaration of Helsinki, and the local ethics committee approved the study protocol. All participants included in the study (Figure 1) provided informed written consent.

**LGE-CMR PROCESSING.** LGE-CMR tests were performed using a 3-T scanner (MAGNETOM Trio, Siemens Healthcare, Erlangen, Germany). Image acquisition is summarized in the Online Appendix. All LGE-CMR images were analyzed using a previously described technique (13). Full LV volume was reconstructed in the axial orientation, and the resulting images were processed with ADAS-3D software (Galgo Medical, Barcelona, Spain). Ten concentric surface layers (from 10% to 90%) were created automatically from the endocardium to the epicardium of the LV wall thickness. A 3-dimensional shell was obtained for each layer. Pixel signal intensity maps based on LGE-CMR images were projected to each shell, following a trilinear interpolation algorithm, and color coded. To identify the scar areas, a pixel signal intensity-based algorithm was applied to characterize the hyperenhanced area as core zone, BZ, or healthy tissue using  $40 \pm 5\%$  and  $60 \pm 5\%$  of the maximum intensity as thresholds (Online Figure 1).

**MYOCARDIAL SCAR CHARACTERIZATION.** Two independent expert investigators analyzed the LGE-CMR images, and a third observer was available in case of discrepancy. The scar mass and areas in each shell (total scar, BZ, and core) were automatically

The authors attest they are in compliance with human studies committees and animal welfare regulations of the authors' institutions and Food and Drug Administration guidelines, including patient consent where appropriate. For more information, visit the [JACC: Clinical Electrophysiology author instructions page](#).

Manuscript received July 12, 2019; revised manuscript received September 19, 2019, accepted October 10, 2019.



measured using ADAS-3D software. Scar heterogeneity was defined as BZ proportion of scar (7). BZCs were defined as continuous corridors of BZ surrounded by scar core or an anatomical barrier (i.e., mitral annulus) that connected 2 areas of healthy tissue (12). If a given channel was identified in the same segment and with the same orientation in adjacent layers, it was considered as a single multilayer channel. The BZC mass was automatically computed using a fully automated tool embedded within ADAS-3D software.

Because tissue characterization is based on a pixel signal intensity algorithm, healthy myocardium cannot be distinguished from areas with a no-reflow phenomenon (n-RP). This is driven by the presence of microvascular obstruction, which is the potential result of different physiopathological events, such as direct endothelial necrosis, reperfusion injury of microvessels, and/or distal atherothrombotic embolization. This obstruction provokes a persistent

hypoenhancement on LGE-CMR images which, in turn, prevents proper tissue characterization of infarcted areas. Therefore, n-RP was considered whenever a hypointense area within the scar was detected on LGE-CMR images. Consequently, in patients with n-RP, no attempt was made to differentiate core and BZ areas inside the scar or to identify BZCs. In these patients, only information regarding LV dimensions and/or function and total scar mass (including n-RP regions inside the total scar mass) was compiled.

Scar location, mass, and area, as well as the presence of BZCs, were compared in the LGE-CMR images at 7 days, 6 months, and 4 years. A given BZC was considered to be stable among studies if it was located in the same myocardial layer and myocardial segment per the American Heart Association 17-segment model, with the same orientation and morphology.



**TABLE 1** Baseline Characteristics of the Study Population

	Total (N = 56)	No-Reflow (n = 16)	p Value*	Nonarrhythmic Scar† (n = 23)	Arrhythmic Scar† (n = 28)	p Value‡
Age, yrs	57 ± 11	53 ± 13	0.11	58 ± 9	56 ± 12	0.64
Men	43 (76.8)	12 (75.0)	0.84	19 (86.4)	20 (69.0)	0.15
Hypertension	22 (39.3)	4 (25.0)	0.17	8 (36.4)	13 (44.8)	0.54
Diabetes mellitus	5 (9.0)	0 (0.0)	0.33	4 (18.2)	1 (3.4)	0.16
Dyslipidemia	11 (19.6)	3 (18.8)	0.92	6 (27.3)	4 (13.8)	0.23
Smoker	27 (48.2)	9 (56.3)	0.28	11 (50.0)	13 (44.8)	0.87
Familiar history of early CAD	32 (57.1)	10 (62.5)	0.61	15 (68.2)	13 (44.8)	0.10
Time to reperfusion	218 ± 175	211 ± 136	0.86	220 ± 211	215 ± 162	0.94
Responsible artery			0.34			0.28
LAD	27 (48.2)	9 (56.3)		8 (36.4)	17 (58.6)	
RCA	22 (39.3)	4 (25.0)		11 (50.0)	9 (31.0)	
Cx	7 (12.5)	3 (18.8)		3 (13.6)	3 (10.3)	
Initial TIMI flow	1.1 ± 1.1	0	0.29	1.3 ± 1.2	1.3 ± 1.2	1.00
Final TIMI flow	2.9 ± 0.3	2.9 ± 0.3	1.00	2.9 ± 0.3	2.9 ± 0.3	0.90
Treatment during the acute phase						
Beta-blockers	48 (85.7)	14 (87.5)	0.71	17 (77.3)	26 (89.7)	0.24
ACE inhibitors/ARB	47 (83.9)	14 (87.5)	0.67	1 (4.5)	1 (3.4)	1.00
Statins	55 (98.2)	16 (100.0)	0.52	22 (100)	28 (96.6)	0.38
LVEF, %	47.1 ± 8.9	42.1 ± 7.4	0.01§	49.9 ± 9.0	46.7 ± 8.2	0.20
iLVEDV, ml/m <sup>2</sup>	83.8 ± 18.1	88.7 ± 22.2	0.21	78.7 ± 14.5	85.4 ± 17.1	0.16
iLVESV, ml/m <sup>2</sup>	44.2 ± 13.8	52.4 ± 17	0.01§	38.5 ± 9.7	45.7 ± 12.0	0.03§
Basal scar mass, g	20.3 ± 14.6	28 ± 13.1	0.01§	12.9 ± 12.5	23.1 ± 14.6	0.02§
Basal BZ mass, g	12.9 ± 9.1	17.9 ± 8.7	0.01§	9.0 ± 8.6	13.5 ± 8.2	0.08
Basal core mass, g	7.5 ± 6.6	10.1 ± 7.1	0.06	3.9 ± 4.2	9.6 ± 7.5	<0.01§

Values are mean ± SD and n (%). \*p Values for the differences between patients with normal reperfusion (n = 40) versus those showing no-reflow phenomenon (n = 16). †Arrhythmic and nonarrhythmic scars are defined as those with and without border zone (BZ) channels 4 years after ST-segment elevation myocardial infarction, respectively. ‡p Values for the differences between patients with non-arrhythmic (n = 23) versus arrhythmic scars (n = 28). §Statistically significant difference (p < 0.05).

ACE = angiotensin-converting enzyme; ARB = angiotensin II receptor blockers; CAD = coronary artery disease; Cx = circumflex artery; iLVEDV = indexed left ventricular end-diastolic volume; iLVESV = indexed left ventricular end-systolic volume; LAD = left anterior descending; LVEF = left ventricular ejection fraction; RCA = right coronary artery; TIMI = Thrombolysis In Myocardial Infarction.

**STATISTICAL ANALYSIS.** Continuous variables are mean ± SD. Categorical variables are total number and proportions. To compare the means of 2 variables, Student's *t*-test or Wilcoxon test were used, as appropriate. Proportions were compared using the chi-square test or Fisher exact test, as appropriate. Differences between repeated sets of continuous variables were evaluated with 1-way repeated measures analysis of variance and paired sample Student's *t*-tests, as appropriate. Testing for differences between repeated sets of proportions was performed using Cochran's Q test. Intraclass correlation coefficient (ICC) estimates and their 95% confident intervals (CIs) were calculated based on a mean rating (*k* = 2), absolute agreement, 2-way mixed-effects model. Receiver-operating curve analyses were used to evaluate the optimal cutoff value of scar mass at 7 days, BZ mass at 7 days, and scar mass relative reduction for predicting the presence of BZCs at 4 years. A *p* value <0.05 was considered significant. Statistical analysis was performed using IBM SPSS Statistics, version 25.0 (IBM Corp.; Armonk, New York).

## RESULTS

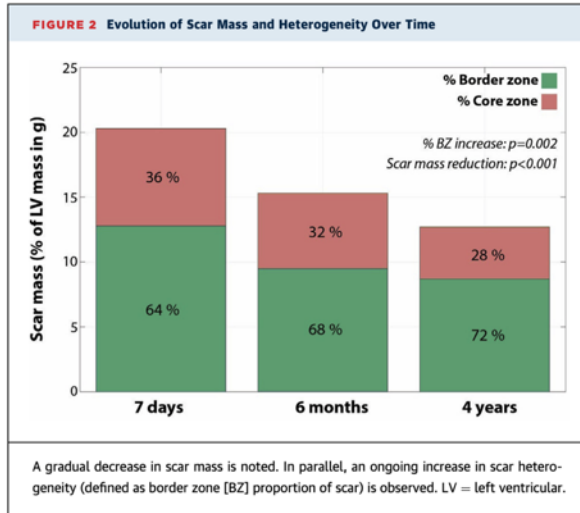
**PATIENT POPULATION.** Of 170 consecutive cases of STEMI, 100 patients met the inclusion criteria. Eight (8%) were initially excluded after the 7-day LGE-CMR because of poor image quality. Another patient (1%) had an aborted SCD with adverse neurological outcome and was also excluded. Of the 91 available patients at 6 months, 56 (61%) were included in the final analysis. The causes of long-term follow-up loss are depicted in [Figure 1](#). One patient had to be excluded due to a repeated MI occurring in the same coronary territory.

Baseline characteristics are listed and summarized in [Table 1](#). Sixteen of 56 (29%) patients showed n-RP at basal CMR imaging. Of these, 7 (13%) still showed n-RP at 6 months and 5 (9%) at 4 years. This n-RP population showed worse LVEFs in the acute phase after STEMI (42.1 ± 7.4% vs. 47.1 ± 8.9%; *p* = 0.01), a higher indexed LV end-systolic volume (52.4 ± 17% vs. 44.2 ± 13.8%; *p* = 0.01), and greater scar mass (28 ± 13.1 g vs. 20.3 ± 14.6 g; *p* = 0.01).

**LV FUNCTION AND MYOCARDIAL REMODELING.** LVEF improved after 6 months (from  $47.5 \pm 8.7\%$  to  $50.9 \pm 9.3\%$ ;  $p < 0.001$ ) and remained stable at 4 years ( $53.3 \pm 16.0\%$ ;  $p = 0.21$ ). Indexed LV end-diastolic volume slightly increased at 6 months (from  $83.5 \pm 18.2$  to  $88.0 \pm 22.2$  ml/m<sup>2</sup>;  $p = 0.05$ ) and remained stable at 4 years ( $88.3 \pm 22.9$  ml/m<sup>2</sup>;  $p = 0.92$ ). The indexed LV end-systolic volume remained stable throughout the study ( $43.9 \pm 13.7$  ml/m<sup>2</sup> at 7 days,  $44.0 \pm 18.7$  ml/m<sup>2</sup> at 6 months, and  $44.2 \pm 21.2$  ml/m<sup>2</sup> at 4 years;  $p = 0.91$ ).

**SCAR CHARACTERIZATION AND REMODELING.** At 7-day CMR, mean scar mass was  $20.3 \pm 14.6$  g, which accounted for  $15.3 \pm 9.2\%$  of the LV mass. Mean core (dense scar) mass was  $7.5 \pm 6.7$  g, BZ mass was  $12.8 \pm 9.2$  g, and scar heterogeneity, as defined previously (14) was  $65.1 \pm 12.3\%$ . The mean scar mass decreased progressively; it was  $15.3 \pm 13.3$  g at 6 months and  $12.7 \pm 11.7$  g at 4 years ( $p < 0.001$  for both comparisons), which was a mean decrease of 41%. BZ and core both decreased consistently, although this reduction was greater for the core mass ( $49 \pm 38\%$  core vs.  $33 \pm 38\%$  BZ;  $p < 0.001$ ). Consequently, the heterogeneity of the scar increased progressively ( $67.7 \pm 3.3$  at 6 months and  $71.7 \pm 12.9$  at 4 years;  $p = 0.02$ ) (Figure 2). Table 2 summarizes the evolution of ventricular and scar remodeling parameters after AMI.

**CHARACTERIZATION OF BZCs.** After excluding 16 initial uncharacterizable cases due to n-RP, a total of 61 BZCs were identified at 7 days in 30 of 40 patients (75%). In these patients without n-RP, a steadily smaller proportion of arrhythmogenic scars was observed at 6 months (27 of 40 patients; 68%) and 4 years (20 of 40 patients; 50%) ( $p = 0.001$ ). Sixteen of 18 (88.9%) patients with a 4-year scar mass  $>10$  g had identifiable BZCs in the 4-year CMR study, which represented 31.4% of the total population. In contrast, only 12 of 28 (36.4%) patients with a 4-year scar mass  $<10$  g had BZCs, which represented 23.5% of the total. The number of BZCs was reduced from a mean of 1.6 channels per patient to 1.3 at 6 months and 0.9 channel per patients at 4 years ( $p < 0.01$  in both cases). Regarding BZC distribution, 40 of 61 BZCs (65%) remained stable at 6 months, but only 26 of 61 (42%) BZCs remained stable after 4 years. Moreover, the degree of BZC transmural, defined as the number of myocardial layers in which given BZCs could be visualized, became progressively lower in the long term. BZCs could be detected at a mean of  $3.6 \pm 2.4$  layers at 7 days,  $3.8 \pm 1.8$  layers at 6 months ( $p = 0.83$ ), and  $2.7 \pm 1.8$  layers at 4 years ( $p = 0.04$ ). Figure 3 shows a typical case of scar remodeling with a decrease in BZC transmural.



In parallel, the BZC mass gradually decreased (Figure 4), with a mean BZC mass reduction of  $72 \pm 35\%$  at 4 years. The mean BZC mass per individual channel decreased from  $3.3 \pm 3.4$  g at 7 days to  $2.1 \pm 1.8$  g at 6 months ( $p = 0.02$ ) and to  $1.7 \pm 1.3$  g at 4 years ( $p = 0.12$ ). The total BZC mass  $>2.4$  g at 7 days predicted the persistence of BZCs at 4 years with a sensitivity of 94% and a specificity of 70% (area under the curve: 0.82; 95% CI: 0.65 to 0.99;  $p = 0.005$ ) (Figure 5A).

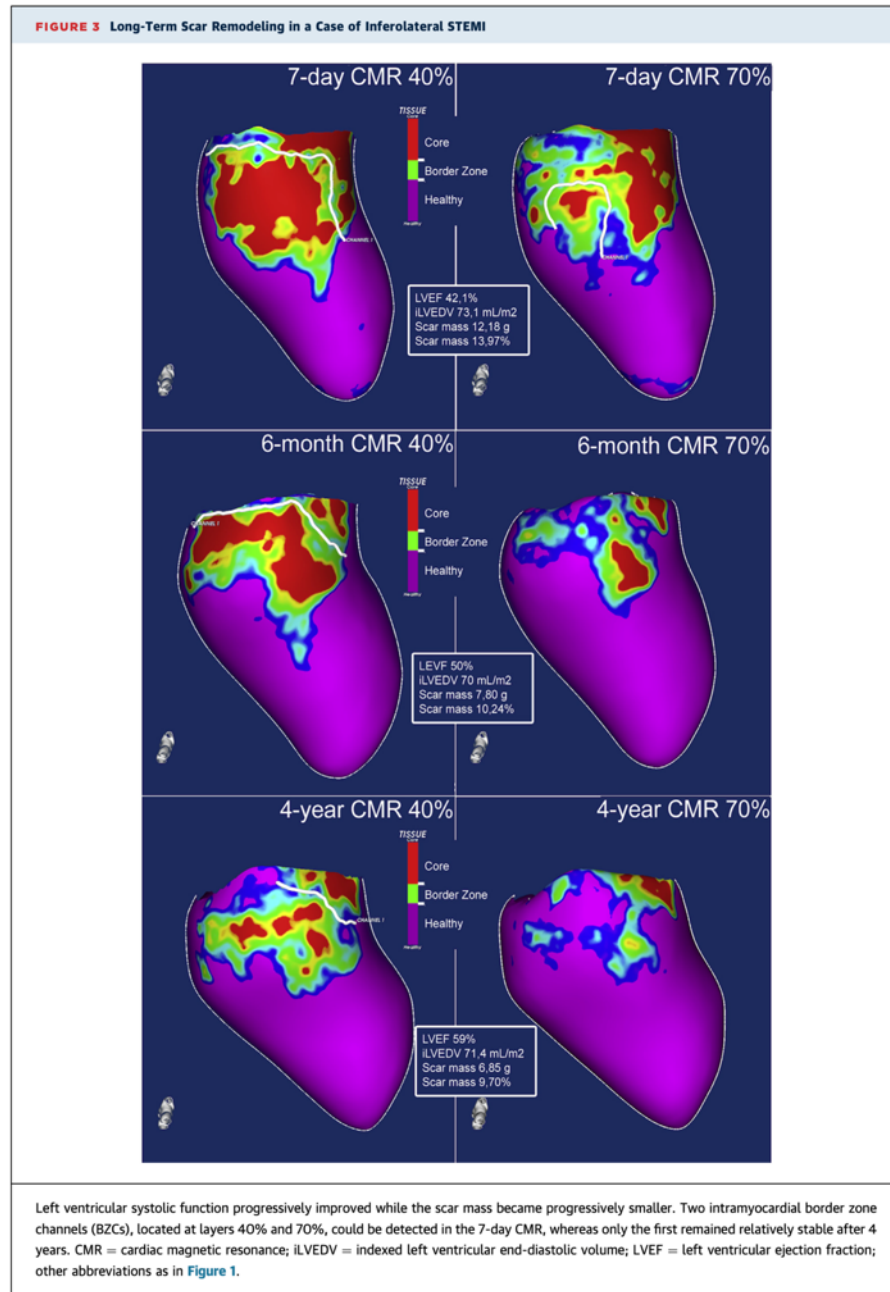
Finally, the degree of correlation and agreement for the number of identified BZCs between the 2 investigators who analyzed the LGE-CMR images was good to excellent for the 7-day study (ICC: 0.91; 95% CI: 0.79 to 0.96;  $p < 0.001$ ) and 6-month CMR study (ICC: 0.91; 95% CI: 0.85 to 0.95;  $p < 0.001$ ), and excellent for the 4-year CMR study (ICC: 0.96; 95% CI: 0.92 to 0.98;  $p < 0.001$ ).

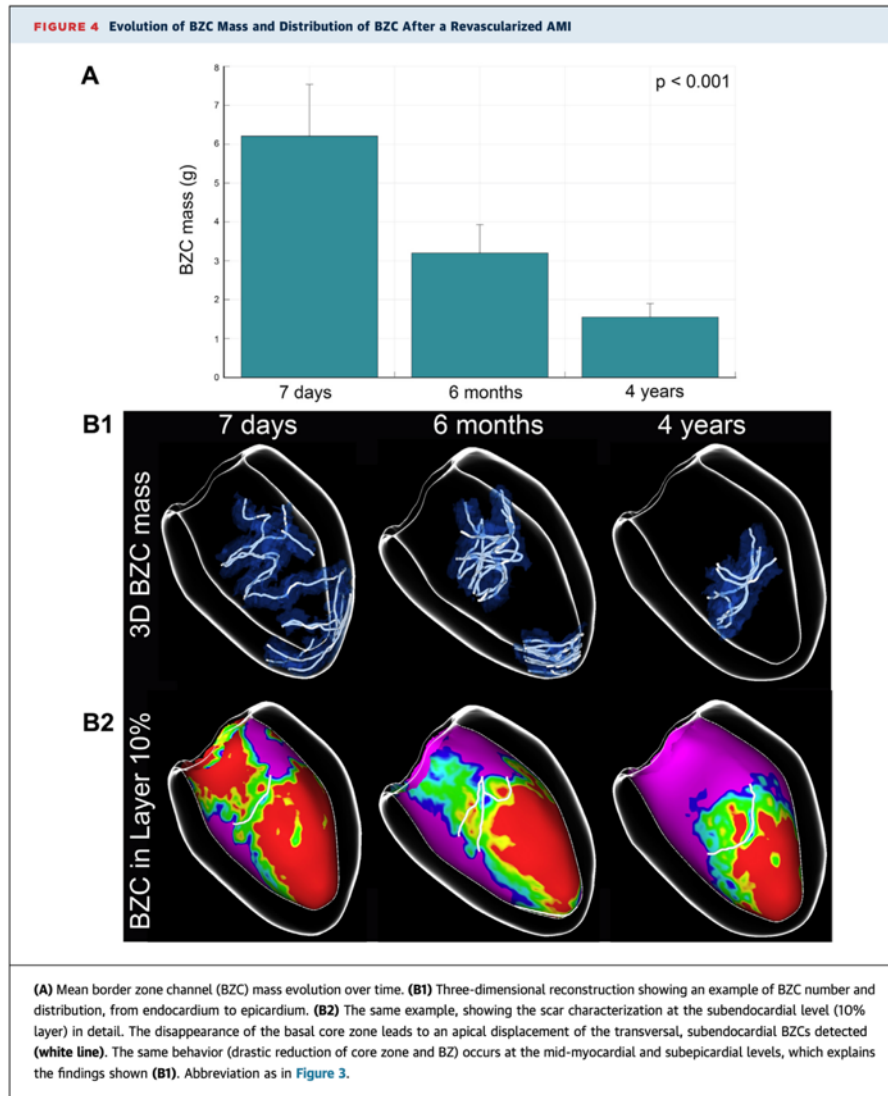
**TABLE 2 Evolution of Ventricular and Scar Remodeling Parameters After AMI**

	7 Days	6 Months	4 Years	p Value*	p Value†
ILVEDV, ml/m <sup>2</sup>	$83.5 \pm 18.2$	$88.0 \pm 22.2$	$88.3 \pm 22.9$	0.05	0.92
ILVESV, ml/m <sup>2</sup>	$43.9 \pm 13.7$	$44.0 \pm 18.7$	$44.2 \pm 21.2$	0.92	0.91
LVEF, %	$47.5 \pm 8.7$	$50.9 \pm 9.3$	$53.3 \pm 16.0$	$<0.001$	0.21
Scar mass, g	$20.3 \pm 14.6$	$15.3 \pm 13.3$	$12.7 \pm 11.7$	$<0.001$	$<0.001$
BZ mass, g	$12.8 \pm 9.2$	$9.5 \pm 7.3$	$8.7 \pm 7.7$	0.001	0.11
Core mass, g	$7.5 \pm 6.7$	$5.8 \pm 6.9$	$4.0 \pm 5.3$	$<0.001$	$<0.001$
N. of BZCs/patient	$1.5 \pm 1.3$	$1.2 \pm 1.3$	$0.8 \pm 1.0$	$<0.01$	$<0.01$
BZCs total mass, g	$6.2 \pm 7.0$	$3.2 \pm 3.9$	$1.5 \pm 1.9$	$<0.01$	0.01

Values are mean  $\pm$  SD. \*p value between 7 days and 6 months. †p Value between 6 months and 4 years.

BZCs = border zone channel; other abbreviations as in Table 1.





**CMR-BASED SCAR CHARACTERIZATION AND ARRHYTHMIA RISK ASSESSMENT.** The presence of a scar mass  $>14.5$  g predicted, with a sensitivity of 70% and a specificity of 70%, the persistence of BZCs at 4 years (area under the curve: 0.75; 95% CI: 0.61 to 0.90;  $p = 0.004$ ) (Figure 5B). Patients (18 of 51; 35%) with a 4-year scar mass  $>10$  g showed a significantly lower

relative reduction of the scar mass compared with the group (33 of 51; 65%) with a 4-year scar mass of  $<10$  g ( $26.4 \pm 27.4\%$  scar mass reduction vs.  $53.9 \pm 30.3\%$  scar mass reduction, respectively;  $p = 0.002$ ). Similarly, this reduction was greater among patients (23 of 51; 45%) without BZCs after 4 years than among those (28 of 51; 55%) with long-term persistence of BZCs ( $57.6 \pm$

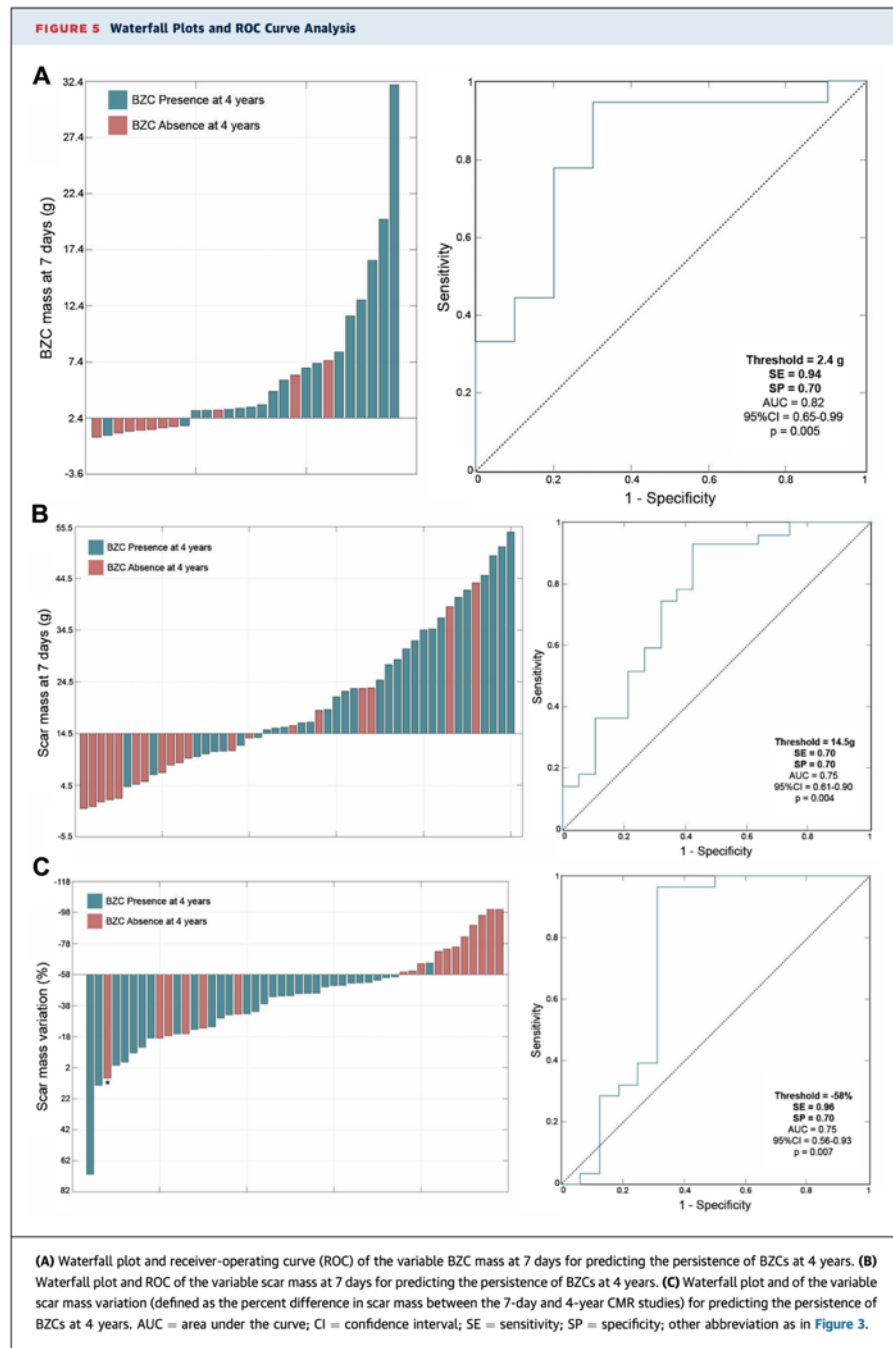


**TABLE 3** Value of 7-Day LGE-CMR for Predicting the Presence or Absence of BZCs at 4 Years

	4-Year CMR		Total
	Absence of BZCs	Presence of BZCs	
7-day CMR			
Absence of BZCs	9 TN	1 FN	10
Presence of BZCs	10 FP	20 TP	30
Total	19	21	40

Sensitivity 95.2%, specificity 47.4%, positive predictive value 66.7%, negative predictive value 90%.  
FN = false negative; FP = false positive; LGE-CMR = late gadolinium enhancement cardiac magnetic resonance; TN = true negative; TP = true positive; other abbreviation as in Table 2.

33.9% vs.  $32.2 \pm 29.0\%$ , respectively;  $p = 0.01$ ). A reduction in the scar mass of  $<58\%$  predicted, with a sensitivity of 96% and specificity of 70%, the persistence of BZCs at 4 years (area under the curve: 0.75; 95% CI: 0.56 to 0.93;  $p = 0.007$ ) (Figure 5C). As depicted in Tables 3 and 4, the usefulness of performing CMR in the acute or subacute phases after STEMI (7 days and 6 months, respectively) relied on the fact that, if the scar showed no BZCs, the negative predictive value for absence of BZCs at 4 years (i.e., non-arrhythmogenic scar) was  $>90\%$ .

**ARRHYTHMIC EVENTS AND FOLLOW-UP.** No arrhythmic events were detected in the study population after a mean follow-up of  $62.5 \pm 7.4$  months. As previously published (4), 2 patients were initially recruited but were excluded early. One patient experienced sustained VT 5 months after STEMI and received an implantable cardioverter-defibrillator; the other patient had an aborted SCD 1 week after hospital discharge and experienced an adverse neurological outcome that contraindicated continuation of the study.

Of the 56 patients finally included in the study, 2 received an implantable cardioverter-defibrillator for primary prevention after the 4-year CMR due to LVEF

**TABLE 4** Value Of 6-Month LGE-CMR for Predicting the Presence or Absence of BZCs at 4 Years

	4-Year CMR		Total
	Absence of BZCs	Presence of BZCs	
6-month CMR			
Absence of BZCs	12	1	13
Presence of BZCs	8	28	36
Total	20	29	49

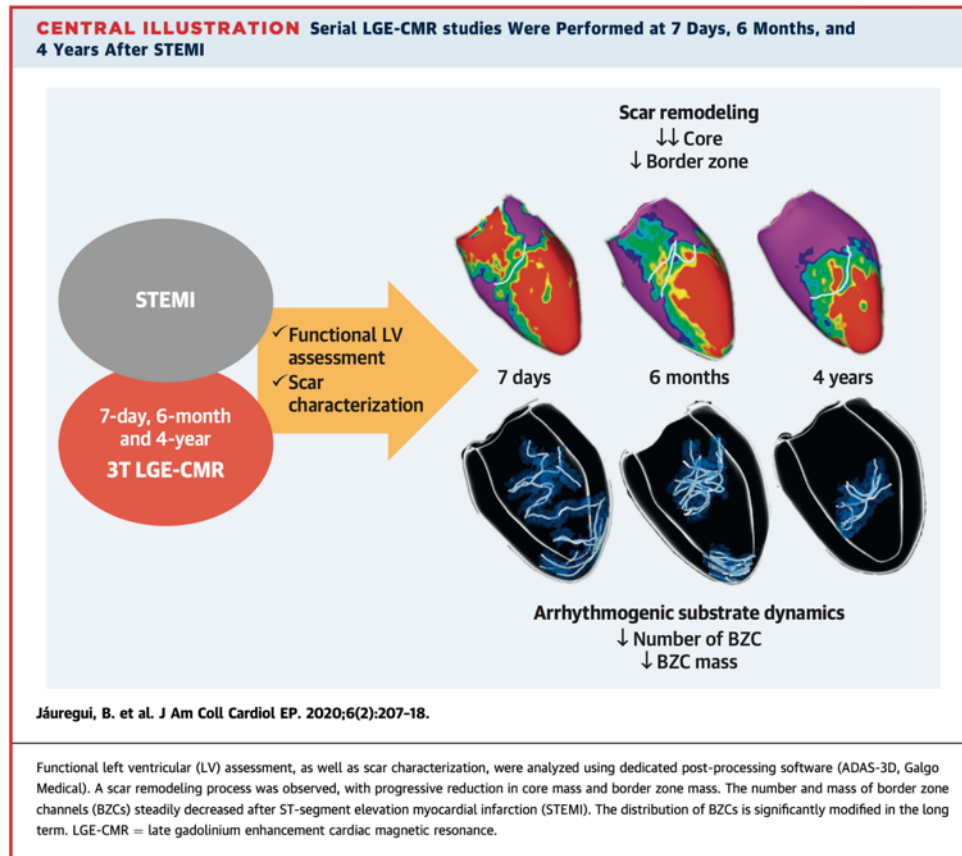
Sensitivity 96.6%, specificity 60%, positive predictive value 77.8%, negative predictive value 92.3%.  
Abbreviations as in Tables 2 and 3.

impairment ( $<30\%$ ). Both showed BZCs at 4 years (2 channels each). No heart failure–related hospitalizations were observed during this follow-up period. One patient experienced unstable angina due to severe right coronary artery stenosis (although the responsible artery for STEMI was the left anterior descending artery).

## DISCUSSION

**THE CONCEPT OF THE POST-MI SCAR REMODELING PROCESS.** This was the first clinical study to evaluate the long-term remodeling process of myocardial scar and the potential underlying arrhythmogenic substrate after STEMI. The main finding of the FOOTPRINT (Follow-Up After Myocardial Infarction to Explore the Stability of Arrhythmogenic Substrate) study was that the scar mass decreased steadily over a 4-year period after the acute coronary event, whereas an increase in scar heterogeneity was observed. (Central Illustration) Therefore, cardiac remodeling after AMI directly affected the scar tissue, and, consequently, should not be considered as exclusively affecting the remote, healthy myocardium. Scar remodeling, as part of the whole cardiac remodeling process, starts within the first 6 months, but lasts during a more chronic phase of the healing process. However, due to edema resorption, LGE-CMR might overestimate the infarct size, although only in the initial phases of scar healing (14). The hyperenhanced area on CMR increased in the first 48 h after AMI and decreased thereafter over an 8-week period, which correlated well with infarct size changes in the same period (15,16). Progressive infarct size reduction during a 3-month period after AMI was clinically observed (17), which was attributed to resolution of the edema. Conversely, previous studies (3) indicated that infarct size continued to decrease slightly, but significantly, during the first year after AMI. Consequently, long-term chronic changes observed in the FOOTPRINT study were unlikely due to edema resorption, were in line with previous investigations, and supported the existence of a continuous and constant scar remodeling process that lasts for years.

**DYNAMICS OF POST-MI SCAR STRUCTURE AND POTENTIAL IMPLICATIONS.** The second innovative finding of the FOOTPRINT study was that the number, degree of transmural, and mass of BZCs (i.e., parameters that can be derived from CMR post-processing) were consistently diminished over a 4-year period after an acute coronary event (Central Illustration). Hence, most of the acutely identified scar mass and corresponding BZCs might not reveal



the real, long-term potential arrhythmogenic substrate. This steady transformation, which affected not only the global scar size but also the number, distribution, and mass of BZCs, might reflect an active, long-term uninterrupted process of biological healing at the injured myocardial area, which could play an important pathophysiological role in arrhythmogenesis. In this regard, analysis of the distribution of BZ tissue could improve arrhythmic event prediction based on CMR information, because this distribution creates BZCs that are the surrogate for conducting channels in electroanatomic maps, act as VT isthmuses when they become active, and constitute substrate ablation targets during interventional procedures (11,12,18,19). In the GAUDI-CRT study (18), the presence of a scar mass <10 g and the absence of BZCs had a 100% negative predictive value for

implantable cardioverter-defibrillator therapies or SCD among candidates for cardiac resynchronization therapy. Sixteen patients in the FOOTPRINT study (31% of the total) had a scar mass of >10 g and identifiable BZCs in the 4-year CMR study, as well as a significantly lower relative reduction of the scar size over time. The clinical relevance of these findings is still to be revealed. In contrast, it should be noted that BZCs in smaller scars might be different in nature or morphologically and could be more difficult to detect using CMR criteria derived from larger scars. Nevertheless, scars of <10 g are unlikely to be arrhythmogenic, in accordance with the previously mentioned results of the GAUDI-CRT study.

**EARLY POST-MI CMR USEFULNESS FOR RISK STRATIFICATION.** Finally, the present study described potential clinical uses for the performance

of CMR studies at different timepoints after AMI: an acute (7-day) detection of a critical BZC mass  $>2.4$  g or a total scar mass  $>14.5$  g were both related to the persistence of BZCs in the long term. In contrast, the lack of BZCs in the 7-day or 6-month CMR scan showed a high negative predictive value ( $>90\%$  in both cases) for the absence of an arrhythmogenic substrate after 4 years. Despite the difficulty in determining the best time to depict scar substrate and establish the risk of developing re-entrant VA after AMI, the potential uses of acute (i.e., first week) or subacute (i.e., after 6 months) CMR studies should be taken into consideration. More research would be required, such as clinical studies with longer follow-up, use of computed deep learning to establish virtual models of scar remodeling, or translational studies using animal models, which are necessary to fully understand the long-term biological processes taking part within the scarred myocardium.

**CLINICAL IMPLICATIONS.** Despite only representing a subset of patients with a favorable medical course after STEMI, the FOOTPRINT study referred to the modern scenario of early successful percutaneous revascularization of STEMI. This population was not considered at high risk for SCD, despite the fact that most cases (in absolute numbers) of SCD after AMI occurred in patients with this profile (LVEF  $>35\%$ ) (20). Their estimated annual incidence of SCD was approximately 0.6% in a recent cohort (21). In the PRESERVE EF (Post Myocardial Infarction Risk Stratification for Sudden Cardiac Death in Patients With Preserved Ejection Fraction) study (22), 9 of 575 post-MI patients with a mean LVEF of 50.8% and no standard indication for a secondary prevention implantable cardioverter-defibrillator had appropriate implantable cardioverter-defibrillator therapies after a mean follow-up of 32 months. The absence of arrhythmic events in the FOOTPRINT population during the follow-up period might reflect the relatively low cumulative incidence of SCD after AMI in the first 5 years (9), which should even be lower in a modern, early revascularized population. However, the absence of arrhythmia events might not only be related to the FOOTPRINT population clinical characteristics (see Table 1). Progressive reduction of scar mass, number, and mass of BZCs over time was translated into a gradually smaller proportion of patients theoretically at risk for VA (from an initial 73% to 55% at 4 years) in agreement with the clinical observation that only a small proportion of patients

developed VA, usually many years after the acute coronary event. In this regard, previous studies (23) showed a mean period from MI until first documented VT as long as  $16 \pm 8$  years. From the present observations, it could be hypothesized that the scar remodeling process might require years until it becomes clinically arrhythmogenic. Longer follow-up would be required to detect arrhythmic events and to characterize the substrate characteristics that lead to scar arrhythmogenicity, at the moment when the arrhythmia occurs.

**STUDY LIMITATIONS.** The patient sample was relatively small, although large enough to observe that long-term duration of the myocardial scar remodeling process after an AMI seems to be the rule in all patients with STEMI included in the FOOTPRINT study. Further studies with larger samples and longer follow-up are needed to clarify the relationship between the presence of BZCs and long-term arrhythmic events. The FOOTPRINT study could only give insight into the myocardial and scar remodeling processes of a selected population with uncomplicated STEMI and relatively preserved LVEFs. There was still some clinical uncertainty due to the absence of VA events during follow-up. In addition, it was possible that arrhythmogenic scars might have different remodeling patterns over time. Regarding CMR studies, T2 sequences for edema, as well as T1 mapping to detect interstitial fibrosis in the remote myocardium, were not available.

## CONCLUSIONS

CMR data post-processing permits a dynamic assessment of quantitative and qualitative post-AMI scar characteristics. The infarcted myocardium undergoes a long-lasting remodeling process characterized by a steady decrease in scar mass and a progressive increase in scar heterogeneity. The number and distribution of BZCs, which constitute the histological substrate for arrhythmogenesis, appear notably changed over a 4-year period and can be reliably assessed with serial CMR. Further studies will be required to understand how, when, and in whom the healing process of the scar leads to a critical substrate capable of generating clinical VA.

**ADDRESS FOR CORRESPONDENCE:** Dr. Antonio Berruezo, Heart Institute, Teknon Medical Center, C/ Vilana, 12, 08022 Barcelona, Spain. E-mail: [antonio.berruezo@quironsalud.es](mailto:antonio.berruezo@quironsalud.es).



## PERSPECTIVES

**COMPETENCY IN MEDICAL KNOWLEDGE:** After AMI, scar size and its components (core zone and BZ) experience a continuous remodeling process that lasts in the long-term and can be reliably assessed with serial CMR. This scar remodeling process is accompanied by measurable anatomic changes within the potential, subjacent arrhythmogenic substrate. Further studies will be required to understand how, when, and who had the healing process of the scar leads to a critical substrate capable of generating clinical VAs. In this regard, serial LGE-CMR could be an optimal tool to understand the pathophysiology of long-term arrhythmogenesis after an acute coronary event.

**TRANSLATIONAL OUTLOOK:** Further clinical studies with longer follow-up, the use of computed deep learning to establish virtual models of scar remodeling, or translational studies using animal models to assess histopathological changes would be required to finally understand the biological processes taking part in the scarred myocardium years after an acute coronary event. The role of certain biomarkers to assess local inflammation, cell signaling, or extracellular matrix turnover may also be of relevance in this setting.

## REFERENCES

- Westman PC, Lipinski MJ, Luger D, et al. Inflammation as a driver of adverse left ventricular remodeling after acute myocardial infarction. *J Am Coll Cardiol* 2016;67:2050-60.
- Frangogiannis NG. Pathophysiology of myocardial infarction. *Compr Physiol* 2015;5:1841-75.
- Pokorney SD, Rodriguez JF, Ortiz JT, Lee DC, Bonow RO, Wu E. Infarct healing is a dynamic process following acute myocardial infarction. *J Cardiovasc Magn Reson* 2012;14:62.
- Penela D, Acosta J, Andreu D, et al. Identification of the potentially arrhythmogenic substrate in the acute phase of ST-segment elevation myocardial infarction. *Heart Rhythm* 2017;14:592-8.
- Klem I, Weinsaft JW, Bahnon TD, et al. Assessment of myocardial scarring improves risk stratification in patients evaluated for cardiac defibrillator implantation. *J Am Coll Cardiol* 2012;60:408-20.
- Izquierdo M, Ruiz-Granell R, Bonanad C, et al. Value of early cardiovascular magnetic resonance for the prediction of adverse arrhythmic cardiac events after a first noncomplicated ST-segment-elevation myocardial infarction. *Circ Cardiovasc Imaging* 2013;6:755-61.
- Fernández-Armenta J, Berrueto A, Mont L, et al. Use of myocardial scar characterization to predict ventricular arrhythmia in cardiac resynchronization therapy. *Europace* 2012;14:1578-86.
- Solomon SD, Zelenkofske S, McMurray JJ, et al., Valsartan in Acute Myocardial Infarction Trial (VALIANT) Investigators. Sudden death in patients with myocardial infarction and left ventricular dysfunction, heart failure, or both. *N Engl J Med* 2005;352:2581-8.
- Berger CJ, Murabito JM, Evans JC, Anderson KM, Levy D. Prognosis after first myocardial infarction: comparison of Q-wave and non-Q-wave myocardial infarction in the Framingham Heart Study. *JAMA* 1992;268:1545-51.
- Kannel WB, Sorlie P, McNamara PM. Prognosis after initial myocardial infarction: the Framingham study. *Am J Cardiol* 1979;44:53-9.
- Piers SR, Tao Q, de Riva Silva M, et al. CMR-based identification of critical isthmus sites of ischemic and nonischemic ventricular tachycardia. *J Am Coll Cardiol* 2014;7:774-84.
- Fernández-Armenta J, Berrueto A, Andreu D, et al. Three-dimensional architecture of scar and conducting channels based on high resolution CE-CMR: insights for ventricular tachycardia ablation. *Circ Arrhythm Electrophysiol* 2013;6:528-37.
- Andreu D, Ortiz-Pérez JT, Fernández-Armenta J, et al. 3D delayed-enhanced magnetic resonance sequences improve conducting channel delineation prior to ventricular tachycardia ablation. *Europace* 2015;17:938-45.
- Dall'Armellina E, Karia N, Lindsay AC, et al. Dynamic changes of edema and late gadolinium enhancement after acute myocardial infarction and their relationship to functional recovery and salvage index. *Circ Cardiovasc Imaging* 2011;4:228-36.
- Rochitte CE, Lima JA, Bluemke DA, et al. Magnitude and time course of microvascular obstruction and tissue injury after acute myocardial infarction. *Circulation* 1998;98:1006-14.
- Fieno DS, Hillenbrand HB, Rehwald WG, et al. Infarct resorption, compensatory hypertrophy, and differing patterns of ventricular remodeling following myocardial infarctions of varying size. *J Am Coll Cardiol* 2004;43:2124-31.
- Hillenbrand HB, Sandstede J, Störk S, et al. Remodeling of the infarct territory in the time course of infarct healing in humans. *Magn Reson Mater Phys* 2011;24:277-84.
- Acosta J, Fernández-Armenta J, Borràs R, et al. Scar characterization to predict life-threatening arrhythmic events and sudden cardiac death in patients with cardiac resynchronization therapy: the GAUDI-CRT study. *J Am Coll Cardiol* 2018;11:561-72.
- Soto-Iglesias D, Acosta J, Penela D, et al. Image-based criteria to identify the presence of epicardial arrhythmogenic substrate in patients with transmural myocardial infarction. *Heart Rhythm* 2018;15:814-21.
- Dagres N, Hindricks G. Risk stratification after myocardial infarction: is left ventricular ejection fraction enough to prevent sudden cardiac death? *Eur Heart J* 2014;34:1964-71.
- Ikedo T, Yoshino H, Sugi K, et al. Predictive value of microvolt T-wave alternans for sudden cardiac death in patients with preserved cardiac function after acute myocardial infarction. results of a collaborative cohort study. *J Am Coll Cardiol* 2006;48:2268-74.
- Gatzoulis KA, Tsiachris D, Arsenos P, et al. Arrhythmic risk stratification in post-myocardial infarction patients with preserved ejection fraction: the PRESERVE EF study. *Eur Heart J* 2019;40:2940-9.
- Acosta J, Fernández-Armenta J, Penela D, et al. Infarct transmural as a criterion for first-line endo-epicardial substrate-guided ventricular tachycardia ablation in ischemic cardiomyopathy. *Heart Rhythm* 2016;13:85-95.

**KEY WORDS** arrhythmogenic substrate, border zone channels, cardiac magnetic resonance, myocardial infarction, ventricular arrhythmias

**APPENDIX** For an expanded Methods section and a supplemental figure, please see the online version of this paper.

## **INTRODUCTION**

Many clinical and experimental studies have been conducted in the field of myocardial remodeling after an acute myocardial infarction (AMI). However, this term usually refers exclusively to the maladaptive changes affecting the remote myocardium and causing progressive heart failure, which, on the other hand, appear not to be completely dependent from initial MI size. (1) Regarding the infarcted myocardium, the histopathophysiology of scar healing has been well described, (2) and can be assessed by means of noninvasive cardiac imaging techniques, such as late gadolinium enhancement cardiac magnetic resonance (LGE-CMR). However, little is known about the time course needed for its completion in human population. (3)

Deeper characterization of the scar size and its components (border zone and core zone) can be performed in the acute phase of STEMI using LGE-CMR (4), and can help stratifying the risk of future arrhythmic events. (5-7) Ventricular arrhythmias (VA) are cause for a high, continuous global sudden cardiac death (SCD) incidence among ischemic population, regardless of LVEF. (8-10) Border zone tissue corridors (BZC) within the scar, identified with LGE-CMR, act as ventricular tachycardia (VT) isthmuses (11), correlating well with slow conducting channels recognized in electroanatomic maps during VT substrate ablation procedures, (12) and thus constitute the arrhythmogenic substrate of the scar.

In the present study, we sought to characterize the long-term remodeling process of post-AMI scar and its components using LGE-CMR, as well as describing the potential changes of the subjacent arrhythmogenic substrate.

## **METHODS**

### **Patient sample**

We report the results of a predefined endpoint of a prospective observational study. (4) Consecutive patients admitted to our institution with a first STEMI, in whom percutaneous revascularization was performed within the first 12 hours from onset of symptoms, were included from September 2012 to June 2014. Patients who met one or more of the following criteria were excluded: STEMI >12 hours from symptom onset; history of prior MI; history of prior structural heart disease; age <18 years; life expectancy <1 year due to noncardiac pathology; classic contraindication for CMR; or clinical contraindication to perform the study within the first week (i.e., persistent Killip III-IV, persistent hemodynamic instability, invasive ventilation, or intra-aortic balloon pump/left ventricular assist device). Patients who were transferred to another institution within 7 days after admission were also excluded. In all patients, LGE-CMR was performed at  $7 \pm 2$  days, 6 months and 4 years post-STEMI. The study complied with the Declaration of Helsinki, and the local ethics committee approved the study protocol. All participants included in the study (Figure 1) provided informed written consent.

### **LGE-CMR processing**

LGE-CMR tests were performed using a 3-Tesla scanner (MAGNETOM Trio, Siemens Healthcare, Erlangen, Germany). Image acquisition is summarized in the Supplementary Material. All LGE-CMR images were analyzed using a previously described technique. (13) Full LV volume was reconstructed in the axial orientation, and the resulting images were processed with ADAS-3D™ software (Galgo Medical, Barcelona, Spain). Ten concentric

surface layers (from 10% to 90%) were created automatically from endocardium to epicardium of the LV wall thickness. A 3D shell was obtained for each layer. Pixel signal intensity maps based on LGE-CMR images were projected to each shell, following a trilinear interpolation algorithm, and color-coded. To identify the scar areas, a pixel signal intensity-based algorithm was applied to characterize the hyperenhanced area as core zone, BZ or healthy tissue using  $40\% \pm 5\%$  and  $60\% \pm 5\%$  of the maximum intensity as thresholds (Supplementary Figure 1).

### **Myocardial scar characterization**

Two independent expert investigators analyzed the LGE-CMR images, and a third observer was available in case of discrepancy. The scar mass and areas in each shell (total scar, BZ, and core) were automatically measured using ADAS-3D™ software. Scar heterogeneity was defined as BZ percentage of scar. (7) The BZC were defined as continuous corridors of BZ surrounded by scar core or an anatomical barrier (mitral annulus) that connects two areas of healthy tissue. (12) If a given channel was identified at the same segment and with the same orientation in adjacent layers, it was considered as a single multilayer channel. The BZC mass was automatically computed using a full-automated tool embedded within the ADAS-3D™ software.

Because tissue characterization is based on a pixel signal intensity algorithm, healthy myocardium cannot be distinguished from areas with “no-reflow” phenomenon (n-RP). This is an occurrence driven by the presence of microvascular obstruction, which is the potential result of different physiopathological events, such as direct endothelial necrosis, reperfusion injury of microvessels, and/or distal atherothrombotic embolization. This

obstruction provokes a persistent hypoenhancement on LGE-CMR images which, in turn, prevents a proper tissue characterization of infarcted areas. Therefore, the n-RP was considered in all cases where any hypointense area within the scar was detected on LGE-CMR images. Consequently, in patients with n-RP no attempt was made to differentiate core and BZ areas inside the scar or to identify BZC. In these patients, only information regarding LV dimensions/function and total scar mass (including n-RP regions inside the total scar mass) were collected.

Scar location, mass, and area as well as the presence of BZC were compared in the LGE-CMR images at 7 days, 6 months and 4 years. A given BZC was considered to be stable among studies if it was located in the same myocardial layer and myocardial segment as per the American Heart Association (AHA) 17-segment model, with the same orientation and morphology.

### **Statistical analysis**

Continuous variables are given as mean  $\pm$  SD. Categorical variables are given as total number and percentages. To compare the means of 2 variables, the Student t-test or Wilcoxon test were used, as appropriate. Proportions were compared using the  $\chi^2$  or Fisher exact test, as appropriate. Friedman analysis of variance by ranks was used for repeated measurements. Testing for differences between repeated sets of proportions was performed using the Cochran's Q test.  $P < 0.05$  was considered significant. Statistical analysis was performed using IBM SPSS Statistics, version 25.0 (IBM Corp. Released 2017; Armonk, NY: IBM Corp.).

## RESULTS

### Patient population

Out of 170 consecutive cases of STEMI, 100 patients met the inclusion criteria. Eight (8%) were initially excluded after the 7-day LGE-CMR because of poor image quality. Another patient (1%) had an aborted SCD with adverse neurologic outcome and was also excluded. From the 91 available patients at 6 months, 56 (61%) were included for the final analysis. The causes of long-term follow-up loss are depicted in Figure 1. One patient had to be excluded due to a repeated MI occurring at the same coronary territory.

Baseline characteristics are listed and summarized in Table 1. Sixteen patients out of 56 (29%) showed no-reflow phenomenon at basal CMR imaging. From them, 7 (13%) still showed n-RP at 6 months, and 5 (9%) at 4 years. These n-RP population showed worse LVEF in the acute phase after STEMI ( $42.1 \pm 7.4\%$  vs.  $47.1 \pm 8.9\%$ ;  $p < 0.01$ ), a higher indexed left-ventricular end-systolic volume (iLVESV) ( $52.4 \pm 17\%$  vs.  $44.2 \pm 13.8\%$ ;  $p < 0.01$ ), and greater scar mass ( $28 \pm 13.1$  g vs.  $20.3 \pm 14.6$  g;  $p < 0.01$ ).

### Left ventricular function and myocardial remodeling

LVEF improved after 6 months (from  $47.5 \pm 8.7$  to  $50.9 \pm 9.3\%$ ,  $p < 0.001$ ), remaining stable at 4 years ( $53.3 \pm 16.0\%$ ,  $p = 0.21$ ). Indexed LV end-diastolic volume (iLVEDV) slightly increased at 6 months (from  $83.5 \pm 18.2$  to  $88.0 \pm 22.2$  mL/m<sup>2</sup>,  $p = 0.05$ ), remaining stable at 4 years ( $88.3 \pm 22.9$  mL/m<sup>2</sup>,  $p = 0.92$ ). The indexed LV end-systolic volume (iLVESV) remained stable throughout the study ( $43.9 \pm 13.7$  mL/m<sup>2</sup> at 7 days,  $44.0 \pm 18.7$  mL/m<sup>2</sup> at 6 months, and  $44.2 \pm 21.2$  mL/m<sup>2</sup> at 4 years;  $p = 0.91$ ).

### **Scar characterization and remodeling**

At 7-day CMR, mean scar mass was  $20.3 \pm 14.6$  g, accounting for  $15.3 \pm 9.2\%$  of LV mass. Mean core (dense scar) mass was  $7.5 \pm 6.7$  g, BZ mass was  $12.8 \pm 9.2$  g, and scar heterogeneity, as defined previously,<sup>25</sup> was  $65.1 \pm 12.3\%$ . The mean scar mass decreased progressively, being  $15.3 \pm 13.3$  g at 6 months and  $12.7 \pm 11.7$  g at 4 years ( $p < 0.001$  for both comparisons), showing a mean decrease of 41%. BZ and core both decreased consistently, although this reduction was greater for the core mass ( $49 \pm 38\%$  core vs.  $33 \pm 38\%$  BZ,  $p < 0.001$ ). Consequently, the heterogeneity of the scar increased progressively ( $67.7 \pm 3.3$  at 6 months, and  $71.7 \pm 12.9$  at 4 years;  $p 0.02$ ) (Figure 2). Table 2 summarizes the evolution of ventricular and scar remodeling parameters after AMI.

### **Characterization of border zone channels**

After excluding 16 uncharacterizable cases due to n-RP, in 30/40 patients (73%), a total of 61 BZC could be identified at 7 days, with a steadily smaller proportion of arrhythmogenic scars observed at 6 months (27/40; 68%) and 4 years (20/40; 50%) ( $p 0.001$ ). The number of BZC was reduced from a mean of 1.6 channels per patient to 1.3 at 6 months and 0.9 at 4 years ( $p < 0.01$  in both cases). Regarding BZC distribution, 40/61 BZC (65%) remained stable at 6 months, but only 26/61 (42%) after 4 years. Moreover, the degree of BZC transmural, defined as the number of myocardial layers in which a given BZC can be visualized, became progressively lower at the long-term; BZC could be detected in a mean of  $3.6 \pm 2.4$  layers at 7 days,  $3.8 \pm 1.8$  at 6 months ( $p = 0.83$ ) and  $2.7 \pm 1.8$  at 4 years ( $p = 0.04$ ). Figure 3 shows a typical case of scar remodeling with decrease of BZC transmural.

In parallel, the BZC mass gradually decreased as shown in Figure 4, with a mean BZC mass reduction of  $72 \pm 35\%$  at 4 years. The mean BZC mass per individual channel decreased from  $3.3 \pm 3.4$  g at 7 days to  $2.1 \pm 1.8$  g at 6 months ( $p$  0.02) and  $1.7 \pm 1.3$  g at 4 years ( $p$  0.12). A total BZC mass  $>2.4$  g at 7 days predicted with sensitivity 94% and specificity 70% the persistence of BZC at 4 years (AUC 0.82; 95% CI 0.65-0.99;  $p$  0.005) (Figure 5A).

### **CMR-based scar characterization and arrhythmia risk assessment**

The presence of a scar mass  $> 14.5$  g predicted, with sensitivity 70% and specificity 70% the persistence of BZC at 4 years (AUC 0.75; 95% CI 0.61-0.90;  $p$  0.004) (Figure 5B). Moreover, it was found that the scar mass reduction over time was greater among patients ( $n = 16$ ) with absence of BZC after 4 years (median  $-69\%$ ) than among those ( $n = 28$ ) with long-term persistence of BZC (median  $-44\%$ ) ( $U = 114$ ;  $p$  0.007). In fact, a reduction in the scar mass  $<58\%$  predicted with sensitivity 96% and specificity 70% the persistence of BZC at 4 years (AUC 0.75; 95% CI 0.56-0.93;  $p$  0.007) (Figure 5C). As depicted in Tables 3 and 4, the usefulness of performing CMR in the acute or subacute phases after STEMI (7 days and 6 months, respectively) relies on the fact that, in case the scar shows no BZC, the negative predictive value for absence of BZC at 4 years (i.e. 'non-arrhythmogenic scar') is  $>90\%$ .

### **Arrhythmic events and follow-up**

No arrhythmic events were detected in the study population after a mean follow-up of  $62.5 \pm 7.4$  months. As previously published, (4) two patients were initially recruited but early excluded: One suffered sustained ventricular tachycardia five months after STEMI and was implanted with an ICD; the other one had an aborted SCD one week after hospital



discharge, suffering adverse neurological outcome that contraindicated continuation of the study.

From the 56 patients finally included, two received an ICD on primary prevention after the 4-year CMR due to impairment of LVEF (<30%). Both showed BZC at 4 years (2 channels each). No heart failure-related hospitalizations were observed during this follow-up period. One patient suffered from unstable angina due to severe right coronary artery stenosis (whereas the responsible artery for STEMI had been the left anterior descendent).

## **DISCUSSION**

This is the first clinical study evaluating the remodeling process of myocardial scar and the potential underlying arrhythmogenic substrate, long-term after STEMI. The main finding of the FOOTPRINT study is that the scar mass decreases steadily over a 4-year period after the acute coronary event, while an increase in scar heterogeneity is observed. Therefore, 'cardiac remodeling' after AMI does directly affect the scar tissue and, consequently, it should not be considered as exclusively affecting the remote, healthy myocardium. Scar remodeling, as part of the whole cardiac remodeling process, starts within the first 6 months, but lasts during a more chronic phase of the healing process. Nevertheless, it should be pointed out that, due to edema resorption, LGE may overestimate the infarct size, however only in the initial phases of scar healing. (14) The hyperenhanced area on CMR increases in the first 48 hours after AMI and decreases thereafter over an 8-week period, correlating well with infarct size changes in the same period. (15,16) Progressive infarct size reduction during a 3-month period after AMI has been clinically observed (17), attributed

to resolution of edema. Conversely, previous studies (18) have already indicated that infarct size continues to decrease slightly but significantly during the first year after AMI. Consequently, long-term chronic changes observed in the FOOTPRINT study are unlikely due to edema resorption, go in line with previous investigations, and support the existence of a continuous and constant scar remodeling process lasting for years.

The second, innovative finding of the FOOTPRINT study is that the number, degree of transmural, and mass of BZC, parameters that can be derived from CMR post-processing, are consistently diminished over a 4-year period after an acute coronary event. Hence, most of the acutely identified scar mass and corresponding BZC may not reveal the real, long-term potential arrhythmogenic substrate. This steady transformation, affecting not only the global scar size but also the number, distribution and mass of BZC, may be reflecting an active, long-term uninterrupted process of biological healing process at the injured myocardial area, which could play an important physiopathological role in arrhythmogenesis. In this regard, it must be remarked that analysis of the distribution of BZ tissue can improve arrhythmic event prediction based on CMR information, as this distribution creates BZC which are the surrogate for conducting channels in the electroanatomic maps, act as VT isthmuses when they become active, and constitute substrate ablation targets during interventional procedures. (11,12,19,20)

Finally, the present study describes potential clinical uses of performing CMR studies at different timepoints after AMI: An acute (7-day) detection of a critical BZC mass >2.4 g or a total scar mass >14.5 g are both related to the persistence of BZC in the long-term. On the contrary, the lack of BZC in the 6-month CMR showed a high negative predictive value (92.3%) for the absence of arrhythmogenic substrate after 4 years. Despite the difficulty of

elucidating when it is the best time to depict scar substrate and establish the risk for the development of reentrant VA after AMI, the potential uses of acute (i.e., first week) or subacute (i.e., after 6 months) CMR studies should be taken into consideration and would require further investigations, such as clinical studies with longer follow-up, the use of computed deep learning to establish virtual models of scar remodeling, or translational studies using animal models, which would be likely required to finally understand the biological, chronic processes taking part within the scarred myocardium.

Despite only representing a subset of patients with favorable medical course after STEMI, the FOOTPRINT study refers to the modern scenario of early, successful percutaneous revascularization of STEMI. Besides, this population is not considered as of high risk for SCD, despite most cases (in absolute numbers) of SCD after AMI occur in patients with its profile (LVEF>35%), (21) the commonest clinical profile in ischemic heart disease. The absence of arrhythmic events in the FOOTPRINT population during the follow-up period may reflect the relatively low cumulative incidence of SCD after AMI in the first 5 years, (22) which should be even lower in a modern, early revascularized population. However, it should be noted that the absence of arrhythmia events may not be only related to the FOOTPRINT population clinical characteristics (see Table 1). Progressive reduction of scar mass, number and mass of BZC over time is translated into a gradually smaller proportion of patients theoretically at risk for VA (from an initial 73% to 50% at 4 years), which is in agreement with the clinical observation that only a small proportion of patients develop VA, usually many years after the acute coronary event. In this regard, previous studies (23) have shown a mean period from MI until first documented VT being as long as of 16 ± 8 years. From the present observations, it can be hypothesized that the scar remodeling process may require years

until it becomes clinically arrhythmogenic. Longer follow-up would be required to detect arrhythmic events and characterize the substrate characteristics leading to scar arrhythmogenicity, just at the moment when the arrhythmia occurs.

### **Study limitations**

The patient sample is relatively small, although enough to make the observation that the myocardial scar remodeling process, occurring during long-term after an AMI, seems to be the rule in all the STEMI patients included in the FOOTPRINT study. Further studies with larger samples and longer follow-up are needed to clarify the relationship between the presence of BZC and long-term arrhythmic events. The FOOTPRINT study can only give insight into myocardial and scar remodeling processes of a selected population with uncomplicated STEMI and a relatively preserved LVEF.

Related to CMR studies, T2 sequences for edema as well as T1 mapping to detect interstitial fibrosis in the remote myocardium were not available.

### **Conclusions**

CMR data post-processing allows to perform a dynamic assessment of quantitative and qualitative post-AMI scar characteristics. The infarcted myocardium undergoes a long-lasting remodeling process characterized by a steady decrease of scar mass, and a progressive increase in scar heterogeneity. The number and distribution of BZC, which constitute the histological substrate for arrhythmogenesis, appear notably changed over a 4-year period and can be reliably assessed with serial CMR. Further studies will be required

to understand how, when, and in whom the healing process of the scar leads to a critical substrate capable of generating clinical VA.

**REFERENCES**

1. Westman PC, Lipinski MJ, Luger D, et al. Inflammation as a Driver of Adverse Left Ventricular Remodeling After Acute Myocardial Infarction. *JACC* 2016;67:2050-2060.
2. Frangogiannis NG. Pathophysiology of myocardial infarction. *Compr Physiol* 2015;5(4):1841-1875.
3. Pokorney SD, Rodriguez JF, Ortiz JT, Lee DC, Bonow RO, Wu E. Infarct healing is a dynamic process following acute myocardial infarction. *J Cardiovasc Magn Reson* 2012;2;14:62.
4. Penela D, Acosta J, Andreu D, et al. Identification of the potentially arrhythmogenic substrate in the acute phase of ST-segment elevation myocardial infarction. *Heart Rhythm* 2017;14:592-598.
5. Klem I, Weinsaft JW, Bahnson TD, et al. Assessment of myocardial scarring improves risk stratification in patients evaluated for cardiac defibrillator implantation. *J Am Coll Cardiol* 2012;60:408-420.
6. Izquierdo M, Ruiz-Granell R, Bonanad C, et al. Value of early cardiovascular magnetic resonance for the prediction of adverse arrhythmic cardiac events after a first noncomplicated ST-segment-elevation myocardial infarction. *Circ Cardiovasc Imaging* 2013;6:755-761.
7. Fernández-Armenta J, Berruezo A, Mont L, et al. Use of myocardial scar characterization to predict ventricular arrhythmia in cardiac resynchronization therapy. *Europace* 2012;14:1578-1586.

8. Solomon SD, Zelenkofske S, McMurray JJ, et al. Valsartan in Acute Myocardial Infarction Trial (VALIANT) Investigators. Sudden death in patients with myocardial infarction and left ventricular dysfunction, heart failure, or both. *N Engl J Med* 2005;352:2581-2588.
9. Berger CJ, Murabito JM, Evans JC, Anderson KM, Levy D. Prognosis after first myocardial infarction: comparison of Q-wave and non-Q-wave myocardial infarction in the Framingham Heart Study. *JAMA* 1992;268:1545-1551.
10. Kannel WB, Sorlie P, McNamara PM. Prognosis after initial myocardial infarction: the Framingham study. *Am J Cardiol* 1979;44:53-59.
11. Piers SR, Tao Q, de Riva Silva M, et al. CMR-based identification of critical isthmus sites of ischemic and nonischemic ventricular tachycardia. *JACC Cardiovasc Imaging* 2014;7:774-784.
12. Fernández-Armenta J, Berruezo A, Andreu D, et al. Three-dimensional architecture of scar and conducting channels based on high resolution ce-CMR: insights for ventricular tachycardia ablation. *Circ Arrhythm Electrophysiol* 2013;6:528-537.
13. Andreu D, Ortiz-Pérez JT, Fernández-Armenta J, et al. 3D delayed-enhanced magnetic resonance sequences improve conducting channel delineation prior to ventricular tachycardia ablation. *Europace* 2015;17:938-945.
14. Dall'Armellina E, Karia N, Lindsay AC, et al. Dynamic changes of edema and late gadolinium enhancement after acute myocardial infarction and their relationship to functional recovery and salvage index. *Circ Cardiovasc Imaging* 2011;4:228-236.
15. Rochitte CE, Lima JA, Bluemke DA, et al. Magnitude and time course of microvascular obstruction and tissue injury after acute myocardial infarction. *Circulation* 1998;98:1006-1014.

16. Fieno DS, Hillenbrand HB, Rehwald WG, et al. Infarct resorption, compensatory hypertrophy, and differing patterns of ventricular remodeling following myocardial infarctions of varying size. *J Am Coll Cardiol* 2004;43:2124-2131.
17. Hillenbrand HB, Sandstede J, Störk S, et al. Remodeling of the infarct territory in the time course of infarct healing in humans. *Magn Reson Mater Phy* 2011;24:277-284.
18. Pokorney SD, Rodriguez JF, Ortiz JT, Lee DC, Bonow RO, Wu E. Infarct healing is a dynamic process following acute myocardial infarction. *J Cardiovasc Magn Reson* 2012;14:62.
19. Acosta J, Fernández-Armenta J, Borràs R, et al. Scar Characterization to Predict Life-Threatening Arrhythmic Events and Sudden Cardiac Death in Patients With Cardiac Resynchronization Therapy: The GAUDI-CRT Study. *JACC Cardiovasc Imaging* 2018;11:561-572.
20. Soto-Iglesias D, Acosta J, Penela D, et al. Image-based criteria to identify the presence of epicardial arrhythmogenic substrate in patients with transmural myocardial infarction. *Heart Rhythm* 2018;15:814-821.
21. Dagues N, Hindricks G. Risk stratification after myocardial infarction: is left ventricular ejection fraction enough to prevent sudden cardiac death? *Eur Heart J* 2014;34:1964-1971.
22. Berger CJ, Murabito JM, Evans JC, Anderson KM, Levy D. Prognosis after first myocardial infarction: comparison of Q-wave and non-Q-wave myocardial infarction in the Framingham Heart Study. *JAMA* 1992;268:1545-1551.
23. Acosta J, Fernández-Armenta J, Penela D, et al. Infarct transmurality as a criterion for first-line endo-epicardial substrate-guided ventricular tachycardia ablation in ischemic cardiomyopathy. *Heart Rhythm* 2016;13:85-95.



## FIGURES AND FIGURE LEGENDS

**Central illustration.** Serial LGE-CMR studies were performed at 7 days, 6 months, and 4 years after STEMI. Functional LV assessment, as well as scar characterization, were analyzed using a dedicated post-processing software (ADAS-3D®, Galgo Medical, Barcelona, Spain). A scar remodeling process is observed, with progressive reduction of core mass and border zone mass. The number and mass of BZC steadily decrease after STEMI. The distribution of BZC is significantly modified in the long-term.

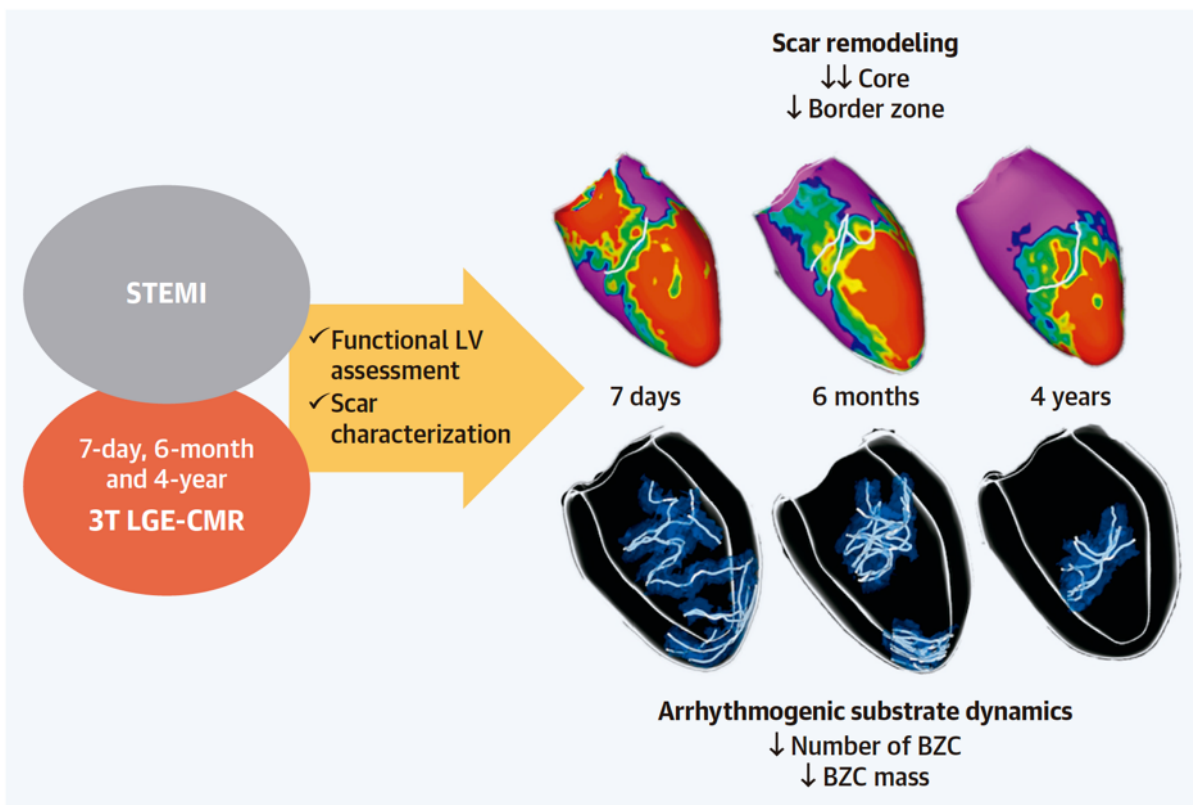


**Fig. 1.** Study inclusion flow diagram.

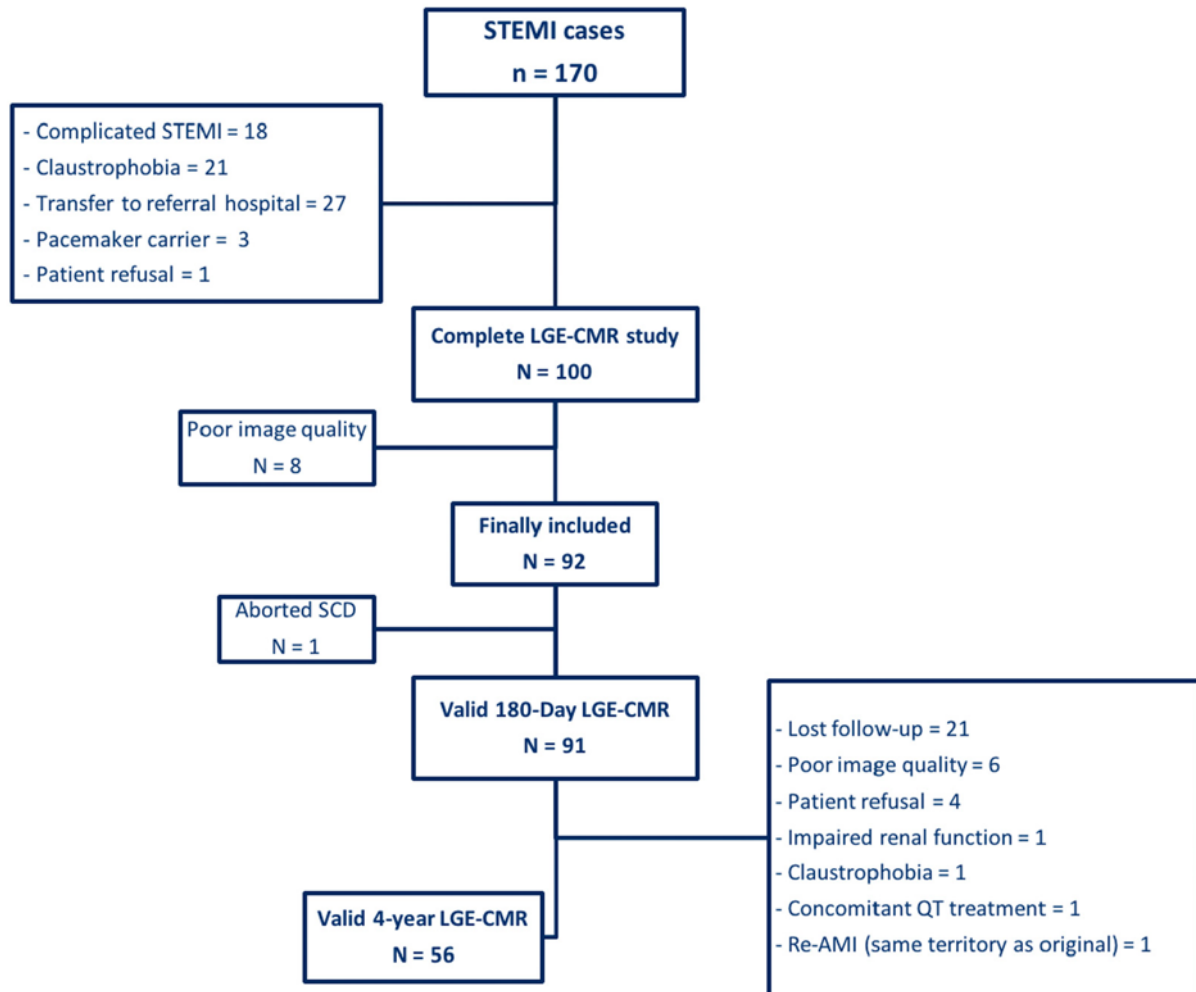


**Fig. 2.** Evolution of scar mass and heterogeneity over time. A gradual decrease in scar mass is noted. Parallely, an ongoing increase in scar heterogeneity (defined as BZ percentage of scar) is observed.

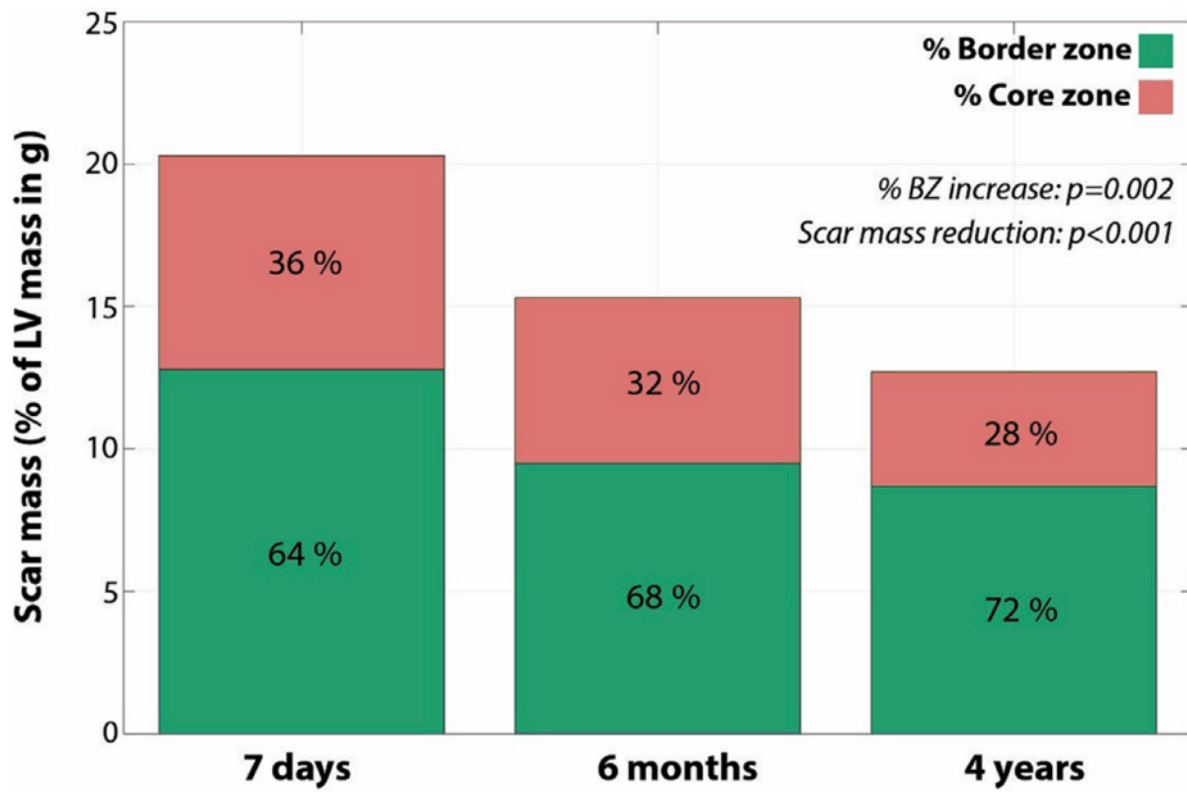


**Fig. 3.** Long-term scar remodeling in a case of inferolateral STEMI. LV systolic function progressively improved while the scar mass became progressively smaller. Two intramyocardial BZC, located at layers 40% and 70%, could be detected in the 7-day CMR, whereas only the first remained relatively stable after 4 years.

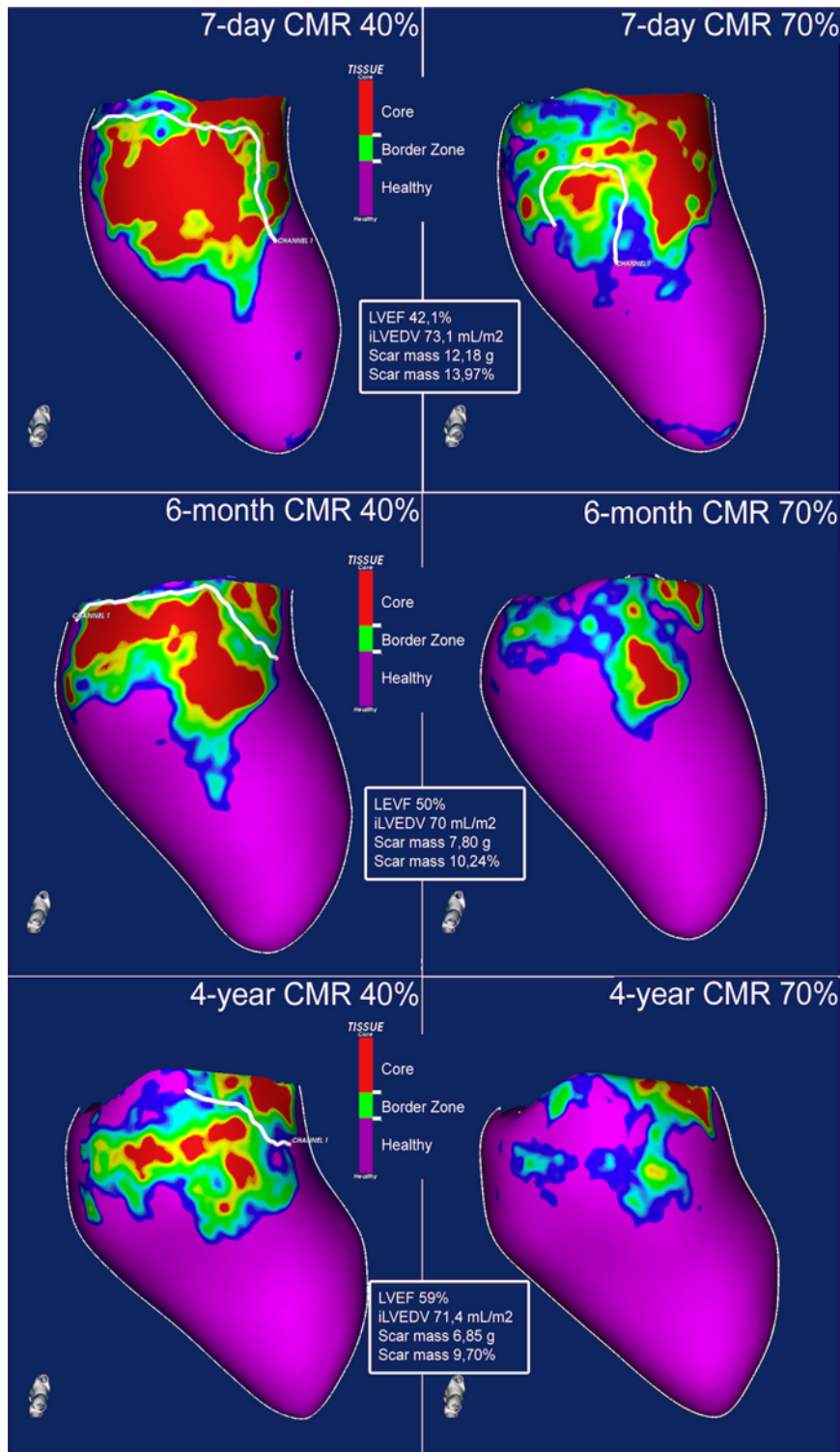


**Fig. 4.** *Panel A:* Mean BZC mass evolution over time. *Panel B1:* 3-D reconstruction showing an example of BZC number and distribution, from endo- to epicardium. *Panel B2:* The same example, showing in detail the scar characterization at the subendocardial level (10%-layer). Noteworthy, the disappearance of the basal core zone leads to an 'apical displacement' of the transversal, subendocardial BZC detected (white line). The same behavior (drastic reduction of core zone and BZ) occurs at the mid-myocardial and subepicardial levels, therefore explaining the findings shown in *panel B1*.

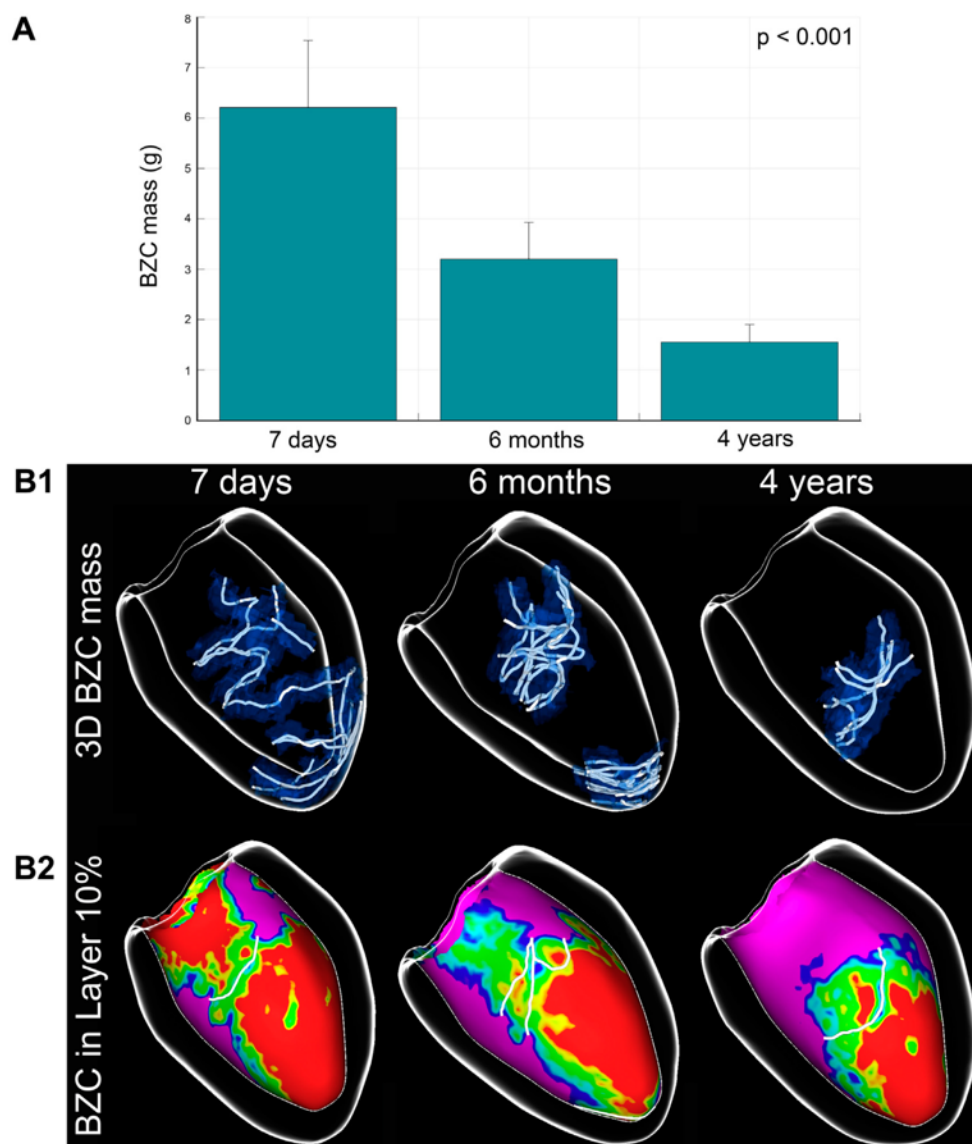
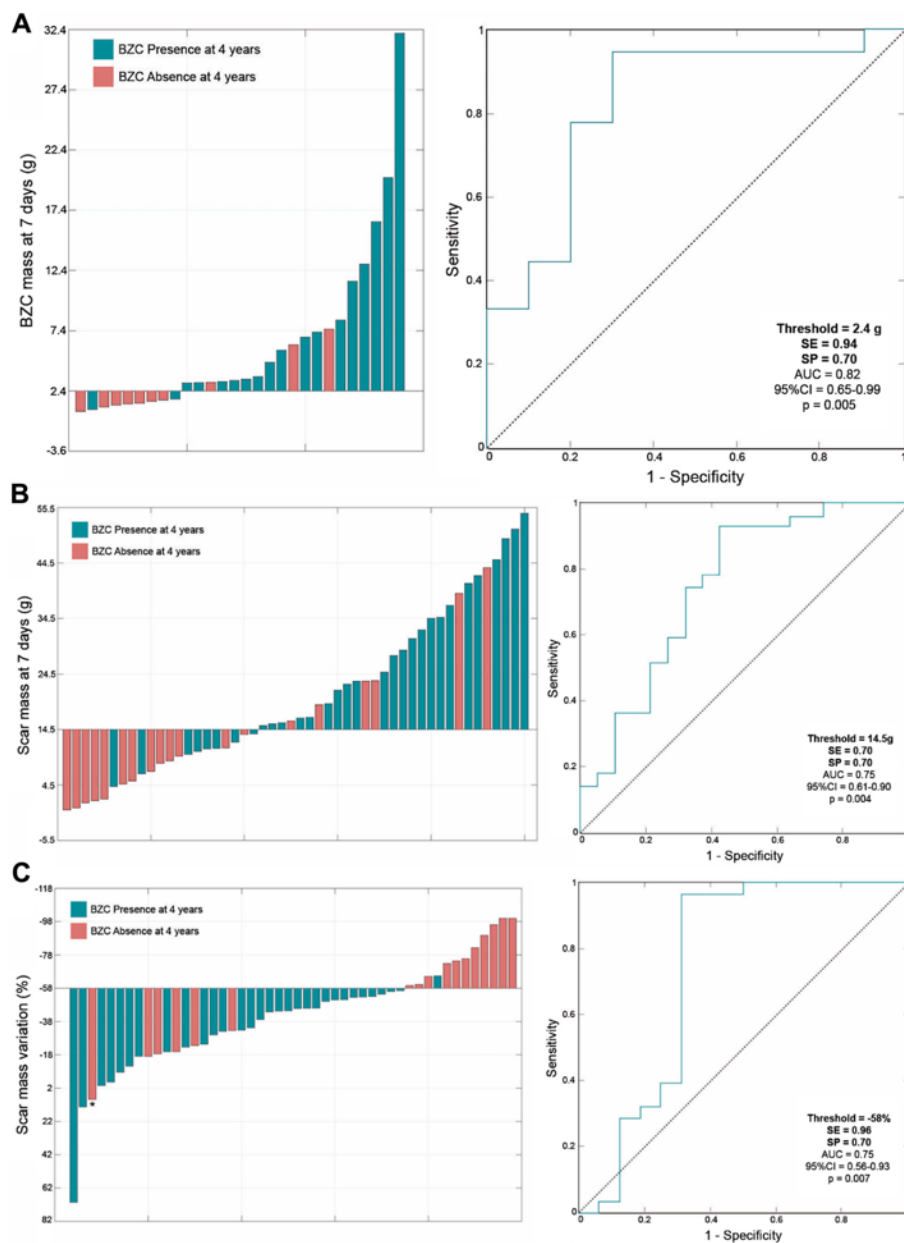


**Fig. 5.** *Panel A:* Waterfall plot and receiver operator curve (ROC) of the variable “BZC mass at 7 days” for predicting the persistence of BZC at 4 years. *Panel B:* Waterfall plot and receiver operator curve (ROC) of the variable “scar mass at 7 days” for predicting the persistence of BZC at 4 years. *Panel C:* Waterfall plot and receiver operator curve (ROC) of the variable “scar mass variation” (defined as the difference of scar mass in % between the 7-day and 4-year CMR studies) for predicting the persistence of BZC at 4 years.



## TABLES

**Table 1:** Baseline characteristics of the study population.

	Total (n = 56)	No-reflow (n = 16)	P-value <sup>†</sup>	Non-Arrhythmic scar <sup>‡</sup> (n = 22)	Arrhythmic scar <sup>‡</sup> (n = 29)	P-value <sup>  </sup>
Age	57 ± 11	53 ± 13	0.11	58 ± 9	56 ± 12	0.64
Men	43 (76.8%)	12 (75%)	0.84	19 (86.4%)	20 (69%)	0.15
Hypertension	22 (39.3%)	4 (25%)	0.17	8 (36.4%)	13 (44.8%)	0.54
Diabetes Mellitus	5 (9%)	0 (0%)	0.33	4 (18.2%)	1 (3.4%)	0.16
Dyslipidemia	11 (19.6%)	3 (18.8%)	0.92	6 (27.3%)	4 (13.8%)	0.23
Smoker	27 (48.2%)	9 (56.3%)	0.28	11 (50%)	13 (44.8%)	0.87
Familiar history of early CAD	32 (57.1%)	10 (62.5%)	0.61	15 (68.2%)	13 (44.8%)	0.1
Time to reperfusion	218 ± 175	211 ± 136	0.86	220 ± 211	215 ± 162	0.94
Responsible artery						
• LADA	27 (48.2%)	9 (56.3%)	0.34	8 (36.4%)	17 (58.6%)	0.28
• RCA	22 (39.3%)	4 (25%)		11 (50%)	9 (31%)	
• CA	7 (12.5%)	3 (18.8%)		(13.6%)	3 (10.3%)	
Initial TIMI flow	1.1 ± 1.1	0	0.29	1.3 ± 1.2	1.3 ± 1.2	1.0
Final TIMI flow	2.9 ± 0.3	2.9 ± 0.3	1.0	2.9 ± 0.3	2.9 ± 0.3	0.9
Treatment during the acute phase						
• Betablockers	48 (85.7%)	14 (87.5%)	0.71	17 (77.3%)	26 (89.7%)	0.24
• ACEI/ARB	47 (83.9%)	14 (87.5%)	0.67	1 (4.5%)	1 (3.4%)	1.0
• Statins	55 (98.2%)	16 (100%)	0.52	22 (100%)	28 (96.6%)	0.38
LVEF (%)	47.1 ± 8.9	42.1 ± 7.4	0.01*	49.9 ± 9.0	46.7 ± 8.2	0.2
iLVEDV (mL/m <sup>2</sup> )	83.8 ± 18.1	88.7 ± 22.2	0.21	78.7 ± 14.5	85.4 ± 17.1	0.16
iLVESV (mL/m <sup>2</sup> )	44.2 ± 13.8	52.4 ± 17	0.01*	38.5 ± 9.7	45.7 ± 12.0	0.03*
Basal scar mass (g)	20.3 ± 14.6	28 ± 13.1	0.01*	12.9 ± 12.5	23.1 ± 14.6	0.02*
Basal BZ mass (g)	12.9 ± 9.1	17.9 ± 8.7	0.01*	9.0 ± 8.6	13.5 ± 8.2	0.08
Basal core mass (g)	7.5 ± 6.6	10.1 ± 7.1	0.06	3.9 ± 4.2	9.6 ± 7.5	<0.01*

\* Statistically significant difference ( $p < 0.05$ ). <sup>†</sup> P-values for the differences between patients with normal reperfusion ( $n = 40$ ) vs. those showing no-reflow phenomenon ( $n = 16$ ). <sup>‡</sup> Arrhythmic and non-arrhythmic scars are defined as those with and without BZ channels 4 years after the STEMI, respectively. <sup>||</sup> P-values for the differences between patients with non-arrhythmic ( $n = 22$ ) vs. arrhythmic scars ( $n = 29$ ).

CAD: Coronary artery disease; LADA: Left anterior descending artery; RCA: Right coronary artery; CA: Circumflex artery; ACEI: Angiotensin-converter enzyme inhibitors; ARB: Angiotensin-II receptor blockers; LVEF: Left ventricular ejection fraction; iLVEDV: Indexed left ventricular end-diastolic volume; iLVESV: Indexed left ventricular end-systolic volume; BZ: Border zone.

**Table 2.** Evolution of ventricular and scar remodeling parameters after AMI.

	<b>7 days</b>	<b>6 months</b>	<b>4 years</b>	<b>P-value*</b>	<b>P-value†</b>
<b>iLVEDV (mL/m<sup>2</sup>)</b>	83.5 ± 18.2	88.0 ± 22.2	88.3 ± 22.9	0.05	0.92
<b>iLVESV (mL/m<sup>2</sup>)</b>	43.9 ± 13.7	44.0 ± 18.7	44.2 ± 21.2	0.92	0.91
<b>LVEF (%)</b>	47.5 ± 8.7	50.9 ± 9.3	53.3 ± 16.0	<0.001	0.21
<b>Scar mass (g)</b>	20.3 ± 14.6	15.3 ± 13.3	12.7 ± 11.7	<0.001	<0.001
<b>BZ mass (g)</b>	12.8 ± 9.2	9.5 ± 7.3	8.7 ± 7.7	0.001	0.11
<b>Core mass (g)</b>	7.5 ± 6.7	5.8 ± 6.9	4.0 ± 5.3	<0.001	<0.001
<b>N. of BZC/patient</b>	1.5 ± 1.3	1.2 ± 1.3	0.8 ± 1.0	<0.01	<0.01
<b>BZC total mass (g)</b>	6.2 ± 7.0	3.2 ± 3.9	1.5 ± 1.9	<0.01	0.01

\* P-value between 7 days and 6 months. † P-value between 6 months and 4 years.

LVEF: Left ventricular ejection fraction; iLVEDV: Indexed left ventricular end-diastolic volume; iLVESV: Indexed left ventricular end-systolic volume; BZ: Border zone; BZC: Border zone channel.

**Table 3.** Value of 7-day LGE-CMR for predicting the presence or absence of BZ channels at 4 years.

		<b>4-year CMR</b>		<b>Total</b>
		<b>Absence of BZC</b>	<b>Presence of BZC</b>	
<b>7-day CMR</b>	<b>Absence of BZC</b>	9	1	10
	<b>Presence of BZC</b>	10	19	29
<b>Total</b>		19	20	39

Sensitivity 65.5%, specificity 47.3%, positive predictive value 65.5%, negative predictive value 90%. CMR: Cardiac magnetic resonance; BZC: Border zone channels.



**Table 4.** Value of 6-month LGE-CMR for predicting the presence or absence of BZ channels at 4 years.

		4-year CMR		Total
		Absence of BZC	Presence of BZC	
6-month CMR	Absence of BZC	12	1	13
	Presence of BZC	9	28	37
Total		21	29	50

Sensitivity 96.6%, specificity 57.1%, positive predictive value 75.7%, negative predictive value 92.3%. CMR: Cardiac magnetic resonance; BZC: Border zone channels.

## **ONLINE APPENDIX**

### **SUPPLEMENTARY METHODS**

#### **LGE-CMR Processing:**

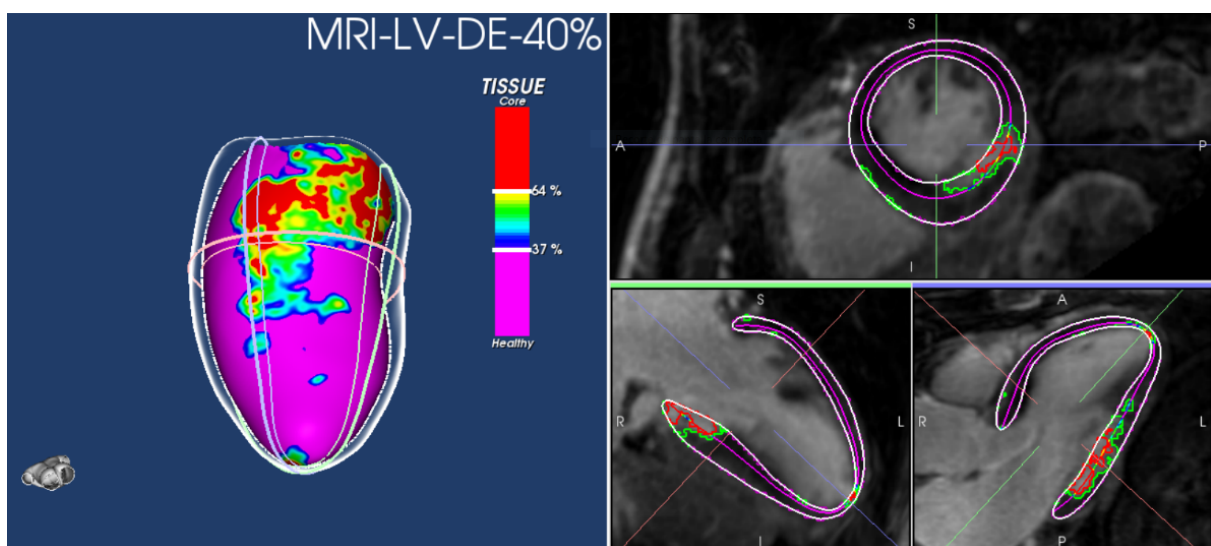
Subjects were imaged in a 3T MAGETOM Trio scanner (Siemens Healthcare, Erlangen, Germany). All images were gated to the electrocardiogram and acquired during repeated breath holds using a 32-element phased-array receiver coil. The imaging protocol included the following:

1. Cine-CMR imaging was acquired with a TrueFISP sequence after appropriate frequency adjustment in sequential 8-mm short axis slices encompassing the entire left ventricle and the 2-, 3- and 4- chambers' views. In case of relevant susceptibility artifacts arising from field inhomogeneities at 3T, a standard FLASH sequence was applied in the same orientation.
2. First-pass perfusion imaging during intravenous administration of a dose of 0.1 mmol/kg of gadodiamide (Omniscan®, Amersham Health). Basal, mid-ventricular and apical 8-mm short axis slices and an additional long axis slice depending on the infarct-related artery were acquired for every heartbeat.
3. An additional dose of 0.1 mmol/kg of gadodiamide was given at first-pass perfusion completion. In project #2 the full dose of 0.2 mmol/kg is given at once.
4. Early enhancement. (only in project #1). In a single breath-hold, a stack of short axis images will be obtained 5 min after contrast injection in identical slice position as in cines. For this purpose, a Single-Shot TrueFISP PSIR-GE sequence will be used.

5. Modified MOLLI sequence (or equivalent) in a mid-ventricular short axis slice with varying TI times (10 images ranging from TI 50 to 1000 msec). Optional.
6. TI scout for optimal myocardial contrast on magnitude images.
7. Viability study. Ten minutes after contrast injection, a navigator- and ECG-gated 3D GE PSIR sequence was applied in the axial orientation with an isotropic spatial resolution of  $2 \times 2 \times 2$  mm. Acquisition time was targeted at below 10 min.
8. Conventional 2D T1-weighted segmented IR-turboFLASH GE imaging with 5 mm slice thickness in sequential short axis slices with no gap between them. Inversion-time was adjusted to null normal myocardium and the typical voxel size was  $1.3 \times 1.3 \times 5$  mm<sup>3</sup>.
9. Finally, a stack of 5-mm slices was performed in the 2- and 4-chamber views in two separate breathholds covering the entire ventricle and using the Single-Shot TrueFISP PSIR-GE sequence. This was used for shifting correction of the 2D viability images. The entire protocol was concluded within 60 to 70 minutes.

**SUPPLEMENTARY FIGURE**

**Supplementary Fig. 1.** Post-processing of CMR images. Right panels: Short-axis, 2-chamber and 4-chamber views. Myocardial borders are contoured in white, scar core in red and border zone in green. The 40%-layer is demarcated with a purple line. Left panel: Automated 3D shell of the 40%-layer, showing core zone in red, border zone in green, and normal myocardium in purple. Tissue characterization thresholds are adjusted according to the raw images in the right panel, within the limits of  $40\% \pm 5\%$  and  $60\% \pm 5\%$ , as described in the text.





## Artículo 2: Monocyte Subsets Are Differently Associated with Infarct Size, Left Ventricular Function, and the Formation of a Potentially Arrhythmogenic Scar in Patients with Acute Myocardial Infarction

Bosch X, **Jáuregui B**, Villamor N, Morales-Ruiz M, Ortiz-Pérez JT, Borràs R, Penela D, Soto-Iglesias D, Perea RJ, Doltra A, Prat-González S, Jiménez W, Mira Á, Lasalvia L, Berruezo A. Monocyte Subsets Are Differently Associated with Infarct Size, Left Ventricular Function, and the Formation of a Potentially Arrhythmogenic Scar in Patients with Acute Myocardial Infarction. *J Cardiovasc Transl Res* 2020;13:722-730. *FACTOR DE IMPACTO (2020): 4.132*.  
*ÁREA DE CONOCIMIENTO: Cardiology and Cardiovascular Medicine. CUARTIL: Q1.*

Los objetivos generales del estudio son:

- Investigar el papel de los monocitos (células del sistema inmune implicadas en procesos de inflamación/reparación tisular) y sus distintas subpoblaciones: clásicos (CLM, CD14<sup>++</sup> CD16<sup>-</sup>), intermedios (INTM, CD14<sup>++</sup> CD16<sup>+</sup>) y no clásicos (no CLM, CD14<sup>+</sup> CD16<sup>++</sup>), en la formación de la cicatriz después de un IAMCEST, evaluada ésta con CRM.
- Evaluar el valor predictivo de cada subpoblación monocitaria en la potencial aparición de eventos clínicos.
- Evaluar el valor predictivo clínico de las diferentes subpoblaciones monocitarias y otros biomarcadores evaluados, en paralelo con el valor predictivo de la CRM, así como el valor incremental de la utilización conjunta de biomarcadores y CRM.
- Identificar nuevos biomarcadores asociados a eventos adversos.

**RESUMEN**

**Objetivos:** Investigar el papel de los monocitos clásicos (CLM, CD14<sup>++</sup> CD16<sup>-</sup>), intermedios (INTM, CD14<sup>++</sup> CD16<sup>+</sup>) y no clásicos (no-CLM, CD14<sup>+</sup> CD16<sup>++</sup>) en la formación de cicatrices miocárdicas después de un IAMCEST, evaluado con RM.

**Métodos:** 102 pacientes consecutivos con un primer IAMCEST se sometieron a análisis de sangre seriados después de 1, 3 y 7 días tras el evento coronario. Se realizó una RMC a los 7 días y 6 meses, analizando la presencia, en la cicatriz, de core (CO), border zone (BZ) y la presencia de canales de BZ.

**Resultados:** Los niveles de CLM e INTM disminuyeron progresivamente; se correlacionaron con la masa de cicatriz, CO y BZ a los 7 días y 6 meses ( $p < 0,05$ ), e inversamente con la fracción de eyección del ventrículo izquierdo (FEVI,  $p < 0,01$ ). Los niveles de no-CLM aumentaron gradualmente; dichos niveles se correlacionaron con la masa de BZ y la presencia de canales de BZ a los 7 días y 6 meses ( $p < 0,001$ ).

**Conclusiones:** CLM e INTM se asocian con tamaño del infarto e inversamente con FEVI, mientras que los no-CLM se asocian con la masa de BZ y la presencia de sustrato potencialmente arritmogénico.



## Monocyte Subsets Are Differently Associated with Infarct Size, Left Ventricular Function, and the Formation of a Potentially Arrhythmogenic Scar in Patients with Acute Myocardial Infarction

Xavier Bosch<sup>1,2</sup> · Beatriz Jáuregui<sup>1,2,3</sup> · Neus Villamor<sup>2,4</sup> · Manuel Morales-Ruiz<sup>2,5,6</sup> · José T. Ortiz-Pérez<sup>1,2</sup> · Roger Borràs<sup>1</sup> · Diego Penela<sup>7</sup> · David Soto-Iglesias<sup>1,3</sup> · Rosario J. Perea<sup>8</sup> · Ada Doltra<sup>1</sup> · Susana Prat-González<sup>1</sup> · Wladimiro Jiménez<sup>2,5,6</sup> · Áurea Mira<sup>2,5</sup> · Luis Lasalvia<sup>9</sup> · Antonio Berrueto<sup>3</sup>

Received: 21 August 2019 / Accepted: 28 November 2019  
 © Springer Science+Business Media, LLC, part of Springer Nature 2019

### Abstract

To investigate the role of classical (CLM, CD14<sup>++</sup>CD16<sup>-</sup>), intermediate (INTM, CD14<sup>++</sup>CD16<sup>+</sup>), and non-classical (Non-CLM, CD14<sup>+</sup>CD16<sup>++</sup>) monocytes in scar formation after ST-elevation myocardial infarction (STEMI), evaluated with cardiac magnetic resonance (CMR). One hundred two patients with a first STEMI had serial blood analyses after 1, 3, and 7 days. A CMR was performed at 7 days and 6 months, depicting scar core (CO), border zone (BZ), and the presence of BZ channels. CLM and INTM levels progressively decreased, correlated with the scar mass, CO, and BZ at 7 days and 6 months ( $p < 0.05$ ), and inversely with left ventricular ejection fraction (LVEF,  $p < 0.01$ ). Non-CLM levels gradually increased, correlated with BZ mass and the presence of BZ channels at 7 days and 6 months ( $p < 0.001$ ). CLM and INTM are associated with infarct size and inversely with LVEF, whereas Non-CLM are associated with BZ mass and the presence of potentially arrhythmogenic substrate.

**Keywords** Monocytes · Myocardial infarction · Left ventricular function · Arrhythmogenic substrate

### Introduction

Monocytes constitute a critical component of the innate immune response to inflammation. Three subsets have been

described in humans: classical CD14<sup>++</sup>CD16<sup>-</sup> monocytes (CLM), intermediate CD14<sup>++</sup>CD16<sup>+</sup> (INTM), and non-classical CD14<sup>+</sup>CD16<sup>++</sup> (Non-CLM). Monocyte subsets have been shown to contribute to scar formation in specific ways

Associate Editor Joost Shuijter oversaw the review of this article.

**Electronic supplementary material** The online version of this article (<https://doi.org/10.1007/s12265-019-09944-8>) contains supplementary material, which is available to authorized users.

✉ Antonio Berrueto  
[antonio.berrueto@quironsalud.es](mailto:antonio.berrueto@quironsalud.es)

<sup>1</sup> Cardiology Department, Cardiovascular Institute, Hospital Clínic, University of Barcelona, Spain, Carrer de Villarroel, 170, 08036 Barcelona, Spain

<sup>2</sup> Institut d'Investigacions Biomèdiques August Pi i Sunyer (IDIBAPS), Barcelona, Spain

<sup>3</sup> Heart Institute, Teknon Medical Center, Barcelona, Spain

<sup>4</sup> Hematopathology Unit, Pathology Department, Hospital Clínic, University of Barcelona, Spain, Barcelona, Spain

<sup>5</sup> Biochemistry and Molecular Genetics Department, Hospital Clínic, University of Barcelona, Spain, Barcelona, Spain

<sup>6</sup> Centro de Investigación Biomédica en Red en Enfermedades Hepáticas y Digestivas (CIBERehd), Barcelona, Spain

<sup>7</sup> Cardiology Department, Ospedale Guglielmo da Saliceto, Piacenza, Italy

<sup>8</sup> Radiology Department, Hospital Clínic, University of Barcelona, Spain, Barcelona, Spain

<sup>9</sup> Siemens Healthcare Diagnostics, New York, NY, USA

Published online: 12 December 2019

Springer



and in a sequential form in a mice model of acute myocardial infarction (AMI) [1]. Ly-6C<sup>high</sup> monocytes, which correspond to CLM in humans, predominate at the site of injury on days 1 to 4 after MI (phase 1) and scavenge necrotic debris by a combination of inflammatory mediator expression, proteolysis, and phagocytosis. Ly-6C<sup>low</sup> monocytes, which correspond to Non-CLM in humans, prevail from day 4 onward (phase 2), and contribute to angiogenesis and fibrosis, propagating repair [1]. It has been suggested that wound healing is delayed if the infarct recruits insufficient numbers of monocytes, because debris is neither cleared nor replaced with granulation tissue and collagen matrix [1]. On the other hand, a prolonged immune response from Ly-6C<sup>high</sup> monocytes can initiate inflammatory cascades and drive autoimmunity, resulting in further tissue damage [2]. Although extensive experimental research has been performed on the role of monocyte subsets in atherosclerosis and myocardial infarction, few clinical studies have been performed in humans on their different contributions to the process of scar formation after AMI, [3–7] especially on the role of INTM and Non-CLM.

Infarct size, as assessed with late gadolinium enhancement cardiac magnetic resonance (LGE-CMR), is an independent predictor of arrhythmic events in patients with AMI [8]. In addition, LGE-CMR can provide accurate 3D information about scar architecture, allowing the identification of core scar (CO), border zone (BZ), and BZ channels [9]. These BZ channels have a reasonably high correlation with conducting channels in the electroanatomic maps obtained during ventricular tachycardia substrate ablation procedures [9] and are related with the ventricular tachycardia isthmuses [10].

The aim of the present study was to determine the temporal evolution of blood levels of monocyte subsets up to 7 days after a ST segment elevation AMI (STEMI), and their role in left ventricular remodeling and the formation of the scar and its potentially arrhythmogenic substrate.

## Methods

### Patients

Inclusion criteria were patients admitted to our institution with a first STEMI and treated with primary percutaneous coronary intervention (PCI) within the first 12 h from symptom onset. Exclusion criteria were early death (within the first week), concomitant structural heart disease, life expectancy < 1 year due to non-cardiac pathology, other underlying inflammatory or fibrotic pathologies affecting major organs (e.g., liver, kidney, and lung), persistent contraindication for LGE-CMR (metallic prosthesis, claustrophobia, or GFR < 30 ml/min/1.73m<sup>2</sup>) or for its use within the first week after STEMI (e.g., due to mechanical ventilation or hemodynamic instability).

PCI was performed by experienced on-call interventional cardiologists following unfractionated heparin, aspirin, and a loading dose of clopidogrel. At the physician's discretion and unless contraindicated, enalapril, bisoprolol, and high-dose atorvastatin were initiated early, usually by 24 h from admission. Baseline characteristics and clinical data were prospectively collected in all cases. The study complied with the Declaration of Helsinki, and the local Ethics Committee (Clinical Research Ethics Committee of the Hospital Clínic de Barcelona; CEIC Hospital Clínic) approved the study protocol. All participants included in the study provided informed written consent.

### Laboratory Measurements

#### Monocyte Subpopulations

Peripheral venous blood was collected at days 1, 3, and 7 after STEMI and processed by flow cytometry within 60 min. Samples of 100 µl of blood were incubated with a combination of CD64-FITC (fluorescein isothiocyanate), CD16-PE (Phycoerythrin), CD45 PerCP (Peridinin Chlorophyll Protein), and CD14-APC (Allophycocyanin), all from BD Biosciences (San Jose, CA), for 15 min, followed by lysis of red cells with FACS Lysing solution (BD Biosciences) and an additional wash with phosphate-buffered saline. At least 50,000 cells of the stained sample were acquired in a FACS Canto II flow cytometer (BD Biosciences). Samples were analyzed with Infinicyt software (Cytognos, Salamanca, Spain). Monocytes were selected based on forward (FSC) and side (SSC) scatter characteristics and CD45 and CD64 expression (Supplementary Fig. S1). Once selected, the percent of monocytes from the total leukocytes, and the percent of each monocyte subpopulation (CD14<sup>++</sup>CD16<sup>-</sup>, CD14<sup>++</sup>CD16<sup>+</sup>, and CD14<sup>+</sup>CD16<sup>++</sup>) were obtained. The absolute numbers of monocytes and their subpopulations were calculated using the values of total leukocytes of the same sample.

#### Biomarkers

Troponin I (TnI), brain natriuretic peptide (BNP), tumor necrosis factor α (TNF-α), matrix metalloproteinase-1 (MMP-1), MMP-2, MMP-9, TIMP-1, beta-C-terminal telopeptide (CITP), and interleukins IL-1β, IL-6, and IL-10 were processed and quantified as described in the Online Supplementary Material.

#### LGE-CMR Processing

LGE-CMR examinations were performed at 7 days and 6 months after STEMI using a 3-T scanner (Magnetom Trio®, Siemens Healthcare, Erlangen, Germany). Image acquisition is summarized in the Online Supplementary

**Material.** All LGE-CMR images were analyzed using a previously described technique [11]. In brief, full left ventricular (LV) volume was reconstructed in the axial orientation and the resulting images were processed with ADAS-VT software (Galgo Medical, Barcelona, Spain). Five concentric surface layers (10%, 25%, 50%, 75%, 90%) were created automatically from endocardium to epicardium of the LV wall thickness. A 3D shell was obtained for each layer. Pixel signal intensity maps obtained from LGE-CMR images were projected to each shell following a trilinear interpolation algorithm and color-coded. To identify the scar areas, a pixel signal intensity-based algorithm was applied to characterize the hyperenhanced area as CO or BZ, using  $40 \pm 5\%$  and  $60 \pm 5\%$  of the maximum intensity as thresholds. Thus, BZ defined by LGE-CMR is an area of the infarct with an intermediate degree of fibrosis with a patient-specific distribution and does not correspond with the anatomical border of the infarct.

### Myocardial Scar Characterization

Two independent investigators analyzed the LGE-CMR images, and a third observer was available in case of discrepancy. The scar mass and areas in each shell (total scar, CO, and BZ) were automatically measured using ADAS-VT software. The BZ channels were defined as continuous corridors of BZ (with the prespecified pixel signal intensity threshold) surrounded by scar core/mitral annulus. A corridor of BZ was considered a channel when connecting 2 areas of normal myocardium. If a given channel was identified at the same location and with the same orientation in adjacent layers, it was considered a single multilayer channel (Fig. 1). When BZ channels into a given scar were identified, the scar was considered potentially arrhythmogenic since they highly correlate with conducting channels in electroanatomic maps [11]. These channels are responsible for slow conduction, a necessary component of re-entry, and have been shown to act as ventricular tachycardia isthmus [10].

As tissue characterization is based on a pixel signal intensity algorithm, normal myocardium cannot be distinguished from areas showing “no reflow” phenomenon; both areas have no hyperenhancement and a very low-intensity signal. Therefore, in 11 patients with no-reflow no attempt was made to identify BZ channels in the 7-day LGE-CMR study, although they were identified at the 6-month follow-up.

### Statistical Analysis

Continuous variables are given as mean value  $\pm$  SD and were compared using Student *t* test or Mann-Whitney *U* test, according to the data distribution (Student *t* test for normal distributed data and Mann-Whitney *U* test for non-parametric data). Categorical variables are given as total number and percentages. Bivariate correlations were performed using

Spearman and Pearson correlation coefficients, according to the data distribution. Since all the data were analyzed at three specific time points (1, 3, and 7 days after MI), a mixed linear model for multiple measurements was used to test for time-dependent changes of total number of monocytes and their subsets, as well as for biomarker levels. The same analysis was used for the comparisons between monocyte subsets and scar characteristics. A *p* value  $< 0.05$  was considered significant. Statistical analysis was performed using R software for Windows version 3.3.0 (R project for statistical computing, Vienna, Austria).

## Results

### Patients

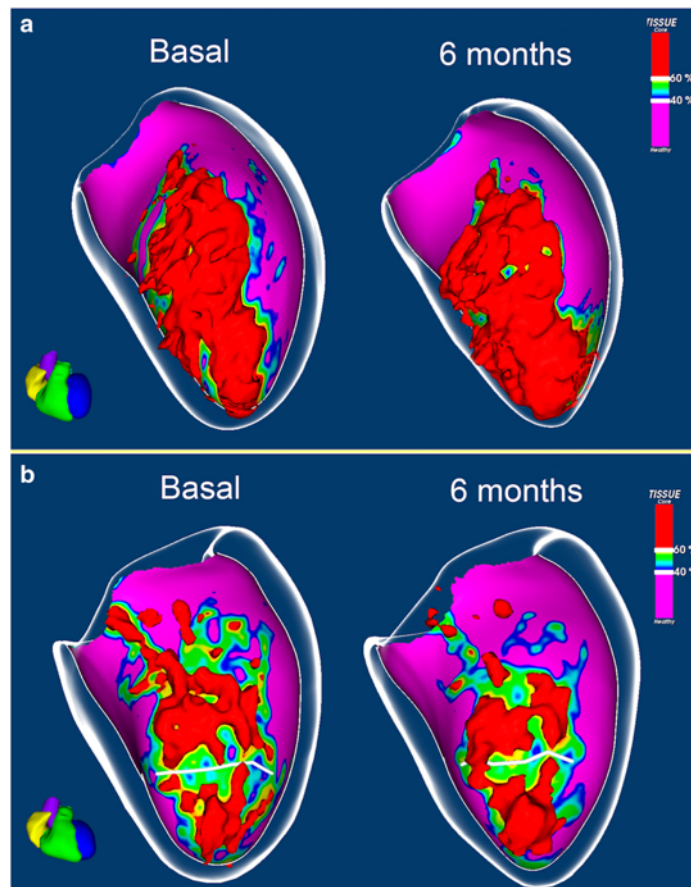
Of the 140 eligible participants, 102 were finally included and formed the study population (Fig. 2). A 7-day LGE-CMR was performed in all patients, although 4 studies had poor image quality and 11 patients showed severe no-reflow phenomenon that precluded tissue characterization and BZ channel identification. At 6-month follow-up, LGE-CMR was performed in 95 patients and tissue characterization in 89 patients.

Clinical baseline characteristics of the 102 patients are reported in Table 1. Median time to reperfusion was 170 (IQR: 160) minutes. Most STEMI were caused by left anterior descending coronary artery thrombosis (48%). The scar mass decreased from  $22 \pm 19$  g at 7 days to  $14 \pm 12$  g at 6 months, while LVEF increased from  $46 \pm 10\%$  to  $51 \pm 10\%$  respectively. BZ channels were identified in 52 of 83 patients at day 7 and in 53 of 89 patients at 6 months.

### Time Course of Monocyte Subset Levels

CLM levels decreased from  $670 \pm 271$  cells/ $\mu$ l at day 1 to  $607 \pm 250$  cells/ $\mu$ l at day 3, and to  $528 \pm 211$  cells/ $\mu$ l at day 7 ( $p < 0.001$  for global changes and  $p < 0.01$  for differences between days 1 to 3, and days 3 to 7) (Fig. 3). CLM represented, respectively, 91.8%, 91.1%, and 91.7% of total monocytes at days 1, 3, and 7 ( $p = 0.99$  for all comparisons). INTM levels also progressively decreased from days 1 and 3 to day 7 ( $44 \pm 44$  to  $41 \pm 32$  to  $28 \pm 23$  cells/ $\mu$ l, respectively;  $p < 0.001$  for global changes and  $p < 0.01$  from day 1 to day 7, and day 3 to day 7). INTM represented, respectively, 6.0%, 6.2%, and 4.9% of total monocytes at days 1, 3, and 7 ( $p = 0.99$  for differences between days 1 and 3, and  $p = 0.92$  for days 3 to 7). Conversely, Non-CLM levels increased progressively from  $16 \pm 14$  to  $18 \pm 18$  to  $20 \pm 20$  cells/ $\mu$ l at days 1, 3, and 7 post-STEMI ( $p = 0.04$  for global changes). Non-CLM represented, respectively, 2.2%, 2.7%, and 3.5% of total monocytes at days 1, 3, and 7 ( $p = 0.95$  for differences between days 1 and 3, and  $p = 0.94$  for days 3 to 7).

**Fig. 1** Example of myocardial scar in two patients with anterior wall STEMI. Automated representation of a myocardial layer in the wall thickness of the left ventricular reconstruction with a color-coded pixel signal intensity map. Normal myocardium is shown in purple, border zone in green, and the core in red. **a** Scar without border zone channels in a patient with low circulating levels of non-classical monocytes. **b** Scar in a patient with high levels of non-classical monocytes. In 7-day and 6-month studies, a border zone channel (white line) can be identified in the same myocardial layer and segment, with the same orientation and morphology



### Monocyte Subsets and Biomarkers

The temporal changes in circulating biomarkers are depicted in Supplementary Fig. S2. IL-6 levels decreased from days 1 and 3 to day 7 ( $p < 0.001$ ), paralleling the circulating dynamics of CLM and INTM, while TNF- $\alpha$ , MMP-1, MMP-2, MMP-9, and TIMP-1 levels increased progressively from day 1 to day 7.

The correlation coefficients observed between the circulating levels of monocyte subsets and biomarkers differed not only according to each monocyte subset and biomarker but also by the specific time since STEMI (Supplementary Fig. S3). CLM and INTM followed a similar pattern and significantly correlated with pro-inflammatory biomarkers during days 1 to 3, especially with IL-6, TNF- $\alpha$ , and CRP. These associations extended to day 7, although to a lesser degree.

They also significantly correlated with markers of extracellular matrix degradation during days 1 to 7: CLM with MMP-9 and TIMP-1, and INTM with MMP-2 and MMP-9. On the other hand, the reparative Non-CLM also was directly correlated with pro-inflammatory biomarkers during days 1 and 3, and with MMP-1, MMP-2, and TIMP-1.

### Association with Left Ventricular Volumes and Ejection Fraction

Peak levels of CLM directly correlated with left ventricular (LV) volumes at day 7, both for end-diastolic volume (LVEDV) ( $r = 0.21$ ,  $p = 0.04$ ), and LV end-systolic volume (LVESV) ( $r = 0.33$ ,  $p = 0.001$ ), resulting in an inverse correlation with LVEF ( $r = -0.30$ ,  $p = 0.003$ ) that was also observed at 6 months ( $r = -0.31$ ,  $p = 0.002$ ). Interestingly, peak

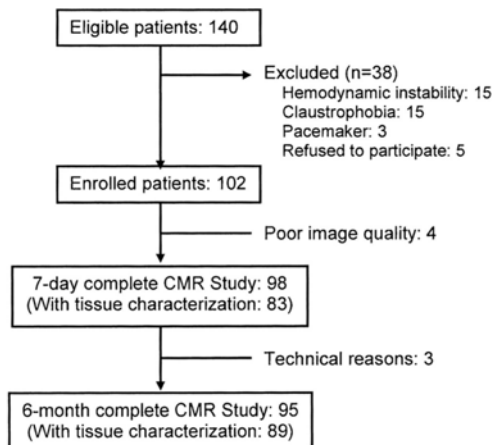


**Fig. 2** Flow chart of the studied patients. LGE-CMR, late gadolinium enhancement cardiac magnetic resonance

**Table 1** Characteristics of the studied population

Age, years	58 ± 11
Sex, female	18 (18)
Coronary risk factors	
Present smoker	51 (50)
Hypertension	42 (41)
Hypercholesterolemia	25 (25)
Diabetes mellitus	13 (13)
Site of MI: anterior	48 (47)
Peak Troponin I, IU/l	128 ± 150
Killip class ≥ 2	9 (9)
Serum creatinine, mg/dl	0.95 ± 0.22
Leucocytes, cells/ $\mu$ l	10,849 ± 2893
Monocytes, cells/ $\mu$ l	729 ± 302
Prior treatment	
ACE-i/ARB	23 (23)
Beta blockers	4 (4)
Statins	21 (21)
CMR at 7 days	
LVEF, %	46 ± 10
Scar mass, g	22 ± 19
CO mass, g	11 ± 10
BZ mass, g	12 ± 10
CMR at 6 months	
LVEF, %	51 ± 10
Scar mass, g	14 ± 12
CO mass, g	7 ± 6
BZ mass, g	8 ± 7

Values are means ± SD or n (%). ACE-I, angiotensin-converting enzyme inhibitors; ARB, angiotensin receptor blockers; BZ, scar border zone; CO, scar core; LVEF, left ventricular ejection fraction

INTM levels also inversely correlated with LV ejection fraction (LVEF) at 7 days ( $r = -0.26$ ,  $p = 0.01$ ) and at 6 months ( $r = -0.27$ ,  $p < 0.01$ ). In contrast, no significant correlations were found between Non-CLM levels and LVEDV, LVESV, or LVEF.

### Monocyte Subsets and Scar Characteristics

Blood levels of monocyte subsets were directly correlated with scar mass and its parts, the CO and BZ, as evaluated by LGE-CMR at 7 days. However, the degree of association was different for every monocyte subset and zone. Thus, while CLM and INTM levels were directly, strongly, and uniformly associated with CO and BZ mass, Non-CLM levels were exclusively associated with the BZ mass (Table 2). Similar although less marked results were obtained at 6 months.

Interestingly, although the BZ mass was directly associated with all monocyte subsets, the presence of BZ channels was strongly associated only with Non-CLM levels, both at 7 days and at 6 months (Table 2 and Fig. 1). Compared with patients without BZ channels, patients with BZ channels had uniformly higher levels of Non-CLM during the first 7 days after STEMI (Fig. 4), higher peak Tn I ( $134 \pm 118$  IU/l vs.  $91 \pm 188$  IU/l,  $p < 0.01$ ), higher BZ mass, and lower LVEF at 6 months ( $50 \pm 9\%$  vs.  $55 \pm 9\%$ ,  $p < 0.05$ ). No differences between patients with and without arrhythmogenic scar were found for other clinical characteristics, MI location, or time to reperfusion ( $235 \pm 185$  min vs.  $215 \pm 188$  min,  $p = 0.39$ ).

### Discussion

This study is the first to analyze the role of circulating monocyte subsets in the process of scar formation after AMI and their relationship with differential tissue characteristics using 3-T LGE-CMR at 7 days and 6 months. Two main findings have been showed: CLM and INTM had a similar pattern of blood kinetics and of association with inflammatory biomarkers, and both were directly associated with infarct size and inversely with LVEF. In contrast, Non-CLM showed different blood kinetics and were strongly associated with the scar BZ and with its potentially arrhythmogenic distribution, creating BZ channels.

Early after MI, monocytes are rapidly released by the splenic reservoir and are rapidly recruited by the ischemic myocardium, matched by rapid (<24 h) cell death [12]. In accordance with these observations and other reports, [5, 6] we found that CLM and INTM showed similar kinetics with a peak on day 1 and a progressive decrease at day 3 and day 7. Although the progressive increase in the circulating levels of Non-CLM from days 1 to 7 after MI has not been observed in other clinical studies, [5, 6] our results are in agreement with experimental studies on Ly-6C<sup>low</sup> monocytes/macrophage

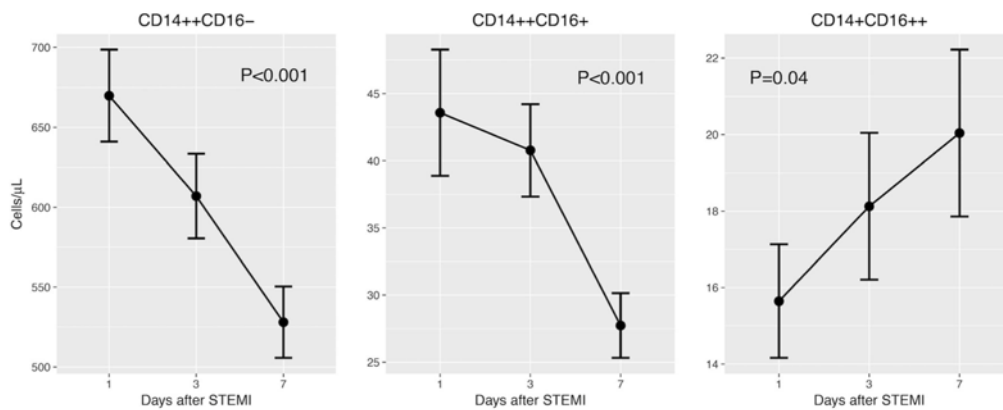


Fig. 3 Circulating levels of monocyte subsets within the first 7 days after myocardial infarction

showing a progressive increase from baseline, with a peak on day 7 after MI [1]. Nevertheless, it should be noted that the total number of monocytes and their subpopulations remained within what is considered the normal range throughout the study [13–16].

**Association Between Monocyte Subsets and Serum Biomarkers**

We found that all monocyte subsets were associated with pro-inflammatory biomarkers during phase 1, suggesting that all of them may have pro-inflammatory effects during this phase [12], in accordance with experimental work reporting that Ly-6C<sup>high</sup> monocytes have proteolytic and inflammatory functions, whereas Ly-6C<sup>low</sup> have also attenuated inflammatory and proangiogenic properties [1]. In this regard, IL-6, which

is involved in the inflammatory injury, progressively decreases as local post-STEMI inflammation does (Supplementary Fig. S2). CLM and INTM were also associated with MMP-9 from day 1 to day 7 after STEMI, and Non-CLM were associated with MMP-1, and MMP-2, markers of extracellular matrix degradation, suggesting that the protease activity involved in the process of extracellular matrix remodeling may continue during the reparative phase 2. In fact, these MMPs showed a progressive increase during the first days after the STEMI (Supplementary Fig. S2).

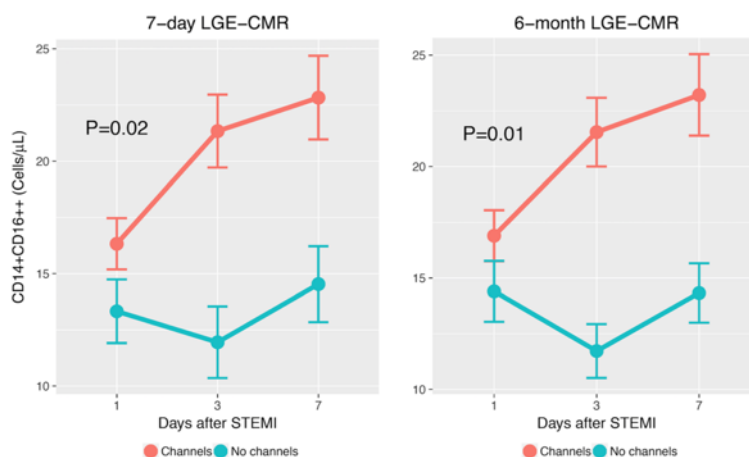
The levels of CLM and INTM significantly correlated with the serum concentrations of TNF-α. This could be justified since TNF-α is an autocrine contributor to myocardial dysfunction and cardiomyocyte death in ischemia-reperfusion injury, either by direct depression of contractility or by induction of myocyte apoptosis [17].

Table 2 Parameter estimation from the lineal model of the association between each monocyte subset and the scar mass and its components at 7 days and 6 months after myocardial infarction

	Scar		Core zone		Border zone		Border zone channels	
	β ± SE	p	β ± SE	p	β ± SE	p	β ± SE	p
Results at 7 days								
CLM	0.017 ± 0.004	0.0001	0.008 ± 0.002	< 0.001	0.009 ± 0.002	0.0002	0.00003 ± 0.0003	0.92
INTM	0.118 ± 0.031	0.0002	0.054 ± 0.016	0.001	0.064 ± 0.017	0.0001	0.005 ± 0.002	0.03
Non-CLM	0.137 ± 0.063	0.03	0.045 ± 0.033	0.17	0.091 ± 0.033	0.006	0.014 ± 0.004	0.0002
Results at 6 months								
CLM	0.005 ± 0.003	0.06	0.002 ± 0.001	0.10	0.003 ± 0.002	0.05	0.00006 ± 0.0003	0.82
INTM	0.060 ± 0.020	0.003	0.021 ± 0.010	0.03	0.038 ± 0.011	< 0.001	0.002 ± 0.002	0.20
Non-CLM	0.062 ± 0.040	0.13	0.013 ± 0.020	0.53	0.050 ± 0.022	0.025	0.012 ± 0.004	< 0.001

CLM, classical human monocytes (CD14++CD16-); INTM, intermediate human monocytes (CD14++CD16+); Non-CLM, non-classical human monocytes (CD14+CD16++)

**Fig. 4** Mean (95% CI) blood levels of non-classical monocytes during the first 7 days after myocardial infarction in patients with and without border zone channels at 7-day and 6-month LGE-CMR



### LV Remodeling and Dysfunction

Maekawa et al. first reported an association between peak monocyte count and LV volumes and LVEF measured by left contrast ventriculography in patients with AMI, suggesting a possible role of monocytes in the development of LV remodeling after MI [3]. In our study, a strong association was found between CLM levels and LV remodeling within 7 days after STEMI, an effect that remained at 6 months. These results are in agreement with experimental research showing that Ly-6C<sup>high</sup> monocytosis 5 days after AMI disturbs resolution of inflammation and enhances LV remodeling [2]. Previous clinical studies have shown conflicting results [4, 7]. In the study by Tsujioka et al. in 30 patients with STEMI, peak levels of CLM were not inversely correlated with basal or 6-month LVEF but with the change in LVEF [4]. The small sample of patients may explain these results. On the other hand, van der Laan et al. also found an association between CLM levels 5 days post-AMI and LVEF [7]. We also observed an inverse correlation between circulating levels of INTM and LVEF at 7 days and 6 months after STEMI, a finding not previously reported. The strong similarities of these two monocyte subsets in phenotype, circulating dynamics, interleukin expression, proinflammatory effects, and transcriptome characteristics also support our results, as INTM seems to be an intermediate stage of differentiation from CLM to Non-CLM.

### Non-classical Monocytes and the Formation of a Potentially Arrhythmogenic Scar

Different results have been also reported on the association between blood levels of monocyte subsets and infarct size [4, 7]. The present study was the first to assess MI size using

3-T LGE-CMR, and the components of the scar and its tissue characterization at 7 days and 6 months. The results showed a strong, direct correlation between CLM and INTM levels and infarct size, as previously reported in experimental studies with Ly-6C<sup>high</sup> monocytes [1, 18]. In addition, the relationship was uniform for both parts of the scar, the CO and the BZ.

More important, we found for the first time a strong direct association between circulating levels of Non-CLM and the BZ mass, and the formation of an adverse myocardial scar defined as a pro-arrhythmogenic scar with BZ channels. Patients with these scar channels had higher levels of Non-CLM at days 3 and 7, and higher BZ mass than patients without BZ channels, suggesting that high Non-CLM levels may affect or influence infarct healing and result in a pro-arrhythmogenic scar.

These results may have important clinical implications and raise some intriguing hypotheses. Indeed, it has been shown that Ly6C<sup>low</sup> macrophages promote transdifferentiation of fibroblasts into secretory and contractile myofibroblasts, and these cells can form electrotonic connections with cardiomyocytes, potentially contributing to arrhythmogenesis [19]. In addition, in an experimental study, mice treated with antibodies towards fractalkine, a mediator for Ly-6C<sup>low</sup> infiltration of the myocardium, had smaller infarct size [20]. Thus, decreased recruitment and infiltration of Non-CLM by direct intervention early after STEMI might have favorable effects on infarct healing.

### Clinical Implications

Further experimental studies at a cellular and molecular level are needed to confirm these results and to provide a mechanistic explanation for each process. Several therapeutic targets

and strategies addressing the inflammatory and immune responses after an AMI have been evaluated. These strategies have tried, for example, to reduce the activity of certain immune cells, such as neutrophils; to inhibit the activity of various inflammatory cytokines using monoclonal antibodies; or to target multiple inflammatory pathways by using stem cells. In this regard, treatment with stem cells, although promising, still faces numerous limitations [21]. A deeper understanding of these mechanisms, for which LGE-CMR constitutes an essential diagnostic tool, may provide a unique opportunity to identify new therapeutic strategies to limit LV remodeling and to modulate the arrhythmogenic substrate early after myocardial infarction.

### Study Limitations

This was a prospective, observational study. Thus, the results do not provide a mechanistic explanation for the association found between the levels of each monocyte subset and the analyzed biomarkers, LV remodeling, infarct size, and the formation of BZ channels. In addition, our study could not determine whether the blood levels of the three monocyte subsets reflect the extent of their infiltration in the ischemic and necrotic myocardium.

### Conclusions

Monocyte subsets have an important role in scar formation early after STEMI. Classical and intermediate monocyte levels were directly correlated with infarct size and inversely with LVEF. Non-classical monocytes were strongly associated with the scar BZ mass and distribution, thus creating a potentially arrhythmogenic substrate. Further experimental studies at a cellular and molecular level are needed to confirm these results and to provide a mechanistic explanation for each process. A deeper understanding of these mechanisms, for which LGE-CMR constitutes an essential diagnostic tool, may provide a unique opportunity to identify new therapeutic strategies to limit LV remodeling and to modulate the arrhythmogenic substrate early after myocardial infarction.

**Acknowledgments** This study was partially supported by Siemens Healthineers GmbH (Dr. Lasalvia).

**Funding Information** This work was supported by Agencia de Gestió d'Ajuts Universitaris i de Recerca (AGAUR), Generalitat de Catalunya [grant number 2014-SGR-471]; Instituto de Salud Carlos III (ISCIII), Centro de Investigación Biomédica en Red: FIS-CIBER16 [grant number CB16/11/00354]; Fondo de Investigación Sanitaria (FIS) [grant numbers PI14/00759, PI17/01968]; and Ministerio de Economía y Competitividad, RETOS [grant numbers RTC-2015-3515-1, RTC-2016-5445-1].

 Springer

### Compliance with Ethical Standards

**Conflict of Interest** Dr. Berruzo is a stockholder in Galgo Medical SL and has received financial support from Siemens Healthcare. Dr. Lasalvia is a stockholder and employee of Siemens Healthcare. The other authors have no other relevant affiliations or financial involvement with any organization or entity with a financial interest in or financial conflict with the subject matter or materials discussed in the manuscript apart from those disclosed.

**Human Subjects/Informed Consent Statement** All procedures followed were in accordance with the ethical standards of the responsible committee on human experimentation (institutional and national) and with the Helsinki Declaration of 1975, as revised in 2000. Informed consent was obtained from all patients for being included in the study.

### References

- Nahrendorf, M., Swirski, F. K., Aikawa, E., Stangenberg, L., Wurdinger, T., Figueiredo, J. L., Libby, P., Weissleder, R., & Pittet, M. J. (2007). The healing myocardium sequentially mobilizes two monocyte subsets with divergent and complementary functions. *The Journal of Experimental Medicine*, 204, 3037–3047.
- Panizzi, P., Swirski, F. K., Figueiredo, J. L., Waterman, P., Sosnovik, D. E., Aikawa, E., Libby, P., Pittet, M., Weissleder, R., & Nahrendorf, M. (2010). Impaired infarct healing in atherosclerotic mice with Ly-6C(hi) monocytes. *Journal of the American College of Cardiology*, 55, 1629–1638.
- Maekawa, Y., Anzai, T., Yoshikawa, T., Asakura, Y., Takahashi, T., Ishikawa, S., Mitamura, H., & Ogawa, S. (2002). Prognostic significance of peripheral monocytes after reperfusion acute myocardial infarction: a possible role for left ventricular remodeling. *Journal of the American College of Cardiology*, 39, 241–246.
- Tsujioka, H., Imanishi, T., Ikejima, H., Kuroi, A., Takarada, S., Tanimoto, T., Kitabata, H., Okochi, K., Arita, Y., Ishibashi, K., Komukai, K., Kataiwa, H., Nakamura, N., Hirata, K., Tanaka, A., & Akasaka, T. (2009). Impact of heterogeneity of human peripheral blood monocyte subsets on myocardial salvage in patients with primary acute myocardial infarction. *Journal of the American College of Cardiology*, 54, 130–138.
- Tapp, L. D., Shantsila, E., Wrigley, B. J., Pamukcu, B., & Lip, G. Y. (2012). The CD14<sup>++</sup>CD16<sup>+</sup> monocyte subset and monocyte-platelet interactions in patients with ST-elevation myocardial infarction. *Journal of Thrombosis and Haemostasis*, 10, 1231–1241.
- Zhou, X., Liu, X. L., Ji, W. J., Liu, J. X., Guo, Z. Z., Ren, D., Ma, Y. Q., Zeng, S., Xu, Z. W., Li, H. X., Wang, P. P., Zhang, Z., Li, Y. M., Benefield, B. C., Zawada, A. M., Thorp, E. B., Lee, D. C., & Heine, G. H. (2016). The kinetics of circulating monocyte subsets and monocyte-platelet aggregates in the acute phase of ST-elevation myocardial infarction: associations with 2-year cardiovascular events. *Medicine*, 95, 1–9.
- Van der Laan, A. M., Hirsch, A., Robbers, L. F., Nijveldt, R., Lommerse, I., Delewi, R., van der Vleuten, P. A., Biemond, B. J., Zwaginga, J. J., van der Giessen, W. J., Zijlstra, F., van Rossum, A. C., Voermans, C., van der Schoot, C. E., & Piek, J. J. (2012). A proinflammatory monocyte response is associated with myocardial injury and impaired functional outcome in patients with ST-segment elevation myocardial infarction. *American Heart Journal*, 163, 57–65.
- Izquierdo, M., Ruiz-Granell, R., Bonanad, C., Chaustre, F., Gomez, C., Ferrero, A., Lopez-Lereu, P., Monmeneu, J. V., Nuñez, J., Chorro, F. J., & Bodi, V. (2013). Value of early cardiovascular magnetic resonance for the prediction of adverse arrhythmic cardiac

- events after a first noncomplicated ST-segment-elevation myocardial infarction. *Circulation. Cardiovascular Imaging*, 6, 755–761.
9. Fernández-Armenta, J., Berruzo, A., Andreu, D., Camara, O., Silva, E., Serra, L., Barbarito, V., Carotenutto, L., Evertz, R., Ortiz-Pérez, J. T., De Caralt, T. M., Perea, R. J., Sitges, M., Mont, L., Frangi, A., & Brugada, J. (2013). Three-dimensional architecture of scar and conducting channels based on high resolution ce-CMR: insights for ventricular tachycardia ablation. *Circulation. Arrhythmia and Electrophysiology*, 6, 528–537.
  10. Estner, H. L., Zviman, M. M., Herzka, D., Miller, F., Castro, V., Nazarian, S., Ashikaga, H., Dori, Y., Berger, R. D., Calkins, H., Lardo, A. C., & Halperin, H. R. (2011). The critical isthmus sites of ischemic ventricular tachycardia are in zones of tissue heterogeneity, visualized by magnetic resonance imaging. *Heart Rhythm*, 8, 1942–1949.
  11. Penela, D., Acosta, J., Andreu, D., Ortiz-Perez, J. T., Bosch, X., Perea, R. J., de Caralt, T. M., Fernández-Armenta, J., Soto-Iglesias, D., Prat-Gonzalez, S., Borrás, R., Mont, L., Hervas, V., Morales-Ruiz, M., Jiménez, W., Mira, A., Donnelly, J., Ekinci, O., Lasalvia, L., & Berruzo, A. (2017). Identification of the potentially arrhythmogenic substrate in the acute phase of ST-segment elevation myocardial infarction. *Heart Rhythm*, 14, 592–598.
  12. Leuschner, F., Rauch, P. J., Ueno, T., Gorbатов, R., Marinelli, B., Lee, W. W., Dutta, P., Wei, Y., Robbins, C., Iwamoto, Y., Sena, B., Chudnovskiy, A., Panizzi, P., Keliher, E., Higgins, J. M., Libby, P., Moskowitz, M. A., Pittet, M. J., Swirski, F. K., Weissleder, R., & Nahrendorf, M. (2012). Rapid monocyte kinetics in acute myocardial infarction are sustained by extramedullary monocytopoiesis. *The Journal of Experimental Medicine*, 209, 123–137.
  13. Selimoglu-Buet, D., Wagner-Ballon, O., Saada, V., Bardet, V., Itzykson, R., Bencheikh, L., Morabito, M., Met, E., Debord, C., Benayoun, E., Nloga, A. M., Fenaux, P., Braun, T., Willekens, C., Quesnel, B., Adès, L., Fontenay, M., Rameau, P., Droin, N., Koscielny, S., Solary, E., & Francophone Myelodysplasia Group. (2015). Characteristic repartition of monocyte subsets as a diagnostic signature of chronic myelomonocytic leukemia. *Blood*, 125, 3618–3626.
  14. Picot, T., Aanei, C. M., Flandrin Gresta, P., Noyel, P., Tondeur, S., Tavernier Tardy, E., Guyotat, D., & Campos, C. L. (2018). Evaluation by flow cytometry of mature monocyte subpopulations for the diagnosis and follow-up of chronic myelomonocytic leukemia. *Frontiers in Oncology*, 8, 109.
  15. Hidraj, D., Vorselaars, A. D., Grutters, J. C., Claessen, A. M., & Rijkers, G. T. (2012). Differential expression of TNFR1 (CD120a) and TNFR2 (CD120b) on subpopulations of human monocytes. *J Inflamm (Lond)*, 9, 38.
  16. Fendl, B., Weiss, R., Eichhorn, T., Spittler, A., Fischer, M. B., & Weber, V. (2019). Storage of human whole blood, but not isolated monocytes, preserves the distribution of monocyte subsets. *Biochemical and Biophysical Research Communications*, 517, 709–714.
  17. Meldrum, D. R. (1998). Tumor necrosis factor in the heart. *The American Journal of Physiology*, 274, R577–R595.
  18. Ruparelia, N., Godec, J., Lee, R., Chai, J. T., Dall'Armellina, E., McAndrew, D., Digby, J. E., Forfar, J. C., Prendergast, B. D., Kharbanda, R. K., Banning, A. P., Neubauer, S., Lygate, C. A., Channon, K. M., Haining, N. W., & Choudhury, R. P. (2015). Acute myocardial infarction activates distinct inflammation and proliferation pathways in circulating monocytes, prior to recruitment, and identified through conserved transcriptional responses in mice and humans. *European Heart Journal*, 36, 1923–1934.
  19. Miragoli, M., Gaudesius, G., & Rohr, S. (2006). Electronic modulation of cardiac impulse conduction by myofibroblasts. *Circulation Research*, 98, 801–810.
  20. Xuan, W., Liao, Y., Chen, B., Huang, Q., Xu, D., Liu, Y., Bin, J., & Kitakaze, M. (2011). Detrimental effect of fractalkine on myocardial ischaemia and heart failure. *Cardiovascular Research*, 92, 385–393.
  21. Rosen, M. R., Myerburg, R. J., Francis, D. P., Cole, G. D., & Marbán, E. (2014). Translating stem cell research to cardiac disease therapies: pitfalls and prospects for improvement. *Journal of the American College of Cardiology*, 64, 922–937.

**Publisher's Note** Springer Nature remains neutral with regard to jurisdictional claims in published maps and institutional affiliations.



## INTRODUCTION

Monocytes constitute a critical component of the innate immune response to inflammation. Three subsets have been described in humans: classical CD14<sup>++</sup>CD16<sup>-</sup> monocytes (CLM), intermediate CD14<sup>++</sup>CD16<sup>+</sup> (INTM), and non-classical CD14<sup>+</sup>CD16<sup>++</sup> (Non-CLM). Monocyte subsets have been shown to contribute to scar formation in specific ways and in a sequential form in a mice model of acute myocardial infarction (AMI). (1) Ly-6Chigh monocytes, which correspond to CLM in humans, predominate at the site of injury on days 1 to 4 after MI (phase 1) and scavenge necrotic debris by a combination of inflammatory mediator expression, proteolysis, and phagocytosis. Ly-6Clow monocytes, which correspond to Non-CLM in humans, prevail from day 4 onward (phase 2), and contribute to angiogenesis and fibrosis, propagating repair. (1) It has been suggested that wound healing is delayed if the infarct recruits insufficient numbers of monocytes, because debris is neither cleared nor replaced with granulation tissue and collagen matrix. (1) On the other hand, a prolonged immune response from Ly-6Chigh monocytes can initiate inflammatory cascades and drive autoimmunity, resulting in further tissue damage. (2) Although extensive experimental research has been performed on the role of monocyte subsets in atherosclerosis and myocardial infarction, few clinical studies have been performed in humans on their different contribution to the process of scar formation after AMI, (3-7) especially on the role of INTM and Non-CLM.

Infarct size, as assessed with late gadolinium enhancement cardiac magnetic resonance (LGE-CMR), is an independent predictor of arrhythmic events in patients with AMI. (8) In addition, LGE-CMR can provide accurate 3D information about scar architecture, allowing the identification of core scar (CO), border zone (BZ), and BZ channels. (9) These BZ

channels have a reasonably high correlation with conducting channels in the electroanatomic maps obtained during ventricular tachycardia substrate ablation procedures (9) and are related with the ventricular tachycardia isthmuses. (10)

The aim of the present study was to determine the temporal evolution of blood levels of monocyte subsets up to 7 days after a ST-segment elevation AMI (STEMI), and their role in left ventricular remodeling and the formation of the scar and its potentially arrhythmogenic substrate.

## **METHODS**

### **Patients**

Inclusion criteria were patients admitted to our institution with a first STEMI and treated with primary percutaneous coronary intervention (PCI) within the first 12 hours from symptom onset. Exclusion criteria were early death (within the first week), concomitant structural heart disease, life expectancy <1 year due to non-cardiac pathology, other underlying inflammatory or fibrotic pathologies affecting major organs (e.g., liver, kidney, and lung), persistent contraindication for LGE-CMR (metallic prosthesis, claustrophobia, or GFR <30ml/min/1.73m<sup>2</sup>) or for its use within the first week after STEMI (e.g., due to mechanical ventilation or hemodynamic instability).

PCI was performed by experienced on-call interventional cardiologists following unfractionated heparin, aspirin, and a loading dose of clopidogrel. At the physician's discretion and unless contraindicated, enalapril, bisoprolol, and high-dose atorvastatin were initiated early, usually by 24 hours from admission. Baseline characteristics and clinical

data were prospectively collected in all cases. The study complied with the Declaration of Helsinki, and the local Ethics Committee (Clinical Research Ethics Committee of the Hospital Clínic de Barcelona; CEIC Hospital Clínic) approved the study protocol. All participants included in the study provided informed written consent.

## **Laboratory measurements**

### ***Monocyte subpopulations***

Peripheral venous blood was collected at days 1, 3, and 7 after STEMI and processed by flow cytometry within 60 min. Samples of 100  $\mu$ L of blood were incubated with a combination of CD64-FITC (fluorescein isothiocyanate), CD16-PE (Phycoerythrin), CD45 PerCP (Peridinin Chlorophyll Protein) and CD14-APC (Allophycocyanin), all from BD Biosciences (San Jose, CA), for 15 minutes, followed by lysis of red cells with FACS Lysing solution (BD Biosciences) and an additional wash with phosphate-buffered saline. At least 50,000 cells of the stained sample were acquired in a FACS Canto II flow cytometer (BD Biosciences). Samples were analyzed with Infinicyt software (Cytognos, Salamanca, Spain). Monocytes were selected based on forward (FSC) and side (SSC) scatter characteristics and CD45 and CD64 expression. (Supplementary Figure S1) Once selected, the percent of monocytes from the total leukocytes, and the percent of each monocyte subpopulation (CD14<sup>++</sup>CD16<sup>-</sup>, CD14<sup>++</sup>CD16<sup>+</sup>, and CD14<sup>+</sup>CD16<sup>++</sup>) were obtained. The absolute numbers of monocytes and their subpopulations was calculated using the values of total leukocytes of the same sample.

### ***Biomarkers***

Troponin I (TnI), brain natriuretic peptide (BNP), tumor necrosis factor  $\alpha$  (TNF- $\alpha$ ), matrix metalloproteinase-1 (MMP-1), MMP-2, MMP-9, TIMP-1, beta-C-terminal telopeptide (CITP), and interleukins IL-1 $\beta$ , IL-6, and IL-10 were processed and quantified as described in the Online Supplementary Material.

### **LGE-CMR processing**

LGE-CMR examinations were performed at 7 days and 6 months after STEMI using a 3-T scanner (Magnetom Trio<sup>®</sup>, Siemens Healthcare, Erlangen, Germany). Image acquisition is summarized in the Online Supplementary Material. All LGE-CMR images were analyzed using a previously described technique. (11) In brief, full left ventricular (LV) volume was reconstructed in the axial orientation and the resulting images were processed with ADAS-VT software (Galgo Medical, Barcelona, Spain). Five concentric surface layers (10%, 25%, 50%, 75%, 90%) were created automatically from endocardium to epicardium of the LV wall thickness. A 3D shell was obtained for each layer. Pixel signal intensity maps obtained from LGE-CMR images were projected to each shell following a trilinear interpolation algorithm and color-coded. To identify the scar areas, a pixel signal intensity-based algorithm was applied to characterize the hyperenhanced area as CO or BZ, using  $40 \pm 5\%$  and  $60 \pm 5\%$  of the maximum intensity as thresholds. Thus, BZ defined by LGE-CMR is an area of the infarct with an intermediate degree of fibrosis with a patient-specific distribution and does not correspond with the anatomical border of the infarct.

### **Myocardial scar characterization**

Two independent investigators analyzed the LGE-CMR images, and a third observer was available in case of discrepancy. The scar mass and areas in each shell (total scar, CO, and BZ) were automatically measured using ADAS-VT software. The BZ channels were defined as continuous corridors of BZ (with the prespecified pixel signal intensity threshold) surrounded by scar core/mitral annulus. A corridor of BZ was considered a channel when connecting 2 areas of normal myocardium. If a given channel was identified at the same location and with the same orientation in adjacent layers, it was considered as a single multilayer channel (Figure 1). When BZ channels into a given scar were identified, the scar was considered potentially arrhythmogenic since they highly correlate with conducting channels in electroanatomic maps. (12) These channels are responsible for slow conduction, a necessary component of re-entry, and have been shown to act as ventricular tachycardia isthmus. (10)

As tissue characterization is based on a pixel signal intensity algorithm, normal myocardium cannot be distinguished from areas showing “no reflow” phenomenon; both areas have no hyperenhancement and a very low-intensity signal. Therefore, in 11 patients with no-reflow no attempt was made to identify BZ channels in the 7-day LGE-CMR study, although they were identified at the 6-month follow-up.

### **Statistical Analysis**

Continuous variables are given as mean value  $\pm$  SD and were compared using Student t test or Mann-Whitney U test, according to the data distribution (Student t test for normal distributed data and Mann-Whitney U test for non-parametric data). Categorical variables are given as total number and percentages. Bivariate correlations were performed using

Spearman and Pearson correlation coefficients, according to the data distribution. Since all the data were analyzed at three specific time points (1, 3 and 7 days after MI), a mixed linear model for multiple measurements was used to test for time-dependent changes of total number of monocytes and their subsets, as well as for biomarker levels. The same analysis was used for the comparisons between monocyte subsets and scar characteristics. A P-value <0.05 was considered significant. Statistical analysis was performed using R software for Windows version 3.3.0 (R project for statistical computing, Vienna, Austria).

## **RESULTS**

### **Patients**

Of the 140 eligible participants, 102 were finally included and formed the study population (Figure 2). A 7-day LGE-CMR was performed in all patients, although 4 studies had poor image quality and 11 patients showed severe no-reflow phenomenon that precluded tissue characterization and BZ channel identification. At 6-month follow-up, LGE-CMR was performed in 95 patients and tissue characterization in 89 patients.

Clinical baseline characteristics of the 102 patients are reported in Table 1. Median time to reperfusion was 170 (IQR: 160) minutes. Most STEMI were caused by left anterior descending coronary artery thrombosis (48%). The scar mass decreased from  $22 \pm 19$  g at 7 days to  $14 \pm 12$  g at 6 months, while LVEF increased from  $46 \pm 10\%$  to  $51 \pm 10\%$  respectively. BZ channels were identified in 52 of 83 patients at day 7 and in 53 of 89 patients at 6 months.

### **Time course of monocyte subset levels**

CLM levels decreased from  $670 \pm 271$  cells/ $\mu$ L at day 1 to  $607 \pm 250$  cells/ $\mu$ L at day 3, and to  $528 \pm 211$  cells/ $\mu$ L at day 7 ( $p < 0.001$  for global changes and  $p < 0.01$  for differences between days 1 to 3, and days 3 to 7), (Figure 3). CLM represented, respectively, 91.8%, 91.1% and 91.7% of total monocytes at days 1, 3, and 7 ( $p = 0.99$  for all comparisons). INTM levels also progressively decreased from days 1 and 3 to day 7 ( $44 \pm 44$  to  $41 \pm 32$  to  $28 \pm 23$  cells/ $\mu$ L, respectively;  $p < 0.001$  for global changes and  $p < 0.01$  from day 1 to day 7, and day 3 to day 7). INTM represented, respectively, 6.0%, 6.2% and 4.9% of total monocytes at days 1, 3, and 7 ( $p = 0.99$  for differences between days 1 to 3, and  $p = 0.92$  for days 3 to 7). Conversely, Non-CLM levels increased progressively from  $16 \pm 14$  to  $18 \pm 18$  to  $20 \pm 20$  cells/ $\mu$ L at days 1, 3 and 7 post-STEMI ( $p = 0.04$  for global changes). Non-CLM represented, respectively, 2.2%, 2.7% and 3.5% of total monocytes at days 1, 3, and 7 ( $p = 0.95$  for differences between days 1 to 3, and  $p = 0.94$  for days 3 to 7).

### **Monocyte subsets and biomarkers**

The temporal changes in circulating biomarkers are depicted in Supplementary Figure S2. IL-6 levels decreased from days 1 and 3 to day 7 ( $p < 0.001$ ), paralleling the circulating dynamics of CLM and INTM, while TNF- $\alpha$ , MMP-1, MMP-2, MMP-9, and TIMP-1 levels increased progressively from day 1 to day 7.

The correlation coefficients observed between the circulating levels of monocyte subsets and biomarkers differed not only according to each monocyte subset and biomarker but also by the specific time since STEMI (Supplementary Figure S3). CLM and INTM followed a similar pattern and significantly correlated with pro-inflammatory biomarkers during days 1

to 3, especially with IL-6, TNF- $\alpha$ , and CRP. These associations extended to day 7, although to a lesser degree. They also significantly correlated with markers of extracellular matrix degradation during days 1 to 7: CLM with MMP-9 and TIMP-1, and INTM with MMP-2 and MMP-9. On the other hand, the reparative Non-CLM also was directly correlated with pro-inflammatory biomarkers during days 1 and 3, and with MMP-1, MMP-2, and TIMP-1.

### **Association with left ventricular volumes and ejection fraction**

Peak levels of CLM directly correlated with left ventricular (LV) volumes at day 7, both for end-diastolic volume (LVEDV), ( $r = 0.21$ ,  $p = 0.04$ ), and LV end-systolic volume (LVESV), ( $r = 0.33$ ,  $p = 0.001$ ), resulting in an inverse correlation with LVEF ( $r = -0.30$ ,  $p = 0.003$ ) that was also observed at 6 months ( $r = -0.31$ ,  $p = 0.002$ ). Interestingly, peak INTM levels also inversely correlated with LV ejection fraction (LVEF) at 7 days ( $r = -0.26$ ,  $p = 0.01$ ) and at 6 months ( $r = -0.27$ ,  $p < 0.01$ ). In contrast, no significant correlations were found between Non-CLM levels and LVEDV, LVESV or LVEF.

### Monocyte subsets and scar characteristics

Blood levels of monocyte subsets were directly correlated with scar mass and its parts, the CO and BZ, as evaluated by LGE-CMR at 7 days. However, the degree of association was different for every monocyte subset and zone. Thus, while CLM and INTM levels were directly, strongly, and uniformly associated with CO and BZ mass, Non-CLM levels were exclusively associated with the BZ mass (Table 2). Similar although less marked results were obtained at 6 months.



Interestingly, although the BZ mass was directly associated with all monocyte subsets, the presence of BZ channels was strongly associated only with Non-CLM levels, both at 7 days and at 6 months (Table 2 and Figure 1). Compared to patients without BZ channels, patients with BZ channels had uniformly higher levels of Non-CLM during the first 7 days after STEMI (Figure 4), higher peak Tn I ( $134 \pm 118$  IU/L vs.  $91 \pm 188$  IU/L,  $p < 0.01$ ), higher BZ mass, and lower LVEF at 6 months ( $50 \pm 9\%$  vs.  $55 \pm 9\%$ ,  $p < 0.05$ ). No differences between patients with and without arrhythmogenic scar were found for other clinical characteristics, MI location, or time to reperfusion ( $235 \pm 185$  min vs.  $215 \pm 188$  min,  $p = 0.39$ ).

## **DISCUSSION**

This study is the first to analyze the role of circulating monocyte subsets in the process of scar formation after AMI and their relationship with differential tissue characteristics using 3-T LGE-CMR at 7 days and 6 months. Two main findings have been showed: CLM and INTM had a similar pattern of blood kinetics and of association with inflammatory biomarkers, and both were directly associated with infarct size and inversely with LVEF. In contrast, Non-CLM showed different blood kinetics and were strongly associated with the scar BZ and with its potentially arrhythmogenic distribution, creating BZ channels.

Early after MI, monocytes are rapidly released by the splenic reservoir and are rapidly recruited by the ischemic myocardium, matched by rapid ( $< 24$  hours) cell death. (13) In accordance with these observations and other reports, (5,6) we found that CLM and INTM showed similar kinetics with a peak on day 1 and a progressive decrease at day 3 and day 7. Although the progressive increase in the circulating levels of Non-CLM from days 1 to 7

after MI has not been observed in other clinical studies, (5,6) our results are in agreement with experimental studies on Ly-6Clow monocytes/macrophage showing a progressive increase from baseline, with a peak on day 7 after MI. (1) Nevertheless, it should be noted that the total number of monocytes and their subpopulations remained within what is considered the normal range throughout the study. (14-17)

### **Association between monocyte subsets and serum biomarkers**

We found that all monocyte subsets were associated with pro-inflammatory biomarkers during phase 1, suggesting that all of them may have pro-inflammatory effects during this phase, (13) in accordance with experimental work reporting that Ly-6Chigh monocytes have proteolytic and inflammatory functions, whereas Ly-6Clow have also attenuated inflammatory and proangiogenic properties. (1) In this regard, IL-6, which is involved in the inflammatory injury, progressively decreases as local post-STEMI inflammation does (Supplementary Figure S2). CLM and INTM were also associated with MMP-9 from day 1 to day 7 after STEMI, and Non-CLM were associated with MMP-1, and MMP-2, markers of extracellular matrix degradation, suggesting that the protease activity involved in the process of extracellular matrix remodeling may continue during the reparative phase 2. In fact, these MMPs showed a progressive increase during the first days after the STEMI (Supplementary Figure S2).

The levels of CLM and INTM significantly correlated with the serum concentrations of TNF- $\alpha$ . This could be justified since TNF- $\alpha$  is an autocrine contributor to myocardial dysfunction and cardiomyocyte death in ischemia-reperfusion injury, either by direct depression of contractility or by induction of myocyte apoptosis. (18)

**LV remodeling and dysfunction**

Maekawa et al. first reported an association between peak monocyte count and LV volumes and LVEF measured by left contrast ventriculography in patients with AMI, suggesting a possible role of monocytes in the development of LV remodeling after MI. (3) In our study, a strong association was found between CLM levels and LV remodeling within 7 days after STEMI, an effect that remained at 6 months. These results are in agreement with experimental research showing that Ly-6Chigh monocytosis 5 days after AMI disturbs resolution of inflammation and enhances LV remodeling. (2) Previous clinical studies have shown conflicting results. (4,7) In the study by Tsujioka et al. in 30 patients with STEMI, peak levels of CLM were not inversely correlated with basal or 6-month LVEF but with the change in LVEF. (4) The small sample of patients may explain these results. On the other hand, van der Laan et al. also found an association between CLM levels 5 days post-AMI and LVEF. (7) We also observed an inverse correlation between circulating levels of INTM and LVEF at 7 days and 6 months after STEMI, a finding not previously reported. The strong similarities of these two monocyte subsets in phenotype, circulating dynamics, interleukin expression, proinflammatory effects, and transcriptome characteristics also support our results, as INTM seems to be an intermediate stage of differentiation from CLM to Non-CLM.

**Non-classical monocytes and the formation of a potentially arrhythmogenic scar**

Different results have been also reported on the association between blood levels of monocyte subsets and infarct size. (4,7) The present study was the first to assess MI size using 3-T LGE-CMR, and the components of the scar and its tissue characterization at 7 days

and 6 months. The results showed a strong, direct correlation between CLM and INTM levels and infarct size, as previously reported in experimental studies with Ly-6Chigh monocytes. (1,19) In addition, the relationship was uniform for both parts of the scar, the CO and the BZ.

More important, we found for the first time a strong direct association between circulating levels of Non-CLM and the BZ mass, and the formation of an adverse myocardial scar defined as a pro-arrhythmogenic scar with BZ channels. Patients with these scar channels had higher levels of Non-CLM at days 3 and 7, and higher BZ mass than patients without BZ channels, suggesting that high Non-CLM levels may affect or influence infarct healing and result in a pro-arrhythmogenic scar.

These results may have important clinical implications and raise some intriguing hypotheses. Indeed, it has been shown that Ly6Clow macrophages promote transdifferentiation of fibroblasts into secretory and contractile myofibroblasts, and these cells can form electrotonic connections with cardiomyocytes, potentially contributing to arrhythmogenesis. (20) In addition, in an experimental study, mice treated with antibodies towards fractalkine, a mediator for Ly-6Clow infiltration of the myocardium, had smaller infarct size. (21) Thus, decreased recruitment and infiltration of Non-CLM by direct intervention early after STEMI might have favorable effects on infarct healing.

### **Clinical implications**

Further experimental studies at a cellular and molecular level are needed to confirm these results and to provide a mechanistic explanation for each process. Several therapeutic targets and strategies addressing the inflammatory and immune responses after an AMI

have been evaluated. These strategies have tried, for example, to reduce the activity of certain immune cells, such as neutrophils; to inhibit the activity of various inflammatory cytokines using monoclonal antibodies, or to target multiple inflammatory pathways by using stem cells. In this regard, treatment with stem cells, although promising, still faces numerous limitations. (22) A deeper understanding of these mechanisms, for which LGE-CMR constitutes an essential diagnostic tool, may provide a unique opportunity to identify new therapeutic strategies to limit LV remodeling and to modulate the arrhythmogenic substrate early after myocardial infarction.

### **Study limitations**

This was a prospective, observational study. Thus, the results do not provide a mechanistic explanation for the association found between the levels of each monocyte subset and the analyzed biomarkers, LV remodeling, infarct size, and the formation of BZ channels. In addition, our study could not determine whether the blood levels of the three monocyte subsets reflect the extent of their infiltration in the ischemic and necrotic myocardium.

### **Conclusions**

Monocyte subsets have an important role in scar formation early after STEMI. Classical and Intermediate monocyte levels were directly correlated with infarct size and inversely with LVEF. Non-classical monocytes were strongly associated with the scar BZ mass and distribution, thus creating a potentially arrhythmogenic substrate. Further experimental studies at a cellular and molecular level are needed to confirm these results and to provide a mechanistic explanation for each process. A deeper understanding of these mechanisms,

for which LGE-CMR constitutes an essential diagnostic tool, may provide a unique opportunity to identify new therapeutic strategies to limit LV remodeling and to modulate the arrhythmogenic substrate early after myocardial infarction.

## **ACKNOWLEDGEMENTS**

This study was partially supported by Siemens Healthineers GmbH (Dr. Lasalvia).

## **SOURCES OF FUNDING**

This work was supported by Agencia de Gestió d'Ajuts Universitaris i de Recerca (AGAUR), Generalitat de Catalunya [grant number 2014-SGR-471]; Instituto de Salud Carlos III (ISCIII), Centro de Investigación Biomédica en Red: FIS-CIBER16 [grant number CB16/11/00354]; Fondo de Investigación Sanitaria (FIS) [grant numbers PI14/00759, PI17/01968]; and Ministerio de Economía y Competitividad, RETOS [grant numbers RTC-2015-3515-1, RTC-2016-5445-1].

## **DISCLOSURES**

Dr. Berruezo is a stockholder in Galgo Medical SL and has received financial support from Siemens Healthcare. Dr. Lasalvia is a stockholder and employee of Siemens Healthcare. The other authors have no other relevant affiliations or financial involvement with any organization or entity with a financial interest in or financial conflict with the subject matter or materials discussed in the manuscript apart from those disclosed.

**REFERENCES**

1. Nahrendorf M, Swirski FK, Aikawa E, Stangenberg L, Wurdinger T, Figueiredo JL, Libby P, Weissleder R, Pittet MJ. The healing myocardium sequentially mobilizes two monocyte subsets with divergent and complementary functions. *J Exp Med* 2007;204:3037-3047.
2. Panizzi P, Swirski FK, Figueiredo JL, Waterman P, Sosnovik DE, Aikawa E, Libby P, Pittet M, Weissleder R, Nahrendorf M. Impaired infarct healing in atherosclerotic mice with Ly-6C(hi) monocytosis. *J Am Coll Cardiol* 2010;55:1629-1638.
3. Maekawa Y, Anzai T, Yoshikawa T, Asakura Y, Takahashi T, Ishikawa S, Mitamura H, Ogawa S. Prognostic significance of peripheral monocytosis after reperfused acute myocardial infarction: a possible role for left ventricular remodeling. *J Am Coll Cardiol* 2002;39:241-246.
4. Tsujioka H, Imanishi T, Ikejima H, Kuroi A, Takarada S, Tanimoto T, Kitabata H, Okochi K, Arita Y, Ishibashi K, Komukai K, Kataiwa H, Nakamura N, Hirata K, Tanaka A, Akasaka T. Impact of heterogeneity of human peripheral blood monocyte subsets on myocardial salvage in patients with primary acute myocardial infarction. *J Am Coll Cardiol* 2009;54:130-138.
5. Tapp LD, Shantsila E, Wrigley BJ, Pamukcu B, Lip GY. The CD14<sup>++</sup>CD16<sup>+</sup> monocyte subset and monocyte-platelet interactions in patients with ST-elevation myocardial infarction. *J Thromb Haemost* 2012;10:1231-1241.
6. Zhou X, Liu XL, Ji WJ, Liu JX, Guo ZZ, Ren D, Ma YQ, Zeng S, Xu ZW, Li HX, Wang PP, Zhang Z, Li YM, Benefield BC, Zawada AM, Thorp EB, Lee DC, Heine GH. The kinetics of circulating monocyte subsets and monocyte-platelet aggregates in the acute phase of ST-

elevation myocardial infarction: Associations with 2-year cardiovascular events. *Medicine* 2016;95:1-9.

7. Van der Laan AM, Hirsch A, Robbers LF, Nijveldt R, Lommerse I, Delewi R, van der Vleuten PA, Biemond BJ, Zwaginga JJ, van der Giessen WJ, Zijlstra F, van Rossum AC, Voermans C, van der Schoot CE, Piek JJ. A proinflammatory monocyte response is associated with myocardial injury and impaired functional outcome in patients with ST-segment elevation myocardial infarction. *Am Heart J* 2012;163:57-65.

8. Izquierdo M, Ruiz-Granell R, Bonanad C, Chaustre F, Gomez C, Ferrero A, Lopez-Lereu P, Monmeneu JV, Nuñez J, Chorro FJ, Bodi V. Value of early cardiovascular magnetic resonance for the prediction of adverse arrhythmic cardiac events after a first noncomplicated ST-segment-elevation myocardial infarction. *Circ Cardiovasc Imaging* 2013;6:755-761.

9. Fernández-Armenta J, Berruezo A, Andreu D, Camara O, Silva E, Serra L, Barbarito V, Carotenutto L, Evertz R, Ortiz-Pérez JT, De Caralt TM, Perea RJ, Sitges M, Mont L, Frangi A, Brugada J. Three-dimensional architecture of scar and conducting channels based on high resolution ce-CMR: insights for ventricular tachycardia ablation. *Circ Arrhythm Electrophysiol* 2013;6:528-537.

10. Estner HL, Zviman MM, Herzka D, Miller F, Castro V, Nazarian S, Ashikaga H, Dori Y, Berger RD, Calkins H, Lardo AC, Halperin HR. The critical isthmus sites of ischemic ventricular tachycardia are in zones of tissue heterogeneity, visualized by magnetic resonance imaging. *Heart Rhythm* 2011;8:1942-1949.

12. Penela D, Acosta J, Andreu D, Ortiz-Perez JT, Bosch X, Perea RJ, de Caralt TM, Fernández-Armenta J, Soto-Iglesias D, Prat-Gonzalez S, Borràs R, Mont L, Hervas V, Morales-



Ruiz M, Jiménez W, Mira A, Donnelly J, Ekinci O, Lasalvia L, Berruezo A. Identification of the potentially arrhythmogenic substrate in the acute phase of ST-segment elevation myocardial infarction. *Heart Rhythm* 2017;14:592-598.

13. Leuschner F, Rauch PJ, Ueno T, Gorbatov R, Marinelli B, Lee WW, Dutta P, Wei Y, Robbins C, Iwamoto Y, Sena B, Chudnovskiy A, Panizzi P, Keliher E, Higgins JM, Libby P, Moskowitz MA, Pittet MJ, Swirski FK, Weissleder R, Nahrendorf M. Rapid monocyte kinetics in acute myocardial infarction are sustained by extramedullary monocytopoiesis. *J Exp Med* 2012;209:123-137.

14. Selimoglu-Buet D, Wagner-Ballon O, Saada V, Bardet V, Itzykson R, Bencheikh L, Morabito M, Met E, Debord C, Benayoun E, Nloga AM, Fenaux P, Braun T, Willekens C, Quesnel B, Adès L, Fontenay M, Rameau P, Droin N, Koscielny S, Solary E; Francophone Myelodysplasia Group. Characteristic repartition of monocyte subsets as a diagnostic signature of chronic myelomonocytic leukemia. *Blood* 2015;125:3618-3626.

15. Picot T, Aanei CM, Flandrin Gresta P, Noyel P, Tondeur S, Tavernier Tardy E, Guyotat D, Campos Catafal L. Evaluation by Flow Cytometry of Mature Monocyte Subpopulations for the Diagnosis and Follow-Up of Chronic Myelomonocytic Leukemia. *Front Oncol* 2018;8:109.

16. Hidraj D, Vorselaars AD, Grutters JC, Claessen AM, Rijkers GT. Differential expression of TNFR1 (CD120a) and TNFR2 (CD120b) on subpopulations of human monocytes. *J Inflamm (Lond)* 2012;9:38.

17. Fendl B, Weiss R, Eichhorn T, Spittler A, Fischer MB, Weber V. Storage of human whole blood, but not isolated monocytes, preserves the distribution of monocyte subsets. *Biochem Biophys Res Commun* 2019;517:709-714.

18. Meldrum DR. Tumor necrosis factor in the heart. *Am J Physiol* 1998;274:R577-595.
19. Ruparelia N, Godec J, Lee R, Chai JT, Dall'Armellina E, McAndrew D, Digby JE, Forfar JC, Prendergast BD, Kharbanda RK, Banning AP, Neubauer S, Lygate CA, Channon KM, Haining NW, Choudhury RP. Acute myocardial infarction activates distinct inflammation and proliferation pathways in circulating monocytes, prior to recruitment, and identified through conserved transcriptional responses in mice and humans. *Eur Heart J* 2015;36:1923-1934.
20. Miragoli M, Gaudesius G, Rohr S. Electrotonic modulation of cardiac impulse conduction by myofibroblasts. *Circ Res* 2006;98:801-810.
21. Xuan W, Liao Y, Chen B, Huang Q, Xu D, Liu Y, Bin J, Kitakaze M. Detrimental effect of fractalkine on myocardial ischaemia and heart failure. *Cardiovasc Res* 2011;92:385-393.
22. Rosen MR, Myerburg RJ, Francis DP, Cole GD, Marbán E. Translating stem cell research to cardiac disease therapies: pitfalls and prospects for improvement. *J Am Coll Cardiol* 2014;64:922-937.

**TABLES****Table 1.** Characteristics of the studied population.

Age, years	58±11
Sex, female	18 (18)
Coronary risk factors	
Present smoker	51 (50)
Hypertension	42 (41)
Hypercholesterolemia	25 (25)
Diabetes mellitus	13 (13)
Site of MI: anterior	48 (47)
Peak Troponin I, IU/l	128±150
Killip class ≥ 2	9 (9)
Serum creatinine, mg/dl	0.95±0.22
Leucocytes, cells/ $\mu$ l	10,849±2,893
Monocytes, cells/ $\mu$ l	729±302
Prior treatment	
ACE-i/ARB	23 (23)
Beta blockers	4 (4)
Statins	21 (21)
CMR at 7 days	
LVEF, %	46±10
Scar mass, g	22±19
CO mass, g	11±10
BZ mass, g	12±10
CMR at 6 months	
LVEF, %	51±10
Scar mass, g	14±12
CO mass, g	7±6
BZ mass, g	8±7

Values are means  $\pm$  SD or n (%). ACE-I: Angiotensin-converting enzyme inhibitors; ARB: Angiotensin receptor blockers; BZ: Scar border zone; CO: Scar core; LVEF: Left ventricular ejection fraction.

**Table 2.** Parameter estimation from the lineal model of the association between each monocyte subset and the scar mass and its components at 7 days and 6 months after myocardial infarction.

	Scar		Core zone		Border zone		Border zone Channels	
	$\beta \pm SE$	P	$\beta \pm SE$	P	$\beta \pm SE$	P	$\beta \pm SE$	P
<b>Results at 7 days</b>								
<b>CLM</b>	0.017 $\pm$ 0.004	0.0001	0.008 $\pm$ 0.002	<0.001	0.009 $\pm$ 0.002	0.0002	0.00003 $\pm$ 0.0003	0.92
<b>INTM</b>	0.118 $\pm$ 0.031	0.0002	0.054 $\pm$ 0.016	0.001	0.064 $\pm$ 0.017	0.0001	0.005 $\pm$ 0.002	0.03
<b>Non-CLM</b>	0.137 $\pm$ 0.063	0.03	0.045 $\pm$ 0.033	0.17	0.091 $\pm$ 0.033	0.006	0.014 $\pm$ 0.004	0.0002
<b>Results at 6 months</b>								
<b>CLM</b>	0.005 $\pm$ 0.003	0.06	0.002 $\pm$ 0.001	0.10	0.003 $\pm$ 0.002	0.05	0.00006 $\pm$ 0.0003	0.82
<b>INTM</b>	0.060 $\pm$ 0.020	0.003	0.021 $\pm$ 0.010	0.03	0.038 $\pm$ 0.011	< 0.001	0.002 $\pm$ 0.002	0.20
<b>Non-CLM</b>	0.062 $\pm$ 0.040	0.13	0.013 $\pm$ 0.020	0.53	0.050 $\pm$ 0.022	0.025	0.012 $\pm$ 0.004	<0.001

CLM: Classical human monocytes (CD14<sup>++</sup>CD16<sup>-</sup>); INTM: Intermediate human monocytes (CD14<sup>++</sup>CD16<sup>+</sup>); Non-CLM: Non-classical human monocytes (CD14<sup>+</sup>CD16<sup>++</sup>).

**FIGURES**

**Figure 1.** Example of myocardial scar in two patients with anterior wall STEMI. Automated representation of a myocardial layer in the wall thickness of the left ventricular reconstruction with a color-coded pixel signal intensity map. Normal myocardium is shown in purple, border zone in green, and the core in red. A: Scar without border zone channels in a patient with low circulating levels of non-classical monocytes. B: Scar in a patient with high levels of non-classical monocytes. In 7-day and 6-month studies, a border zone channel (white line) can be identified in the same myocardial layer and segment, with the same orientation and morphology.

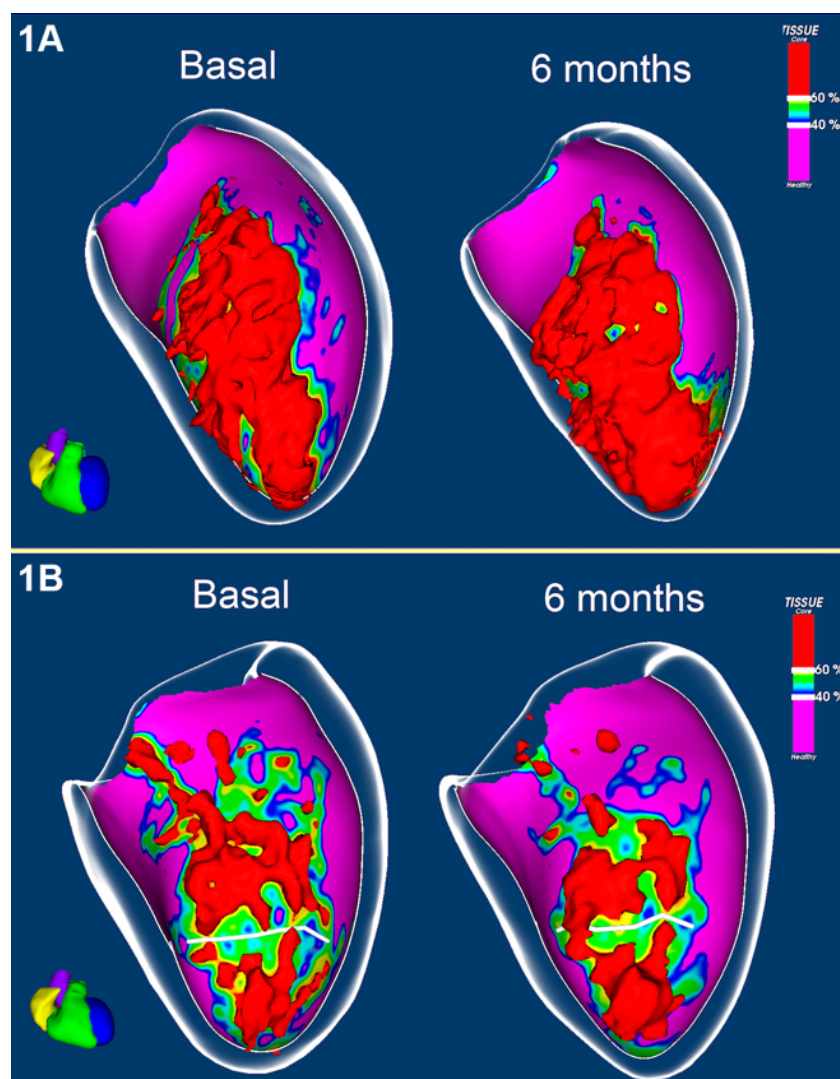


**Figure 2.** Flow-chart of the studied patients. LGE-CMR, late gadolinium enhancement cardiac magnetic resonance.

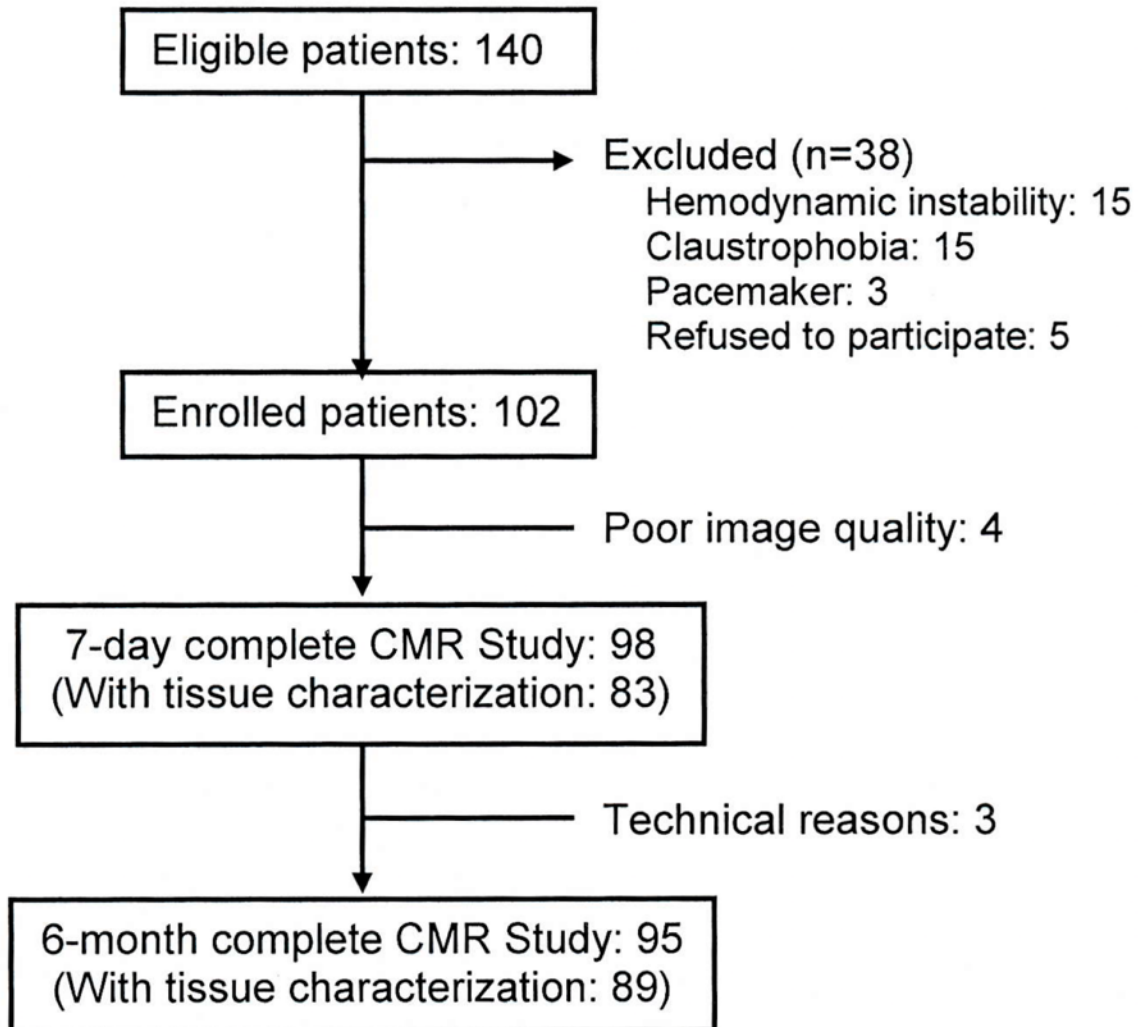


**Figure 3.** Circulating levels of monocyte subsets within the first 7 days after myocardial infarction.

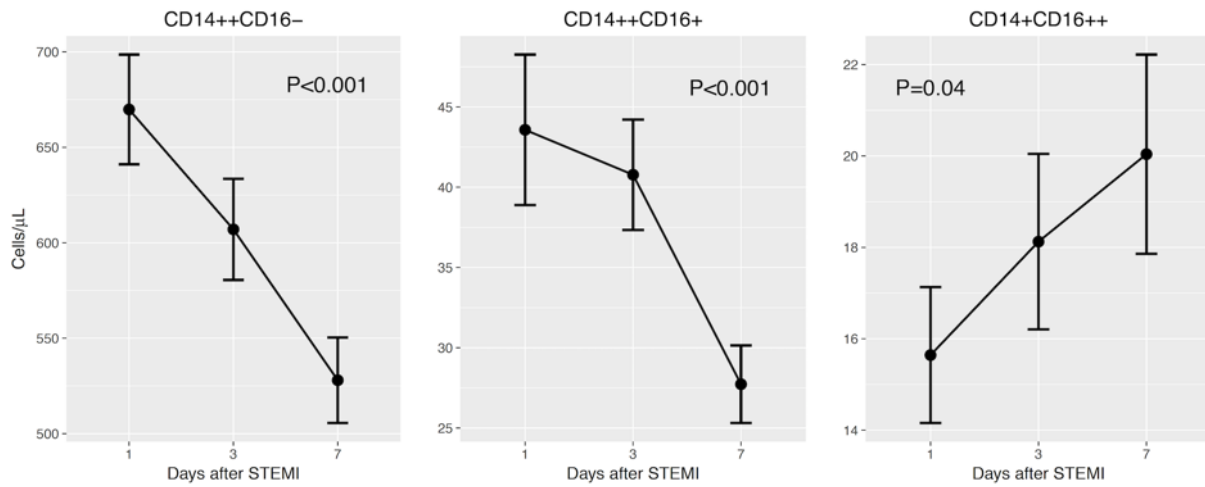
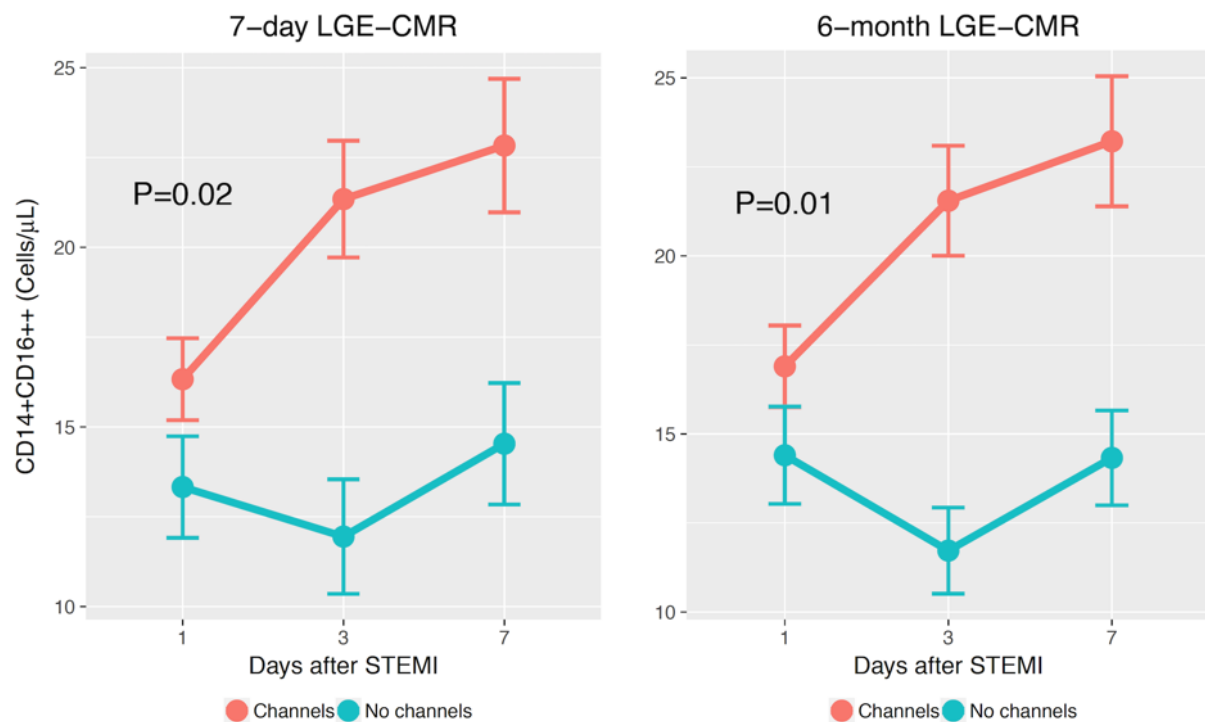


**Figure 4.** Mean (95% CI) blood levels of non-classical monocytes during the first 7 days after myocardial infarction in patients with and without border zone channels at 7-day and 6-month LGE-CMR.



## **SUPPLEMENTARY MATERIAL**

### **METHODS**

#### **Laboratory measurements:**

Blood samples were obtained from study participants at days 1, 3 and 7 after STEMI and collected into plain or heparin/EDTA-coated blood collection tubes. After centrifugation at 3,000 rpm for 15 minutes, serum or plasma samples were stored at -80°C until analysis. Troponin I (TnI) was determined in heparin plasma samples using chemiluminometric immunoassays run on the DIMENSION EXL System (Siemens Healthcare Diagnostics, Tarrytown, NY, USA). Tumor necrosis factor  $\alpha$  (TNF- $\alpha$ ), and interleukins IL-1 $\beta$  and IL-6 were measured in serum samples using an IMMULITE 1000 Immunoassay system (Siemens Healthcare Diagnostics, Tarrytown, NY, USA). Serum matrix metalloproteinase-1 (MMP-1), MMP-2, MMP-9 (Quantikine Human; R&D Systems, Minneapolis, MN), were quantified by manual colorimetric ELISA assays. The intra-assay and inter-assay coefficient of variation were lower than 5% and 10%, respectively, in all cases. All the parameters were measured according to the manufacturer's instructions. Other biochemical and haematological parameters were measured by standard procedures at the Core Laboratory of the Biomedical Diagnostic Centre of the Hospital Clinic of Barcelona.

#### **CMR protocol:**

Short axis cine images encompassing the ventricles and long axis (2-, 3- and 4-chamber views) were acquired using conventional steady-state free precession sequence, during end-expiratory apnea, using retrospective gating, (repetition time 3.1 ms; echo time 1.4 ms;



flip angle 50°; section thickness 6 mm; matrix 208 x 184; field of view 380 x 360 mm<sup>2</sup>; bandwidth, 1335 Hz/px; parallel processing factor (GRAPPA) 2; and number of phases 30). LGE imaging was obtained 10 minutes after a 0.2 mmol/kg intravenous bolus of Gadobutrol (Gadovist®, Bayer Hispania, Barcelona, Spain) applying a standard 2D segmented gradient-echo inversion-recovery sequence (Turbo-FLASH). The inversion time was adjusted for optimal nulling of remote normal myocardium. Sequential 6 mm slices with no gap between them were prescribed to cover both ventricles in the short-axis orientation in addition to the 2-, 3-, and 4-chamber views. Typical parameters were: repetition time 800 ms; echo time 2 ms; flip angle 20°; bandwidth 140 Hz/px; 35–45 k space lines filled every other heartbeat, needing 10–15 heartbeats per slice; parallel processing factor (GRAPPA) 2. The mean in-plane resolution was 1.4 x 1.4 mm, and the voxel size was 11.80 mm<sup>3</sup>.

*Image analysis:*

CMR analysis was performed by an experienced reader. Ventricular volumes and ejection fraction (EF) were calculated on an external workstation (Leonardo, Siemens Medical Solutions, Erlangen, Germany) equipped with a dedicated cardiac post-processing software (Argus, Syngo, Siemens Medical Solutions, Erlangen, Germany). Endocardial end-diastolic and end-systolic borders were manually traced from the stack of contiguous short axis images.

*Myocardial infarct size quantification:*

The infarcted myocardium at baseline and at 180 days was delimited in the delayed-enhanced 2D segmented gradient-echo inversion-recovery sequence (Turbo-FLASH) in all

short-axis slices by using a self-developed customized segmentation tool (TCTK®) as previously described. Infarct mass was computed as infarct volume, the sum of all hyperenhanced voxels, multiplied by the myocardium density and expressed as LV mass.

## SUPPLEMENTARY FIGURES

**Figure S1.** Gating strategy to identify the monocytes subsets. First, gate was drawn in FSC vs. SSC around the leukocytes followed by a gate in SSC vs. CD45 to exclude the remaining debris (plots A and B). For the selection of monocytes, a gate that included cells with intermediate SSC and dim to high CD64 expression was done (plot C). Finally, the monocytes included in the previous gate were plotted for CD14 vs CD16 and the three monocytes subsets were identified according to their expression on both markers (plot D).

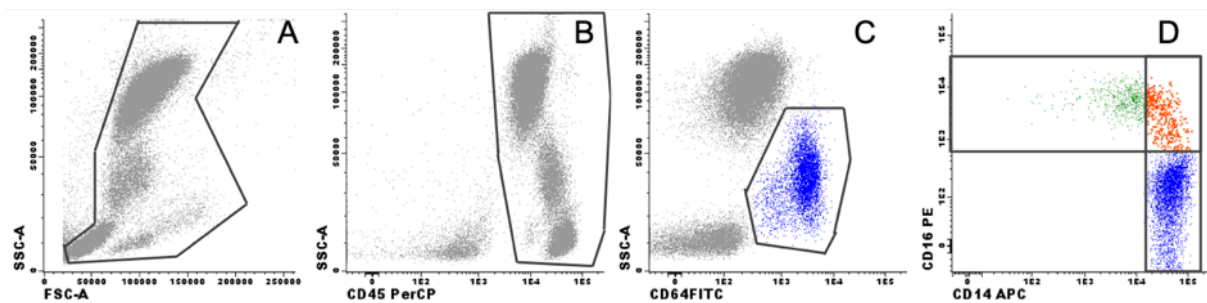


**Figure S2.** Dynamics of biomarkers of inflammation and extracellular matrix degradation.

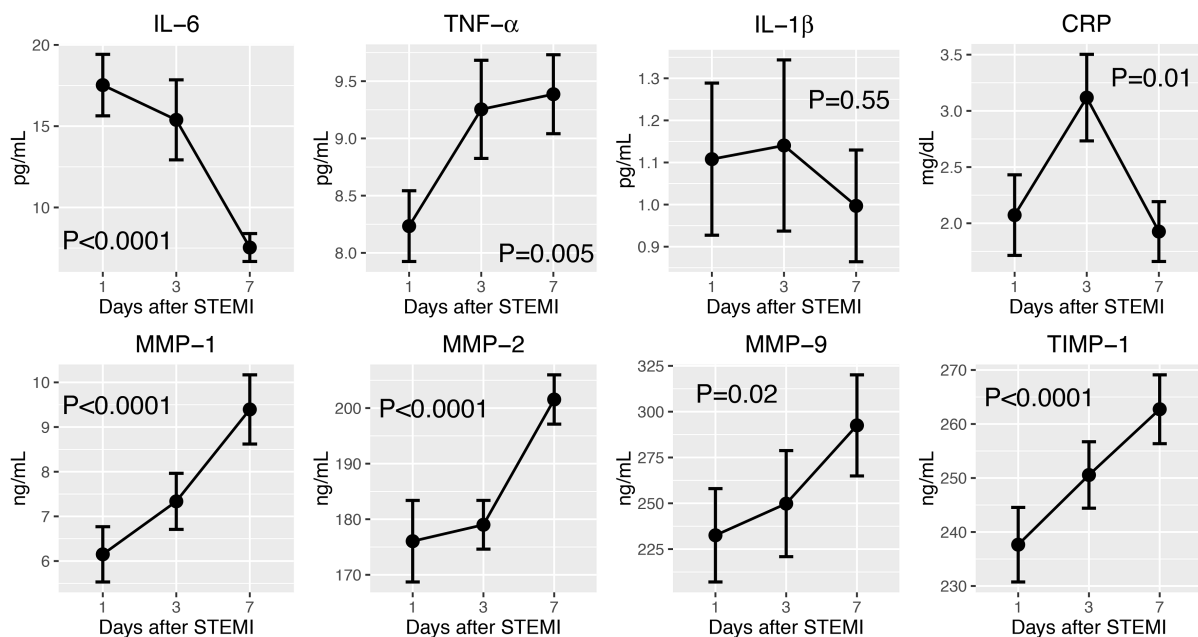
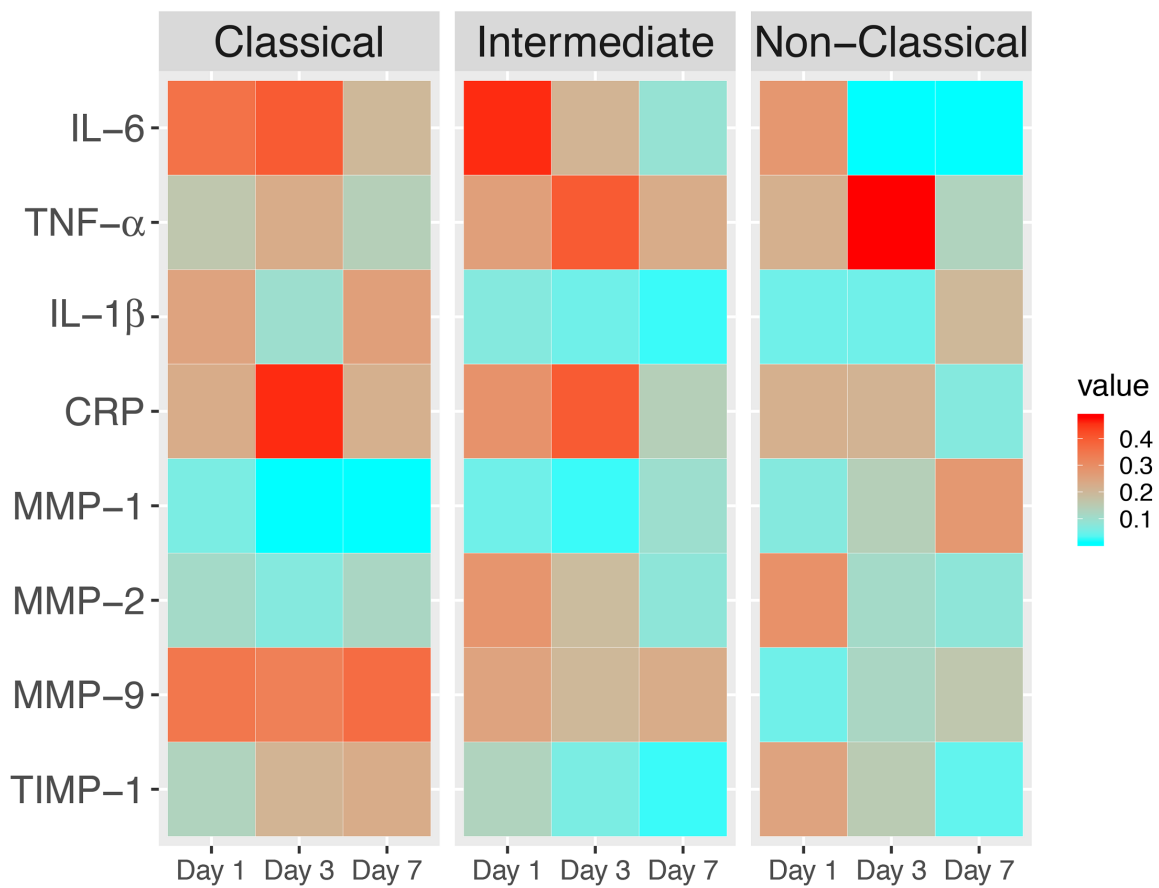


**Figure S3.** Heatmap of the correlation coefficients between levels of each monocyte subset and biomarkers of inflammation and extracellular matrix degradation at each time period after myocardial infarction.  $P < 0.05$  for  $r$  between 0.20 and 0.27;  $p < 0.01$  for  $r$  between 0.28 and 0.33;  $p < 0.001$  for  $r > 0.33$ .





**Artículo 3: Arrhythmogenic substrate detection in chronic ischaemic patients undergoing ventricular tachycardia ablation using multidetector cardiac computed tomography: compared evaluation with cardiac magnetic resonance**

**Jáuregui B**, Soto-Iglesias D, Zucchelli G, Penela D, Ordóñez A, Terés C, Chauca A, Acosta J, Fernández-Armenta J, Linhart M, Perea RJ, Dolta A, Ortiz-Pérez JT, Bosch X, Berruezo A. Arrhythmogenic Substrate Detection in Ischemic Patients Undergoing Ventricular Tachycardia Ablation using Multi-Detector Computed Tomography. Compared Evaluation with Cardiac Magnetic Resonance. *Europace* 2021;23:82-90. **FACTOR DE IMPACTO (2020): 5.214. ÁREA DE CONOCIMIENTO: Cardiology and Cardiovascular Medicine. CUARTIL: Q1.**

El objetivo general del estudio fue investigar el rendimiento general de la tomografía computarizada (TC) para identificar la presencia de sustrato arritmogénico en pacientes con infarto crónico de miocardio, comparado con el rendimiento de la resonancia magnética cardiaca (RMC), técnica de imagen *gold standard*.

## RESUMEN ESTRUCTURADO

**Objetivos:** La resonancia magnética cardíaca con realce tardío de gadolinio (RMC-RTG) permite caracterizar las cicatrices isquémicas, detectando los HTC que constituyen el sustrato arritmogénico. La RM-RTG también mejora la supervivencia libre de arritmias cuando se utiliza para guiar la ablación de sustrato de TV. Sin embargo, su disponibilidad puede ser limitada. Buscamos evaluar el rendimiento de la TAC para identificar los HTC detectados por RM-RTG en pacientes isquémicos sometidos a ablación de sustrato de TV.

**Métodos:** Se incluyeron treinta pacientes isquémicos sometidos tanto a RM-RTG como a TAC antes de la ablación de sustrato de TV. Utilizando un software de post-procesamiento dedicado, dos operadores ciegos, asignados al análisis RM-RTG o TAC, caracterizaron la presencia de canales de RM y de TAC, respectivamente. Los canales de RM se clasificaron como endocárdicos (capas <50%), epicárdicos (capas  $\geq$  50%) o transmurales. Se consideró la concordancia entre los canales de RM y de TAC cuando mostraran la misma orientación y se localizaban en el mismo segmento de la AHA (*American Heart Association*).

**Resultados:** La edad media fue de  $69 \pm 10$  años; El 90% eran hombres. La FEVI media fue de  $35 \pm 10\%$ . Todos los pacientes tenían canales de RMC ( $n = 76$ ), mientras que sólo 26/30 (86,7%) tenían canales de TAC ( $n = 91$ ). La sensibilidad global (Se) y los valores predictivos positivos (VPP) para detectar canales de RM fueron 61,8% y 51,6%, respectivamente. El rendimiento de la TAC mejoró en pacientes con canales de RM epicárdicos (Se 80,5%) y cicatrices transmurales (Se 72,2%). En 4/11 (36%) pacientes con infarto de miocardio subendocárdico, la TAC no pudo identificar la presencia de sustrato arritmogénico.

**Conclusiones:** En comparación con la RM-RTG, la evaluación del grosor de la pared miocárdica mediante TAC no detecta la presencia de sustrato arritmogénico en el 36% de

los pacientes con infarto de miocardio subendocárdico, mostrando una sensibilidad moderada para identificar HTC pero un mejor desempeño en pacientes con cicatrices transmurales.





ESC  
European Society  
of Cardiology

Europace (2020) 0, 1–9  
doi:10.1093/europace/ea237

CLINICAL RESEARCH

## Arrhythmogenic substrate detection in chronic ischaemic patients undergoing ventricular tachycardia ablation using multidetector cardiac computed tomography: compared evaluation with cardiac magnetic resonance

Beatriz Jáuregui<sup>1,2</sup>, David Soto-Iglesias<sup>1,2</sup>, Giulio Zucchelli<sup>3</sup>, Diego Penela<sup>1,2</sup>, Augusto Ordóñez<sup>1</sup>, Cheryl Terés<sup>1</sup>, Alfredo Chauca<sup>1</sup>, Juan Acosta<sup>4</sup>, Juan Fernández-Armenta<sup>5</sup>, Markus Linhart<sup>6</sup>, Rosario J. Perea<sup>2</sup>, Susana Prat-González<sup>2</sup>, Xavier Bosch<sup>2</sup>, José T. Ortiz-Pérez<sup>2</sup>, Lluís Mont<sup>2</sup>, and Antonio Berruezo<sup>1,2\*</sup>

<sup>1</sup>Heart Institute, Teknon Medical Center, C/Vilana, 12, 08022 Barcelona, Spain; <sup>2</sup>Clinic Cardiovascular Institute, Hospital Clínic, C/Villarroel, 170, 08036 Barcelona, Spain; <sup>3</sup>Cardiac Thoracic and Vascular Department, Azienda Ospedaliero-Universitaria Pisana, Via Roma, 67, 56126 Pisa, Italy; <sup>4</sup>Arrhythmia Unit, Hospital Universitario Virgen del Rocío, Avda. Manuel Siurot, s/n, 41013, Sevilla, Spain; <sup>5</sup>Arrhythmia Unit, Hospital Puerta del Mar, Avda. Ana de Viya, 21, 11009 Cádiz, Spain; and <sup>6</sup>Arrhythmia Section, University Hospital of Girona Dr. Josep Trueta, Avda. de Francia, s/n, 17007, Girona, Spain

Received 8 December 2019; editorial decision 11 July 2020; accepted after revision 21 July 2020

### Aims

Late gadolinium enhancement cardiac magnetic resonance (LGE-CMR) permits characterizing ischaemic scars, detecting heterogeneous tissue channels (HTCs) which constitute the arrhythmogenic substrate (AS). Late gadolinium enhancement cardiac magnetic resonance also improves the arrhythmia-free survival when used to guide ventricular tachycardia (VT) substrate ablation. However, its availability may be limited. We sought to evaluate the performance of multidetector cardiac computed tomography (MDCT) imaging in identifying HTCs detected by LGE-CMR in ischaemic patients undergoing VT substrate ablation.

### Methods and results

Thirty ischaemic patients undergoing both LGE-CMR and MDCT before VT substrate ablation were included. Using a dedicated post-processing software, two blinded operators, assigned either to LGE-CMR or MDCT analysis, characterized the presence of CMR and computed tomography (CT) channels, respectively. Cardiac magnetic resonance channels were classified as endocardial (layers < 50%), epicardial (layers ≥ 50%), or transmural. Cardiac magnetic resonance- vs. CT-channel concordance was considered when showing the same orientation and American Heart Association (AHA) segment. Mean age was 69 ± 10 years; 90% were male. Mean left ventricular ejection fraction was 35 ± 10%. All patients had CMR channels (*n* = 76), whereas only 26/30 (86.7%) had CT channels (*n* = 91). Global sensitivity (Se) and positive predictive values for detecting CMR channels were 61.8% and 51.6%, respectively. MDCT performance improved in patients with epicardial CMR channels (Se 80.5%) and transmural scars (Se 72.2%). In 4/11 (36%) patients with subendocardial myocardial infarction (MI), MDCT was unable to identify the AS.

### Conclusions

Compared to LGE-CMR, myocardial wall thickness assessment using MDCT fails to detect the presence of AS in 36% of patients with subendocardial MI, showing modest sensitivity identifying HTCs but a better performance in patients with transmural scars.

### Keywords

Cardiac magnetic resonance • Multidetector cardiac computed tomography • Arrhythmogenic substrate • Ventricular tachycardia • Image-guided substrate ablation • Conducting channels

\*Corresponding author. Tel: +34 932 90 62 00; fax: +34 932 11 26 90. E-mail address: antonio.berruezo@quironsalud.es  
Published on behalf of the European Society of Cardiology. All rights reserved. © The Author(s) 2020. For permissions, please email: journals.permissions@oup.com.

### What's new?

- Whereas multidetector cardiac computed tomography (MDCT) is able to detect ridges and sinks of myocardial tissue within the scar, late gadolinium enhancement cardiac magnetic resonance (LGE-CMR) is capable of distinguishing viable myocardial tissue, irrespective of its relative thickness.
- Compared to scar characterization using LGE-CMR, wall thickness assessment using MDCT shows only a modest sensitivity in identifying the presence of heterogeneous tissue channels (HTCs), being unable to detect the presence of arrhythmogenic substrate (AS) in 36% of subendocardial myocardial infarction (MI) scars.
- MDCT wall thickness-derived scar analysis performance improves in patients with transmural MI scars and in the identification of non-endocardial (i.e. subepicardial or transmural) HTCs embedded within the scar.
- MDCT wall thickness-derived scar analysis may be proposed as a useful pre-procedural imaging technique to aid ventricular tachycardia (VT) substrate ablation procedures in patients with transmural MI scars, better if combined with CMR information. For only subendocardial MI scars, LGE-CMR should be considered as the best imaging tool to depict the potential AS and to plan VT substrate ablation procedures.

## Introduction

Ventricular tachycardia (VT) substrate ablation is an effective treatment for scar-dependent VT<sup>1,2</sup> but recurrence rate remains high with standard approaches.<sup>3-5</sup> Recent studies<sup>6,7</sup> have shown that aiding or guiding VT substrate ablation procedures with integrated colour-coded pixel signal intensity (PSI) maps, obtained from pre-procedural late gadolinium enhancement cardiac magnetic resonance (LGE-CMR) imaging, results in less need for radiofrequency delivery and an improved VT recurrence-free survival. Late gadolinium enhancement cardiac magnetic resonance shows great accuracy when characterizing the scarred tissue<sup>8,9</sup> and is able to identify further arrhythmogenic substrate (AS) as compared with endocardial or epicardial surface electroanatomic maps (EAM) alone.<sup>6</sup> However, the use of LGE-CMR may be limited in certain situations, such as patient's claustrophobia, inability to perform long breath-holds, presence of image artefacts in carriers of cardiac implantable electronic devices, etc. Moreover, CMR may not be broadly available for all centres to be used routinely as part of the pre-procedural work-up for patients undergoing VT ablation.

Wall thickness assessment using MDCT has recently arisen as an alternative cardiac imaging method to identify the AS before VT ablation procedures. Wall thinning (WT) is a useful parameter that has proven to correlate with low voltage areas (LVA) and distribution of local abnormal ventricular activities (LAVAs).<sup>10,11</sup> Computed tomography (CT)-defined ridges of thicker myocardial tissue within the scar can be considered as appropriate ablation targets.<sup>12</sup> However, in cases of ischaemic cardiomyopathy (ICM) with transmural substrate the agreement with epicardial LVA has been shown to be significantly higher for CMR than for MDCT.<sup>13</sup> In the present study, we sought to evaluate the general performance of MDCT imaging in identifying the

heterogeneous tissue channels (HTCs) detected by CMR in patients with ICM undergoing VT substrate ablation.

## Methods

### Patient sample

This is a retrospective study, including 30 consecutive patients with ICM referred for a first catheter ablation of scar-related sustained monomorphic VT. As previously reported,<sup>6,7</sup> substrate mapping was guided by the information from the three-dimensional (3D) LGE-CMR-derived reconstructions (i.e. PSI maps) integrated into the navigation system, after merging a fast-anatomical map of the aorta or the right ventricle with the corresponding structure from the 3D cardiac MDCT-derived reconstructions. The study complied with the Declaration of Helsinki. The local Ethics Committee approved the study protocol and all included participants signed the informed consent.

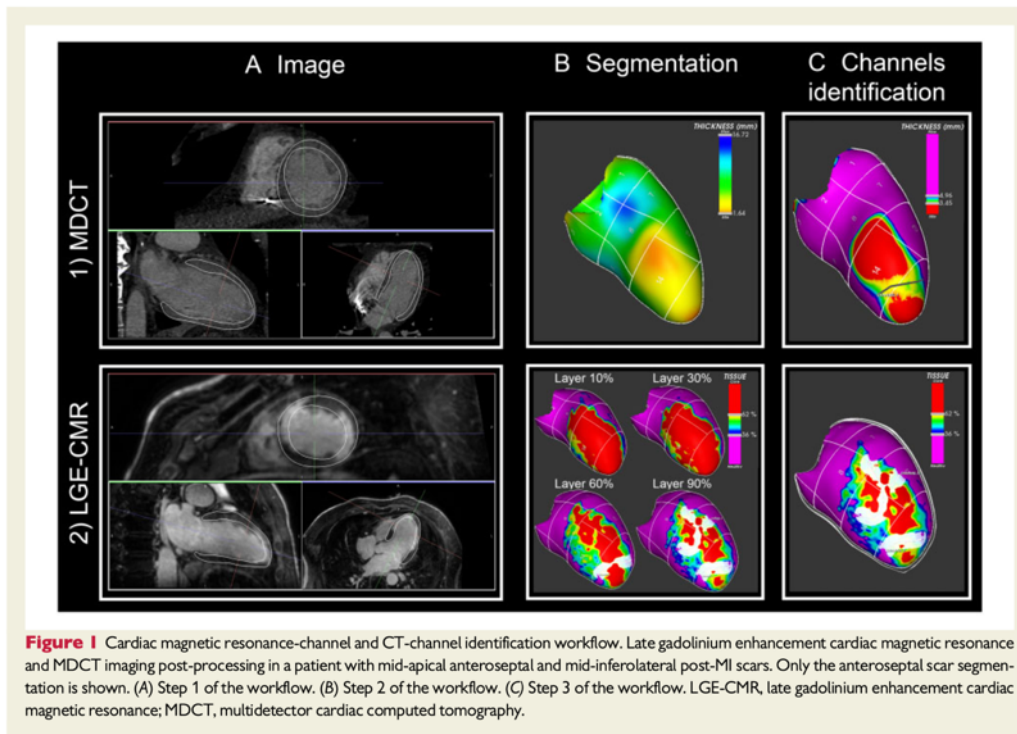
### Late gadolinium enhancement cardiac magnetic resonance acquisition and segmentation

A pre-procedural LGE-CMR study was performed either in a 3-Tesla scanner (MAGNETOM Trio<sup>TM</sup>, Siemens Healthcare, Erlangen, Germany) or a 1.5-Tesla scanner (MAGNETOM Aera<sup>TM</sup>, Siemens Healthcare). For patients previously implanted with an implantable cardiac defibrillator (ICD), the 1.5-Tesla scanner was used with a specific 'wideband' sequence in order to avoid device artefacts, although some ICD carriers underwent a 3-Tesla CMR immediately before implantation, as pre-implantation imaging is our routine clinical practice. For acquisition details, see [Supplementary material online](#).

Late gadolinium enhancement cardiac magnetic resonance images were analysed using a previously described technique.<sup>6,7</sup> The 3D left ventricle (LV) was segmented from the whole image volume using ADAS-3D<sup>TM</sup> software (Galgo Medical, Barcelona, Spain). The LV was automatically divided into 10 layers from endocardium to epicardium, each one representing 10% of the total LV wall thickness. Pixel signal intensity was projected onto each layer following a trilinear interpolation algorithm. Myocardial tissue was classified into core zone (CZ), border zone (BZ), and healthy tissue using  $60 \pm 5\%$  and  $40 \pm 5\%$  of the maximum intensity signal of the scar as thresholds.<sup>14</sup> Finally, different scar areas (CZ and BZ) were automatically quantified in each myocardial layer. On the LGE-CMR PSI maps, HTCs were defined as continuous corridors of BZ surrounded by scar core or scar core and an anatomical barrier (i.e. mitral annulus) connecting two areas of healthy tissue. Heterogeneous tissue channels were obtained automatically by the ADAS-3D<sup>TM</sup> software. Heterogeneous tissue channels were classified as: (i) subendocardial (layers from 10% to 50%); (ii) subepicardial (layers from 60% to 90%); and (iii) transmural (from layer 10% to 90%). Additionally, HTC entrances were defined as the areas where HTC connect with healthy tissue.

### Multidetector cardiac computed tomography acquisition and segmentation

In all patients, a pre-procedural MDCT electrocardiogram-gated study was performed on a 128 x 2-slice CT scanner (SOMATOM Definition Flash<sup>TM</sup>, Siemens Healthcare). Acquisition details are summarized in [Supplementary material online](#). MDCT images were retrospectively analysed using ADAS-3D<sup>TM</sup> software. The endocardial and epicardial surfaces of the LV were segmented using an algorithm based on initial alignment of a standard cardiac model, followed by manual corrections. The myocardial wall thickness was automatically computed as the



distance between each point on the endocardial and epicardial surfaces of the model. A 3D colour-coded surface mesh of the LV myocardial wall thickness was automatically obtained with the software.

### Ablation procedure

CARTO3™ electroanatomical navigation system (Biosense Webster, Diamond Bar, CA, USA) was used for guiding ablation. An open-irrigated 3.5-mm tip ablation catheter (ThermoCool™ SmartTouch™, Biosense Webster) was used for mapping and ablation. A transeptal access was performed in all patients for LV endocardial mapping. An epicardial approach was considered whenever the presence of LGE involved  $\geq 75\%$  of the myocardial wall thickness.<sup>15</sup> Ablation was performed according to the scar dechanneling technique,<sup>5</sup> considering all CMR-channel entrances (CMR entrances) as ablation targets. A CMR-guided approach<sup>7</sup> was used; this approach has already been proven to be feasible, safe, and effective in terms of post-ablation inducibility and VT recurrence rates.<sup>7</sup>

### Comparison between cardiac magnetic resonance channels and computed tomography channels

Two operators, blinded to any clinical or procedural information of the patients, were randomly assigned either to CMR or MDCT *post hoc* analysis. The CMR operator characterized the presence of CMR channels (i.e. HTC) in terms of disposition (longitudinal, transversal, or diagonal), degree of transmuralty, and location defined by the 17-segment American Heart Association (AHA) model. The MDCT operator examined the

area with a myocardial thickness  $< 5$  mm and analysed, hand raking the wall thickness thresholds in order to detect myocardial ridges. These ridges, named CT channels, were defined as channel-shaped edges inside the MDCT scar showing a thickness that exceeded the surrounding myocardium by  $\geq 1$  mm<sup>11</sup> (Figure 1). Finally, disposition and location were annotated for CT channels in the same manner as for CMR channels. Both operators annotated the total number of channels observed, as well as the number and location of the corresponding channel entrances, which are considered ablation targets according to the scar dechanneling technique.<sup>5</sup> MDCT findings were compared to those derived from CMR, considering this last imaging technique as the gold standard for AS evaluation. Channel concordance was considered whenever a CT channel showed the same disposition and was located in the same AHA segment as a corresponding CMR channel.

### Statistical analysis

Continuous variables are presented as mean values  $\pm$  standard deviations. Categorical variables are presented as total numbers and percentages. Populations were compared by the Wilcoxon–Mann–Whitney or Fisher's exact test, as appropriate. A  $P$ -value  $\leq 0.05$  was considered for statistical significance. Statistics were obtained using IBM SPSS Statistics, version 25.0 (IBM Corp. Released 2017; Armonk, NY, USA: IBM Corp.), and Matlab statistics toolbox (Matlab R2010a, The Mathworks, Inc., Natick, MA, USA).

**Table 1** Baseline characteristics

	Total population (n = 30)	Subendocardial MI (n = 11)	Transmural MI (n = 19)	P-value
Age (years)	69 ± 10	69 ± 10	68 ± 10	0.85
Men (%)	27 (90%)	11 (100%)	16 (84.2%)	0.16
Hypertension (%)	24 (80%)	8 (72.7%)	16 (84.2%)	0.45
Dyslipidaemia (%)	22 (73.3%)	8 (72.7%)	14 (73.7%)	0.95
Diabetes mellitus (%)	13 (43.3%)	7 (63.6%)	6 (31.6%)	0.09
Smokers (%)	5 (16.7%)	3 (27.3%)	2 (10.5%)	0.23
LVEF (%)	35 ± 9	35 ± 11	34 ± 9	0.82
LVEDD (mm)	61 ± 7	63 ± 9	60 ± 6	0.39
Scar localization				
Anterior	14 (6.7%)	3 (27.3%)	11 (57.9%)	0.22
Inferior	13 (43.3%)	7 (63.6%)	6 (31.6%)	
Lateral	3 (10%)	1 (9.1%)	2 (10.5%)	
CAD extension and severity				
Single-vessel	7/18 (39%)	2/4 (50%)	5/14 (36%)	0.14
Two-vessel	7/18 (39%)	0	7/14 (50%)	
Three-vessel	4/18 (22%)	2/4 (50%)	2/14 (14%)	
Complete CAD revascularization	14/18 (78%)	3/4 (75%)	11/14 (79%)	0.64
Coronary CTO	2/18 (11%)	0	2/14 (14%)	0.78
Time since MI (months)	21 ± 9	25 ± 12	20 ± 7	0.41
NYHA class (%)	1.94 ± 0.64	2.13 ± 0.64	1.80 ± 0.63	0.28
Previous ICD (%)	24 (80%)	9 (81.8%)	15 (78.9%)	0.85
Appropriate ICD therapies (ATP + shocks), n	9 ± 21	1 ± 1	15 ± 27	0.31
Arrhythmia storm (%)	3 (10%)	2 (18.2%)	1 (5.3%)	0.26
Previous treatment				
Betablockers	20 (66.7%)	6 (54.5%)	14 (73.7%)	0.11
Sotalol	0 (0%)	0 (0%)	0 (0%)	–
Amiodarone	15 (50%)	7 (63.6%)	8 (42.1%)	0.32

ATP, anti-tachycardia pacing; CAD, coronary artery disease; CTO, chronic total occlusion; ICD, implantable cardiac defibrillator; LVEDD, left ventricular end-diastolic diameter; LVEF, left ventricular ejection fraction; MI, myocardial infarction; NYHA, New York Heart Association.

## Results

### Patient characteristics

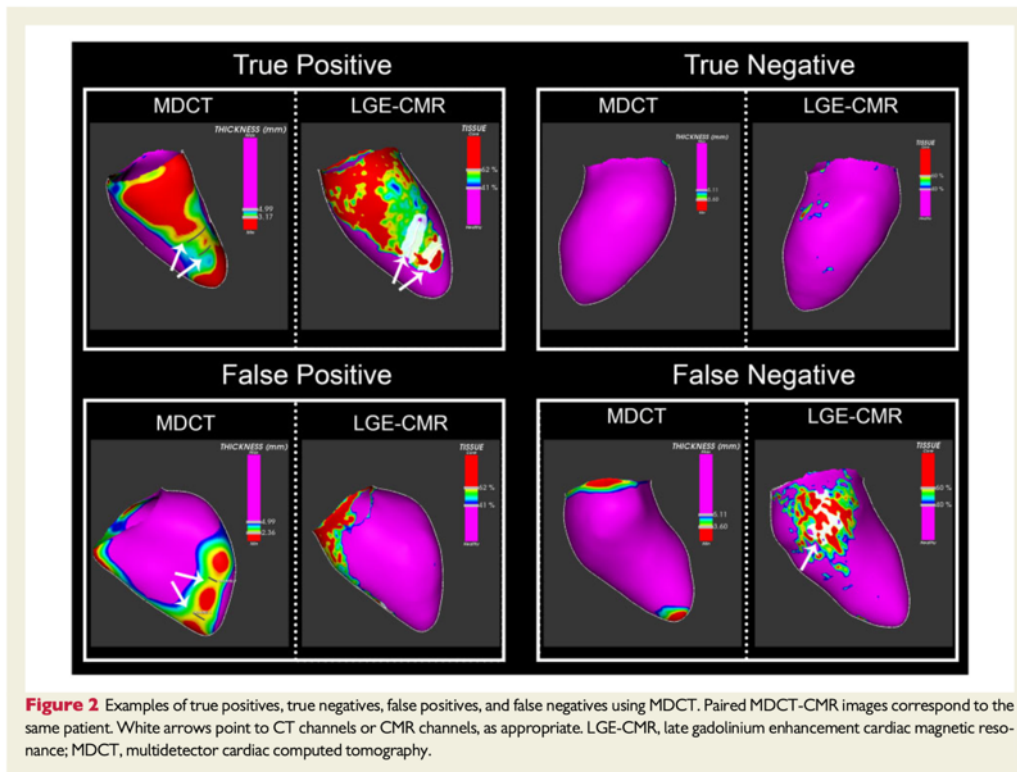
Mean age was 69 ± 10 years; 94% were male. Mean left ventricular ejection fraction was 35 ± 10%. Using classical imaging criteria,<sup>16</sup> 19/30 (63%) patients showed a transmural myocardial infarction (MI) (hyperenhancement involving ≥75% of the wall thickness), whereas 11/30 (37%) had only a subendocardial MI. Baseline characteristics of the population are summarized in Table 1.

### Multimodality image-based assessment of arrhythmogenic substrate

An example of CT-channel identification workflow is shown in Figure 1. The mean area of significant myocardial WT (5-mm cut-off)<sup>17</sup> was 62.3 ± 40.4 cm<sup>2</sup>, corresponding to a mean of 30.7 ± 17.0% of the total LV endocardial area. Patients with a transmural MI presented a larger area of significant myocardial WT than those with a subendocardial MI (36.9 ± 13.1% vs. 21.9 ± 18.4%, *P* = 0.016). A total of 91 CT channels were identified in 26/30 (86.7%) patients, with a

mean of 3.0 ± 2.0 CT channels per patient. The mean WT thresholds employed to detect the CT channels were 3.66 ± 0.96 and 4.31 ± 0.58 mm for the lower and upper limits, respectively, with 91/91 (100%) of the myocardial ridges found in the areas with <5-mm thickness, which was considered the MDCT area of interest for analysis. A total of 190 CT-channel entrances (CT entrances) were identified, corresponding to a mean of 6.3 ± 4.1 CT entrances per patient.

Thirteen out of 30 (43%) patients underwent a 1.5-Tesla CMR using a wideband sequence. The mean scar mass evaluated with CMR was 34.5 ± 12.1 g, corresponding to a mean of 20.6 ± 6.4% of the total LV mass. Patients with a transmural MI presented a higher scar mass than those with a subendocardial MI (22.7 ± 5.7% vs. 17.3 ± 6.5%, *P* = 0.030). Using standard thresholds<sup>14</sup> for BZ and core characterization, 76 CMR channels were identified in 30/30 (100%) patients, with a mean of 2.4 ± 1.2 CMR channels per patient. Thirty-six out of 76 (47.4%) CMR channels were classified as non-endocardial (i.e. epimural or transmural). A total of 275 CMR entrances were identified, corresponding to a mean of 8.9 ± 4.9 CMR entrances per patient.



### Comparison of multidetector cardiac computed tomography-based vs. cardiac magnetic resonance-based evaluation of arrhythmogenic substrate

A total of 47/91 (51.6%) CT channels were also detected as CMR channels, and therefore identified as CT true positives. On the contrary, 44/91 (48.4%) CT channels were considered as false positives. In particular, 19/91 (20.9%) CT channels were identified outside the boundaries of the CMR scar. Moreover, 29/76 (38.2%) CMR channels could not be identified on the CT (false negatives) (Figure 2).

A total of 29/36 (80.5%) non-endocardial CMR channels were also identified on MDCT analysis. A significantly higher proportion of non-endocardial CMR channels could be identified with MDCT, when compared to only-endocardial CMR channels (80.5% vs. 45%;  $P=0.002$ ) (Table 2).

There were 91/190 (47.9%) true positive CT entrances after matching with their corresponding CMR entrances. On the other hand, 99/190 (52.1%) CT entrances were considered false positives, and 184/275 (66.9%) CMR entrances could not be identified using CT (false negatives). The estimated global sensitivity values for detection of channels and channel entrances using MDCT were 61.8% and 33.1%, respectively (Figure 3).

Notably, in 4/11 (36%) patients with subendocardial MI, MDCT was unable to identify the presence of AS.

### Performance of multidetector cardiac computed tomography in patients with transmural myocardial infarction

Among patients with transmural MI ( $n=19$ , 63.3%), there were 39/73 (53.4%) CT channels considered as true positives, whereas 34/73 (46.6%) were identified as false positives. Fifteen out of 54 (27.8%) CMR channels could not be detected on CT (false negatives).

A significantly higher proportion of CMR channels can be identified with MDCT in patients with transmural MI ( $n=19$ ), as compared to non-transmural MI ( $n=11$ ) (72.2% vs. 36.4%;  $P=0.004$ ) (Table 2 and Figure 4). Moreover, there is also a non-significant trend towards a better detection performance of MDCT for endocardial CMR channels in patients with transmural MI as compared with non-transmural (55.6% vs. 36.4%;  $P=0.37$ ) (Table 3).

There were 76/153 (49.7%) true positive CT entrances after matching with their corresponding CMR entrances. On the other hand, 77/153 (50.3%) CT entrances were considered false positives, and 117/191 (61.3%) CMR entrances could not be identified using CT (false negatives). Concerning channel entrance detection, there is

a non-significant trend to a lower rate of false positives when comparing transmural with non-transmural MI (50.3% vs. 59.5%;  $P=0.31$ ). Furthermore, the rate of false negatives was significantly lower in transmural MI (61.3% vs. 79.8%;  $P=0.002$ ). In this population, the estimated sensitivity values for detection of CMR channels and their entrances using MDCT were 72.2% and 39.7%, respectively. These sensitivity values are significantly higher in patients with transmural MI: 72.2% vs. 36.4% ( $P=0.004$ ) for the detection of channels, and 39.4% vs. 18.3% ( $P<0.001$ ) for the identification of channel entrances. In both cases, these differences may be ascribed to the lower rate of false negatives encountered. A summary of the most important findings of the study can be found in Table 4.

**Table 2** Multidetector cardiac computed tomography detection performance for endocardial vs. non-endocardial (i.e. epicardial or transmural) CMR channels, and for transmural vs. non-transmural MI

	Total CMR channels	MDCT-detected CMR channels	P-value
All CMR channels	76	47 (61.8%)	–
Non-endocardial CMR channels	36	29 (80.5%)	0.002
Endocardial CMR channels	40	18 (45%)	
All patients (n = 30)	76	47 (61.8%)	–
Transmural MI (n = 19)	54	39 (72.2%)	0.004
Non-transmural MI (n = 11)	22	8 (36.4%)	

CMR, cardiac magnetic resonance; MDCT, multidetector cardiac computed tomography; MI, myocardial infarction.

## Discussion

To the best of our knowledge, this is the first clinical study comparing two different non-invasive methods for identification of the AS within post-infarction scarred tissue: (i) detection of anatomical, thickened myocardial ridges identified using MDCT vs. (ii) detection of HTC (BZ corridors) using LGE-CMR.

The main findings of the study are that (i) MDCT fails to detect the presence of HTCs in ~36% of patients with only subendocardial scars (Figure 4); (ii) MDCT assessment of WT is only moderately capable (61.8% sensitivity) of identifying the presence of HTCs; (iii) in patients with transmural MI, MDCT sensitivity improves significantly (72.2%) due to a lower false negative rate; and (iv) WT evaluation with MDCT shows a poor sensitivity in identifying HTC entrances (33.1%), mainly due to a very high false negative rate that slightly improves in patients with transmural MI.

### Cardiac magnetic resonance, the imaging reference for arrhythmogenic substrate characterization

Late gadolinium enhancement cardiac magnetic resonance constitutes a highly accurate tool to characterize and delimit the scarred tissue within the entire myocardial thickness.<sup>8</sup> Moreover, it has proven to be capable of identifying additional AS compared with endocardial or epicardial surface EAM alone,<sup>6</sup> as well as to improve the acute and long-term VT substrate ablation outcomes when guiding such procedures, without the need for an EAM reconstruction.<sup>7</sup> In this regard, it has been shown that patients with HTCs identified by CMR that are not targeted for ablation (i.e. with normal electrograms at EAM, due to a far-field effect from the surrounding healthy myocardium), suffer from more VT recurrences after  $20 \pm 19$  months of follow-up.<sup>6</sup> Furthermore, a previous study from Yamashita et al.<sup>13</sup> demonstrated

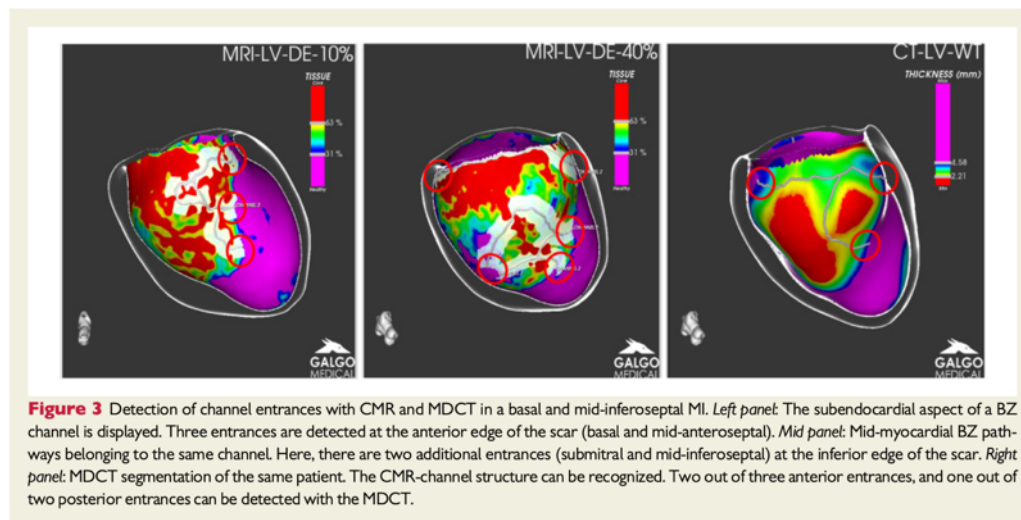


**Figure 3** Detection of channel entrances with CMR and MDCT in a basal and mid-inferoseptal MI. *Left panel:* The subendocardial aspect of a BZ channel is displayed. Three entrances are detected at the anterior edge of the scar (basal and mid-anteroseptal). *Mid panel:* Mid-myocardial BZ pathways belonging to the same channel. Here, there are two additional entrances (submitral and mid-inferoseptal) at the inferior edge of the scar. *Right panel:* MDCT segmentation of the same patient. The CMR-channel structure can be recognized. Two out of three anterior entrances, and one out of two posterior entrances can be detected with the MDCT.

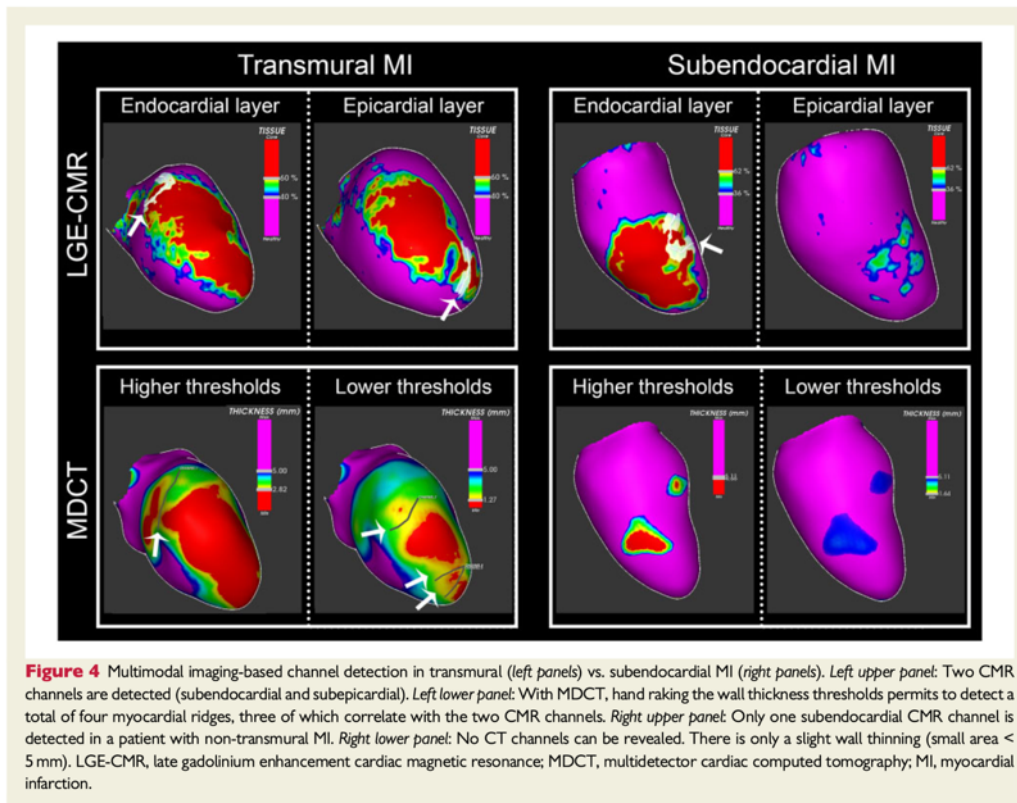


**Table 3** Multidetector cardiac computed tomography detection performance for endocardial vs. non-endocardial (i.e. epicardial or transmural) CMR channels with respect to MI transmural

	Total CMR channels	MDCT-detected CMR channels	P-value
Transmural MI (n = 19)	54	39 (72.2%)	0.05
Non-endocardial CMR channels	36	29 (80.5%)	
Endocardial CMR channels	18	10 (55.6%)	
Non-transmural MI (n = 11)	22	8 (36.4%)	–
Non-endocardial CMR channels	0	0 (0%)	
Endocardial CMR channels	22	8 (36.4%)	

CMR, cardiac magnetic resonance; MDCT, multidetector cardiac computed tomography; MI, myocardial infarction.

that the agreement between detection of structural substrate in imaging and low voltage zones (areas with peak-to-peak amplitude <1.5 mV of bipolar voltage) was higher for CMR than for MDCT when evaluating epicardial substrate ( $73 \pm 7\%$  vs.  $60 \pm 13\%$ ,  $P = 0.002$ ) in ICM.

In order to improve the characterization of the AS using EAM, different multi-electrode catheters and high-density mapping systems

have been tested. In previous studies, the use of a grid mapping catheter<sup>18</sup> allowed to identify late potentials or LAVAs only in 72% of the sites that had been identified as VT mid-isthmuses after VT induction, whereas the use of a multi-basket catheter<sup>19</sup> allowed to identify only 50% of the critical isthmuses of all induced VTs. More recently, Tung *et al.*<sup>20</sup> have described, after simultaneous VT mapping from endocardium and epicardium, how VT isthmuses are frequently 3D, while

**Table 4** Multidetector cardiac computed tomography performance in detection of heterogeneous tissue channels and their entrances, as compared with CMR

		Global (n = 30)	Transmural MI (n = 19)	Non-transmural MI (n = 11)	P-value
CC detection	True positives	47/91 (51.6%)	39/73 (53.4%)	8/18 (44.4%)	0.49
	False positives	44/91 (48.4%)	34/73 (46.6%)	10/18 (55.6%)	0.49
	False negatives	29/76 (38.2%)	15/54 (27.8%)	14/22 (63.6%)	0.004
	Sensitivity	61.8%	72.2%	36.4%	0.004
	PPV	51.6%	53.4%	44.4%	0.49
CC entrances' detection	True positives	91/190 (47.9%)	76/153 (49.7%)	15/37 (40.5%)	0.31
	False positives	99/190 (52.1%)	77/153 (50.3%)	22/37 (59.5%)	0.31
	False negatives	184/275 (66.9%)	117/191 (61.3%)	67/84 (79.8%)	0.002
	Sensitivity	33.1%	39.4%	18.3%	<0.001
	PPV	47.9%	49.7%	40.5%	0.31

CC, conducting channel; CMR, cardiac magnetic resonance; MDCT, multidetector cardiac computed tomography; MI, myocardial infarction; PPV, positive predictive value.

recognizing that conventional EAM results in a limited two-dimensional representation of the re-entrant circuit. All these aspects have been pondered over when considering CMR as the imaging reference to identify VT substrate in ICM.

### Usefulness of wall thinning evaluation using multidetector cardiac computed tomography for substrate detection in ischaemic cardiomyopathy

As previously ascertained, MDCT is capable of only modestly identifying the presence of HTCs detected with CMR (61.8% sensitivity). However, the relationship between the regional myocardial WT assessed with MDCT and the presence of AS in ICM has been well recognized before,<sup>13</sup> aside from MDCT ability to detect critical ablation sites, identified as ridges of myocardial tissue dividing areas of VT.<sup>12,21</sup> Recently, Takigawa et al.<sup>21</sup> studied nine post-infarction patients and found that 100% of their VT isthmuses were found inside CT channels. However, this finding refers only to the 10/32 induced VTs whose circuit could be fully characterized, that is, only 31% of the VTs could be fully mapped using EAM. Considering the small size of the studied population and that, in our study, MDCT could not detect the presence of AS in 36% of the patients with subendocardial MI, we would take this sensitivity with caution.

The AS information depicted by MDCT is different from that provided by CMR; whereas MDCT is able to detect ridges and sinks of myocardial tissue within the scar, CMR is capable of distinguishing viable myocardial tissue, irrespective of its relative thickness. Notwithstanding, these two imaging techniques also have similarities: effective ablation sites are most often found in the thicker ridges in MDCT<sup>12</sup> and are also most frequently located in HTC (BZ channels) detected with CMR.<sup>6</sup> Moreover, the ridges with effective ablation sites are predominantly located in the BZ scar (areas with a bipolar voltage of 0.5–1.5 mV).<sup>12</sup>

The fact that MDCT shows better accuracy at identifying the AS depicted by CMR in patients with transmural MI (72.2% sensitivity) and/or in the presence of epicardial or transmural channels, is in line with these considerations. Transmural scars show greater WT, probably making it easier to detect potential 'ridges and sinks' of

myocardial tissue. Small subendocardial scars may not always modify the myocardial thickness at the injured zone in such a magnitude that these ridges can reflect the whole 3D structure of the AS. Heterogeneous tissue channels are complex, branched structures connecting with healthy tissue at several entrances that show specific electrogram properties and are target for ablation.<sup>4</sup> These entrances, usually found at BZ areas of the scar, can barely be identified with MDCT in patients with subendocardial scars (18.3% sensitivity). In fact, MDCT cannot detect the presence of AS in up to 36% of the patients with a subendocardial MI.

Nevertheless, MDCT still constitutes a valuable tool depicting AS characteristics that help when performing scar-related VT ablation procedures,<sup>10-13,20-22</sup> although CMR seems to be a more precise tool to depict the whole AS 3D structure and guide ablation procedures.<sup>7</sup> Finally, it cannot be ignored that MDCT-derived cardiac anatomy integration during ablation procedures impacts on safety and helps with procedural management.<sup>10,13,15</sup> MDCT may be proposed as a useful pre-procedural imaging technique to aid VT substrate ablation procedures in patients with a transmural MI, better if combined with CMR information. For subendocardial scars, CMR should be considered as the best imaging tool to depict the AS and plan these procedures.

### Study limitations

Since ablation was performed using a CMR-guided approach, only limited EAM data were available.<sup>7</sup> The analysis of channel entrances, where MDCT showed a remarkably poor sensitivity, was considered useful as these constitute ablation targets in the scar dechanneling technique. Yet, when only channel detection is considered the main message remains the same, thus making the results applicable to other ablation approaches. Finally, imaging data on substrate detection could be potentially influenced by CMR/MDCT image quality.

### Conclusions

Compared to LGE-CMR, wall thickness assessment and identification of myocardial ridges within the scar using MDCT shows only a modest sensitivity in identifying the presence of HTCs, being unable to



detect the presence of AS, as depicted by CMR, in 36% of patients with subendocardial MI scars. MDCT performance improves in patients with transmural MI and in the identification of non-endocardial (i.e. subepicardial or transmural) channels. For subendocardial scars, CMR should be considered as the best imaging tool to depict the AS and to plan ablation procedures.

## Supplementary material

Supplementary material is available at *Europace* online.

**Conflict of interest:** A.B. is a stockholder in Galgo Medical SL. All other authors declared no conflict of interest.

## Data availability

The data underlying this article cannot be shared publicly due to the fact that it belongs to the patients who participated in the study and the institution where the research was conducted (Hospital Clinic, University of Barcelona), as the corresponding author moved to another Institution (Teknon Medical Center). The data that support the findings of this study are available from the corresponding author, [A.B.], upon reasonable request.

## References

- Reddy VY, Reynolds MR, Neuzil P, Richardson AW, Taborsky M, Jongnarangsin K et al. Prophylactic catheter ablation for the prevention of defibrillator therapy. *N Engl J Med* 2007;**357**:2657–65.
- Kuck KH, Schaumann A, Eckardt L, Willems S, Ventura R, Delacretaz E et al. Catheter ablation of stable ventricular tachycardia before defibrillator implantation in patients with coronary heart disease (VTACH): a multicentre randomised controlled trial. *Lancet* 2010;**375**:31–40.
- Jais P, Maury P, Khairy P, Sacher F, Nault I, Komatsu Y et al. Elimination of local abnormal ventricular activities: a new end point for substrate modification in patients with scar-related ventricular tachycardia. *Circulation* 2012;**125**:2184–96.
- Di Biase L, Santangeli P, Burkhardt DJ, Bai R, Mohanty P, Carbuicchio C et al. Endo-epicardial homogenization of the scar versus limited substrate ablation for the treatment of electrical storms in patients with ischemic cardiomyopathy. *J Am Coll Cardiol* 2012;**60**:132–41.
- Berrueto A, Fernández-Armenta J, Andreu D, Penela D, Herczku C, Evertz R et al. Scar dechanneling: new method for scar-related left ventricular tachycardia substrate ablation. *Circ Arrhythm Electrophysiol* 2015;**8**:326–36.
- Andreu D, Penela D, Acosta J, Fernández-Armenta J, Perea RJ, Soto-Iglesias D et al. Cardiac magnetic resonance-aided scar dechanneling: influence on acute and long-term outcomes. *Heart Rhythm* 2017;**14**:1121–8.
- Soto-Iglesias D, Penela D, Jáuregui B, Acosta J, Fernández-Armenta J, Linhart M et al. Cardiac magnetic resonance-guided ventricular tachycardia substrate ablation. *JACC Clin Electrophysiol* 2020;**6**:436–47.
- Fernández-Armenta J, Berrueto A, Andreu D, Camara O, Silva E, Serra L et al. Three-dimensional architecture of scar and conducting channels based on high resolution ce-CMR: insights for ventricular tachycardia ablation. *Circ Arrhythm Electrophysiol* 2013;**6**:528–37.
- Perez-David E, Arenal A, Rubio-Guivernau JL, del Castillo R, Atea L, Arbelo E et al. Noninvasive identification of ventricular tachycardia-related conducting channels using contrast-enhanced magnetic resonance imaging in patients with chronic myocardial infarction: comparison of signal intensity scar mapping and endocardial voltage mapping. *J Am Coll Cardiol* 2011;**57**:184–94.
- Tian J, Jeudy J, Smith MF, Jimenez A, Yin X, Bruce PA et al. Three-dimensional contrast-enhanced multidetector CT for anatomic, dynamic, and perfusion characterization of abnormal myocardium to guide ventricular tachycardia ablations. *Circ Arrhythm Electrophysiol* 2010;**3**:496–504.
- Komatsu Y, Cochet H, Jadidi A, Sacher F, Shah A, Derval N et al. Regional myocardial wall thinning at multidetector computed tomography correlates to arrhythmogenic substrate in postinfarction ventricular tachycardia: assessment of structural and electrical substrate. *Circ Arrhythm Electrophysiol* 2013;**6**:342–50.
- Ghannam M, Cochet H, Jais P, Sermesant M, Patel S, Siontis KC et al. Correlation between computer tomography-derived scar topography and critical ablation sites in postinfarction ventricular tachycardia. *J Cardiovasc Electrophysiol* 2018;**29**:438–45.
- Yamashita S, Sacher F, Mahida S, Berte B, Lim HS, Komatsu Y et al. Image integration to guide catheter ablation in scar-related ventricular tachycardia. *J Cardiovasc Electrophysiol* 2016;**27**:699–708.
- Andreu D, Berrueto A, Ortiz-Pérez JT, Silva E, Mont L, Borrás R et al. Integration of 3D electroanatomic maps and magnetic resonance scar characterization into the navigation system to guide ventricular tachycardia ablation. *Circ Arrhythm Electrophysiol* 2011;**4**:674–83.
- Soto-Iglesias D, Acosta J, Penela D, Fernández-Armenta J, Cabrera M, Martínez M et al. Image-based criteria to identify the presence of epicardial arrhythmogenic substrate in patients with transmural myocardial infarction. *Heart Rhythm* 2018;**15**:814–21.
- Alexandre J, Saloux E, Dugué AE, Lebon A, Lemaître A, Roule V et al. Scar extent evaluated by late gadolinium enhancement CMR: a powerful predictor of long-term appropriate ICD therapy in patients with coronary artery disease. *J Cardiovasc Magn Reson* 2013;**15**:12.
- Stolzmann P, Scheffel H, Leschka S, Schertler T, Frauenfelder T, Kaufmann PA et al. Reference values for quantitative left ventricular and left atrial measurements in cardiac computed tomography. *Eur Radiol* 2008;**18**:1625–34.
- Okubo K, Frontera A, Bisceglia C, Paglino G, Radinovic A, Foppoli L et al. Grid mapping catheter for ventricular tachycardia ablation. *Circ Arrhythm Electrophysiol* 2019;**12**:e007500.
- Nührich JM, Kaiser L, Akbulak RÖ, Schäffer BN, Eickholt C, Schwarzl M et al. Substrate characterization and catheter ablation in patients with scar-related ventricular tachycardia using ultra high-density 3D mapping. *J Cardiovasc Electrophysiol* 2017;**28**:1058–67.
- Tung R, Raiman M, Liao H, Zhan X, Chung FP, Nagel R et al. Simultaneous endocardial and epicardial delineation of 3D reentrant ventricular tachycardia. *J Am Coll Cardiol* 2020;**75**:884–9.
- Takigawa M, Duchateau J, Sacher F, Martin R, Vlachos K, Kitamura T et al. Are wall thickness channels defined by computed tomography predictive of isthmuses of postinfarction ventricular tachycardia? *Heart Rhythm* 2019;**16**:1661–8.
- Bourier F, Martin R, Martin CA, Takigawa M, Kitamura T, Frontera A et al. Is it feasible to offer 'targeted ablation' of ventricular tachycardia circuits with better understanding of isthmus anatomy and conduction characteristics? *Europace* 2019;**21**:27–33.

## **INTRODUCTION**

Ventricular tachycardia (VT) substrate ablation is an effective treatment for scar-dependent VT (1,2) but recurrence rate remains high with standard approaches (3-5). Recent studies (6,7) have shown that aiding or guiding VT-substrate ablation procedures with integrated color-coded pixel signal intensity (PSI) maps, obtained from pre-procedural late gadolinium enhancement cardiac magnetic resonance (LGE-CMR) imaging, results in less need for RF delivery and an improved VT recurrence-free survival. LGE-CMR shows great accuracy when characterizing the scarred tissue, (8,9) and is able to identify further arrhythmogenic substrate (AS) as compared with endocardial or epicardial surface electroanatomic maps (EAM) alone. (6) However, the use of LGE-CMR may be limited in certain situations, such as patient's claustrophobia, inability to perform long breath-holds, presence of image artifacts in carriers of cardiac implantable electronic devices (CIED), etc. Moreover, CMR may not be broadly available for all centers to be used routinely as part of the pre-procedural work-up for patients undergoing VT ablation.

Wall thickness assessment using multidetector cardiac tomography (MDCT) has recently arisen as an alternative cardiac imaging method to identify the AS before VT ablation procedures. Wall thinning (WT) is a useful parameter that has proven to correlate with low voltage areas (LVA) and distribution of local abnormal ventricular activities (LAVA). (10,11) CT-defined ridges of thicker myocardial tissue within the scar can be considered as appropriate ablation targets. (12) However, in cases of ischemic cardiomyopathy (ICM) with transmural substrate the agreement with epicardial low voltage areas has been shown to be significantly higher for CMR than for MDCT. (13) In the present study, we sought to evaluate

the general performance of MDCT imaging in identifying the heterogeneous tissue channels (HTCs) detected by CMR in patients with ICM undergoing VT substrate ablation.

## **METHODS**

### **Patient sample**

This is a retrospective study, including 30 consecutive patients with ICM referred for a first catheter ablation of scar-related sustained monomorphic VT. As previously reported, (6,7) substrate mapping was guided by the information from the 3D LGE-CMR-derived reconstructions (i.e. pixel signal intensity maps) integrated into the navigation system, after merging a fast-anatomical map (FAM) of the aorta or the right ventricle with the corresponding structure from the 3D cardiac MDCT-derived reconstructions. The study complied with the Declaration of Helsinki. The local Ethics Committee approved the study protocol and all included participants signed the informed consent.

### **LGE-CMR acquisition and segmentation**

A pre-procedural LGE-CMR study was performed either in a 3-Tesla scanner (MAGNETOM Trio™, Siemens Healthcare, Erlangen, Germany) or a 1.5-Tesla scanner (MAGNETOM Aera™; Siemens Healthcare, Erlangen, Germany). For patients previously implanted with an implantable cardiac defibrillator (ICD), the 1.5-Tesla scanner was used with a specific 'wideband' sequence in order to avoid device artefacts, although some ICD carriers underwent a 3-Tesla CMR immediately before implantation, as preimplantation imaging is our routine clinical practice. For acquisition details, see Supplementary material.

LGE-CMR images were analyzed using a previously described technique. (6,7) The 3D left ventricle (LV) was segmented from the whole image volume using ADAS-3D™ software (Galgo Medical, Barcelona, Spain). The LV was automatically divided into 10 layers from endo- to epicardium, each one representing 10% of the total LV wall thickness. PSI was projected onto each layer following a trilinear interpolation algorithm. Myocardial tissue was classified into core zone (CZ), border zone (BZ), and healthy tissue using  $60 \pm 5\%$  and  $40 \pm 5\%$  of the maximum intensity signal of the scar as thresholds. (14) Finally, different scar areas (core and BZ) were automatically quantified in each myocardial layer. On the LGE-CMR PSI maps, HTC were defined as continuous corridors of BZ surrounded by scar core or scar core and an anatomical barrier (i.e. mitral annulus) connecting two areas of healthy tissue. HTCs were obtained automatically by the ADAS-3D™ software. HTCs were classified as: 1) sub-endocardial (layers from 10 to 50%); 2) sub-epicardial (layers from 60 to 90%); and 3) transmural (from layer 10 to 90%). Additionally, HTC entrances were defined as the areas where HTC connect with healthy tissue.

### **Multidetector CT (MDCT) acquisition and segmentation**

In all patients, a preprocedural MDCT ECG-gated study was performed on a 128 x 2-slice CT scanner (SOMATOM Definition Flash®, Siemens Healthcare, Erlangen, Germany). Acquisition details are summarized in Supplementary material. MDCT images were retrospectively analyzed using ADAS-3D™ software. The endo- and epicardial surfaces of the LV were segmented using an algorithm based on initial alignment of a standard cardiac model, followed by manual corrections. The myocardial wall thickness was automatically computed as the distance between each point on the endo- and epicardial surfaces of the

model. A 3D color-coded surface mesh of the LV myocardial wall thickness was automatically obtained with the software.

### **Ablation procedure**

CARTO3<sup>®</sup> electroanatomical navigation system (Biosense Webster, Diamond Bar, CA, USA) was used for guiding ablation. An open-irrigated 3.5-mm tip ablation catheter (ThermoCool<sup>®</sup> SmartTouch<sup>®</sup>, Biosense Webster, Diamond Bar, CA, USA) was used for mapping and ablation. A transeptal access was performed in all patients for LV endocardial mapping. An epicardial approach was considered whenever the presence of LGE involved  $\geq 75\%$  of the myocardial wall thickness. (15) Ablation was performed according to the scar dechanneling technique (5), considering all CMR-channel entrances ('CMR-entrances') as ablation targets. A CMR-guided approach (7) was used; this approach has already been proven to be feasible, safe and effective in terms of post-ablation inducibility and VT recurrence rates. (7)

### **Comparison between CMR-channels and CT-channels**

Two operators, blinded to any clinical or procedural information of the patients, were randomly assigned either to CMR or MDCT post-hoc analysis. The CMR operator characterized the presence of CMR-channels (i.e. HTC) in terms of disposition (longitudinal, transversal, or diagonal), degree of transmural, and location defined by the 17-segment American Heart Association (AHA) model. The MDCT operator examined the area with a myocardial thickness  $< 5$  mm and analyzed, hand-raking the wall thickness thresholds in order to detect myocardial ridges. These ridges, named CT-channels, were defined as

channel-shaped edges inside the MDCT scar showing a thickness that exceeded the surrounding myocardium by  $\geq 1$  mm (11) (Figure 1) Finally, disposition and location were annotated for CT-channels in the same manner as for CMR-channels. Both operators annotated the total number of channels observed, as well as the number and location of the corresponding channel entrances, which are considered ablation targets according to the scar dechanneling technique. (5) MDCT findings were compared to those derived from CMR, considering this last imaging technique as the gold standard for AS evaluation. Channel concordance was considered whenever a CT-channel showed the same disposition and was located in the same AHA segment as a corresponding CMR-channel.

### **Statistical analysis**

Continuous variables are presented as mean values  $\pm$  standard deviations. Categorical variables are presented as total numbers and percentages. Populations were compared by the Wilcoxon-Mann-Whitney or Fisher exact test, as appropriate. A p-value  $\leq 0.05$  was considered for statistical significance. Statistics were obtained using IBM SPSS Statistics, version 25.0 (IBM Corp. Released 2017; Armonk, NY: IBM Corp.), and Matlab statistics toolbox (Matlab R2010a, The Mathworks, Inc., Natick, MA, USA).

## **RESULTS**

### **Patient characteristics**

Mean age was  $69 \pm 10$  years; 94% were male. Mean LVEF was  $35 \pm 10\%$ . Using classical imaging criteria (16), 19/30 (63%) patients showed a transmural MI (hyperenhancement involving  $\geq 75\%$  of the wall thickness), whereas 11/30 (37%) had only a subendocardial MI. Baseline characteristics of the population are summarized in Table 1.

### **Multimodality image-based assessment of arrhythmogenic substrate (AS)**

An example of CT-channel identification workflow is shown in Figure 1. The mean area of significant myocardial WT (5-mm cut-off) (17) was  $62.3 \pm 40.4$  cm<sup>2</sup>, corresponding to a mean of  $30.7 \pm 17.0\%$  of the total LV endocardial area. Patients with a transmural MI presented a larger area of significant myocardial WT than those with a subendocardial MI ( $36.9 \pm 13.1\%$  vs  $21.9 \pm 18.4\%$ ,  $p = 0.016$ ). A total of 91 CT-channels were identified in 26/30 (86.7%) patients, with a mean of  $3.0 \pm 2.0$  CT-channels per patient. The mean WT thresholds employed to detect the CT-channels were  $3.66 \pm 0.96$  mm and  $4.31 \pm 0.58$  mm for the lower and upper limits, respectively, with 91/91 (100%) of the myocardial ridges found in the areas with  $< 5$ -mm thickness, which was considered the MDCT area of interest for analysis. A total of 190 CT-channel entrances ('CT-entrances') were identified, corresponding to a mean of  $6.3 \pm 4.1$  CT-entrances per patient.

Thirteen out of 30 (43%) patients underwent a 1.5 Tesla CMR using a wideband sequence. The mean scar mass evaluated with CMR was  $34.5 \pm 12.1$  g, corresponding to a mean of  $20.6 \pm 6.4\%$  of the total LV mass. Patients with a transmural MI presented a higher scar mass than those with a subendocardial MI ( $22.7 \pm 5.7\%$  vs  $17.3 \pm 6.5\%$ ,  $p = 0.030$ ). Using standard thresholds (14) for BZ and core characterization, 76 CMR-channels were identified

in 30/30 (100%) patients, with a mean of  $2.4 \pm 1.2$  CMR-channels per patient. Thirty-six out of 76 (47.4%) CMR-channels were classified as non-endocardial (i.e. epi- or transmural). A total of 275 CMR-entrances were identified, corresponding to a mean of  $8.9 \pm 4.9$  CMR-entrances per patient.

### **Comparison of MDCT-based vs. CMR-based evaluation of AS**

A total of 47/91 (51.6%) CT-channels were also detected as CMR-channels, and therefore identified as CT true positives. On the contrary, 44/91 (48.4%) CT-channels were considered as false positives. In particular, 19/91 (20.9%) CT-channels were identified outside the boundaries of the CMR scar. Moreover, 29/76 (38.2%) CMR-channels could not be identified on the CT (false negatives). (Figure 2).

A total of 29/36 (80.5%) non-endocardial CMR-channels were also identified on MDCT analysis. A significantly higher proportion of non-endocardial CMR-channels could be identified with MDCT, when compared to only-endocardial CMR-channels (80.5% vs. 45%;  $p = 0.002$ ) (Table 2).

There were 91/190 (47.9%) true positive CT-entrances after matching with their corresponding CMR-entrances. On the other hand, 99/190 (52.1%) CT-entrances were considered false positives, and 184/275 (66.9%) CMR-entrances could not be identified using CT (false negatives). The estimated global sensitivity values for detection of channels and channel entrances using MDCT were 61.8% and 33.1%, respectively (Figure 3).



Notably, in 4/11 (36%) patients with subendocardial MI, MDCT was unable to identify the presence of AS.

### **Performance of MDCT in patients with transmural MI**

Among patients with transmural MI ( $n = 19$ , 63.3%), there were 39/73 (53.4%) CT-channels considered as true positives, whereas 34/73 (46.6%) were identified as false positives. Fifteen out of 54 (27.8%) CMR-channels could not be detected on CT (false negatives).

A significantly higher proportion of CMR-channels can be identified with MDCT in patients with transmural MI ( $n = 19$ ), as compared to non-transmural MI ( $n = 11$ ) (72.2% vs. 36.4%;  $p = 0.004$ ) (Table 2 and Figure 4). Moreover, there is also a non-significant trend towards a better detection performance of MDCT for endocardial CMR channels in patients with transmural MI as compared with non-transmural (55.6% vs 36.4%;  $p = 0.37$ ) (Table 3).

There were 76/153 (49.7%) true positive CT-entrances after matching with their corresponding CMR-entrances. On the other hand, 77/153 (50.3%) CT-entrances were considered false positives, and 117/191 (61.3%) CMR-entrances could not be identified using CT (false negatives). Concerning channel entrance detection, there is a non-significant trend to a lower rate of false positives when comparing transmural with non-transmural MI (50.3% vs. 59.5%;  $p = 0.31$ ). Furthermore, the rate of false negatives was significantly lower in transmural MI (61.3% vs. 79.8%;  $p=0.002$ ). In this population, the estimated sensitivity values for detection of CMR-channels and their entrances using MDCT were 72.2% and 39.7%, respectively. These sensitivity values are significantly higher in patients with

transmural MI: 72.2% vs. 36.4% ( $p = 0.004$ ) for the detection of channels, and 39.4% vs. 18.3% ( $p < 0.001$ ) for the identification of channel entrances. In both cases, these differences may be ascribed to the lower rate of false negatives encountered. A summary of the most important findings of the study can be found in Table 4.

## **DISCUSSION**

To the best of our knowledge, this is the first clinical study comparing two different non-invasive methods for identification of the AS within post-infarction scarred tissue: i) Detection of anatomical, thickened myocardial ridges identified using MDCT, versus ii) detection of HTC (border zone corridors) using LGE-CMR.

The main findings of the study are that: i) MDCT fails to detect the presence of HTCs in about 36% of patients with only subendocardial scars (Figure 4); ii) MDCT assessment of WT is only moderately capable (61.8% sensitivity) of identifying the presence of HTCs; iii) in patients with transmural MI, MDCT sensitivity improves significantly (72.2%) due to a lower false negative rate; and iv) WT evaluation with MDCT shows a poor sensitivity in identifying HTC entrances (33.1%), mainly due to a very high false negative rate that slightly improves in patients with transmural MI.

### **CMR, the imaging reference for AS characterization**

LGE-CMR constitutes a highly accurate tool to characterize and delimit the scarred tissue within the entire myocardial thickness. (8) Moreover, it has proven to be capable of

identifying additional AS compared with endocardial or epicardial surface electroanatomic maps (EAM) alone, (6) as well as to improve the acute and long-term VT substrate ablation outcomes when guiding such procedures, without the need for an EAM reconstruction. (7) In this regard, it has been shown that patients with HTCs identified by CMR that are not targeted for ablation (i.e. with normal electrograms at EAM, due to a far-field effect from the surrounding healthy myocardium), suffer from more VT recurrences after  $20 \pm 19$  months of follow-up. (6) Furthermore, a previous study from Yamashita et al. (13) demonstrated that the agreement between detection of structural substrate in imaging and low voltage zones (areas with peak-to-peak amplitude  $< 1.5$  mV of bipolar voltage) was higher for CMR than for MDCT when evaluating epicardial substrate ( $73 \pm 7\%$  vs.  $60 \pm 13\%$ ,  $p = 0.002$ ) in ICM. In order to improve the characterization of the AS using EAM, different multi-electrode catheters and high-density mapping systems have been tested. In previous studies, the use of a grid mapping catheter (18) allowed to identify late potentials or LAVAs only in 72% of the sites that had been identified as VT mid-isthmuses after VT induction, whereas the use of a multi-basket catheter (19) allowed to identify only 50% of the critical isthmuses of all induced VTs. More recently, Tung R et al. (20) have described, after simultaneous VT mapping from endo- and epicardium, how VT isthmuses are frequently 3-dimensional, while recognizing that conventional EAM results in a limited 2D representation of the reentrant circuit. All these aspects have been pondered over when considering CMR as the imaging reference to identify VT substrate in ICM.

### **Usefulness of VT evaluation using MDCT for substrate detection in ICM**

As previously ascertained, MDCT is capable of only modestly identifying the presence of HTCs detected with CMR (61.8% sensitivity). However, the relationship between the regional myocardial WT assessed with MDCT and the presence of AS in ICM has been well recognized before, (13) aside from MDCT ability to detect critical ablation sites, identified as ridges of myocardial tissue dividing areas of WT. (12,21) Recently, Takigawa M et al. (21) studied 9 postinfarction patients and found that 100% of their VT isthmuses were found inside CT channels. However, this finding refers only to the 10/32 induced VTs whose circuit could be fully characterized, that is, only 31% of the VTs could be fully mapped using EAM. Considering the small size of the studied population and that, in our study, MDCT could not detect the presence of AS in 36% of the patients with subendocardial MI, we would take this sensitivity with caution.

The AS information depicted by MDCT is different from that provided by CMR; whereas MDCT is able to detect ridges and sinks of myocardial tissue within the scar, CMR is capable of distinguishing viable myocardial tissue, irrespective of its relative thickness. Notwithstanding, these two imaging techniques also have similarities: effective ablation sites are most often found in the thicker ridges in MDCT (12) and are also most frequently located in HTC (BZ channels) detected with CMR. (6) Moreover, the ridges with effective ablation sites are predominantly located in the BZ scar (areas with a bipolar voltage of 0.5-1.5 mV). (12)

The fact that MDCT shows better accuracy at identifying the AS depicted by CMR in patients with transmural MI (72.2% sensitivity) and/or in the presence of epicardial or transmural

channels, is in line with these considerations. Transmural scars show greater WT, probably making it easier to detect potential 'ridges and sinks' of myocardial tissue. Small subendocardial scars may not always modify the myocardial thickness at the injured zone in such a magnitude that these ridges can reflect the whole 3-D structure of the AS. HTC are complex, branched structures connecting with healthy tissue at several entrances that show specific electrogram properties and are target for ablation. (6) These entrances, usually found at BZ areas of the scar, can barely be identified with MDCT in patients with subendocardial scars (18.3% sensitivity). In fact, MDCT cannot detect the presence of AS in up to 36% of the patients with a subendocardial MI.

Nevertheless, MDCT still constitutes a valuable tool depicting AS characteristics that help when performing scar-related VT ablation procedures, (10-13,20-22) although CMR seems to be a more precise tool to depict the whole AS 3D structure and guide ablation procedures. (7) Finally, it cannot be ignored that MDCT-derived cardiac anatomy integration during ablation procedures impacts on safety and helps with procedural management. (10,13,15) MDCT may be proposed as a useful pre-procedural imaging technique to aid VT substrate ablation procedures in patients with a transmural MI, better if combined with CMR information. For subendocardial scars, CMR should be considered as the best imaging tool to depict the AS and plan these procedures.

### **Study limitations**

Since ablation was performed using a CMR-guided approach, only limited EAM data were available. (7) The analysis of channel entrances, where MDCT showed a remarkably poor

sensitivity, was considered useful as these constitute ablation targets in the scar dechanneling technique. Yet, when only channel detection is considered the main message remains the same, thus making the results applicable to other ablation approaches. Finally, imaging data on substrate detection could be potentially influenced by CMR/MDCT image quality.

## **Conclusions**

Compared to LGE-CMR, wall thickness assessment and identification of myocardial ridges within the scar using MDCT shows only a modest sensitivity in identifying the presence of HTC, being unable to detect the presence of AS, as depicted by CMR, in 36% of patients with subendocardial MI scars. MDCT performance improves in patients with transmural MI and in the identification of non-endocardial (i.e. subepicardial or transmural) channels. For subendocardial scars, CMR should be considered as the best imaging tool to depict the AS and to plan ablation procedures.

## **ACKNOWLEDGEMENTS**

None.

## **FUNDING**

This research received no specific grant from any funding agency in the public, commercial, or not-for-profit sectors.

**CONFLICT OF INTEREST**

Dr. Berruezo is a stockholder in Galgo Medical SL. The other authors have no other relevant affiliations or financial involvement with any organization or entity with a financial conflict with the subject matter or materials discussed in the manuscript apart from those disclosed.

**REFERENCES**

1. Reddy VY, Reynolds MR, Neuzil P, Richardson AW, Taborsky M, Jongnarangsin K, et al. Prophylactic catheter ablation for the prevention of defibrillator therapy. *N Engl J Med* 2007;357:2657-2665.
2. Kuck KH, Schaumann A, Eckardt L, Willems S, Ventura R, Delacrétaz E, et al. Catheter ablation of stable ventricular tachycardia before defibrillator implantation in patients with coronary heart disease (VTACH): a multicentre randomised controlled trial. *Lancet* 2010;375:31-40.
3. Jaïs P, Maury P, Khairy P, Sacher F, Nault I, Komatsu Y, et al. Elimination of local abnormal ventricular activities: a new end point for substrate modification in patients with scar-related ventricular tachycardia. *Circulation* 2012;125:2184-2196.
4. Di Biase L, Santangeli P, Burkhardt DJ, Bai R, Mohanty P, Carbucicchio C, et al. Endo-epicardial homogenization of the scar versus limited substrate ablation for the treatment of electrical storms in patients with ischemic cardiomyopathy. *J Am Coll Cardiol* 2012, 60:132-141.
5. Berruezo A, Fernández-Armenta J, Andreu D, Penela D, Herczku C, Evertz R, et al. Scar dechanneling: new method for scar-related left ventricular tachycardia substrate ablation. *Circ Arrhythm Electrophysiol* 2015;8:326-336.
6. Andreu D, Penela D, Acosta J, Fernández-Armenta J, Perea RJ, Soto-Iglesias D, et al. Cardiac magnetic resonance-aided scar dechanneling: Influence on acute and long-term outcomes. *Heart Rhythm* 2017;14:1121-1128.



7. Soto-Iglesias D, Penela D, Jáuregui B, Acosta J, Fernández-Armenta J, Linhart M, et al. Cardiac Magnetic Resonance-Guided Ventricular Tachycardia Substrate Ablation. *JACC Clin Electrophysiol* 2020;6:436-447.
8. Fernández-Armenta J, Berruezo A, Andreu D, Camara O, Silva E, Serra L, et al. Three-dimensional architecture of scar and conducting channels based on high resolution ce-CMR: insights for ventricular tachycardia ablation. *Circ Arrhythm Electrophysiol* 2013;6:528-537.
9. Perez-David E, Arenal A, Rubio-Guivernau JL, del Castillo R, Atea L, Arbelo E, et al. Noninvasive identification of ventricular tachycardia-related conducting channels using contrast-enhanced magnetic resonance imaging in patients with chronic myocardial infarction: comparison of signal intensity scar mapping and endocardial voltage mapping. *J Am Coll Cardiol* 2011;57:184-194.
10. Tian J, Jeudy J, Smith MF, Jimenez A, Yin X, Bruce PA, et al. Three-dimensional contrast-enhanced multidetector CT for anatomic, dynamic, and perfusion characterization of abnormal myocardium to guide ventricular tachycardia ablations. *Circ Arrhythm Electrophysiol* 2010;3:496-504.
11. Komatsu Y, Cochet H, Jadidi A, Sacher F, Shah A, Derval N, et al. Regional myocardial wall thinning at multidetector computed tomography correlates to arrhythmogenic substrate in postinfarction ventricular tachycardia: assessment of structural and electrical substrate. *Circ Arrhythm Electrophysiol* 2013;6:342-350.
12. Ghannam M, Cochet H, Jais P, Sermesant M, Patel S, Siontis KC, et al. Correlation between computer tomography-derived scar topography and critical ablation sites in postinfarction ventricular tachycardia. *J Cardiovasc Electrophysiol* 2018;29:438-445.

13. Yamashita S, Sacher F, Mahida S, Berte B, Lim HS, Komatsu Y, et al. Image Integration to Guide Catheter Ablation in Scar-Related Ventricular Tachycardia. *J Cardiovasc Electrophysiol* 2016;27:699-708.
14. Andreu D, Berruezo A, Ortiz-Pérez JT, Silva E, Mont L, Borràs R, et al. Integration of 3D Electroanatomic Maps and Magnetic Resonance Scar Characterization Into the Navigation System to Guide Ventricular Tachycardia Ablation. *Circ Arrhythm Electrophysiol* 2011;4:674-683.
15. Soto-Iglesias D, Acosta J, Penela D, Fernández-Armenta J, Cabrera M, Martínez M, et al. Image-based criteria to identify the presence of epicardial arrhythmogenic substrate in patients with transmural myocardial infarction. *Heart Rhythm* 2018;15:814-821.
16. Alexandre J, Saloux E, Dugué AE, Lebon A, Lemaitre A, Roule V, et al. Scar extent evaluated by late gadolinium enhancement CMR: A powerful predictor of long-term appropriate ICD therapy in patients with coronary artery disease. *J Cardiovasc Magn Reson* 2013;15:12.
17. Stolzmann P, Scheffel H, Leschka S, Schertler T, Frauenfelder T, Kaufmann PA, et al. Reference values for quantitative left ventricular and left atrial measurements in cardiac computed tomography. *Eur Radiol* 2008;18:1625-1634.
18. Okubo K, Frontera A, Bisceglia C, Paglino G, Radinovic A, Foppoli L, et al. Grid Mapping Catheter for Ventricular Tachycardia Ablation. *Circ Arrhythm Electrophysiol* 2019;12:e007500.
19. Nührich JM, Kaiser L, Akbulak RÖ, Schäffer BN, Eickholt C, Schwarzl M, et al. Substrate characterization and catheter ablation in patients with scar-related ventricular

tachycardia using ultra high-density 3D mapping. *J Cardiovasc Electrophysiol* 2017;28:1058-1067.

20. Tung R, Raiman M, Liao H, Zhan X, Chung FP, Nagel R, et al. Simultaneous Endocardial and Epicardial Delineation of 3D Reentrant Ventricular Tachycardia. *J Am Coll Cardiol* 2020;75:884-889.

21. Takigawa M, Duchateau J, Sacher F, Martin R, Vlachos K, Kitamura T, et al. Are wall thickness channels defined by computed tomography predictive of isthmuses of postinfarction ventricular tachycardia? *Heart Rhythm* 2019;16:1661-1668.

22. Bourier F, Martin R, Martin CA, Takigawa M, Kitamura T, Frontera A, et al. Is it feasible to offer 'targeted ablation' of ventricular tachycardia circuits with better understanding of isthmus anatomy and conduction characteristics? *Europace* 2019;21(Supplement\_1):i27-i33.

## TABLES

**Table 1.** Baseline characteristics.

	<b>Total population (n = 30)</b>	<b>Subendocardial MI (n = 11)</b>	<b>Transmural MI (n = 19)</b>	<b>P-value</b>
<b>Age, years</b>	69 ± 10	69 ± 10	68 ± 10	0.85
<b>Men (%)</b>	27 (90%)	11 (100%)	16 (84.2%)	0.16
<b>Hypertension (%)</b>	24 (80%)	8 (72.7%)	16 (84.2%)	0.45
<b>Dyslipidemia (%)</b>	22 (73.3%)	8 (72.7%)	14 (73.7%)	0.95
<b>Diabetes mellitus (%)</b>	13 (43.3%)	7 (63.6%)	6 (31.6%)	0.09
<b>Smokers (%)</b>	5 (16.7%)	3 (27.3%)	2 (10.5%)	0.23
<b>LVEF, %</b>	35 ± 9	35 ± 11	34 ± 9	0.82
<b>LVEDD, mm</b>	61 ± 7	63 ± 9	60 ± 6	0.39
<b>Scar localization</b>				
- Anterior	14 (6.7%)	3 (27.3%)	11 (57.9%)	0.22
- Inferior	13 (43.3%)	7 (63.6%)	6 (31.6%)	
- Lateral	3 (10%)	1 (9.1%)	2 (10.5%)	
<b>CAD extension &amp; severity</b>				
- Single-vessel	7/18 (39%)	2/4 (50%)	5/14 (36%)	0.14
- Two-vessel	7/18 (39%)	0	7/14 (50%)	
- Three-vessel	4/18 (22%)	2/4 (50%)	2/14 (14%)	
<b>Complete CAD revascularization</b>	14/18 (78%)	3/4 (75%)	11/14 (79%)	0.64
<b>Coronary CTO</b>	2/18 (11%)	0	2/14 (14%)	0.78
<b>Time since MI, months</b>	21 ± 9	25 ± 12	20 ± 7	0.41
<b>NYHA class (%)</b>	1.94 ± 0.64	2.13 ± 0.64	1.80 ± 0.63	0.28
<b>Previous ICD (%)</b>	24 (80%)	9 (81.8%)	15 (78.9%)	0.85
<b>Appropriate ICD therapies (ATP + shocks), n</b>	9 ± 21	1 ± 1	15 ± 27	0.31
<b>Arrhythmia storm (%)</b>	3 (10%)	2 (18.2%)	1 (5.3%)	0.26
<b>Previous treatment</b>				
- Betablockers	20 (66.7%)	6 (54.5%)	14 (73.7%)	0.11
- Sotalol	0 (0%)	0 (0%)	0 (0%)	-
- Amiodarone	15 (50%)	7 (63.6%)	8 (42.1%)	0.32

MI: Myocardial infarction; LVEF: Left ventricular ejection fraction; LVEDD: Left ventricular end-diastolic diameter; CAD: Coronary artery disease; CTO: Chronic total occlusion; NYHA: New York Heart Association; ICD: Implantable cardiac defibrillator; ATP: Anti-tachycardia pacing.

**Table 2.** MDCT detection performance for endocardial vs. non-endocardial (i.e. epicardial or transmural) CMR-channels, and for transmural vs. non-transmural MI.

	<b>Total CMR-channels</b>	<b>MDCT-detected CMR-channels</b>	<b>P-value</b>
<b>All CMR-channels</b>	76	47 (61.8%)	-
• <b>Non-endocardial CMR-channels</b>	36	29 (80.5%)	0.002
• <b>Endocardial CMR-channels</b>	40	18 (45%)	
<b>All patients (n = 30)</b>	76	47 (61.8%)	-
• <b>Transmural MI (n = 19)</b>	54	39 (72.2%)	0.004
• <b>Non-transmural MI (n = 11)</b>	22	8 (36.4%)	

*MDCT: Multidetector cardiac tomography; MI: Myocardial infarction; CMR: Cardiac magnetic resonance.*

**Table 3.** MDCT detection performance for endocardial vs. non-endocardial (i.e. epicardial or transmural) CMR-channels with respect to MI transmurality.

	<b>Total CMR-channels</b>	<b>MDCT-detected CMR-channels</b>	<b>P-value</b>
<b>Transmural MI (n = 19)</b>	54	39 (72.2%)	0.05
• <b>Non-endocardial CMR-channels</b>	36	29 (80.5%)	
• <b>Endocardial CMR-channels</b>	18	10 (55.6%)	
<b>Non-transmural MI (n = 11)</b>	22	8 (36.4%)	-
• <b>Non-endocardial CMR-channels</b>	0	0 (0%)	
• <b>Endocardial CMR-channels</b>	22	8 (36.4%)	

*MDCT: Multidetector cardiac tomography; CMR: Cardiac magnetic resonance; MI: Myocardial infarction.*

**Table 4.** MDCT performance in detection of heterogeneous tissue channels and their entrances, as compared with CMR.

		<b>Global (n = 30)</b>	<b>Transmural MI (n = 19)</b>	<b>Non-transmural MI (n = 11)</b>	<b>P-value</b>
<b>CC detection</b>	True positives	47/91 (51.6%)	39/73 (53.4%)	8/18 (44.4%)	0.49
	False positives	44/91 (48.4%)	34/73 (46.6%)	10/18 (55.6%)	0.49
	False negatives	29/76 (38.2%)	15/54 (27.8%)	14/22 (63.6%)	0.004
	<b>Sensitivity</b>	<b>61.8%</b>	<b>72.2%</b>	<b>36.4%</b>	<b>0.004</b>
	<b>PPV</b>	<b>51.6%</b>	<b>53.4%</b>	<b>44.4%</b>	<b>0.49</b>
<b>CC entrances' detection</b>	True positives	91/190 (47.9%)	76/153 (49.7%)	15/37 (40.5%)	0.31
	False positives	99/190 (52.1%)	77/153 (50.3%)	22/37 (59.5%)	0.31
	False negatives	184/275 (66.9%)	117/191 (61.3%)	67/84 (79.8%)	0.002
	<b>Sensitivity</b>	<b>33.1%</b>	<b>39.4%</b>	<b>18.3%</b>	<b>&lt; 0.001</b>
	<b>PPV</b>	<b>47.9%</b>	<b>49.7%</b>	<b>40.5%</b>	<b>0.31</b>

MDCT: Multidetector cardiac tomography; CMR: Cardiac magnetic resonance; MI: Myocardial infarction; CC: Conducting channel; PPV: Positive predictive value.

**FIGURES**

**Figure 1.** CMR-channel and CT-channel identification workflow. LGE-CMR and MDCT imaging post-processing in a patient with mid-apical anteroseptal and mid-inferolateral post-MI scars. Only the anteroseptal scar segmentation is shown.

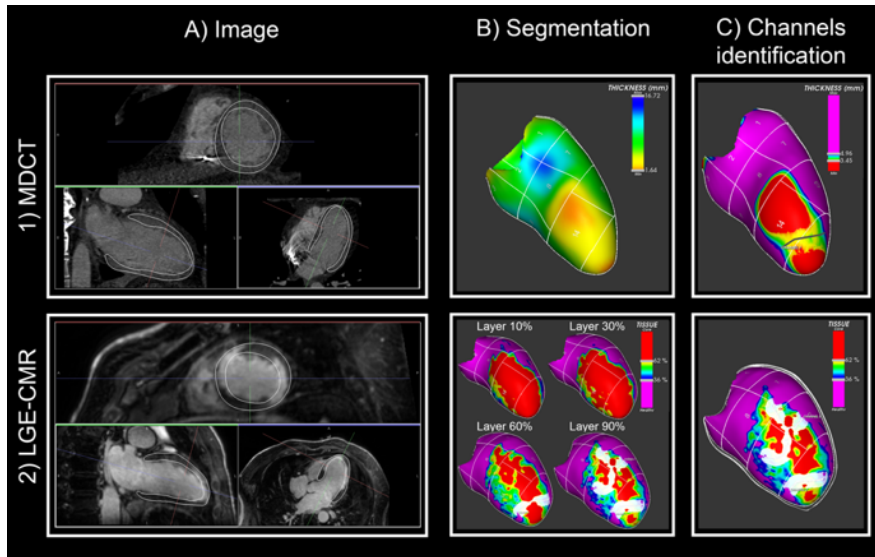


**Figure 2.** Examples of true positives, true negatives, false positives, and false negatives using MDCT. Paired MDCT-CMR images correspond to the same patient. White arrows point to CT-channels or CMR-channels, as appropriate.

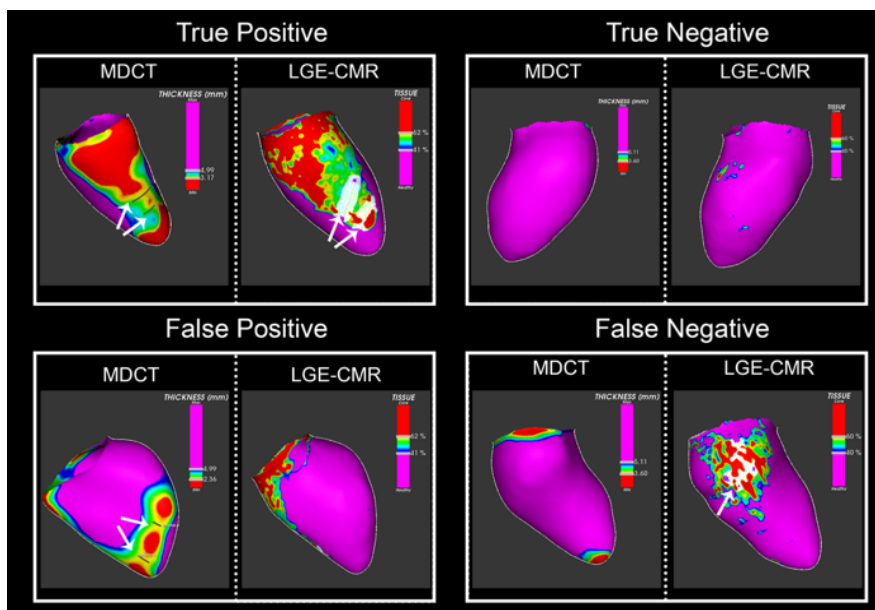


**Figure 3.** Detection of channel entrances with CMR and MDCT in a basal and mid-inferoseptal MI. Left panel: The subendocardial aspect of a BZ channel is displayed. Three entrances are detected at the anterior edge of the scar (basal and mid-anteroseptal). Mid panel: Mid-myocardial BZ pathways belonging to the same channel. Here, there are two additional entrances (submitral and mid-inferoseptal) at the inferior edge of the scar. Right panel: MDCT segmentation of the same patient. The CMR-channel structure can be recognized. Two out of three anterior entrances, and one out of two posterior entrances can be detected with the MDCT.

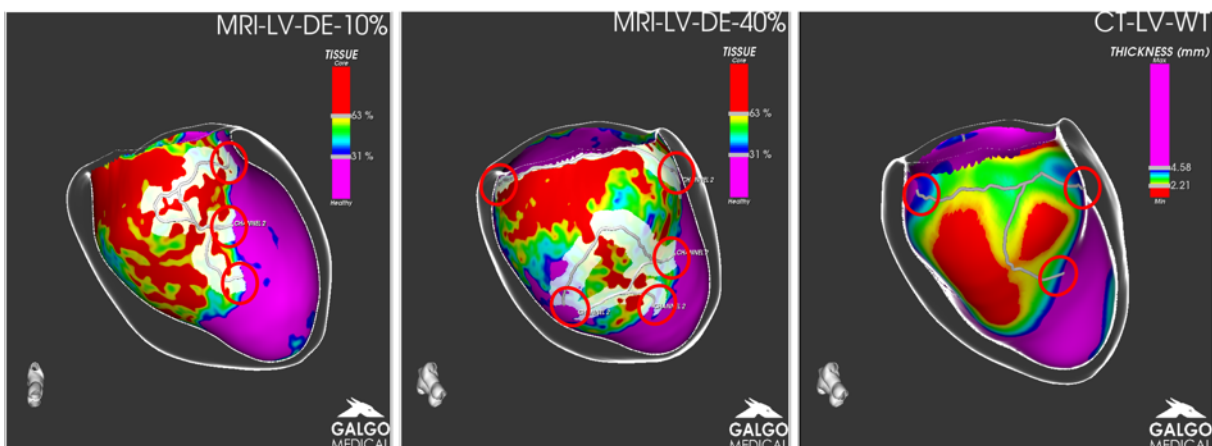
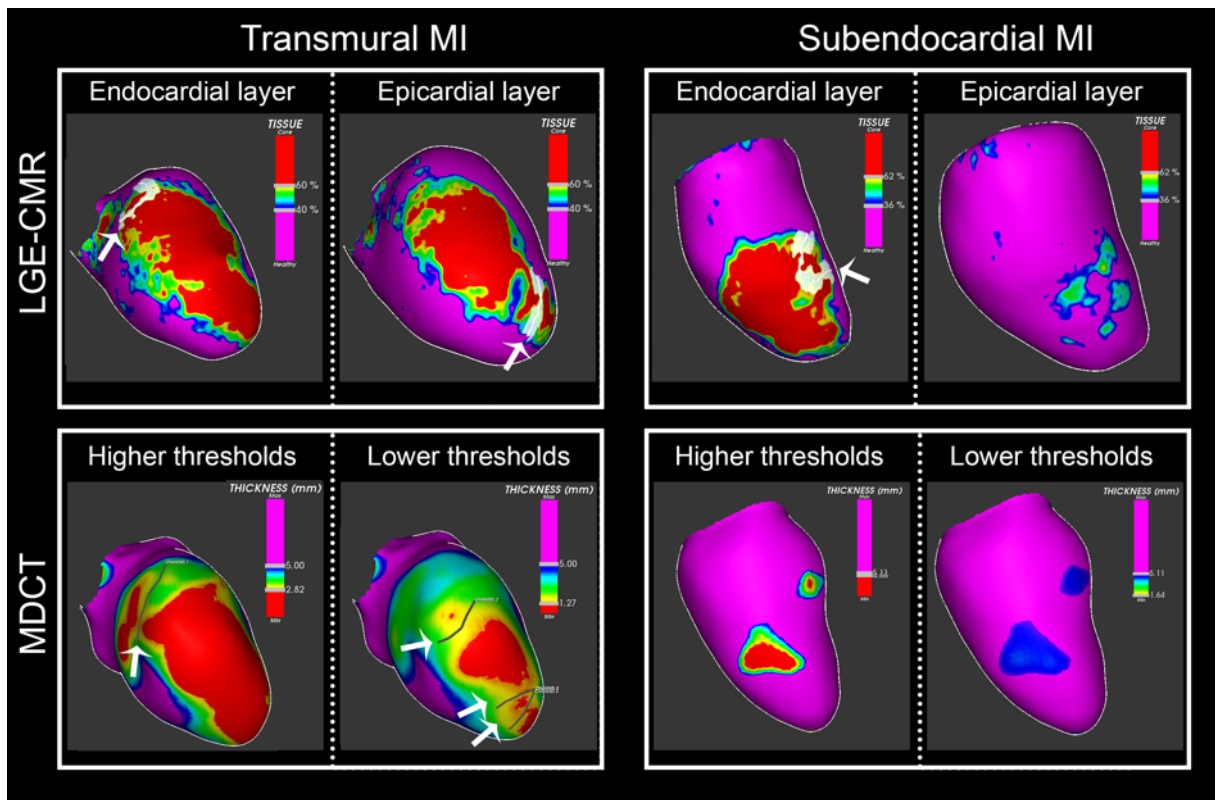


**Figure 4 (representative figure).** Multimodal imaging-based channel detection in transmural (left panels) vs. subendocardial MI (right panels). Left upper panel: Two CMR-channels are detected (subendocardial and subepicardial). Left lower panel: With MDCT, hand-raking the wall thickness thresholds permits to detect a total of four myocardial ridges, three of which correlate with the two CMR-channels. Right upper panel: Only one subendocardial CMR channel is detected in a patient with non-transmural MI. Right lower



panel: No CT-channels can be revealed. There is only a slight wall thinning (small area < 5 mm).



## **SUPPLEMENTARY METHODS**

### **LGE-CMR acquisition**

Contrast-enhanced images were acquired 10 minutes after bolus injection of 0.2 mmol/Kg Gadobutrol (Gadovist □, Bayer Hispania, Barcelona, Spain) using a commercially available, free-breathing, ECG-gated, navigator-gated, 3D inversion-recovery, gradient-echo technique. Slice thickness was 1.4 mm, with no gap between slices. The field of view was set at 360 mm and matrix size was kept to 256 x 256 pixels to yield an isotropic spatial resolution of 1.4 x 1.4 x 1.4 mm.

### **Wideband sequence acquisition**

In patients previously implanted with an intracardiac device the LGE-CMR was performed with a 1.5-Tesla scanner (MAGNETOM Aera □, Siemens, Erlangen, Germany). Using a 2D turboFLASH gradient-echo sequence, the sort-axis contrast-enhanced images were acquired synchronized with the ECG. Slice thickness was 5 mm, with no gap between slices, with iPAT accelerator factor x2. Typical parameters were: Repetition time 948.8 ms; echo time 1.39 ms; bandwidth 592 Hx/Px; flip angle 25°; and matrix size 256 x 144 pixels. The mean in-plane resolution was 1.4 x 1.4 mm, and the voxel size was 9.80 mm<sup>3</sup>.

### **MDCT acquisition**

Images were acquired during an inspiratory breath-hold using retrospective ECG-gating technique with tube current modulation set between 50% and 100% of the cardiac cycle. CT angiographic images were acquired during the injection of a 100 mL bolus of Iopromide 370 mg I/mL (Ultravist □, Bayer Hispania, Barcelona, Spain) at a rate of 3 mL/s.



## SUBPROYECTO 2. UTILIDAD DE LA CARDIORRESONANCIA EN LA ESTRATIFICACIÓN DE RIESGO ARRÍTMICO EN EL POST-INFARTO CRÓNICO DE MIOCARDIO.

### Artículo 4: Cardiovascular Magnetic Resonance Determinants of Ventricular Arrhythmic Events After Myocardial Infarction

**Jáuregui B**, Soto-Iglesias D, Penela D, Acosta J, Fernández-Armenta J, Linhart M, Chauca A, Carreño JM, Scherer C, Falasconi G, Prat-González S, Perea RJ, Mont L, Bosch X, Ortiz-Pérez JT, Berruezo A. Cardiovascular Magnetic Resonance Determinants of Ventricular Arrhythmic Events After Myocardial Infarction. *Europace* 2021;euab275. [Online Ahead of Print] *FACTOR DE IMPACTO (2020): 5.214. ÁREA DE CONOCIMIENTO: Cardiology and Cardiovascular Medicine. CUARTIL: Q1.*

## RESUMEN

**Objetivos:** Caracterizar de forma no invasiva, mediante resonancia magnética cardíaca con realce tardío de gadolinio (LGE-CMR), las diferencias de cicatriz y las posibles variables asociadas a la aparición de TV en pacientes crónicos post-IM.

**Métodos y resultados:** Se diseñó un estudio de casos y controles retrospectivo a través del análisis de datos de LGE-CMR en pacientes crónicos post-IM: i) derivados consecutivamente para ablación de sustrato después de un primer episodio de TV (n = 66), y ii) de un grupo de control (n = 84) sin evidencia de arritmia. El miocardio se caracterizó diferenciando core, border zone (BZ) y canales de BZ (BZC) utilizando la plataforma de post-procesamiento de imágenes ADAS 3D. Las características clínicas y de las cicatrices se compararon entre ambos grupos. Se incluyeron 150 pacientes post-IM. Se crearon cuatro modelos de Cox de riesgos proporcionales para la masa total de cicatriz, la de BZ, la de core y la de BZC, ajustándolas por edad, sexo y FEVI. Un punto de corte de 5,15 g de masa de BZC identificó los casos con una sensibilidad del 92,4% y una especificidad del 86,9% [AUC 0,93 (0,89 - 0,97);  $p < 0,001$ ], con un aumento significativo en el AUC en comparación con otros parámetros de la cicatriz ( $p < 0,001$  para todas las comparaciones por pares). La adición de masa de BZC a la FEVI permitió reclasificar el 33,3% de los casos y el 39,3% de los controles [NRI = 0,73 (0,71 - 0,74)].

**Conclusiones:** La masa de BZC es la variable independiente más fuerte asociada con la ocurrencia de TVMS clínica en pacientes post-infarto de miocardio después del ajuste de covariables por edad, sexo y FEVI. La medición de la masa de BZC podría permitir una estratificación del riesgo de TV más precisa que la FEVI en pacientes crónicos tras un IM.



ESC  
European Society  
of Cardiology

Europace (2021) 00, 1–10  
<https://doi.org/10.1093/europace/euab275>

CLINICAL RESEARCH

## Cardiovascular magnetic resonance determinants of ventricular arrhythmic events after myocardial infarction

Beatriz Jáuregui <sup>1,2</sup>, David Soto-Iglesias <sup>1,2</sup>, Diego Penela <sup>1,2</sup>, Juan Acosta <sup>3</sup>, Juan Fernández-Armenta <sup>4</sup>, Markus Linhart <sup>5</sup>, Augusto Ordóñez <sup>1</sup>, Rodolfo San Antonio <sup>1</sup>, Cheryl Terés <sup>1</sup>, Alfredo Chauca <sup>1</sup>, José M. Carreño <sup>1</sup>, Claudia Scherer <sup>1</sup>, Giulio Falasconi <sup>1</sup>, Susana Prat-González <sup>2</sup>, Rosario J. Perea <sup>2</sup>, Lluís Mont <sup>2</sup>, Xavier Bosch <sup>2</sup>, José T. Ortiz-Pérez <sup>2</sup>, and Antonio Berruezo <sup>1,2\*</sup>

<sup>1</sup>Arrhythmia Department, Heart Institute, Teknon Medical Center, C/Vilana 12, 08022 Barcelona, Spain; <sup>2</sup>Arrhythmia Department, Hospital Clínic, University of Barcelona, C/ Villarroel 170, 08024 Barcelona, Spain; <sup>3</sup>Arrhythmia Department, Virgen del Rocío University Hospital, Avda. Manuel Siurot s/n, 41013 Sevilla, Spain; <sup>4</sup>Arrhythmia Department, Puerta del Mar University Hospital, Avda. Ana de Viya 21, 11009 Cádiz, Spain; and <sup>5</sup>Arrhythmia Department, Josep Trueta University Hospital, Avda. de França s/n, 17007 Girona, Spain

Received 14 May 2021; editorial decision 22 October 2021; accepted after revision 26 October 2021

### Aims

To non-invasively characterize, by means of late gadolinium enhancement cardiac magnetic resonance (LGE-CMR), scar differences, and potential variables associated with ventricular tachycardia (VT) occurrence in chronic post-myocardial infarction (MI) patients.

### Methods and results

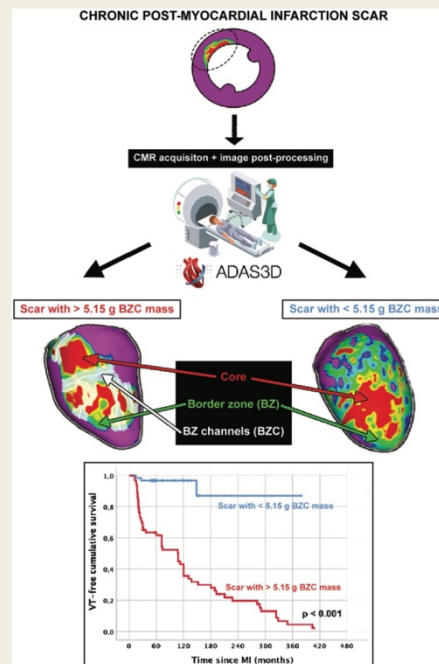
A case-control study was designed through retrospective LGE-CMR data analysis of chronic post-MI patients (i) consecutively referred for VT substrate ablation after a first VT episode ( $n=66$ ) and (ii) from a control group ( $n=84$ ) with no arrhythmia evidence. The myocardium was characterized differentiating core, border zone (BZ), and BZ channels (BZCs) using the ADAS 3D post-processing imaging platform. Clinical and scar characteristics, including a novel parameter, the BZC mass, were compared between both groups. One hundred and fifty post-MI patients were included. Four multivariable Cox proportional hazards regression models were created for total scar mass, BZ mass, core mass, and BZC mass, adjusting them by age, sex, and left ventricular ejection fraction (LVEF). A cut-off of 5.15 g of BZC mass identified the cases with 92.4% sensitivity and 86.9% specificity [area under the ROC curve (AUC) 0.93 (0.89–0.97);  $P<0.001$ ], with a significant increase in the AUC compared to other scar parameters ( $P<0.001$  for all pairwise comparisons). Adding BZC mass to LVEF allowed to reclassify 33.3% of the cases and 39.3% of the controls [net reclassification improvement = 0.73 (0.71–0.74)].

### Conclusions

The mass of BZC is the strongest independent variable associated with the occurrence of sustained monomorphic ventricular tachycardia in post-MI patients after adjustment for age, sex, and LVEF. Border zone channel mass measurement could permit a more accurate VT risk stratification than LVEF in chronic post-MI patients.

\*Corresponding author. Tel: +34 932 90 62 00; fax: +34 932 11 26 90. E-mail address: antonio.berruezo@quironsalud.es  
Published on behalf of the European Society of Cardiology. All rights reserved. © The Author(s) 2021. For permissions, please email: journals.permissions@oup.com.

## Graphical Abstract



## Keywords

Myocardial infarction • Arrhythmogenic substrate • Scar arrhythmogenicity • Cardiac magnetic resonance • Border zone channels • Ventricular arrhythmias

## Introduction

The presence of viable strands of cardiomyocytes embedded within fibrotic tissue is known to be the substrate for the appearance of scar-related re-entrant ventricular arrhythmias (VA) in chronic ischaemic cardiomyopathy.<sup>1</sup> Late gadolinium enhancement cardiac magnetic resonance (LGE-CMR) has proven to be a useful technique in the non-invasive characterization of the scarred tissue and the underlying arrhythmogenic substrate.<sup>2</sup> Previous studies identified the CMR-derived infarct mass as a better predictor of sustained monomorphic ventricular tachycardia (SMVT) inducibility during an electrophysiologic study (EPS), when compared to left ventricular ejection fraction (LVEF).<sup>3</sup> In fact, the presence of significant scarring [ $>5\%$  of the left ventricular (LV) mass] is an independent predictor of adverse outcome in patients being considered for implantable cardioverter-defibrillator (ICD) placement.<sup>4</sup> On the other hand, in inducible patients for SMVT during EPS, more heterogeneous scars [i.e. with greater border zone (BZ) mass] can be found.<sup>5</sup> Similarly, the presence of heterogeneous

tissue channels, which correlate with voltage channels after endocardial voltage mapping of the scar, can be more frequently observed in patients suffering from SMVT than in matched controls for age, sex, infarct location, and LVEF.<sup>6</sup> However, the lack of solid evidence and randomized trials makes LVEF still the main decision parameter when assessing suitability for ICD implantation in primary prevention.<sup>7,8</sup> In the present study, we sought to characterize scar differences and potential variables associated with arrhythmogenicity in post-myocardial infarction (MI) patients using a commercially available, post-processing imaging platform with Food and Drug Administration (FDA) (USA) 510(k) Clearance and CE Mark approval.

## Methods

## Study population

Figure 1 shows the flow diagram of the study population. A case-control study was designed through retrospective LGE-CMR data analysis from our imaging database. In brief, cases were recruited from: (i) a prospective

**What's new?**

- This is the first report describing the border zone channel (BZC) mass as a powerful non-invasive, CMR-derived parameter that may improve arrhythmia risk stratification in chronic post-myocardial infarction (MI) patients.
- BZC mass is the strongest independent scar-derived variable associated with the appearance of clinical sustained monomorphic VTs in chronic post-MI patients after covariate adjustment for age, sex, and left ventricular ejection fraction (LVEF).
- Adding the information of CMR-derived BZC mass to LVEF could improve the accuracy of ventricular tachycardia risk stratification in chronic post-MI patients.
- The BZC mass is intrinsically linked to the qualitative structure of the scar, its heterogeneity, and spatial distribution, and is related to the presence and amount of slow conducting channels within the scar.

cohort of post-MI patients referred for ventricular tachycardia (VT) substrate ablation after a first SMVT episode and (ii) an additional prospective cohort of post-MI patients who underwent ICD implantation in primary prevention and had any documented episode of SMVT thereafter. All the cases had undergone a CMR study right before substrate ablation or before ICD implantation (which is regular practice in our institution).

On the other hand, controls were selected from: (i) a cohort of consecutive post-MI patients with no arrhythmia evidence, either in terms of standard clinical follow-up for those with LVEF >35%, or after periodic ICD interrogations (at least once per year) for those with ICD in primary prevention (LVEF ≤ 35%) and (ii) a prospective cohort of post-MI patients undergoing ICD implantation in primary prevention, with no documented SMVT episodes thereafter. All the controls had to have a CMR study performed at least 4 years after the MI (which is regular practice in our institution), or right before the ICD implantation, when indicated.

All patients were treated according to clinical guidelines, and none of them had been pre-treated with antiarrhythmic drugs. Sustained monomorphic ventricular tachycardia was defined as any ventricular rhythm faster than 100 beats per minute, lasting ≥30 s or requiring termination due to haemodynamic instability or by antitachycardia pacing or shocks.

The study complied with the Declaration of Helsinki, and the local ethics committee approved the study protocol.

**Late gadolinium enhancement cardiac magnetic resonance processing**

Late gadolinium enhancement cardiac magnetic resonance tests were performed using a 3-Tesla scanner (MAGNETOM Trio, Siemens Healthcare, Erlangen, Germany), or 1.5-Tesla scanners (ACHIEVA, Philips, The Netherlands; and MAGNETOM Aera, Siemens Healthcare, Erlangen, Germany). In patients previously implanted with an ICD, LGE-CMR was performed using a specific wideband sequence to avoid device artefacts. Image acquisition protocol is summarized in the [Supplementary material online, Methods](#). All LGE-CMR images were analysed using a previously described protocol.<sup>9</sup> A full LV volume was reconstructed in the axial orientation, and the resulting images were processed with ADAS 3D LV software (ADAS3D Medical, Barcelona, Spain). Ten concentric surface layers (from 10% to 90%) were created automatically from endocardium to epicardium of the LV wall thickness, obtaining a 3D shell for each layer. Colour-coded pixel signal intensity (PSI) maps based on LGE-CMR images were projected to each shell, following a trilinear interpolation algorithm. A PSI-based algorithm was applied to characterize the hyperenhanced area as core zone, BZ or healthy tissue using 40% ± 5% and 60% ± 5% of the maximum PSI as thresholds.<sup>9</sup>

**Myocardial scar characterization**

The total scar mass, BZ mass, and core mass in each shell were automatically measured using the ADAS 3D LV software. BZ channels (BZCs) were defined as continuous corridors of BZ surrounded by scar core or an anatomical barrier (i.e. mitral annulus) connecting two areas of healthy tissue. The BZC mass, defined as grams of BZ tissue that make up BZC, was obtained by multiplying the number of image voxels within the identified BZC by the voxel volume and a myocardial density of 1.05 g/cm<sup>3</sup> (see [Supplementary material online, Methods](#) for rationale and calculation method), using a full-automated tool embedded within the ADAS 3D LV software.

**Statistical analysis**

Continuous variables are given as mean ± standard deviation or median (interquartile range, IQR), as appropriate. Categorical variables are given as total number and percentages. To compare the means of two variables, the Student's *t*-test or Wilcoxon test were used, when applicable. Proportions were compared using the  $\chi^2$  or Fisher's exact test, as fitted. Time-dependent receiver operating characteristic (ROC) curve analyses were used to evaluate the optimal cut-off value of BZC mass for

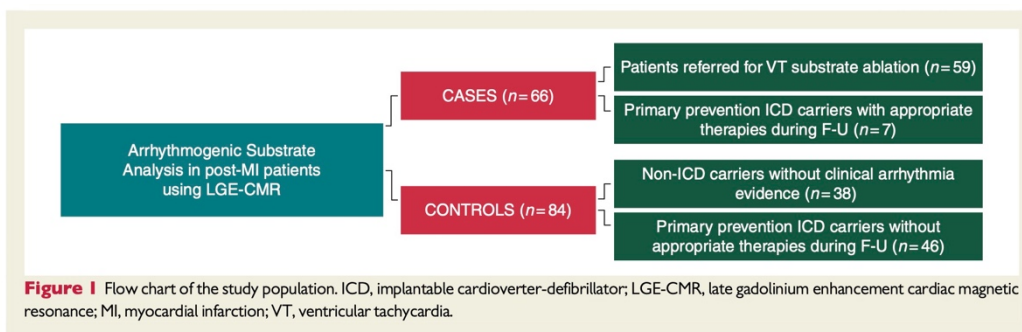




**Table 1** Clinical and scar characteristics of the patient population

	Total (n = 150)	Cases (n = 66)	Controls (n = 84)	P-value
Age (years)	64 ± 11	67 ± 9	62 ± 11	0.007 <sup>a</sup>
Male sex	133 (89%)	63 (96%)	70 (83%)	0.02 <sup>a</sup>
Hypertension	89 (65%)	46 (78%)	43 (54%)	0.004 <sup>a</sup>
Diabetes mellitus	41 (30%)	21 (36%)	20 (25%)	0.14
Dyslipidaemia	81 (59%)	44 (75%)	37 (47%)	0.001 <sup>a</sup>
Smoker	27 (20%)	5 (9%)	22 (28%)	0.005 <sup>a</sup>
Atrial fibrillation	6 (4%)	1 (2%)	5 (6%)	0.20
LVEF (%)	36 ± 13	34 ± 10	38 ± 14	0.07
MI location (anterior)	65 (44%)	26 (40%)	39 (46%)	0.46
Time since MI (months)	58 (31–120)	72 (22–151)	57 (51–115)	0.89
Betablockers	112 (81%)	43 (73%)	69 (87%)	0.03 <sup>a</sup>
ACEI/ARB	97 (70%)	37 (63%)	60 (76%)	0.08
Diuretics	64 (46%)	29 (49%)	35 (44%)	0.54
MRA	72 (52%)	36 (61%)	36 (46%)	0.07
Statins	130 (94%)	58 (98%)	72 (91%)	0.07
Total scar mass (g)	26.4 ± 17.0	33.5 ± 15.5	20.9 ± 16.1	<0.001 <sup>a</sup>
BZ mass (g)	15.7 ± 10.9	20.9 ± 9.5	11.7 ± 10.1	<0.001 <sup>a</sup>
Core mass (g)	10.6 ± 8.7	12.4 ± 8.3	9.2 ± 8.8	0.03 <sup>a</sup>
BZC mass (g)	5.8 ± 5.1	9.7 ± 4.2	3.4 ± 2.8	<0.001 <sup>a</sup>

ACEI, angiotensin-converting enzyme inhibitor; ARB, angiotensin receptor blocker; BZ, border zone; BZC, border zone channel; LVEF, left ventricular ejection fraction; MI, myocardial infarction; MRA, mineralocorticoid-receptor antagonists.

<sup>a</sup>Statistically significant differences ( $P < 0.05$ ).

predicting occurrence of VT. Comparisons of area under the ROC curves (AUCs) were performed using the De Long's test. Kaplan–Meier curves and the log-rank test were used to assess cumulative survival. Cox proportional hazard models were used to assess relative risks. The overall discriminatory capacity of the Cox models was assessed by using the Harrell concordance index (C-index), which was validated by bootstrapping with 1000 replications. Propensity scores (PSs) were calculated for cases and controls using a multivariable regression model that included the following clinical variables: age, sex, and LVEF. Pairing was performed using a greedy protocol 1:1 (calliper 0.01), with no replacement, and adequate goodness of fit was assumed if standardized differences were <10%. Predictive capabilities were further evaluated using continuous net reclassification improvement (NRI), and integrated discrimination improvement (IDI).  $P$ -value <0.05 was considered of statistical significance. Statistical analysis was performed using IBM SPSS Statistics, version 26.0 (IBM Corp. Released 2019; Armonk, NY, USA: IBM Corp.), MedCalc Statistical Software version 16.4.3 (MedCalc Software bv, Ostend, Belgium), and SAS 9.3 (SAS Institute, Inc., Cary, NC, USA).

## Results

### Patient population

One hundred and fifty chronic post-MI patients were included for analysis (Figure 1). There were 66 cases; 59/66 (89%) were patients referred for VT substrate ablation after a first documented SMVT, and 7/66 (11%) had any documented SMVT episode after ICD implantation in primary prevention. The median time from MI until the first VT episode was 72 (IQR 22–151, range 13–404) months, whereas the median time from MI until the CMR acquisition in this

group was 37 (22–131) months. Among those referred for VT ablation, 37/59 (63%) had a previously implanted ICD. From them, 23/37 (62%) underwent a 3-Tesla CMR before the ICD implantation, and 14/37 (38%) underwent a 1.5-Tesla CMR before ablation using a wideband sequence to avoid ICD artefacts.

There were 84 controls; 38/84 (45%) were patients with no arrhythmia evidence, and 46/84 (55%) were ICD carriers in primary prevention with no arrhythmia evidence after a median follow-up of 31 (IQR 12–64) months post-implantation (Figure 1). The median time from MI until study inclusion was 57 (IQR 51–115, range 48–408) months ( $P = 0.89$  for the comparison with cases, Table 1). For the controls, all the CMR studies were performed at least 4 years after the MI.

### Baseline characteristics and scar characterization

Baseline characteristics of the total population can be found in Table 1. Mean LVEF was  $36 \pm 13\%$ , being similar between cases and controls ( $34 \pm 10$  vs.  $38 \pm 14\%$ ;  $P = 0.07$ ). Compared to controls, cases were significantly older ( $67 \pm 9$  vs.  $62 \pm 11$  years;  $P = 0.007$ ), had more cardiovascular risk factors and were more frequently male (96% vs. 83%,  $P = 0.02$ ) (Table 1). Regarding scar characteristics, cases had a greater scar mass ( $33.5 \pm 15.5$  vs.  $20.9 \pm 16.1$  g;  $P < 0.001$ ), BZ mass ( $20.9 \pm 9.5$  vs.  $11.7 \pm 10.1$  g;  $P < 0.001$ ), core mas ( $12.4 \pm 8.3$  vs.  $9.2 \pm 8.8$  g;  $P = 0.03$ ), and BZC mass ( $9.7 \pm 4.1$  vs.  $2.8 \pm 3.4$  g;  $P < 0.001$ ) (Table 1). These differences were also found in a PS-adjusted population ( $n = 132$ ; 66 cases and 66 controls), controlling for relevant clinical covariates (age, sex, and LVEF) (Supplementary

**Table 2** Multivariable Cox proportional hazards regression models to identify independent variables associated with VT events in the study population

	Covariate adjustment			PS as covariate 'doubly robust'	
	HR (95% CI)	P-value	c-statistic	HR (95% CI)	P-value
Multivariable model 1					
Age (years)	1.02 (0.99–1.06)	0.13	0.69	1.06 (1.01–1.12)	0.02 <sup>a</sup>
Male sex	1.07 (0.32–3.59)	0.92		1.06 (0.31–3.60)	0.50
LVEF (%)	1.00 (0.98–1.03)	0.83		1.00 (0.97–1.03)	0.93
Total scar mass (g)	1.03 (1.02–1.05)	<0.001 <sup>a</sup>		1.03 (1.02–1.05)	<0.001 <sup>a</sup>
Multivariable model 2					
Age (years)	1.02 (0.99–1.05)	0.23	0.73	1.05 (1.00–1.11)	0.047 <sup>a</sup>
Male sex	0.85 (0.25–2.91)	0.80		0.85 (0.24–2.92)	0.57
LVEF (%)	0.99 (0.97–1.02)	0.56		0.99 (0.96–1.02)	0.32
BZ mass (g)	1.06 (1.04–1.09)	<0.001 <sup>a</sup>		1.06 (1.04–1.09)	<0.001 <sup>a</sup>
Multivariable model 3					
Age (years)	1.03 (1.00–1.06)	0.05	0.61	1.02 (0.99–1.05)	0.31
Male sex	1.53 (0.47–4.99)	0.48		1.53 (0.47–4.99)	0.40
LVEF (%)	0.99 (0.96–1.01)	0.24		0.98 (0.96–1.01)	0.26
Core mass (g)	1.00 (0.97–1.03)	0.94		1.00 (0.97–1.04)	0.85
Multivariable model 4					
Age (years)	1.02 (0.99–1.05)	0.31	0.77	1.04 (0.99–1.09)	0.13
Male sex	0.94 (0.28–3.18)	0.92		0.94 (0.27–3.18)	0.51
LVEF (%)	0.99 (0.97–1.02)	0.58		0.99 (0.96–1.02)	0.54
BZC mass (g)	1.12 (1.07–1.17)	<0.001 <sup>a</sup>		1.11 (1.07–1.16)	<0.001 <sup>a</sup>

BZ, border zone; BZC, border zone channel; CI, confidence interval; HR, hazard ratio; LVEF, left ventricular ejection fraction; PS, propensity score; VT, ventricular tachycardia.  
<sup>a</sup>Statistically significant differences ( $P < 0.05$ ).

material online, Table S1). There was only a slight negative linear correlation between scar mass and LVEF ( $r^2 = 0.18$ ;  $P < 0.001$ ), suggesting that not only the scar mass but also remodelling of the remote myocardium is contributing to the decrease in LVEF after MI. On the contrary, there was a strong positive linear association between scar mass and BZ mass ( $r^2 = 0.80$ ;  $P < 0.001$ ), and a mild positive linear association between scar mass and BZC mass ( $r^2 = 0.37$ ;  $P < 0.001$ ), suggesting a different spatial distribution of BZ tissue in scars with the same total scar mass.

### Scar variables associated with ventricular tachycardia events

Four multivariable Cox proportional hazards regression models were created for total scar mass (model 1), BZ mass (model 2), core mass (model 3), and BZC mass (model 4). All of them were adjusted by age, sex, and LVEF (Table 2). In the corresponding models, only total scar mass, BZ mass, core mass, and BZC mass were independent variables associated with the development of VT, with similar findings after a doubly robust estimation weighting for the calculated PSs (Table 2). Supplementary material online, Figure S1 shows the distribution of calculated BZC mass values between cases and controls. The overall diagnostic performance of BZC mass to differentiate cases and controls was excellent, with an AUC of 0.93 [95% confidence interval (CI) 0.89–0.97;  $P < 0.001$ ]. From De Long's test, all pairwise comparisons of AUCs between BZC mass and total scar mass, BZ mass, and core mass showed statistical significance ( $P < 0.001$ ). Time-dependent ROC

curves for all the scar parameters analysed are shown in Figure 2. For BZC mass, a cut-off point of  $>5.15$  g showed 92% sensitivity and 87% specificity values for the identification of patients with documented VT. A visual example of the scar characteristics and differences between cases and controls is shown in Figure 3.

Interestingly, 49/66 (74%) of the cases had transmural scars, as opposed to only 48/84 (57%) of the controls ( $P = 0.03$ ) (Supplementary material online, Figure S2). Total scar mass, BZ mass, core mass, and BZC mass were significantly higher for transmural substrates as compared to non-transmural scars ( $P < 0.001$  for all comparisons) (Supplementary material online, Table S2).

### Border zone channel mass vs. left ventricular ejection fraction for prediction of ventricular tachycardia events

Out of 67 (45%) patients having an LVEF  $>35\%$ , 29 (43%) had a BZC mass  $>5.15$  g. Of them, 26 (90%) were cases. On the contrary, out of 83 (55%) patients with LVEF  $\leq 35\%$ , 40 (48%) had a BZC mass  $\leq 5.15$  g and, from them, 36 (90%) were controls. Cumulative survival curves from MI until first documented SMVT episode according to the used LVEF and BZC mass cut-off points are shown in Figure 4.

An LVEF  $\leq 35\%$  would have classified at a significant arrhythmia risk only 39/66 (59%) of the cases. Conversely, an LVEF  $>35\%$  would not have identified 44/84 (52%) of the controls. Patients fulfilling the combined criterium of LVEF  $>35\%$  and BZC mass  $\leq 5.15$  g ( $n = 38$ ) were mostly controls (37/38, 93%). Adding BZC mass to LVEF to stratify

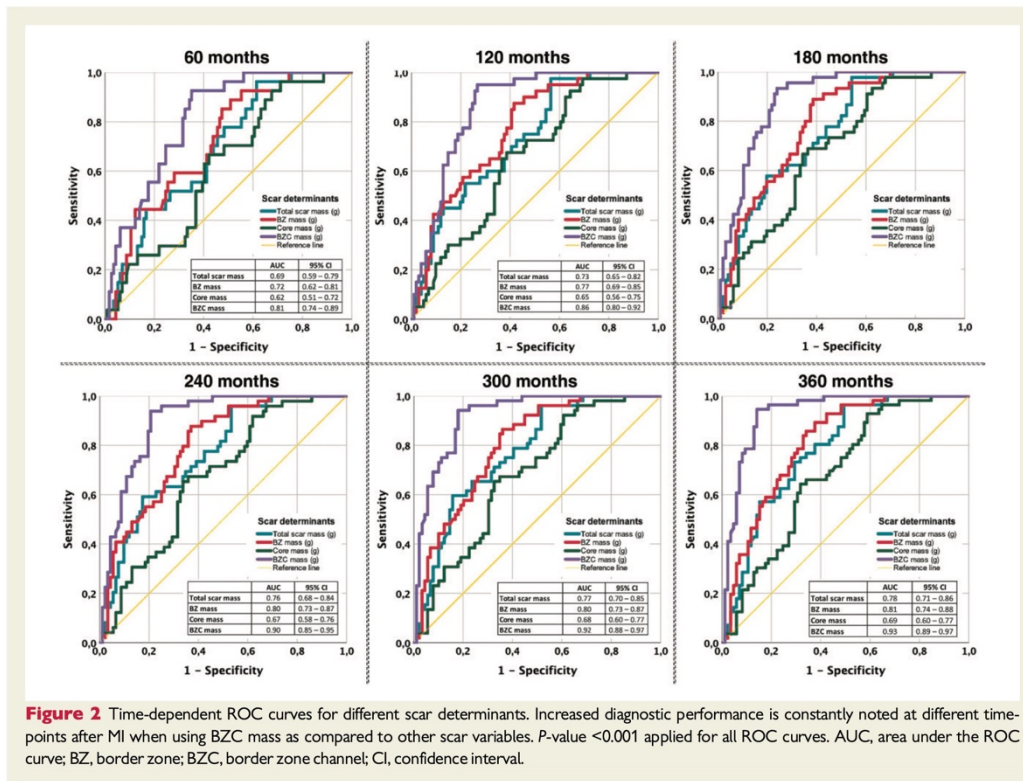


**Figure 2** Time-dependent ROC curves for different scar determinants. Increased diagnostic performance is constantly noted at different time-points after MI when using BZC mass as compared to other scar variables.  $P$ -value  $< 0.001$  applied for all ROC curves. AUC, area under the ROC curve; BZ, border zone; BZC, border zone channel; CI, confidence interval.

the VT occurrence risk allowed to reclassify 33.3% of the cases and 39.3% of the controls. The NRI was 0.73 (95% CI 0.71–0.74), which amounted to 36.7% of all cases being reclassified (Figure 5). Compared with a VT risk stratification purely based on LVEF [ $c$ -index = 0.55 (95% CI 0.46–0.63)], there was a significant improvement in discrimination by using the BZC mass, confirmed by a  $c$ -index difference of 0.39 (95% CI 0.29–0.48;  $P < 0.001$ ). The diagnostic performance of LVEF [AUC = 0.46 (95% CI 0.36–0.55)] was significantly improved by combining it with the BZC mass (IDI = 0.62,  $P < 0.001$ ). Combined diagnostic performance of LVEF and BZC mass for predicting the occurrence of SMVT episodes in the study population is shown in Table 3.

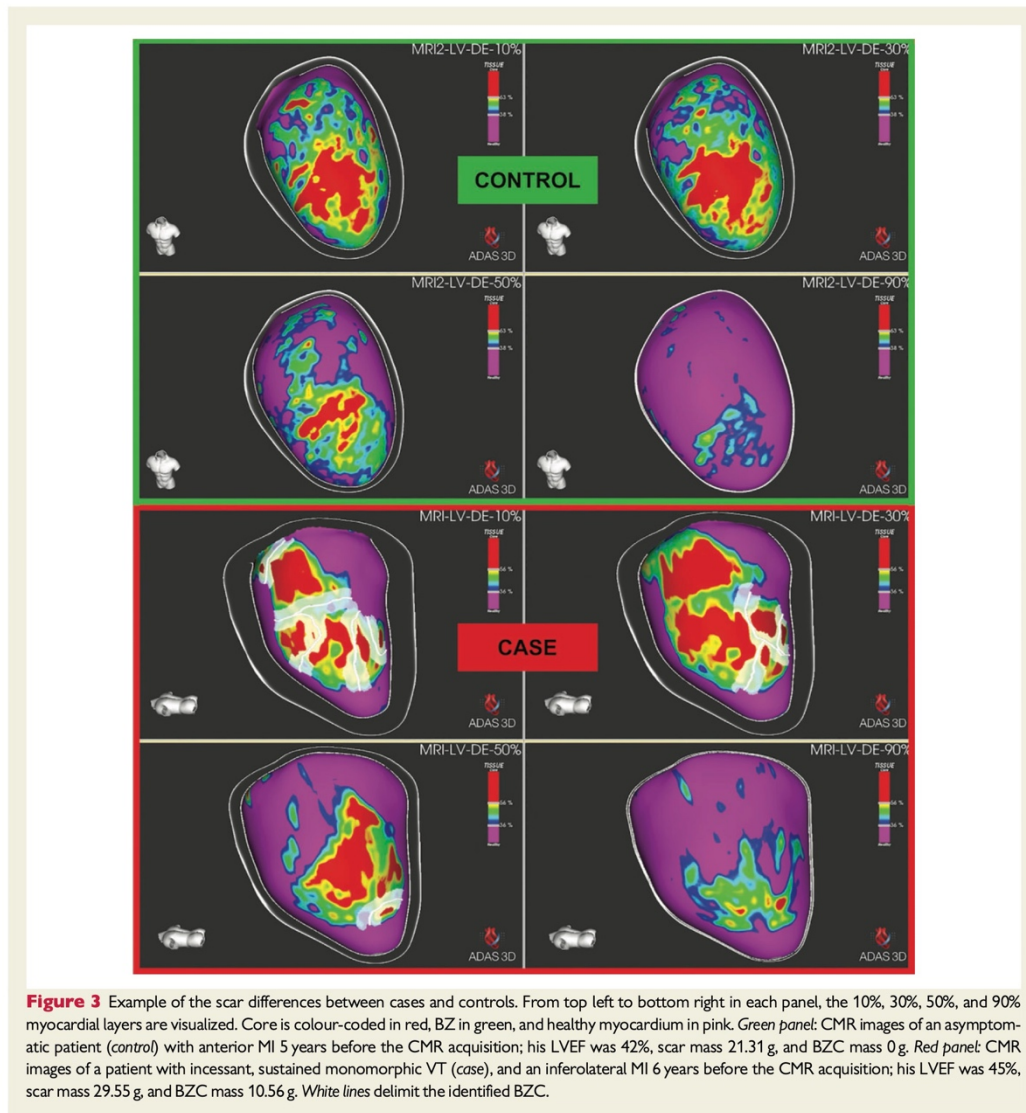
## Discussion

### Main findings

This study is the first report describing the BZC mass as a powerful non-invasive, CMR-derived parameter that can be easily quantified and may improve arrhythmia risk stratification in chronic post-MI patients. It is also the first clinical study to report the feasibility of calculating the BZC mass in an automated way, using a commercially available cardiac imaging post-processing platform with FDA 510(k) Clearance and CE Mark approval.

The BZC mass is intrinsically linked to the qualitative structure of the scar, its heterogeneity, and spatial distribution, and is related to the presence and amount of slow conducting channels within the scar.<sup>6,10</sup> In a previous prospective study on cardiac resynchronization therapy patients (the GAUDI study),<sup>11</sup> the dichotomic presence of BZC had already a similar positive predictive value for arrhythmia events (24–25%) to that of an increased BZ (not BZC) mass ( $> 5.35$  g in that study). Although the presence of BZC and BZ mass showed a better diagnostic performance than total scar mass, in the present study the quantitative BZC mass has shown to be the most accurate parameter above all.

On the other hand, the relative higher proportion of VA among patients with severely depressed LVEF may be explained because, the greater the scar, the higher the probability of LV systolic dysfunction, although this correlation is weak.<sup>12</sup> Similarly, the greater the scar, the higher the probability of having a greater mass of BZ and BZC. The BZC mass was, among all the scar determinants analysed, the variable most highly associated with VT occurrence, after covariate adjustment for age, sex, and LVEF. Most likely, the BZC mass constitutes the characteristic that gets closer to the true histological substrate that gives rise to post-MI scar-related re-entrant VTs, that is, the basis of scar arrhythmogenicity.



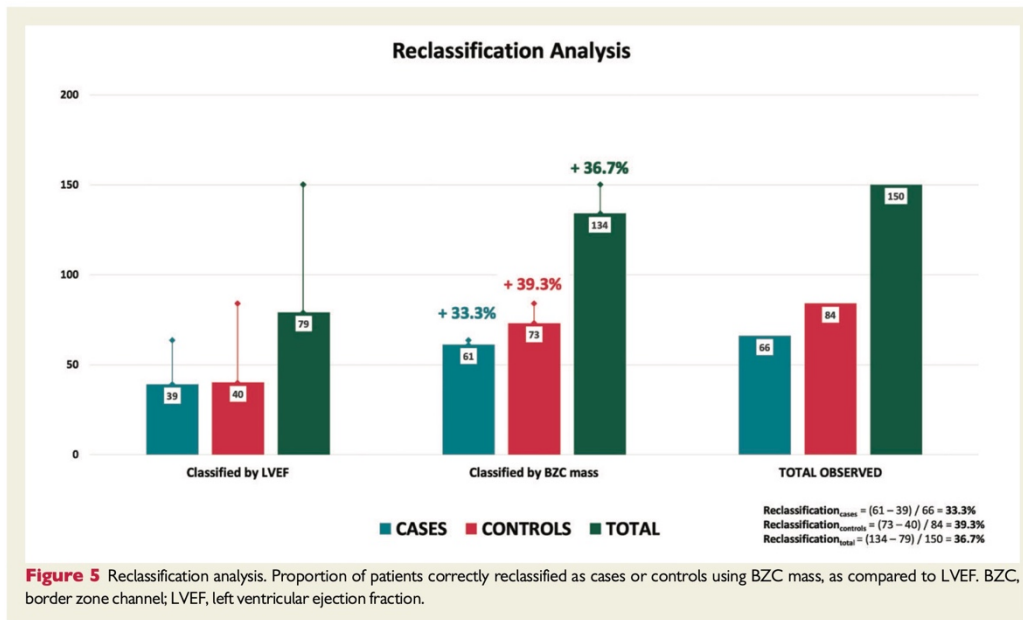
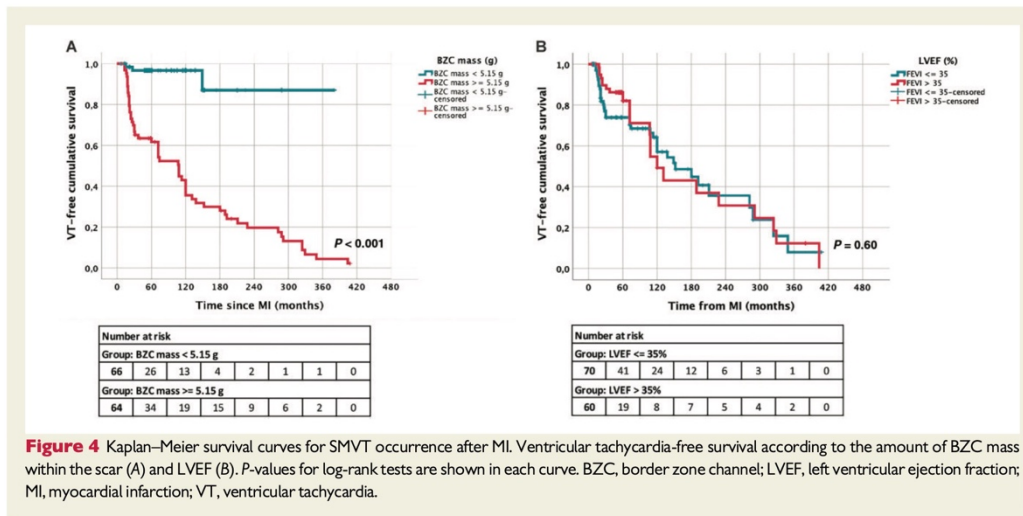
The major findings of the study can be summarized as the following:

i. Among all the scar parameters analysed, BZC mass was the strongest independent variable associated with the appearance of clinical SMVT in chronic post-MI patients after covariate adjustment for age, sex, and LVEF. The overall diagnostic performance of BZC mass to identify post-MI patients with SMVT was very high (sensitivity 92.4% and specificity 86.9% for the cut-off value of >5.15 g).

ii. Adding the information of CMR-derived BZC mass to LVEF could improve the accuracy of VT risk stratification in chronic post-MI patients, as shown by significant increases in AUC with respect to other scar determinants, IDI, and NRI.

### Rationale for the quantitative evaluation of the border zone channel mass

Late gadolinium enhancement cardiac magnetic resonance is recognized as the gold standard technique to determine the location and



extent of myocardial scar.<sup>13</sup> The CMR-defined scar has a good correlation with low-voltage areas in the electroanatomical maps (EAM).<sup>10,14</sup> Moreover, the size and heterogeneity of the post-MI scar, as evaluated with CMR, are variables that, unlike LVEF, have been associated with VT inducibility,<sup>3,5</sup> arrhythmia events, and even mortality.<sup>2,4,15</sup> In a recently published, retrospective study, the

presence of 'grey zone' 13 fibrosis (i.e. BZ mass) >5.0g showed an 84% sensitivity and 72% specificity to predict the occurrence of sudden cardiac death (SCD) in chronic post-MI patients.<sup>16</sup> Moreover, post-MI patients with documented SMVT had more conducting channels, as evaluated during EAM, when compared to controls.<sup>17</sup> Cardiac magnetic resonance permits to identify BZC that correlate

**Table 3** Diagnostic performance of LVEF, BZC mass, and a combination of both for predicting the occurrence of SMVT episodes in the study population

	Case	Control	Total
LVEF performance			
LVEF ≤ 35% (high risk)	39	44	83
LVEF > 35% (low risk)	27	40	67
Total	66	84	150
Se = 59.1%; Sp = 47.6%			
BZC mass performance			
BZC mass > 5.15 g (high risk)	61	11	72
BZC mass ≤ 5.15 g (low risk)	5	73	78
Total	66	84	150
Se = 92.4%; Sp = 86.9%			
Combined performance (LVEF + BZC mass)			
LVEF ≤ 35% and BZC mass > 5.15 g (high risk)	35	8	43
LVEF > 35% and BZC mass ≤ 5.15 g (low risk)	1	37	38
Total	36	45	81
Se = 97.2%; Sp = 82.2%			

BZC, border zone channel; LVEF, left ventricular ejection fraction; Se, sensitivity; SMVT, sustained monomorphic ventricular tachycardia; Sp, specificity.

well with the EAM conducting channels within the scar.<sup>10</sup> In fact, the presence of BZC has been associated<sup>11</sup> with a higher risk of VA/SCD, and could help deciding whether to implant an ICD in candidates for cardiac resynchronization therapy. In addition, CMR-guided VT substrate ablation approaches, which are based on the ablation of BZC identified on CMR, have shown improvement in arrhythmia-free survival during follow-up.<sup>18</sup> The assessment of the clinical value of BZC mass quantification in the present study has been the necessary next step to set up future prospective studies to confirm the role of CMR in improving risk stratification for VA and SCD in post-MI patients.

### Clinical implications for sudden cardiac death risk stratification

In chronic post-MI patients, VA causing SCD are mostly re-entrant SMVT. Therefore, identification of scars with arrhythmogenic characteristics could help better identify patients at a higher risk of SCD. In previous reports, LVEF has shown low-specificity in differentiating the risk of SCD from risk of death associated with comorbidities or the evolution of heart failure.<sup>15</sup> With the current, LVEF-based decision algorithms used for primary prevention of SCD with ICDs, the contemporary rate of appropriated therapies is very low, inferior than in classical ICD implantation trials that provided the evidence for current recommendations. Therefore, a more accurate identification of patients at risk is urgently needed. Upon further validation, the use of BZC mass may help improving the selection of post-MI patients for ICD implantation (i.e. in cardiac resynchronization therapy candidates),<sup>11</sup> or contribute to decide closer monitoring or to carry out additional screening tests (i.e. electrophysiological studies) in those patients at higher arrhythmic risk, regardless of their LVEF.<sup>11</sup> Yet, it shall be reminded that most cases of SCD in post-MI patients occur with normal or moderately reduced LVEF.<sup>19</sup> Larger cohort

studies would be necessary to prospectively evaluate the use of BZC mass and its predictive accuracy for the appearance of VA and SCD.

### Study limitations

Despite the inherent limitations of a case-control design, it can be acceptable to propose new variables to be tested when a low event rate is observed. However, the generated risk and effect of the scar variables analysed could have been overestimated. On the other hand, post-MI scar may suffer structural changes in the long-term,<sup>20</sup> being therefore unknown which would be the best timing for a BZC mass screening. Ventricular tachycardia screening capacity was limited for those patients who were not ICD carriers, as no continuous monitoring was available. Finally, optimal CMR quality should be a requisite to obtain reliable BZC mass measurements. Medical decision-making based on the BZC mass should be supported by external clinical validation in prospective studies. Finally, it shall be reminded that SCD in post-MI patients may not be always due to SMVT degenerating into ventricular fibrillation (VF).

### Conclusions

The mass of BZC is the strongest independent variable associated with the occurrence of SMVT in post-MI patients after adjustment for sex, LVEF, and total scar mass. The determination of BZC could be used to assess the risk of having SMVT, although it is still unclear its precise role in estimating the global risk of SCD.

### Supplementary material

Supplementary material is available at *Europace* online.

**Conflicts of interest:** A.B. and L.M. are stockholders of ADAS 3D Medical. D.S.-I. is an employee of Biosense Webster Inc. A.B. has received financial support from Siemens Healthineers. All other authors declared no conflict of interest.

## Data availability

The data that support the findings of this study are available from the corresponding author (A.B.) upon reasonable request.

## References

- De Bakker JMT, Van Capelle FJL, Janse MJ, Wilde AAM, Coronel R, Becker AE et al. Reentry as a cause of ventricular tachycardia in patients with chronic ischemic heart disease: electrophysiology and anatomic correlation. *Circulation* 1988;**77**:589–606.
- Yan AT, Shayne AJ, Brown KA, Gupta SN, Chan CV, Luu TM et al. Characterization of the peri-infarct zone by contrast-enhanced cardiac magnetic resonance imaging is a powerful predictor of post-myocardial infarction mortality. *Circulation* 2006;**114**:32–9.
- Bello D, Fieno DS, Kim RJ, Pereles FS, Passman R, Song G et al. Infarct morphology identifies patients with substrate for sustained ventricular tachycardia. *J Am Coll Cardiol* 2005;**45**:1104–8.
- Klem I, Weinsaft JW, Bahnson TD, Hegland D, Kim HW, Hayes B et al. Assessment of myocardial scarring improves risk stratification in patients evaluated for cardiac defibrillator implantation. *J Am Coll Cardiol* 2012;**60**:408–20.
- Schmidt A, Azevedo CF, Cheng A, Gupta SN, Bluemke DA, Foo TK et al. Infarct tissue heterogeneity by magnetic resonance imaging identifies enhanced cardiac arrhythmia susceptibility in patients with left ventricular dysfunction. *Circulation* 2007;**115**:2006–14.
- Perez-David E, Arenal Á, Rubio-Guivernau JL, Del Castillo R, Atea L, Arbelo E et al. Noninvasive identification of ventricular tachycardia-related conducting channels using contrast-enhanced magnetic resonance imaging in patients with chronic myocardial infarction: comparison of signal intensity scar mapping and endocardial voltage mapping. *J Am Coll Cardiol* 2011;**57**:184–94.
- Moss AJ, Zareba W, Hall WJ, Klein H, Wilber DJ, Cannom DS et al; Multicenter Automatic Defibrillator Implantation Trial II Investigators. Prophylactic implantation of a defibrillator in patients with myocardial infarction and reduced ejection fraction. *N Engl J Med* 2002;**346**:877–83.
- Bardy GH, Lee KL, Mark DB, Poole JE, Packer DL, Boineau R et al; Sudden Cardiac Death in Heart Failure Trial (SCD-HeFT) Investigators. Amiodarone or an implantable cardioverter-defibrillator for congestive heart failure. *N Engl J Med* 2005;**352**:225–37.
- Andreu D, Ortiz-Pérez JT, Fernández-Armenta J, Guiu E, Acosta J, Prat-González S et al. 3D delayed-enhanced magnetic resonance sequences improve conducting channel delineation prior to ventricular tachycardia ablation. *Europace* 2015;**17**:938–45.
- Fernández-Armenta J, Berrueto A, Andreu D, Camara O, Silva E, Serra L et al. Three-dimensional architecture of scar and conducting channels based on high resolution ce-CMR: insights for ventricular tachycardia ablation. *Circ Arrhythm Electrophysiol* 2013;**6**:528–37.
- Acosta J, Fernández-Armenta J, Borràs R, Anguera I, Bisbal F, Martí-Almor J et al. Scar characterization to predict life-threatening arrhythmic events and sudden cardiac death in patients with cardiac resynchronization therapy: the GAUDI-CRT study. *JACC Cardiovasc Imaging* 2018;**11**:561–72.
- Palazzuoli A, Beltrami M, Gennari L, Dastidar AG, Nuti R, McAlindon E et al. The impact of infarct size on regional and global left ventricular systolic function: a cardiac magnetic resonance imaging study. *Int J Cardiovasc Imaging* 2015;**31**:1037–44.
- Cronin EM, Bogun FM, Maury P, Peichl P, Chen M, Nambodiri N et al. 2019 HRS/EHRA/APHRS/LAHS expert consensus statement on catheter ablation of ventricular arrhythmias. *Europace* 2019;**21**:1143–4.
- Gupta S, Desjardins B, Baman T, Ilg K, Good E, Crawford T et al. Delayed-enhanced MR scar imaging and intraprocedural registration into an electroanatomical mapping system in post-infarction patients. *JACC Cardiovasc Imaging* 2012;**5**:207–10.
- Disertori M, Rigoni M, Pace N, Casolo G, Masè M, Gonzini L et al. Myocardial fibrosis assessment by LGE is a powerful predictor of ventricular tachyarrhythmias in ischemic and nonischemic LV dysfunction: a meta-analysis. *JACC Cardiovasc Imaging* 2016;**9**:1046–55.
- Abbasin Z, Osita O, Joseph D. B, Manish K, Mauro L, Howard M et al. Myocardial fibrosis as a predictor of sudden death in patients with coronary artery disease. *J Am Coll Cardiol* 2021;**77**:29–41.
- Haqqani HM, Kalman JM, Roberts-Thomson KC, Balasubramanian RN, Rosso R, Snowdon RL et al. Fundamental differences in electrophysiologic and electroanatomic substrate between ischemic cardiomyopathy patients with and without clinical ventricular tachycardia. *J Am Coll Cardiol* 2009;**54**:166–73.
- Soto-Iglesias D, Penela D, Jáuregui B, Acosta J, Fernández-Armenta J, Linhart M et al. Cardiac magnetic resonance-guided ventricular tachycardia substrate ablation. *JACC Clin Electrophysiol* 2020;**6**:436–47.
- Huikuri HV, Castellanos A, Myerburg RJ. Sudden death due to cardiac arrhythmias. *N Engl J Med* 2001;**345**:1473–82.
- Jáuregui B, Soto-Iglesias D, Penela D, Acosta J, Fernández-Armenta J, Linhart M et al. Follow-up after myocardial infarction to explore the stability of arrhythmogenic substrate: the footprint study. *JACC Clin Electrophysiol* 2020;**6**:207–18.

## **INTRODUCTION**

The presence of viable strands of cardiomyocytes embedded within fibrotic tissue is known to be the substrate for the appearance of scar-related reentrant ventricular arrhythmias (VA) in chronic ischemic cardiomyopathy (ICM).(1) Late gadolinium enhancement cardiac magnetic resonance (LGE-CMR) has proven to be a useful technique in the non-invasive characterization of the scarred tissue and the underlying arrhythmogenic substrate.(2-4) Previous studies identified the CMR-derived infarct mass as a better predictor of sustained monomorphic ventricular tachycardia (SMVT) inducibility during an electrophysiologic study (EPS), when compared to left ventricular ejection fraction (LVEF).(5) In fact, the presence of significant scarring (>5% of the LV mass) is an independent predictor of adverse outcome in patients being considered for implantable cardioverter-defibrillator (ICD) placement.(6) On the other hand, in inducible patients for SMVT during EPS, more heterogeneous scars (i.e. with greater border zone mass) can be found.(3) Similarly, the presence of heterogeneous tissue channels, which correlate with voltage channels after endocardial voltage mapping of the scar, can be more frequently observed in patients suffering from SMVT than in matched controls for age, sex, infarct location, and LVEF.(7) However, the lack of solid evidence and randomized trials makes LVEF still the main decision parameter when assessing suitability for ICD implantation in primary prevention.(8,9) In the present study, we sought to characterize scar differences and potential variables associated with arrhythmogenicity in post-myocardial infarction (MI) patients using a commercially available, post-processing imaging platform with FDA 510(k) Clearance and CE Mark approval.



## **METHODS**

### **Study population**

A case-control study was designed through retrospective LGE-CMR data analysis of: i) a prospective cohort of chronic post-MI patients with documented sustained monomorphic VTs (SMVT); and ii), a prospective control group of consecutive chronic post-MI patients with no arrhythmia evidence, either in terms of standard clinical follow-up for those with LVEF > 35%, or after periodic ICD interrogations (at least once per year) for those with ICD in primary prevention due to LVEF  $\leq$  35%.

Figure 1 shows the flow diagram of the study population. All the controls had to have a CMR study performed at least 4 years after the MI (which is regular practice in our institution), or before a primary prevention ICD implantation procedure, when indicated.

All patients were treated according to clinical guidelines, and none of them had been pre-treated with antiarrhythmic drugs. SMVT was defined as any ventricular rhythm faster than 100 beats per minute, lasting  $\geq$  30 s or requiring termination due to hemodynamic instability or by antitachycardia pacing (ATP) or shocks. The study complied with the Declaration of Helsinki, and the local ethics committee approved the study protocol.

### **LGE-CMR processing**

LGE-CMR tests were performed using a 3-Tesla scanner (MAGNETOM Trio, Siemens Healthcare, Erlangen, Germany), or 1.5-Tesla scanners (ACHIEVA, Philips, The Netherlands; and MAGNETOM Aera, Siemens Healthcare, Erlangen, Germany). In patients previously

implanted with an ICD, LGE-CMR was performed using a specific wide-band sequence to avoid device artefacts. Image acquisition protocol is summarized in the Supplementary Methods. All LGE-CMR images were analyzed using a previously described protocol.<sup>(10)</sup> A full left ventricular (LV) volume was reconstructed in the axial orientation, and the resulting images were processed with ADAS 3D LV software (ADAS3D Medical, Barcelona, Spain). Ten concentric surface layers (from 10% to 90%) were created automatically from endocardium to epicardium of the LV wall thickness, obtaining a 3D shell for each layer. Color-coded pixel signal intensity (PSI) maps based on LGE-CMR images were projected to each shell, following a trilinear interpolation algorithm. A PSI-based algorithm was applied to characterize the hyperenhanced area as core zone, border zone (BZ) or healthy tissue using  $40\% \pm 5\%$  and  $60\% \pm 5\%$  of the maximum PSI as thresholds.<sup>(10)</sup>

### **Myocardial scar characterization**

The total scar mass, BZ mass, and core mass in each shell were automatically measured using the ADAS 3D LV software. BZ channels (BZCs) were defined as continuous corridors of BZ surrounded by scar core or an anatomical barrier (i.e. mitral annulus) connecting two areas of healthy tissue.<sup>(12)</sup> The BZC mass was automatically computed (see Supplementary Methods) using a full-automated tool embedded within the ADAS 3D LV software.

### **Statistical analysis**

Continuous variables are given as mean  $\pm$  standard deviation or median (interquartile range, IQR), as appropriate. Categorical variables are given as total number and percentages. To compare the means of 2 variables, the Student t-test or Wilcoxon test were

used, when applicable. Proportions were compared using the  $\chi^2$  or Fisher exact test, as fitted. Time-dependent receiver-operating characteristic (ROC) curve analyses were used to evaluate the optimal cut-off value of BZC mass for predicting occurrence of VT. Comparisons of AUCs were performed using the De Long's test. Kaplan-Meier curves and the log-rank test were used to assess cumulative survival. Cox proportional hazard models were used to assess relative risks. The overall discriminatory capacity of the Cox models was assessed by using the Harrell concordance index (C-index), which was validated by bootstrapping with 1000 replications. Propensity scores (PS) were calculated for cases and controls using a multivariable regression model that included the following clinical variables: age, sex, and LVEF. Pairing was performed using a greedy protocol 1:1 (caliper 0.01), with no replacement, and adequate goodness of fit was assumed if standardized differences were  $< 10\%$ . Predictive capabilities were further evaluated using continuous net reclassification improvement (NRI), and integrated discrimination improvement (IDI).  $P < 0.05$  was considered of statistical significance. Statistical analysis was performed using IBM SPSS Statistics, version 26.0 (IBM Corp. Released 2019; Armonk, NY: IBM Corp.), MedCalc Statistical Software version 16.4.3 (MedCalc Software bv, Ostend, Belgium), and SAS 9.3 (SAS Institute, Inc., Cary, NC).

## **RESULTS**

### **Patient population**

One hundred and fifty chronic post-MI patients were included for analysis (figure 1). There were 66 cases; 59/66 (89%) were patients referred for VT substrate ablation after a first

documented SMVT, and 7/66 (11%) had any documented SMVT episode after ICD implantation in primary prevention. The median time from MI until the first VT episode was 72 (IQR 22 - 151, range 13 - 404) months. Among those referred for VT ablation, 37/59 (63%) had a previously implanted ICD. From them, 23/37 (62%) underwent a 3-Tesla CMR before the ICD implantation, and 14/37 (38%) underwent a 1.5-Tesla CMR before ablation using a wideband sequence to avoid ICD artifacts.

There were 84 controls; 38/84 (45%) were patients with no arrhythmia evidence, and 46/84 (55%) were ICD carriers in primary prevention with no arrhythmia evidence after a median follow-up of 31 (IQR 12 - 64) months post-implantation (figure 1). The median time from MI until study inclusion was 57 (IQR 51 - 115, range 48 - 408) months ( $p = 0.89$  for the comparison with cases, table 1). For the controls, all the CMR studies were performed at least 4 years after the MI.

### **Baseline characteristics and scar characterization**

Baseline characteristics of the total population can be found in table 1. Mean LVEF was  $36 \pm 13\%$ , being similar between cases and controls ( $34 \pm 10$  vs.  $38 \pm 14\%$ ;  $p = 0.07$ ). Compared to controls, cases were significantly older ( $67 \pm 9$  vs.  $62 \pm 11$  years;  $p = 0.007$ ), had more cardiovascular risk factors and were more frequently male ( $96\%$  vs.  $83\%$ ,  $p = 0.02$ ) (table 1). Regarding scar characteristics, cases had a greater scar mass ( $33.5 \pm 15.5$  vs.  $20.9 \pm 16.1$  g;  $p < 0.001$ ), BZ mass ( $20.9 \pm 9.5$  vs.  $11.7 \pm 10.1$  g;  $p < 0.001$ ), core mas ( $12.4 \pm 8.3$  vs.  $9.2 \pm 8.8$  g;  $p = 0.03$ ), and BZC mass ( $9.7 \pm 4.1$  vs.  $2.8 \pm 3.4$  g;  $p < 0.001$ ) (table 1). These differences were also found in a propensity score-adjusted population ( $n = 132$ ; 66 cases

and 66 controls), controlling for relevant clinical covariates (age, sex, and LVEF) (supplementary table 1). There was only a slight negative linear correlation between scar mass and LVEF ( $r^2$  0.18;  $p < 0.001$ ), suggesting that not only the scar mass but also remodeling of the remote myocardium is contributing to the decrease in LVEF after MI. On the contrary, there was a strong positive linear association between scar mass and BZ mass ( $r^2$  0.80;  $p < 0.001$ ), and a mild positive linear association between scar mass and BZC mass ( $r^2$  0.37;  $p < 0.001$ ), suggesting a different spatial distribution of BZ tissue in scars with the same total scar mass.

### **Scar variables associated with VT events**

Four multivariable Cox proportional hazards regression models were created for total scar mass (model 1), BZ mass (model 2), core mass (model 3), and BZC mass (model 4). All of them were adjusted by age, sex, and LVEF (table 2). In the corresponding models, only total scar mass, BZ mass, core mass, and BZC mass were independent variables associated with the development of VT, with similar findings after a doubly robust estimation weighting for the calculated propensity scores (table 2). Figure 2 shows the distribution of calculated BZC mass values between cases and controls. The overall diagnostic performance of BZC mass to differentiate cases and controls was excellent, with an area under the ROC curve (AUC) of 0.93 [95% CI 0.89 to 0.97;  $p < 0.001$ ]. From De Long's test, all pairwise comparisons of AUCs between BZC mass and total scar mass, BZ mass, and core mass showed statistical significance ( $p < 0.001$ ). Time-dependent ROC curves for all the scar parameters analyzed are shown in figure 3. For BZC mass, a cut-off point of  $> 5.15$  g showed 92% sensitivity and 87% specificity values for the identification of patients with documented VT. A visual

example of the scar characteristics and differences between cases and controls is shown in figure 4.

### **BZC mass vs. LVEF for prediction of VT events**

Out of 67 (45%) patients having a LVEF > 35%, 29 (43%) had a BZC mass  $\geq$  5.15 g. Of them, 26 (90%) were cases. On the contrary, out of 83 (55%) patients with LVEF  $\leq$  35%, 40 (48%) had a BZC mass < 5.15 g and, from them, 36 (90%) were controls. Cumulative survival curves from MI until first documented SMVT episode according to the used LVEF and BZC mass cut-off points are shown in figure 5.

A LVEF  $\leq$  35% would have classified at a significant arrhythmia risk only 39/66 (59%) of the cases. Conversely, a LVEF > 35% would not have identified 44/84 (52%) of the controls. Patients fulfilling the combined criterium of LVEF > 35% and BZC mass < 5.15 g (n = 38) were mostly controls (37/38, 93%). Adding BZC mass to LVEF to stratify the VT occurrence risk allowed to reclassify 33.3% of the cases and 39.3% of the controls. The NRI was 0.73 (95% CI 0.71 to 0.74), which amounted to 36.7% of all cases being reclassified (figure 6). Compared with a VT risk stratification purely based on LVEF [c-index = 0.55 (95% CI 0.46 to 0.63)], there was a significant improvement in discrimination by using the BZC mass, confirmed by a c-index difference of 0.39 (95% CI 0.29 to 0.48; p < 0.001). The diagnostic performance of LVEF [AUC = 0.46 (95% CI 0.36 to 0.55)] was significantly improved by combining it with the BZC mass (IDI = 0.62, p < 0.001). Combined diagnostic performance of LVEF and BZC mass for predicting the occurrence of SMVT episodes in the study population is shown on table 3.

## **DISCUSSION**

### **Main findings**

This study is the first report describing the BZC mass as a powerful noninvasive, CMR-derived parameter that can be easily quantified and may improve arrhythmia risk stratification in chronic post-MI patients. It is also the first clinical study to report the feasibility of calculating the BZC mass in an automated way, using a commercially available cardiac imaging post-processing platform with FDA 510(k) Clearance and CE Mark approval.

The BZC mass is intrinsically linked to the qualitative structure of the scar, its heterogeneity and spatial distribution, and is related to the presence and amount of slow conducting channels within the scar. (7,11) In a previous prospective study on CRT patients (the GAUDI study), (12) the dichotomic presence of BZC had already a similar positive predictive value for arrhythmia events (24-25%) to that of an increased BZ mass (> 5.35 g in that study). Although the presence of BZC and BZ mass showed a better diagnostic performance than total scar mass, in the present study the quantitative BZC mass has shown to be the most accurate parameter above all.

On the other hand, the relative higher proportion of VA among patients with severely depressed LVEF may be explained because, the greater the scar, the higher the probability of LV systolic dysfunction, although this correlation is weak. (13) Similarly, the greater the

scar, the higher the probability of having a greater mass of BZ and BZC. The BZC mass was, among all the scar determinants analyzed, the variable most highly associated with VT occurrence, after covariate adjustment for age, sex, and LVEF. Most likely, the BZC mass constitutes the characteristic that gets closer to the true histological substrate that gives rise to post-MI scar-related reentrant VTs, that is, the basis of scar arrhythmogenicity.

The major findings of the study can be summarized as the following:

- i. Among all the scar parameters analyzed, BZC mass was the strongest independent variable associated with the appearance of clinical SMVT in chronic post-MI patients after covariate adjustment for age, sex, and LVEF. The overall diagnostic performance of BZC mass to identify post-MI patients with SMVT was very high (sensitivity 92.4% and specificity 86.9% for the cut-off value of > 5.15 g).
- ii. Adding the information of CMR-derived BZC mass to LVEF could improve the accuracy of VT risk stratification in chronic post-MI patients, as shown by significant increases in AUC with respect to other scar determinants, IDI, and NRI.

### **Rationale for the quantitative evaluation of the BZC mass**

LGE-CMR is recognized as the gold standard technique to determine the location and extent of myocardial scar.(14) The CMR-defined scar has a good correlation with low-voltage areas in the electroanatomical maps (EAM).(11,15) Moreover, the size and heterogeneity of the post-MI scar, as evaluated with CMR, are variables that, unlike LVEF, have been associated with VT inducibility,(3,5) arrhythmia events, and even mortality.(4,6,16-18) In a recently published, retrospective study, the presence of 'grey



zone' fibrosis (i.e. BZ mass) > 5.0 g showed an 84% sensitivity and 72% specificity to predict the occurrence of sudden cardiac death (SCD) in chronic post-MI patients.(19) Moreover, post-MI patients with documented SMVT had more conducting channels, as evaluated during EAM, when compared to controls.(20) CMR permits to identify BZC (21) that correlate well with the EAM conducting channels within the scar.(11) In fact, the presence of BZC has been associated with a higher risk of VA/SCD, and could help deciding whether to implant an ICD in candidates for cardiac resynchronization therapy.(12) In addition, CMR-aided or CMR-guided VT substrate ablation approaches, which are based on the ablation of BZC identified on CMR, have shown improvement in arrhythmia-free survival during follow-up.(22,23) The assessment of the clinical value of BZC mass quantification in the present study has been the necessary next step to set up future prospective studies to confirm the role of CMR in improving risk stratification for VA and SCD in post-MI patients.(24)

### **Clinical implications for SCD risk stratification**

It has been shown, in autopsy series of sudden deaths occurring during recreational sports, that coronary atherosclerotic disease was present in about 50% of the autopsies and that half of them showed chronic post-MI scars.(25) In chronic post-MI patients, VA causing SCD are mostly reentrant SMVT.(26) Therefore, identification of scars with arrhythmogenic characteristics could help better identify patients at a higher risk of SCD.

In previous reports, LVEF has shown low-specificity in differentiating the risk of SCD from risk of death associated with comorbidities or the evolution of heart failure.(18) With the

current, LVEF-based decision algorithms used for primary prevention of SCD with ICDs, the contemporary rate of appropriated therapies is very low, and much inferior than in classical ICD implantation trials that provided the evidence for current recommendations.(27) Therefore, a more accurate identification of patients at risk is urgently needed. Upon further validation, the use of BZC mass may help improving the selection of post-MI patients for ICD implantation (i.e., in cardiac resynchronization therapy candidates), (12) or contribute to deciding closer monitoring or carrying out additional screening tests (i.e. electrophysiological studies) in those patients at higher arrhythmic risk, regardless of their LVEF.(12,28,29) Yet, it shall be reminded that most cases of SCD in post-MI patients occur with normal or moderately reduced LVEF.(30) Larger cohort studies would be necessary to prospectively evaluate the use of BZC mass and its predictive accuracy for the appearance of VA and SCD.

### **Study limitations**

Despite the inherent limitations of a case-control design, it can be acceptable to propose new variables to be tested when a low event rate is observed. However, the generated risk and effect of the scar variables analyzed could have been overestimated. On the other hand, post-MI scar may suffer structural changes in the long-term, (31) being therefore unknown which would be the best timing for a BZC mass screening. VT screening capacity was limited for those patients who were not ICD carriers, as no continuous monitoring was available. Finally, optimal CMR quality should be a requisite to obtain reliable BZC mass measurements. Medical decision-making based on the BZC mass should be supported by

external clinical validation in prospective studies. Lastly, it shall be reminded that SCD in post-MI patients may not be always due to SMVT degenerating into VF.

## **Conclusions**

The mass of BZC, automatically obtained with a commercially available CMR post-processing software, is the strongest independent variable associated with the occurrence of clinical SMVT in post-MI patients after covariate adjustment for sex, LVEF, and total scar mass. The determination of BZC could be used to assess the risk of having SMVT, although it is still unclear its precise role in estimating the global risk of SCD.

## **ACKNOWLEDGEMENTS**

None.

## **FUNDING**

This research received no specific grant from any funding agency in the public, commercial, or not-for-profit sectors.

**REFERENCES**

1. De Bakker JMT, Van Capelle FJL, Janse MJ, et al. Reentry as a cause of ventricular tachycardia in patients with chronic ischemic heart disease: Electrophysiology and anatomic correlation. *Circulation*. 1988;77(3):589-606.
2. Wu E, Judd RM, Vargas JD, Klocke FJ, Bonow RO, Kim RJ. Visualisation of presence, location, and transmural extent of healed Q-wave and non-Q-wave myocardial infarction. *Lancet*. 2001;357(9249):21-8.
3. Schmidt A, Azevedo CF, Cheng A, et al. Infarct tissue heterogeneity by magnetic resonance imaging identifies enhanced cardiac arrhythmia susceptibility in patients with left ventricular dysfunction. *Circulation*. 2007;115(15):2006-14.
4. Yan AT, Shayne AJ, Brown KA, et al. Characterization of the peri-infarct zone by contrast-enhanced cardiac magnetic resonance imaging is a powerful predictor of post-myocardial infarction mortality. *Circulation*. 2006;114(1):32-9.
5. Bello D, Fieno DS, Kim RJ, et al. Infarct morphology identifies patients with substrate for sustained ventricular tachycardia. *J Am Coll Cardiol*. 2005;45(7):1104-8.
6. Klem I, Weinsaft JW, Bahnson TD, et al. Assessment of myocardial scarring improves risk stratification in patients evaluated for cardiac defibrillator implantation. *J Am Coll Cardiol*. 2012;60(5):408-20.
7. Perez-David E, Arenal Á, Rubio-Guivernau JL, et al. Noninvasive identification of ventricular tachycardia-related conducting channels using contrast-enhanced magnetic resonance imaging in patients with chronic myocardial infarction: Comparison of signal intensity scar mapping and endocardial voltage mappin. *J Am Coll Cardiol*. 2011;57(2):184-94.

8. Moss AJ, Zareba W, Hall WJ, et al. Prophylactic Implantation of a Defibrillator in Patients with Myocardial Infarction and Reduced Ejection Fraction. *N Engl J Med.* 2002;346(12):877-83.
9. Bardy GH, Lee KL, Mark DB, et al. Amiodarone or an Implantable Cardioverter-Defibrillator for Congestive Heart Failure. *N Engl J Med.* 2005 Jan;352(3):225-37.
10. Andreu D, Ortiz-Pérez JT, Fernández-Armenta J, et al. 3D delayed-enhanced magnetic resonance sequences improve conducting channel delineation prior to ventricular tachycardia ablation. *Europace.* 2015;17(6):938-45.
11. Fernández-Armenta J, Berruezo A, Andreu D, et al. Three-dimensional architecture of scar and conducting channels based on high resolution ce-CMR: Insights for ventricular tachycardia ablation. *Circ Arrhythmia Electrophysiol.* 2013;6(3):528-37.
12. Acosta J, Fernández-Armenta J, Borràs R, et al. Scar Characterization to Predict Life-Threatening Arrhythmic Events and Sudden Cardiac Death in Patients With Cardiac Resynchronization Therapy: The GAUDI-CRT Study. *JACC Cardiovasc Imaging.* 2018;11(4):561-72.
13. Palazzuoli A, Beltrami M, Gennari L, et al. The impact of infarct size on regional and global left ventricular systolic function: a cardiac magnetic resonance imaging study. *Int J Cardiovasc Imaging.* 2015;31(5):1037-44.
14. Cronin EM, Bogun FM, Maury P, et al. 2019 HRS/EHRA/APHRS/LAHRS expert consensus statement on catheter ablation of ventricular arrhythmias. *Heart Rhythm.* 2020;17(1):e2-154.

15. Gupta S, Desjardins B, Baman T, et al. Delayed-enhanced MR scar imaging and intraprocedural registration into an electroanatomical mapping system in post-infarction patients. Vol. 5, JACC: Cardiovascular Imaging. 2012. p. 207-10.
16. Kwon DH, Asamoto L, Popovic ZB, et al. Infarct characterization and quantification by delayed enhancement cardiac magnetic resonance imaging is a powerful independent and incremental predictor of mortality in patients with advanced ischemic cardiomyopathy. *Circ Cardiovasc Imaging*. 2014;7(5):796-804.
17. Ganesan AN, Gunton J, Nucifora G, McGavigan AD, Selvanayagam JB. Impact of Late Gadolinium Enhancement on mortality, sudden death and major adverse cardiovascular events in ischemic and nonischemic cardiomyopathy: A systematic review and meta-analysis. *Int J Cardiol*. 2018;254:230-7.
18. Disertori M, Rigoni M, Pace N, et al. Myocardial Fibrosis Assessment by LGE Is a Powerful Predictor of Ventricular Tachyarrhythmias in Ischemic and Nonischemic LV Dysfunction: A Meta-Analysis. *JACC Cardiovasc Imaging*. 2016;9(9):1046-55.
19. Abbasin Z, Osita O, Joseph de B, et al. Myocardial Fibrosis as a Predictor of Sudden Death in Patients With Coronary Artery Disease. *J Am Coll Cardiol* [Internet]. 2021 Jan 5;77(1):29-41. Available from: <https://doi.org/10.1016/j.jacc.2020.10.046>
20. Haqqani HM, Kalman JM, Roberts-Thomson KC, et al. Fundamental Differences in Electrophysiologic and Electroanatomic Substrate Between Ischemic Cardiomyopathy Patients With and Without Clinical Ventricular Tachycardia. *J Am Coll Cardiol*. 2009;54(2):166-73.

21. Andreu D, Berruezo A, Ortiz-Pérez JT, et al. Integration of 3D electroanatomic maps and magnetic resonance scar characterization into the navigation system to guide ventricular tachycardia ablation. *Circ Arrhythmia Electrophysiol.* 2011;4(5):674-83.
22. Andreu D, Penela D, Acosta J, et al. Cardiac magnetic resonance-aided scar dechanneling: Influence on acute and long-term outcomes. *Heart Rhythm.* 2017;14(8):1121-8.
23. Soto-Iglesias D, Penela D, Jáuregui B, et al. Cardiac Magnetic Resonance-Guided Ventricular Tachycardia Substrate Ablation. *JACC Clin Electrophysiol.* 2020;6(4):436-47.
24. Al-Khatib SM, Stevenson WG, Ackerman MJ, et al. 2017 AHA/ACC/HRS guideline for management of patients with ventricular arrhythmias and the prevention of sudden cardiac death: Executive summary: A Report of the American College of Cardiology/American Heart Association Task Force on Clinical Practice Gui. *Heart Rhythm.* 2018;15(10):e190-252.
25. Suárez-Mier MP, Aguilera B, Mosquera RM, Sánchez-de-León MS. Pathology of sudden death during recreational sports in Spain. *Forensic Sci Int.* 2013;226(1-3):188-96.
26. Mehta D, Curwin J, Gomes JA, Fuster V. Sudden death in coronary artery disease: Acute ischemia versus myocardial substrate. Vol. 96, *Circulation.* 1997. p. 3215-23.
27. Sabbag A, Suleiman M, Laish-Farkash A, et al. Contemporary rates of appropriate shock therapy in patients who receive implantable device therapy in a real-world setting: From the Israeli ICD Registry. *Heart Rhythm.* 2015;12(12):2426-33.
28. Crespo C, Linhart M, Acosta J, et al. Optimisation of cardiac resynchronisation therapy device selection guided by cardiac magnetic resonance imaging: Cost-effectiveness analysis. *Eur J Prev Cardiol.* 2020;27(6):622-32.

29. Goldenberg I, Vyas AK, Hall WJ, et al. Risk Stratification for Primary Implantation of a Cardioverter-Defibrillator in Patients With Ischemic Left Ventricular Dysfunction. *J Am Coll Cardiol.* 2008;51(3):288-96.
30. Huikuri HV, Castellanos A, Myerburg RJ. Sudden Death Due to Cardiac Arrhythmias. *N Engl J Med.* 2001;345(20):1473-82.
31. Jáuregui B, Soto-Iglesias D, Penela D, et al. Follow-Up After Myocardial Infarction to Explore the Stability of Arrhythmogenic Substrate: The Footprint Study. *JACC Clin Electrophysiol.* 2020;6(2):207-18.



## FIGURES

**Graphical Abstract.** Main findings of the study. CMR permits to identify and characterize the components of the myocardial scar after a MI. Using a dedicated software, post-processed CMR images allow to quantify the mass (in grams) of the different scar components. A BZC mass > 5.15 g has shown to be strongly associated with the occurrence of VT events (survival curve). Examples of scars with and without critical BZC mass are shown.

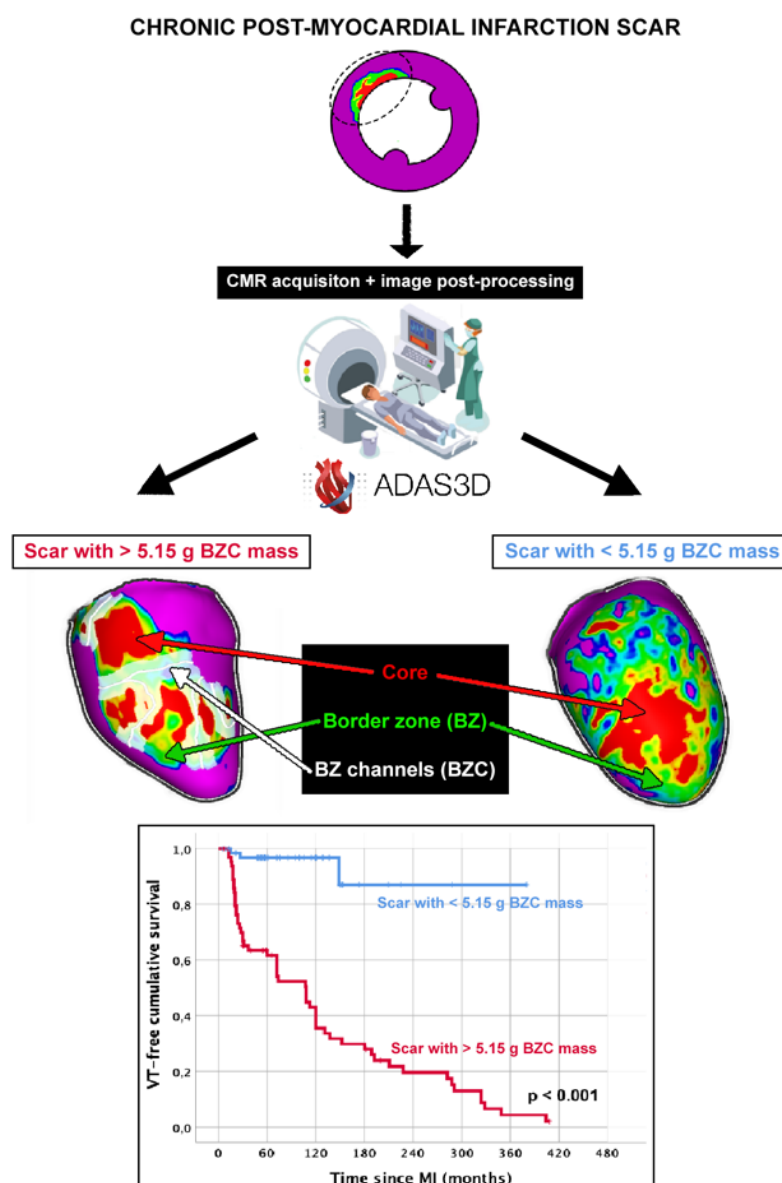


**Figure 1.** Flow chart of the study population.



**Figure 2.** Distribution of BZC mass between cases and controls. Waterfall plot presenting the distribution of BZC mass (in grams) between post-MI patients with and without documented clinical VT. The black line is located at a cut-off point of 5.15 g (see text for details).

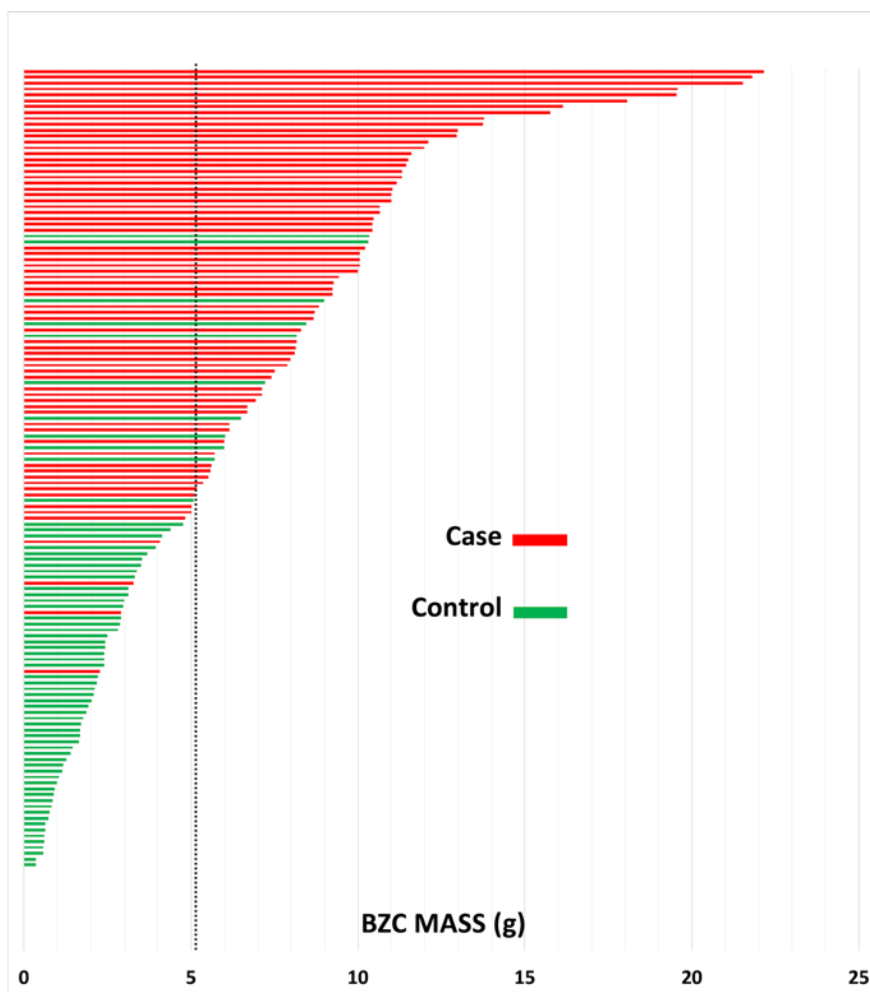


**Figure 3.** Time-dependent ROC curves for different scar determinants. Increased diagnostic performance is constantly noted at different time-points after MI when using BZC mass as compared to other scar variables.  $P < 0.001$  applied for all ROC curves.

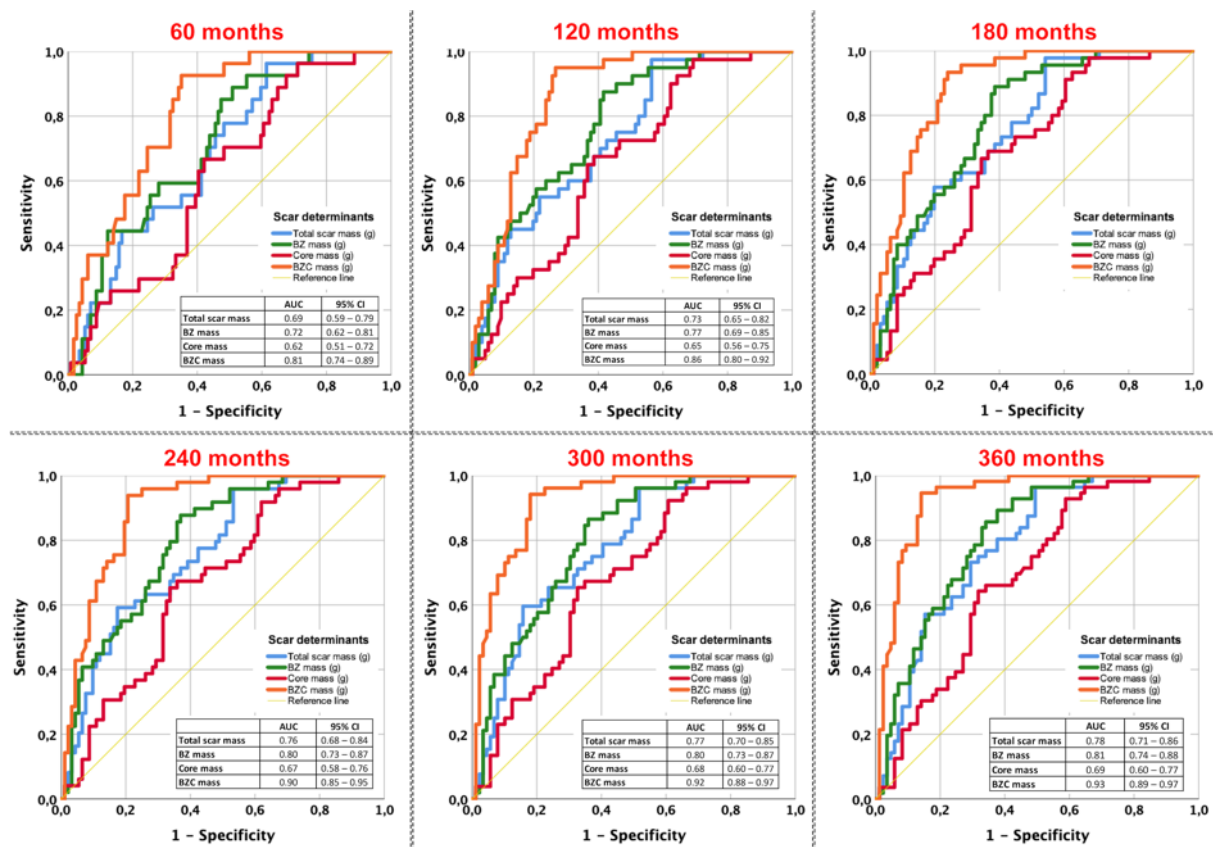


**Figure 4.** Example of the scar differences between cases and controls. From top left to bottom right in each panel, the 10%, 30%, 50%, and 90% myocardial layers are visualized. Core is color-coded in red, BZ in green, and healthy myocardium in pink. Green panel: CMR images of an asymptomatic patient (control) with anterior MI 5 years before the CMR acquisition; his LVEF was 42%, scar mass 21.31 g and BZC mass 0 g. Red panel: CMR images of a patient with incessant, sustained monomorphic VT (case), and an inferolateral MI 6 years

before the CMR acquisition; his LVEF was 45%, scar mass 29.55 g and BZC mass 10.56 g.

White lines delimit the identified BZC.

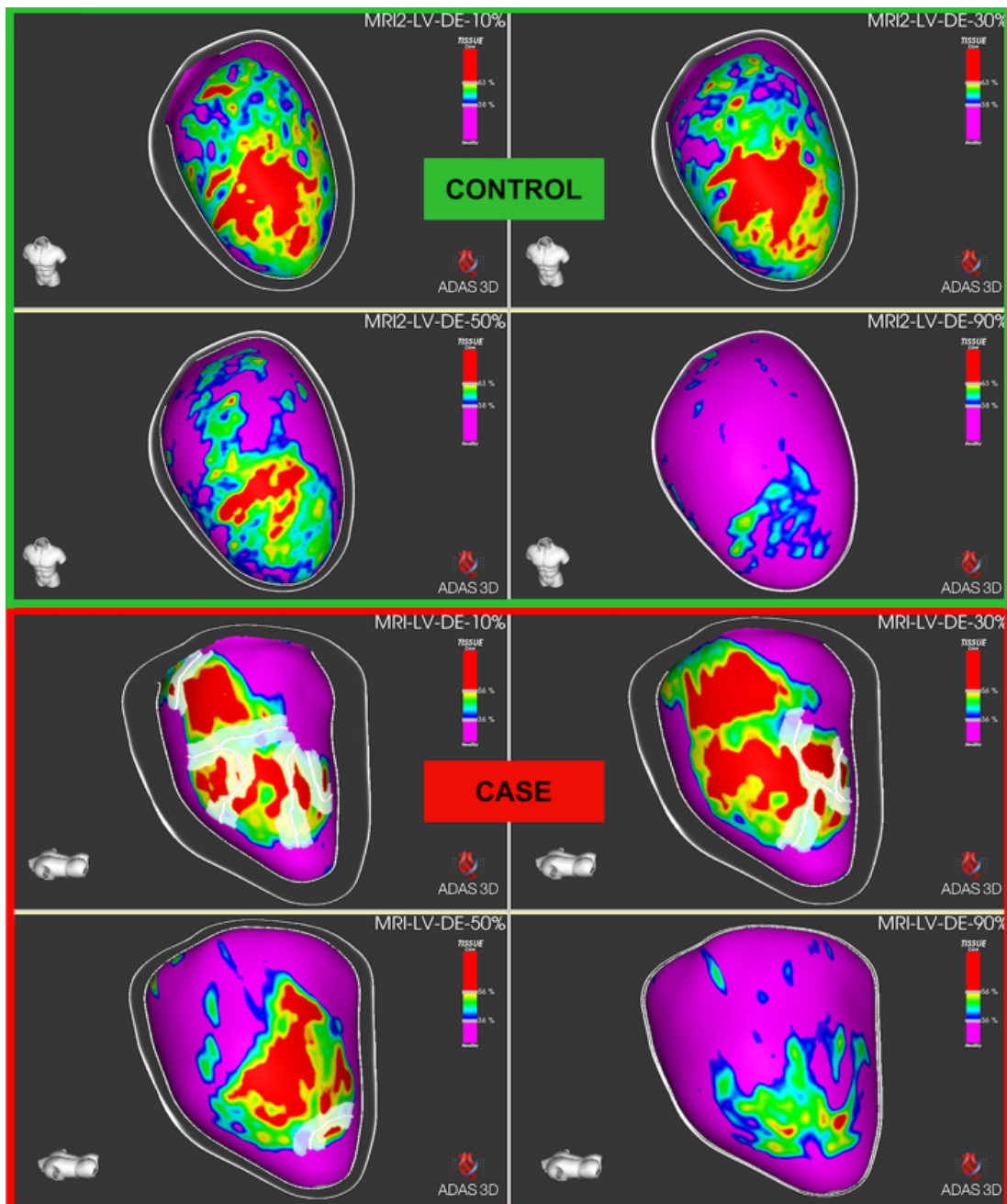


**Figure 5.** Kaplan-Meier survival curves for SMVT occurrence after MI. VT-free survival according to the amount of BZC mass within the scar (panel A), and LVEF (panel B). P-values for log-rank tests are shown in each curve.

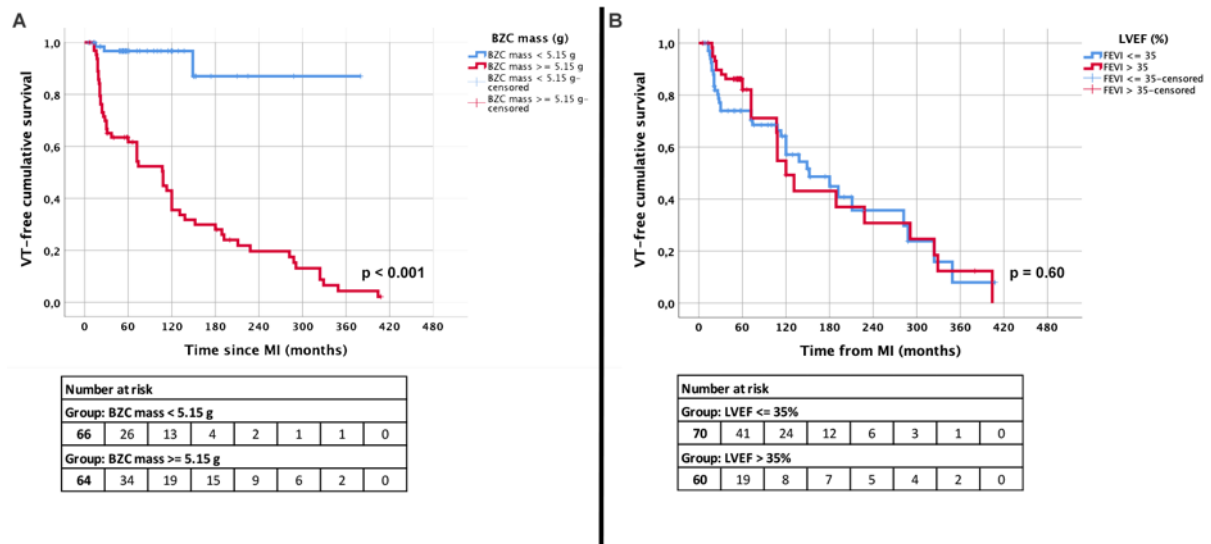
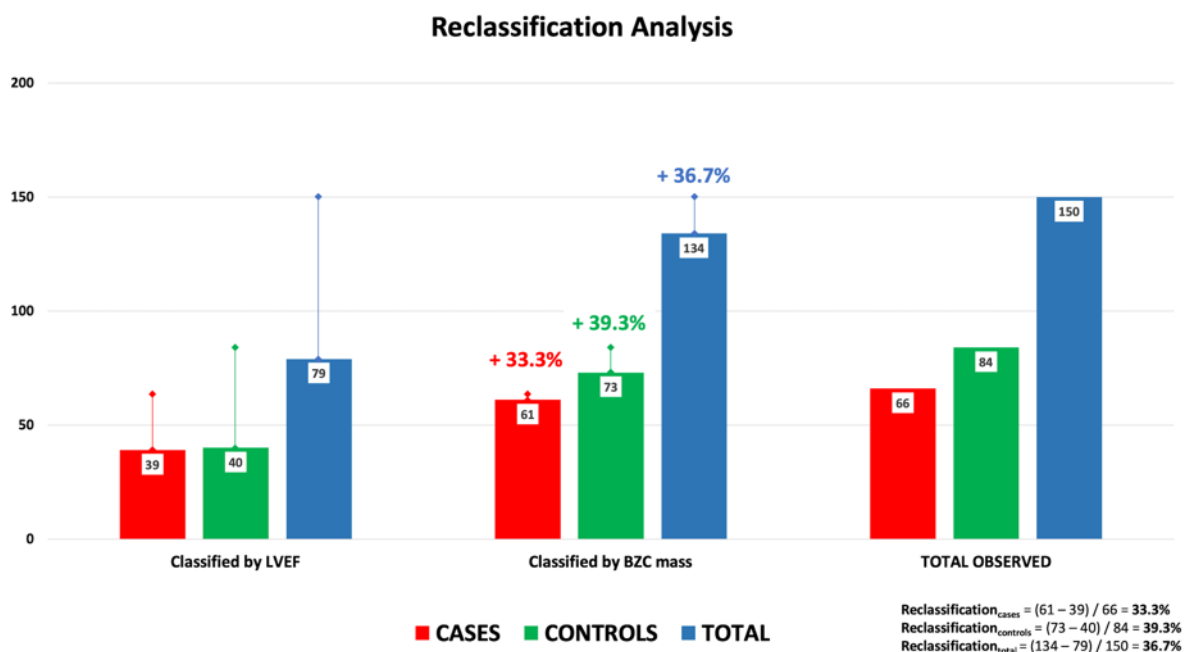


**Figure 6.** Reclassification analysis. Proportion of patients correctly reclassified as cases or controls using BZC mass, as compared to LVEF.



## TABLES

**Table 1.** Clinical and scar characteristics of the patient population.

	<b>TOTAL</b> <b>(n = 150)</b>	<b>CASES</b> <b>(n = 66)</b>	<b>CONTROLS</b> <b>(n = 84)</b>	<b>P</b>
<b>Age (years)</b>	64 ± 11	67 ± 9	62 ± 11	0.007*
<b>Male sex</b>	133 (89%)	63 (96%)	70 (83%)	0.02*
<b>Hypertension</b>	89 (65%)	46 (78%)	43 (54%)	0.004*
<b>Diabetes mellitus</b>	41 (30%)	21 (36%)	20 (25%)	0.14
<b>Dyslipidemia</b>	81 (59%)	44 (75%)	37 (47%)	0.001*
<b>Smoker</b>	27 (20%)	5 (9%)	22 (28%)	0.005*
<b>Atrial fibrillation</b>	6 (4%)	1 (2%)	5 (6%)	0.20
<b>LVEF (%)</b>	36 ± 13	34 ± 10	38 ± 14	0.07
<b>MI location (anterior)</b>	65 (44%)	26 (40%)	39 (46%)	0.46
<b>Time since MI (months)</b>	58 (31 – 120)	72 (22 – 151)	57 (51 – 115)	0.89
<b>Betablockers</b>	112 (81%)	43 (73%)	69 (87%)	0.03*
<b>ACEI/ARB</b>	97 (70%)	37 (63%)	60 (76%)	0.08
<b>Diuretics</b>	64 (46%)	29 (49%)	35 (44%)	0.54
<b>MRA</b>	72 (52%)	36 (61%)	36 (46%)	0.07
<b>Statins</b>	130 (94%)	58 (98%)	72 (91%)	0.07
<b>Total scar mass (g)</b>	26.4 ± 17.0	33.5 ± 15.5	20.9 ± 16.1	< 0.001*
<b>BZ mass (g)</b>	15.7 ± 10.9	20.9 ± 9.5	11.7 ± 10.1	< 0.001*
<b>Core mass (g)</b>	10.6 ± 8.7	12.4 ± 8.3	9.2 ± 8.8	0.03*
<b>BZC mass (g)</b>	5.8 ± 5.1	9.7 ± 4.2	3.4 ± 2.8	< 0.001*

*MI: Myocardial infarction; LVEF: left ventricular ejection fraction; ACEI: angiotensin-converting enzyme inhibitor; ARB: angiotensin receptor blocker; MRA: mineralocorticoid-receptor antagonists; BZ: border zone; BZC: border zone channel. \* Statistically significant differences (p < 0.05).*

**Table 2.** Multivariable Cox proportional hazards regression models to identify independent variables associated with VT events in the study population.

<b><u>MULTIVARIABLE MODEL 1</u></b>					
	<b>Covariate adjustment</b>			<b>PS as covariate “doubly robust”</b>	
	<b>HR (95% CI)</b>	<b>P</b>	<b>c-statistic</b>	<b>HR (95% CI)</b>	<b>p</b>
<b>Age (years)</b>	1.02 (0.99 – 1.06)	0.13	0.69	1.06 (1.01 – 1.12)	0.02*
<b>Male sex</b>	1.07 (0.32 – 3.59)	0.92		1.06 (0.31 – 3.60)	0.50
<b>LVEF (%)</b>	1.00 (0.98 – 1.03)	0.83		1.00 (0.97 – 1.03)	0.93
<b>Total scar mass (g)</b>	1.03 (1.02 – 1.05)	< 0.001*		1.03 (1.02 – 1.05)	< 0.001*
<b><u>MULTIVARIABLE MODEL 2</u></b>					
	<b>Covariate adjustment</b>			<b>PS as covariate “doubly robust”</b>	
	<b>HR (95% CI)</b>	<b>p</b>	<b>c-statistic</b>	<b>HR (95% CI)</b>	<b>p</b>
<b>Age (years)</b>	1.02 (0.99 – 1.05)	0.23	0.73	1.05 (1.00 – 1.11)	0.047*
<b>Male sex</b>	0.85 (0.25 – 2.91)	0.80		0.85 (0.24 – 2.92)	0.57
<b>LVEF (%)</b>	0.99 (0.97 – 1.02)	0.56		0.99 (0.96 – 1.02)	0.32
<b>BZ mass (g)</b>	1.06 (1.04 – 1.09)	< 0.001*		1.06 (1.04 – 1.09)	< 0.001*

<b>MULTIVARIABLE MODEL 3</b>					
	<b>Covariate adjustment</b>			<b>PS as covariate “doubly robust”</b>	
	<b>HR (95% CI)</b>	<b>p</b>	<b>c-statistic</b>	<b>HR (95% CI)</b>	<b>p</b>
<b>Age (years)</b>	1.03 (1.00 – 1.06)	0.05	0.61	1.02 (0.99 – 1.05)	0.31
<b>Male sex</b>	1.53 (0.47 – 4.99)	0.48		1.53 (0.47 – 4.99)	0.40
<b>LVEF (%)</b>	0.99 (0.96 – 1.01)	0.24		0.98 (0.96 – 1.01)	0.26
<b>Core mass (g)</b>	1.00 (0.97 – 1.03)	0.94		1.00 (0.97 – 1.04)	0.85
<b>MULTIVARIABLE MODEL 4</b>					
	<b>Covariate adjustment</b>			<b>PS as covariate “doubly robust”</b>	
	<b>HR (95% CI)</b>	<b>p</b>	<b>c-statistic</b>	<b>HR (95% CI)</b>	<b>p</b>
<b>Age (years)</b>	1.02 (0.99 – 1.05)	0.31	0.77	1.04 (0.99 – 1.09)	0.13
<b>Male sex</b>	0.94 (0.28 – 3.18)	0.92		0.94 (0.27 – 3.18)	0.51
<b>LVEF (%)</b>	0.99 (0.97 – 1.02)	0.58		0.99 (0.96 – 1.02)	0.54
<b>BZC mass (g)</b>	1.12 (1.07 – 1.17)	< 0.001*		1.11 (1.07 – 1.16)	< 0.001*

*LVEF: left ventricular ejection fraction; BZ: border zone; BZC: border zone channel; HR: hazard ratio; CI: confidence interval; PS: propensity score. \*Statistically significant differences ( $p < 0.05$ ).*



**Table 3.** Diagnostic performance of LVEF, BZC mass and a combination of both for predicting the occurrence of SMVT episodes in the study population.

<b><u>LVEF performance</u></b>	<b>CASE</b>	<b>CONTROL</b>	<b>TOTAL</b>
LVEF $\leq$ 35% (high risk)	27	44	71
LVEF $>$ 35% (low risk)	39	40	79
<b>TOTAL</b>	<b>66</b>	<b>84</b>	<b>150</b>
<b><u>Se = 40.9%; Sp 47.6%</u></b>			
<b><u>BZC mass performance</u></b>	<b>CASE</b>	<b>CONTROL</b>	<b>TOTAL</b>
BZC mass $>$ 5.15 g (high risk)	61	11	72
BZC mass $\leq$ 5.15 g (low risk)	5	73	78
<b>TOTAL</b>	<b>66</b>	<b>84</b>	<b>150</b>
<b><u>Se = 92.4%; Sp = 86.9%</u></b>			
<b><u>Combined performance (LVEF + BZC mass)</u></b>	<b>CASE</b>	<b>CONTROL</b>	<b>TOTAL</b>
LVEF $\leq$ 35% and BZC mass $>$ 5.15 g (high risk)	35	8	43
LVEF $>$ 35% and BZC mass $\leq$ 5.15 g (low risk)	1	37	38
<b>TOTAL</b>	<b>36</b>	<b>45</b>	<b>81</b>
<b><u>Se = 97.2%; Sp = 82.2%</u></b>			

*LVEF: Left ventricular ejection fraction; BZC: border zone channel; Se: Sensitivity; Sp: specificity.*

## **SUPPLEMENTARY MATERIAL**

### **SUPPLEMENTARY METHODS**

#### **LGE-CMR Acquisition**

Contrast-enhanced images were acquired 10 minutes after bolus injection of 0.2 mmol/Kg Gadobutrol (Gadovist<sup>®</sup>, Bayer Hispania, Barcelona, Spain) using a commercially available, free-breathing, ECG-gated, navigator-gated, 3D inversion-recovery, gradient-echo technique. Slice thickness was 1.4 mm, with no gap between slices. The field of view was set at 360 mm and matrix size was kept to 256 x 256 pixels to yield an isotropic spatial resolution of 1.4 x 1.4 x 1.4 mm.

#### **Wideband sequence acquisition**

In patients previously implanted with an intracardiac device the LGE-CMR was performed with a 1.5-Tesla scanner (MAGNETOM Aera<sup>®</sup>, Siemens, Erlangen, Germany). Using a 2D turboFLASH gradient-echo sequence, the short-axis contrast-enhanced images were acquired synchronized with the ECG. Slice thickness was 5 mm, with no gap between slices, with iPAT accelerator factor x2. Typical parameters were: Repetition time 948.8 ms; echo time 1.39 ms; bandwidth 592 Hz/Px; flip angle 25°; and matrix size 256 x 144 pixels. The mean in-plane resolution was 1.4 x 1.4 mm, and the voxel size was 9.80 mm<sup>3</sup>.

#### **BZC mass calculation**

In order to calculate the BZC mass, the ADAS 3D LV software includes an algorithm that first calculates the BZC paths within the myocardium, which result in BZC 'centerlines'. Then, the

BZC center lines are processed to obtain the surrounding total BZ volume, and converted into mass (grams). A tissue characterization step is first applied to all myocardial layers individually to identify the three types of tissue involved (core, BZ, and healthy tissue); then, a topological detection algorithm<sup>1</sup> is applied to each layer to obtain BZC on the layers. A final check is done on the detected corridors to guarantee that they consider the surrounding tissue outside each layer.

The automatically calculated BZC centerline is displayed over the surface of a layer (supplementary figures 3-7). The centerline starts at the transition between BZ tissue and healthy myocardium and passes through BZ in between core regions, ending at another healthy myocardium zone. The software uses this centerline as the center of a cylindrical tube to define the maximum extent of BZ to be taken into consideration for the mass computation. The radius of the tube has been set at a maximum of 5 mm from the centerline, since it was previously established that the mean maximum width of BZ channels identified on CMR was  $5.8 \pm 2.5$  mm.<sup>2</sup> The tube centered around the centerline extends itself beyond the surface of the layer (supplementary figure 3).

This cylindrical tube encloses the BZ voxels of the original CMR image that will contribute to the BZC mass. Supplementary figure 4 shows: a) a short-axis slice intersecting the LV surface layer and the corridor centerline and tube, and b) the short-axis slice is shown with the color-coded myocardium, as well as the surrounding cylindrical tube contours (white). The myocardium is shown in three colors: core in red, BZ in yellow and healthy in blue. The BZ voxels enclosed in the tube are shown in green, and these are the voxels that will be

counted toward the BZ corridor mass. See Supplementary figures 5 and 6 for additional 3D views of the BZC volume, the core volume and the slices from the CMR volume.

The final BZC mass is obtained by multiplying the number of voxels of BZ enclosed in the cylindrical tube and contiguous to the centerline, by the voxel volume and a tissue density of  $1.05 \text{ g/cm}^3$ . Supplementary figure 7 shows a detail on a CMR plane, in which the BZC volume intersection is seen in green, enclosed in the 5-mm tube, and its relation to the other structures.

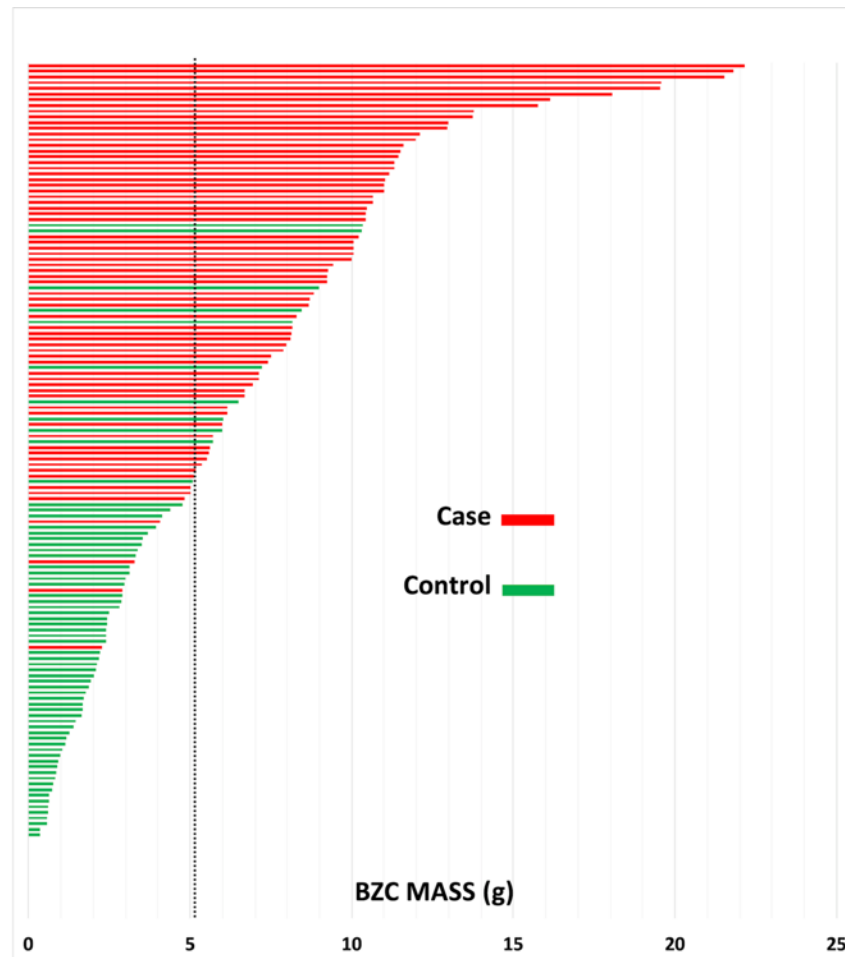
In the example of Supplementary figures 3-7, the corridor had a volume of 745 voxels, which resulted in a BZC mass of 2.18 g. Each voxel had a size of  $2.788 \text{ mm}^3$  ( $1.4063 \times 1.4063 \times 1.4100 \text{ mm}$ ), so the total volume was  $2077.45 \text{ mm}^3$  and thus the total mass was 2.18 g. The total scar mass was 24.43 g, BZ was 19.4 g, and core was 5.04 g.

**SUPPLEMENTARY REFERENCES**

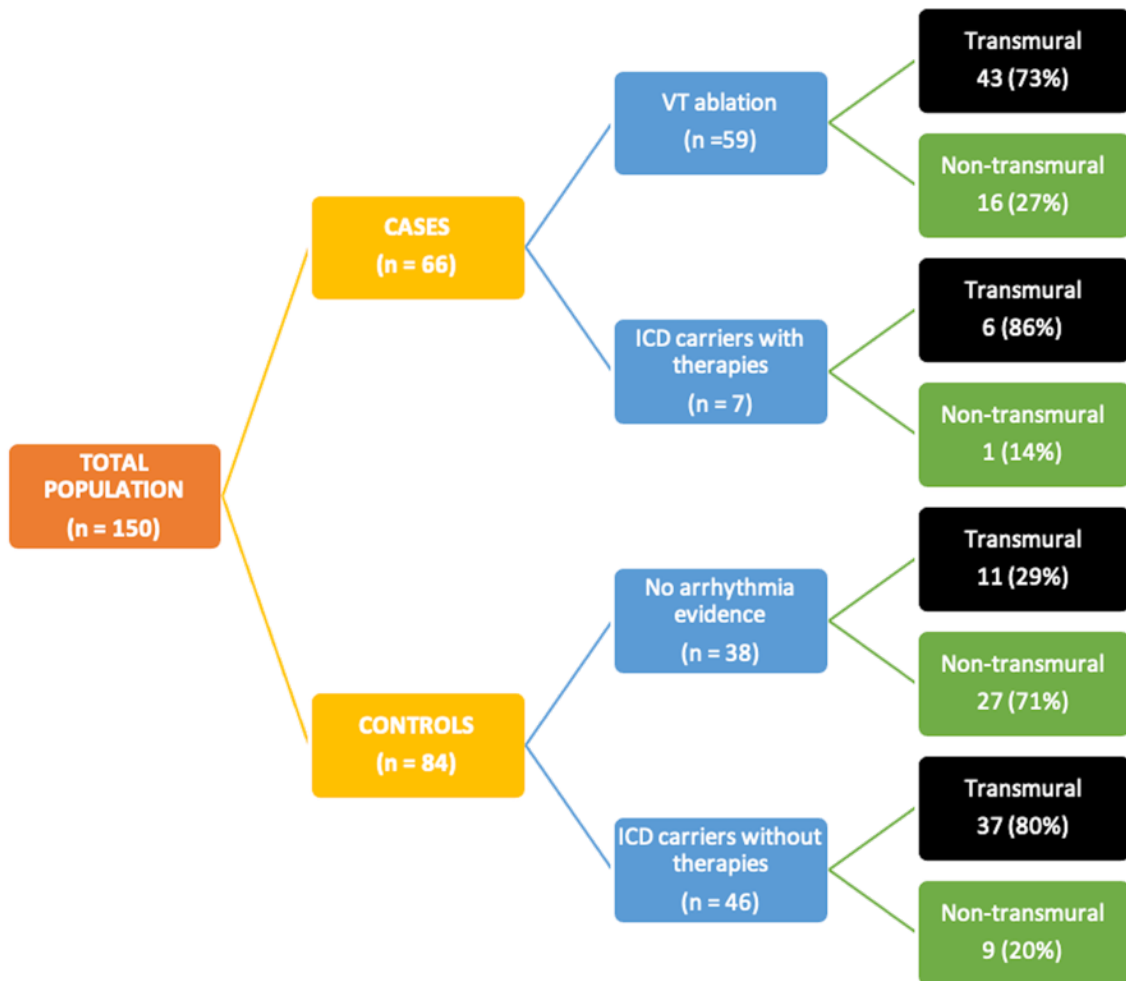
1. Steghöfer M, Serra L, Brugada J, Mont JL, Berruezo A, inventors; ADAS3D Medical SL, Hospital Clinic de Barcelona, Universitat de Barcelona, assignees. A computer implemented method for identifying channels from representative data in a 3D volume and a computer program product implementing the method. US Patent 10,304,185. European Patent EP2950270B1. 2015.
2. Fernández-Armenta J, Berruezo A, Andreu D, Camara O, Silva E, Serra L, Barbarito V, Carotenutto L, Evertz R, Ortiz-Pérez JT, De Caralt TM, Perea RJ, Sitges M, Mont L, Frangi A, Brugada J. Three-dimensional architecture of scar and conducting channels based on high resolution ce-CMR: insights for ventricular tachycardia ablation. *Circ Arrhythm Electrophysiol* 2013;6:528-537.

**SUPPLEMENTARY FIGURES**

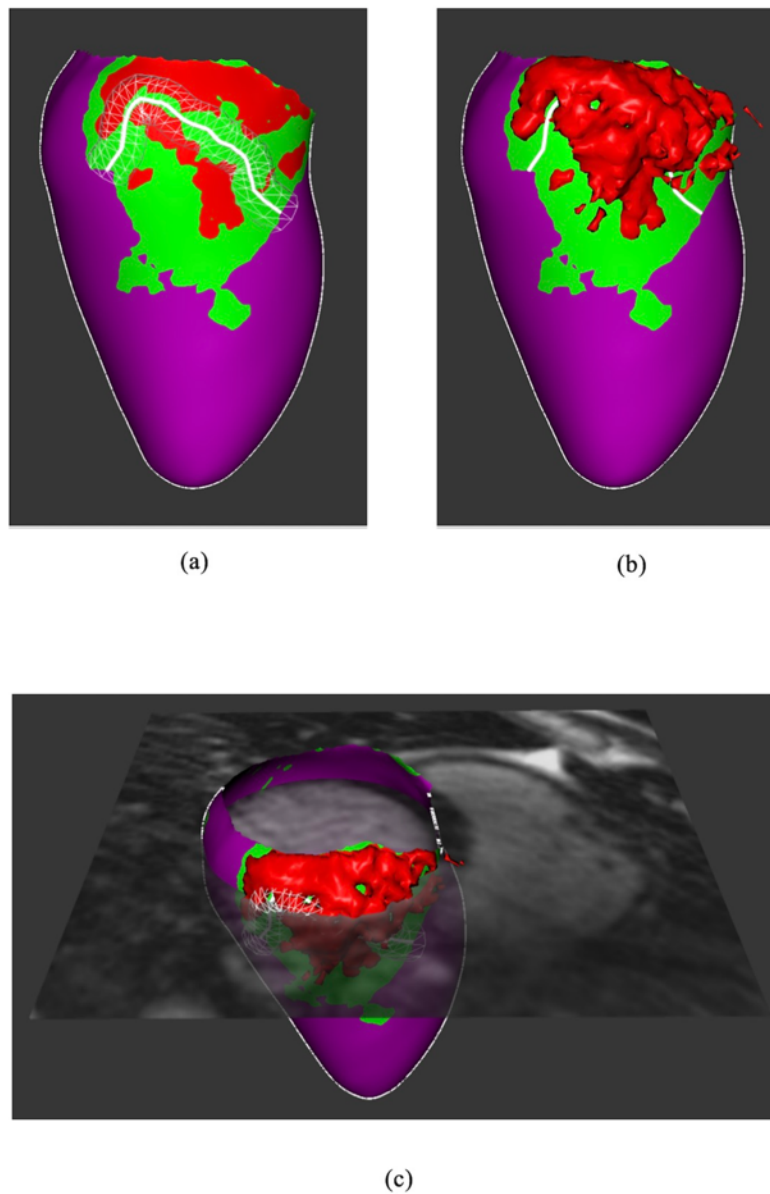
**Supplementary Fig. 1.** Waterfall plot presenting the distribution of BZC mass (in grams) between post-MI patients with and without documented clinical VT. The *black line* is located at a cut-off point of 5.15 g (see text for details).



**Supplementary Fig. 2.** Distribution of transmural substrates in the study subgroups, defined as the presence of LGE beyond 75% of the myocardial wall thickness.

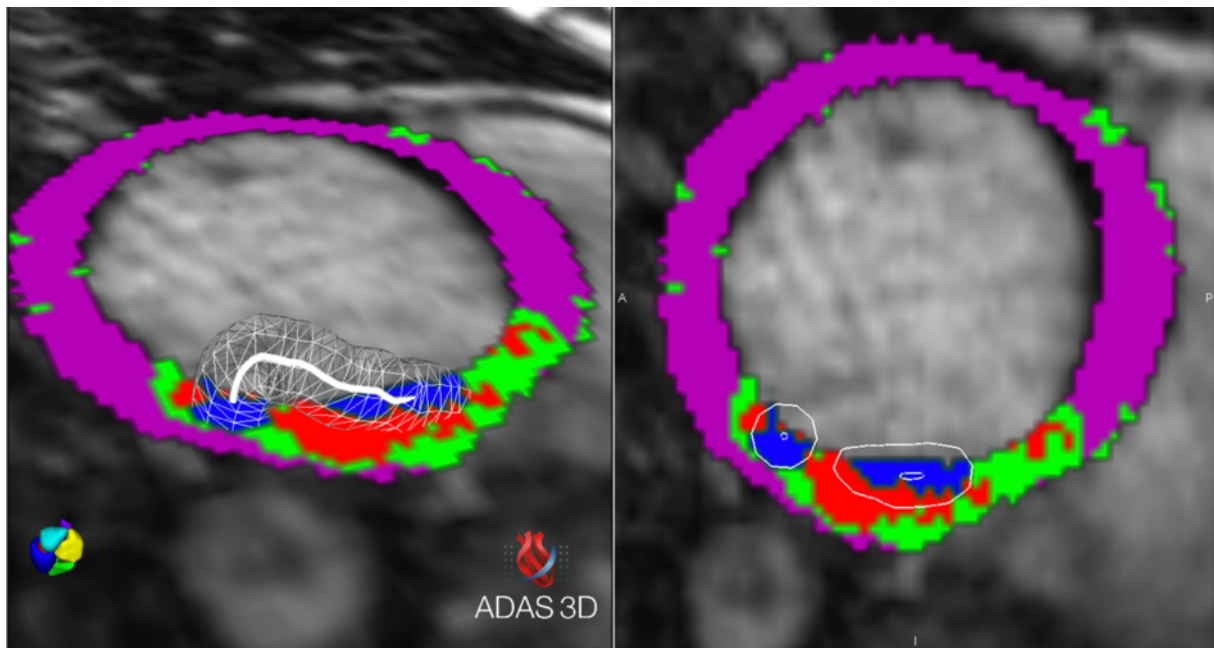


**Supplementary Fig. 3.** Panel (a): Myocardial surface layer showing a corridor centerline (*white*) surrounded by a tube of 5-mm radius (seen as a *wireframe mesh*). Panel (b): 3D core surface added (*red*). Panel (c): CMR short-axis slice showing the intersection with the segmented myocardium.

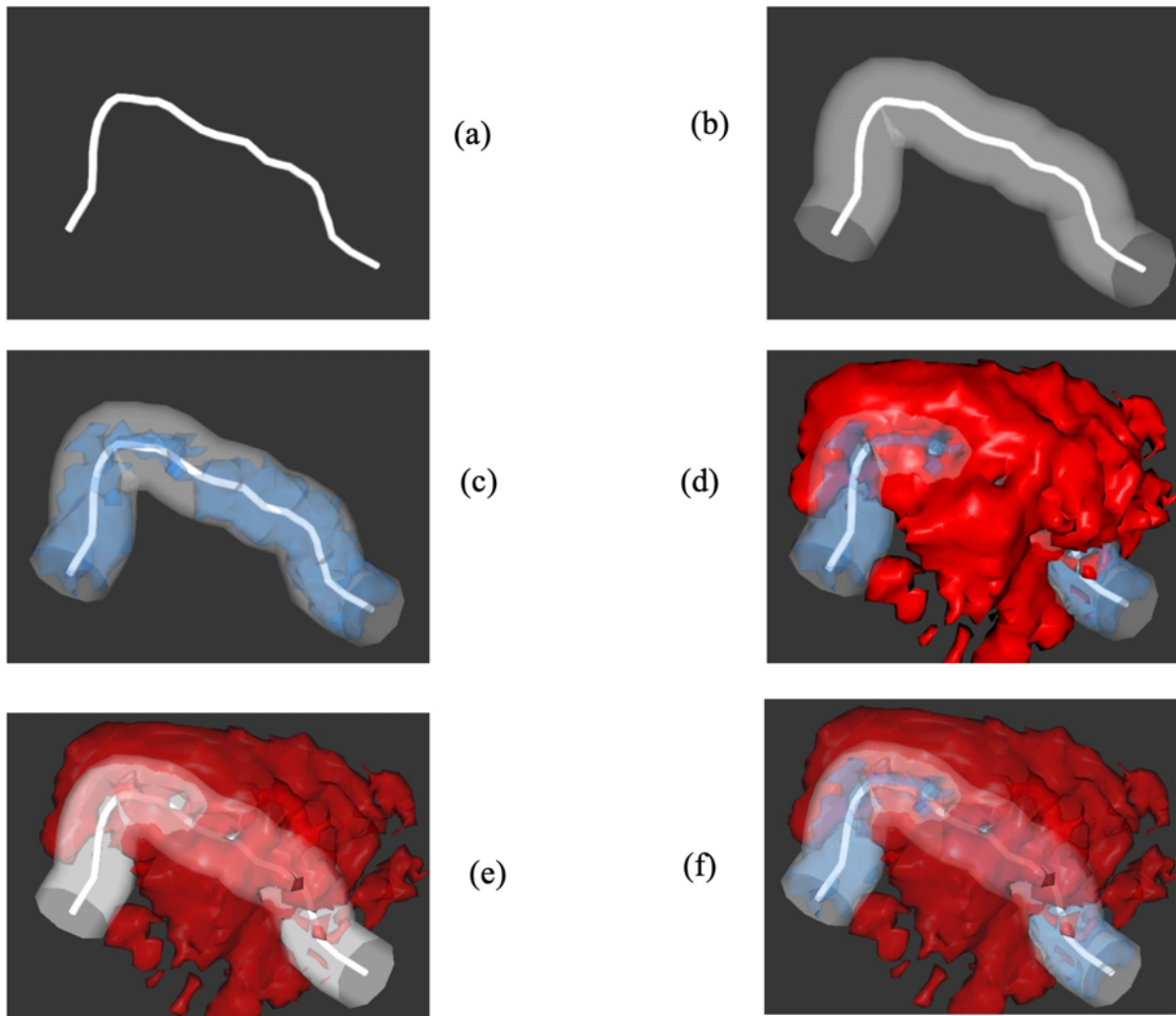




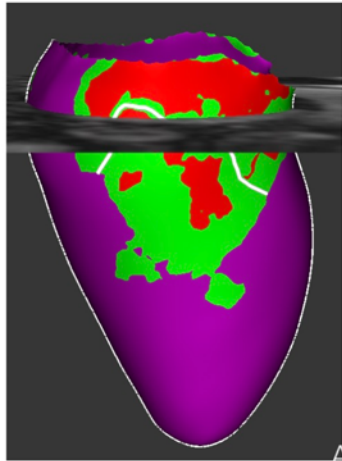
**Supplementary Fig. 4.** CMR short-axis slice showing the intersection with the segmented myocardium. The corridor centerline is seen as a *white line* emerging from the slice, showing the 5-mm tube (wireframe). Tissue in this case is colored as healthy (*pink*), core (*red*) and BZ (*green*). In *blue* is the BZC tissue within the 5-mm radius of the corridor centerline.



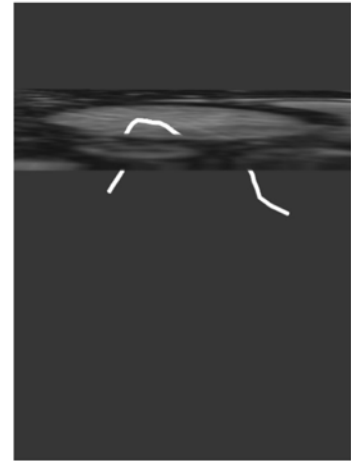
**Supplementary Fig. 5.** Panel (a): Original corridor centerline. Panel (b): 5-mm tube around the corridor. Panel (c): BZC volume contained inside the 5-mm tube (blue). Panel (d): Core surface (red) surrounding the BZC volume. Panel (e): Semitransparent core surface with the corridor centerline and 5-mm tube. Panel (f): Semitransparent core surface with the BZC volume contained inside the 5-mm tube (blue).



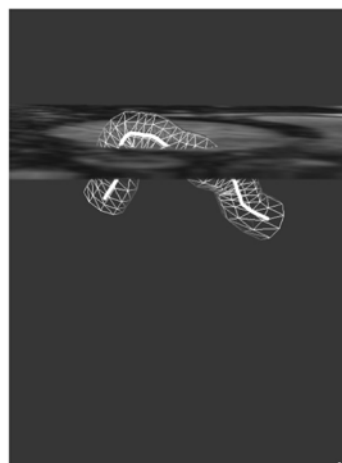
**Supplementary Fig. 6.** Relationships of the CMR short-axis slice with the myocardial layer [panel (a)], the BZC centerline [panel (b)], the BZC 5-mm tube [panel (c)], and the BZC tube embedded within the 3D core [panel (d)].



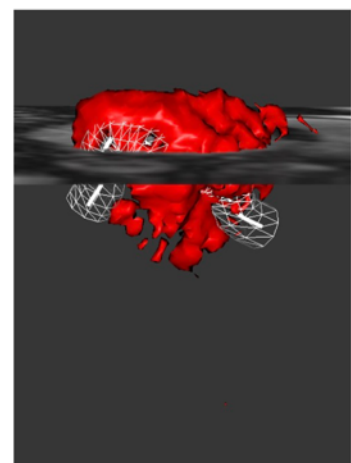
(a)



(b)

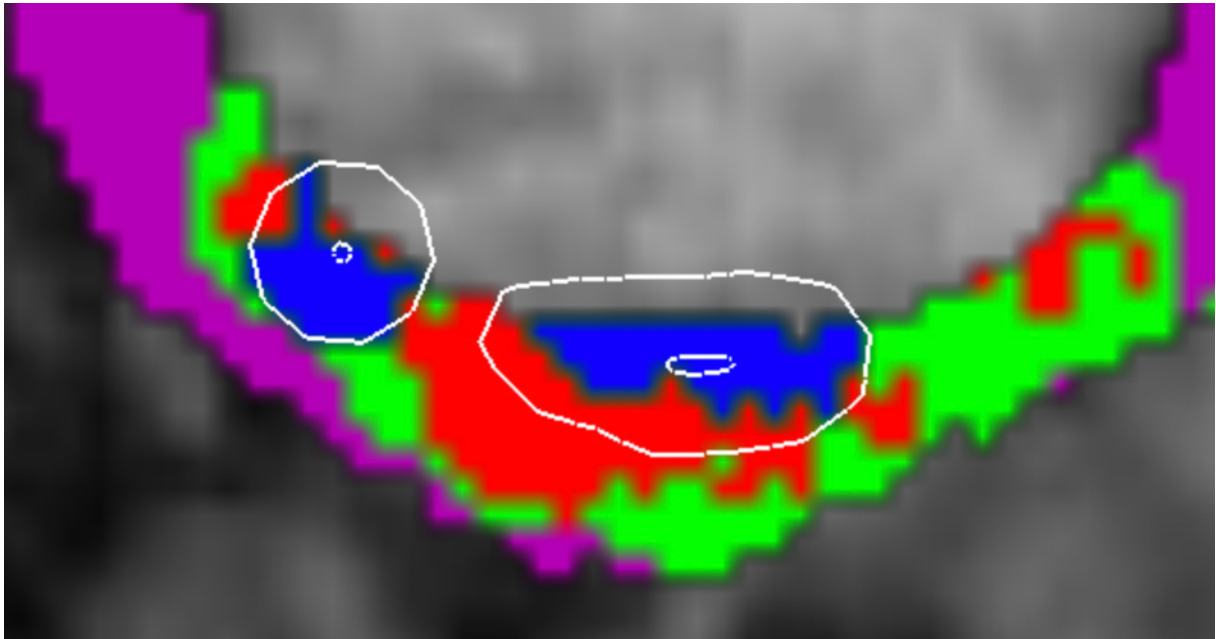


(c)



(d)

**Supplementary Fig. 7.** Detail of the different surfaces intersecting the short-axis slice. *Red*: Core zone. *Green*: border zone. *Pink*: healthy myocardium. *Blue*: BZC 5-mm tube.



**SUPPLEMENTARY TABLES**

**Supplementary table 1.** Main characteristics analyzed in the propensity score-adjusted population (66 cases + 66 controls), showing an adequate goodness of fit with respect to the adjusted clinical covariates (age, sex, LVEF):

<b>PROPENSITY SCORE-ADJUSTED POPULATION</b>					
	<b>TOTAL (n = 132)</b>	<b>CASES (n = 66)</b>	<b>CONTROLS (n = 66)</b>	<b>P</b>	<b>Standardized differences (%)</b>
<b>Age (years)</b>	67 ± 9	67 ± 9	66 ± 9	0.66	+7.9
<b>Male sex</b>	127 (96%)	63 (96%)	64 (97%)	0.76	-7.9
<b>LVEF (%)</b>	34 ± 11	34 ± 10	33 ± 13	0.79	+4.6
<b>MI location (anterior)</b>	56 (42%)	26 (39%)	30 (45%)	0.49	-10.0
<b>Time since MI (months)</b>	64 (27 - 141)	72 (22 - 149)	58 (52 - 121)	0.82	+8.4
<b>Total scar mass (g)</b>	27.6 ± 15.9	33.5 ± 15.5	21.8 ± 14.2	< 0.001*	+73.3†
<b>BZ mass (g)</b>	16.3 ± 10.3	20.9 ± 9.5	11.7 ± 9.0	< 0.001*	+90.0†
<b>Core mass (g)</b>	11.3 ± 8.5	12.4 ± 8.3	10.2 ± 8.6	0.13	+26.3†
<b>BZC mass (g)</b>	6.1 ± 5.3	9.7 ± 4.2	2.5 ± 3.5	< 0.001*	+136.5†

\*Statistically significant differences ( $p < 0.05$ ). †Inadequate goodness of fit (standardized differences > 10%). The sign of the differences refers to the comparison of cases with respect to controls.

**Supplementary table 2.** Distribution of the analyzed scar parameters in transmural vs. non-transmural substrates. Transmurality was defined as the presence of LGE beyond 75% of the myocardial wall thickness.

	<b>Transmural scars</b>	<b>Non-transmural scars</b>	<b>p</b>
<b>Scar mass (g)</b>	34.13 ± 15.66	12.35 ± 7.81	< 0.001
<b>BZ mass (g)</b>	19.96 ± 10.73	8.03 ± 5.57	< 0.001
<b>Core mass (g)</b>	14.07 ± 8.83	4.32 ± 3.32	< 0.001
<b>BZC mass (g)</b>	6.86 ± 5.42	3.95 ± 3.74	< 0.001

*BZ: border zone; BZC: border zone channel. \*Statistically significant differences ( $p < 0.05$ ).*



## SUBPROYECTO 3. UTILIDAD DE LA CARDIORRESONANCIA EN EL TRATAMIENTO DE LAS ARRITMIAS VENTRICULARES EN EL POST-INFARTO CRÓNICO DE MIOCARDIO.

### Artículo 5: Cardiac Magnetic Resonance–Guided Ventricular Tachycardia Substrate Ablation

Soto-Iglesias D, Penela D, **Jáuregui B**, Acosta J, Fernández-Armenta J, Linhart M, Zucchelli G, Syrovnev V, Zaraket F, Terés C, Perea RJ, Prat-González S, Doltra A, Ortiz-Pérez JT, Bosch X, Cámara Ó, Berruezo A. Cardiac Magnetic Resonance–Guided Ventricular Tachycardia Substrate Ablation. *JACC Clin Electrophysiol* 2020;6:436–447. *FACTOR DE IMPACTO (2020): 6.375. ÁREA DE CONOCIMIENTO: Cardiology and Cardiovascular Medicine. CUARTIL: Q1.*

El objetivo general del trabajo es evaluar la viabilidad y el beneficio potencial de realizar los procedimientos de ablación de sustrato de TV guiando la ablación con los mapas de intensidad de señales de píxeles (PSI) derivados de la CRM.



## RESUMEN

**Antecedentes:** La ablación de TV asistida por resonancia magnética cardíaca (CMR-aided) mediante mapas de PSI a partir de RMC-RTG, y fusionada con la información del EAM, ha demostrado mejorar los resultados de la ablación de sustrato de TV.

**Objetivos:** Evaluar la viabilidad y el beneficio potencial de realizar procedimientos de ablación de sustrato de TV guiados por mapas PSI derivados de RM (CMR-guided).

**Métodos:** Se incluyeron en el estudio 84 pacientes con TV monomórfica dependiente de cicatriz que se sometieron a ablación de sustrato. En los últimos 28 (33%) pacientes consecutivos el procedimiento fue guiado por RM. Se compararon los datos del procedimiento, así como los resultados agudos y de seguimiento entre los pacientes guiados por RM y dos grupos de control: 1) pacientes en los que se disponía de mapas PSI pero en los que se adquirió EAM y éste se utilizó para seleccionar los objetivos de ablación (CMR-aided); y 2) pacientes sin mapas de PSI disponibles (No-CMR).

**Resultados:** La duración media del procedimiento fue menor en la ablación del sustrato guiada por RM en comparación con la ablación CMR-aided y No-CMR ( $107 \pm 59$  frente a  $203 \pm 68$  min y  $227 \pm 52$ ;  $p < 0,001$  para ambas comparaciones). La CMR-guided requirió menos tiempo de fluoroscopia que la CMR-aided y No-CMR ( $10 \pm 4$  frente a  $23 \pm 11$  min y  $20 \pm 9$  min, respectivamente;  $p < 0,001$  para ambas comparaciones) y menos tiempo de radiofrecuencia (RF) ( $15 \pm 8$  vs.  $20 \pm 15$  y  $26 \pm 10$  min;  $p = 0,16$  y  $p < 0,001$  respectivamente). Después de la ablación de sustrato, la inducibilidad para TV fue menor en la CMR-guided en comparación con la CMR-aided y No-CMR (18 vs. 32% y 46%;  $p = 0,35$  y  $p = 0,04$  respectivamente), sin diferencias significativas en las complicaciones. Después de 18

meses, la recurrencia de TV fue menor en la CMR-guided en comparación con la No-CMR (rango logarítmico = 0,019), sin diferencias con la ablación CMR-aided.

**Conclusiones:** La ablación de TV guiada por RM es factible y segura, reduciendo significativamente el tiempo de procedimiento, fluoroscopia y RF, y se asocia a una mayor tasa de no inducibilidad y menor recurrencia de TV después de la ablación de sustrato.

## VENTRICULAR ARRHYTHMIAS

# Cardiac Magnetic Resonance-Guided Ventricular Tachycardia Substrate Ablation



David Soto-Iglesias, PhD,<sup>a,b,\*</sup> Diego Penela, MD, PhD,<sup>c,\*</sup> Beatriz Jáuregui, MD,<sup>a</sup> Juan Acosta, MD, PhD,<sup>d</sup> Juan Fernández-Armenta, MD, PhD,<sup>e</sup> Markus Linhart, MD,<sup>b</sup> Giulio Zucchelli, MD, PhD,<sup>f</sup> Vladimir Syrovnev, MD,<sup>b</sup> Fatima Zaraket, MD,<sup>b</sup> Cheryl Terés, MD,<sup>a</sup> Rosario J. Perea, MD, PhD,<sup>b</sup> Susana Prat-González, MD, PhD,<sup>b</sup> Ada Doltra, MD, PhD,<sup>b</sup> José T. Ortiz-Pérez, MD, PhD,<sup>b</sup> Xavier Bosch, MD, PhD,<sup>b</sup> Oscar Camara, PhD,<sup>g</sup> Antonio Berruezo, MD, PhD<sup>a,b</sup>

### ABSTRACT

**OBJECTIVES** This study assessed the feasibility and potential benefit of performing ventricular tachycardia (VT) substrate ablation procedures guided by cardiac magnetic resonance (CMR)-derived pixel signal intensity (PSI) maps.

**BACKGROUND** CMR-aided VT ablation using PSI maps from late gadolinium enhancement-CMR (LGE-CMR), together with electroanatomical map (EAM) information, has been shown to improve outcomes of VT substrate ablation.

**METHODS** Eighty-four patients with scar-dependent monomorphic VT who underwent substrate ablation were included in the study. In the last 28 (33%) consecutive patients, the procedure was guided by CMR. Procedural data, as well as acute and follow-up outcomes, were compared between patients who underwent guided CMR and 2 control groups: 1) patients who had PSI maps were available but the EAM was acquired and used to select the ablation targets (CMR aided); and 2) patients with no CMR-derived PSI maps available (no CMR).

**RESULTS** Mean procedure duration was lower in CMR-guided substrate ablation compared with CMR-aided and no CMR (107 ± 59 min vs. 203 ± 68 min and 227 ± 52 min;  $p < 0.001$  for both comparisons). CMR-guided ablation required less fluoroscopy time than CMR-aided ablation and no CMR (10 ± 4 min vs. 23 ± 11 min and 20 ± 9 min, respectively;  $p < 0.001$  for both comparisons) and less radiofrequency time (15 ± 8 min vs. 20 ± 15 min and 26 ± 10 min;  $p = 0.16$  and  $p < 0.001$ , respectively). After substrate ablation, VT inducibility was lower in CMR-guided ablation compared with CMR-aided ablation and no CMR (18% vs. 32% and 46%;  $p = 0.35$  and  $p = 0.04$ , respectively), without significant differences in complications. After 12 months, VT recurrence was lower in those who underwent CMR-guided ablation compared with no CMR (log-rank: 0.019), with no differences with CMR-aided ablation.

**CONCLUSIONS** CMR-guided VT ablation is feasible and safe, significantly reduces the procedural, fluoroscopy, and radiofrequency times, and is associated with a higher noninducibility rate and lower VT recurrence after substrate ablation. (J Am Coll Cardiol EP 2020;6:436–47) © 2020 by the American College of Cardiology Foundation.

From the <sup>a</sup>Heart Institute, Teknon Medical Center, Barcelona, Spain; <sup>b</sup>Clinic Cardiovascular Institute, Hospital Clínic, Barcelona, Spain; <sup>c</sup>Ospedale Guglielmo da Saliceto, Piacenza, Italy; <sup>d</sup>Hospital Universitario Virgen del Rocío, Sevilla, Spain; <sup>e</sup>Hospital Puerta del Mar, Cádiz, Spain; <sup>f</sup>Azienda Ospedaliero-Universitaria Pisana, Pisa, Italy; and <sup>g</sup>Physense, DTIC, Universitat Pompeu Fabra, Barcelona, Spain. \*Drs. Soto-Iglesias and Penela contributed equally to this work and are joint first authors. This work was supported by Agencia de Gestió d'Ajuts Universitaris i de Recerca, Generalitat de Catalunya (grant 2014-SGR-471), Instituto de Salud Carlos III, Centro de Investigación Biomédica en Red: FIS-CIBER16 (grant CB16/11/00354), Fondo de Investigación Sanitaria (grants PI14/00759 and PI17/01968), and Ministerio de Economía y Competitividad, RETOS (grants RTC-2015-3515-1 and RTC-2016-5445-1). Dr. Berruezo holds stock in Galgo Medical SL; and has received financial support from Siemens Healthcare. All other authors have reported that they have no relationships relevant to the contents of this paper to disclose.

ISSN 2405-500X/\$36.00

<https://doi.org/10.1016/j.jacep.2019.11.004>

Ventricular tachycardia (VT) substrate ablation is an effective treatment for patients with recurrent episodes of scar-dependent VT (1,2) but recurrence rates remain high (3,4). Moreover, despite the adoption of substrate-based mapping and ablation as the technique of choice for VT suppression in the last decade (5), the procedure is still considered challenging and time-consuming.

Recent studies (6,7) have shown that aiding VT substrate ablation with color-coded pixel signal intensity (PSI) maps obtained from pre-procedural late gadolinium enhancement–cardiac magnetic resonance (LGE-CMR) imaging results in less need for radiofrequency (RF) delivery and improved VT recurrence–free survival. The accuracy of LGE-CMR for scar tissue characterization and delimitation within the entire myocardial thickness (8), as well as its ability to identify additional arrhythmogenic substrates, compared with endocardial or epicardial surface electroanatomic maps (EAMs) alone (6), would suggest better outcomes with this approach. However, in these previous studies, selection of the ablation targets was still based on EAM findings rather than on LGE-CMR information. Data on the appropriateness of selecting ablation target sites based exclusively on information provided by PSI maps is lacking.

The objective of the present study was to evaluate the feasibility and potential benefits of performing VT substrate ablation guided by PSI maps obtained from LGE-CMR imaging.

## METHODS

**PATIENT SAMPLE.** This is a prospective, experimental, nonrandomized, and pilot study performed in 2 centers. Between March 2017 and June 2018, 28 consecutive patients referred for catheter ablation of left ventricular (LV) scar-related sustained monomorphic VT were included. Patients were included if they had incessant or repetitive ( $\geq 2$ ) VT episodes but also if they had a first episode of slow monomorphic VT. VT substrate ablation was guided by PSI map information (CMR guided) in each case. Procedural data, as well as acute and follow-up outcomes, were compared with 2 historical control groups selected consecutively (inclusion period from April 2011 to

March 2017) and matched by LV ejection fraction (LVEF), etiology of cardiomyopathy, and need for an epicardial approach: 1) 28 patients who had VT substrate ablation was performed without LGE-CMR information (no CMR); and 2) 28 patients who had PSI maps were obtained, integrated into the navigation system, and combined with the electroanatomical map (EAM), selecting the ablation target based on the EAM information (CMR aided). The study complied with the Declaration of Helsinki. The local ethics committee approved the study protocol, and all participants signed the informed consent.

**IMAGE PROCESSING.** Pre-procedural LGE-CMR was obtained using a 3-T scanner (MAGNETOM Trio, Siemens Healthcare, Erlangen, Germany). In patients previously implanted with an implantable cardioverter-defibrillator (ICD), LGE-CMR was performed with a 1.5-T scanner (MAGNETOM Aera; Siemens Healthcare) using a specific wide-band sequence to avoid device artefacts. Pre-procedural multidetector computer tomography (MDCT) was also obtained, in absence of contraindication, using a dual-source SOMATOM Definition Flash, 128-slice CT scanner (Siemens Healthcare). For acquisition details, see the [Supplemental Appendix](#).

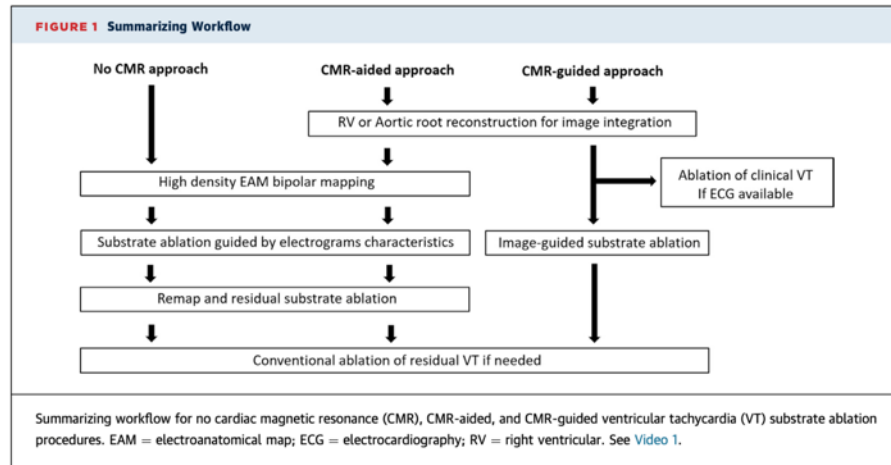
All LGE-CMR images were processed using a previously described approach (9). Briefly, a full LV volume was reconstructed in the axial orientation, and the resulting images were processed with ADAS-VT (Galgo Medical, Barcelona, Spain) software. The LV was divided into 10 layers from the endocardium to the epicardium, and a 3-dimensional shell was obtained for each layer. PSI maps were obtained from LGE-CMR images, color-coded, and projected to each of the shells following a trilinear interpolation algorithm. To characterize the scar areas, a PSI-based algorithm was applied to define the hyperenhanced area as a scar core or border zone, using  $40 \pm 5\%$  and  $60 \pm 5\%$  of the maximum intensity as thresholds (10). In the LGE-CMR PSI maps, heterogeneous tissue channels (HTCs) were defined as continuous corridors of border zone surrounded by scar core or scar core and an anatomical barrier (mitral annulus) connecting 2 areas of healthy tissue. HTCs were obtained

## ABBREVIATIONS AND ACRONYMS

CC	= conducting channel
CMR	= cardiac magnetic resonance
EAM	= electroanatomical map
ECG	= electrocardiography
EGM	= electrogram
HSC	= hidden slow conduction
HTC	= heterogeneous tissue channel
ICD	= implantable cardioverter-defibrillator
LGE-CMR	= late gadolinium enhancement cardiac magnetic resonance
LV	= left ventricular
LVEF	= left ventricular ejection fraction
MDCT	= multidetector cardiac tomography
PSI	= pixel signal intensity
SR	= sinus rhythm

The authors attest they are in compliance with human studies committees and animal welfare regulations of the authors' institutions and Food and Drug Administration guidelines, including patient consent where appropriate. For more information, visit the [JACC: Clinical Electrophysiology author instructions page](#).

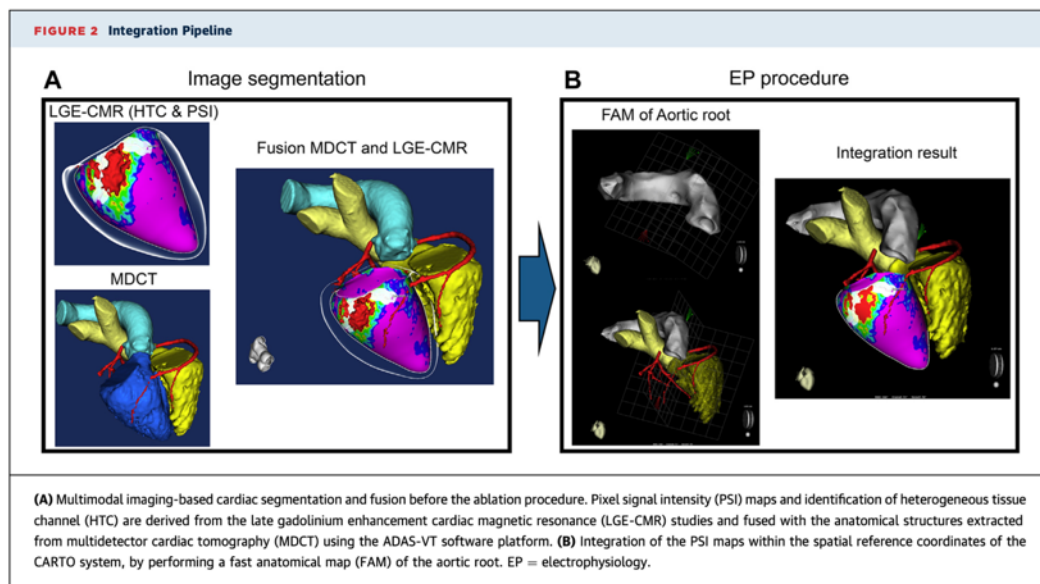
Manuscript received June 26, 2019; revised manuscript received November 8, 2019, accepted November 11, 2019.



automatically by the ADAS-VT software. HTCs were classified as: 1) sub-endocardial (layers from 10% to 50%); 2) sub-epicardial (layers from 60% to 90%); and 3) transmural (layers from 10% to 90%).

**ABLATION PROCEDURE.** The CARTO3 system (Biosense Webster, Diamond Bar, California) was used for ablation. An open, irrigated 3.5-mm tip ablation catheter (NaviStar ThermoCool or ThermoCool SmartTouch, Biosense Webster) was used for mapping and ablation. A transseptal approach was used

for LV endocardial mapping. In patients with LGE-CMR information (CMR guided and CMR aided), an epicardial approach was performed when a scar area  $\geq 14 \text{ cm}^2$  was found in the 90% epicardial layer (11,12). In the no CMR group, the need for an epicardial approach was estimated based on VT morphology on the electrocardiography (ECG), mapping, and ablation data, the etiology of cardiomyopathy, and multimodal imaging techniques, as previously published by Acosta et al. (11).



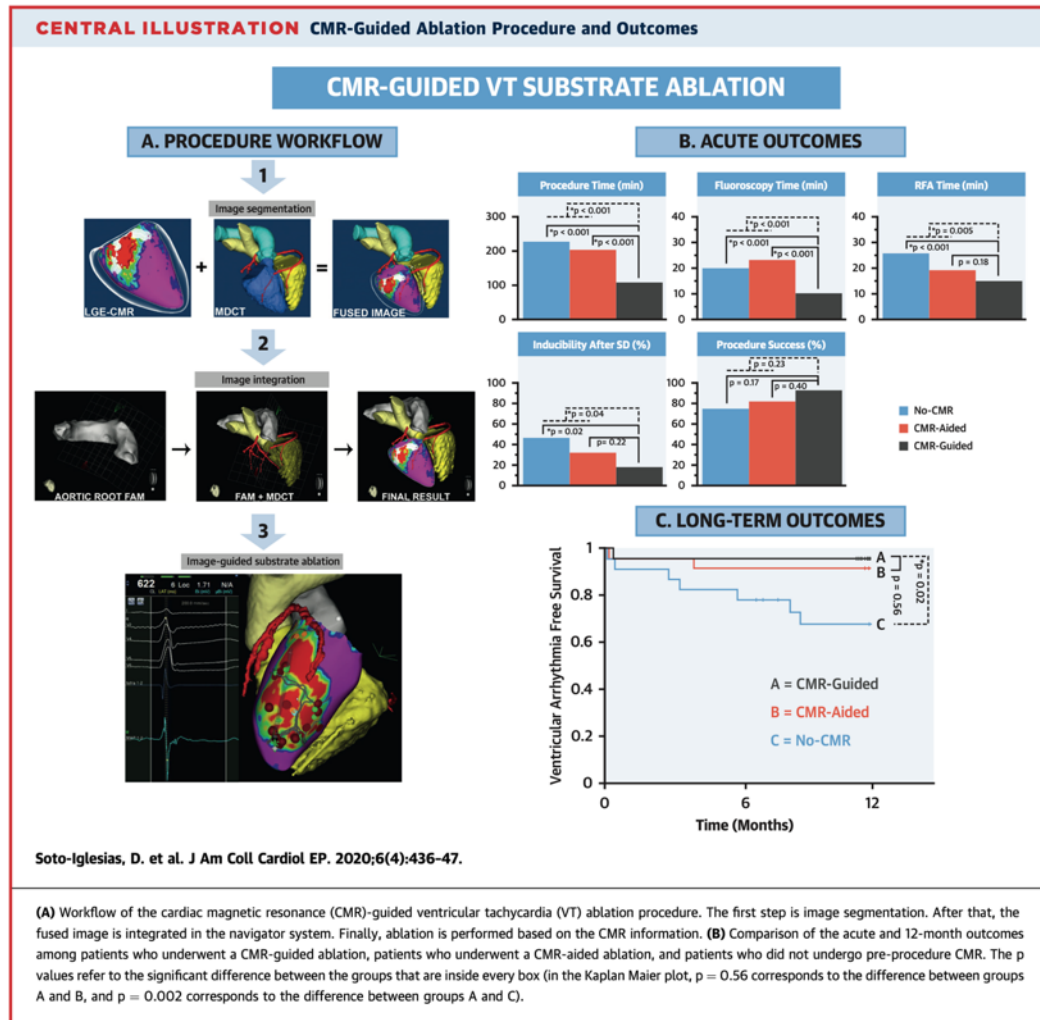
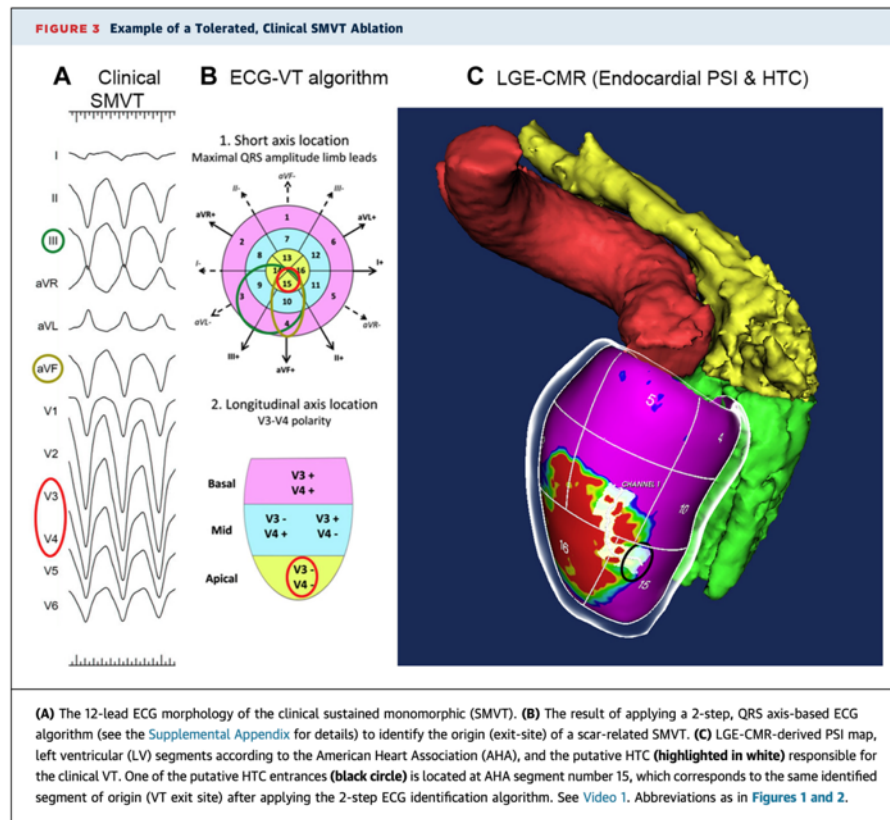


Figure 1 shows the procedure workflow in the 3 groups. The first step of the procedure in both CMR-guided and -aided ablation was the acquisition of a fast anatomical map of the aorta or the right ventricle and pulmonary artery. This fast anatomical map was then used to integrate the MDCT cardiac reconstruction and PSI maps within the spatial reference coordinates of the CARTO System (Figure 2). In the CMR-guided group, the next step after PSI map integration was RF delivery at the target ablation sites directly selected from the CMR information, without

acquisition of any EAM, as shown in the Central Illustration. In the CMR-aided group, a high-density bipolar EAM was acquired, and CMR information was used to focus mapping in areas of interest (scar and HTC on the PSI map) to facilitate the identification of target ablation sites, as previously described (6). In the no CMR group, the procedure started with acquisition of a high-density bipolar EAM of the entire ventricle, and, as described previously (6), substrate ablation was entirely guided by electrographic characteristics. In a subgroup of 10 patients

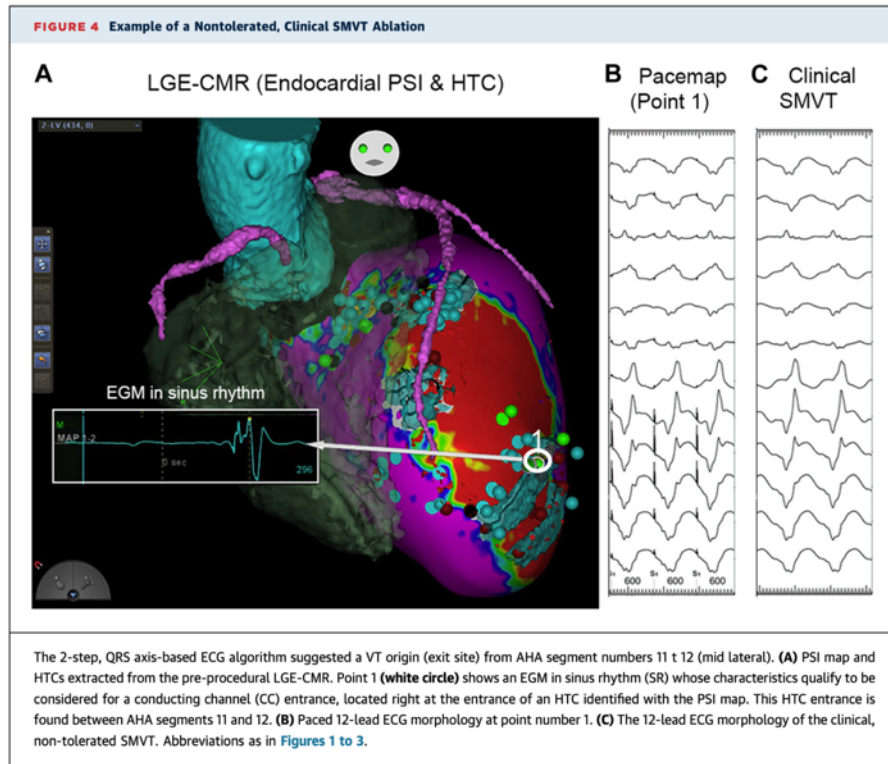


from the CMR-guided group, who had available ECG information on clinical VT, a baseline programmed ventricular stimulation was performed to induce clinical VT (see the following). No attempt was made for clinical VT induction at the beginning of the procedure in the remaining 74 patients, and programmed ventricular stimulation was performed after substrate elimination (13).

**SELECTION OF TARGET ABLATION SITES.** In the CMR-guided group, RF was delivered at the entrance of the HTCs identified on the PSI maps. RF was applied, regardless of the presence or not of a pathological electrogram (EGM) of the targeted sites identified by CMR. When the ablation catheter was positioned at a target ablation site according to the PSI map, the EGM information was analyzed before applying RF to avoid applications: 1) in EGM with His or fascicular EGM characteristics; and 2) at sites with an EGM amplitude

>3 mV or between 1.5 and 3 mV without delayed components, either during sinus rhythm (SR) or after application of multiple extrastimuli to check for the presence of hidden slow conduction (HSC), as previously described (14). RF applications were power-controlled (50 W, 45°C) for 30 s. In HTCs located beyond the 50% myocardial layer, RF applications were prolonged up to 45 s, and contact force was >20 g. For each HTC entrance, >1 application was delivered to eliminate the pathological EGM (if present) or to cover the HTC's wide entrance.

In the no CMR and CMR-aided groups, target ablation sites were selected after a complete LV EAM in the first case or focused on the scar area in the latter case. EGMs that were considered conducting channel (CC) entrances, according to the scar de-channeling technique, were targeted (15). See the [Supplemental Appendix](#) for details.



**CMR-GUIDED CLINICAL VT ABLATION.** In a subgroup of 10 patients (36%) from the CMR-guided group who had an available 12-lead ECG of clinical VT, the putative channel responsible for the VT was identified in the PSI map before the procedure, according to the ECG characteristics of the VT. For this purpose, the LV was automatically divided into 16 segments (following the American Heart Association Model) over the PSI map information and a previously described (16) 2-step, QRS axis-based ECG algorithm was used to identify the segment most likely to be related with the VT exit. Afterward, the PSI map was analyzed to identify any HTC entrance within the designated segment (Figure 3, Video 1). The ECG algorithm is explained in detail in the Supplemental Appendix.

In these 10 patients, after image integration, the first step of the procedure was induction and ablation of clinical VT. Mapping of the induced VT was accurately directed to the entrance (isthmus exit site during VT) of the identified putative channel within the scar. When the VT was hemodynamically not tolerated, the

VT exit site was located by pace mapping (Figure 4) focused on the identified putative channel. Video 1 shows an example of clinical VT ablation. After reaching non-inducibility of the clinical VT with programmed ventricular stimulation, ablation of the remaining HTC entrances was performed.

#### PROCEDURE ENDPOINTS, SUCCESS, AND FOLLOW-UP.

The intended endpoint of all procedures was the complete elimination of all EGMs corresponding to CC entrances by applying RF during SR (scar dechanneling technique) (15), either guided by EGM characteristics after performing an EAM of the substrate (no CMR and CMR-aided approaches), or by applying RF to all HTC entrances identified with the CMR-derived PSI maps (CMR-guided). In all cases, substrate ablation was not considered complete until disappearance of all pathological EGMs in SR, as well as after checking for the absence of HSC (performing a multiple extrastimuli technique) (14). For this, the CC (EAM-derived) or HTC (PSI map-derived) neighboring sites directed to the center of the scar were tested



**TABLE 1** Baseline Characteristics Based on the VT Ablation Procedure

	Total (N = 84)	No CMR (n = 28)	CMR-Aided (n = 28)	CMR-Guided (n = 28)	p Value*	p Value†
Age, yrs	67 ± 10	70 ± 8	66 ± 8	64 ± 14	0.04	0.4
Male	79 (94)	26 (93)	26 (93)	27 (96)	1.00	1.00
HT	62 (74)	22 (79)	21 (75)	19 (68)	0.55	0.77
DLP	44 (52)	13 (46)	17 (61)	14 (50)	0.58	0.78
DM	22 (26)	6 (21)	7 (25)	9 (32)	0.36	0.55
LVEF, %	38 ± 12	39 ± 14	38 ± 11	37 ± 11	0.71	0.87
LVEDD, mm	62 ± 7	62 ± 7	60 ± 8	62 ± 7	0.72	0.65
LVESD, mm	43 ± 12	45 ± 9	42 ± 11	41 ± 17	0.47	0.88
IHD	69 (82)	24 (86)	22 (79)	23 (82)	0.45	0.37
Mean VT cycle length	333 ± 126	331 ± 116	317 ± 125	364 ± 151	0.503	0.859
Patients with an ICD at the ablation time	75 (89)	27 (96)	24 (86)	24 (86)	0.160	0.160
NYHA functional class						
I	26 (31)	7 (25)	13 (46)	6 (21)	0.894	0.138
II	46 (55)	17 (61)	11 (39)	18 (65)		
III	12 (14)	4 (14)	4 (15)	4 (14)		
IV	0 (0)	0 (0)	0 (0)	0 (0)		
Approach					0.95	0.44
Endo	58 (69)	19 (68)	17 (65)	20 (71)		
Endo/Epi	26 (31)	9 (32)	9 (32)	8 (29)		
Indication						
Incessant VT	5 (6)	2 (7)	2 (7)	1 (4)	0.99	0.99
Arrhythmic storm	13 (16)	5 (18)	2 (7)	6 (21)	0.99	0.14

Values are mean ± SD or n (%). \*Difference between cardiac magnetic resonance (CMR)-guided and no-CMR. †Difference between CMR-guided and CMR-aided.  
CMR = cardiac magnetic resonance; DLP = dyslipidemia; DM = diabetes mellitus; HT = hypertension; ICD = implantable cardioverter-defibrillator; IHD = ischemic heart disease; LVEF = left ventricular ejection fraction; LVEDD = left ventricular end-diastolic diameter; LVESD = left ventricular end-systolic diameter; NYHA = New York Heart Association; VT = ventricular tachycardia.

both during SR and after applying multiple extra-stimuli to discard remaining HSCs.

After achieving a complete substrate ablation, programmed ventricular stimulation was performed in all patients to assess for residual inducible VTs (Figure 1). Any induced sustained VT was targeted for ablation either by activation mapping (if tolerated) or pace mapping maneuvers. Inducibility was checked again after each residual VT ablation. Acute success was defined as noninducibility of any sustained monomorphic VT at the end of the procedure. Partial success was considered when the clinical VT was successfully ablated but other monomorphic VTs remained inducible.

All patients were discharged with an ICD, and the first VT zone was programmed at 15 beats/min slower than clinical VT. Clinical evaluation, together with ICD interrogation, was scheduled every 6 months. Ventricular arrhythmia-free survival was compared between groups. Follow-up data were limited to the first 12 months after the procedure to avoid differences in follow-up duration between groups. Any episode of sustained ventricular arrhythmia or appropriate ICD therapy was considered a VT recurrence.

**STATISTICAL ANALYSIS.** Continuous variables are presented as mean ± SD. Means of 2 variables were

compared using Student's *t*-test, Mann-Whitney *U*, or analysis of variance tests, when appropriate. Categorical variables were expressed as total numbers (proportions) and compared between groups using the chi-square test. Kaplan-Meier analysis was used to analyze ventricular arrhythmia-free survival, and the log-rank test was used to detect significant differences between groups. For all tests, a *p* value <0.05 was considered statistically significant. Statistics were obtained using the Matlab statistics toolbox (Matlab R2010a; Mathworks, Inc., Natick, Massachusetts).

## RESULTS

A total of 84 patients (mean age: 67 ± 11 years; 79 [94%] were men, 69 [82%] had ischemic heart disease) were included in the study. CMR-guided ablation was performed in the last 28 consecutively included patients. In this group (CMR-guided), the mean age was 64 ± 14 years; 27 (96%) patients were men, and 23 (82%) had ischemic heart disease. Table 1 summarizes the baseline characteristics of the population according to the type of ablation procedure. There were no significant differences between groups according to LVEF, indication for ablation, etiology of

cardiomyopathy, New York Heart Association functional class, or presence of cardiovascular risk factors. There was a significant difference in age between the no CMR and CMR-guided groups.

**CMR-GUIDED ABLATION.** In this group of patients (n = 28), the mean total procedure time was 107 ± 59 min. Fifteen (54%) patients underwent a 3-T LGE-CMR, whereas 13 of 26 (46%) patients underwent wide-band 1.5-T LGE-CMR because of a previously implanted ICD (n = 11) or for logistic reasons (n = 2). [Supplemental Figure 1](#) shows an example of 1.5- and 3-T acquisition. A MDCT scan was also performed in 27 of 28 (96%) patients to obtain key anatomical information (e.g., coronary arteries, papillary muscles, and aortic arch). The integration of CMR and MDCT images was performed before the ablation procedure, using the ADAS-VT software platform, and then imported into the CARTO system ([Figure 2](#)).

The first step of the procedure was the acquisition of a fast anatomical map, either of the aorta or the right ventricle and pulmonary artery, to integrate the multimodality pre-procedural cardiac imaging (MDCT cardiac reconstructions and 3-dimensional CMR-derived PSI maps) within the spatial reference coordinates of CARTO. In 25 of 28 (89%) patients, this integration was achieved using the fast anatomical map of the aortic root, using a mean time of 7.4 ± 2 min for this step. In 3 (11%) patients for whom a MDCT scan was not available or a retro-aortic access was not possible, the integration was performed using the right ventricle and pulmonary artery fast anatomical map, using a mean time of 32 ± 23 min.

**CMR-guided clinical VT ablation.** The second step of the procedure in the 10 of 28 (36%) patients with a documented 12-lead ECG of the VT was clinical VT ablation. For this purpose, the ablation catheter was positioned at the entrance of the previously identified putative channel responsible for the clinical VT, based on analysis of the 12-lead ECG of the VT ([Figures 3 and 4](#)). In all cases, a pathological EGM was found at the entrance of the putative channel during SR. In 5 of 10 (50%) cases, the local EGM showed CC entrance characteristics, with a mean voltage of 0.49 ± 0.21 mV and a mean delay of 8.4 ± 4.27 ms between both components of the EGM. In the other 5 of 10 (50%) cases, the local EGM showed no delay between the far field and the local component during SR; the mean voltage was 1.26 ± 0.61 mV. In these latter cases, multiple extrastimuli were delivered from the right ventricular apex to check for HSC, according to a previously explained technique (14).

After induction, the VT isthmus exit site of the clinical VT was located using activation mapping, if

**TABLE 2 Acute Results of VT Substrate Ablation Procedures**

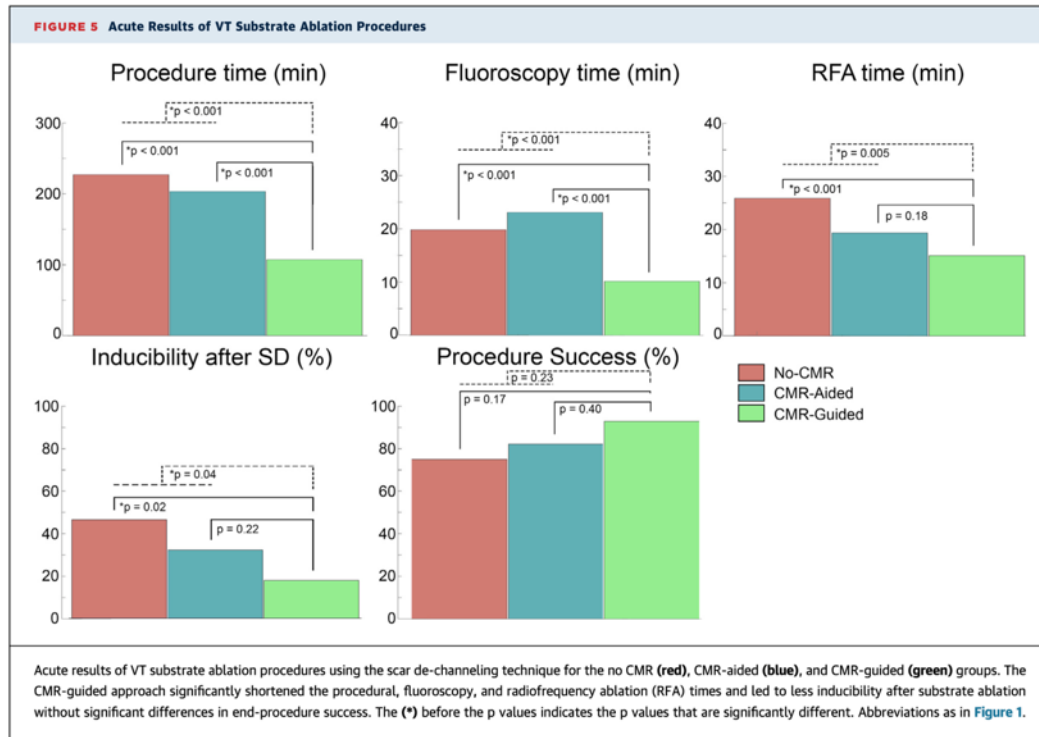
	Total (N = 84)	No CMR (n = 28)	CMR-Aided (n = 28)	CMR-Guided (n = 28)	p Value*	p Value†
Procedure time, min	179 ± 79	227 ± 52	203 ± 68	107 ± 59	<0.001*	<0.001*
RF time, min	20 ± 12	26 ± 11	20 ± 15	15 ± 8	<0.001*	0.16
RF applications	31 ± 18	35 ± 14	29 ± 22	29 ± 20	0.26	0.96
Fluoroscopy time, min	18 ± 10	20 ± 9	23 ± 11	10 ± 4	<0.001*	<0.001*
Residual VT after substrate ablation	27 (32)	13 (46)	9 (32)	5 (18)	0.04*	0.35
Induced VT	1.27 ± 1.24	1.36 ± 1.35	1.35 ± 1.36	1.04 ± 0.99	0.34	0.36
Complications	5 (6)	1 (4)	3 (10)	1 (4)	0.75	0.35
Final procedure success					0.17	0.39
Total	70 (84)	21 (75)	23 (82)	26 (93)		
Partial	12 (14)	6 (21)	4 (14)	2 (7)		
No	2 (2)	1 (4)	1 (4)	0 (0)		

Values are mean ± SD or n (%). \*Difference between CMR-guided groups and no CMR. †Difference between CMR-guided and CMR-aided groups.

RF = radiofrequency; other abbreviations as in [Table 1](#).

tolerated (2 of 10 [20%] patients), or otherwise, using pace mapping (8 of 10 [80%] patients). When activation mapping was used, a limited activation map (22 ± 2.8 mean points) focused into the putative channel entrance was performed to identify the VT isthmus exit site during VT. After that, clinical VT was stopped during RF as shown in [Video 1](#). In patients who had the VT isthmus was identified by pace mapping, the minimum level of concordance with the 12-lead ECG of the clinical VT was a 10 of 12 lead match. No patient was inducible for clinical VT after this step. The mean time required from the beginning of the procedure to clinical VT ablation was 36 ± 15 min. More details of procedural outcomes in this group are shown in [Supplemental Table 1](#).

**CMR-guided substrate ablation.** Complete substrate ablation based on information from the PSI maps was performed in all patients (n = 28) of the CMR-guided group. A combined endo-epicardial approach was performed in 8 of 28 (29%) patients. The mean number of HTCs identified per patient in the LGE-CMR-derived PSI map was 1.71 ± 0.97 (29 of 48 [60%] of them were sub-endocardial, 5 of 48 [10%] were subepicardial, and 14 of 48 [30%] were transmural), with a mean number of HTC entrances per patient of 9.3 ± 5.4 (mean of 4.7 ± 3.5 entrances per each HTC). The mean HTC entrance width was 9.5 ± 4 mm. In 177 of 225 (79%) of the identified HTC entrances, a pathological EGM was found; 59% of them showed HSC conduction characteristics, whereas 41% showed delayed components during SR. The mean number of RF applications per patient was 29 ± 20, requiring a mean of 4.1 ± 3.7 applications for each



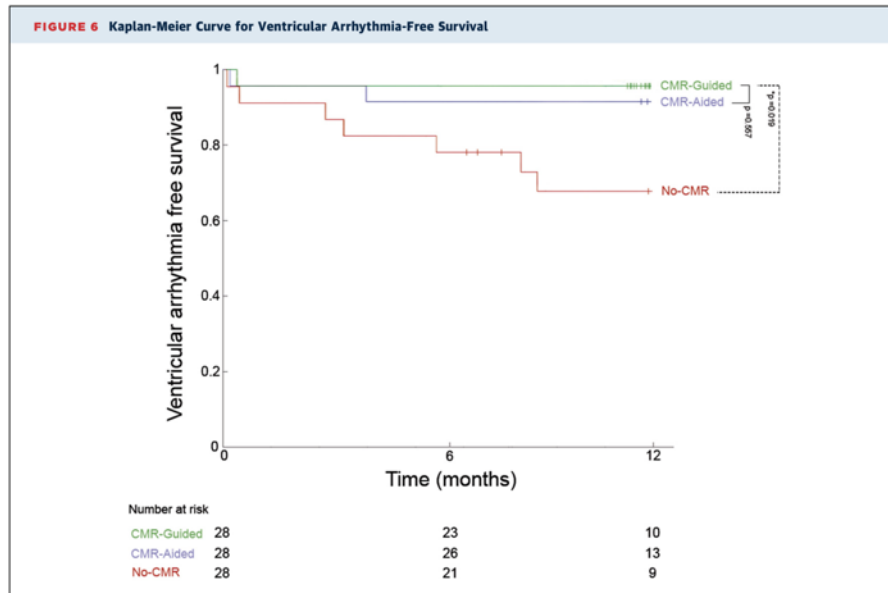
HTC entrance. An example of HTC with multiple entrances can be seen in Supplemental Figure 2.

**COMPARISON OF ACUTE AND FOLLOW-UP OUTCOMES.** The differences in acute outcomes after substrate ablation between groups are summarized in Table 2 and Figure 5. The CMR-guided group required less procedural time than the CMR-aided and no CMR groups ( $107 \pm 59$  min vs.  $203 \pm 68$  min and  $227 \pm 52$  min, respectively;  $p < 0.001$  for both), as well as less fluoroscopy time than the CMR-aided and no CMR groups ( $10 \pm 4$  min vs.  $23 \pm 11$  min and  $20 \pm 9$  min, respectively;  $p < 0.001$  for both). Moreover, the CMR-guided group required less RF time than the no CMR group ( $15 \pm 8$  min vs.  $26 \pm 10$  min;  $p < 0.001$ ) and CMR-aided group, without reaching statistical significance in this latter case ( $15 \pm 8$  min vs.  $20 \pm 15$  min;  $p = 0.16$ ).

In the CMR-guided group, 5 of 28 (18%) patients were inducible for residual VTs after completion of substrate ablation. At the end of the procedure only 2 of 26 (7%) patients were still inducible for fast, nontolerated, nonclinical VTs. The final end procedure success rate (after ablation of any residual VTs) in this group was 93%.

Compared with the no CMR group, there was a lower inducibility rate of residual substrate ablation in the CMR-guided group (18% vs. 46%;  $p = 0.04$ ), with a higher, although statistically nonsignificant, end procedure success rate (93% vs. 79%;  $p = 0.17$ ). Compared with the CMR-aided group, no differences were found in the inducibility rate after substrate ablation (18% vs. 32%  $p = 0.35$ ) or in the end procedure success rate (93% vs. 86%;  $p = 0.39$ ). Five of 84 (6%) patients had complications without any significant difference between groups (Table 2). In the CMR-guided group, 1 patient experienced a fistula. In the CMR-aided group, 1 patient experienced phrenic paralysis and 2 patients had an atrioventricular block. Finally, in the no CMR group, 1 patient had cardiac tamponade.

After a mean follow-up of 12 months, 10 (12%) patients had arrhythmia recurrence (1 [4%] patient in the CMR-guided group, 2 [7%] patients in the CMR-aided group, and 7 [25%] patients in the no CMR group;  $p = 0.024$ ). The Kaplan-Meier curves for ventricular arrhythmia-free survival (Figure 6) showed a lower recurrence rate in the CMR-guided



group compared with the no CMR group (log-rank: 0.019) with no significant differences in recurrence rates between the CMR-guided and CMR-aided groups. Patients censored in the Kaplan-Meier curves represent those lost to follow-up (4 in the no CMR group and 2 in the CMR-aided group) or patients who had the last follow-up occurred before 12 months. No patient died or underwent cardiac transplantation during the study period, and there were no differences in the mean follow-up duration among the groups ( $11.9 \pm 0.3$  months in the CMR-guided group,  $11.9 \pm 0.1$  months in the CMR-aided group and  $11.4 \pm 1.6$  months in the no CMR group;  $p = 0.10$ ). Neither procedure success nor recurrence rate differed based on CMR image acquisition (1.5-T scanner vs. 3-T scanner) (Supplemental Table 2).

## DISCUSSION

The present study reported, for the first time, the feasibility of performing VT substrate ablation procedures guided by LGE-CMR, without requiring an EAM. This approach was safe and allowed a significant shortening of the procedural, fluoroscopy, and RF delivery times, which made it more efficient compared with the classical EAM-based procedure and with the previously reported CMR-aided VT substrate ablation

approach (6). Moreover, CMR-guided VT substrate ablation was also associated with an improvement in acute outcomes compared with no CMR by reducing the inducibility rate after substrate ablation and a lower recurrence rate during follow-up, which, in turn, suggested better identification of the arrhythmogenic substrate and target ablation sites.

It was previously shown that scar distribution across the myocardial wall, as assessed by LGE-CMR, was useful in deciding the best approach (endocardial, epicardial, or combined) for VT ablation to reach the whole VT substrate (11,12). Integration of CMR-derived PSI maps in the electromagnetic navigation system was also previously shown to improve the acute and long-term outcomes of VT substrate ablation using combined CMR-EAM information (6,7).

**EFFICIENCY OF CMR-GUIDED VT SUBSTRATE ABLATION.** CMR-guided ablation was shown to be more efficient due to a significant shortening of procedural, fluoroscopy, and RF time needed to completely eliminate the VT substrate. In patients who underwent the CMR-guided procedure, no EAM was obtained, either of the whole LV (no CMR group) or the scar area (CMR-aided group). According to a previous study from our group (6), the mean time spent for acquiring the EAM was approximately 36 min, which might partially explain the remarkable

shortening of procedural times. Moreover, the need for a re-map, acquired in the no CMR and CMR-aided groups, to identify residual pathological EGMs, was no longer present and could partially explain the remaining saved time. Additional RF target selection in the CMR-guided group was based on the PSI map information (i.e., checking for neighboring sites adjacent to the identified HTC entrances). Furthermore, only 18% of patients who underwent the CMR-guided procedure needed additional mapping due to VT inducibility after substrate ablation, which was a lower proportion compared with the CMR-aided (32%) and no CMR (46%) groups.

A lower inducibility rate found after CMR-guided substrate ablation suggested an improvement in VT substrate identification. CMR-derived PSI maps might enable a better identification of the real CC entrances located in the border zone between dense scar and healthy tissue as defined by conventional voltage criteria in the EAM (14). This is a region that cannot usually be well-defined by the EAM due to the far-field effect of the surrounding healthy myocardium, which leads to an EAM-derived, low-voltage area smaller than the PSI-derived (anatomical) scar area (10). A higher number of CC entrances was described previously (6) in areas with a bipolar voltage of  $>1.5$  mV when PSI information was used. A better characterization of these transitional areas between healthy and border zone tissue with LGE-CMR explained a more extensive substrate elimination in the CMR-guided group and better acute outcomes (6,17).

In addition, CMR-derived information could be used to obtain PSI maps from the whole myocardial thickness, permitting characterization of the substrate into different tissue layers, from endocardium to epicardium. One of the main limitations of EAM is the lack of sensitivity to analyze local EGMs generated deeper than the subendocardium due to a far-field effect of the surrounding tissue. This might explain why, in the present study, 21% of HTC entrances detected in the CMR-guided procedures showed an apparently normal EGM. Clinical support for this hypothesis comes from the previous study by Andreu et al. (6), in which patients with undetected CMR-derived HTCs in the EAM, which were therefore not targeted for ablation, showed an increased VT recurrence rate after 18 months.

More accurate arrhythmogenic substrate identification with the PSI maps, both at the edge of the scar and deep within the myocardial wall, could explain the lower inducibility rate after substrate ablation, as well as the lower recurrence rate when the procedure was guided by CMR information compared with the no CMR group. Although PSI information was available in

the CMR-aided group for substrate characterization, the selection of ablation targets was exclusively guided by EAM information. Thus, HTCs depicted in the PSI maps, but not identified in the EAM, were not targeted for ablation. A complete substrate ablation was achieved using a pure CMR-guided approach, which showed a trend toward lower inducibility after substrate ablation and a lower VT recurrence rate compared with the CMR-aided approach; however, this did not reach statistical significance.

**EFFICIENCY OF CMR-GUIDED CLINICAL VT ABLATION.** The present study defined a new approach for clinical VT ablation guided by imaging and looking for the putative channel based on ECG morphology during VT, as described previously (16). The mean procedure time needed for ablating a clinical VT was only  $36 \pm 15$  min, a vast reduction in the time taken by a conventional approach using EAMs. Moreover, in all cases in which clinical VT ablation was performed (before completing substrate ablation), a local pathological EGM was found at the entrance (exit during VT) of the HTC responsible for the VT, corroborating the accuracy of CMR imaging for identifying the arrhythmogenic substrate.

**CLINICAL IMPLICATIONS.** Over the past decade, a substrate-based approach for VT ablation has steadily increased (5) in both high-volume and non-high-volume centers (18). Despite the need to corroborate the results of this study in a multicenter study to check for reproducibility, consolidation of this approach could help simplify a procedure considered challenging and time-consuming. Moreover, the CMR-guided clinical VT ablation approach could be an attractive option in selected patients who had the exclusive elimination of clinical VT as the endpoint, that is, recurrent VT in patients with a high risk of complications and comorbidities.

**STUDY LIMITATIONS.** The main limitation of this study is the lack of randomization, although we tried to make groups comparable by matching them for the key outcome predictors after substrate ablation. The procedures were performed in different time periods because only the final 28 consecutive patients underwent CMR-guided ablation. Substrate ablation techniques only differed among the groups in the selection of the target ablation site for RF applications. However, we could not completely exclude that the results might have been influenced by technical developments that we did not take into account. We could not provide data of unipolar EGMs. As consequence, a direct comparison between unipolar maps and CMR-derived PSI maps was not performed. Contact force and multielectrode catheters were not

systematically used for EAM. Accuracy of CMR-guided ablation might have been influenced by the CMR acquisition technique, spatial resolution, and image quality. All the structural abnormalities present in the scar tissue under the current spatial resolution of the CMR could not be characterized, as previously reported (8). Even if fluoroscopy time was significantly lower in the CMR-guided group, radiation exposure due to MDCT could reduce this benefit. Finally, we used the scar de-channeling technique for substrate ablation in all patients. Further studies are needed to analyze CMR-guided approach reproducibility by other groups, in other substrate ablation modalities, or using different post-processing tools.

### CONCLUSIONS

CMR-guided VT ablation halves the time required for the procedure, significantly reduces the need of fluoroscopy and RF delivery, and is associated with a higher rate of non-inducibility after substrate ablation and a higher ventricular arrhythmia-free survival.

### REFERENCES

- Reddy VY, Reynolds MR, Neuzil P, et al. Prophylactic catheter ablation for the prevention of defibrillator therapy. *N Engl J Med* 2007;357:2657-65.
- Kuck KH, Schaumann A, Eckardt L, et al. Catheter ablation of stable ventricular tachycardia before defibrillator implantation in patients with coronary heart disease (VTACH): a multicentre randomised controlled trial. *Lancet* 2010;375:31-40.
- Sacher F, Tedrow UB, Field ME, et al. Ventricular tachycardia ablation: evolution of patients over 8 years. *Circ Arrhythm Electrophysiol* 2008;1:153-61.
- Stevenson WG, Wilber DJ, Natale A, et al. Multicenter Thermocool VT Ablation Trial Investigators. Irrigated radiofrequency catheter ablation guided by electroanatomic mapping for recurrent ventricular tachycardia after myocardial infarction: the Multicenter Thermocool Ventricular Tachycardia Ablation Trial. *Circulation* 2008;118:2773-82.
- Palaniswamy C, Kolte D, Hari Krishnan P, et al. Catheter ablation of postinfarction ventricular tachycardia: ten-year trends in utilization, in-hospital complications, and in-hospital mortality in the United States. *Heart Rhythm* 2014;11:2056-63.
- Andreu D, Penela D, Acosta J, et al. Cardiac magnetic resonance-aided scar dechanneling: influence on acute and long-term outcomes. *Heart Rhythm* 2017;14:1121-8.
- Zghalib T, Ipek EG, Hansford R, et al. Standard ablation versus magnetic resonance-guided

ablation in the treatment of ventricular tachycardia. *Circ Arrhythm Electrophysiol* 2018;11:e005973.

8. Fernández-Armenta J, Berrueto A, Andreu D, et al. Three-dimensional architecture of scar and conducting channels based on high resolution CE-CMR: insights for ventricular tachycardia ablation. *Circ Arrhythm Electrophysiol* 2013;6:528-37.

9. Andreu D, Ortiz-Pérez JT, Fernández-Armenta J, et al. 3D delayed enhanced magnetic resonance sequences improve conducting channel delineation prior to ventricular tachycardia ablation. *Europace* 2015;17:938-45.

10. Andreu D, Berrueto A, Ortiz-Pérez JT, et al. Integration of 3D electroanatomic maps and magnetic resonance scar characterization into the navigation system to guide ventricular tachycardia ablation. *Circ Arrhythm Electrophysiol* 2011;4:674-83.

11. Acosta J, Fernández-Armenta J, Penela D, et al. Infarct transmural as a criterion for first-line endo-epicardial substrate-guided ventricular tachycardia ablation in ischemic cardiomyopathy. *Heart Rhythm* 2016;13:85-95.

12. Soto-Iglesias D, Acosta J, Penela D, et al. Image-based criteria to identify the presence of epicardial arrhythmogenic substrate in patients with transmural myocardial infarction. *Heart Rhythm* 2018;15:814-21.

13. Fernández-Armenta J, Penela D, Acosta J, et al. Substrate modification or ventricular tachycardia induction, mapping, and ablation as the first step? A randomized study. *Heart Rhythm* 2016;13:1589-95.

14. Acosta J, Andreu D, Penela D, et al. Elucidation of hidden slow conduction by double ventricular extrastimuli: a method for further arrhythmic substrate identification in ventricular tachycardia ablation procedures. *Europace* 2018;20:337-46.

15. Berrueto A, Fernández-Armenta J, Andreu D, et al. Scar dechanneling: a new method for scar-related left ventricular tachycardia substrate ablation. *Circ Arrhythm Electrophysiol* 2015;8:326-36.

16. Andreu D, Fernández-Armenta J, Acosta J, et al. A QRS axis-based algorithm to identify the origin of scar-related ventricular tachycardia in an American Heart Association 17-segment model. *Heart Rhythm* 2018;15:1491-7.

17. Andreu D, Ortiz-Pérez JT, Boussy T, et al. Usefulness of contrast-enhanced cardiac magnetic resonance in identifying the ventricular arrhythmic substrate and the approach needed for ablation. *Eur Heart J* 2014;35:1316-26.

18. Katz DF, Turakhia MP, Sauer WH, et al. Safety of ventricular tachycardia ablation in clinical practice: findings from 9699 hospital discharge records. *Circ Arrhythm Electrophysiol* 2015;8:362-70.

**KEY WORDS** cardiac magnetic resonance, conducting channels, image-guided ablation, substrate ablation

**APPENDIX** For an expanded Methods section, supplemental tables, figures, and a video, please see the online version of this paper.

**ADDRESS FOR CORRESPONDENCE:** Dr. Antonio Berrueto, Heart Institute, Teknon Medical Center, C/Vilana, 12, 08022 Barcelona, Spain. E-mail: [antonio.berrueto@quironsalud.es](mailto:antonio.berrueto@quironsalud.es).

### PERSPECTIVES

**COMPETENCY IN MEDICAL KNOWLEDGE:** The present study constitutes the first report on the feasibility of VT substrate ablation guided by LGE-CMR information (PSI maps), without requiring an EAM during the procedures. CMR-guided VT ablation halves the time needed for the procedure, reduces the need for fluoroscopy, and RF delivery, and is associated with higher rates of non-inducibility and lower VT recurrence after substrate ablation.

**TRANSLATIONAL OUTLOOK:** Although these results warrant confirmation in further multicenter studies, the consolidation of a CMR-guided approach for VT substrate ablation could simplify and improve the outcomes of a procedure considered challenging and time-consuming.

## **INTRODUCTION**

Ventricular tachycardia (VT) substrate ablation is an effective treatment for patients that suffer from recurrent episodes of scar-dependent VT (1,2) but recurrence rates remain high (3,4). Moreover, despite the adoption of substrate-based mapping and ablation as the technique of choice for VT suppression in the last decade (5), the procedure is still considered challenging and time-consuming.

Recent studies (6,7) have shown that aiding VT substrate ablation with color-coded pixel signal intensity (PSI) maps obtained from pre-procedural LGE-CMR imaging, results in less need for RF delivery and improved VT recurrence-free survival. The accuracy of LGE-CMR for scar tissue characterization and delimitation within the entire myocardial thickness, (8) as well as its ability to identify additional arrhythmogenic substrate compared with endocardial or epicardial surface electroanatomic maps (EAM) alone (6), would suggest better outcomes with this approach. However, in these previous studies, selection of the ablation targets was still based on EAM findings rather than on LGE-CMR information. Data on the appropriateness of selecting ablation target sites based exclusively on information provided by PSI maps is lacking.

The objective of the present study was to evaluate the feasibility and potential benefits of performing VT substrate ablation guided by PSI maps obtained from LGE-CMR imaging.

## **METHODS**

### **Patient Sample**

This is a prospective, experimental, non-randomized, and pilot study performed in two centers. From March 2017, 28 consecutive patients referred for catheter ablation of left ventricle (LV) scar-related sustained monomorphic VT were included. Patients were included if they had incessant or repetitive ( $\geq 2$ ) VT episodes but also in case of first episode of slow monomorphic VT. VT substrate ablation was guided by PSI map information (CMR-Guided) in each case. Procedural data, acute and follow-up outcomes were compared with two historical control groups consecutively selected (inclusion period from April 2011 to March 2017) and matched by LV ejection fraction (LVEF), etiology of cardiomyopathy and need for an epicardial approach: 1) 28 patients in whom VT substrate ablation was performed without LGE-CMR information (No-CMR), and 2) 28 patients in whom PSI maps were obtained, integrated into the navigation system and fused with the EAM, selecting the ablation target based on the EAM information (CMR-Aided). The study complied with the Declaration of Helsinki. The local Ethics Committee approved the study protocol and all participants signed the informed consent.

### **Image Processing**

A pre-procedural LGE-CMR was obtained using a 3T scanner (MAGNETOM® Trio®, Siemens Healthcare, Erlangen, Germany). In patients previously implanted with an implantable cardiac defibrillator (ICD), the LGE-CMR was performed with a 1.5T scanner (MAGNETOM®



Aera®; Siemens Healthcare, Erlangen, Germany) using a specific 'wideband' sequence in order to avoid device artefacts. A pre-procedural multi-detector cardiac tomography (MDCT) was also obtained, in absence of contraindication, using a dual source SOMATOM® Definition Flash, 128-slice, CT scanner (Siemens Healthcare, Erlangen, Germany). For acquisition details, see supplemental material.

All LGE-CMR images were processed using a previously described approach (9). Briefly, a full LV volume was reconstructed in the axial orientation and the resulting images were processed with ADAS-VT™ (Galgo Medical, Barcelona, Spain) software. The LV was divided into 10 layers from endocardium to epicardium and a 3D shell was obtained for each layer. PSI maps were obtained from LGE-CMR images, color-coded and projected to each of the shells following a trilinear interpolation algorithm. To characterize the scar areas, a PSI-based algorithm was applied to define the hyperenhanced area as scar core or border zone (BZ), using  $40 \pm 5\%$  and  $60 \pm 5\%$  of the maximum intensity as thresholds. (10) In the LGE-CMR PSI maps, heterogeneous tissue channels (HTCs) were defined as continuous corridors of BZ surrounded by scar core or scar core and an anatomical barrier (mitral annulus) connecting two areas of healthy tissue. HTCs were obtained automatically by the ADAS-VT™ software. HTCs were classified as: 1) sub-endocardial (layers from 10 to 50%); 2) sub-epicardial (layers from 60 to 90%); and 3) transmural (from layer 10 to 90%).

### **Ablation Procedure**

The CARTO3® system (Biosense Webster, Diamond Bar, CA, USA) was used for ablation. An open irrigated 3.5-mm tip ablation catheter (NaviStar® ThermoCool® or ThermoCool®

SmartTouch™, Biosense Webster, Diamond Bar, CA, USA) was used for mapping and ablation. A transeptal approach was used for LV endocardial mapping. In patients with LGE-CMR information [CMR-Guided and CMR-Aided] an epicardial approach was performed when a scar area  $\geq 14$  cm<sup>2</sup> was found in the 90% epicardial layer. (11,12) In the No-CMR group the need for an epicardial approach was estimated based on VT morphology in the ECG, mapping and ablation data, the etiology of the cardiomyopathy and multimodal imaging techniques, as previously published by Acosta et al. (11)

Figure 1 summarizes the procedure workflow in the three groups. The first step of the procedure in CMR-Guided and CMR-Aided ablation was the acquisition of a fast-anatomical map (FAM) of the aorta or the right ventricle and pulmonary artery. This FAM was then used to integrate the MDCT cardiac reconstruction and PSI maps within the spatial reference coordinates of the CARTO system, as shown in Figure 2. In the CMR-Guided group, the immediate next step after PSI map integration was RF delivery at the target ablation sites directly selected from the CMR information, without acquisition of any EAM. In the CMR-Aided group, a high-density bipolar EAM was acquired and the CMR information was used to focus mapping in areas of interest (scar and HTC in the PSI map) to facilitate the identification of target ablation sites, as previously described (6). In the No-CMR group, the procedure started with the acquisition of a high-density bipolar EAM of the entire ventricle and, as described before (6), substrate ablation was entirely guided by electrogram characteristics. In a subgroup of 10 patients from the CMR-guided group, in whom ECG information of the clinical VT was available, a baseline programmed ventricular stimulation was performed in order to induce the clinical VT (see below). In the remaining 74 patients,

no attempt was made for clinical VT induction at the beginning of the procedure, and programmed ventricular stimulation was performed after substrate elimination (13).

### **Selection of target ablation sites**

In the CMR-Guided group, RF was delivered at the entrance of the HTC's identified in the PSI maps. Radiofrequency was applied regardless of the presence or not of a pathological electrogram (EGM) of the targeted sites identified by the CMR. When the ablation catheter was positioned at a target ablation site according to the PSI map, the EGM information was analyzed before applying RF in order to avoid applications: 1) in EGM with His or fascicular electrogram characteristics, and 2) at sites with an EGM amplitude  $>3\text{mV}$  or between  $1.5\text{-}3\text{mV}$  without delayed components, either during sinus rhythm (SR) or after application of multiple extrastimuli to check for the presence of hidden slow conduction (HSC), as previously described. (14) Radiofrequency applications were power-controlled ( $50\text{W}$ ,  $45^\circ\text{C}$ ) for a duration of 30 seconds. In HTC's located beyond 50% myocardial layer, RF applications were prolonged up to 45 seconds and contact force was intended to be  $>20$  grams. For each HTC's entrance, more than one application was delivered in order to eliminate pathological EGM (if present) or to cover the HTC's wide entrance.

In the No-CMR and CMR-Aided groups, target ablation sites were selected after a complete LV EAM in the first case, or focused on the scar area in the latter case. The EGMs that qualified to be considered as conducting channel (CC) entrances, according to the 'scar dechanneling' technique, were targeted (15). See Supplemental Material for details.

### **CMR-guided clinical VT ablation**

In a subgroup of 10 patients (36%) from the CMR-Guided group in whom the 12-lead ECG of the clinical VT was available, the 'putative' channel responsible for the VT was identified in the PSI map before the procedure, according to the ECG characteristics of the VT. For this purpose, the LV was automatically divided into 16 segments [following the American Heart Association (AHA) Model] over the PSI map information and a previously described, (16) two-step QRS axis-based ECG algorithm was used to identify the segment most likely to be related with the VT exit. Afterwards, the PSI map was analyzed to identify any HTC entrance within the designated segment (Figure 3). The ECG algorithm is explained in detail in Supplemental Material.

In these 10 patients, after image integration, the first step of the procedure was induction and ablation of the clinical VT. Mapping of the induced VT was accurately directed to the entrance (isthmus exit site during VT) of the identified 'putative' channel within the scar. When the VT was hemodynamically not tolerated, the VT exit site was located by using pace mapping (Figure 4) focused on the identified 'putative' channel. The Supplemental Video shows an example of clinical VT ablation. After reaching non-inducibility of the clinical VT with programmed ventricular stimulation, ablation of the remaining HTC entrances was performed.

### **Procedure endpoints, success and follow-up**

The intended endpoint of all procedures was the complete elimination of all EGMs corresponding to CC entrances by applying RF during SR ['scar dechanneling' technique

(15)], either guided by EGM characteristics after performing an EAM of the substrate (No-CMR and CMR-Aided approaches), or by applying RF to all HTC entrances identified with the CMR-derived PSI maps (CMR-Guided). In all cases, substrate ablation was not considered complete until disappearance of all pathological EGMs in SR, as well as after checking for the absence of HSC [performing a multiple extrastimuli technique (14)]. For this, the CC (EAM-derived) or HTC (PSI map-derived) neighboring sites directed to the center of the scar were tested both during SR and after applying multiple extrastimuli to discard remaining HSC.

After achieving a complete substrate ablation, programmed ventricular stimulation was performed in all patients to assess for residual inducible VTs (Figure 1). Any induced sustained VT was targeted for ablation either by activation mapping (if tolerated) or pace-mapping maneuvers. Inducibility was checked again after each residual VT ablation. Acute success was defined as non-inducibility of any sustained monomorphic VT at the end of the procedure. Partial success was considered when the clinical VT was successfully ablated but other monomorphic VTs remained inducible.

All patients were discharged with an ICD and the first VT zone was programmed 15 bpm slower than clinical VT. Clinical evaluation together with ICD interrogation was scheduled every 6 months. Ventricular arrhythmia-free survival was compared between groups. Follow-up data was limited to the first 18 months after the procedure to avoid differences in follow-up duration between groups. Any episode of sustained ventricular arrhythmia or appropriate ICD therapy was considered as a VT recurrence.

## Statistical Analysis

Continuous variables are presented as mean  $\pm$  standard deviation. Means of two variables were compared using Student's T, Mann-Whitney U or ANOVA tests, where appropriate. Categorical variables were expressed as total numbers (percentages) and compared between groups using the Chi-square test. The Kaplan-Meier analysis was used to analyze ventricular arrhythmia-free survival, and log-rank test to detect significant differences between groups. For all tests, a p-value  $<0.05$  was considered statistically significant. Statistics were obtained using the Matlab<sup>®</sup> statistics toolbox (Matlab<sup>®</sup> R2010a, The Mathworks, Inc., Natick, MA, USA).

## RESULTS

A total of 84 patients [mean age  $67 \pm 11$  years old, 79 (94%) men, 69 (82%) with ischemic heart disease (IHD)] were included in the study. A CMR-guided ablation was performed in the last 28 consecutively included patients. In this group (CMR-Guided), the mean age was  $64 \pm 14$  years, 27 (96%) men and 23 (82%) had IHD. Table 1 summarizes the baseline characteristics of the population according to the type of ablation procedure. There were no significant differences between groups according to LVEF, indication for ablation, etiology of cardiomyopathy, New York Heart Association (NYHA) functional class, or presence of cardiovascular risk factors. There was a significant difference in age between No-CMR and CMR-guided groups. However, we considered this difference will not affect

the ablation results since the presence of VTs has been related with the scar characteristics rather than age.

### **CMR-Guided ablation**

In this group of patients (n = 28), the mean total procedure time was  $107 \pm 59$  minutes. Fifteen (54%) patients underwent a 3-Tesla LGE-CMR, whereas 13/26 (46%) undertook a 'wideband' 1.5-Tesla LGE-CMR because of a previously implanted ICD (11 patients) or for logistic reasons (2 patients). Supplemental Figure 1 shows an example of 1.5 and 3 tesla acquisition. In 27/28 (96%) patients a MDCT scan was also obtained for obtaining key anatomical information such as coronary arteries, papillary muscles and aortic arch. The integration of CMR and MDCT images was performed before the ablation procedure, using the ADAS-VT™ software platform, and then imported into the CARTO® system, as shown in Figure 2.

The first step of the procedure was the acquisition of a FAM, either of the aorta or the RV and pulmonary artery, to integrate the multimodality pre-procedural cardiac imaging (MDCT cardiac reconstructions and 3D CMR-derived PSI maps) within the spatial reference coordinates of CARTO®. In 25/28 (89%) patients this integration was achieved using the FAM of the aortic root, employing a mean time of  $7.4 \pm 2$  minutes for this step. In 3 (11%) patients in which a MDCT scan was not available or a retroaortic access was not possible the integration was performed using the RV and pulmonary artery FAM, employing in this case a mean time of  $32 \pm 23$  minutes.

**CMR-Guided clinical VT ablation**

The second step of the procedure in the 10/28 (36%) patients with a documented 12-lead ECG of the VT was clinical VT ablation. For this purpose, the ablation catheter was positioned at the entrance of the previously identified 'putative' channel responsible for the clinical VT, based on analysis of the 12-lead ECG of the VT, as shown in Figures 3 and 4. In all cases, a pathological EGM was found at the entrance of the 'putative' channel during SR. In 5/10 (50%) cases the local EGM showed CC entrance characteristics, with a mean voltage of  $0.49 \pm 0.21$  mV and a mean delay of  $8.4 \pm 4.27$  ms between both components of the EGM. In the other 5/10 (50%) cases, the local EGM showed no delay between the far field and the local component during SR, and a mean voltage was  $1.26 \pm 0.61$  mV. In these latter cases, multiple extrastimuli were delivered from the right ventricular apex to check for HSC, according to a previously explained technique. (14)

After induction, the VT-isthmus exit site of the clinical VT was located using activation mapping if tolerated [2/10 (20%) patients] or, otherwise, using pacemapping [8/10 (80%) patients]. When activation mapping was used, a limited activation map ( $22 \pm 2.8$  mean points) focused into the 'putative' channel entrance was performed to identify the VT-isthmus exit site during VT. After that, clinical VT was stopped during RF as shown in the Supplemental Video. In patients in whom the VT isthmus was identified by pacemapping, the minimum level of concordance with the 12-lead ECG of the clinical VT was a 10/12 lead match. No patient was inducible for clinical VT after this step. The mean time required from the beginning of the procedure to clinical VT ablation was  $36 \pm 15$  minutes. More details of procedural outcomes in this group are shown in Supplemental Table 1.



### **CMR-Guided substrate ablation**

Complete substrate ablation based on information of the PSI maps was performed in all patients ( $n = 28$ ) of the CMR-Guided group. A combined endo-epicardial approach was performed in 8/28 (29%). The mean number of HTC identified per patient in the LGE-CMR-derived PSI map was  $1.71 \pm 0.97$  [29/48 (60%) of them were sub-endocardial, 5/48 (10%) sub-epicardial, and 14/48 (30%) transmural], with a mean number of HTC entrances per patient of  $9.3 \pm 5.4$  (mean of  $4.7 \pm 3.5$  entrances per each HTC). The mean HTC entrance width was  $9.5 \pm 4$  mm. In 177/225 (79%) of the identified HTC entrances a pathological EGM was found, 59% of them showed HSC conduction characteristics, whereas 41% showed delayed components during SR. The mean number of RF applications per patient was  $29 \pm 20$ , requiring a mean of  $4.1 \pm 3.7$  applications for each HTC entrance. An example of HTC with multiple entrances can be seen in Supplemental Figure S2.

### **Comparison of acute and follow-up outcomes**

The differences in acute outcomes after substrate ablation between groups are summarized in Table 2 and Figure 5. The CMR-Guided group required less procedure time than CMR-Aided and No-CMR ( $107 \pm 59$  vs.  $203 \pm 68$  min and  $227 \pm 52$  min, respectively;  $p < 0.001$  for both), as well as less fluoroscopy time than CMR-Aided and No-CMR ( $10 \pm 4$  vs.  $23 \pm 11$  min and  $20 \pm 9$  min, respectively;  $p < 0.001$  for both). Moreover, CMR-Guided required less RF time than No-CMR ( $15 \pm 8$  vs.  $26 \pm 10$  min;  $p < 0.001$ ) and CMR-Aided, without reaching statistical significance in this latter case ( $15 \pm 8$  vs.  $20 \pm 15$  min;  $p 0.16$ ).

In CMR-guided, 5/28 (18%) patients were inducible for residual VTs after completion of substrate ablation. At the end of the procedure only 2/26 (7%) patients were still inducible for fast, non-tolerated, non-clinical VTs. The final end-procedure success rate (after ablation of any residual VTs) in this group was 93%.

When compared with the No-CMR group there was a lower inducibility rate of residual substrate ablation in the CMR-Guided group (18% vs. 46%,  $p$  0.04), with a higher, although statistically non-significant, end-procedure success rate (93% vs. 79%;  $p$  0.17). When compared with the CMR-Aided group, no differences were found in the inducibility rate after substrate ablation (18% vs. 32%,  $p$  0.35) or in the end-procedure success rate (93% vs. 86%;  $p$  0.39). The complication rate was 5/84 (6%) without any significant difference between groups, Table 2. In the CMR-guided group 1 patient suffered a fistula. In the CMR-Aided group 1 patient suffered a phrenic paralysis and 2 patients suffered an atrioventricular block. Finally, in the No-CMR group 1 patient suffered a cardiac tamponade. After a mean follow-up period of 18 months, 10 (12%) patients had arrhythmia recurrence [1 (4%) patient in the CMR-Guided, 2 (7%) patients in the CMR-Aided and 7 (25%) patients in the No-CMR group,  $p=0.024$ ]. The Kaplan-Meier curves for ventricular arrhythmia-free survival (Figure 6) show a lower recurrence rate in the CMR-Guided compared with the No-CMR group (log-rank=0.019) with no significant differences in recurrence rate between CMR-Guided and CMR-Aided groups. Neither procedure success nor recurrence rate differed based on CMR image acquisition (1.5 vs 3 Tesla scanner), as Supplemental Table 2 shows.

## **DISCUSSION**

The present study reports, for the first time, the feasibility of performing VT substrate ablation procedures guided by LGE-CMR, without requiring an EAM. This approach was safe, allowing a significant shortening of the procedure, fluoroscopy and RF delivery times, making it more efficient as compared with the classical EAM-based procedure and even compared with the previously reported CMR-aided VT substrate ablation approach. (6) Moreover, CMR-guided VT substrate ablation is also associated with an improvement in acute outcomes when compared with No-CMR by reducing the inducibility rate after substrate ablation, and a lower recurrence rate during follow-up, which in turn suggests a better identification of the arrhythmogenic substrate and target ablation sites.

With this regard, it has already been shown that scar distribution across the myocardial wall, assessed by LGE-CMR, is useful to decide on the best approach (endocardial, epicardial, or combined) for VT ablation to reach the whole VT substrate. (11,12) Besides, integration of CMR-derived PSI maps in the electromagnetic navigation system has already been shown to improve the acute and long-term outcomes of VT substrate ablation using combined CMR-EAM information. (6,7)

### **Efficiency of CMR-Guided VT substrate ablation**

CMR-Guided ablation has been shown to be more efficient due to a significant shortening of procedure, fluoroscopy and RF time needed to completely eliminate the VT substrate. In CMR-Guided patients no EAM was obtained, either of the whole LV (No-CMR group) or

focused on the scar area (CMR-Aided). According to a previous study from our group (6), the mean time spent for acquiring the EAM was about 36 min, which may explain in part the remarkable shortening of procedure times found. Moreover, the need for a remap, acquired in the No-CMR and CMR-Aided approaches whenever inducibility was demonstrated, in order to identify residual pathological EGMs, is no longer present and could partially explain the remaining 'saved time'. Additional RF target selection in the CMR-Guided group was based on the PSI map information, i.e., checking for neighboring sites adjacent to the identified HTC entrances. Furthermore, only 18% of CMR-Guided patients needed additional mapping due to VT inducibility after substrate ablation, a lower proportion when compared to CMR-Aided (32%) and No-CMR (46%) groups.

A lower inducibility rate found after CMR-Guided substrate ablation suggests an improvement in VT substrate identification. CMR-derived PSI maps may enable a better identification of the real CC entrances, located in the BZ between dense scar and healthy tissue as defined by conventional voltage criteria in the EAM (14). This is a region that cannot usually be well defined by the EAM due to the far-field effect of the surrounding healthy myocardium, thus leading to an EAM-derived low-voltage area smaller than the PSI-derived ('anatomical') scar area (10). A higher number of CC entrances has been described previously (6) in areas with bipolar voltage  $>1.5$  mV when PSI information is used. A better characterization of these transitional areas between healthy and BZ tissue with the LGE-CMR explains a more extensive substrate elimination in the CMR-Guided group and better acute outcomes (6,17).

Additionally, CMR-derived information can be used to obtain PSI maps from the whole myocardial thickness, permitting characterization of the substrate into different tissue layers, from endocardium to epicardium. One of the main limitations of EAM is the lack of sensitivity to analyze local EGMs generated deeper than the subendocardium due to a far-field effect of the surrounding tissue. This may explain why, in the present study, 21% of HTC entrances detected in the CMR-Guided procedures showed an apparently normal EGM. Clinical support for this hypothesis comes from the previous study by Andreu D et al. (6) in which patients with 'undetected' CMR-derived HTC in the EAM, therefore not targeted for ablation, showed an increased VT recurrence rate after 18 months.

More accurate arrhythmogenic substrate identification with the PSI maps, both at the edge of the scar and deep within the myocardial wall, can explain the lower inducibility rate after substrate ablation, as well as the lower recurrence rate when the procedure was guided by the CMR information compared with the No-CMR group. Although PSI information was available in the CMR-Aided group for substrate characterization, the selection of ablation targets was exclusively guided by the EAM information. Thus, HTC depicted in the PSI maps but not identified in the EAM were not targeted for ablation. A complete substrate ablation is achievable using a pure CMR-Guided approach, showing a trend towards lower inducibility after substrate ablation and lower VT recurrence rate when compared to the CMR-Aided approach, although without reaching statistical significance.

### **Efficiency of CMR-Guided clinical VT ablation**

The present study defines a new approach for clinical VT ablation guided by imaging, looking for the putative channel based on ECG morphology during VT, as described previously (16). The mean procedure time needed for ablating a clinical VT was only  $36 \pm 15$  minutes, a vast reduction in the time taken by a conventional approach using EAMs. Moreover, in all cases where clinical VT ablation was performed (before completing substrate ablation), a local pathological EGM was found at the entrance (exit during VT) of the HTC responsible for the VT, corroborating the accuracy of CMR imaging at identifying arrhythmogenic substrate.

### **Clinical implications**

Over the past decade, a substrate-based approach for VT ablation has steadily increased (5), in both high-volume and non-high-volume centers (18). Despite the need to corroborate the results of this study in a multicenter study to check for reproducibility, consolidation of this approach could help simplify a procedure considered as challenging and time-consuming. Moreover, the CMR-guided clinical VT ablation approach described could be an attractive option in selected patients in whom the exclusive elimination of clinical VT is the endpoint, i.e., recurrent VT in patients with a high-risk of complications and comorbidities.

### **Study limitations**

The main limitation of this study is the lack of randomization, although we tried to make groups comparable by matching them for the key outcome predictors after substrate ablation. The procedures were performed in different time periods and therefore only the

final 28 consecutive patients underwent CMR-guided ablation. However, the substrate ablation technique only differed between groups in the selection of the target ablation site for radiofrequency applications. Contact force as well as multielectrode catheters were not systematically used for electroanatomical mapping. Accuracy of CMR-guided ablation could be influenced by the CMR acquisition technique, spatial resolution and image quality. Moreover, we used Scar dechanneling technique for substrate ablation in all patients. Further studies are needed for analyzing CMR-guided approach reproducibility by other groups, in other substrate ablation modalities or using different postprocessing tools.

## **Conclusion**

CMR-guided VT ablation halves the time required for the procedure, significantly reduces the need of fluoroscopy and radiofrequency delivery and is associated with a higher rate of noninducibility after substrate ablation and a higher ventricular arrhythmia-free survival.

**REFERENCES**

1. Reddy VY, Reynolds MR, Neuzil P, et al. Prophylactic Catheter Ablation for the Prevention of Defibrillator Therapy. *N Engl J Med* 2007;357:2657-2665.
2. Kuck KH, Schaumann A, Eckardt L, et al. Catheter ablation of stable ventricular tachycardia before defibrillator implantation in patients with coronary heart disease (VTACH): a multicentre randomised controlled trial. *Lancet* 2010;375:31-40.
3. Sacher F, Tedrow UB, Field ME, et al. Ventricular Tachycardia Ablation: Evolution of Patients Over 8 Years. *Circ Arrhythm Electrophysiol* 2008;1:153-161.
4. Stevenson WG, Wilber DJ, Natale A, et al. Multicenter Thermocool VT Ablation Trial Investigators. Irrigated radiofrequency catheter ablation guided by electroanatomic mapping for recurrent ventricular tachycardia after myocardial infarction: the multicenter Thermocool ventricular tachycardia ablation trial. *Circulation* 2008;118:2773-2782.
5. Palaniswamy C, Kolte D, Harikrishnan P, et al. Catheter ablation of postinfarction ventricular tachycardia: ten-year trends in utilization, in-hospital complications, and in-hospital mortality in the United States. *Heart Rhythm* 2014;11:2056-2063.
6. Andreu D, Penela D, Acosta J, et al. Cardiac magnetic resonance-aided scar dechanneling: Influence on acute and long-term outcomes. *Heart Rhythm* 2017;14:1121-1128.
7. Zghaib T, Ipek EG, Hansford R, et al. Standard Ablation Versus Magnetic Resonance Imaging-Guided Ablation in the Treatment of Ventricular Tachycardia. *Circ Arrhythm Electrophysiol* 2018;11:e005973.

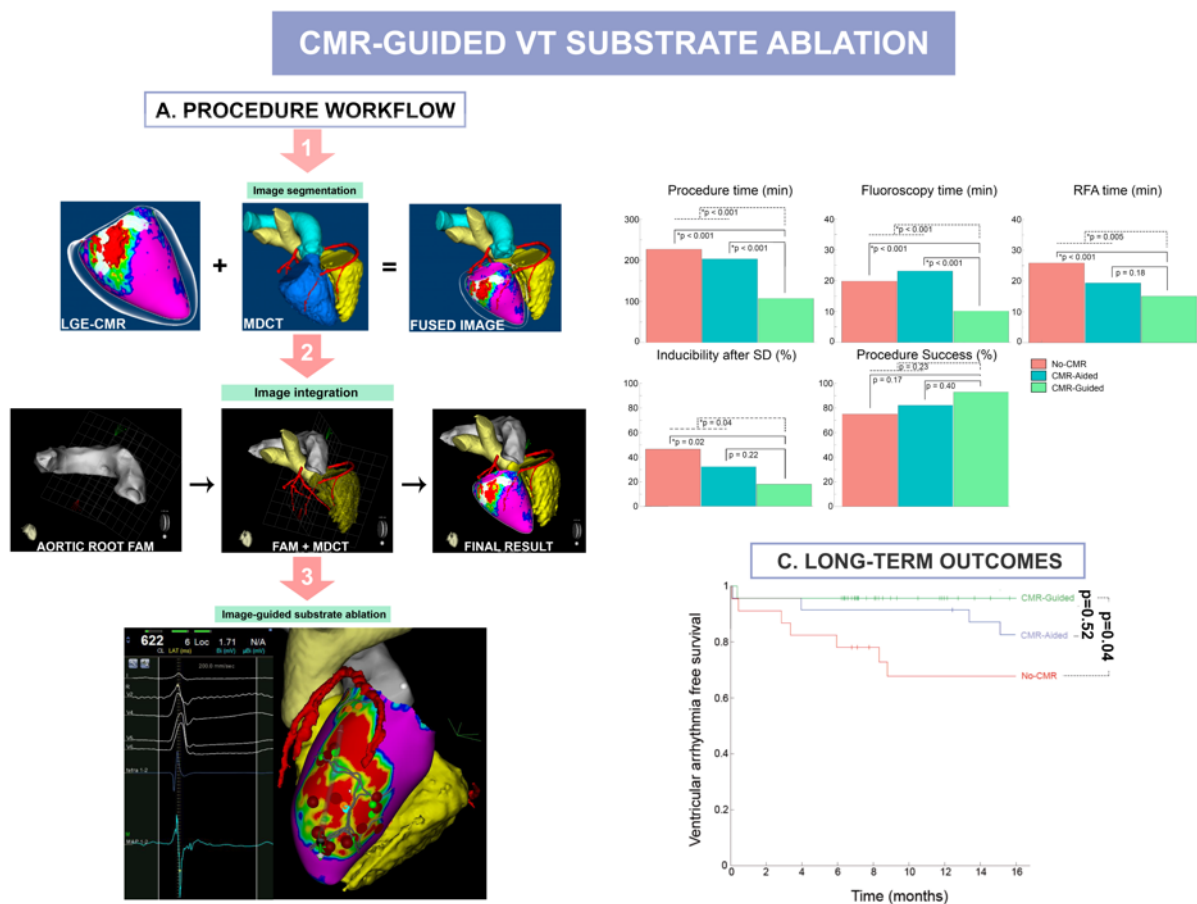


8. Fernández-Armenta J, Berruezo A, Andreu D, et al. Three-dimensional architecture of scar and conducting channels based on high resolution ce-CMR: insights for ventricular tachycardia ablation. *Circ Arrhythm Electrophysiol.* 2013;6:528-537.
9. Andreu D, Ortiz-Pérez JT, Fernández-Armenta J, et al. 3D delayed enhanced magnetic resonance sequences improve conducting channel delineation prior to ventricular tachycardia ablation. *Europace* 2015;17:938-945.
10. Andreu D, Berruezo A, Ortiz-Perez JT, et al. Integration of 3D Electroanatomic Maps and Magnetic Resonance Scar Characterization Into the Navigation System to Guide Ventricular Tachycardia Ablation. *Circ Arrhythm Electrophysiol* 2011;4:674-683.
11. Acosta J, Fernández-Armenta J, Penela D, et al. Infarct transmuralty as a criterion for first-line endo-epicardial substrate-guided ventricular tachycardia ablation in ischemic cardiomyopathy. *Heart Rhythm* 2016;13:85-95.
12. Soto-Iglesias D, Acosta J, Penela D, et al. Image-based criteria to identify the presence of epicardial arrhythmogenic substrate in patients with transmural myocardial infarction. *Heart Rhythm* 2018;15:814-821.
13. Fernández-Armenta J, Penela D, Acosta J, et al. Substrate modification or ventricular tachycardia induction, mapping, and ablation as the first step? A randomized study. *Heart Rhythm.* 2016;13:1589-95.
14. Acosta J, Andreu D, Penela D, et al. Elucidation of hidden slow conduction by double ventricular extrastimuli: a method for further arrhythmic substrate identification in ventricular tachycardia ablation procedures. *Europace* 2018;20:337-346.

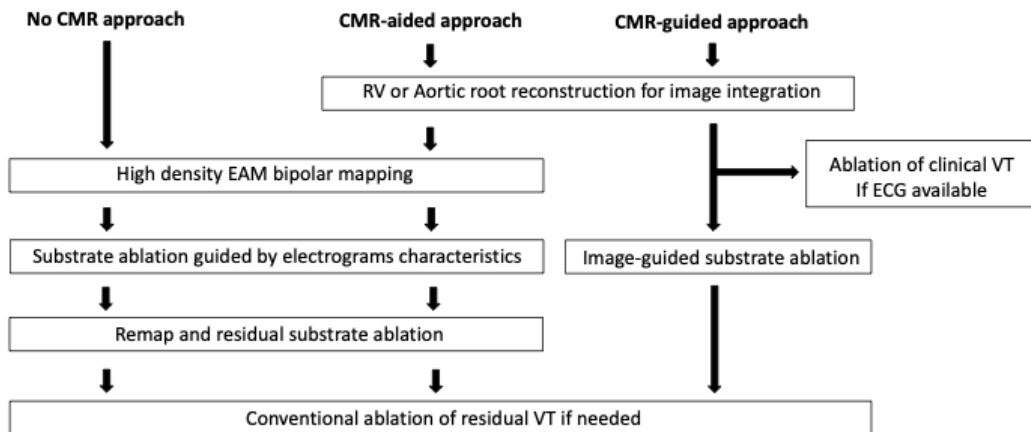
15. Berruezo A, Fernandez-Armenta J, Andreu D, et al. Scar dechanneling: a new method for scar-related left ventricular tachycardia substrate ablation. *Circ Arrhythm Electrophysiol* 2015;8:326-336.
16. Andreu D, Fernández-Armenta J, Acosta J, et al. A QRS axis-based algorithm to identify the origin of scar-related ventricular tachycardia in an American Heart Association 17-segment model. *Heart Rhythm* 2018. doi: 10.1016/j.hrthm.2018.06.013. [Epub ahead of print]
17. Andreu D, Ortiz-Perez JT, Boussy T, et al. Usefulness of contrast-enhanced cardiac magnetic resonance in identifying the ventricular arrhythmia substrate and the approach needed for ablation. *Eur Heart J* 2014;35:1316-1326.
- 18.. Katz DF, Turakhia MP, Sauer WH, et al. Safety of ventricular tachycardia ablation in clinical practice: findings from 9699 hospital discharge records. *Circ Arrhythm Electrophysiol* 2015;8:362-370.

**FIGURES**

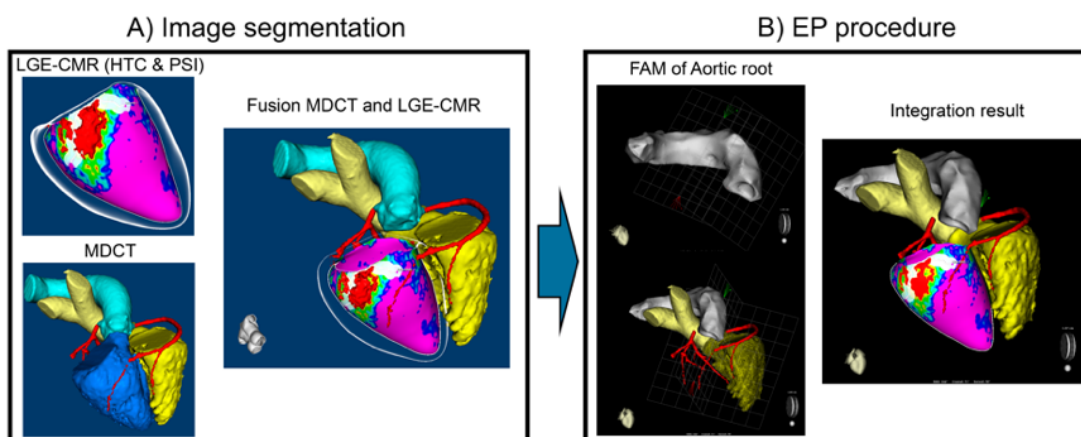
**Central illustration.** On the left: workflow of the CMR-Guided VT ablation procedure. The first step is image segmentation. After that, the fused image is integrated in the navigator system. Finally, ablation is performed based on the CMR information. On the right: comparison of the acute and 18 months outcomes between patients with a CMR-Guided ablation, patients with a CMR-Aided ablation and patients without pre-procedure CMR.



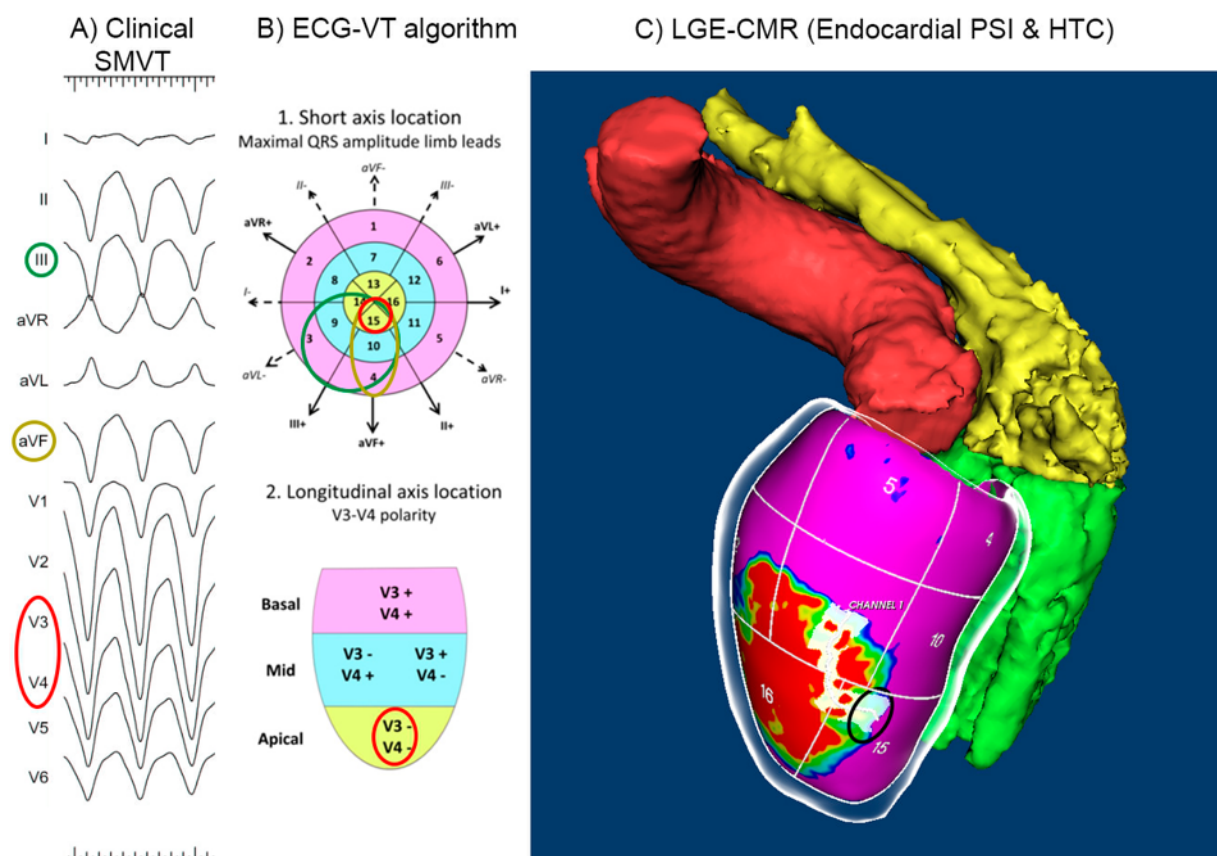
**Figure 1.** Summarizing workflow for No-CMR, CMR-Aided and CMR-Guided VT substrate ablation procedures.



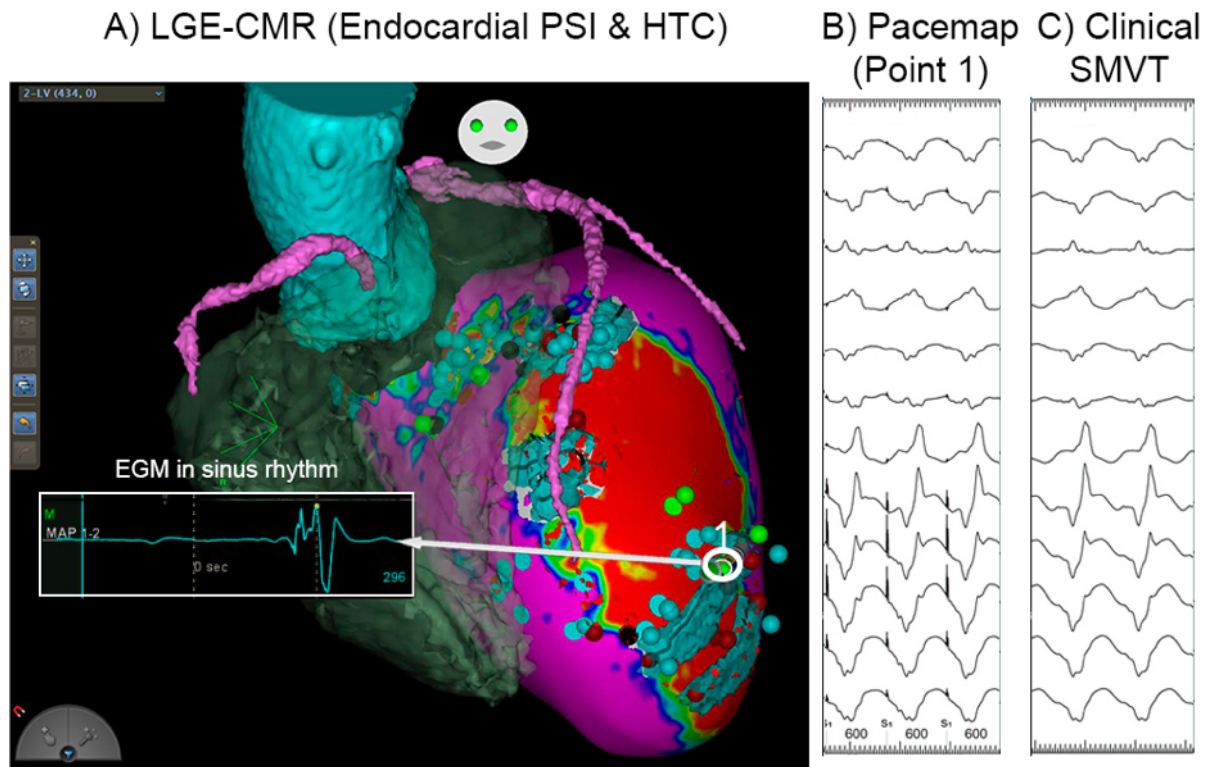
**Figure 2.** Integration pipeline. Panel A represents the multimodal imaging-based cardiac segmentation and fusion before the ablation procedure. PSI maps and identification of HTC are derived from the LGE-CMR studies and fused with the anatomical structures extracted from MDCT using the ADAS-VT™ software platform. Panel B shows integration of the PSI maps within the spatial reference coordinates of the CARTO® system, by performing a fast anatomical map (FAM) of the aortic root.



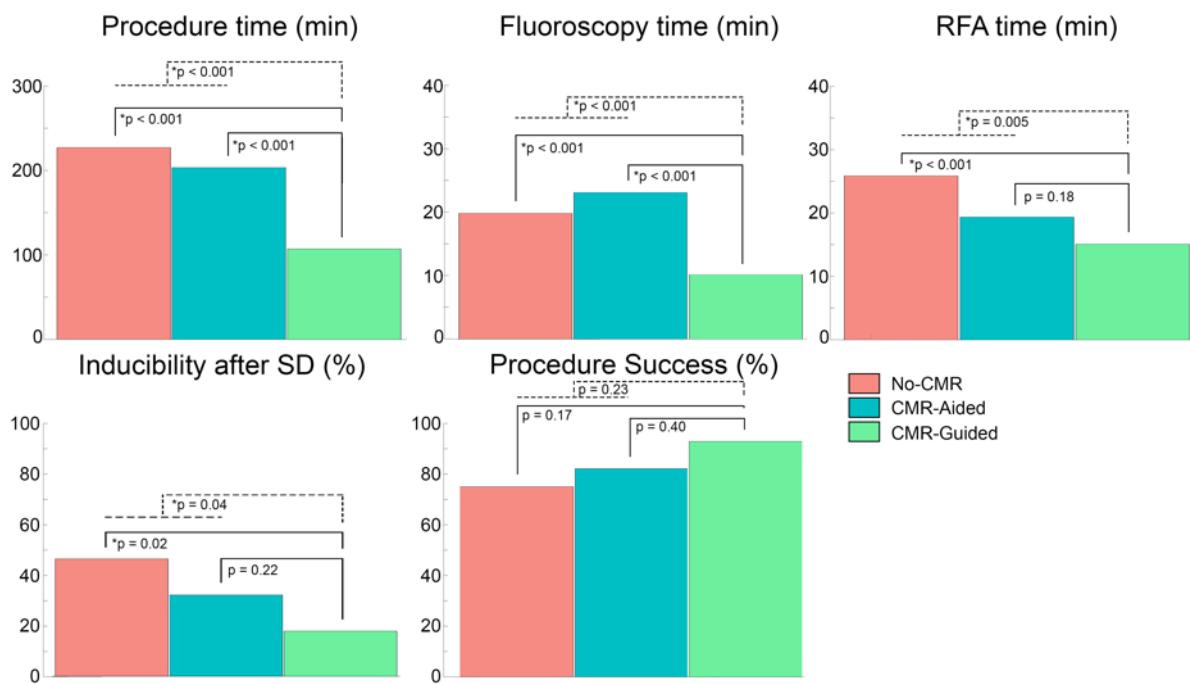
**Figure 3.** Example of a tolerated, clinical sustained monomorphic VT (SMVT) ablation. Panel A represents the 12-lead ECG morphology of the clinical SMVT. Panel B represents the result of applying a two-step, QRS axis-based ECG algorithm (see Supplemental Material for details) to identify the origin (exit-site) of a scar-related SMVT. Panel C represents the LGE-CMR-derived PSI map, LV AHA segments, and the 'putative' HTC (highlighted in white) responsible for the clinical VT. One of the 'putative' HTC entrances (black circle) is located at AHA segment number 15, which corresponds to the same identified segment of origin (VT exit site) after applying the two-step ECG identification algorithm.

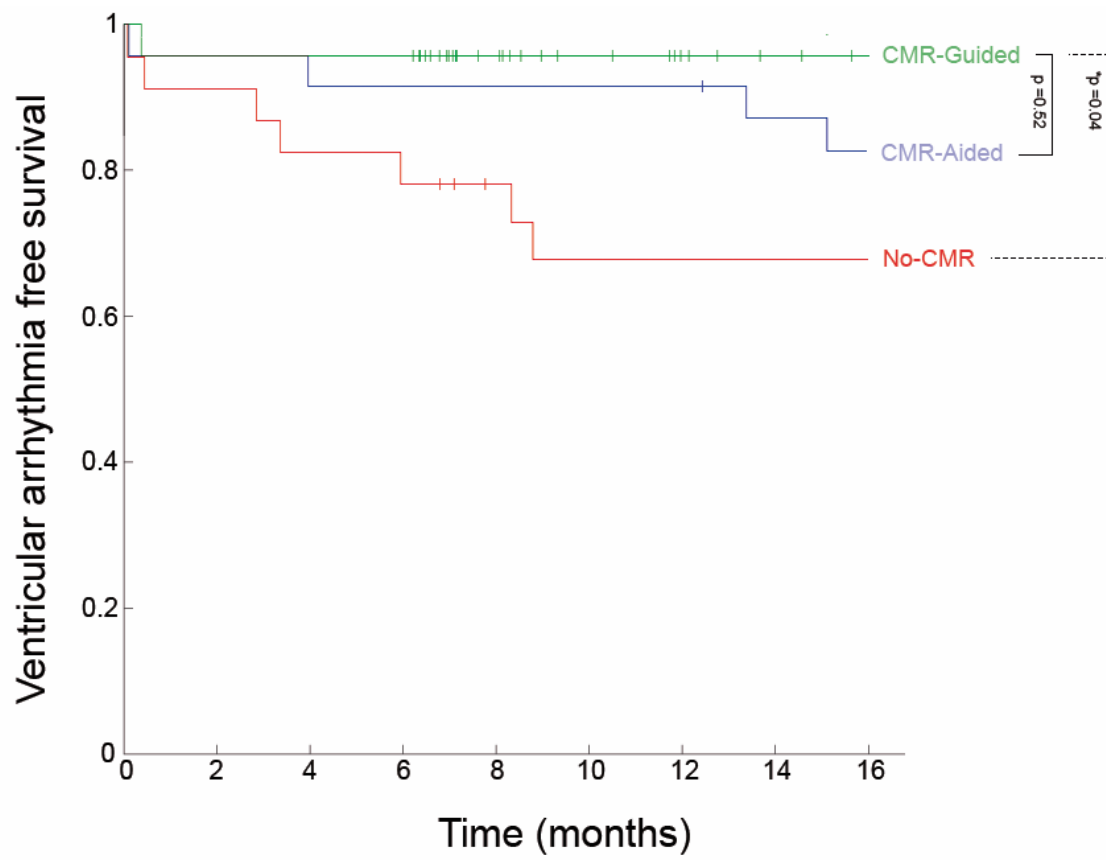


**Figure 4.** Example of a non-tolerated, clinical sustained monomorphic VT (SMVT) ablation. The two-step, QRS axis-based ECG algorithm suggested a VT origin (exit site) from AHA segment number 11-12 (mid lateral). Panel A shows the PSI map and HTC extracted from the pre-procedural LGE-CMR. Point 1 (white circle) shows an EGM in SR whose characteristics qualify to be considered for a CC entrance, located right at the entrance of an HTC identified with the PSI map. This HTC entrance is found between AHA segments 11 and 12. Panel B represents the paced 12-lead ECG morphology at point number 1. Panel C represents the 12-lead ECG morphology of the clinical, non-tolerated SMVT.



**Figure 5.** Acute results of VT substrate ablation procedures using the 'scar dechanneling' technique for the No-CMR (red), CMR-Aided (blue) and CMR-Guided (green) groups. The CMR-Guided approach significantly shortens the procedure, fluoroscopy and RFA times and leads to less inducibility after substrate ablation without significant differences in end-procedure success.



**Figure 6.** Kaplan-Maier curve for ventricular arrhythmia-free survival.



## TABLES

**Table 1.** Baseline characteristics based on the VT ablation procedure.

	Total n=84	No- CMR n=28	CMR- Aided n=28	CMR- Guided n=28	P-value*	P-value**
Age, y	67±10	70±8	66±8	64±14	0.04	0.4
Male, n (%)	79 (94)	26 (93)	26 (93)	27 (96)	1.00	1.00
HT, n (%)	62 (74)	22 (79)	21 (75)	19 (68)	0.55	0.77
DLP, n (%)	44 (52)	13 (46)	17 (61)	14 (50)	0.58	0.78
DM, n (%)	22 (26)	6 (21)	7 (25)	9 (32)	0.36	0.55
LVEF, %	38±12	39±14	38±11	37±11	0.71	0.87
LVEDD, mm	62±7	62±7	60±8	62±7	0.72	0.65
LVESD, mm	43±12	45±9	42±11	41±17	0.47	0.88
IHD, n (%)	69 (82)	24 (86)	22 (79)	23 (82)	0.45	0.37
Mean VT cycle length	333±126	331±116	317±125	364±151	0.503	0.859
Patients with an ICD at the ablation time [n (%)]	75 (89)	27 (96)	24 (86)	24 (86)	0.160	0.160
NYHA						
• I, n (%)	26 (31)	7 (25)	13 (46)	6 (21)		
• II, n (%)	46 (55)	17 (61)	11 (39)	18 (65)	0.894	0.138
• III, n (%)	12 (14)	4 (14)	4 (15)	4 (14)		
• IV, n (%)	0	0	0	0		
Approach						
• Endo, n (%)	58 (69)	19 (68)	17 (65)	20 (71)	0.95	0.44
• Endo/Epi, n (%)	26 (31)	9 (32)	9 (32)	8 (29)		
Indication						
• Incessant VT, n (%)	5 (6)	2 (7)	2 (7)	1 (4)	0.99	0.99
• Arrhythmic storm, n (%)	13 (16)	5 (18)	2 (7)	6 (21)	0.99	0.14

CMR: cardiac magnetic resonance; DLP: dyslipidemia; DM: diabetes mellitus; HT: hypertension; IHD: ischemic heart disease; LVEF: left ventricle ejection fraction; LVEDD: left ventricle end-diastolic diameter; LVESD: left ventricle end-systolic diameter; NYHA: New York Heart Association class; VT: ventricular tachycardia.

\* Difference between CMR-guided and No-CMR; \*\*Difference between CMR-Guided and CMR-Aided.

**Table 2.** Acute results of VT substrate ablation procedures.

	<b>Total n=84</b>	<b>No-CMR n=28</b>	<b>CMR- Aided n=28</b>	<b>CMR- Guided n=28</b>	<b>P- value*</b>	<b>P- value**</b>
<b>Procedure time (min)</b>	179±79	227±52	203±68	107±59	<0.001*	<0.001*
<b>RF time (min)</b>	20±12	26±11	20±15	15±8	<0.001*	0.16
<b>RF applications (n)</b>	31±18	35±14	29±22	29±20	0.26	0.96
<b>Fluoroscopy time (min)</b>	18±10	20±9	23±11	10±4	<0.001*	<0.001*
<b>Residual VT after substrate ablation, n (%)</b>	27 (32)	13 (46)	9 (32)	5 (18)	0.04*	0.35
<b>Induced VT (n)</b>	1.27±1.24	1.36±1.35	1.35±1.36	1.04±0.99	0.34	0.36
<b>Complications (%)</b>	5 (6)	1 (4)	3(10)	1 (4)	0.75	0.35
<b>Final procedure success (n, %)</b>						
• <b>Total</b>	70 (84)	21 (75)	23 (82)	26 (93)		
• <b>Partial</b>	12 (14)	6 (21)	4 (14)	2 (7)	0.17	0.39
• <b>No</b>	2 (2)	1 (4)	1 (4)	0 (0)		

**RF:** radiofrequency; **VT:** ventricular tachycardia. \*Difference between CMR-guided and No-CMR; \*\*Difference between CMR-Guided and CMR-Aided groups.

## **ONLINE APPENDIX**

### **SUPPLEMENTAL METHODS**

#### **LGE-CMR acquisition**

LGE-CMR was performed in a 3T scanner (Magnetom Trio™-Tim®, Siemens, Erlangen, Germany). Contrast-enhanced images were acquired 10 minutes after bolus injection of 0.2 mmol/kg Gadobutrol (Gadovist®, Bayer Hispania, Barcelona, Spain) using a commercially available, free-breathing, ECG-gated, navigator-gated, 3D inversion-recovery, gradient-echo technique. Slice thickness was 1.4 mm, with no gap between slices. The field of view was set at 360 mm and matrix size was kept to 256x256 pixels in order to yield an isotropic resolution of 1.4x1.4x1.4 mm.

#### **Wide band sequence acquisition**

In those patients previously implanted with an intracardiac device the LGE-CMR was performed with a 1.5T scanner (Magnetom Aera®, Siemens, Erlangen, Germany). Using a 2D turbo flash gradient echo sequence the sort-axis contrast-enhanced images were acquired synchronized with the ECG. Slice thickness was 5 mm, with no gap between slices iPAT accelerator factor x2. Typical parameters were: Repetition time 948,8 msec; Echo time 1,39 msec; Bandwidth 592 Hx/Px; Flip angle 25°; and Matrix size 256x144 pixels. The mean in-plane resolution was 1.4x1.4 mm, and the voxel size was 9.80 mm<sup>3</sup>.

#### **MDCT acquisition**

MDCT ECG-gated study was performed on a 128x2-slice computed tomography (CT) scanner (Somatom Definition Flash, Siemens Healthcare, Erlangen, Germany). Images were acquired during an inspiratory breath-hold using retrospective ECG-gating technique with tube current modulation set between 50% and 100% of the cardiac cycle. CT angiographic images were acquired during the injection of a 100 mL bolus of Iopromide 370 mg I/mL (Ultravist, Bayer Hispania, Barcelona, Spain) at a rate of 3 mL/s.

### **A QRS basis algorithm to identify the origin of scar-related ventricular tachycardia in an American Heart Association 17-segment model**

The algorithm uses the QRS axis in the frontal plane to locate the VT origin in the LV short axis (inferior vs anterior, septal vs lateral) and the polarity in V3-V4 for its location in the LV longitudinal plane (basal, medial or apical).

Two steps are needed to define the segment of origin (SgO) of a VT using the proposed algorithm (18), as follows:

1) Identify the lead limbs with the highest voltage magnitude (positive or negative). If this magnitude is I, II, or III, the adjacent leads must be considered, as the major axis is facing the boundary between two groups of segments. The adjacent limb lead with higher magnitude will determine the group of segments where the VT may originate. In cases where there was not a clear lead with R or QS pattern, the Q, R or S wave with the higher amplitude was taken into the account. In Figure 3, the highest QRS magnitude (negative) is in lead III. The QRS magnitude in aVL (positive) and aVF (negative) should be compared. As

the absolute amplitude of QRS in aVF is higher than in aVL, the potential SgO are segments 4, 10 and 15.

2) Identify the positivity or negativity of the precordial leads V3 and V4; concordance indicates a basal or apical origin, respectively. Other combinations indicate a middle origin. Figure 3 shows an example of a VT in which the algorithm correctly identified the SOO in segment 15.

### **Substrate ablation protocol in the control group**

A four-step ablation protocol was performed as previously described.(5,17-19). Briefly, an endocardial and/or epicardial substrate map was acquired first. Electrograms with delayed components (E-DCs) were tagged and differentiated between inner and conducting channel (CC) entrance electrograms, depending on the DC precocity during sinus rhythm. The CC entrance was defined as the E-DC with the shortest delay between the far-field component of healthy/BZ muscle and the local, pathological component corresponding to the local activation of myocardial fibers within the scar. Second, radiofrequency was delivered at target ablation sites, which were the CC entrances identified in the EAM as described in the previous step. Third, a remap was acquired in order to document complete substrate elimination or to identify residual E-DCs if that were the case. Residual E-DCs were identified in the same way as in the first step and RF ablation was delivered to eliminate all of them.

**SUPPLEMENTAL TABLES**

**Online Table 1.** Procedural outcomes based on whether ablation of clinical VT was performed or not.

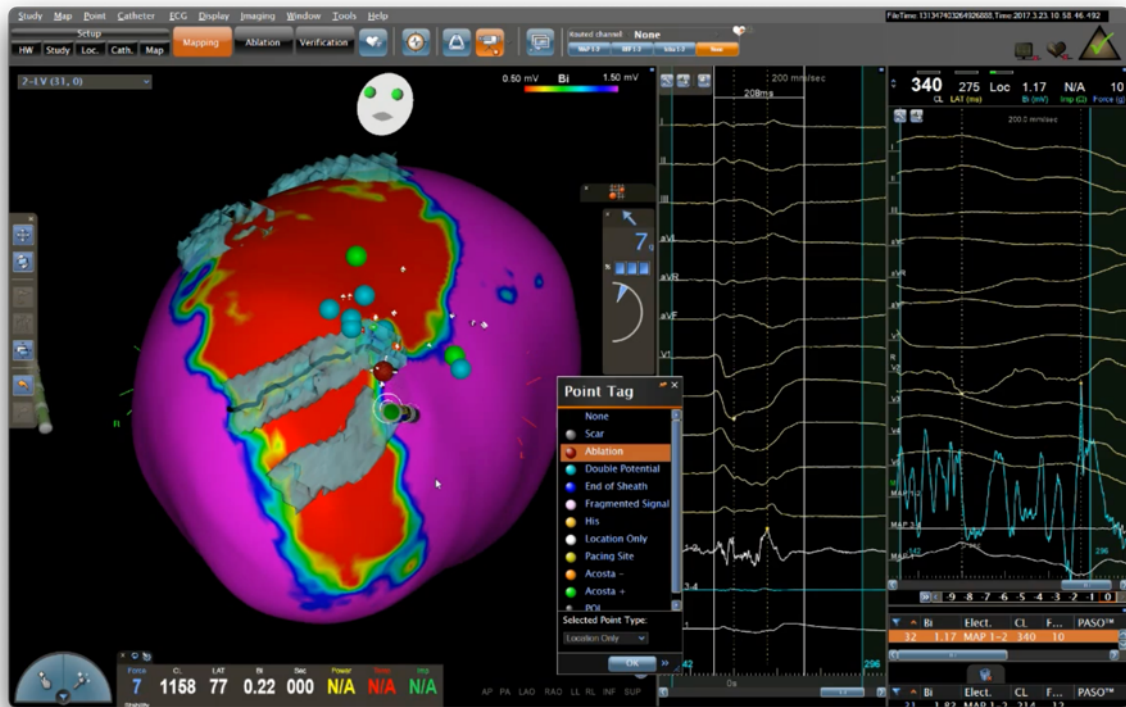
	<b>Without 12-lead N = 18</b>	<b>With 12-Lead N = 10</b>	<b>P-value**</b>
<b>Procedure time (min)</b>	121.56 ± 64.09	81.10 ± 41.10	0.085
<b>RF time (min)</b>	15.56 ± 7.35	14.03 ± 9.84	0.645
<b>RF applications (n)</b>	30.83 ± 17.87	25.4 ± 21.36	0.478
<b>Fluoroscopy time (min)</b>	9.89 ± 4.16	10.50 ± 4.06	0.710
<b>Residual VT after substrate ablation, n (%)</b>	2 (11%)	3 (30%)	0.211
<b>Induced VT (n)</b>	0.83 ± 9.85	1.40 ± 0.97	0.154
<b>Final procedure success (n, %)</b>			
• <b>Total</b>	• 18 (100%)	• 8 (80)	0.050
• <b>Partial</b>	• 0	• 2 (20)	
• <b>No</b>	• 0	• 0	
<b>Recurrence rate (n, %)</b>	1 (5%)	0	0.448

**Online Table 2.** Main outcomes after CMR-guided ablation based on the CMR field strength (1.5 vs 3 Tesla scanner).

	<b>1.5-T CMR N = 13</b>	<b>3-T CMR N = 15</b>	<b>P-value**</b>
<b>Procedure time (min)</b>	109.23 ± 60.33	105.27 ± 60.81	0.864
<b>RF time (min)</b>	13.08 ± 5.30	16.68 ± 9.93	0.253
<b>RF applications, n</b>	27.15 ± 16.59	30.40 ± 21.30	0.660
<b>Fluoroscopy time (min)</b>	8.85 ± 3.29	11.20 ± 4.44	0.128
<b>Residual VT after substrate ablation, n (%)</b>	2 (15%)	3 (20%)	0.750
<b>Induced VT (n)</b>	0.92 ± 1.04	1.13 ± 0.99	0.588
<b>Final procedure success, n (%)</b>			
• <b>Total</b>	• 12(92%)	• 14(93%)	0.916
• <b>Partial</b>	• 1 (8%)	• 1 (7%)	
• <b>No</b>	• 0	• 0	
<b>Recurrence rate, n (%)</b>	1 (7.7%)	0 (0%)	0.274
<b>Number of HTC</b>	1.54 ± 0.78	2.07 ± 1.03	0.143
<b>Number of HTC entrances</b>	7.77 ± 6.34	8.93 ± 4.46	0.575

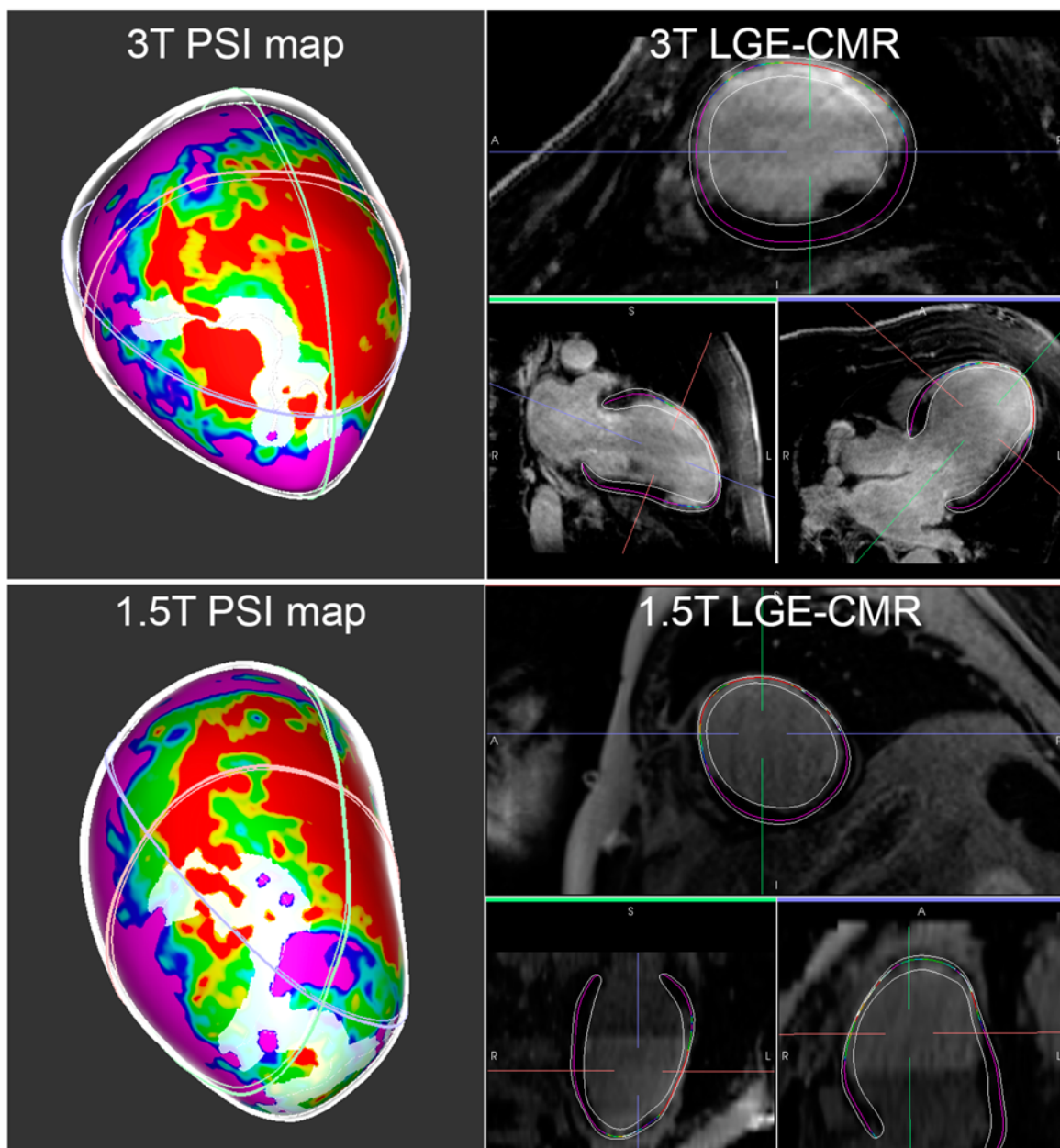
**SUPPLEMENTAL VIDEO**

**Supplemental video.** Supplemental video shows an example of clinical VT ablation.



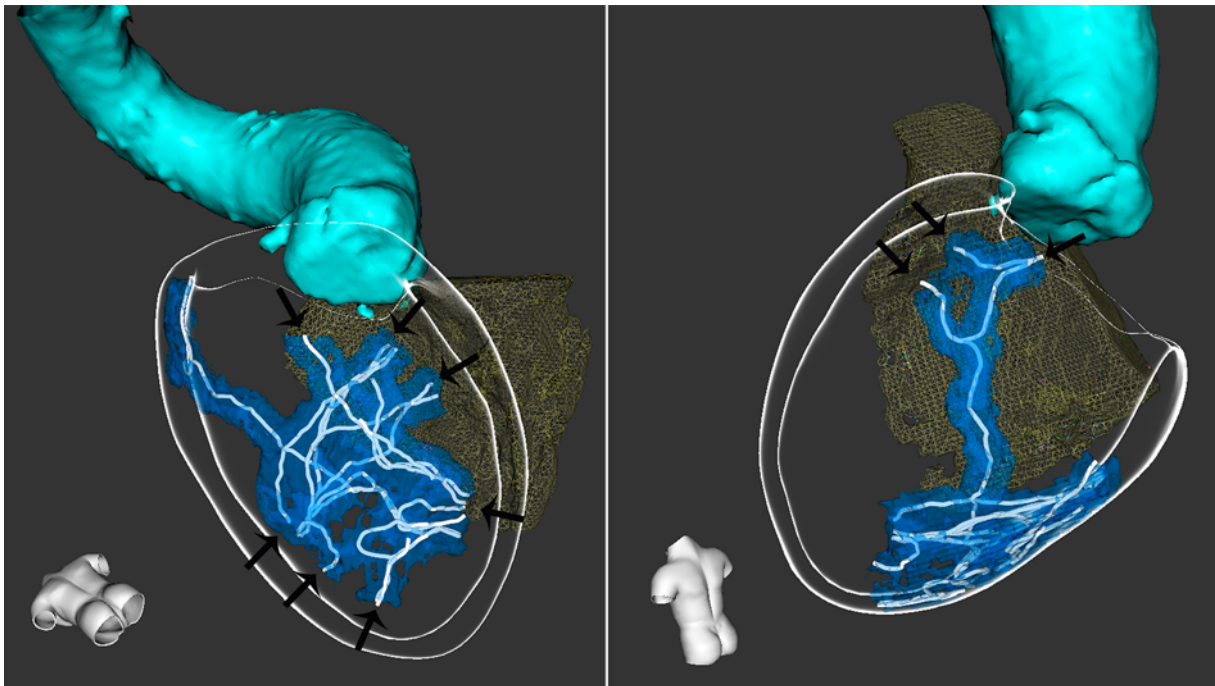
**SUPPLEMENTAL FIGURES**

**Online Figure 1.** Late gadolinium enhancement cardiac magnetic resonance (LGE- CMR) and delivered pixel signal intensity (PSI) in a patient with a prior anterior myocardial infarction. On top a study performed with a 3 Tesla scanner. On the bottom, a study performed with a 1.5 Tesla scanner in the same patient. Both studies identified a heterogeneous tissue channel in the septal portion of the scar with the same morphology and distribution.





**Online Figure 2.** Example of a post myocardial infarction patient with an inferior heterogeneous tissue channel (HTC) with multiple entrances (black arrows).







# 7. DISCUSIÓN

## a. Hallazgos principales de la Tesis

La presente Tesis analiza la utilidad clínica de la RM, una técnica de diagnóstico por imagen no invasiva, en un amplio espectro de aplicaciones para pacientes con CI, atendiendo a los distintos momentos evolutivos de esta patología desde el evento isquémico agudo: i) análisis de la presencia y evolución histológica de la cicatriz post-IAM y su potencial sustrato arritmogénico, así como comparación de su utilidad respecto a la TAC; ii) evaluación de las características de la cicatriz post-IAM que le confieren un potencial arritmogénico y, por tanto, utilidad de la RM-RTG para estratificar mejor el riesgo arrítmico respecto a la FEVI; y iii) rendimiento y utilidad de la RM-RTG para guiar de forma directa los procedimientos de ablación del sustrato arritmogénico en pacientes que ya han tenido AV relacionadas con la cicatriz.

De manera resumida, los principales hallazgos de la Tesis son los siguientes:

1. La RM permite una evaluación dinámica de las características cuantitativas y cualitativas de las cicatrices post-IAM a lo largo del tiempo.
2. El miocardio infartado experimenta un proceso de remodelación de larga duración (años) que se caracteriza por una disminución constante de la masa total de cicatriz y un aumento progresivo en su heterogeneidad, es decir, un aumento en la proporción de tejido heterogéneo dentro de la misma.

3. El número y distribución de los canales de tejido heterogéneo (HTC/BZC), que constituyen el sustrato histológico de la arritmogénesis, cambian notablemente durante años (al menos, 4) tras el IAM, y estos cambios pueden evaluarse de forma fiable con RM seriadas.
4. En la fase aguda tras el IAM, se inicia una cascada de procesos inmunes que implican el reclutamiento de distintas subpoblaciones monocitarias y la expresión de diversos biomarcadores detectables en suero.
5. Algunas subpoblaciones monocitarias (monocitos "clásicos" e "intermedios") se relacionan de forma positiva con el tamaño de la cicatriz de IAM, y de manera inversa con la FEVI resultante. Por el contrario, los monocitos "no clásicos", relacionados con el control de la inflamación, parecen asociarse de forma positiva con una mayor heterogeneidad de la cicatriz y la presencia de canales de tejido heterogéneo.
6. La RM-RTG, en comparación con la TAC, es la técnica de imagen más precisa a la hora de evaluar, de forma no invasiva, las características de la cicatriz post-IAM y su potencial arritmogenicidad. La TAC no es capaz de detectar la presencia de BZC en aproximadamente un 36% de los pacientes que tienen cicatrices post-IAM sólo subendocárdicas.
7. La masa de BZC de la cicatriz en el IM crónico, un parámetro cuantificable con RM, es la variable independiente que se correlaciona más fuertemente con la aparición de AV, tras ajustar por variables de confusión como la edad, la FEVI o la masa total de cicatriz. Su utilización podría mejorar la estratificación del riesgo de AV en pacientes con CI crónica, en comparación con la FEVI.

8. En pacientes con CI y AV, es posible y seguro realizar procedimientos de ablación de sustrato guiándolos exclusivamente mediante la información derivada de los mapas de PSI de la RM, sin necesidad de adquirir EAM completos. Este abordaje es, además, más eficaz y eficiente que si no se dispusiera de la RM-RTG.

## **b. Utilidad de la Resonancia Magnética en la Evaluación de la Presencia y Evolución del Sustrato Arritmogénico**

Como primer aspecto novedoso aportado, esta Tesis demuestra que la RM puede permitir el análisis evolutivo de la cicatriz post-IAM, viniendo además a modificar la creencia pre-establecida de que la cicatriz post-IAM no se modifica a largo plazo. En la CI, a diferencia de otras miocardiopatías (figura 23), cuando evoluciona en ausencia de nuevos eventos isquémicos (es decir, cuando la EAC permanece estable) no se observa un aumento progresivo de la fibrosis macroscópica. El resto de miocardiopatías, bien con base genética o tóxico-metabólicas, van afectar habitualmente de manera progresiva a la estructura del miocardio y se asocian también con una progresión de la fibrosis macroscópica. Por tanto, ser capaces de visualizar la anatomía evolutiva de la cicatriz post-IAM mediante RM-RTG equivale a poder analizar el efecto histológico directo de los mecanismos reparativos (mediados por el sistema inmune) sobre el tejido dañado.

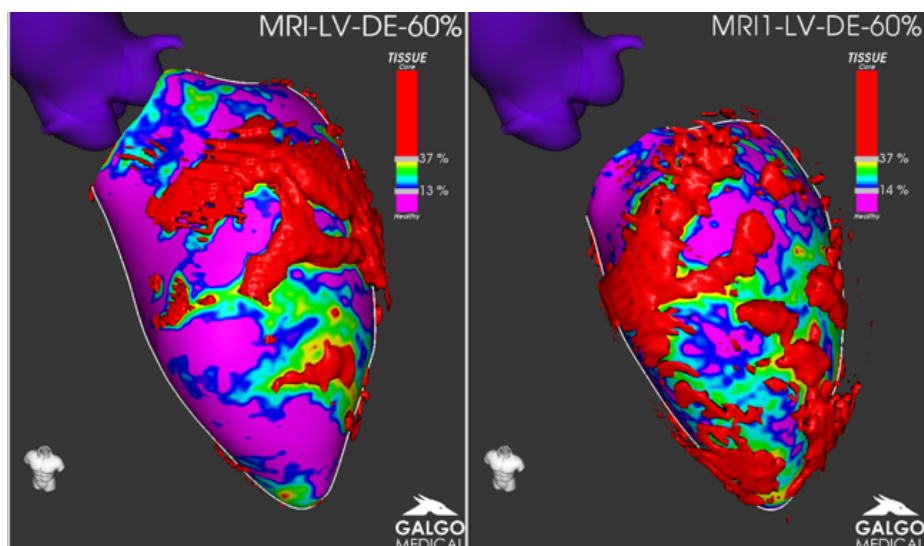


Figura 23. Mapas de PSI a partir de RM-RTG seriadas, separadas en el tiempo 4 años, en un paciente diagnosticado de miocardiopatía dilatada NO isquémica de origen genético. El paciente no había tenido AV documentadas, y su FEVI estaba moderadamente deprimida, sin indicación para DAI en prevención primaria. Nótese visualmente cómo, a diferencia de lo que se demuestra en el artículo 1 de la Tesis (301) para pacientes con CI, la progresión de la fibrosis macroscópica, evaluada mediante RTG, es hacia su aumento, afectando progresivamente a una mayor masa del VI. Figura original.

### b.1 Cambios histológicos tras la isquemia y formación de la cicatriz post-IAM

La información que disponemos sobre los procesos celulares e histológicos que ocurren tras un IAM se basa fundamentalmente en modelos experimentales con animales. Durante los primeros días y semanas tras el evento isquémico agudo, los miocitos muertos son reemplazados gradualmente por una cicatriz de colágeno. Esta progresión de la cicatrización de la "lesión miocárdica" es un proceso dinámico que generalmente se divide en 3 etapas: i) inflamación/necrosis, ii) fibrosis/proliferación y iii) remodelación/maduración a largo plazo. (302-305)

La fase inflamatoria ocurre durante los primeros días en animales pequeños y la primera semana o más en animales más grandes y en humanos. (306-309) Varias células inflamatorias, incluidos neutrófilos, monocitos/macrófagos y linfocitos, invaden el área

isquémica ya en las primeras horas después del evento coronario agudo, alcanzando su concentración máxima varios días después. (308,309) Estas células juegan un papel central en el proceso de cicatrización, estando involucradas en tareas de señalización celular, funciones de remodelación, proteólisis y fagocitosis. (310) El artículo 2 de la presente Tesis (311) describe la cinética de las distintas subpoblaciones de monocitos circulantes (CLM, non-CLM e INTM) en el proceso de formación de la cicatriz post-IAM, complementando la relativa ausencia de datos al respecto en el ser humano. (312-316)

La remodelación estructural del área isquémica se inicia cuando las células inflamatorias y los miocitos necróticos secretan y activan las metaloproteinasas de la matriz (MMPs) (figura 24). (317-319) Estas enzimas degradan el material de la matriz y las células que ayudan a los macrófagos fagocíticos en la reabsorción del tejido necrótico. Una proporción de los macrófagos, la que no incluye los macrófagos residentes tisulares, proceden de la diferenciación de los monocitos séricos, una vez han penetrado en el tejido dañado. (320) En el artículo 2 de la Tesis (311) se analizó la relación entre las distintas subpoblaciones monocitarias y los niveles de ciertos biomarcadores séricos, incluyendo las MMPs (MMP-1, 2 y 9), relacionadas con la degradación de la matriz extracelular, pero también otras moléculas como las interleukinas 6 (IL-6) y 1 $\beta$  (IL-1 $\beta$ ), relacionadas con la inflamación; el factor de necrosis tumoral  $\alpha$  (TNF- $\alpha$ ), relacionado con la apoptosis celular; el inhibidor tisular de las MMPs (TIMP) y la proteína C reactiva (CRP), relacionada también con la inflamación.



En relación a la fase inflamatoria inicial, si bien la nueva acumulación de colágeno no es evidente en los primeros días, a medida que los miocitos necróticos se reabsorben, se deposita en su lugar un tejido de granulación provisional que consiste en fibrina, fibronectina, laminina, glicosaminoglicanos y nueva matriz. (306,317,321) En el artículo 2 de la Tesis, (311) el hecho de disponer del análisis anatómico de la cicatriz a los 7 días del IAM mediante post-procesado de las imágenes de RM permitió evaluar las características visibles de esta fase inflamatoria, poniendo en relación el posible papel de la expresión diferencial de las subpoblaciones monocitarias con las características del tejido cicatricial en la RM.

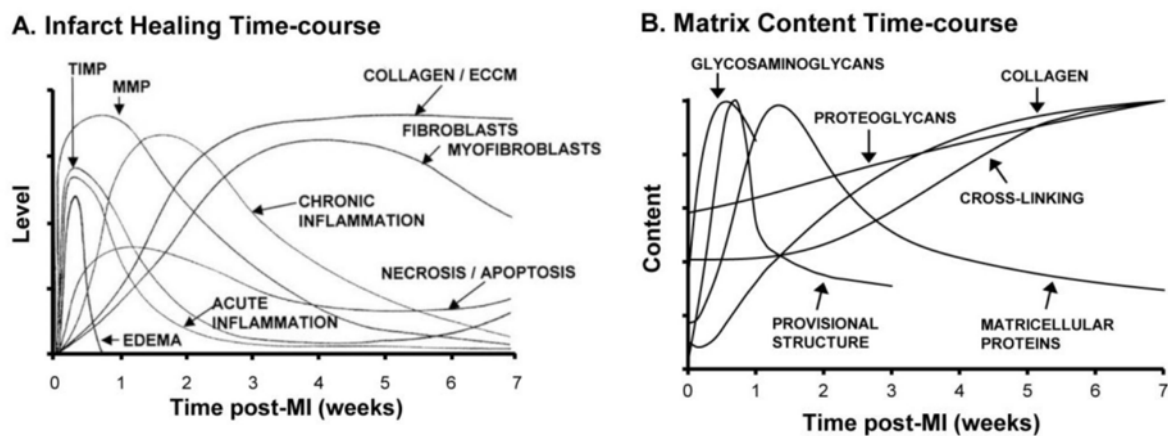


Figura 24. Eventos moleculares y celulares clave que intervienen en la formación de la cicatriz post-IAM (panel A) y proceso de maduración de la matriz extracelular de colágeno (panel B). De Richardson et al. (305)

En la fase de fibrosis, que suele durar varias semanas, (306–309) comienza una proliferación y migración de fibroblastos, que son las células más abundantes del corazón sano, (304,322) hacia la zona isquémica, donde se produce su diferenciación celular hacia miofibroblastos. Estos miofibroblastos, que también surgen por diferenciación de otras

células aparte de los fibroblastos, como células madre del corazón, pericitos, células de músculo liso vascular y células endoteliales, (322-324) se caracterizan por una elevada expresión de  $\alpha$ -actina, (323) una proteína que interviene en la función contráctil de los sarcómeros. Justo cuando comienza la proliferación de miofibroblastos, la concentración de MMPs empieza su descenso por activación del TIMP (figura 24). En el artículo 2 de la Tesis (311) se recoge precisamente el aumento progresivo de los niveles de TIMP ya durante la fase inflamatoria, que es lo que provocará el descenso progresivo de la concentración de MMPs. Los miofibroblastos expresan (y secretan, hacia la matriz extracelular) pro-colágeno (principalmente de los tipos I y III, aunque también IV y VI), alcanzando el pico máximo de expresión de estas moléculas hacia la semana post-IAM. (325-331) Esta expresión de pro-colágeno provoca a su vez aumentos de hasta 10 veces en el contenido de colágeno miocárdico, que se estabiliza varias semanas a meses después del IAM. (304,326,332-337)

Por último, la fase de remodelación, que dura varias semanas en animales pequeños y meses en animales grandes y humanos, (306-309) consiste en la "estabilización" del nuevo colágeno de la matriz extracelular, por un fenómeno denominado de "*cross-linking*" entre las fibras y por la unión de las fibras de colágeno a proteoglicanos (figura 24). (302,322,331,337-343) En el artículo 2 de la Tesis, (311) se escogió como momento temporal para realizar la segunda RM seriada 6 meses después del evento coronario, con la intención de reflejar precisamente los cambios histológicos ocurridos durante las fases de fibrosis y remodelado de la cicatriz, un aspecto novedoso y que pone en íntima relación el trabajo con el artículo 1 de la Tesis, (301) tal y como se abordará en el siguiente apartado.

Los niveles de monocitos clásicos e intermedios (CLM e INTM), como se ha demostrado en la Tesis, se correlacionan de manera positiva, sobre todo en los primeros 3 días después del IAM, con los niveles de IL-6, TNF- $\alpha$ , and CRP, moléculas de señalización paracrina que intervienen directamente en la inflamación. La cinética y los niveles de monocitos no clásicos (non-CLM) se correlacionaron con los niveles de MMPs, en relación a los procesos de degradación de la matriz extracelular.

Finalmente, no debemos olvidar que, en comparación con los modelos animales clásicos de IAM no reperfundido, estudios más recientes han modificado este modelo hacia uno basado en la isquemia-reperfusión. Gracias a la aparición de las estrategias de perfusión temprana (angioplastia coronaria), este tipo de modelo experimental es mucho más semejante a lo que ocurre en el ser humano hoy en día, como la población incluida en el artículo 2 de la Tesis. (311) Gracias a estos modelos de isquemia-reperfusión, se ha demostrado que la perfusión temprana acelera la reabsorción de tejido necrótico, aumenta la cantidad de células inflamatorias, aumenta la cantidad de vasos sanguíneos y disminuye la cantidad de miofibroblastos dentro de la herida, (344,345) presumiblemente por aumento del flujo sanguíneo en la zona reperfundida. Estructuralmente, estos cambios provocan la supervivencia de un mayor número de miocardiocitos y una menor densidad de colágeno en el área infartada, así como una menor densidad de enlaces cruzados (*cross-linking*) dentro de la matriz de colágeno. (346) Faltaría por demostrar, pues, si una perfusión más temprana se podría relacionar con posibles diferencias en la respuesta inmune (p. ej., en la expresión diferencial de unas subpoblaciones monocitarias u otras) a

la injuria miocárdica, y si esto puede tener un papel en la modificación ulterior de las características histológicas (“más o menos arritmogénicas”) de la cicatriz.

## **b.2 Papel de la Resonancia Magnética en la evaluación de los cambios histológicos post-IAM e implicaciones clínicas**

Inmediatamente después del IAM se ponen en marcha una serie de procesos biológicos con implicación directa del sistema inmune, tal y como se ha analizado en el artículo 2 de esta Tesis, (311) que van a influir en la reparación tisular de la zona dañada. La dificultad del estudio de estos procesos en el ser humano estriba en la dificultad de obtener muestras biológicas autópsicas en distintos momentos tras el IAM, aparte de la imposibilidad obvia de comparar muestras histológicas de un mismo sujeto en distintos momentos evolutivos. Aquí es donde la RM va a jugar el papel fundamental de permitir analizar estos cambios de manera no invasiva.

El artículo 1 de la Tesis (301) viene a indagar precisamente en la capacidad de la RM, como técnica diagnóstica no invasiva, de detectar los cambios evolutivos de la cicatriz isquémica en el ser humano. Además de confirmar la capacidad de la RM para detectar estos cambios, el artículo 1 (301) supone la primera evidencia descrita en la literatura que confirma que el proceso de remodelado del tejido cicatricial no cesa en los primeros meses tras el evento isquémico agudo, sino que continúa ocurriendo a lo largo de mucho más tiempo, como se comprueba al comparar RM realizadas 4 años después del IAM con las realizadas al cabo de una semana y a los 6 meses. En este punto, merece la pena recordar que, debido a la

aparición de edema lesional, es conocido que la RM-RTG podría sobreestimar el tamaño del infarto en las fases iniciales de cicatrización. (347) De hecho, el área con RTG puede aumentar en las primeras 48 h después del IAM y luego disminuir durante un período de hasta 8 semanas, hallazgos ambos correlacionados con los cambios en el tamaño del infarto durante el mismo periodo. (348,349) Paralelamente, existe evidencia de que, en el ser humano, se observa una reducción progresiva del tamaño del infarto durante los primeros 3 meses después del evento isquémico agudo, (350) habiendo sido atribuido este hecho a la resolución del edema. Por el contrario, otros estudios (351) han indicado que el tamaño del infarto continúa disminuyendo leve, pero significativamente, durante el primer año. En consecuencia, los cambios crónicos a largo plazo observados en el estudio FOOTPRINT (primer artículo de la Tesis) (301) no pueden ser explicados sólo por la supuesta reabsorción del edema, sino que van en la línea de investigaciones previas (351) y respaldan la existencia de un proceso continuo y constante de remodelado de las cicatrices isquémicas que dura años.

La metodología de post-procesado de las imágenes de RM utilizada en el artículo 1 de la Tesis (301) y sucesivos (311,352-354) merece un comentario para justificar la manera en la que se ha llevado a cabo la caracterización tisular y cuantificación de los componentes de la cicatriz post-IAM a lo largo de la Tesis. Al fin y al cabo, del correcto y preciso análisis de las imágenes dependen las conclusiones que se extraigan posteriormente. En todos los artículos, se utilizó el software de post-procesamiento ADAS3D LV (ADAS3D Medical SL, Barcelona), desarrollado con la colaboración del Hospital Clínic y comercialmente disponible. Cuenta actualmente con marcado CE (*Conformité Européenne*, de la Unión

Europea), aprobación por la FDA (*Food and Drug Administration*, de los EEUU) y dispone de un algoritmo patentado para la detección automática de HTC/BZC (*US Patent 10,304,185* y *European Patent EP2950270B1.2015*). Con este software, el único paso estrictamente manual del post-procesamiento de las imágenes es la delimitación de los bordes endocárdico y epicárdico del VI, una tarea sencilla que puede ser aprendida rápidamente tras unos pocos casos procesados. Posteriormente, el software elabora automáticamente los mapas 3D de PSI, mostrándolos en distintas capas, todas ellas codificadas en colores (configurables por el usuario, pero habitualmente referidas como las capas del 10%, 20%, 30%, 40%, 50%, 60%, 70%, 80% y 90% del espesor miocárdico total, desde endocardio hacia epicardio) (figura 25). Para la elaboración de los mapas PSI, como ya se ha comentado, se eligen automáticamente los umbrales de PSI correspondientes al 40% ( $\pm 5\%$ ) y 60% ( $\pm 5\%$ ) de la MSI, pues previamente han demostrado ser los que mejor correlacionan los componentes de la cicatriz (core y BZ) con las zonas de bajo voltaje ( $< 0,5$  mV y entre 0,5 y 1,5 mV, respectivamente) identificables en los EAM. (220) En este punto, merece la pena recordar sin embargo que, hasta la fecha, la única validación histológica los mapas EAM para la detección de cicatrices surge de modelos de IM en animales, (355) por lo que los EAM no deberían ser considerados "gold standard" en la identificación de la cicatriz post-IM.

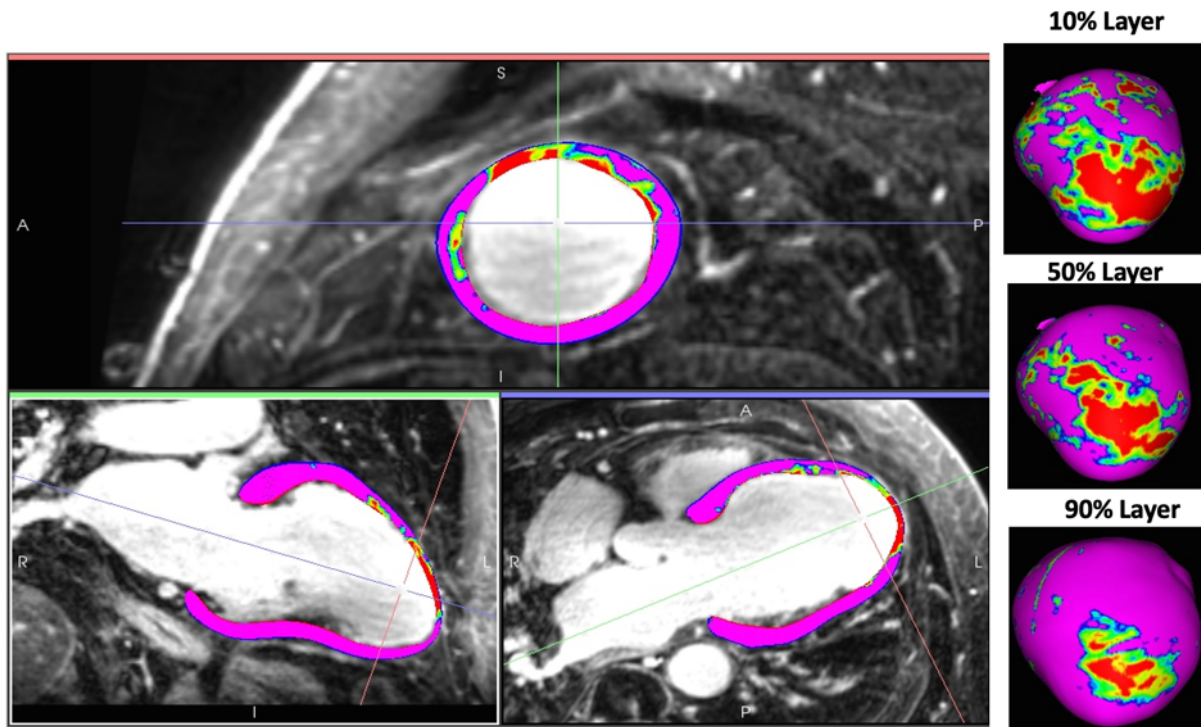


*Figura 25. Identificación del miocardio sano (púrpura) y los componentes de la cicatriz (rojo, core; amarillo-verde, BZ) mediante análisis automático de las intensidades de señal de píxeles (PSI) y utilización de los puntos de corte de  $40 \pm 5\%$  y  $60 \pm 5\%$  respecto a la máxima intensidad de señal (MSI). A la derecha, reconstrucciones 3D de los mapas PSI para las capas del 10% (subendocardio), 50% (medio-miocardio) y 90% (subepicardio). Se utilizó el software ADAS3D LV (ADAS 3D Medical, Barcelona) en todos los artículos de la Tesis. Figura original.*

Además de la identificación automática de los componentes principales de la cicatriz (core y BZ), la utilización del software ADAS3D nos ha permitido cuantificar, de una manera completamente automatizada, la masa de BZC (figura 26). Esto ha sido de especial relevancia para los artículos 1 (301) y 3 (354) de la presente Tesis. El artículo 1 (301) no sólo demuestra que el remodelado de la cicatriz ocurre a mucho más largo plazo de lo que previamente se creía, sino que este trabajo describe además, por primera vez, un cambio sustancial a largo plazo en la morfología y distribución de los BZC, así como una disminución progresiva y generalizada en la masa de estos canales (figura 27). La significación de este hecho permanece incierta al no haber documentado eventos arrítmicos durante el seguimiento de los pacientes incluidos en el estudio, pero abre la hipótesis sobre si estos cambios a largo plazo en el sustrato arritmogénico subyacente

podrían tener que ver con el hecho de que las AV por reentrada suelen ocurrir en muchos casos años después del evento isquémico. En este sentido, ha sido descrita una media de tiempo desde el IAM hasta la arritmia de  $16 \pm 8$  años. (283) La ausencia de eventos arrítmicos en la población de los artículos 1 y 2 de la Tesis (301,311) durante el período de seguimiento podría reflejar la relativamente baja incidencia acumulada de MSC en los primeros 5 años después de un IAM según estudios clásicos (cohorte Framingham), (56) y que aún se esperaría que fuera menor en poblaciones modernas, donde se dispone de la posibilidad de tratamiento mediante revascularización coronaria precoz.

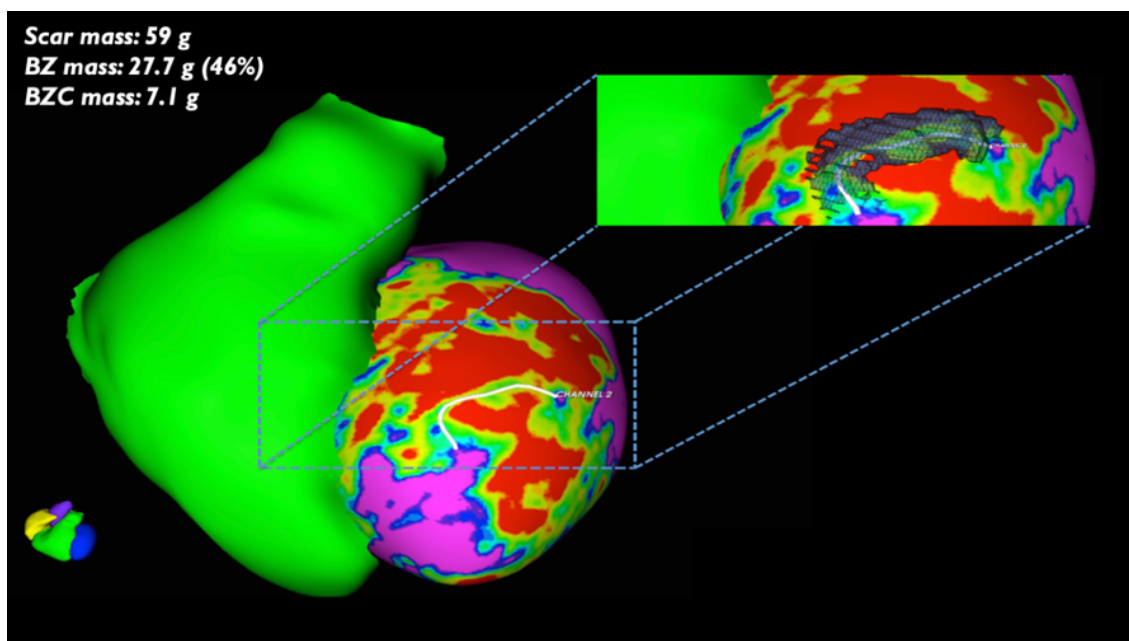


Figura 26. Ejemplo de un paciente con antecedentes de IAM anterior y TVMS por reentrada en relación a la cicatriz. La RM post-procesada muestra la presencia de una gran cicatriz (59 g), con abundante presencia de tejido heterogéneo (27,7 g de BZ) y un gran BZC de 7,1 g (línea blanca), responsable del circuito de reentrada. Rojo: core; verde-amarillo: BZ; púrpura: miocardio sano; malla azul: volumen calculado para el BZC; cámara verde: ventrículo derecho. Figura original.



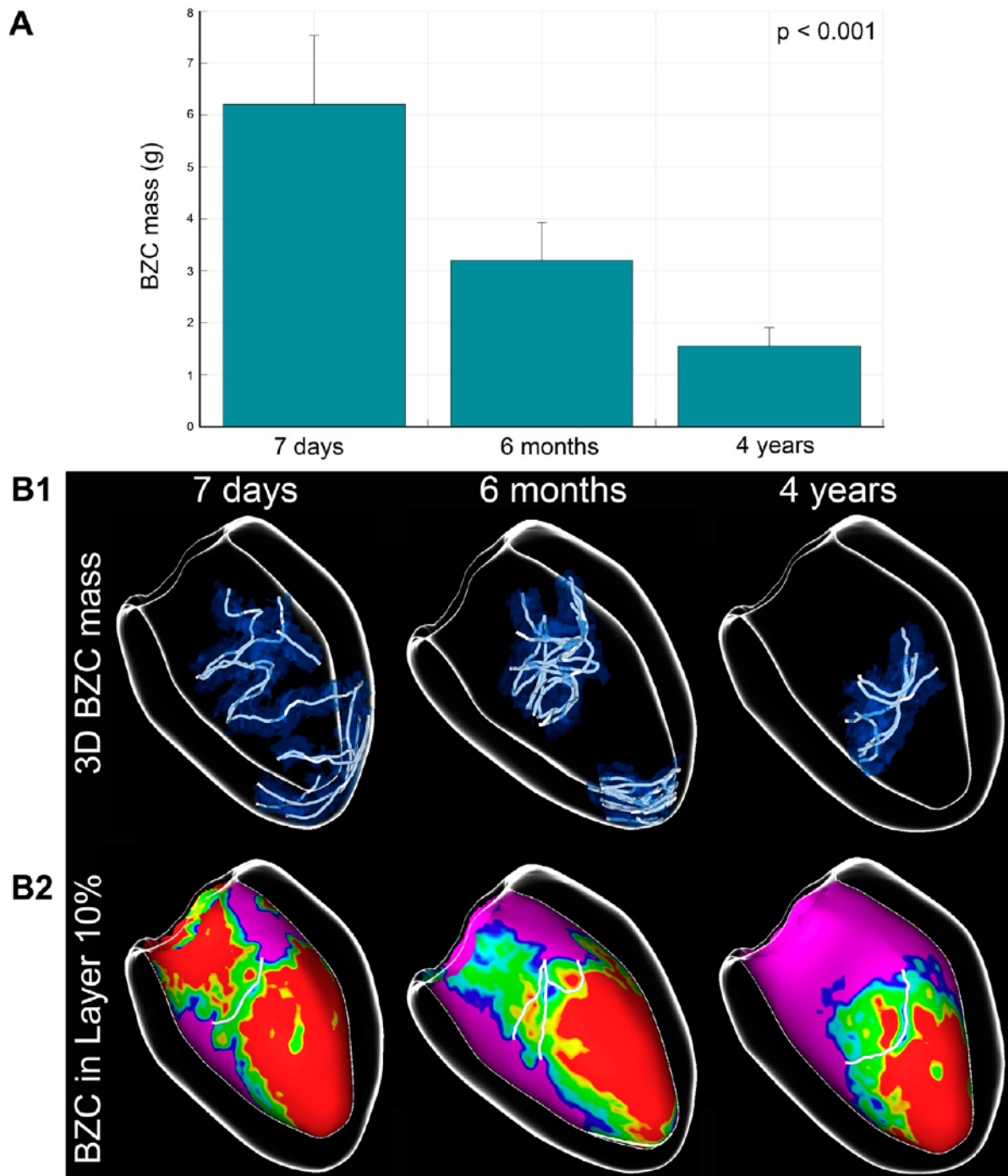


Figura 27. Disminución progresiva y generalizada en la masa de BZC tras un IAM (panel A). Panel B1) Reconstrucción 3D que muestra la evolución temporal en el número y distribución de los BZC en todas las capas del miocardio, en un paciente con IAM anterior. Panel B2) Mismo paciente, mostrando en detalle los componentes de la cicatriz y BZC sólo a nivel subendocárdico (capa del 10%). La desaparición de la zona más basal de core provoca un aparente “desplazamiento” apical de los BZC subendocárdicos (líneas blancas del panel B2). Este mismo comportamiento (reducción drástica de la zona de core y BZ) ocurre también a nivel medio-miocárdico y subepicárdico, lo que explica los hallazgos mostrados en el panel B1. De Jáuregui et al. (301)

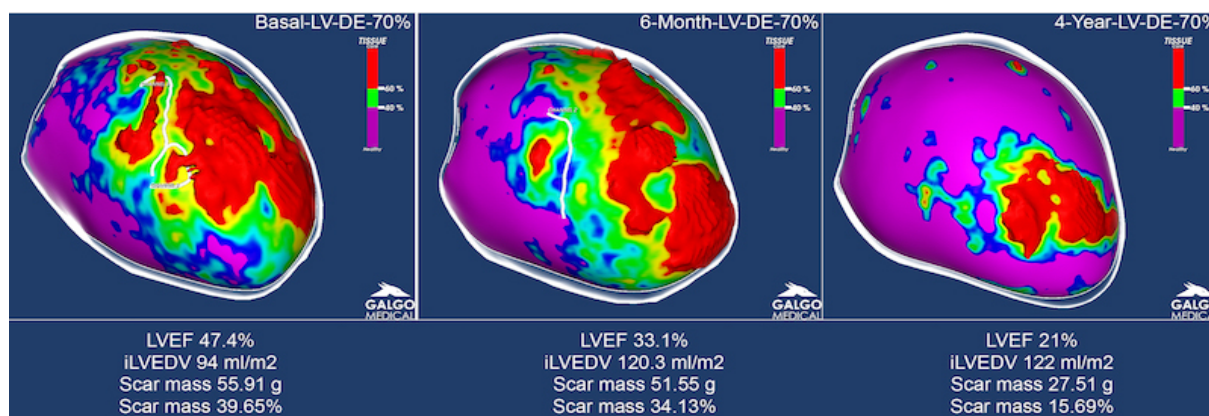


Figura 28. Paciente con IAM anterior. De izquierda a derecha, mapas de PSI a partir RM seriadas a los 7 días, 6 meses y 4 años del evento isquémico. Se muestra la capa del 70% del miocardio (intramiocárdica). Cualitativa y cuantitativamente, se aprecia una disminución progresiva de la masa total de cicatriz. A los 4 años, desaparece un BZC (línea blanca) por desaparición del área de BZ (verde-amarillo) del borde septal de la cicatriz. Persiste una zona cicatricial con predominio de core (rojo) en el extremo más apical de la cicatriz original. Nótese que, a pesar de una disminución de la masa de cicatriz, el VI sufre un remodelado adverso “paradójico”, con aumento progresivo del volumen telediastólico y caída de la FEVI. De acuerdo a las guías de práctica clínica, el paciente se remitió para implante de DAI en prevención primaria. Figura original.

Por otra parte, en el artículo 1 de la Tesis, (301) pasados 4 años del IAM hasta un 31% de los pacientes tenían cicatrices de un tamaño considerable (> 10 g de masa total) y con presencia de BZC. Aunque no pueden extraerse más conclusiones sobre este hecho al no haber documentado AV clínicas, merece la pena recordar en este punto que, en el estudio GAUDI-CRT, (356) la presencia de cicatriz > 10 g y BZC demostró predecir con un 100% de sensibilidad, 64,6% de especificidad y 24,5% de valor predictivo positivo la aparición de AV en pacientes isquémicos, en este caso candidatos a implante de dispositivo de resincronización cardiaca.

Como ya se mencionó en la Introducción de esta Tesis, la aparición de un IAM va a provocar, y esto sí es ampliamente conocido en la literatura, un proceso de remodelado del VI (incluido el miocardio remoto a la zona de la cicatriz) que, en algunos casos, podrá ser causa de IC (figura 28). De hecho, otros trabajos previos (357) han descrito la utilidad de la

medición de la fibrosis difusa en el miocardio remoto a la cicatriz post-IAM, como parte de ese remodelado del VI, medido con RM y puesto en relación con ciertos biomarcadores séricos, como la galectina-3. (357) Además, y como también se mencionó en la introducción, la RM es una técnica más precisa, en comparación con la ecocardiografía, para la evaluación de las dimensiones del VI y la FEVI. (161) En el artículo 2 de la Tesis (311) se encontró una fuerte asociación entre los niveles de monocitos CLM e INTM y el remodelado adverso del VI dentro de los 7 días posteriores al IAM, efecto que se mantuvo a los 6 meses. Este proceso de remodelado se evaluó, mediante la adquisición de imágenes de cine-RM, como un aumento de los diámetros telediastólico y telesistólico del VI junto con una disminución de la FEVI en esos 6 meses. No obstante, el efecto mecanístico no es posible demostrarlo con nuestro trabajo, pues, entre otros aspectos, resulta difícil establecer si el hecho de tener un IAM de mayores dimensiones es lo que condiciona una mayor concentración de estas subpoblaciones monocitarias y si, a su vez, esto es lo que provoca un peor remodelado; o si, por el contrario, es el aumento relativo de estas subpoblaciones el que condiciona verdaderamente dicho remodelado adverso.

En estudios experimentales previos en roedores, ya había sido descrita la correlación entre una mayor presencia de monocitos clásicos y el tamaño del IAM y sus componentes (core, BZ) (figura 29). (310,358) Por otra parte, y también en roedores, se ha investigado el efecto del tratamiento con determinados anticuerpos que interfieren en la infiltración tisular monocitaria, relacionándose esta menor infiltración con una disminución del tamaño de los infartos. (359) Los hallazgos de nuestro trabajo son, por tanto, generadores de hipótesis

para la realización de futuros estudios relacionados con este tema, y para el análisis de potenciales dianas terapéuticas anti-inflamación tras el IAM.

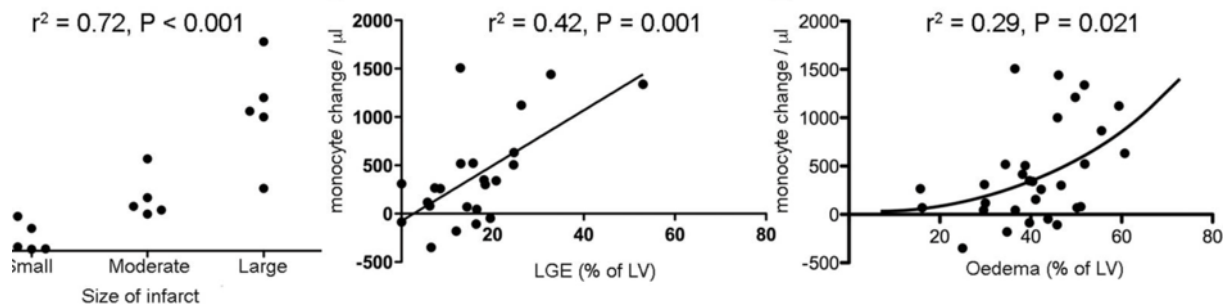


Figura 29. El grado de respuesta monocitaria depende del tamaño del IAM (panel de la izquierda, modelo en ratones) y se correlaciona con la cantidad de fibrosis (RTG en RM) a los 6 meses del mismo (panel central, modelo en humanos). Por el contrario, la correlación entre la respuesta monocitaria y la cantidad de edema en fase aguda (48 h) del IAM, medida mediante secuencias T2 de RM, es débil (panel de la derecha, modelo en humanos). Esto podría reflejar que la respuesta monocitaria está favorecida por la extensión de tejido que ha sufrido una lesión irreversible. LGE: late gadolinium enhancement; LV: left ventricle. De Ruparelia et al. (358)

Por otro lado, el artículo 2 de esta Tesis (311) demuestra, por primera vez en la literatura y al haber aplicado las técnicas de post-procesado de imágenes de RM para la caracterización de la cicatriz y cuantificación de sus componentes, una fuerte asociación entre los niveles de monocitos non-CLM y la masa de BZ en la cicatriz, así como entre éstos y la formación de BZC, el sustrato arritmogénico para el desarrollo de AV por reentrada. Estos resultados, nuevamente, abren la puerta a nuevos estudios que confirmen la causalidad de dicha asociación. En este sentido, es conocido que, en roedores, (360) los monocitos no clásicos promueven la diferenciación celular de los fibroblastos en miofibroblastos contráctiles y secretores de pro-colágeno; los miofibroblastos, además, pueden formar conexiones electrotónicas con los miocardiocitos del tejido sano circundante, contribuyendo potencialmente a la arritmogénesis. (360)

A modo de resumen, los dos primeros artículos de la Tesis abren preguntas clínicas no resueltas pero muy relevantes, como p. ej. ¿por qué la mayoría de AV relacionadas con la cicatriz (TVMS reentrantes) ocurren años después de un IAM? ¿Podrían influir los mecanismos reparadores/inmunes de los primeros momentos (fase aguda) tras el IAM en el curso evolutivo histológico de la cicatriz? ¿Podrían jugar un papel estos mecanismos en la aparición de AV a largo plazo en estos pacientes? Es más, ¿podrían desarrollarse nuevas estrategias terapéuticas que modificaran el curso evolutivo de la cicatriz y potencialmente previnieran la aparición de AV?

Por último, continuaría siendo una incógnita el conocer cuándo es el mejor momento evolutivo post-IAM para identificar y caracterizar el sustrato arritmogénico pues, como se ha demostrado, éste parece ser cambiante durante años. No obstante, en el artículo 1 (301) se demostró igualmente que la no identificación de BZC en las RM realizadas a los 7 días y 6 meses tras el IAM mostró un alto valor predictivo negativo (> 90% en ambos casos) para la ausencia de un sustrato arritmogénico a los 4 años. La RM, por tanto, podría ayudar a clasificar a los pacientes isquémicos con bajo riesgo arrítmico desde fases relativamente tempranas tras el evento coronario agudo, aunque harían falta más estudios al respecto que confirmaran esta hipótesis.

### **b.3 Evaluación del sustrato arritmogénico mediante otras técnicas de imagen: Comparación de la Tomografía Computarizada frente a la Resonancia Magnética**

Como ya se ha mencionado previamente, la RM tiene algunas limitaciones potenciales; p. ej. el hecho de ser una técnica no ampliamente disponible en algunos centros hospitalarios, la necesidad de contar con radiólogos y técnicos bien entrenados en la adquisición de imágenes cardíacas, la imposibilidad de completar los estudios en pacientes con severa claustrofobia, o la aparición de artefactos en relación a la presencia de dispositivos de estimulación cardíaca (marcapasos y DAI). Aunque se pueden adquirir imágenes de calidad óptima no sólo con máquinas de 3 Tesla, sino también con las de 1,5 Tesla, o se pueden utilizar secuencias de banda ancha (*wideband*) para eliminar o disminuir los artefactos de los dispositivos de estimulación, estos son algunos motivos por los que otros grupos de investigación han analizado el rol de la TAC, una técnica de imagen más accesible, para identificar y caracterizar el sustrato arritmogénico en CI. En este sentido, con el tercer artículo de la Tesis (352) pretendimos evaluar el comportamiento de la TAC respecto a la RM a la hora de evaluar el sustrato arritmogénico en pacientes con CI, con el objeto de valorar si lo que ya había sido estudiado en los artículos 1 y 2 (301,311) podía ser igualmente analizado con la TAC. Otras técnicas de medicina nuclear aplicadas a imagen cardíaca, como el SPECT y, en menor medida, el PET, han sido utilizadas también para predecir la recuperación funcional y el remodelado ventricular post-IAM, así como para determinar la presencia y extensión de la fibrosis miocárdica. El problema de estas técnicas, que sobrepasan los objetivos de esta Tesis, es su limitada resolución espacial (5-8 mm) en comparación con la TAC, en un rango mucho mayor que el que se precisa para la evaluación de los corredores de tejido heterogéneo.

La evaluación del espesor de la pared miocárdica mediante TAC ha surgido recientemente como un método alternativo de imagen cardíaca para identificar el sustrato arritmogénico en pacientes con CI. El IAM provoca una pérdida neta de tejido (por apoptosis celular) y su sustitución por fibrosis, esto es, acumulación de colágeno en la zona dañada. El resultado macroscópico es el adelgazamiento de la pared miocárdica, más o menos patente en función del tamaño del infarto. Basándose en los valores normales de grosor miocárdico del VI previamente descritos para población sana, (361) un grupo de investigación de Burdeos analizó (295) la relación entre las áreas de bajo voltaje identificadas en el EAM y las zonas de adelgazamiento significativo de la pared miocárdica, definido como  $< 5$  mm. Para poder hacer esto, los investigadores utilizaron un software de post-procesamiento que, de manera análoga a como se ha venido realizando en los artículos que componen esta Tesis, permitía crear reconstrucciones 3D del VI y codificar mediante colores la información obtenida, en este caso, el grosor de la pared por TAC (figura 30). Los autores detectaron que todas las LAVA estaban presentes en la zona de adelgazamiento significativo de la pared ( $< 5$  mm), o sólo hasta 23 mm fuera de su borde. (295) Además, las LAVA en el endocardio se encontraban principalmente zonas con grosor miocárdico de entre 3 y 5 mm, mientras que en el epicardio se encontraban en las zonas con adelgazamiento muy significativo ( $< 3$  mm).

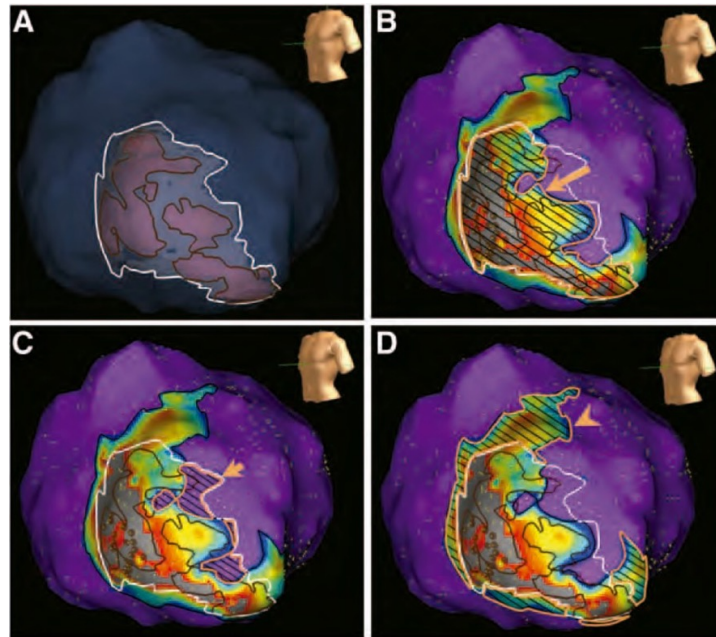


Figura 30. Comparación de las áreas adelgazamiento de la pared miocárdica y zonas de bajo voltaje en el EAM. A) Áreas de adelgazamiento con  $< 5$  mm (línea blanca) y  $< 3$  mm (línea marrón). B) Área de superposición (flecha larga) entre la zona de adelgazamiento con  $< 5$  mm y voltaje  $< 1,5$  mV. C) Área de adelgazamiento con  $< 5$  mm pero sin bajo voltaje (flecha corta). D) Zona con voltaje  $< 1,5$  mV pero sin adelgazamiento significativo (punta de flecha). Las regiones de LAVA (puntos marrones) se encuentran dentro de las áreas con grosor de pared  $< 5$  mm y  $< 3$  mm. De Komatsu et al. (295)

Gracias al análisis de las imágenes de TAC mediante mapas 3D de grosor miocárdico codificados en color, se pudieron identificar inhomogeneidades en dicho grosor, dentro de la zona afectada por la cicatriz post-IAM. Estas diferencias locales de grosor, que definiremos como "crestas" (*ridges*) en ocasiones originan canales-cresta delimitados por "valles" de tejido más adelgazado, y se han correlacionado con los istmos responsables de AV por reentrada (figura 31). (300,362) Histológicamente, estas crestas representan corredores de tejido miocárdico viable que, al tener una mayor celularidad respecto al entorno de cicatriz densa (*core*), origina un mayor grosor visible de pared.



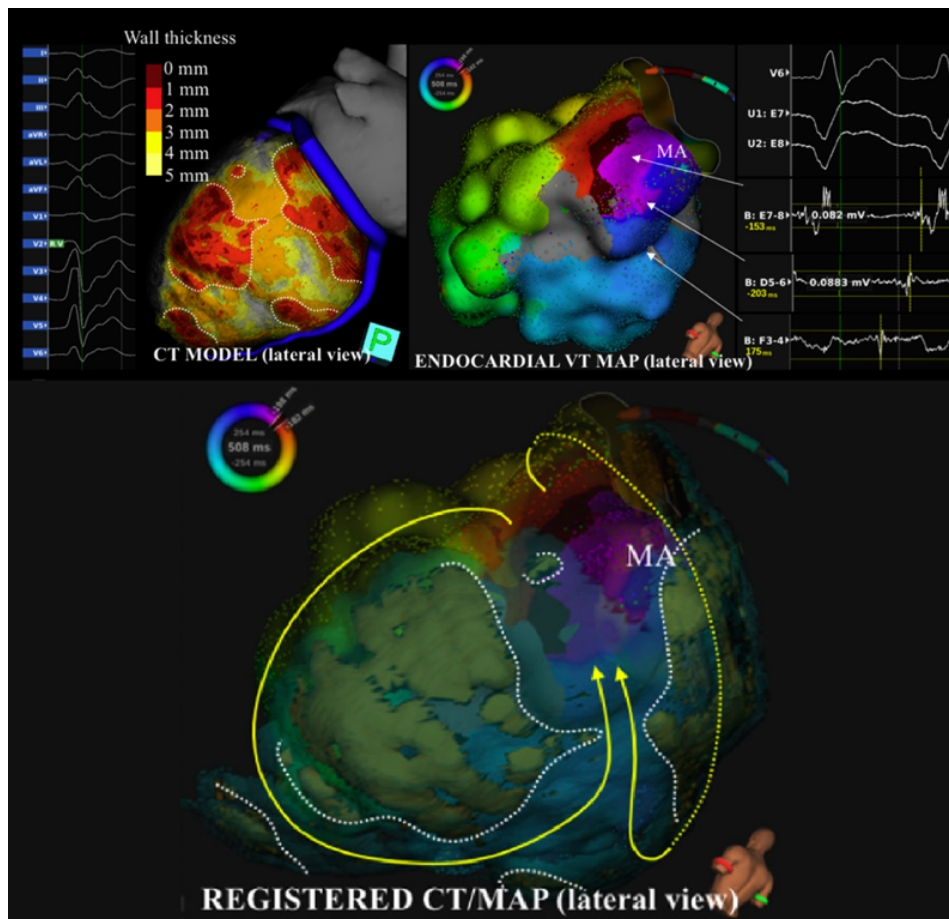


Figura 31. IAM inferolateral. Mapa de canales (ridges) de TAC (arriba a la izquierda) vs. EAM con mapa de activación de una TV (arriba a la derecha). Debajo se muestra la fusión entre ambos mapas. Un canal-ridge de TAC con grosor de 2-4 mm y rodeado por zonas de < 2 mm corresponde con el istmo del circuito de reentrada (obsérvese la activación diastólica en los 3 EGM mostrados arriba a la derecha). Modificado de Takigawa et al. (300)

El punto de partida para la realización del artículo 3 de la presente Tesis (352) fue el constatar la ausencia de una comparación real entre la TAC y la RM en pacientes con CI y sustrato arritmogénico verificado (es decir, pacientes que ya han tenido AV por reentrada en relación a la cicatriz post-IAM). Dado que existe evidencia que demuestra que, en IAM transmurales, la concordancia entre el mapa de adelgazamiento de la TAC (< 5 mm) y el área de bajo voltaje epicárdico en el EAM (< 1,5 mV) es peor que cuando se compara esta última con la zona de cicatriz identificada por RM (figura 32) (298) , planteamos un estudio comparativo entre ambas técnicas de imagen tomando como *gold standard* la RM.

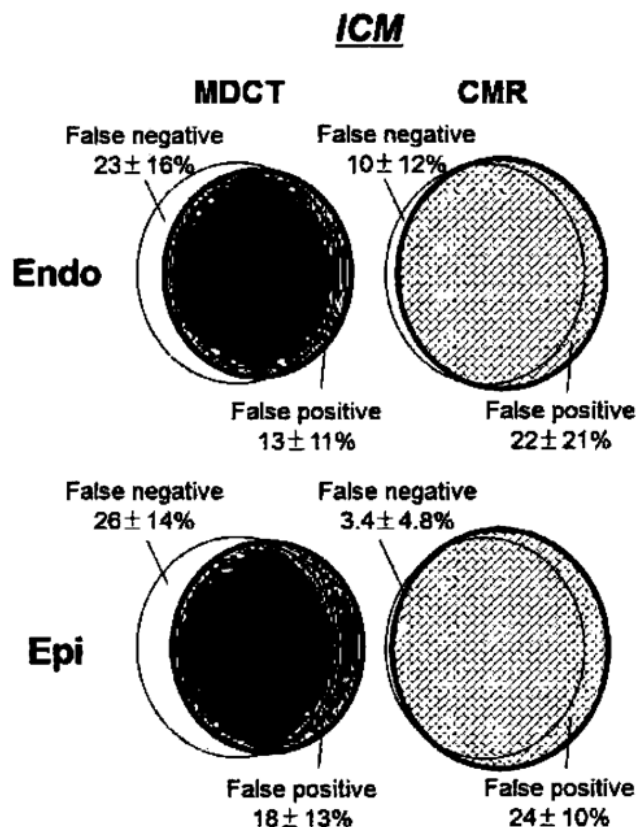


Figura 32. Correlación entre el área de sustrato estructural identificado por imagen (RM y TAC) y por mapeo de voltaje (EAM). La concordancia se muestra tanto para el endocardio como para el epicardio. Las áreas de falsos positivos y falsos negativos se expresan en % respecto al área del sustrato identificada por imagen. ICM: ischemic cardiomyopathy; MDCT: multidetector cardiac tomography; CMR: cardiac magnetic resonance. Modificado de Yamashita et al. (298)

En el tercer artículo de la Tesis (352) se demuestra que la TAC, comparada con la RM, no es capaz de detectar la presencia de sustrato arritmogénico en un porcentaje muy elevado de pacientes (más de un tercio) que tienen IAM no transmurales, sino subendocárdicos. La definición de transmuralidad por TAC se ha determinado clásicamente como la presencia de áreas de adelgazamiento con grosor < 5 mm de pared. (361) El análisis de la presencia de "crestas" miocárdicas en la cicatriz fue sólo moderadamente capaz (sensibilidad del 61,8%) de identificar los BZC que se identifican por RM. (352) Por otro lado, la sensibilidad de la TAC mejoró significativamente, aun siendo todavía modesta (72,2%), en casos de IAM

transmurales, debido a una menor tasa de falsos negativos. En cuanto a la identificación de las entradas de canal, un aspecto particularmente útil a la hora de plantear una ablación de sustrato mediante la técnica de *scar dechanneling*, (263,286,353) la TAC mostró baja sensibilidad (33,1%).

Anatómicamente, resultaría lógico esperar que las zonas de entrada de canal muestren una gradación de grosores miocárdicos mucho más "suave" que la que se va a encontrar en las zonas del interior del canal (el "istmo protegido" correspondiente al potencial circuito de reentrada de TV); las "crestas" y "valles" de tejido se suavizarían en los bordes de la cicatriz. Seguramente por este motivo, establecer umbrales de grosor que identifiquen zonas correspondientes a *ridge* en los extremos de unión de un corredor de miocardio viable con el miocardio sano resulte más difícil. En resumen, de alguna manera la TAC nos permite identificar un sustrato arritmogénico "simplificado" en comparación con la RM-RTG (figuras 33 y 34), siendo una técnica potencialmente útil como ayuda durante la realización de procedimientos de ablación (p. ej., para focalizar la zona de mapeo y ahorrar tiempo, e identificar el curso de las arterias coronarias en los procedimientos de ablación epicárdica), (295,298-300,362,363) pero que no debería reemplazar la información obtenida mediante una RM-RTG. Adelantándonos a lo que se discutirá posteriormente en relación al artículo 5 de la Tesis (353), la RM sí ha demostrado, además de identificar el sustrato arritmogénico con mayor precisión que la TAC, (352) ser capaz de identificar sustrato adicional comparado con los EAM endo-epicárdicos. (191,286) La RM permite, a diferencia de los EAM, identificar, representar y reconstruir los componentes de la cicatriz en todo su espesor 3D,

superando las limitaciones de la representación (incompleta) 2D de los circuitos de reentrada con los EAM. (248)

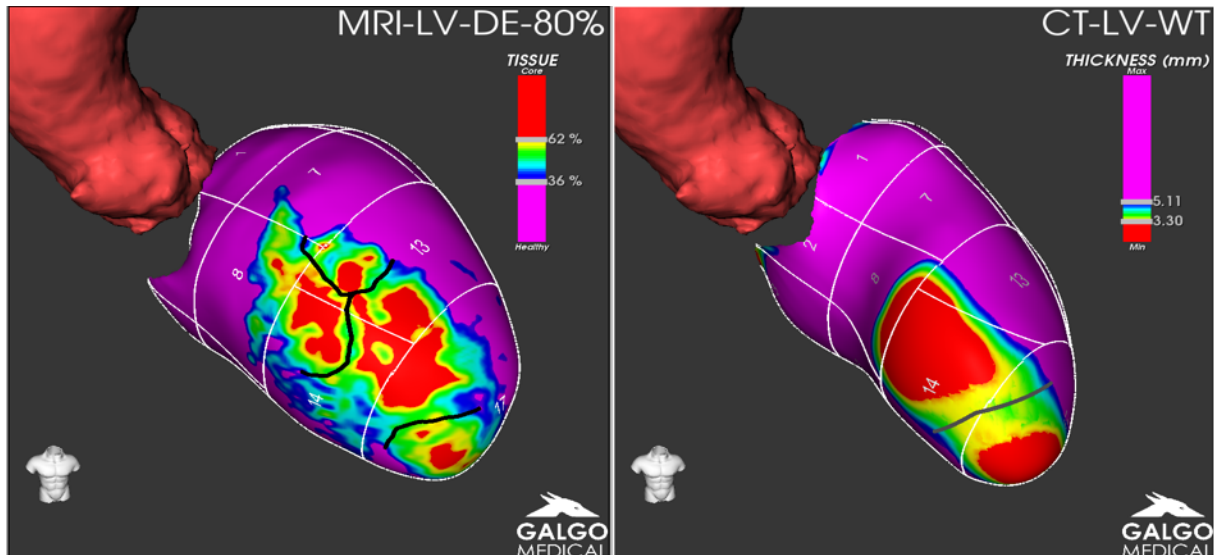


Figura 33. IAM anteroseptal transmural. Se muestra, a la izquierda, el mapa de PSI derivado de RM-RTG correspondiente a la capa del 80% del espesor miocárdico (subepicardio); en rojo se muestra el core, en amarillo-verde la BZ, en púrpura el miocardio sano, y las líneas negras corresponden a BZC identificados con el software ADAS3D. A la derecha, se muestra un mapa codificado en colores del grosor parietal por TAC. Los umbrales de grosor para los distintos colores se modifican manualmente para identificar los “ridges”, estableciendo como límite entre miocardio sano y zona cicatricial el corte de 5 mm. Nótese como la TAC identifica razonablemente bien la zona de cicatriz, pero sólo parcialmente el sustrato arritmogénico: detecta un corredor de tejido viable (BZC en RM, ridge en TAC) en el extremo más apical (línea gris), pero no es capaz de detectar otro corredor situado en la vertiente más basal de la cicatriz, que sí se visualiza con RM. Figura original.

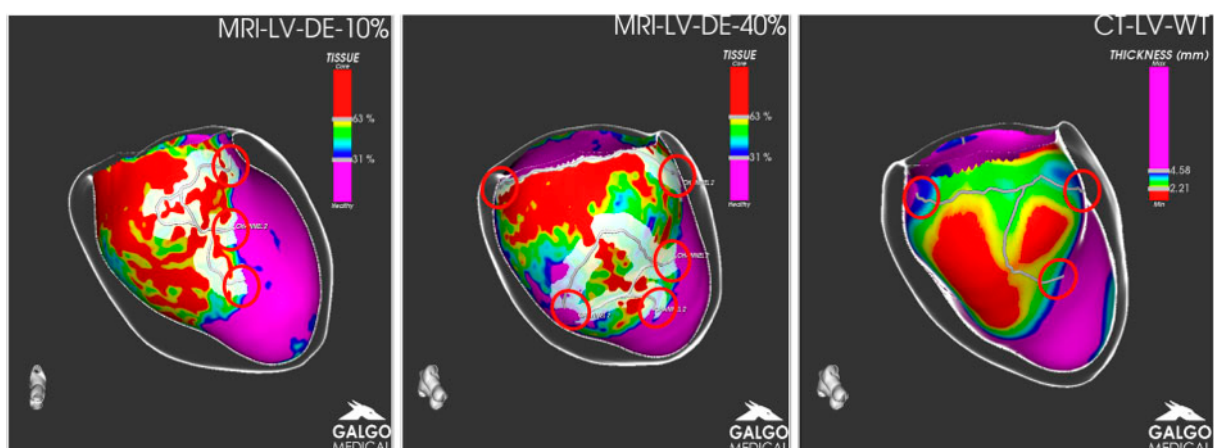


Figura 34. IAM inferoseptal. Detección de entradas de canales con RM y TAC. Panel izquierdo: BZC subendocárdico (en la capa miocárdica del 10%) identificado por RM (línea blanca), que muestra 3 entradas (círculos rojos). Panel medio: Capa del 40% del miocardio (medio-miocardio) por RM. Esta capa muestra varios BZC (uno de ellos, submitral) que realmente corresponden a ramificaciones del BZC anterior en el espesor de la cicatriz; estas ramificaciones aportan 2 entradas adicionales que conectan al canal con el miocardio sano. Panel derecho: mapa de grosor por TAC en el mismo paciente. La

*TAC reconoce muy bien la zona de cicatriz y la estructura simplificada del canal ramificado visible por RM, pero sólo identifica 3 de las 5 entradas del mismo. De Jáuregui et al. (352)*

A pesar de lo expuesto, la integración de la anatomía cardíaca reconstruida mediante post-procesado de las imágenes obtenidas con TAC durante los procedimientos de ablación no deja de ser útil, pues tiene un impacto en la seguridad y resultados del procedimiento (figuras 35 y 36). (298,299,364) Para pacientes con IAM transmural, la utilización de la TAC como técnica para identificación del sustrato puede ser útil, aunque mejor si se combina con la información de la RM. En conclusión, la RM debe ser considerada, la mejor herramienta de imagen para evaluar la presencia y evolución del sustrato arritmogénico, así como para planificar los procedimientos de ablación. La TAC permite contar con una reconstrucción 3D de alta resolución de las cámaras cardíacas y otras estructuras relevantes, siendo la combinación de ambas técnicas de imagen el "ideal" para la planificación de los procedimientos de ablación de sustrato de TV.

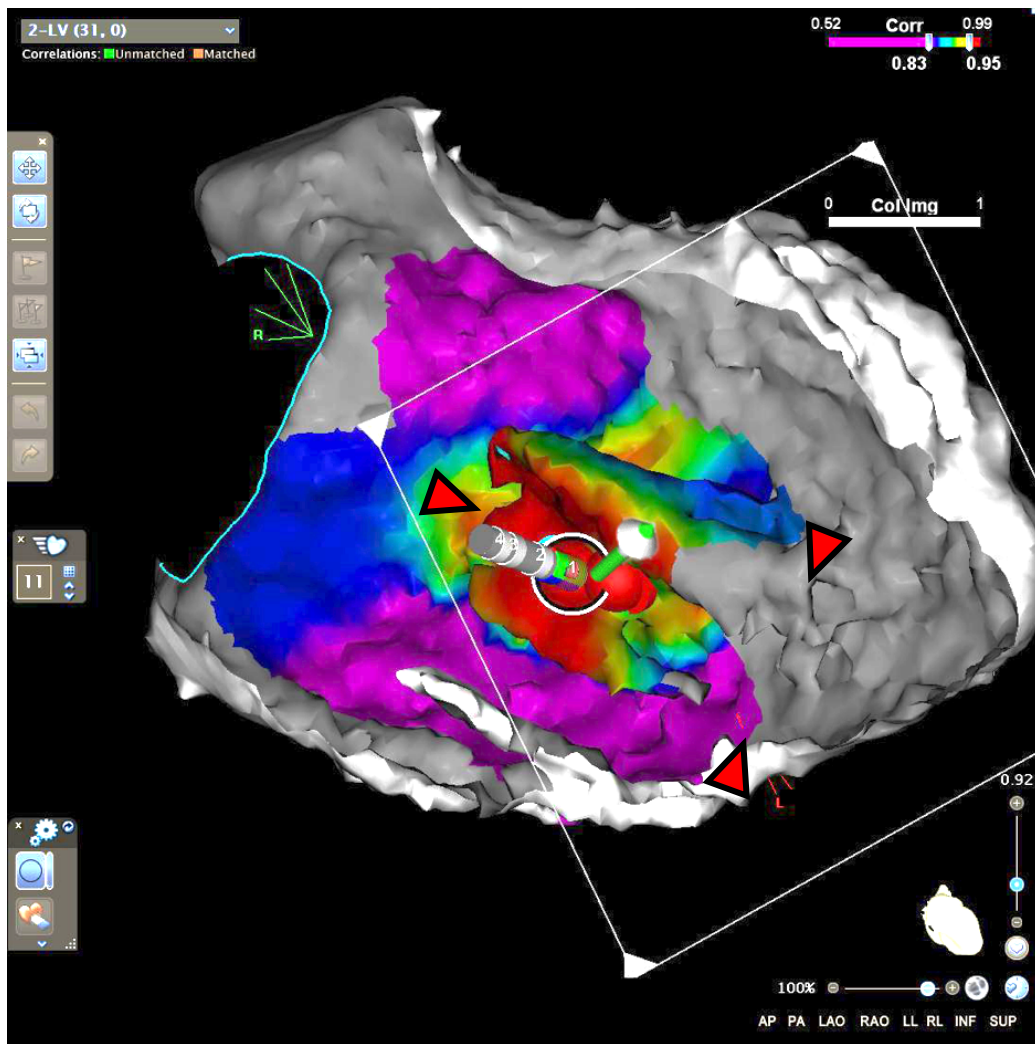


Figura 35. Paciente con antecedentes de IAM anterolateral y afectación del músculo papilar adyacente (estructura 3D con base y vértice delimitados por los triángulos rojos). El paciente presentaba extrasistolia ventricular monotópica de muy alta densidad (> 30% en Holter) relacionada con automatismo anormal en la zona de cicatriz del papilar. La TAC ayuda a delimitar con gran resolución espacial (0,5 mm) las estructuras cardiacas, ayudando a localizar la punta del catéter y a dirigir su apoyo (flecha verde) hacia el sitio diana de ablación. Figura original.

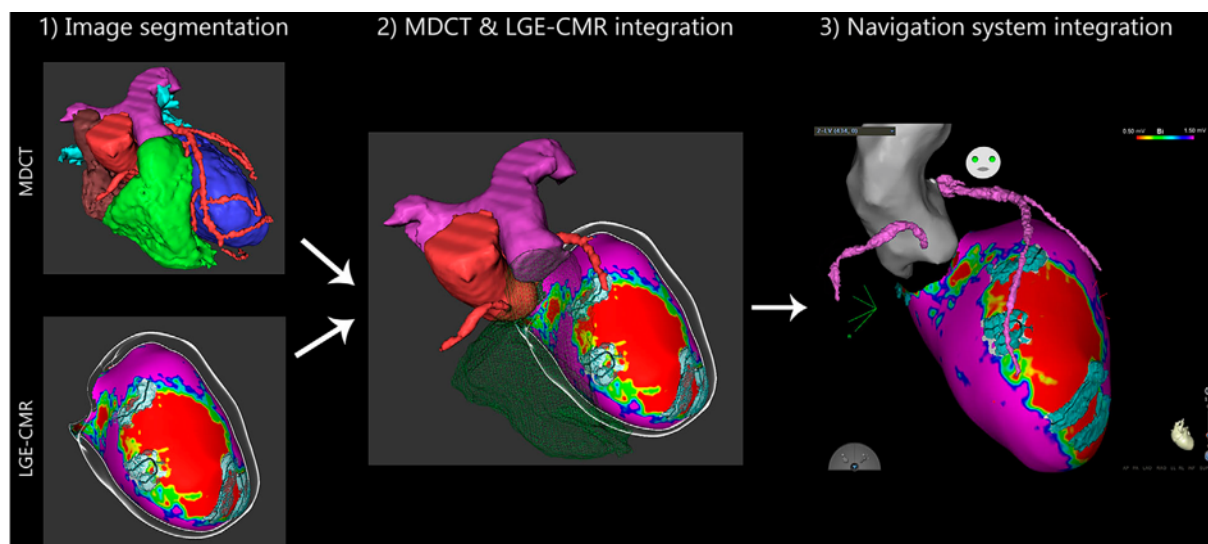


Figura 36. Integración multimodal de imágenes cardiacas para la planificación de procedimientos de ablación de sustrato de TV. A la izquierda y arriba, TAC previa al procedimiento; la alta resolución espacial permite identificar el trayecto de las arterias coronarias, un aspecto importante cuando se realiza ablación desde el epicardio, para evitar dañarlas al aplicar radiofrecuencia. En la parte inferior e izquierda, el mapa de PSI obtenido a partir de RM-RTG permite identificar una gran cicatriz anterior y 3 BZC (líneas negras). En el panel central, resultado de la fusión entre las estructuras anatómicas extraídas de la TAC y la RM. A la derecha, integración de esta información dentro de las coordenadas espaciales de referencia del sistema de navegación con el que se obtienen los EAM y se realiza la ablación. De Berruezo et al. (224)

### c. Utilidad de la Resonancia Magnética en la Estratificación del Riesgo Arrítmico en Cardiopatía Isquémica

El cuarto artículo de la Tesis (354) pretende abordar una de las cuestiones o dificultades más relevantes de la Cardiología actual, como es la estratificación del riesgo de AV y MSC en pacientes con CI. Tal y como se detalló en mayor profundidad en la Introducción, la FEVI no es un marcador de riesgo óptimo, ni en CI ni en miocardiopatías no isquémicas. (60,61,76-78) A pesar de ello, continúa siendo el criterio principal en el que se basan las recomendaciones actuales para determinar la indicación de implante de DAI en prevención primaria de MSC. Dicha indicación se establece hoy en día para pacientes con FEVI < 35%. (3,60-62)

El papel de la RM en la estratificación del riesgo arrítmico ha sido ya evaluado tanto para pacientes con CI como miocardiopatías no isquémicas. A pesar de que existe evidencia de la relación entre la presencia de RTG y una mayor incidencia de eventos arrítmicos (tabla 2), (164,193) y que la extensión y heterogeneidad de la cicatriz miocárdica parece ser un buen predictor de AV y mortalidad (tabla 3), (193) la RM aún no ha podido demostrar su capacidad para guiar de manera fidedigna la toma de decisiones clínicas. Ello es debido principalmente, además de a la baja disponibilidad de la técnica en algunos centros hospitalarios, a tres limitaciones importantes que discutiremos a continuación:

- i) desconocimiento sobre qué parámetro/s de la cicatriz derivados de la RM pueden ser más útiles para estratificar el riesgo;
- ii) falta de evidencia sobre el uso de herramientas de post-procesado de las imágenes de RM; y
- iii) ausencia de protocolos normalizados para su adquisición y validación histológica.

En relación al tercer punto, la ausencia de protocolos normalizados de adquisición, un trabajo previo de nuestro grupo de investigación (190) ya demostró que la obtención de imágenes con una secuencia de adquisición de eco de gradiente 3D ("3D-GRE") con libre respiración (ver apartado f.2 "*Secuencias de adquisición en Resonancia Magnética*" de la Introducción) es superior a las secuencias convencionales 2D para representar el sustrato arritmogénico (figura 37). La mejor resolución obtenida con las secuencias 3D permite revelar mejor la presencia de BZC y su estructura ramificada, (225) aunque también precisan mayores tiempos de adquisición y procesamiento. (190) Las secuencias 2D-GRE, a pesar de



su peor resolución, pueden ser una alternativa razonable debido a que necesitan menores tiempos de adquisición y procesamiento. En aquellos casos en los que el tiempo de adquisición con 3D-GRE e incluso 2D-GRE pudiera resultar problemático (p. ej., claustrofobia, pacientes con patología respiratoria), la secuencia 2D-SSFP (*steady-state-free-precession*) podría ser una opción útil, aunque la sensibilidad de esta secuencia es mucho más modesta. (190) En consecuencia, el análisis del sustrato con RM en todos los artículos de la presente Tesis se ha realizado empleando secuencias 3D-GRE, preferentemente, o 2D-GRE. Los aspectos más técnicos de las adquisiciones se han detallado convenientemente en cada uno de los artículos compilados en la Tesis.

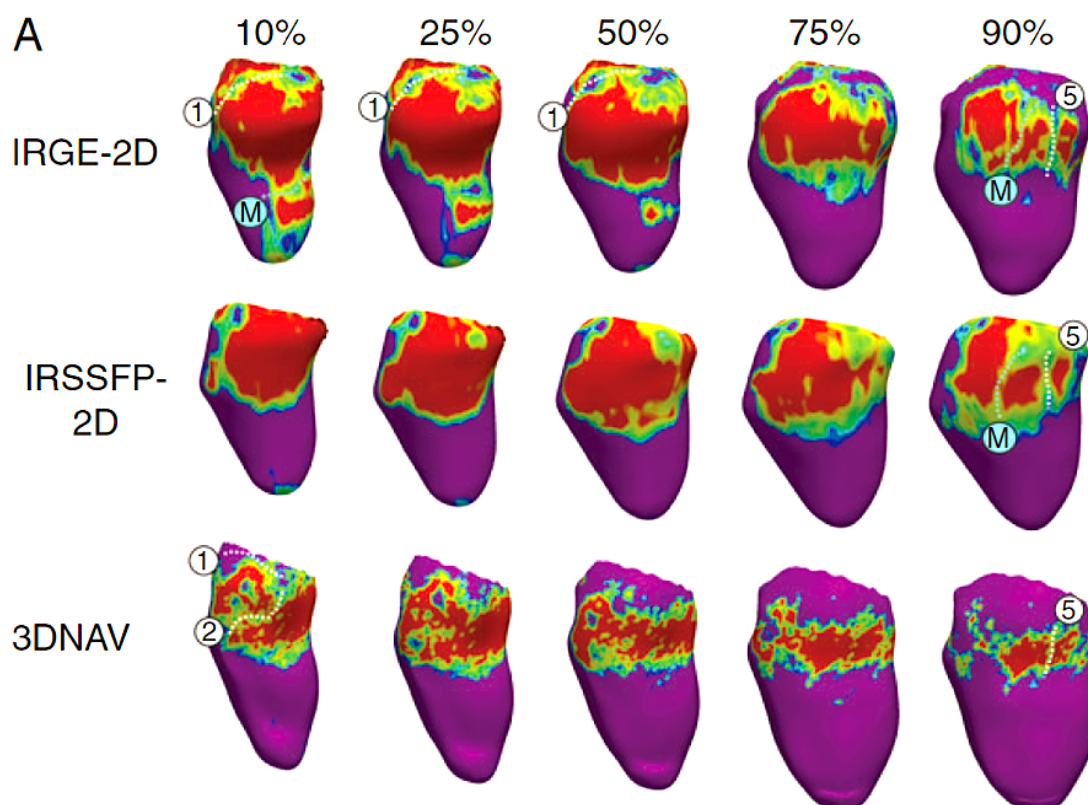
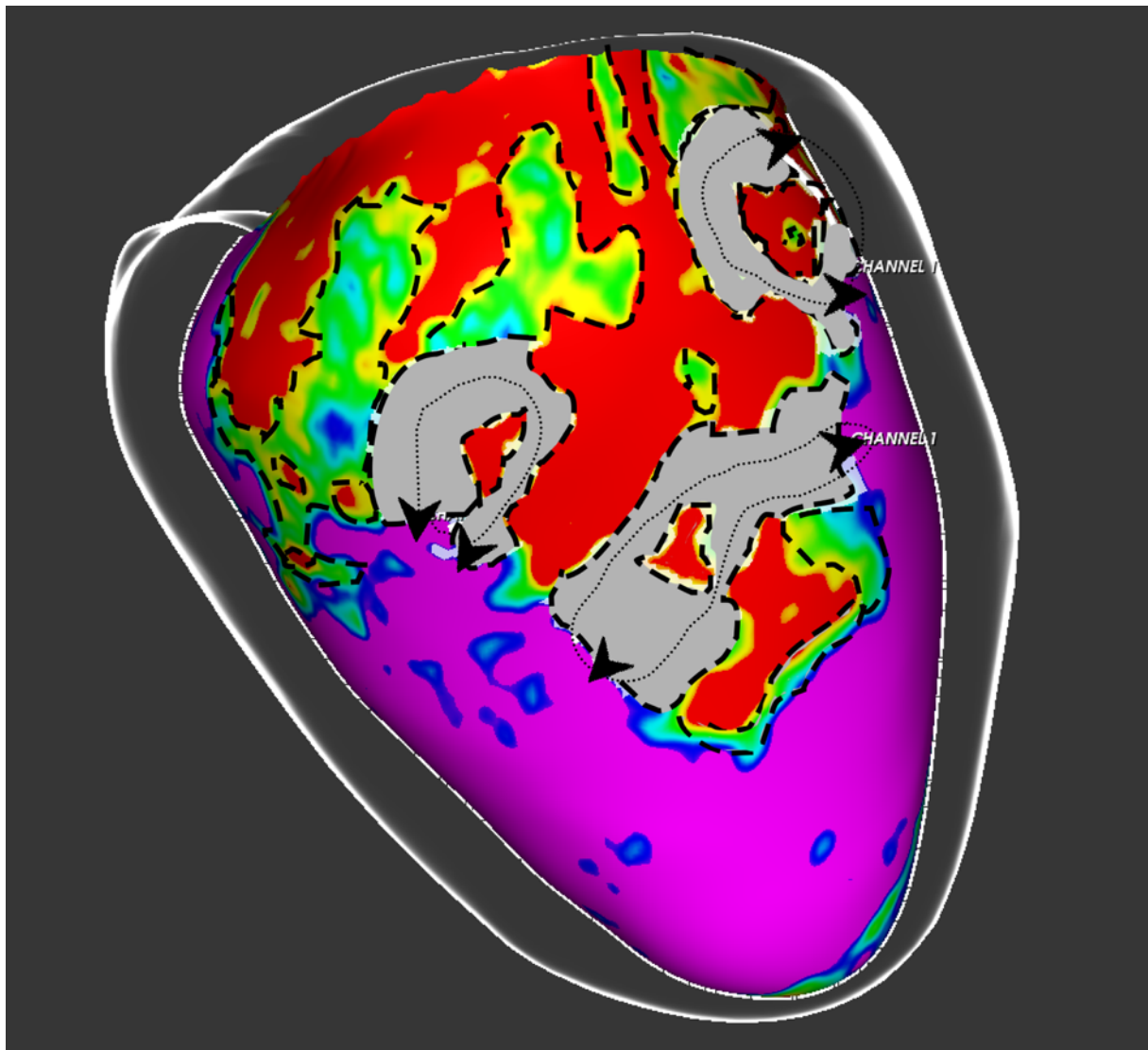


Figura 37. Paciente con IAM inferior transmural. Se muestran capas al 10%, 25%, 50%, 75% y 90% del espesor de la pared del VI. Todos los BZC (líneas de puntos blancos, números 1, 2 y 5) identificados en la reconstrucción 3D del VI utilizando la secuencia 3D-GRE (3DNAV) se habían observado en el EAM mediante análisis de EGM con componentes retrasados (es decir, los BZC correspondían a canales de conducción lenta). Con las otras secuencias 2D (IRGE-2D e IRSSFP-2D) sólo se identificaron parcialmente esos canales. Los canales “M” de las secuencias 2D no se observaron ni la 3D ni en el EAM (falsos positivos). Modificada de Andreu et al. (190)

El artículo 4 de la Tesis (354) viene, pues, a tratar de resolver los problemas identificados en los puntos anteriores i) y ii). Es decir, pretende identificar los parámetros derivados del análisis estructural de la cicatriz relacionados de forma más directa con la arritmogénesis y, por otra parte, pretende describir la cuantificación automatizada de los componentes de la cicatriz con un software de post-procesamiento de imágenes comercialmente disponible, patentado, con marcado CE y aprobado por la FDA. El objetivo, finalmente, fue tratar de estandarizar el análisis de los datos que se pueden obtener con la RM, así como identificar las características anatómico-histológicas que verdaderamente confieren a la cicatriz post-IAM propiedades arritmogénicas.

La cicatriz definida por RM-RTG ha demostrado una buena correlación con las áreas de bajo voltaje ( $< 1,5$  mV) en los EAM. (191,365) Por otro lado, tanto el tamaño como la heterogeneidad de la cicatriz post-IAM, evaluados con RM, son variables que, a diferencia de la FEVI, se han asociado con la inducibilidad de TV en el EEF, (185,186) aparición de AV e incluso mortalidad. (164,165,216,366,367) En nuestro trabajo, (354) de todos los parámetros analizados con RM en pacientes con cicatriz post-IAM (masa total de cicatriz, de BZ, de core y de BZC), la masa de BZC fue la variable más fuertemente asociada a la aparición de TVMS (causa de la mayoría de casos de MSC arrítmica), (368) con una sensibilidad del 92,4% y especificidad del 86,9% para el punto de corte de  $> 5,15$  g.

La masa de BZC, un parámetro cuantitativo, estaría intrínsecamente ligada a la estructura cualitativa de la cicatriz, su heterogeneidad y distribución espacial, y se relacionaría con la presencia y cantidad de canales de conducción lenta dentro de la cicatriz. (188,191) En este sentido, en el estudio prospectivo GAUDI-CRT, (356) llevado a cabo en pacientes con FEVI severamente deprimida ( $< 35\%$ ) e indicación para TRC, la presencia de BZC (evaluada como variable dicotómica) ya tenía un valor predictivo positivo para la aparición de AV (24-25%) similar al de una masa de BZ aumentada ( $> 5,35$  g en ese estudio), demostrando en cualquier caso ambas variables un mejor comportamiento que la simple evaluación de la masa cicatricial total. Esto va en la línea de otro reciente estudio, (193) en el que la presencia de una "grey zone fibrosis" (es decir, la masa de BZ)  $> 5,0$  g mostró una sensibilidad del 84% y una especificidad del 72% para predecir la aparición de MSC en pacientes con CI crónica. La masa de BZC, al relacionarse de manera directa con los istmos anatómicos de reentrada (figura 38), parecería aportar un "plus" de sensibilidad y especificidad respecto a la masa total de BZ.



*Figura 38. Cicatriz post-IM potencialmente arritmogénica. Se han delimitado (líneas discontinuas gruesas) los bordes del core (rojo) y BZ (amarillo-verde). En gris, se marca todo el tejido de BZ que forma parte de la masa de BZC. Las puntas de flecha negras señalan las entradas (puntos de unión con el miocardio sano, en púrpura) de los BZC. Las líneas finas de puntos representan los potenciales circuitos de reentrada que podrían originarse en la cicatriz representada. Figura original.*

Por otro lado, en nuestro estudio, (354) la mejoría del software de post-procesamiento ADAS3D nos permitió calcular de manera automática la masa de BZC, que ha demostrado ser el parámetro más preciso en la predicción de la aparición de TV por reentrada. La **figura 39**, incluida en el artículo, (354) demuestra de forma visual el paradigma de lo que parece conferir “arritmogenicidad” a la cicatriz: no es tanto la cantidad de la misma o de BZ, sino su distribución espacial conformando canales de tejido heterogéneo (BZC/HTC). El hecho

de disponer de una “masa crítica” de BZC elevaría las posibilidades de sufrir una TV por reentrada, independientemente de que otros *triggers* pudieran ser necesarios, como se comentó en la Introducción (factores neurohormonales, mecánicos, alteraciones hidroelectrolíticas, etc.). (87,88)

Aunque haría falta una validación externa, el análisis de la masa de BZC podría ayudar a mejorar la selección de pacientes con CI crónica candidatos a implante de DAI en prevención primaria, (81) de forma similar a como se demostró el valor (incluso en términos de coste-efectividad) de la RM para decidir el implante de un DAI-TRC versus marcapasos-TRC en el estudio GAUDI-CRT. (356,369) También, el análisis de la masa de BZC podría ayudar a decidir realizar un seguimiento clínico más estrecho de determinados pacientes “en riesgo”, o a llevar a cabo pruebas de detección adicionales (p. ej. un EEF) independientemente de la FEVI. (370) Serían necesarios estudios de cohortes más grandes para evaluar prospectivamente el uso de la masa de BZC, evaluada con RM-RTG, y su precisión predictiva para la aparición de AV y MSC.

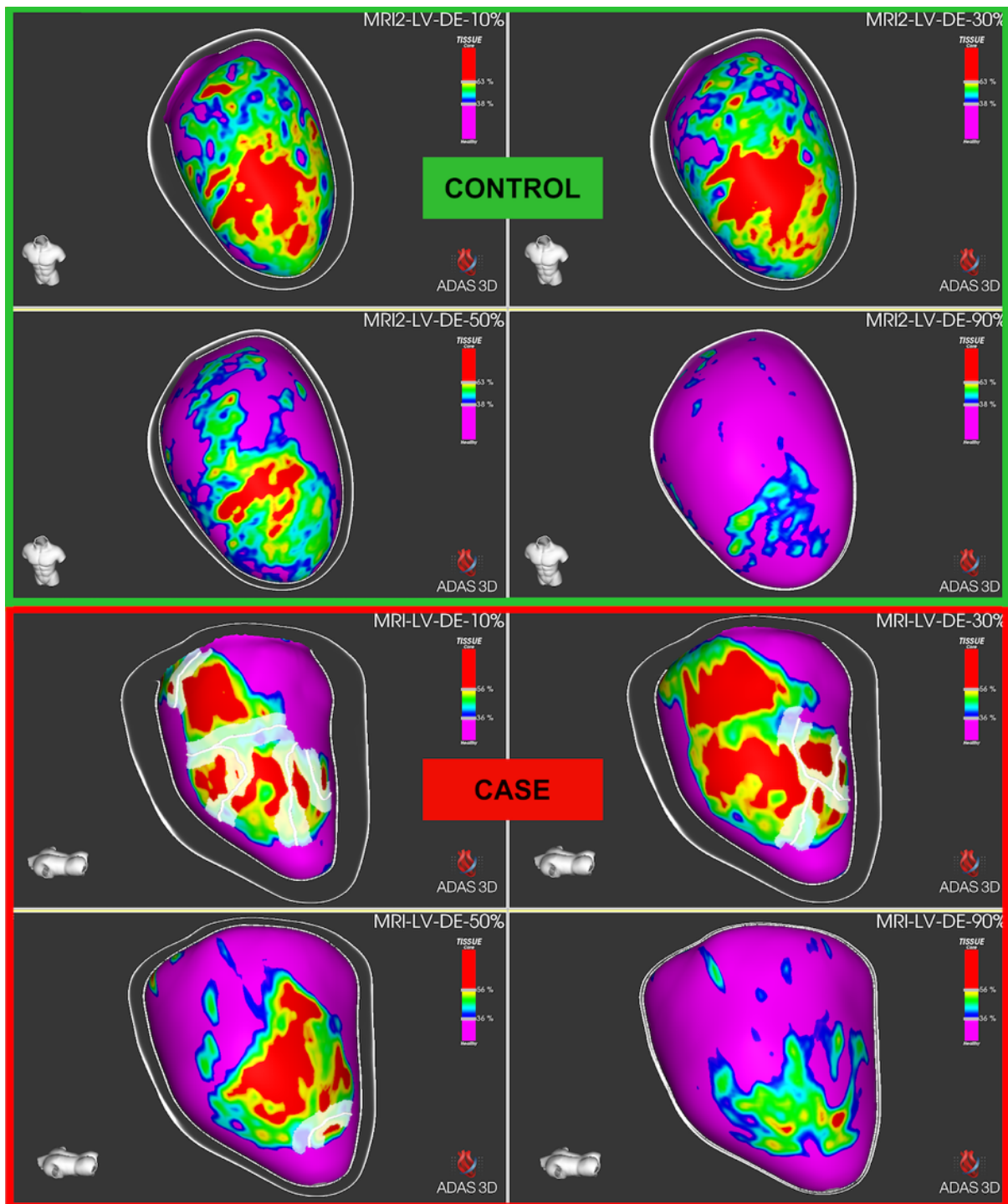


Figura 39. Ejemplos de cicatriz arritmogénica (case) y no arritmogénica (control). Se trata de dos pacientes con cicatriz post-LAM de similares dimensiones, masa y composición en BZ/core (verde/rojo, respectivamente). Sin embargo, el paciente-case, que presentó una TVMS sincopal, presentaba una distribución de la BZ en forma de canales (líneas blancas, BZC), con una masa de BZC significativa que lo predisponía a mantener circuitos de reentrada. En el paciente-control, que no había sufrido eventos arrítmicos, la masa de BZC era de 0 g aun teniendo una masa de BZ similar, pues toda la BZ se encontraba “rodeando” el core, sin formar canales. De Jáuregui et al. (354)

En cuanto al diseño del trabajo presentado en el artículo 4 de la Tesis, (354) a pesar de las limitaciones inherentes de los estudios de casos y controles, este tipo de estudios son aceptables cuando la tasa de eventos de interés (en este caso, aparición de TV en pacientes con CI crónica) es baja. Por otra parte, este trabajo se puede poner en relación con el primer artículo de la Tesis, (301) pues continúa siendo una incógnita cuál sería el mejor momento para realizar el “cribado” de la masa de BZC mediante RM, ya que también hemos demostrado que la cicatriz post-IAM sufre un proceso de remodelado a largo plazo, que afecta directamente a la estructura del sustrato arritmogénico, y que hasta ahora no era conocido. (301)

Una de las fortalezas del estudio es que se emplearon RM de diferentes fabricantes y con distintas intensidades de campo (1,5 y 3 Tesla), por lo que el método propuesto de identificación del sustrato arritmogénico parece poder exportarse a la práctica clínica habitual, independientemente del tipo de máquina de RM disponible, y siempre y cuando la calidad de las imágenes sea suficientemente buena.

Por último, harán falta estudios prospectivos que validen el punto de corte de masa de BZC  $> 5,15$  g y respalden su utilidad en la toma de decisiones clínicas. Además, sabemos ya, por lo que se ha explicado a lo largo de la Tesis, que la MSC en CI no siempre (aunque sí mayoritariamente) se debe a la aparición de TV por reentrada.

## d. Utilidad de la Resonancia Magnética para guiar los Procedimientos de Ablación de Sustrato de Taquicardias Ventriculares

Una vez discutido el papel de la RM como mejor técnica de imagen para la identificación y caracterización del sustrato arritmogénico en CI, (352) su carácter evolutivo tras el IAM (remodelado de la cicatriz) (301,311) y el posible rol del cálculo de la masa de BZC en la estratificación de riesgo arrítmico, (354) el artículo 5 de la Tesis (353) ahonda en las posibilidades de la RM como herramienta para guiar de forma directa los procedimientos de ablación de sustrato de TV en pacientes con CI crónica que ya han presentado eventos arrítmicos (prevención secundaria).

El último artículo de la Tesis (353) demuestra, por primera vez en la literatura y a diferencia de trabajos previos, (285,286) que es posible realizar una ablación de sustrato guiada exclusivamente por la información derivada de los mapas PSI de la RM-RTG, sin necesidad de realizar un EAM completo, consiguiendo procedimientos eficaces, seguros y más eficientes (en menor tiempo). La tasa de inducibilidad para TV residual tras la ablación de sustrato fue significativamente más baja en los procedimientos guiados por RM, por lo que se requirieron menos aplicaciones adicionales de RF para dar por finalizado el procedimiento. Estos resultados se reflejan igualmente al analizar la supervivencia libre de TV al año de la ablación; ésta fue significativamente superior respecto a la de los procedimientos donde no se disponía de la información de la RM (96% vs. 75%, log rank = 0,019), sin diferencias respecto a los procedimientos donde sí se utilizó la RM, pero las dianas de ablación se seleccionaron en base a la información del EAM (96% vs. 93%, log rank = 0,557).



Uno de los primeros motivos por los que la utilización de la RM durante los procedimientos de ablación resulta útil y mejora los resultados del procedimiento reside en la mejor capacidad de planificar la intervención y decidir el mejor abordaje posible en cada caso. La cicatriz de IAM tiene una estructura piramidal, de base más ancha que la zona superior, pues el subendocardio es el que primero sufre la isquemia en el SCA. (41) La realización de un abordaje combinado endo-epicárdico se ha relacionado con una menor tasa de recurrencia arrítmica durante el seguimiento, ya sea como estrategia de primera línea o después de una ablación endocárdica previamente fallida (figura 40). (260,282) El motivo de esto es que se consigue alcanzar con las aplicaciones de RF la vertiente más profunda (subepicárdica) de la cicatriz, eliminando el sustrato situado a dicho nivel. Sin embargo, cuando se realiza el abordaje combinado de manera sistemática, (260) o bien sólo atendiendo al fracaso previo del abordaje endocárdico, (282) se encuentra una significativa proporción de pacientes sin sustrato epicárdico ablacionable, por lo que en algunos casos se habría realizado una técnica fútil y potencialmente peligrosa. En un trabajo previo de nuestro grupo de investigación, (283) se observó que basar la decisión sobre un abordaje endo-epicárdico según el cumplimiento de los criterios clásicos de transmuralidad de la cicatriz por imagen (p. ej. > 75% de la pared con RTG positivo, o grosor < 5 mm en el TAC) mejoraba los resultados tras la ablación, pero, aun así, un 12,5% de los pacientes con cicatrices transmurales continuaban sin presentar sustrato arritmogénico ablacionable en el epicardio cuando se mapeaba la zona con el catéter. Con el objetivo de mejorar la selección de pacientes para el abordaje combinado, otro trabajo de nuestro grupo (364) encontró que la presencia de un área de cicatriz > 14 cm<sup>2</sup> en la capa del 90% de los mapas

PSI de RM tenía una sensibilidad y especificidad ambas del 100% para la detección de sustrato ablacionable en el epicardio. En este sentido, el disponer de la RM pre-procedimiento y aplicar ya este criterio de decisión en los pacientes del artículo 5 de la Tesis (353) probablemente influyó en la mejoría de los resultados clínicos.

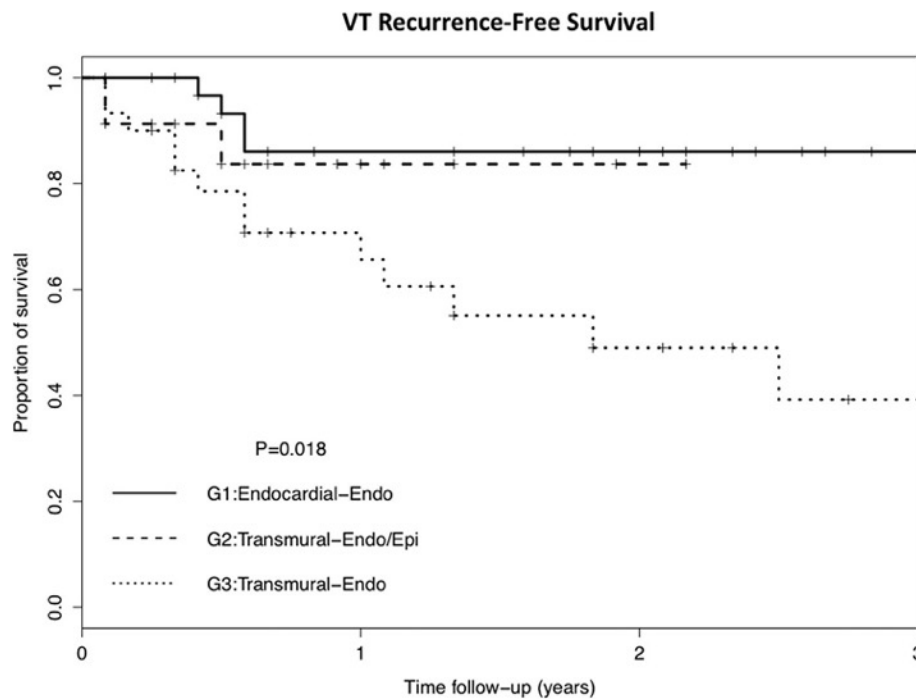


Figura 40. Curvas de supervivencia (Kaplan-Meier) libre de TV tras ablación de sustrato en pacientes con G1: sustrato endocárdico y ablación endocárdica; G2: sustrato transmural y ablación combinada endo-epicárdica; y G3: sustrato transmural pero ablación sólo endocárdica. El grupo G3 presenta una supervivencia significativamente peor que los otros grupos. De Acosta et al. (283)

Por otro lado, ya en un trabajo previo de Andreu et al., (286) donde se analizó la utilidad de la RM para “ayudar” en la ablación, se observó que no sólo la mejor selección del abordaje influía en los resultados clínicos, sino que la propia integración de los mapas PSI en los sistemas de navegación aportaba eficacia adicional. De hecho, los pacientes en los que sí se integraron los mapas PSI pero en los que se detectaron BZC que no se ablacionaron por no haber sido identificados como canales de conducción lenta en el EAM, hubo una mayor tasa de recurrencias a los 20 ± 19 meses (29% vs. 14%, log-rank = 0,027). (286) Esto es

indicativo de que la RM-RTG permite, en algunos casos, identificar sustrato adicional que no es detectable mediante el EAM. Por otra parte, la RM facilita la interpretación 3D de los EGM patológicos encontrados en el mapeo de sustrato, ayudando a una mejor identificación de las entradas de canal (figura 41), un aspecto particularmente importante cuando se utiliza la técnica de *scar dechanneling*, (262-264) pero que igualmente puede ser aplicable a otras técnicas de ablación de sustrato. (257-261)

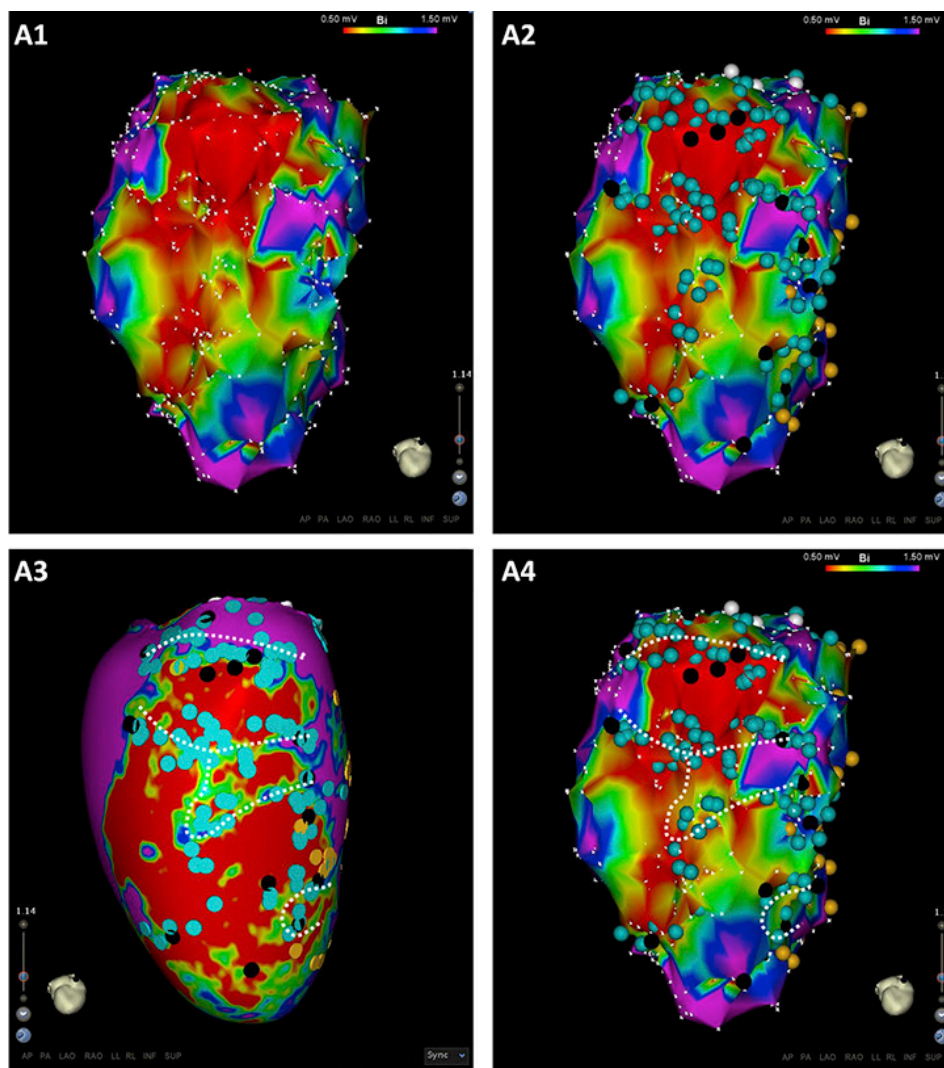


Figura 41. Ablación de sustrato ayudada por RM en paciente con CI. Panel A1: Mapa de voltaje bipolar (EAM) con umbrales estándar (rojo:  $< 0,5 \text{ mV}$ ; púrpura:  $> 1,5 \text{ mV}$ ). El mapa de voltaje no permite identificar canales de tejido con voltajes intermedios. Panel A2: Identificación (puntos azules) de los lugares con EGM con componentes retrasados indicativos de conducción lenta; los EGM con componentes con retraso más corto (puntos negros) representan las entradas de los canales de conducción lenta. La identificación espacial de los canales resulta difícil. Panel A3: Mapa de PSI del VI a partir de RM-RTG. Las líneas discontinuas blancas representan los BZC identificados, que se correlacionan de manera casi perfecta con la distribución de EGM patológicos del EAM (panel A4). De Andreu et al. (286)

En resumen, el artículo 5 de la Tesis, (353) que es la “continuación natural” del trabajo previo de Andreu et al., (286) confirma la fiabilidad de los mapas de PSI obtenidos a partir de la RM-RTG, de tal manera que es posible y seguro realizar una ablación completa y eficaz del sustrato arritmogénico sin obtener un EAM, tan sólo “aislando” los BZC identificados por RM del resto de miocardio sano mediante aplicación de RF en sus entradas (*scar dechanneling*). (262-264) Por otro lado, la eficiencia de los procedimientos, tal y como se describen en el artículo 5, (353) se explica también en parte por el hecho de que no se realiza test de inducibilidad antes de empezar la ablación, sino que se realiza todo el procedimiento en ritmo sinusal (evitando la inestabilización hemodinámica del paciente), (267) y sólo al finalizar se comprueba la inducibilidad para TV residuales. En caso de inducibilidad positiva, se mapearía el sustrato en busca de *targets* adicionales de ablación. Este método no es inferior, y sí más seguro, en comparación con realizar protocolos repetidos de inducción antes y durante la ablación. (267,274,371)

También debemos hacer notar que, en todos los casos de ablación de sustrato, aunque no se obtuviera un mapa completo de la superficie del VI, siempre que se observaran EGM fragmentados se realizaba un “análisis funcional” del sustrato mediante la técnica de aplicación de múltiple extraestímulo, que pretende desenmascarar la presencia de conducción lenta (decremental) oculta en ritmo sinusal. La descripción de esta técnica (275,278) y otras similares, (276,277,279) que han demostrado mejorar los resultados de la ablación de sustrato, escapan no obstante los objetivos de la presente Tesis.

Otro aspecto interesante de nuestro trabajo es la confirmación de la notable eficiencia que supone disponer de una RM pre-procedimiento; en pacientes donde interese ablacionar una sola morfología de TV concreta y no todo el sustrato (p. ej. pacientes añosos, “tormenta arritmogénica” por una TV monomórfica incesante, etc.) se puede completar el procedimiento en una media de  $36 \pm 15$  min. (353) La identificación previa del *exit site* del circuito de la TV responsable se realiza mediante el análisis de la morfología del QRS de la TV en el ECG, existiendo algoritmos sencillos, como el de Andreu et al., (372) que permiten identificar el segmento AHA correspondiente a dicho *exit site* en sólo dos pasos visuales. Con los mapas de PSI a partir de la RM-RTG, se puede identificar el BZC cuya “entrada” (en RS) se localiza en el segmento AHA predicho por el ECG de la TV, y que actuaría como *exit site* del circuito de reentrada. Con toda esta información disponible antes del procedimiento de ablación, ésta consistiría básicamente en realizar el acceso vascular correspondiente, dirigir el catéter al segmento AHA diana y a la entrada del BZC responsable, aplicando RF en dicha zona (figuras 42 y 43) y realizando toda la intervención en ritmo sinusal. Esto permite explicar la corta duración de los procedimientos realizados mediante la metodología que se describe en el último artículo de la Tesis. (353)

Finalmente, en la figura 44 se muestra un ejemplo de la correlación fisiopatológica real entre el sustrato arritmogénico identificado por RM y el circuito real de una TVMS inducida espontáneamente durante un procedimiento de ablación de sustrato, con la información de los mapas PSI integrada en el sistema de navegación.

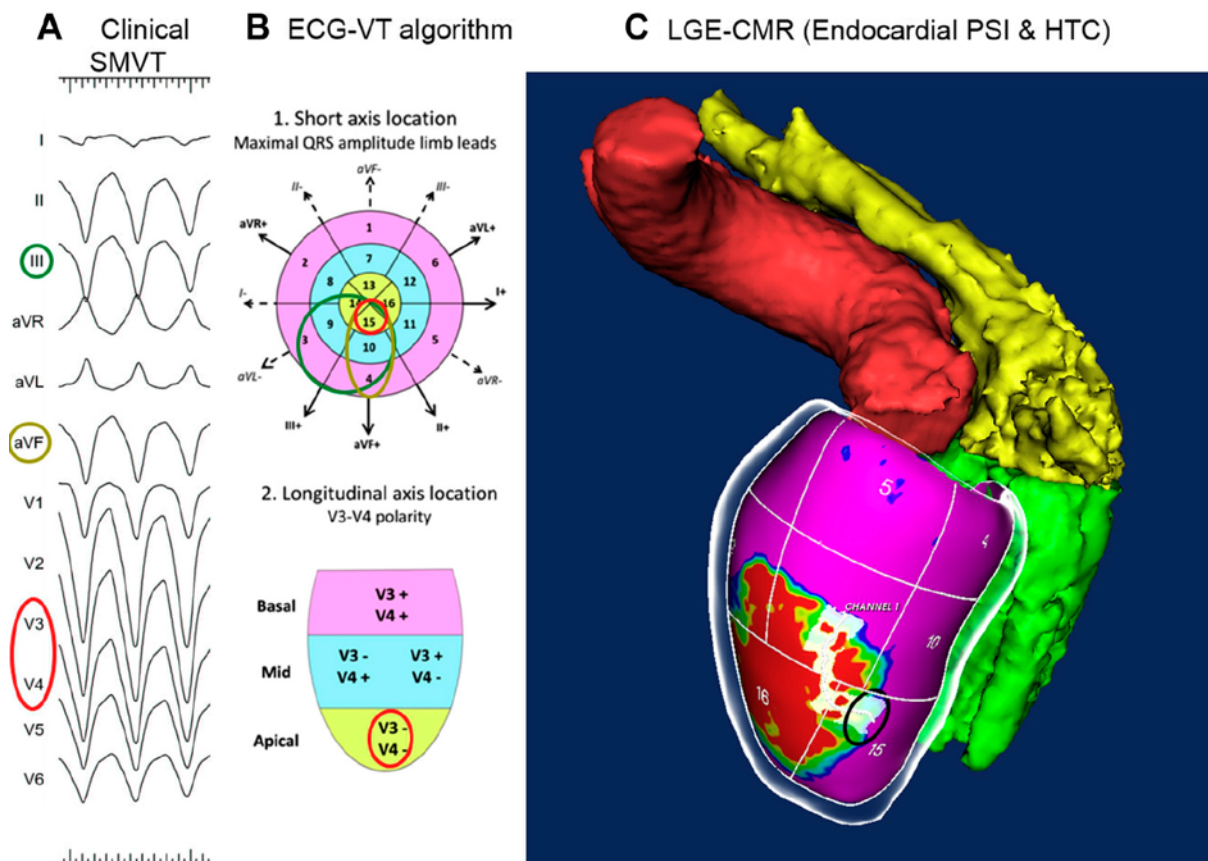


Figura 42. (A) Morfología de una TVMS en el ECG de 12 derivaciones en un paciente con CI. (B) Tras aplicar un algoritmo de análisis del ECG descrito previamente por Andreu et al. (372) se identifica el exit site de la TV clínica en el segmento AHA nº 15 (apical inferior). (C) Mapa de PSI derivado de la RM-RTG con los segmentos AHA marcados y el teórico BZC (resaltado en blanco) responsable de la TV clínica. La entrada identificada en el segmento AHA nº 15 (círculo negro) es el exit site de la TV, y la ablación con RF en dicho lugar consiguió volver no inducible la TV. De Soto-Iglesias et al. (353)

Como limitaciones de nuestro estudio, (353) debemos reconocer que no se trata de un estudio aleatorizado, sino que es observacional prospectivo y utiliza controles históricos (los pacientes que, o bien no tenían RM pre-procedimiento, o en los que se realizó la ablación “facilitada por”, pero no “guiada por” la RM), de manera que otras variables (referentes a mejora de la técnica) podrían haber influido en la mejora de resultados. Por otra parte, no se utilizaron catéteres multielectrodo. Los avances tecnológicos han permitido desarrollar nuevos catéteres que disponen de múltiples electrodos, mini-electrodos o micro-electrodos; no obstante, su diseño puede modificar el “campo de visión” (mm de tejido al que se refiere la señal registrada), la relación señal-ruido, los valores

de voltaje "anómalo" (que son específicos para cada catéter), la capacidad para detectar canales de conducción, la densidad de puntos adquiridos por unidad de tiempo, y también el coste-eficacia de los procedimientos. (373)

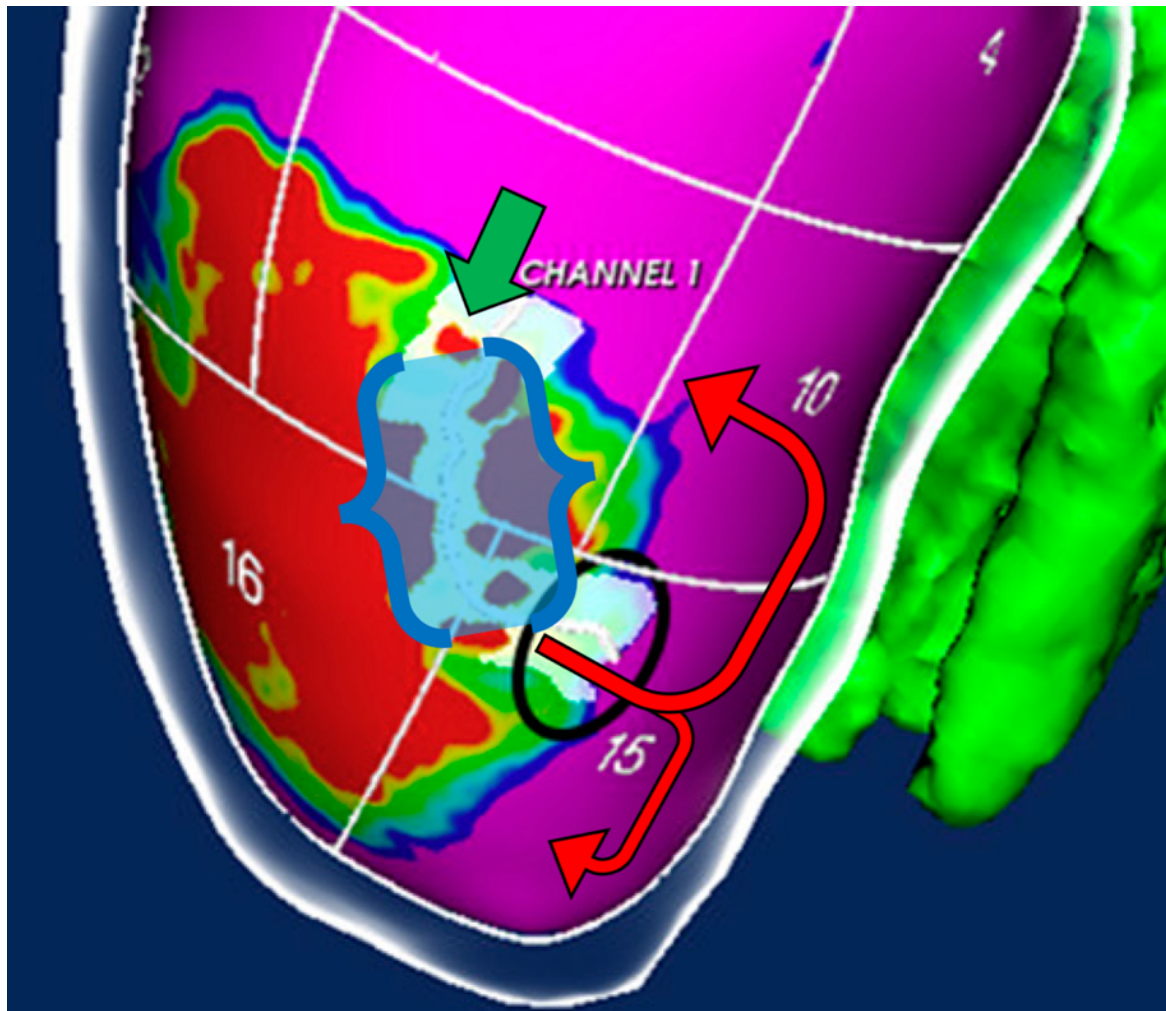


Figura 43. Detalle ampliado de la figura 42. El BZC tiene dos entradas anatómicas, de las cuales la situada en el segmento AHA nº 15 (círculo negro) se co-localiza con el exit site predicho tras el análisis de la morfología de la TV clínica. Las flechas rojas indicarían el sentido de la despolarización miocárdica predicha en TV; la flecha verde la entrada del impulso en el canal; los corchetes azules delimitarían el istmo protegido predicho para el circuito de reentrada, que se co-localiza con el BZC responsable. Modificado de Soto-Iglesias et al. (353)

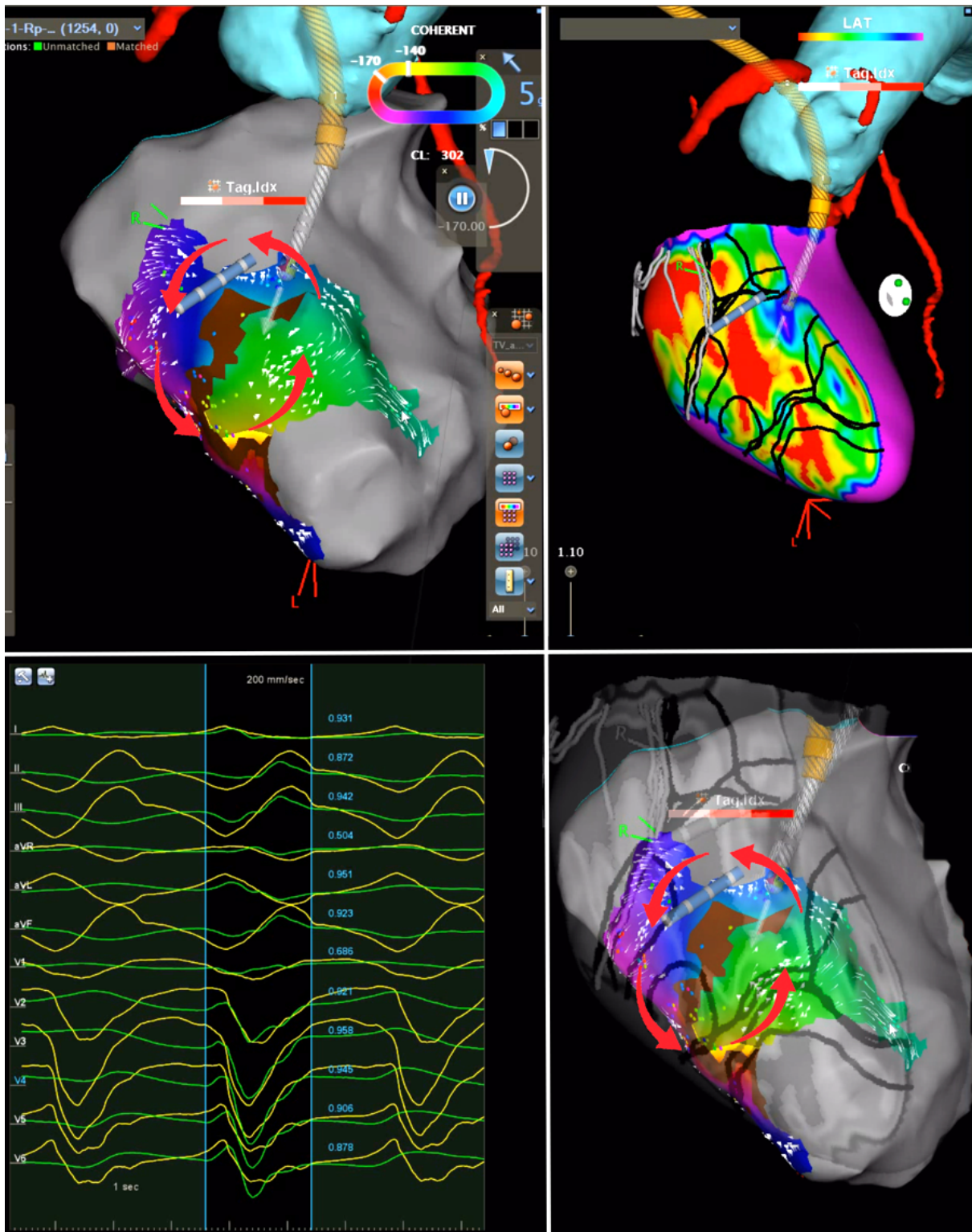


Figura 44. Ablación de sustrato guiada por RM en un paciente con CI. Arriba a la derecha se muestra el mapa de PSI de la capa del 10% del miocardio, integrada en el navegador. Los BZC identificados en negro con el software ADAS3D corresponden a canales situados en el subendocardio (< 50 % del espesor miocárdico). Los canales en gris son, por el contrario, subepicárdicos (> 50%). Durante la intervención, el paciente presentó una TVMS espontánea con la morfología que se muestra abajo a la izquierda. Mediante un catéter multipolar diagnóstico, se mapeó el circuito de reentrada (mapa de activación), registrando la secuencia de activación que señalan las flechas rojas en el panel situado arriba a la izquierda. Cuando se superponen (abajo a la derecha) el mapa de PSI y el mapa de activación de la TV, se observa una correlación espacial perfecta entre el istmo de la TV y el BZC situado a nivel más apical, transversal al eje largo del VI. La ablación en la entrada más anterior de dicho BZC volvió la TV no inducible. Figura original.



Otros grupos de investigación, basándose en la rapidez de mapeo que ofrecen los catéteres multielectrodo, abogan por realizar las ablaciones de TV no basadas en el sustrato en RS, sino identificando el "*diastolic pathway*" (es decir, el istmo del circuito de reentrada), (374,375) incluso en TV mal toleradas hemodinámicamente, gracias a la rapidez de mapeo con dichos catéteres. Estos grupos defienden que el mapeo de sustrato en RS sería incompleto, al no existir siempre una correlación perfecta entre las zonas con conducción lenta que se observarían en RS y en TV ("sustrato dinámico"). (376) En cualquier caso, el mapeo de sustrato en RS o en TV, utilizando catéteres convencionales o nuevos catéteres con múltiples electrodos, diferentes tamaños de electrodo, o diferentes distancias inter-electrodo, continuaría estando sujeto a: i) las limitaciones técnicas inherentes al mapeo electroanatómico, que no permite caracterizar de forma completa ni el sustrato ni los circuitos de TV, que son 3D y en ocasiones afectan a capas profundas de la pared miocárdica; ii) las limitaciones técnicas propias al tipo de catéter empleado, y su coste-eficacia; y iii) la tolerabilidad hemodinámica de las TV, el número de TV inducibles, y los riesgos añadidos para el paciente como resultado de la prolongación del tiempo de las intervenciones. Nuestro trabajo va pues más allá, al considerar como sustrato ablacionable, y potencialmente involucrado en la génesis de la reentrada, todos aquellos BZC/HTC identificados en la RM-RTG, independientemente de que los EGM registrados con el catéter puedan ser considerados patológicos o no. La reentrada precisa de un sustrato anatómico subyacente; lo que varía es la resolución con que somos capaces de identificarlo. La RM, en virtud de los resultados que se han venido discutiendo a lo largo de la Tesis, parece una buena técnica para identificar el sustrato arritmogénico post-IAM, analizar su evolución y tratar las AV que de él se derivan.





## 8. CONCLUSIONES

Las principales conclusiones de la Tesis se detallan a continuación:

1. La RM permite una evaluación de las características cuantitativas y cualitativas de la cicatriz post-IAM de manera dinámica, esto es, permite evaluar los cambios que ocurren a nivel histológico en el tejido dañado a lo largo del tiempo tras el evento coronario agudo.
2. El miocardio infartado presenta un proceso de remodelación de larga duración (años) que se caracteriza por una disminución constante de la masa total de cicatriz y un aumento progresivo en su heterogeneidad, es decir, un aumento en la proporción de tejido heterogéneo dentro de la misma.
3. El número y distribución de los canales de tejido heterogéneo (HTC/BZC), que constituyen el sustrato histológico de la arritmogénesis, cambian notablemente durante años (al menos, 4) tras el IAM, y estos cambios pueden evaluarse de forma fiable con RM seriadas.
4. Tras el IAM, se inicia una cascada de procesos inmunes que implican la expresión de diversos biomarcadores detectables en suero y que están relacionados con la inflamación (IL-6), la degradación de la matriz extracelular (metaloproteinasas) y la apoptosis celular (TNF- $\alpha$ ). Además, se produce un reclutamiento de distintas subpoblaciones monocitarias, células inmunes directamente involucradas en todos estos procesos.

5. Existen 3 subpoblaciones monocitarias: monocitos clásicos (CLM), no clásicos (non-CLM) e intermedios (INTM). Los CLM (los más numerosos) y los INTM presentan una cinética de reclutamiento similar tras el IAM, aumentando su número rápidamente (horas) tras el evento coronario y disminuyendo progresivamente con el paso de los siguientes 7 días. Por el contrario, los non-CLM van aumentando de manera progresiva a lo largo de este periodo.
6. Los monocitos CLM e INTM, relacionados con la pro-inflamación, parecen asociarse de forma positiva con el tamaño de la cicatriz de IAM, y de manera inversa con la FEVI resultante. Por el contrario, los monocitos non-CLM, relacionados con el control de la inflamación, parecen asociarse de forma positiva con una mayor heterogeneidad de la cicatriz y la presencia de canales de tejido heterogéneo.
7. La RM es la técnica de imagen más precisa a la hora de evaluar, de forma no invasiva, las características de la cicatriz post-IAM y su potencial arritmogenicidad. La TAC, otra técnica de imagen ampliamente utilizada por otros grupos de investigación, no es capaz de detectar la presencia de BZC en aproximadamente un 36% de los pacientes que tienen cicatrices sólo subendocárdicas, y sólo es capaz de aproximarse mejor a la RM (aunque con pobres valores de sensibilidad) en casos con cicatrices transmurales, que provocan un adelgazamiento significativo de la pared miocárdica y permiten diferenciar mejor las variaciones locales de grosor en la zona infartada.
8. El post-procesamiento de las imágenes de RM permite caracterizar y cuantificar, en gramos, la masa de los distintos componentes de la cicatriz e incluso la masa de BZC. Esta última, la masa de BZC, es la variable independiente que se correlaciona

- más fuertemente con la aparición de AV en pacientes con cicatriz post-IAM, tras ajustar por variables de confusión como la edad, la FEVI o la masa total de cicatriz.
9. Existe una fuerte correlación positiva entre la masa total de cicatriz y la masa de BZ, pero no así entre la masa total de cicatriz y la de BZC. Esto refleja que no sólo la abundancia relativa de tejido heterogéneo (BZ) en la cicatriz es importante para la estratificación de riesgo de AV tras un IAM, como ya ha sido analizado por otros grupos, sino más bien su distribución cualitativa en forma de canales (BZC). En este sentido, la masa de BZC viene a reflejar precisamente esa distribución espacial, que es la que confiere arritmogenicidad a la cicatriz.
  10. La utilización de la masa de BZC podría mejorar la estratificación del riesgo de AV en pacientes con CI. La masa de BZC, en comparación con la FEVI, permite reclasificar correctamente como de "alto riesgo" a más de un tercio de los pacientes con AV clínicas, y como de "bajo riesgo" también a más de un tercio de los pacientes sin AV documentadas en el seguimiento. Por otro lado, el uso de dos criterios de "alto riesgo arrítmico", como son el tener una FEVI  $\leq 35\%$  y masa de BZC  $> 5,15$  g, permite detectar (sensibilidad) a más del 97% de los pacientes con AV clínicas. Por el contrario, el uso de dos criterios de "bajo riesgo" (FEVI  $> 35\%$  y masa de BZC  $\leq 5,15$  g) permite detectar (especificidad) a más 82% de los controles.
  11. Dado que la RM permite identificar con gran fiabilidad la presencia de BZC y, por tanto, es capaz de ofrecer un mapa preciso del sustrato arritmogénico de la cicatriz post-IAM, hemos demostrado que es posible y seguro realizar procedimientos de ablación de sustrato con RF guiándolos exclusivamente mediante la información derivada de los mapas de PSI de la RM, sin necesidad de adquirir EAM completos.

12. Llevar a cabo procedimientos de ablación de sustrato guiados exclusivamente por la información obtenida a partir de una RM pre-procedimiento es, además, más eficaz (menos recurrencias clínicas durante el seguimiento), probablemente debido a que la RM permite identificar mejor el sustrato arritmogénico evitando las limitaciones de los EAM. Por otra parte, este abordaje permite ahorrar tiempos de mapeo, de RF y de procedimiento, haciendo las intervenciones más eficientes.
13. En casos de pacientes donde se plantee realizar sólo una ablación de la TV clínica (no el sustrato completo), el disponer de una RM previa permite identificar, de antemano y gracias al análisis de la morfología de la TV en el ECG, el BZC responsable (istmo) de mantener el circuito de reentrada de la TV clínica, permitiendo realizar el procedimiento de manera segura, eficaz y muy eficiente.







# 9. BIBLIOGRAFÍA

1. Castellanos A. *Clinical Cardiac Electrophysiology: Techniques and Interpretations*. vol. 78. 5th ed. Philadelphia: Wolters Kluwer; 1980.
2. Verma N., Knight BP. Classification of ventricular tachycardias. *ESC CardioMed*. 2018. p. 2253-6.
3. Al-Khatib SM., Stevenson WG., Ackerman MJ., et al. 2017 AHA/ACC/HRS guideline for management of patients with ventricular arrhythmias and the prevention of sudden cardiac death: Executive summary: A Report of the American College of Cardiology/American Heart Association Task Force on Clinical Practice Guid. *Hear Rhythm* 2018;15(10):e190-252. Doi: 10.1016/j.hrthm.2017.10.035.
4. Issa ZF., Miller JM., Zipes DP. *Clinical arrhythmology and electrophysiology: A companion to Braunwald's heart disease*. 2018.
5. Cronin EM., Bogun FM., Maury P., et al. 2019 HRS/EHRA/APHRS/LAQRS expert consensus statement on catheter ablation of ventricular arrhythmias. *Hear Rhythm* 2020;17(1):e2-154. Doi: 10.1016/j.hrthm.2019.03.002.
6. Natale A., Raviele A., Al-Ahmad A., et al. Venice chart international consensus document on ventricular tachycardia/ventricular fibrillation ablation: Special article. *J Cardiovasc Electrophysiol* 2010;339-79. Doi: 10.1111/j.1540-8167.2009.01686.x.
7. Sakata T., Tanner H., Stuber T., Delacrétaiz E. His-Purkinje system re-entry in patients with clustering ventricular tachycardia episodes. *Europace* 2008;10(3):289-93. Doi: 10.1093/europace/eun004.

8. Markowitz SM., Lerman BB. Mechanisms of focal ventricular tachycardia in humans. *Hear Rhythm* 2009;6(8 SUPPL.). Doi: 10.1016/j.hrthm.2009.02.034.
9. Zipes DP., Jalife J., Stevenson WG. *Cardiac Electrophysiology: From Cell to Bedside: Seventh Edition*. 2017.
10. Iwai S., Cantillon DJ., Kim RJ., et al. Right and left ventricular outflow tract tachycardias: Evidence for a common electrophysiologic mechanism. *J Cardiovasc Electrophysiol* 2006;17(10):1052-8. Doi: 10.1111/j.1540-8167.2006.00539.x.
11. Asirvatham SJ. Correlative anatomy for the invasive electrophysiologist: Outflow tract and supra-valvular arrhythmia. *J Cardiovasc Electrophysiol* 2009:955-68. Doi: 10.1111/j.1540-8167.2009.01472.x.
12. Ho SY. Anatomic insights for catheter ablation of ventricular tachycardia. *Hear Rhythm* 2009;6(8 SUPPL.). Doi: 10.1016/j.hrthm.2009.02.008.
13. Burch GE., Giles TD., Colcolough HL. Ischemic cardiomyopathy. *Am Heart J* 1970;79(3):291-2. Doi: 10.1016/0002-8703(70)90416-3.
14. Briceno N., Schuster A., Lumley M., Perera D. Ischaemic cardiomyopathy: Pathophysiology, assessment and the role of revascularisation. *Heart* 2016;102(5):397-406. Doi: 10.1136/heartjnl-2015-308037.
15. Vanoverschelde JLJ., Melin JA. The pathophysiology of myocardial hibernation: Current controversies and future directions. *Prog Cardiovasc Dis* 2001;43(5):387-98. Doi: 10.1053/pcad.2001.20655.
16. Page BJ., Banas MD., Suzuki G., et al. Revascularization of chronic hibernating myocardium stimulates myocyte proliferation and partially reverses chronic adaptations to ischemia. *J Am Coll Cardiol* 2015;65(7):684-97. Doi:

- 10.1016/j.jacc.2014.11.040.
17. Carluccio E., Biagioli P., Alunni G., et al. Patients with hibernating myocardium show altered left ventricular volumes and shape, which revert after revascularization: Evidence that dyssynergy might directly induce cardiac remodeling. *J Am Coll Cardiol* 2006;47(5):969-77. Doi: 10.1016/j.jacc.2005.09.064.
  18. Khan MA., Hashim MJ., Mustafa H., et al. Global Epidemiology of Ischemic Heart Disease: Results from the Global Burden of Disease Study. *Cureus* 2020. Doi: 10.7759/cureus.9349.
  19. Ponikowski P., Voors AA., Anker SD., et al. 2016 ESC Guidelines for the diagnosis and treatment of acute and chronic heart failure. *Eur Heart J* 2016:2129-2200m. Doi: 10.1093/eurheartj/ehw128.
  20. Ibáñez B., Heusch G., Ovize M., Van De Werf F. Evolving therapies for myocardial ischemia/reperfusion injury. *J Am Coll Cardiol* 2015:1454-71. Doi: 10.1016/j.jacc.2015.02.032.
  21. Rizzello V., Poldermans D., Biagini E., et al. Prognosis of patients with ischaemic cardiomyopathy after coronary revascularisation: Relation to viability and improvement in left ventricular ejection fraction. *Heart* 2009;95(15):1273-7. Doi: 10.1136/hrt.2008.163972.
  22. Shah BN. Geometry or function for the prediction of prognosis following revascularization in ischaemic cardiomyopathy: Beyond the ejection fraction. *Eur J Echocardiogr* 2011:807. Doi: 10.1093/ejehocardi/jer131.
  23. Bart BA., Shaw LK., McCants CB., et al. Clinical determinants of mortality in patients with angiographically diagnosed ischemic or nonischemic cardiomyopathy. *J Am*

- Coll Cardiol 1997;30(4):1002-8. Doi: 10.1016/S0735-1097(97)00235-0.
24. Heusch G. Molecular basis of cardioprotection signal transduction in ischemic pre-, post-, and remote conditioning. *Circ Res* 2015;674-99. Doi: 10.1161/CIRCRESAHA.116.305348.
  25. Burchfield JS., Xie M., Hill JA. Pathological ventricular remodeling: Mechanisms: Part 1 of 2. *Circulation* 2013;128(4):388-400. Doi: 10.1161/CIRCULATIONAHA.113.001878.
  26. Gaasch WH., Delorey DE., St. John Sutton MG., Zile MR. Patterns of Structural and Functional Remodeling of the Left Ventricle in Chronic Heart Failure. *Am J Cardiol* 2008;102(4):459-62. Doi: 10.1016/j.amjcard.2008.03.081.
  27. Draper TS., Silver JS., Gaasch WH. Adverse structural remodeling of the left ventricle and ventricular arrhythmias in patients with depressed ejection fraction. *J Card Fail* 2015;21(2):97-102. Doi: 10.1016/j.cardfail.2014.10.018.
  28. Muhlestein JB. Adverse left ventricular remodelling after acute myocardial infarction: Is there a simple treatment that really works? *Eur Heart J* 2014;144-6. Doi: 10.1093/eurheartj/ehq505.
  29. Roger VL. Epidemiology of heart failure. *Circ Res* 2013;113(6):646-59. Doi: 10.1161/CIRCRESAHA.113.300268.
  30. Groenewegen A., Rutten FH., Mosterd A., Hoes AW. Epidemiology of heart failure. *Eur J Heart Fail* 2020;1342-56. Doi: 10.1002/ejhf.1858.
  31. Flachskampf FA., Schmid M., Rost C., Achenbach S., Demaria AN., Daniel WG. Cardiac imaging after myocardial infarction. *Eur Heart J* 2011;272-83. Doi: 10.1093/eurheartj/ehq446.

32. Hung J., Teng THK., Finn J., et al. Trends from 1996 to 2007 in incidence and mortality outcomes of heart failure after acute myocardial infarction: A population-based study of 20 812 patients with first acute myocardial infarction in Western Australia. *J Am Heart Assoc* 2013;2(5). Doi: 10.1161/JAHA.113.000172.
33. Sulo G., Iglund J., Vollset SE., et al. Heart failure complicating acute myocardial infarction; burden and timing of occurrence: A nation-wide analysis including 86 771 patients from the cardiovascular disease in Norway (CVDNOR) project. *J Am Heart Assoc* 2016;5(1):1-8. Doi: 10.1161/JAHA.115.002667.
34. Gerber Y., Weston SA., Enriquez-Sarano M., et al. Mortality Associated with Heart Failure after Myocardial Infarction: A Contemporary Community Perspective. *Circ Hear Fail* 2016;9(1). Doi: 10.1161/CIRCHEARTFAILURE.115.002460.
35. Felker GM., Thompson RE., Hare JM., et al. Underlying Causes and Long-Term Survival in Patients with Initially Unexplained Cardiomyopathy. *N Engl J Med* 2000;342(15):1077-84. Doi: 10.1056/nejm200004133421502.
36. Packer M., Bristow MR., Cohn JN., et al. The Effect of Carvedilol on Morbidity and Mortality in Patients with Chronic Heart Failure. *N Engl J Med* 1996;334(21):1349-55. Doi: 10.1056/nejm199605233342101.
37. Fletcher RD., Cintron GB., Johnson G., Orndorff J., Carson P., Cohn JN. Enalapril decreases prevalence of ventricular tachycardia in patients with chronic congestive heart failure. *Circulation* 1993;87(6 SUPPL. 1).
38. Pitt B., Zannad F., Remme WJ., et al. The Effect of Spironolactone on Morbidity and Mortality in Patients with Severe Heart Failure. *N Engl J Med* 1999;341(10):709-17. Doi: 10.1056/nejm199909023411001.

39. Pablo A. Olavegogeoascoechea. De la evidencia a la práctica en la insuficiencia cardíaca. *Rev Argentina Med* 2017;5(2):132-3. Doi: 10.1056/NEJMoa1409077.
40. McMurray JJV., Solomon SD., Inzucchi SE., et al. Dapagliflozin in patients with heart failure and reduced ejection fraction. *N Engl J Med* 2019;381(21):1995-2008. Doi: 10.1056/NEJMoa1911303.
41. Zipes DP., Libby P., Bonow RO., Mann DL., Tomaselli GF. *Braunwald's Heart Disease E-Book: A Textbook of Cardiovascular Medicine*. Elsevier Health Sciences; 2018.
42. Adabag AS., Luepker R V., Roger VL., Gersh BJ. Sudden cardiac death: Epidemiology and risk factors. *Nat Rev Cardiol* 2010:216-25. Doi: 10.1038/nrcardio.2010.3.
43. Priori SG., Aliot E., Blomstrom-Lundqvist C., et al. Task Force on sudden cardiac death of the European Society of Cardiology. *Eur Heart J* 2001;22(16):1374-450. Doi: 10.1053/euhj.2001.2824.
44. Zheng ZJ., Croft JB., Giles WH., Mensah GA. Sudden cardiac death in the United States, 1989 to 1998. *Circulation* 2001;104(18):2158-63. Doi: 10.1161/hc4301.098254.
45. Rosamond W., Flegal K., Furie K., et al. Heart disease and stroke statistics-2008 Update: A report from the American heart association statistics committee and stroke statistics subcommittee. *Circulation* 2008. Doi: 10.1161/CIRCULATIONAHA.107.187998.
46. Cobb LA., Fahrenbruch CE., Olsufka M., Copass MK. Changing incidence of out-of-hospital ventricular fibrillation, 1980-2000. *J Am Med Assoc* 2002;288(23):3008-13. Doi: 10.1001/jama.288.23.3008.
47. Chugh SS., Jui J., Gunson K., et al. Current burden of sudden cardiac death: Multiple

- source surveillance versus retrospective death certificate-based review in a large U.S. community. *J Am Coll Cardiol* 2004;44(6):1268-75. Doi: 10.1016/j.jacc.2004.06.029.
48. Nichol G., Thomas E., Callaway CW., et al. Regional variation in out-of-hospital cardiac arrest incidence and outcome. *JAMA - J Am Med Assoc* 2008;300(12):1423-31. Doi: 10.1001/jama.300.12.1423.
49. Myerburg RJ. Sudden cardiac death: Exploring the limits of our knowledge. *J Cardiovasc Electrophysiol* 2001;369-81. Doi: 10.1046/j.1540-8167.2001.00369.x.
50. Davies MJ. Anatomic features in victims of sudden coronary death: Coronary artery pathology. *Circulation*, vol. 85. 1992.
51. Virmani R., Burke A., Farb A. Coronary risk factors and plaque morphology in men with coronary disease who died suddenly. *Eur Heart J* 1998;678-80. Doi: 10.1056/nejm199705013361802.
52. Farb A., Tang AL., Burke AP., Sessums L., Liang Y., Virmani R. Sudden coronary death: Frequency of active coronary lesions, inactive coronary lesions, and myocardial infarction. *Circulation* 1995;92(7):1701-9. Doi: 10.1161/01.CIR.92.7.1701.
53. Pouleur AC., Barkoudah E., Uno H., et al. Pathogenesis of sudden unexpected death in a clinical trial of patients with myocardial infarction and left ventricular dysfunction, heart failure, or both. *Circulation* 2010;122(6):597-602. Doi: 10.1161/CIRCULATIONAHA.110.940619.
54. Bonny A., Ditah I., Tonga N. Implantable cardioverter defibrillators after myocardial infarction. *Cardiovasc J Afr* 2009;20(4):223. Doi: 10.1056/nejmra0803409.
55. Solomon SD., Zelenkofske S., McMurray JJV., et al. Sudden Death in Patients with Myocardial Infarction and Left Ventricular Dysfunction, Heart Failure, or Both. *N Engl*



- J Med 2005;352(25):2581-8. Doi: 10.1056/nejmoa043938.
56. Berger CJ., Murabito JM., Evans JC., Anderson KM., Levy D. Prognosis After First Myocardial Infarction: Comparison of Q-Wave and Non-Q-Wave Myocardial Infarction in the Framingham Heart Study. *JAMA J Am Med Assoc* 1992;268(12):1545-51. Doi: 10.1001/jama.1992.03490120059029.
  57. Cairns JA., Connolly SJ., Roberts R., Gent M. Randomised trial of outcome after myocardial infarction in patients with frequent or repetitive ventricular premature depolarisations: CAMIAT. *Lancet* 1997;349(9053):675-82. Doi: 10.1016/S0140-6736(96)08171-8.
  58. Huikuri H V., Tapanainen JM., Lindgren K., et al. Prediction of sudden cardiac death after myocardial infarction in the beta-blocking era. *J Am Coll Cardiol* 2003;42(4):652-8. Doi: 10.1016/S0735-1097(03)00783-6.
  59. Mehta RH., Starr AZ., Lopes RD., et al. Incidence of and outcomes associated with ventricular tachycardia or fibrillation in patients undergoing primary percutaneous coronary intervention. *JAMA - J Am Med Assoc* 2009;301(17):1779-89. Doi: 10.1001/jama.2009.600.
  60. Moss AJ., Zareba W., Hall WJ., et al. Prophylactic Implantation of a Defibrillator in Patients with Myocardial Infarction and Reduced Ejection Fraction. *N Engl J Med* 2002;346(12):877-83. Doi: 10.1056/nejmoa013474.
  61. Bardy GH., Lee KL., Mark DB., et al. Amiodarone or an Implantable Cardioverter-Defibrillator for Congestive Heart Failure. *N Engl J Med* 2005;352(3):225-37. Doi: 10.1056/nejmoa043399.
  62. Priori SG., Blomstrom-Lundqvist C., Mazzanti A., et al. 2015 ESC Guidelines for the

- management of patients with ventricular arrhythmias and the prevention of sudden cardiac death the Task Force for the Management of Patients with Ventricular Arrhythmias and the Prevention of Sudden Cardiac Death of the Europea. *Eur Heart J* 2015;36(41):2793-2867l. Doi: 10.1093/eurheartj/ehv316.
63. Zaman S., Sivagangabalan G., Narayan A., Thiagalingam A., Ross DL., Kover P. Outcomes of early risk stratification and targeted implantable cardioverter-defibrillator implantation after st-elevation myocardial infarction treated with primary percutaneous coronary intervention. *Circulation* 2009;120(3):194-200. Doi: 10.1161/CIRCULATIONAHA.108.836791.
64. Adabag AS., Therneau TM., Gersh BJ., Weston SA., Roger VL. Sudden death after myocardial infarction. *JAMA - J Am Med Assoc* 2008;300(17):2022-9. Doi: 10.1001/jama.2008.553.
65. Marcus FI., Cobb LA., Edwards JE., et al. Mechanism of death and prevalence of myocardial ischemic symptoms in the terminal event after acute myocardial infarction. *Am J Cardiol* 1988;61(1):8-15. Doi: 10.1016/0002-9149(88)91295-7.
66. Mäkikallio TH., Barthel P., Schneider R., et al. Frequency of sudden cardiac death among acute myocardial infarction survivors with optimized medical and revascularization therapy. *Am J Cardiol* 2006;97(4):480-4. Doi: 10.1016/j.amjcard.2005.09.077.
67. de Diego C., González-Torres L., Núñez JM., et al. Effects of angiotensin-neprilysin inhibition compared to angiotensin inhibition on ventricular arrhythmias in reduced ejection fraction patients under continuous remote monitoring of implantable defibrillator devices. *Hear Rhythm* 2018;15(3):395-402. Doi:

- 10.1016/j.hrthm.2017.11.012.
68. Fernandes GC., Fernandes A., Cardoso R., et al. Association of SGLT2 inhibitors with arrhythmias and sudden cardiac death in patients with type 2 diabetes or heart failure: A meta-analysis of 34 randomized controlled trials. *Heart Rhythm* 2021;18(7):1098-105. Doi: 10.1016/j.hrthm.2021.03.028.
69. Zhang H., Huang T., Shen W., et al. Efficacy and safety of sacubitril-valsartan in heart failure: a meta-analysis of randomized controlled trials. *ESC Heart Fail* 2020;7(6):3841-50. Doi: 10.1002/ehf2.12974.
70. Zelniker TA., Braunwald E. Mechanisms of Cardiorenal Effects of Sodium-Glucose Cotransporter 2 Inhibitors: JACC State-of-the-Art Review. *J Am Coll Cardiol* 2020;422-34. Doi: 10.1016/j.jacc.2019.11.031.
71. Colombo G., Casella R., Cazzaniga A., Casiraghi C. Dapagliflozin in patients with heart failure and reduced ejection fraction. *Intern Emerg Med* 2020;15(3):515-7. Doi: 10.1007/s11739-020-02297-0.
72. Myerburg RJ., Reddy V., Castellanos A. Indications for Implantable Cardioverter-Defibrillators Based on Evidence and Judgment. *J Am Coll Cardiol* 2009;747-63. Doi: 10.1016/j.jacc.2009.03.078.
73. Mukharji J., Rude RE., Poole WK., et al. Risk factors for sudden death after acute myocardial infarction: Two-year follow-up. *Am J Cardiol* 1984;54(1):31-6. Doi: 10.1016/0002-9149(84)90299-6.
74. Singh JP., Hall WJ., McNitt S., et al. Factors influencing appropriate firing of the implanted defibrillator for ventricular tachycardia/fibrillation: Findings from the Multicenter Automatic Defibrillator Implantation Trial II (MADIT-II). *J Am Coll Cardiol*

- 2005;46(9):1712-20. Doi: 10.1016/j.jacc.2005.05.088.
75. Goldberger JJ., Cain ME., Hohnloser SH., et al. American Heart Association/American College of Cardiology Foundation/Heart Rhythm Society scientific statement on noninvasive risk stratification techniques for identifying patients at risk for sudden cardiac death: A scientific statement from the American Heart Association. *Circulation* 2008;118:1497-518. Doi: 10.1161/CIRCULATIONAHA.107.189375.
76. De Vreede-Swagemakers JJM., Gorgels APM., Dubois-Arbouw WI., et al. Out-of-hospital cardiac arrest in the 1990s: A population-based study in the Maastricht area on incidence, characteristics and survival. *J Am Coll Cardiol* 1997;30(6):1500-5. Doi: 10.1016/S0735-1097(97)00355-0.
77. Gorgels APM., Gijsbers C., De Vreede-Swagemakers J., Lousberg A., Wellens HJJ. Out-of-hospital cardiac arrest - The relevance of heart failure. The Maastricht Circulatory Arrest Registry. *Eur Heart J* 2003;24(13):1204-9. Doi: 10.1016/S0195-668X(03)00191-X.
78. Stecker EC., Vickers C., Waltz J., et al. Population-based analysis of sudden cardiac death with and without left ventricular systolic dysfunction: Two-year findings from the Oregon sudden unexpected death study. *J Am Coll Cardiol* 2006;47(6):1161-6. Doi: 10.1016/j.jacc.2005.11.045.
79. Buxton AE., Lee KL., Hafley GE., et al. Limitations of Ejection Fraction for Prediction of Sudden Death Risk in Patients With Coronary Artery Disease. Lessons From the MUSTT Study. *J Am Coll Cardiol* 2007;50(12):1150-7. Doi: 10.1016/j.jacc.2007.04.095.
80. Buxton AE. Risk stratification for sudden death in patients with coronary artery

- disease. *Hear Rhythm* 2009;6(6):836–47. Doi: 10.1016/j.hrthm.2009.02.016.
81. Goldenberg I., Vyas AK., Hall WJ., et al. Risk Stratification for Primary Implantation of a Cardioverter-Defibrillator in Patients With Ischemic Left Ventricular Dysfunction. *J Am Coll Cardiol* 2008;51(3):288–96. Doi: 10.1016/j.jacc.2007.08.058.
82. Levy WC., Lee KL., Hellkamp AS., et al. Maximizing survival benefit with primary prevention implantable cardioverter-defibrillator therapy in a heart failure population. *Circulation* 2009;120(10):835–42. Doi: 10.1161/CIRCULATIONAHA.108.816884.
83. Adabag AS., Grandits GA., Prineas RJ., Crow RS., Bloomfield HE., Neaton JD. Relation of Heart Rate Parameters During Exercise Test to Sudden Death and All-Cause Mortality in Asymptomatic Men. *Am J Cardiol* 2008;101(10):1437–43. Doi: 10.1016/j.amjcard.2008.01.021.
84. McLenachan JM., Dargie HJ. Left Ventricular Hypertrophy as a Factor in Arrhythmias and Sudden Death. *Am J Hypertens* 1989;2(2):128–31. Doi: 10.1093/ajh/2.2.128.
85. Carmeliet E. Cardiac ionic currents and acute ischemia: From channels to arrhythmias. *Physiol Rev* 1999;917–1017. Doi: 10.1152/physrev.1999.79.3.917.
86. David O A., Bullinga JR., Martins JB. Role of the purkinje system in spontaneous ventricular tachycardia during acute ischemia in a canine model. *Circulation* 1997;96(7):2421–9. Doi: 10.1161/01.cir.96.7.2421.
87. Wu TJ., Ong JJC., Hwang C., et al. Characteristics of wave fronts during ventricular fibrillation in human hearts with dilated cardiomyopathy: Role of increased fibrosis in the generation of reentry. *J Am Coll Cardiol* 1998;32(1):187–96. Doi: 10.1016/S0735-1097(98)00184-3.

88. Beuckelmann DJ., Näbauer M., Erdmann E. Alterations of K<sup>+</sup> currents in isolated human ventricular myocytes from patients with terminal heart failure. *Circ Res* 1993;73(2):379-85. Doi: 10.1161/01.RES.73.2.379.
89. Grant AO. Cardiac ion channels. *Circ Arrhythmia Electrophysiol* 2009:185-94. Doi: 10.1161/CIRCEP.108.789081.
90. Nattel S., Carlsson L. Innovative approaches to anti-arrhythmic drug therapy. *Nat Rev Drug Discov* 2006:1034-49. Doi: 10.1038/nrd2112.
91. Mangoni ME., Nargeot J. Genesis and regulation of the heart automaticity. *Physiol Rev* 2008:919-82. Doi: 10.1152/physrev.00018.2007.
92. Gaztañaga L., Marchlinski FE., Betensky BP. Mecanismos de las arritmias cardíacas. *Rev Esp Cardiol* 2012;65(2):174-85. Doi: 10.1016/j.recesp.2011.09.018.
93. Engelen DJ., Gressin V., Krucoff MW., et al. Usefulness of frequent arrhythmias after epicardial recanalization in anterior wall acute myocardial infarction as a marker of cellular injury leading to poor recovery of left ventricular function. *Am J Cardiol* 2003;92(10):1143-9. Doi: 10.1016/j.amjcard.2003.07.020.
94. Issa ZF., Miller JM., Zipes DP. Electrophysiological Mechanisms of Cardiac Arrhythmias. *Clinical Arrhythmology and Electrophysiology*. 2019. p. 51-80.
95. Zipes DP. Mechanisms of clinical arrhythmias. *Hear Rhythm* 2004:C4-18. Doi: 10.1016/j.hrthm.2004.10.015.
96. Wit AL. Afterdepolarizations and triggered activity as a mechanism for clinical arrhythmias. *PACE - Pacing Clin Electrophysiol* 2018:883-96. Doi: 10.1111/pace.13419.
97. Jalife J., Delmar M., Anumonwo J., Berenfeld O., Kalifa J. Basic Cardiac

- Electrophysiology for the Clinician: Second Edition. 2009.
98. Bijl M., Verheugt FWA. Extreme QT prolongation solely due to reversible myocardial ischemia in single-vessel coronary disease. *Am Heart J* 1992;123(2):524-6. Doi: 10.1016/0002-8703(92)90672-I.
  99. De Bakker JMT., Van Capelle FJL., Janse MJ., et al. Reentry as a cause of ventricular tachycardia in patients with chronic ischemic heart disease: Electrophysiology and anatomic correlation. *Circulation* 1988;77(3):589-606. Doi: 10.1161/01.CIR.77.3.589.
  100. Harris P., Lysitsas D. Ventricular arrhythmias and sudden cardiac death. *BJA Educ* 2016;16(7):221-9. Doi: 10.1093/bjaed/mkv056.
  101. Lazzara R., Scherlag BJ. Mechanisms of monomorphic ventricular tachycardia in coronary artery disease. *J Interv Card Electrophysiol* 2003:87-92. Doi: 10.1023/A:1023651231389.
  102. Benito B., Josephson ME. Taquicardia ventricular en la enfermedad coronaria. *Rev Esp Cardiol* 2012;65(10):939-55. Doi: 10.1016/j.recesp.2012.03.027.
  103. De Bakker JMT., Van Capelle FJL., Janse MJ., et al. Slow conduction in the infarcted human heart: "Zigzag" course of activation. *Circulation* 1993;88(3):915-26. Doi: 10.1161/01.CIR.88.3.915.
  104. Wellens HJ., Schuilenburg RM., Durrer D. Electrical stimulation of the heart in patients with ventricular tachycardia. *Circulation* 1972;46(2):216-26. Doi: 10.1161/01.CIR.46.2.216.
  105. Almendral JM., Rosenthal ME., Stamato NJ., et al. Analysis of the resetting phenomenon in sustained uniform ventricular tachycardia: Incidence and relation to termination. *J Am Coll Cardiol* 1986;8(2):294-300. Doi: 10.1016/S0735-

- 1097(86)80043-2.
106. Rosenthal ME., Stamato NJ., Almendral JM., Gottlieb CD., Josephson ME. Resetting of ventricular tachycardia with electrocardiographic fusion: Incidence and significance. *Circulation* 1988;77(3):581-8. Doi: 10.1161/01.CIR.77.3.581.
  107. Almendral JM., Gottlieb CD., Rosenthal ME., et al. Entrainment of ventricular tachycardia: Explanation for surface electrocardiographic phenomena by analysis of electrograms recorded within the tachycardia circuit. *Circulation* 1988;77(3):569-80. Doi: 10.1161/01.CIR.77.3.569.
  108. Professor Hein J.J. Wellens: 33 Years of Cardiology and Arrhythmology. 2000.
  109. Myerburg RJ., Fenster J., Velez M., et al. Impact of community-wide police car deployment of automated external defibrillators on survival from out-of-hospital cardiac arrest. *Circulation* 2002;106(9):1058-64. Doi: 10.1161/01.CIR.0000028147.92190.A7.
  110. Bailey JJ., Berson AS., Handelsman H., Hodges M. Utility of current risk stratification tests for predicting major arrhythmic events after myocardial infarction. *J Am Coll Cardiol* 2001;38(7):1902-11. Doi: 10.1016/S0735-1097(01)01667-9.
  111. Kusmirek SL., Gold MR. Sudden cardiac death: The role of risk stratification. *Am Heart J* 2007;153(4 SUPPL.):25-33. Doi: 10.1016/j.ahj.2007.01.024.
  112. Sanz G., Castañer A., Betriu A., et al. Determinants of Prognosis in Survivors of Myocardial Infarction. *N Engl J Med* 1982;306(18):1065-70. Doi: 10.1056/nejm198205063061801.
  113. Risk Stratification and Survival after Myocardial Infarction. *N Engl J Med* 1983;309(6):331-6. Doi: 10.1056/nejm198308113090602.



114. Halkin A., Stone GW., Dixon SR., et al. Impact and determinants of left ventricular function in patients undergoing primary percutaneous coronary intervention in acute myocardial infarction. *Am J Cardiol* 2005;96(3):325-31. Doi: 10.1016/j.amjcard.2005.03.069.
115. Sjöblom J., Muhrbeck J., Witt N., Alam M., Frykman-Kull V. Evolution of left ventricular ejection fraction after acute myocardial infarction implications for implantable cardioverter-defibrillator eligibility. *Circulation* 2014;743-8. Doi: 10.1161/CIRCULATIONAHA.114.009924.
116. Rouleau JL., Talajic M., Sussex B., et al. Myocardial infarction patients in the 1990s - Their risk factors, stratification and survival in Canada: The Canadian Assessment of Myocardial Infarction (CAMI) study. *J Am Coll Cardiol* 1996;27(5):1119-27. Doi: 10.1016/0735-1097(95)00599-4.
117. Yee GY., Duong T., Bland JM., et al. Optimising the dichotomy limit for left ventricular ejection fraction in selecting patients for defibrillator therapy after myocardial infarction. *Heart* 2007;93(7):832-6. Doi: 10.1136/hrt.2006.102186.
118. Waks JW., Buxton AE. Risk Stratification for Sudden Cardiac Death after Myocardial Infarction. *Annu Rev Med* 2018;69:147-64. Doi: 10.1146/annurev-med-041316-090046.
119. Farrell TG., Bashir Y., Cripps T., et al. Risk stratification for arrhythmic events in postinfarction patients based on heart rate variability, ambulatory electrocardiographic variables and the signal-averaged electrocardiogram. *J Am Coll Cardiol* 1991;18(3):687-97. Doi: 10.1016/0735-1097(91)90791-7.
120. Richards DAB. What is the best predictor of spontaneous ventricular tachycardia and

- sudden death after myocardial infarction? *Circulation* 1991;83(3):756-63. Doi: 10.1161/01.CIR.83.3.756.
121. Bourke JP., Richards DAB., Ross DL., Wallace EM., McGuire MA., Uther JB. Routine programmed electrical stimulation in survivors of acute myocardial infarction for prediction of spontaneous ventricular tachyarrhythmias during follow-up: Results, optimal stimulation protocol and cost-effective screening. *J Am Coll Cardiol* 1991;18(3):780-8. Doi: 10.1016/0735-1097(91)90802-G.
122. Hohnloser SH., Klingenhöfen T., Zabel M., Schopferl M., Mauss O. Prevalence, characteristics and prognostic value during long-term follow-up of nonsustained ventricular tachycardia after myocardial infarction in the thrombolytic era. *J Am Coll Cardiol* 1999;33(7):1895-902. Doi: 10.1016/S0735-1097(99)00108-4.
123. Buxton AE., Lee KL., Hafley GE., et al. Relation of ejection fraction and inducible ventricular tachycardia to mode of death in patients with coronary artery disease: An analysis of patients enrolled in the multicenter unsustained tachycardia trial. *Circulation* 2002;106(19):2466-72. Doi: 10.1161/01.CIR.0000037224.15873.83.
124. Bauer A., Guzik P., Barthel P., et al. Reduced prognostic power of ventricular late potentials in post-infarction patients of the reperfusion era. *Eur Heart J* 2005;26(8):755-61. Doi: 10.1093/eurheartj/ehi101.
125. Exner D V., Kavanagh KM., Slawnych MP., et al. Noninvasive Risk Assessment Early After a Myocardial Infarction. The REFINE Study. *J Am Coll Cardiol* 2007;50(24):2275-84. Doi: 10.1016/j.jacc.2007.08.042.
126. Bauer A., Barthel P., Schneider R., et al. Improved Stratification of Autonomic Regulation for risk prediction in post-infarction patients with preserved left ventricular

- function (ISAR-Risk). *Eur Heart J* 2009;30(5):576–83. Doi: 10.1093/eurheartj/ehn540.
127. Mäkikallio TH., Barthel P., Schneider R., et al. Prediction of sudden cardiac death after acute myocardial infarction: Role of Holter monitoring in the modern treatment era. *Eur Heart J* 2005;26(8):762–9. Doi: 10.1093/eurheartj/ehi188.
128. Hohnloser SH., Kuck KH., Dorian P., et al. Prophylactic use of implantable cardioverter defibrillator after acute myocardial infarction: Commentary. *Indian Heart J* 2004;56(6):687. Doi: 10.1056/NEJMoa041489.
129. Gatzoulis KA., Tsiachris D., Arsenos P., et al. Arrhythmic risk stratification in post-myocardial infarction patients with preserved ejection fraction: The PRESERVE EF study. *Eur Heart J* 2019;40(35):2940–9. Doi: 10.1093/eurheartj/ehz260.
130. Moss AJ., Hall WJ., Cannom DS., et al. Improved Survival with an Implanted Defibrillator in Patients with Coronary Disease at High Risk for Ventricular Arrhythmia. *N Engl J Med* 1996;335(26):1933–40. Doi: 10.1056/nejm199612263352601.
131. Bigger JT. Prophylactic Use of Implanted Cardiac Defibrillators in Patients at High Risk for Ventricular Arrhythmias after Coronary-Artery Bypass Graft Surgery. *N Engl J Med* 1997;337(22):1569–75. Doi: 10.1056/nejm199711273372201.
132. Buxton AE., Lee KL., DiCarlo L., et al. Electrophysiologic Testing to Identify Patients with Coronary Artery Disease Who Are at Risk for Sudden Death. *N Engl J Med* 2000;342(26):1937–45. Doi: 10.1056/nejm200006293422602.
133. Tracy CM., Winkler J., Brittain E., Leon MB., Epstein SE., Bonow RO. Determinants of ventricular arrhythmias in mildly symptomatic patients with coronary artery disease and influence of inducible left ventricular dysfunction on arrhythmia frequency. *J Am Coll Cardiol* 1987;9(3):483–8. Doi: 10.1016/S0735-1097(87)80039-6.

134. Elhendy A., Chapman S., Porter TR., Windle J. Association of myocardial ischemia with mortality and implantable cardioverter-defibrillator therapy in patients with coronary artery disease at risk of arrhythmic death. *J Am Coll Cardiol* 2005;46(9):1721-6. Doi: 10.1016/j.jacc.2005.04.065.
135. Uretsky BF., Thygesen K., Armstrong PW., et al. Acute coronary findings at autopsy in heart failure patients with sudden death: Results from the assessment of treatment with lisinopril and survival (ATLAS) trial. *Circulation* 2000;102(6):611-6. Doi: 10.1161/01.CIR.102.6.611.
136. Denes P., Gillis AM., Pawitan Y., et al. Prevalence, characteristics and significance of ventricular premature complexes and ventricular tachycardia detected by 24-hour continuous electrocardiographic recording in the Cardiac Arrhythmia Suppression Trial. *Am J Cardiol* 1991;68(9):887-96. Doi: 10.1016/0002-9149(91)90404-9.
137. Maggioni AP., Zuanetti G., Franzosi MG., et al. Prevalence and prognostic significance of ventricular arrhythmias after acute myocardial infarction in the fibrinolytic era: GISSI-2 results. *Circulation* 1993;87(2):312-22. Doi: 10.1161/01.CIR.87.2.312.
138. Høfsten DE., Wachtell K., Lund B., Mølgaard H., Egstrup K. Prevalence and prognostic implications of non-sustained ventricular tachycardia in ST-segment elevation myocardial infarction after revascularization with either fibrinolysis or primary angioplasty. *Eur Heart J* 2007;28(4):407-14. Doi: 10.1093/eurheartj/ehl476.
139. Wellens HJJ. Value and limitations of programmed electrical stimulation of the heart in the study and treatment of tachycardias. *Circulation* 1978;845-53. Doi: 10.1161/01.CIR.57.5.845.
140. Waldo AL., Akhtar M., Brugada P., et al. The minimally appropriate electrophysiologic

- study for the initial assessment of patients with documented sustained monomorphic ventricular tachycardia. *J Am Coll Cardiol* 1985;6(5):1174-7. Doi: 10.1016/S0735-1097(85)80329-6.
141. Bourke JP., Richards DAB., Ross DL., McGuire MA., Uther JB. Does the induction of ventricular flutter or fibrillation at electrophysiologic testing after myocardial infarction have any prognostic significance? *Am J Cardiol* 1995;75(7):431-5. Doi: 10.1016/S0002-9149(99)80576-1.
142. Marchlinski FE., Buxton AE., Waxman HL., Josephson ME. Identifying patients at risk of sudden death after myocardial infarction: Value of the response to programmed stimulation, degree of ventricular ectopic activity and severity of left ventricular dysfunction. *Am J Cardiol* 1983;52(10):1190-6. Doi: 10.1016/0002-9149(83)90572-6.
143. Nogami A., Aonuma K., Takahashi A., et al. Usefulness of early versus late programmed ventricular stimulation in acute myocardial infarction. *Am J Cardiol* 1991;68(1):13-20. Doi: 10.1016/0002-9149(91)90702-M.
144. Richards DA., Cody D V., Denniss AR., Russell PA., Young AA., Uther JB. Ventricular electrical instability: A predictor of death after myocardial infarction. *Am J Cardiol* 1983;51(1):75-80. Doi: 10.1016/S0002-9149(83)80014-9.
145. Marchand E., Theroux P., Waters DD. Programmed ventricular stimulation in survivors of an acute myocardial infarction. *Circulation* 1985;72(3):487-94. Doi: 10.1161/01.cir.72.3.487.
146. Buxton AE., Lee KL., Fisher JD., Josephson ME., Prystowsky EN., Hafley G. A randomized study of the prevention of sudden death in patients with coronary artery

- disease. Multicenter Unsustained Tachycardia Trial Investigators. *N Engl J Med* 1999;341(25):1882-90.
147. De Ferrari GM., Rordorf R., Frattini F., Petracci B., De Filippo P., Landolina M. Predictive value of programmed ventricular stimulation in patients with ischaemic cardiomyopathy: Implications for the selection of candidates for an implantable defibrillator. *Europace* 2007;9(12):1151-7. Doi: 10.1093/europace/eum230.
148. Daubert JP., Zareba W., Hall WJ., et al. Predictive value of ventricular arrhythmia inducibility for subsequent ventricular tachycardia or ventricular fibrillation in multicenter automatic defibrillator implantation trial (MADIT) II patients. *J Am Coll Cardiol* 2006;47(1):98-107. Doi: 10.1016/j.jacc.2005.08.049.
149. Zaman S., Narayan A., Thiagalingam A., et al. Long-term arrhythmia-free survival in patients with severe left ventricular dysfunction and no inducible ventricular tachycardia after myocardial infarction. *Circulation* 2014;129(8):848-54. Doi: 10.1161/CIRCULATIONAHA.113.005146.
150. Levy WC., Mozaffarian D., Linker DT., et al. The Seattle Heart Failure Model: Prediction of survival in heart failure. *Circulation* 2006;113(11):1424-33. Doi: 10.1161/CIRCULATIONAHA.105.584102.
151. Shadman R., Poole JE., Dardas TF., et al. A novel method to predict the proportional risk of sudden cardiac death in heart failure: Derivation of the Seattle Proportional Risk Model. *Heart Rhythm* 2015;12(10):2069-77. Doi: 10.1016/j.hrthm.2015.06.039.
152. Breithardt G., Cain ME., el-Sherif N., et al. Standards for analysis of ventricular late potentials using high-resolution or signal-averaged electrocardiography. A statement by a Task Force Committee of the European Society of Cardiology, the

- American Heart Association, and the American College of Ca. *Circulation* 1991;83(4):1481-8. Doi: 10.1161/01.cir.83.4.1481.
153. Gomes JA., Cain ME., Buxton AE., Josephson ME., Lee KL., Hafley GE. Prediction of long-term outcomes by signal-averaged electrocardiography in patients with unsustained ventricular tachycardia, coronary artery disease, and left ventricular dysfunction. *Circulation* 2001;104(4):436-41. Doi: 10.1161/hc2901.093197.
154. Nearing BD., Verrier RL. Modified moving average analysis of T-wave alternans to predict ventricular fibrillation with high accuracy. *J Appl Physiol* 2002;92(2):541-9. Doi: 10.1152/jappphysiol.00592.2001.
155. Walker ML., Rosenbaum DS. Repolarization alternans: Implications for the mechanism and prevention of sudden cardiac death. *Cardiovasc Res* 2003:599-614. Doi: 10.1016/S0008-6363(02)00737-X.
156. Weiss JN., Karma A., Shiferaw Y., Chen PS., Garfinkel A., Qu Z. From pulsus to pulseless: The saga of cardiac alternans. *Circ Res* 2006:1244-53. Doi: 10.1161/01.RES.0000224540.97431.f0.
157. Gold MR., Ip JH., Costantini O., et al. Role of microvolt T-wave alternans in assessment of arrhythmia vulnerability among patients with heart failure and systolic dysfunction primary results from the T-wave alternans sudden cardiac death in heart failure trial substudy. *Circulation* 2008;118(20):2022-8. Doi: 10.1161/CIRCULATIONAHA.107.748962.
158. Chow T., Kereiakes DJ., Onufer J., et al. Does Microvolt T-Wave Alternans Testing Predict Ventricular Tachyarrhythmias in Patients With Ischemic Cardiomyopathy and Prophylactic Defibrillators?. The MASTER (Microvolt T Wave Alternans Testing for Risk

- Stratification of Post-Myocardial Infarction Pa. *J Am Coll Cardiol* 2008;52(20):1607-15. Doi: 10.1016/j.jacc.2008.08.018.
159. Costantini O., Hohnloser SH., Kirk MM., et al. The ABCD (Alternans Before Cardioverter Defibrillator) Trial. Strategies Using T-Wave Alternans to Improve Efficiency of Sudden Cardiac Death Prevention. *J Am Coll Cardiol* 2009;53(6):471-9. Doi: 10.1016/j.jacc.2008.08.077.
160. Lahiri MK., Kannankeril PJ., Goldberger JJ. Assessment of Autonomic Function in Cardiovascular Disease. Physiological Basis and Prognostic Implications. *J Am Coll Cardiol* 2008;52(1):1725-33. Doi: 10.1016/j.jacc.2008.01.038.
161. Bellenger NG., Davies LC., Francis JM., Coats AJS., Pennell DJ. Reduction in sample size for studies of remodeling in heart failure by the use of cardiovascular magnetic resonance. *J Cardiovasc Magn Reson* 2000;2(4):271-8. Doi: 10.3109/10976640009148691.
162. Von Knobelsdorff-Brenkenhoff F., Schulz-Menger J. Role of cardiovascular magnetic resonance in the guidelines of the European Society of Cardiology. *J Cardiovasc Magn Reson* 2016;18(1). Doi: 10.1186/s12968-016-0225-6.
163. Von Knobelsdorff-Brenkenhoff F., Pilz G., Schulz-Menger J. Representation of cardiovascular magnetic resonance in the AHA / ACC guidelines. *J Cardiovasc Magn Reson* 2017;19(1). Doi: 10.1186/s12968-017-0385-z.
164. Disertori M., Rigoni M., Pace N., et al. Myocardial Fibrosis Assessment by LGE Is a Powerful Predictor of Ventricular Tachyarrhythmias in Ischemic and Nonischemic LV Dysfunction: A Meta-Analysis. *JACC Cardiovasc Imaging* 2016;9(9):1046-55. Doi: 10.1016/j.jcmg.2016.01.033.



165. Klem I., Weinsaft JW., Bahnson TD., et al. Assessment of myocardial scarring improves risk stratification in patients evaluated for cardiac defibrillator implantation. *J Am Coll Cardiol* 2012;60(5):408-20. Doi: 10.1016/j.jacc.2012.02.070.
166. Roes SD., Borleffs CJW., Van Der Geest RJ., et al. Infarct tissue heterogeneity assessed with contrast-enhanced mri predicts spontaneous ventricular arrhythmia in patients with ischemic cardiomyopathy and implantable cardioverter-defibrillator. *Circ Cardiovasc Imaging* 2009;2(3):183-90. Doi: 10.1161/CIRCIMAGING.108.826529.
167. Boyé P., Abdel-Aty H., Zacharzowsky U., et al. Prediction of life-threatening arrhythmic events in patients with chronic myocardial infarction by contrast-enhanced CMR. *JACC Cardiovasc Imaging* 2011;4(8):871-9. Doi: 10.1016/j.jcmg.2011.04.014.
168. De Haan S., Meijers TA., Knaapen P., Beek AM., Van Rossum AC., Allaart CP. Scar size and characteristics assessed by CMR predict ventricular arrhythmias in ischaemic cardiomyopathy: Comparison of previously validated models. *Heart* 2011;97(23):1951-6. Doi: 10.1136/heartjnl-2011-300060.
169. Alexandre J., Saloux E., Dugué AE., et al. Scar extent evaluated by late gadolinium enhancement CMR: A powerful predictor of long term appropriate ICD therapy in patients with coronary artery disease. *J Cardiovasc Magn Reson* 2013;15(1). Doi: 10.1186/1532-429X-15-12.
170. Demirel F., Adiyaman A., Timmer JR., et al. Myocardial scar characteristics based on cardiac magnetic resonance imaging is associated with ventricular tachyarrhythmia in patients with ischemic cardiomyopathy. *Int J Cardiol* 2014;177(2):392-9. Doi: 10.1016/j.ijcard.2014.08.132.
171. Assomull RG., Prasad SK., Lyne J., et al. Cardiovascular Magnetic Resonance, Fibrosis,

- and Prognosis in Dilated Cardiomyopathy. *J Am Coll Cardiol* 2006;48(10):1977-85. Doi: 10.1016/j.jacc.2006.07.049.
172. Iles L., Pfluger H., Lefkovits L., et al. Myocardial fibrosis predicts appropriate device therapy in patients with implantable cardioverter-defibrillators for primary prevention of sudden cardiac death. *J Am Coll Cardiol* 2011;57(7):821-8. Doi: 10.1016/j.jacc.2010.06.062.
173. Leyva F., Taylor RJ., Foley PWX., et al. Left ventricular midwall fibrosis as a predictor of mortality and morbidity after cardiac resynchronization therapy in patients with nonischemic cardiomyopathy. *J Am Coll Cardiol* 2012;60(17):1659-67. Doi: 10.1016/j.jacc.2012.05.054.
174. Gulati A., Jabbour A., Ismail TF., et al. Association of fibrosis with mortality and sudden cardiac death in patients with nonischemic dilated cardiomyopathy. *JAMA - J Am Med Assoc* 2013;309(9):896-908. Doi: 10.1001/jama.2013.1363.
175. Neilan TG., Coelho-Filho OR., Danik SB., et al. CMR quantification of myocardial scar provides additive prognostic information in nonischemic cardiomyopathy. *JACC Cardiovasc Imaging* 2013;6(9):944-54. Doi: 10.1016/j.jcmg.2013.05.013.
176. Müller KAL., Müller I., Kramer U., et al. Prognostic Value of Contrast-enhanced Cardiac Magnetic Resonance Imaging in Patients with Newly Diagnosed Non-Ischemic Cardiomyopathy: Cohort Study. *PLoS One* 2013;8(2). Doi: 10.1371/journal.pone.0057077.
177. Perazzolo Marra M., De Lazzari M., Zorzi A., et al. Impact of the presence and amount of myocardial fibrosis by cardiac magnetic resonance on arrhythmic outcome and sudden cardiac death in nonischemic dilated cardiomyopathy. *Hear Rhythm*

- 2014;11(5):856-63. Doi: 10.1016/j.hrthm.2014.01.014.
178. Masci PG., Doulaptsis C., Bertella E., et al. Incremental prognostic value of myocardial fibrosis in patients with non-ischemic cardiomyopathy without congestive heart failure. *Circ Hear Fail* 2014;7(3):448-56. Doi: 10.1161/CIRCHEARTFAILURE.113.000996.
179. Fernández-Armenta J., Berruezo A., Mont L., et al. Use of myocardial scar characterization to predict ventricular arrhythmia in cardiac resynchronization therapy. *Europace* 2012;14(11):1578-86. Doi: 10.1093/europace/eus104.
180. Gao P., Yee R., Gula L., et al. Prediction of arrhythmic events in ischemic and dilated cardiomyopathy patients referred for implantable cardiac defibrillator evaluation of multiple scar quantification measures for late gadolinium enhancement magnetic resonance imaging. *Circ Cardiovasc Imaging* 2012;5(4):448-56. Doi: 10.1161/CIRCIMAGING.111.971549.
181. Wu KC., Gerstenblith G., Guallar E., et al. Combined cardiac magnetic resonance imaging and C-reactive protein levels identify a cohort at low risk for defibrillator firings and death. *Circ Cardiovasc Imaging* 2012;5(2):178-86. Doi: 10.1161/CIRCIMAGING.111.968024.
182. Mordi I., Jhund PS., Gardner RS., et al. LGE and NT-proBNP identify low risk of death or arrhythmic events in patients with primary prevention ICDs. *JACC Cardiovasc Imaging* 2014;7(6):561-9. Doi: 10.1016/j.jcmg.2013.12.014.
183. Almehmadi F., Joncas SX., Nevis I., et al. Prevalence of myocardial fibrosis patterns in patients with systolic dysfunction: Prognostic significance for the prediction of sudden cardiac arrest or appropriate implantable cardiac defibrillator therapy. *Circ*

- Cardiovasc Imaging 2014;7(4):593-600. Doi: 10.1161/CIRCIMAGING.113.001768.
184. Iles LM., Ellims AH., Llewellyn H., et al. Histological validation of cardiac magnetic resonance analysis of regional and diffuse interstitial myocardial fibrosis. *Eur Heart J Cardiovasc Imaging* 2015;16(1):14-22. Doi: 10.1093/ehjci/jeu182.
185. Schmidt A., Azevedo CF., Cheng A., et al. Infarct tissue heterogeneity by magnetic resonance imaging identifies enhanced cardiac arrhythmia susceptibility in patients with left ventricular dysfunction. *Circulation* 2007;115(15):2006-14. Doi: 10.1161/CIRCULATIONAHA.106.653568.
186. Bello D., Fieno DS., Kim RJ., et al. Infarct morphology identifies patients with substrate for sustained ventricular tachycardia. *J Am Coll Cardiol* 2005;45(7):1104-8. Doi: 10.1016/j.jacc.2004.12.057.
187. Bogun FM., Desjardins B., Good E., et al. Delayed-Enhanced Magnetic Resonance Imaging in Nonischemic Cardiomyopathy. Utility for Identifying the Ventricular Arrhythmia Substrate. *J Am Coll Cardiol* 2009;53(13):1138-45. Doi: 10.1016/j.jacc.2008.11.052.
188. Perez-David E., Arenal Á., Rubio-Guivernau JL., et al. Noninvasive identification of ventricular tachycardia-related conducting channels using contrast-enhanced magnetic resonance imaging in patients with chronic myocardial infarction: Comparison of signal intensity scar mapping and endocardial voltage mappin. *J Am Coll Cardiol* 2011;57(2):184-94. Doi: 10.1016/j.jacc.2010.07.043.
189. Andreu D., Ortiz-Pérez JT., Boussy T., et al. Usefulness of contrast-enhanced cardiac magnetic resonance in identifying the ventricular arrhythmia substrate and the approach needed for ablation. *Eur Heart J* 2014;35(20):1316-26. Doi:

- 10.1093/eurheartj/eht510.
190. Andreu D., Ortiz-Pérez JT., Fernández-Armenta J., et al. 3D delayed-enhanced magnetic resonance sequences improve conducting channel delineation prior to ventricular tachycardia ablation. *Europace* 2015;17(6):938-45. Doi: 10.1093/europace/euu310.
  191. Fernández-Armenta J., Berruezo A., Andreu D., et al. Three-dimensional architecture of scar and conducting channels based on high resolution ce-CMR: Insights for ventricular tachycardia ablation. *Circ Arrhythmia Electrophysiol* 2013;6(3):528-37. Doi: 10.1161/CIRCEP.113.000264.
  192. Piers SRD., Tao Q., De Riva Silva M., et al. CMR-based identification of critical isthmus sites of ischemic and nonischemic ventricular tachycardia. *JACC Cardiovasc Imaging* 2014;7(8):774-84. Doi: 10.1016/j.jcmg.2014.03.013.
  193. Zegard A., Okafor O., de Bono J., et al. Myocardial Fibrosis as a Predictor of Sudden Death in Patients With Coronary Artery Disease. *J Am Coll Cardiol* 2021;77(1):29-41. Doi: 10.1016/j.jacc.2020.10.046.
  194. Deng D., Arevalo H., Pashakhanloo F., et al. Accuracy of prediction of infarct-related arrhythmic circuits from image-based models reconstructed from low and high resolution MRI. *Front Physiol* 2015;6(OCT). Doi: 10.3389/fphys.2015.00282.
  195. Bloch F. Nuclear induction. *Phys Rev* 1946;70(7-8):460-74. Doi: 10.1103/PhysRev.70.460.
  196. Bloch F., Hansen WW., Packard M. The nuclear induction experiment. *Phys Rev* 1946;70(7-8):474-85. Doi: 10.1103/PhysRev.70.474.
  197. San Román JA., Fernández RS., García ER., Fernández-Avilés F. Conocimientos

- básicos necesarios para realizar resonancia magnética en cardiología. *Rev Esp Cardiol Supl* 2006;6(E). Doi: 10.1157/13092054.
198. Young AER., Zorab JSM. Magnetic resonance imaging (MRI). *European Journal of Anaesthesiology*. Doi: 10.1017/S026502159725057X.
199. Balaban RS., Peters DC. Basic Principles of Cardiovascular Magnetic Resonance. *Cardiovascular Magnetic Resonance*. 2019. p. 1-14.e2.
200. Hutchinson JMS., Sutherland RJ., Mallard JR. NMR imaging: Image recovery under magnetic fields with large non-uniformities. *J Phys E* 1978;11(3):217-21. Doi: 10.1088/0022-3735/11/3/012.
201. Edelstein WA., Hutchison JMS., Johnson G., Redpath T. Spin warp NMR imaging and applications to human whole-body imaging. *Phys Med Biol* 1980;25(4):751-6. Doi: 10.1088/0031-9155/25/4/017.
202. Nielles-Vallespin S. Cardiovascular magnetic resonance physics, techniques, and contrast agents. *ESC CardioMed*. 2018. p. 503-5.
203. Fieno DS., Kim RJ., Chen EL., Lomasney JW., Klocke FJ., Judd RM. Contrast-enhanced magnetic resonance imaging of myocardium at risk: Distinction between reversible and irreversible injury throughout infarct healing. *J Am Coll Cardiol* 2000;36(6):1985-91. Doi: 10.1016/S0735-1097(00)00958-X.
204. Hunold P., Schlosser T., Vogt FM., et al. Myocardial late enhancement in contrast-enhanced cardiac MRI: Distinction between infarction scar and non-infarction-related disease. *American Journal of Roentgenology*, vol. 184. 2005. p. 1420-6.
205. Kellman P., Arai AE. Cardiac imaging techniques for physicians: Late enhancement. *J Magn Reson Imaging* 2012:529-42. Doi: 10.1002/jmri.23605.

206. Kim RJ., Fieno DS., Parrish TB., et al. Relationship of MRI delayed contrast enhancement to irreversible injury, infarct age, and contractile function. *Circulation* 1999;100(19):1992-2002. Doi: 10.1161/01.CIR.100.19.1992.
207. Prince MR. Gadolinium-enhanced MR aortography. *Radiology* 1994;191(1):155-64. Doi: 10.1148/radiology.191.1.8134563.
208. Atkinson DJ., Burstein D., Edelman RR. First-pass cardiac perfusion: Evaluation with ultrafast MR imaging. *Radiology* 1990;757-62. Doi: 10.1148/radiology.174.3.2305058.
209. Cowper SE., Robin HS., Steinberg SM., Su LD., Gupta S., LeBoit PE. Scleromyxoedema-like cutaneous diseases in renal-dialysis patients. *Lancet* 2000;356(9234):1000-1. Doi: 10.1016/S0140-6736(00)02694-5.
210. Canga A., Kislikova M., Martínez-Gálvez M., et al. Función renal, fibrosis sistémica nefrogénica y otras reacciones adversas asociadas a los medios de contraste basados en el gadolinio. *Nefrología* 2014;34(4):428-38. Doi: 10.3265/Nefrologia.pre2014.Apr.12375.
211. Prince MR., Arnoldus C., Frisoli JK. Nephrotoxicity of high-dose gadolinium compared with iodinated contrast. *J Magn Reson Imaging* 1996;6(1):162-6. Doi: 10.1002/jmri.1880060129.
212. McNamara MT., Tscholakoff D., Revel D., et al. Differentiation of reversible and irreversible myocardial injury by MR imaging with and without gadolinium-DTPA. *Radiology* 1986;158(3):765-9. Doi: 10.1148/radiology.158.3.3945751.
213. Kelle S., Roes SD., Klein C., et al. Prognostic Value of Myocardial Infarct Size and Contractile Reserve Using Magnetic Resonance Imaging. *J Am Coll Cardiol*

- 2009;54(19):1770-7. Doi: 10.1016/j.jacc.2009.07.027.
214. Fieno DS., Jaffe WC., Simonetti OP., Judd RM., Finn JP. TrueFISP: Assessment of accuracy for measurement of left ventricular mass in an animal model. *J Magn Reson Imaging* 2002;15(5):526-31. Doi: 10.1002/jmri.10107.
215. Kramer CM., Barkhausen J., Flamm SD., Kim RJ., Nagel E. Standardized cardiovascular magnetic resonance imaging (CMR) protocols, society for cardiovascular magnetic resonance: board of trustees task force on standardized protocols. *J Cardiovasc Magn Reson* 2008. Doi: 10.1186/1532-429X-10-35.
216. Yan AT., Shayne AJ., Brown KA., et al. Characterization of the peri-infarct zone by contrast-enhanced cardiac magnetic resonance imaging is a powerful predictor of post-myocardial infarction mortality. *Circulation* 2006;114(1):32-9. Doi: 10.1161/CIRCULATIONAHA.106.613414.
217. Kim HW., Farzaneh-Far A., Kim RJ. Cardiovascular Magnetic Resonance in Patients With Myocardial Infarction. Current and Emerging Applications. *J Am Coll Cardiol* 2009;1-16. Doi: 10.1016/j.jacc.2009.06.059.
218. Schelbert EB., Hsu LY., Anderson SA., et al. Late gadolinium-enhancement cardiac magnetic resonance identifies postinfarction myocardial fibrosis and the border zone at the near cellular level in ex vivo rat heart. *Circ Cardiovasc Imaging* 2010;3(6). Doi: 10.1161/CIRCIMAGING.108.835793.
219. Amado LC., Gerber BL., Gupta SN., et al. Accurate and objective infarct sizing by contrast-enhanced magnetic resonance imaging in a canine myocardial infarction model. *J Am Coll Cardiol* 2004;44(12):2383-9. Doi: 10.1016/j.jacc.2004.09.020.
220. Andreu D., Berruezo A., Ortiz-Pérez JT., et al. Integration of 3D electroanatomic maps



- and magnetic resonance scar characterization into the navigation system to guide ventricular tachycardia ablation. *Circ Arrhythmia Electrophysiol* 2011;4(5):674-83. Doi: 10.1161/CIRCEP.111.961946.
221. de Baker JMT., Coronel R., Tasseron S., et al. Ventricular tachyrdia in the infarcted, Langendorff-perfused human heart: Role of the arrangement of surviving cardiac fibers. *J Am Coll Cardiol* 1990;15(7):1594-607. Doi: 10.1016/0735-1097(90)92832-M.
222. Estner HL., Zviman MM., Herzka D., et al. The critical isthmus sites of ischemic ventricular tachycardia are in zones of tissue heterogeneity, visualized by magnetic resonance imaging. *Hear Rhythm* 2011;8(12):1942-9. Doi: 10.1016/j.hrthm.2011.07.027.
223. Franco E., Hernández-Madrid A., Arreo V., Matía R., Sánchez I., Moreno J. Mecanismos generales de las taquicardias. *Cuad Estimul Card* 2015;8(22):3-16.
224. Berruezo A., Penela D., Jáuregui B., Soto-Iglesias D. The role of imaging in catheter ablation of ventricular arrhythmias. *PACE - Pacing Clin Electrophysiol* 2021:1115-25. Doi: 10.1111/pace.14183.
225. Ashikaga H., Sasano T., Dong J., et al. Magnetic resonance-based anatomical analysis of scar-related ventricular tachycardia: Implications for catheter ablation. *Circ Res* 2007;101(9):939-47. Doi: 10.1161/CIRCRESAHA.107.158980.
226. McAnulty J., Halperin B., Kron J., et al. A Comparison of Antiarrhythmic-Drug Therapy with Implantable Defibrillators in Patients Resuscitated from Near-Fatal Ventricular Arrhythmias. *N Engl J Med* 1997;337(22):1576-84. Doi: 10.1056/nejm199711273372202.

227. Connolly SJ., Gent M., Roberts RS., et al. Canadian implantable defibrillator study (CIDS): A randomized trial of the implantable cardioverter defibrillator against amiodarone. *Circulation* 2000;101(11):1297-302. Doi: 10.1161/01.CIR.101.11.1297.
228. Kuck KH., Cappato R., Siebels J., Ruppel R. Randomized comparison of antiarrhythmic drug therapy with implantable defibrillators in patients resuscitated from cardiac arrest: The cardiac arrest study hamburg (CASH). *Circulation* 2000;102(7):748-54. Doi: 10.1161/01.CIR.102.7.748.
229. Connolly SJ., Hallstrom AP., Cappato R., et al. Meta-analysis of the implantable cardioverter defibrillator secondary prevention trials. *Eur Heart J* 2000;21(24):2071-8. Doi: 10.1053/euhj.2000.2476.
230. Ortiz M., Martin A., Arribas F., et al. Randomized comparison of intravenous procainamide vs. intravenous amiodarone for the acute treatment of tolerated wide QRS tachycardia: The PROCAMIO study. *Eur Heart J* 2017;38(17):1329-35. Doi: 10.1093/eurheartj/ehw230.
231. Jáuregui-Garrido B. Procainamida, mejor opción en taquicardia ventricular bien tolerada. Estudio PROCAMIO. In: Fernández-Lozano I, Gómez de Diego JJ, López-Lluya MT, Marzal-Martín D, Murga-Eizagaetzabarría N, and Vidal-Pérez R, editors. *Cardiología hoy 2016: Resumen anual de los avances en investigación y cambios en la práctica clínica*. 1st ed. Madrid: Sociedad Española de Cardiología; 2016. p. 590-3.
232. Preliminary Report: Effect of Encainide and Flecainide on Mortality in a Randomized Trial of Arrhythmia Suppression after Myocardial Infarction. *N Engl J Med* 1989;321(6):406-12. Doi: 10.1056/nejm198908103210629.

233. D.Sc. EMVWDM. Classification of antidysrhythmic drugs. *Pharmacol Ther Part B Gen Syst* 1975;1(1):115-38. Doi: 10.1016/0306-039X(75)90019-7.
234. Julian DG., Camm AJ., Frangin G., et al. Randomised trial of effect of amiodarone on mortality in patients with left-ventricular dysfunction after recent myocardial infarction: EMIAT. *Lancet* 1997;349(9053):667-74. Doi: 10.1016/S0140-6736(96)09145-3.
235. Josephson ME., Harken AH., Horowitz LN. Endocardial excision: A new surgical technique for the treatment of recurrent ventricular tachycardia. *Circulation* 1979;60(7):1430-9. Doi: 10.1161/01.CIR.60.7.1430.
236. Mukaddirov M., Demaria RG., Perrault LP., Frapier JM., Albat B. Reconstructive surgery of postinfarction left ventricular aneurysms: techniques and unsolved problems. *Eur J Cardio-Thoracic Surg* 2008:256-61. Doi: 10.1016/j.ejcts.2008.03.061.
237. Sartipy U., Albåge A., Insulander P., Lindblom D. Surgery for ventricular tachycardia in patients undergoing surgical ventricular restoration: The Karolinska approach. *J Interv Card Electrophysiol* 2007:171-8. Doi: 10.1007/s10840-007-9152-7.
238. Moran JM., Kehoe RF., Loeb JM., Lichtenthal PR., Sanders JH., Michaelis LL. Extended Endocardial Resection for the Treatment of Ventricular Tachycardia and Ventricular Fibrillation. *Ann Thorac Surg* 1982;34(5):538-52. Doi: 10.1016/S0003-4975(10)63001-9.
239. Rastegar H., Link MS., Foote CB., Wang PJ., Manolis AS., Mark Estes NA. Perioperative and long-term results with mapping-guided subendocardial resection and left ventricular endoaneurysmorrhaphy. *Circulation* 1996;94(5):1041-8. Doi:

- 10.1161/01.CIR.94.5.1041.
240. Page PL., Cardinal R., Shenasa M., Kaltenbrunner W., Cossette R., Nadeau R. Surgical treatment of ventricular tachycardia: Regional cryoablation guided by computerized epicardial and endocardial mapping. *Circulation* 1989;80(3 SUPPL. I).
241. Krishnan SC., Josephson ME. Surgery for postinfarction ventricular tachycardia: Is it obsolete? *PACE - Pacing Clin Electrophysiol* 2000:1295-301. Doi: 10.1111/j.1540-8159.2000.tb00948.x.
242. Hartzler GO. Electrode catheter ablation of refractory focal ventricular tachycardia. *J Am Coll Cardiol* 1983;2(6):1107-13. Doi: 10.1016/S0735-1097(83)80337-4.
243. Morady F. Radio-Frequency Ablation as Treatment for Cardiac Arrhythmias. *N Engl J Med* 1999;340(7):534-44. Doi: 10.1056/nejm199902183400707.
244. Gepstein L., Hayam G., Ben-Haim SA. A novel method for nonfluoroscopic catheter-based electroanatomical mapping of the heart: In vitro and in vivo accuracy results. *Circulation* 1997;95(6):1611-22. Doi: 10.1161/01.CIR.95.6.1611.
245. Guandalini GS., Liang JJ., Marchlinski FE. Ventricular Tachycardia Ablation: Past, Present, and Future Perspectives. *JACC Clin Electrophysiol* 2019:1363-83. Doi: 10.1016/j.jacep.2019.09.015.
246. Stevenson WG., Friedman PL., Sager PT., et al. Exploring postinfarction reentrant ventricular tachycardia with entrainment mapping. *J Am Coll Cardiol* 1997:1180-9. Doi: 10.1016/S0735-1097(97)00065-X.
247. Tung R. Challenges and Pitfalls of Entrainment Mapping of Ventricular Tachycardia. *Circ Arrhythmia Electrophysiol* 2017;10(4). Doi: 10.1161/CIRCEP.116.004560.
248. Tung R., Raiman M., Liao H., et al. Simultaneous Endocardial and Epicardial

- Delineation of 3D Reentrant Ventricular Tachycardia. *J Am Coll Cardiol* 2020;75(8):884-97. Doi: 10.1016/j.jacc.2019.12.044.
249. Shirai Y., Liang JJ., Santangeli P., et al. Comparison of the Ventricular Tachycardia Circuit between Patients with Ischemic and Nonischemic Cardiomyopathies: Detailed Characterization by Entrainment. *Circ Arrhythmia Electrophysiol* 2019;12(7). Doi: 10.1161/CIRCEP.119.007249.
250. Josephson ME., Waxman HL., Cain ME., Gardner MJ., Buxton AE. Ventricular activation during ventricular endocardial pacing. II. Role of pace-mapping to localize origin of ventricular tachycardia. *Am J Cardiol* 1982;50(1):11-22. Doi: 10.1016/0002-9149(82)90003-0.
251. De Chillou C., Groben L., Magnin-Poull I., et al. Localizing the critical isthmus of postinfarct ventricular tachycardia: The value of pace-mapping during sinus rhythm. *Hear Rhythm* 2014;11(2):175-81. Doi: 10.1016/j.hrthm.2013.10.042.
252. Tung R., Mathuria N., Michowitz Y., et al. Functional pace-mapping responses for identification of targets for catheter ablation of scar-mediated ventricular tachycardia. *Circ Arrhythmia Electrophysiol* 2012;5(2):264-72. Doi: 10.1161/CIRCEP.111.967976.
253. Gerstenfeld EP., Dixit S., Callans DJ., Rajawat Y., Rho R., Marchlinski FE. Quantitative comparison of spontaneous and paced 12-lead electrocardiogram during right ventricular outflow tract ventricular tachycardia. *J Am Coll Cardiol* 2003;41(11):2046-53. Doi: 10.1016/S0735-1097(03)00427-3.
254. Chang YT., Lin YJ., Chung FP., et al. Ablation of ventricular arrhythmia originating at the papillary muscle using an automatic pacemapping module. *Hear Rhythm* 2016;13(7):1431-40. Doi: 10.1016/j.hrthm.2016.03.017.

255. Marchlinski FE., Callans DJ., Gottlieb CD., Zado E. Linear ablation lesions for control of unmappable ventricular tachycardia in patients with ischemic and nonischemic cardiomyopathy. *Circulation* 2000;101(11):1288-96. Doi: 10.1161/01.CIR.101.11.1288.
256. Briceño DF., Romero J., Gianni C., et al. Substrate Ablation of Ventricular Tachycardia: Late Potentials, Scar Dechanneling, Local Abnormal Ventricular Activities, Core Isolation, and Homogenization. *Card Electrophysiol Clin* 2017:81-91. Doi: 10.1016/j.ccep.2016.10.014.
257. Arenal A., Glez-Torrecilla E., Ortiz M., et al. Ablation of electrograms with an isolated, delayed component as treatment of unmappable monomorphic ventricular tachycardias in patients with structural heart disease. *J Am Coll Cardiol* 2003;41(1):81-92. Doi: 10.1016/S0735-1097(02)02623-2.
258. Vergara P., Trevisi N., Ricco A., et al. Late potentials abolition as an additional technique for reduction of arrhythmia recurrence in scar related ventricular tachycardia ablation. *J Cardiovasc Electrophysiol* 2012;23(6):621-7. Doi: 10.1111/j.1540-8167.2011.02246.x.
259. Jaïs P., Maury P., Khairy P., et al. Elimination of local abnormal ventricular activities : A new end point for substrate modification in patients with scar-related ventricular tachycardia. *Circulation* 2012;125(18):2184-96. Doi: 10.1161/CIRCULATIONAHA.111.043216.
260. Di Biase L., Santangeli P., Burkhardt DJ., et al. Endo-epicardial homogenization of the scar versus limited substrate ablation for the treatment of electrical storms in patients with ischemic cardiomyopathy. *J Am Coll Cardiol* 2012;60(2):132-41. Doi:

- 10.1016/j.jacc.2012.03.044.
261. Tzou WS., Frankel DS., Hegeman T., et al. Core isolation of critical arrhythmia elements for treatment of multiple scar-based ventricular tachycardias. *Circ Arrhythmia Electrophysiol* 2015;8(2):353-61. Doi: 10.1161/CIRCEP.114.002310.
262. Berruezo A., Acosta J., Fernández-Armenta J., et al. Safety, long-term outcomes and predictors of recurrence after first-line combined endoepicardial ventricular tachycardia substrate ablation in arrhythmogenic cardiomyopathy. Impact of arrhythmic substrate distribution pattern. A prospective multicentre st. *Europace* 2017;19(4):607-16. Doi: 10.1093/europace/euw212.
263. Berruezo A., Fernández-Armenta J., Andreu D., et al. Scar dechanneling. *Circ Arrhythmia Electrophysiol* 2015;8(2):326-36. Doi: 10.1161/CIRCEP.114.002386.
264. Fernandez-Armenta J., Berruezo A., Mont L., et al. Scar dechanneling in scar-related ventricular tachycardia. *Hear Rhythm* 2013;10(5):S139.
265. Di Biase L., Burkhardt JD., Lakkireddy D., et al. Ablation of Stable VTs Versus Substrate Ablation in Ischemic Cardiomyopathy the VISTA Randomized Multicenter Trial. *J Am Coll Cardiol* 2015;66(25):2872-82. Doi: 10.1016/j.jacc.2015.10.026.
266. Bricenõ DF., Romero J., Villablanca PA., et al. Long-term outcomes of different ablation strategies for ventricular tachycardia in patients with structural heart disease: Systematic review and meta-analysis. *Europace* 2018:104-15. Doi: 10.1093/europace/eux109.
267. Santangeli P., Muser D., Zado ES., et al. Acute hemodynamic decompensation during catheter ablation of scar-related ventricular tachycardia: Incidence, predictors, and impact on mortality. *Circ Arrhythmia Electrophysiol* 2015;8(1):68-75. Doi:

- 10.1161/CIRCEP.114.002155.
268. Reddy VY., Reynolds MR., Neuzil P., et al. Prophylactic Catheter Ablation for the Prevention of Defibrillator Therapy. *N Engl J Med* 2007;357(26):2657-65. Doi: 10.1056/nejmoa065457.
269. Kuck KH., Schaumann A., Eckardt L., et al. Catheter ablation of stable ventricular tachycardia before defibrillator implantation in patients with coronary heart disease (VTACH): a multicentre randomised controlled trial. *Lancet* 2010;375(9708):31-40. Doi: 10.1016/S0140-6736(09)61755-4.
270. Al-Khatib SM., Daubert JP., Anstrom KJ., et al. Catheter ablation for ventricular tachycardia in patients with an implantable cardioverter defibrillator (CALYPSO) pilot trial. *J Cardiovasc Electrophysiol* 2015;26(2):151-7. Doi: 10.1111/jce.12567.
271. Sapp JL., Wells GA., Parkash R., et al. Ventricular Tachycardia Ablation versus Escalation of Antiarrhythmic Drugs. *N Engl J Med* 2016;375(2):111-21. Doi: 10.1056/nejmoa1513614.
272. Kuck KH., Tilz RR., Deneke T., et al. Impact of substrate modification by catheter ablation on implantable cardioverter-defibrillator interventions in patients with unstable ventricular arrhythmias and coronary artery disease: Results from the multicenter randomized controlled SMS (Substrate . *Circ Arrhythmia Electrophysiol* 2017;10(3). Doi: 10.1161/CIRCEP.116.004422.
273. Tilz RR., Eitel C., Lyan E., et al. Preventive ventricular tachycardia ablation in patients with ischaemic cardiomyopathy: Meta-analysis of randomised trials. *Arrhythmia Electrophysiol Rev* 2019;8(3):173-9. Doi: 10.15420/aer.2019.31.3.
274. Fernandez-Armenta J., Soto-Iglesias D., Silva E., et al. Safety and Outcomes of



- Ventricular Tachycardia Substrate Ablation During Sinus Rhythm: A Prospective Multicenter Registry. *JACC Clin Electrophysiol* 2020;6(11):1435-48. Doi: 10.1016/j.jacep.2020.07.028.
275. Acosta J., Andreu D., Penela D., et al. Elucidation of hidden slow conduction by double ventricular extrastimuli: A method for further arrhythmic substrate identification in ventricular tachycardia ablation procedures. *Europace* 2018;20(2):337-46. Doi: 10.1093/europace/euw325.
276. Jackson N., Gizurason S., Viswanathan K., et al. Decrement Evoked Potential Mapping: Basis of a Mechanistic Strategy for Ventricular Tachycardia Ablation. *Circ Arrhythmia Electrophysiol* 2015;8(6):1433-42. Doi: 10.1161/CIRCEP.115.003083.
277. de Riva M., Naruse Y., Ebert M., et al. Targeting the Hidden Substrate Unmasked by Right Ventricular Extrastimulation Improves Ventricular Tachycardia Ablation Outcome After Myocardial Infarction. *JACC Clin Electrophysiol* 2018;4(3):316-27. Doi: 10.1016/j.jacep.2018.01.013.
278. Acosta J., Soto-Iglesias D., Jáuregui B., et al. Long-term outcomes of ventricular tachycardia substrate ablation incorporating hidden slow conduction analysis. *Hear Rhythm* 2020;17(10):1696-703. Doi: 10.1016/j.hrthm.2020.05.017.
279. Porta-Sánchez A., Jackson N., Lukac P., et al. Multicenter Study of Ischemic Ventricular Tachycardia Ablation With Decrement-Evoked Potential (DEEP) Mapping With Extra Stimulus. *JACC Clin Electrophysiol* 2018;4(3):307-15. Doi: 10.1016/j.jacep.2017.12.005.
280. Shariat MH., Gupta D., Gul EE., et al. Ventricular substrate identification using close-coupled paced electrogram feature analysis. *Europace* 2019;21(3):492-501. Doi:

- 10.1093/europace/euy265.
281. Njeim M., Yokokawa M., Frank L., et al. Value of Cardiac Magnetic Resonance Imaging in Patients with Failed Ablation Procedures for Ventricular Tachycardia. *J Cardiovasc Electrophysiol* 2016;27(2):183-9. Doi: 10.1111/jce.12848.
282. Tung R., Michowitz Y., Yu R., et al. Epicardial ablation of ventricular tachycardia: An institutional experience of safety and efficacy. *Hear Rhythm* 2013;10(4):490-8. Doi: 10.1016/j.hrthm.2012.12.013.
283. Acosta J., Fernández-Armenta J., Penela D., et al. Infarct transmuralidad as a criterion for first-line endo-epicardial substrate-guided ventricular tachycardia ablation in ischemic cardiomyopathy. *Hear Rhythm* 2016;13(1):85-95. Doi: 10.1016/j.hrthm.2015.07.010.
284. Yamashita S., Cochet H., Sacher F., et al. Impact of new technologies and approaches for post-myocardial infarction ventricular tachycardia ablation during long-term follow-up. *Circ Arrhythmia Electrophysiol* 2016;9(7). Doi: 10.1161/CIRCEP.116.003901.
285. Zghaib T., Ipek EG., Hansford R., et al. Standard Ablation Versus Magnetic Resonance Imaging-Guided Ablation in the Treatment of Ventricular Tachycardia. *Circ Arrhythmia Electrophysiol* 2018;11(1). Doi: 10.1161/CIRCEP.117.005973.
286. Andreu D., Penela D., Acosta J., et al. Cardiac magnetic resonance-aided scar dechanneling: Influence on acute and long-term outcomes. *Hear Rhythm* 2017;14(8):1121-8. Doi: 10.1016/j.hrthm.2017.05.018.
287. Nazarian S., Hansford R., Roguin A., et al. A prospective evaluation of a protocol for magnetic resonance imaging of patients with implanted cardiac devices. *Ann Intern*

- Med 2011;155(7):415-24. Doi: 10.7326/0003-4819-155-7-201110040-00004.
288. Russo RJ., Costa HS., Silva PD., et al. Assessing the Risks Associated with MRI in Patients with a Pacemaker or Defibrillator. *N Engl J Med* 2017;376(8):755-64. Doi: 10.1056/nejmoa1603265.
289. Do DH., Eyvazian V., Bayoneta AJ., et al. Cardiac magnetic resonance imaging using wideband sequences in patients with nonconditional cardiac implanted electronic devices. *Hear Rhythm* 2018;15(2):218-25. Doi: 10.1016/j.hrthm.2017.10.003.
290. Roca-Luque I., Van Breukelen A., Alarcon F., et al. Ventricular scar channel entrances identified by new wideband cardiac magnetic resonance sequence to guide ventricular tachycardia ablation in patients with cardiac defibrillators. *Europace* 2020;22(4):598-606. Doi: 10.1093/europace/euaa021.
291. Yamashita S., Sacher F., Mahida S., et al. Role of high-resolution image integration to visualize left phrenic nerve and coronary arteries during epicardial ventricular tachycardia ablation. *Circ Arrhythmia Electrophysiol* 2015;8(2):371-80. Doi: 10.1161/CIRCEP.114.002420.
292. Van Huls Van Taxis CF., Wijnmaalen AP., Piers SR., Van Der Geest RJ., Schalij MJ., Zeppenfeld K. Real-time integration of MDCT-derived coronary anatomy and epicardial fat: Impact on epicardial electroanatomic mapping and ablation for ventricular arrhythmias. *JACC Cardiovasc Imaging* 2013;6(1):42-52. Doi: 10.1016/j.jcmg.2012.05.016.
293. Rivera S., De La Paz Ricapito M., Tomas L., et al. Results of cryoenergy and radiofrequency-based catheter ablation for treating ventricular arrhythmias arising from the papillary muscles of the left ventricle, guided by intracardiac

- echocardiography and image integration. *Circ Arrhythmia Electrophysiol* 2016;9(4).  
Doi: 10.1161/CIRCEP.115.003874.
294. Esposito A., Palmisano A., Antunes S., et al. Cardiac CT With Delayed Enhancement in the Characterization of Ventricular Tachycardia Structural Substrate: Relationship Between CT-Segmented Scar and Electro-Anatomic Mapping. *JACC Cardiovasc Imaging* 2016;9(7):822-32. Doi: 10.1016/j.jcmg.2015.10.024.
295. Komatsu Y., Cochet H., Jadidi A., et al. Regional myocardial wall thinning at multidetector computed tomography correlates to arrhythmogenic substrate in postinfarction ventricular tachycardia: Assessment of structural and electrical substrate. *Circ Arrhythmia Electrophysiol* 2013;6(2):342-50. Doi: 10.1161/CIRCEP.112.000191.
296. Gerber BL., Belge B., Legros GJ., et al. Characterization of acute and chronic myocardial infarcts by multidetector computed tomography: Comparison with contrast-enhanced magnetic resonance. *Circulation* 2006;113(6):823-33. Doi: 10.1161/CIRCULATIONAHA.104.529511.
297. Lardo AC., Cordeiro MAS., Silva C., et al. Contrast-enhanced multidetector computed tomography viability imaging after myocardial infarction: Characterization of myocyte death, microvascular obstruction, and chronic scar. *Circulation* 2006;113(3):394-404. Doi: 10.1161/CIRCULATIONAHA.105.521450.
298. Yamashita S., Sacher F., Mahida S., et al. Image integration to guide catheter ablation in scar-related ventricular tachycardia. *J Cardiovasc Electrophysiol* 2016;27(6):699-708. Doi: 10.1111/jce.12963.
299. Tian J., Jeudy J., Smith MF., et al. Three-dimensional contrast-enhanced

- multidetector CT for anatomic, dynamic, and perfusion characterization of abnormal myocardium to guide ventricular tachycardia ablations. *Circ Arrhythmia Electrophysiol* 2010;3(5):496-504. Doi: 10.1161/CIRCEP.109.889311.
300. Takigawa M., Duchateau J., Sacher F., et al. Are wall thickness channels defined by computed tomography predictive of isthmuses of postinfarction ventricular tachycardia? *Hear Rhythm* 2019;16(11):1661-8. Doi: 10.1016/j.hrthm.2019.06.012.
301. Jáuregui B., Soto-Iglesias D., Penela D., et al. Follow-Up After Myocardial Infarction to Explore the Stability of Arrhythmogenic Substrate: The Footprint Study. *JACC Clin Electrophysiol* 2020;6(2):207-18. Doi: 10.1016/j.jacep.2019.10.002.
302. Dobaczewski M., Gonzalez-Quesada C., Frangogiannis NG. The extracellular matrix as a modulator of the inflammatory and reparative response following myocardial infarction. *J Mol Cell Cardiol* 2010:504-11. Doi: 10.1016/j.yjmcc.2009.07.015.
303. Holmes JW., Borg TK., Covell JW. Structure and mechanics of healing myocardial infarcts. *Annu Rev Biomed Eng* 2005:223-53. Doi: 10.1146/annurev.bioeng.7.060804.100453.
304. Jugdutt BI. Remodeling of the myocardium and potential targets in the collagen degradation and synthesis pathways. *Curr Drug Targets - Cardiovasc Haematol Disord* 2003:1-30. Doi: 10.2174/1568006033337276.
305. Richardson WJ., Clarke SA., Alexander Quinn T., Holmes JW. Physiological implications of myocardial scar structure. *Compr Physiol* 2015;5(4):1877-909. Doi: 10.1002/cphy.c140067.
306. Dewald O., Ren G., Duerr GD., et al. Of Mice and Dogs: Species-Specific Differences in the Inflammatory Response Following Myocardial Infarction. *Am J Pathol*

- 2004;164(2):665-77. Doi: 10.1016/s0002-9440(10)63154-9.
307. Fishbein MC., Maclean D., Maroko PR. The histopathologic evolution of myocardial infarction. *Chest* 1978;73(6):843-9. Doi: 10.1378/chest.73.6.843.
308. Fishbein MC., Maclean D., Maroko PR. Experimental myocardial infarction in the rat. Qualitative and quantitative changes during pathologic evolution. *Am J Pathol* 1978;90(1):57-70.
309. Yang F., Liu YH., Yang XP., Xu J., Kapke A., Carretero OA. Myocardial infarction and cardiac remodelling in mice. *Exp Physiol* 2002;87(5):547-55. Doi: 10.1113/eph8702385.
310. Nahrendorf M., Swirski FK., Aikawa E., et al. The healing myocardium sequentially mobilizes two monocyte subsets with divergent and complementary functions. *J Exp Med* 2007;204(12):3037-47. Doi: 10.1084/jem.20070885.
311. Bosch X., Jáuregui B., Villamor N., et al. Monocyte Subsets Are Differently Associated with Infarct Size, Left Ventricular Function, and the Formation of a Potentially Arrhythmogenic Scar in Patients with Acute Myocardial Infarction. *J Cardiovasc Transl Res* 2020;13(5):722-30. Doi: 10.1007/s12265-019-09944-8.
312. Maekawa Y., Anzai T., Yoshikawa T., et al. Prognostic significance of peripheral monocytosis after reperfused acute myocardial infarction: A possible role for left ventricular remodeling. *J Am Coll Cardiol* 2002;39(2):241-6. Doi: 10.1016/S0735-1097(01)01721-1.
313. Tsujioka H., Imanishi T., Ikejima H., et al. Impact of Heterogeneity of Human Peripheral Blood Monocyte Subsets on Myocardial Salvage in Patients With Primary Acute Myocardial Infarction. *J Am Coll Cardiol* 2009;54(2):130-8. Doi:

- 10.1016/j.jacc.2009.04.021.
314. Tapp LD., Shantsila E., Wrigley BJ., Pamukcu B., Lip GYH. The CD14++CD16+ monocyte subset and monocyte-platelet interactions in patients with ST-elevation myocardial infarction. *J Thromb Haemost* 2012;10(7):1231-41. Doi: 10.1111/j.1538-7836.2011.04603.x.
315. Zhou X., Liu XL., Ji WJ., et al. The kinetics of circulating monocyte subsets and monocyte-platelet aggregates in the acute phase of st-elevation myocardial infarction associations with 2-year cardiovascular events. *Med (United States)* 2016;95(18):e3466. Doi: 10.1097/MD.0000000000003466.
316. Van Der Laan AM., Hirsch A., Robbers LFHJ., et al. A proinflammatory monocyte response is associated with myocardial injury and impaired functional outcome in patients with ST-segment elevation myocardial infarction: Monocytes and myocardial infarction. *Am Heart J* 2012;163(1). Doi: 10.1016/j.ahj.2011.09.002.
317. Lindsey ML., Zamilpa R. Temporal and spatial expression of matrix metalloproteinases and tissue inhibitors of metalloproteinases following myocardial infarction. *Cardiovasc Ther* 2012:31-41. Doi: 10.1111/j.1755-5922.2010.00207.x.
318. Vanhoutte D., Schellings M., Pinto Y., Heymans S. Relevance of matrix metalloproteinases and their inhibitors after myocardial infarction: A temporal and spatial window. *Cardiovasc Res* 2006:604-13. Doi: 10.1016/j.cardiores.2005.10.002.
319. Zamilpa R., Lindsey ML. Extracellular matrix turnover and signaling during cardiac remodeling following MI: Causes and consequences. *J Mol Cell Cardiol* 2010:558-63. Doi: 10.1016/j.yjmcc.2009.06.012.
320. van Furth R., Cohn ZA. The origin and kinetics of mononuclear phagocytes. *J Exp Med*

- 1968;128(3):415-35. Doi: 10.1084/jem.128.3.415.
321. Ursell PC., Gardner PI., Albala A., Fenoglio JJ., Wit AL. Structural and electrophysiological changes in the epicardial border zone of canine myocardial infarcts during infarct healing. *Circ Res* 1985;56(3):436-51. Doi: 10.1161/01.RES.56.3.436.
322. Ma Y., De Castro Brás LE., Toba H., et al. Myofibroblasts and the extracellular matrix network in post-myocardial infarction cardiac remodeling. *Pflugers Arch Eur J Physiol* 2014;1113-27. Doi: 10.1007/s00424-014-1463-9.
323. Daskalopoulos EP., Janssen BJA., Blankesteyn WM. Myofibroblasts in the infarct area: Concepts and challenges. *Microscopy and Microanalysis*, vol. 18. 2012. p. 35-49.
324. Goldsmith EC., Bradshaw AD., Spinale FG. Cellular mechanisms of tissue fibrosis. 2. Contributory pathways leading to myocardial fibrosis: Moving beyond collagen expression. *Am J Physiol - Cell Physiol* 2013;304(5). Doi: 10.1152/ajpcell.00347.2012.
325. Bryant JE., Shamhart PE., Luther DJ., et al. Cardiac myofibroblast differentiation is attenuated by  $\alpha 3$  integrin blockade: Potential role in post-MI remodeling. *J Mol Cell Cardiol* 2009;46(2):186-92. Doi: 10.1016/j.yjmcc.2008.10.022.
326. Cleutjens JPM., Kandala JC., Guarda E., Guntaka R V., Weber KT. Regulation of collagen degradation in the rat myocardium after infarction. *J Mol Cell Cardiol* 1995;27(6):1281-92. Doi: 10.1016/S0022-2828(05)82390-9.
327. Morishita N., Kusachi S., Yamasaki S., Kondo J., Tsuji T. Sequential changes in laminin and type IV collagen in the infarct zone - immunohistochemical study in rat myocardial infarction. *Circ J* 1996;60(2):108-14. Doi: 10.1253/jcj.60.108.



328. Peterson JT., Li H., Dillon L., Bryant JW. Evolution of matrix metalloprotease and tissue inhibitor expression during heart failure progression in the infarcted rat. *Cardiovasc Res* 2000;46(2):307-15. Doi: 10.1016/S0008-6363(00)00029-8.
329. Sun Y., Zhang JQ., Zhang J., Lamparter S. Cardiac remodeling by fibrous tissue after infarction in rats. *J Lab Clin Med* 2000;135(4):316-23. Doi: 10.1067/mlc.2000.105971.
330. Yamanishi A., Kusachi S., Nakahama M., et al. Sequential changes in the localization of the type IV collagen  $\alpha$  chain in the infarct zone: Immunohistochemical study of experimental myocardial infarction in the rat. *Pathol Res Pract* 1998;194(6):413-22. Doi: 10.1016/S0344-0338(98)80032-0.
331. Zimmerman SD., Thomas DP., Velleman SG., Li X., Hansen TR., McCormick RJ. Time course of collagen and decorin changes in rat cardiac and skeletal muscle post-MI. *Am J Physiol - Hear Circ Physiol* 2001;281(4 50-4). Doi: 10.1152/ajpheart.2001.281.4.h1816.
332. Blom AS., Pilla JJ., Arkles J., et al. Ventricular Restraint Prevents Infarct Expansion and Improves Borderzone Function After Myocardial Infarction: A Study Using Magnetic Resonance Imaging, Three-Dimensional Surface Modeling, and Myocardial Tagging. *Ann Thorac Surg* 2007;84(6):2004-10. Doi: 10.1016/j.athoracsur.2007.06.062.
333. Gupta KB., Ratcliffe MB., Fallert MA., Edmunds LH., Bogen DK. Changes in passive mechanical stiffness of myocardial tissue with aneurysm formation. *Circulation* 1994;89(5):2315-26. Doi: 10.1161/01.CIR.89.5.2315.
334. Jugdutt BI., Amy RWM. Healing after myocardial infarction in the dog: Changes in infarct hydroxyproline and topography. *J Am Coll Cardiol* 1986;7(1):91-102. Doi:

- 10.1016/S0735-1097(86)80265-0.
335. Jugdutt BI., Joljart MJ., Khan MI. Rate of Collagen Deposition during Healing and Ventricular Remodeling after Myocardial Infarction in Rat and Dog Models. *Circulation* 1996;94(1):94-101. Doi: 10.1161/01.CIR.94.1.94.
336. Jugdutt BI., Schwarz-Michorowski BL., Khan MI. Effect of long-term captopril therapy on left ventricular remodeling and function during healing of canine myocardial infarction. *J Am Coll Cardiol* 1992;19(3):713-21. Doi: 10.1016/S0735-1097(10)80298-0.
337. McCormick RJ., Musch TI., Bergman BC., Thomas DP. Regional differences in LV collagen accumulation and mature cross-linking after myocardial infarction in rats. *Am J Physiol - Hear Circ Physiol* 1994;266(1 35-1). Doi: 10.1152/ajpheart.1994.266.1.h354.
338. Doi M., Kusachi S., Murakami T., et al. Time-dependent changes of decorin in the infarct zone after experimentally induced myocardial infarction in rats: Comparison with biglycan. *Pathol Res Pract* 2000;196(1):23-33. Doi: 10.1016/S0344-0338(00)80018-7.
339. Fomovsky GM., Holmes JW. Evolution of scar structure, mechanics, and ventricular function after myocardial infarction in the rat. *Am J Physiol - Hear Circ Physiol* 2010;298(1). Doi: 10.1152/ajpheart.00495.2009.
340. Lerman RH., Apstein CS., Kagan HM., et al. Myocardial healing and repair after experimental infarction in the rabbit. *Circ Res* 1983;53(3):378-88. Doi: 10.1161/01.RES.53.3.378.
341. Vivaldi MT., Eyre DR., Kloner RA., Schoen FJ. Effects of methylprednisolone on

- collagen biosynthesis in healing acute myocardial infarction. *Am J Cardiol* 1987;60(4):424-5. Doi: 10.1016/0002-9149(87)90277-3.
342. Westermann D., Mersmann J., Melchior A., et al. Biglycan is required for adaptive remodeling after myocardial infarction. *Circulation* 2008;117(10):1269-76. Doi: 10.1161/CIRCULATIONAHA.107.714147.
343. Yamamoto K., Kusachi S., Ninomiya Y., et al. Increase in the expression of biglycan mRNA expression co-localized closely with that of type I collagen mRNA in the infarct zone after experimentally-induced myocardial infarction in rats. *J Mol Cell Cardiol* 1998;30(9):1749-56. Doi: 10.1006/jmcc.1998.0737.
344. Reimer KA., Heide RSV., Richard VJ. Reperfusion in acute myocardial infarction: Effect of timing and modulating factors in experimental models. *Am J Cardiol* 1993;72(19). Doi: 10.1016/0002-9149(93)90102-I.
345. Vandervelde S., Van Amerongen MJ., Tio RA., Petersen AH., Van Luyn MJA., Harmsen MC. Increased inflammatory response and neovascularization in reperfused vs. nonreperfused murine myocardial infarction. *Cardiovasc Pathol* 2006;15(2):83-90. Doi: 10.1016/j.carpath.2005.10.006.
346. Connelly CM., Vogel WM., Wiegner AW., et al. Effects of reperfusion after coronary artery occlusion on post-infarction scar tissue. *Circ Res* 1985;57(4):562-77. Doi: 10.1161/01.RES.57.4.562.
347. Dall'Armellina E., Karia N., Lindsay AC., et al. Dynamic changes of edema and late gadolinium enhancement after acute myocardial infarction and their relationship to functional recovery and salvage index. *Circ Cardiovasc Imaging* 2011;4(3):228-36. Doi: 10.1161/CIRCIMAGING.111.963421.

348. Rochitte CE., Lima JAC., Bluemke DA., et al. Magnitude and time course of microvascular obstruction and tissue injury after acute myocardial infarction. *Circulation* 1998;98(10):1006-14. Doi: 10.1161/01.CIR.98.10.1006.
349. Fieno DS., Hillenbrand HB., Rehwald WG., et al. Infarct resorption, compensatory hypertrophy, and differing patterns of ventricular remodeling following myocardial infarctions of varying size. *J Am Coll Cardiol* 2004;43(11):2124-31. Doi: 10.1016/j.jacc.2004.01.043.
350. Hillenbrand HB., Sandstede J., Störk S., et al. Remodeling of the infarct territory in the time course of infarct healing in humans. *Magn Reson Mater Physics, Biol Med* 2011;24(5):277-84. Doi: 10.1007/s10334-011-0262-y.
351. Pokorney SD., Rodriguez JF., Ortiz JT., Lee DC., Bonow RO., Wu E. Infarct healing is a dynamic process following acute myocardial infarction. *J Cardiovasc Magn Reson* 2012;14(1). Doi: 10.1186/1532-429X-14-62.
352. Jáuregui B., Soto-Iglesias D., Zucchelli G., et al. Arrhythmogenic substrate detection in chronic ischaemic patients undergoing ventricular tachycardia ablation using multidetector cardiac computed tomography: Compared evaluation with cardiac magnetic resonance. *Europace* 2021;23(1):82-90. Doi: 10.1093/europace/euaa237.
353. Soto-Iglesias D., Penela D., Jáuregui B., et al. Cardiac Magnetic Resonance-Guided Ventricular Tachycardia Substrate Ablation. *JACC Clin Electrophysiol* 2020;6(4):436-47. Doi: 10.1016/j.jacep.2019.11.004.
354. Jauregui B., Soto-Iglesias D., Penela D., et al. Cardiovascular magnetic resonance determinants of ventricular arrhythmic events after myocardial infarction. *EP Eur* 2021;23(Supplement\_3). Doi: 10.1093/europace/euab116.374.

355. Reddy VY., Malchano ZJ., Holmvang G., et al. Integration of cardiac magnetic resonance imaging with three-dimensional electroanatomic mapping to guide left ventricular catheter manipulation: Feasibility in a porcine model of healed myocardial infarction. *J Am Coll Cardiol* 2004;44(11). Doi: 10.1016/j.jacc.2004.08.063.
356. Acosta J., Fernández-Armenta J., Borràs R., et al. Scar Characterization to Predict Life-Threatening Arrhythmic Events and Sudden Cardiac Death in Patients With Cardiac Resynchronization Therapy: The GAUDI-CRT Study. *JACC Cardiovasc Imaging* 2018;11(4):561-72. Doi: 10.1016/j.jcmg.2017.04.021.
357. Perea RJ., Morales-Ruiz M., Ortiz-Perez JT., et al. Utility of galectin-3 in predicting post-infarct remodeling after acute myocardial infarction based on extracellular volume fraction mapping. *Int J Cardiol* 2016;223. Doi: 10.1016/j.ijcard.2016.08.070.
358. Ruparelia N., Godec J., Lee R., et al. Acute myocardial infarction activates distinct inflammation and proliferation pathways in circulating monocytes, prior to recruitment, and identified through conserved transcriptional responses in mice and humans. *Eur Heart J* 2015;36(29):1923-34. Doi: 10.1093/eurheartj/ehv195.
359. Xuan W., Liao Y., Chen B., et al. Detrimental effect of fractalkine on myocardial ischaemia and heart failure. *Cardiovasc Res* 2011;92(3):385-93. Doi: 10.1093/cvr/cvr221.
360. Miragoli M., Gaudesius G., Rohr S. Electrotonic modulation of cardiac impulse conduction by myofibroblasts. *Circ Res* 2006;98(6):801-10. Doi: 10.1161/01.RES.0000214537.44195.a3.
361. Stolzmann P., Scheffel H., Leschka S., et al. Reference values for quantitative left ventricular and left atrial measurements in cardiac computed tomography. *Eur Radiol*

- 2008;18(8):1625-34. Doi: 10.1007/s00330-008-0939-4.
362. Ghannam M., Cochet H., Jais P., et al. Correlation between computer tomography-derived scar topography and critical ablation sites in postinfarction ventricular tachycardia. *J Cardiovasc Electrophysiol* 2018;29(3):438-45. Doi: 10.1111/jce.13441.
363. Bourier F., Martin R., Martin CA., et al. Is it feasible to offer "targeted ablation" of ventricular tachycardia circuits with better understanding of isthmus anatomy and conduction characteristics? *Europace* 2019;127-33. Doi: 10.1093/europace/euy173.
364. Soto-Iglesias D., Acosta J., Penela D., et al. Image-based criteria to identify the presence of epicardial arrhythmogenic substrate in patients with transmural myocardial infarction. *Heart Rhythm* 2018;15(6):814-21. Doi: 10.1016/j.hrthm.2018.02.007.
365. Gupta S., Desjardins B., Baman T., et al. Delayed-enhanced MR scar imaging and intraprocedural registration into an electroanatomical mapping system in post-infarction patients. *JACC Cardiovasc Imaging* 2012;207-10. Doi: 10.1016/j.jcmg.2011.08.021.
366. Kwon DH., Asamoto L., Popovic ZB., et al. Infarct characterization and quantification by delayed enhancement cardiac magnetic resonance imaging is a powerful independent and incremental predictor of mortality in patients with advanced ischemic cardiomyopathy. *Circ Cardiovasc Imaging* 2014;7(5):796-804. Doi: 10.1161/CIRCIMAGING.114.002077.
367. Ganesan AN., Gunton J., Nucifora G., McGavigan AD., Selvanayagam JB. Impact of Late Gadolinium Enhancement on mortality, sudden death and major adverse cardiovascular events in ischemic and nonischemic cardiomyopathy: A systematic

- review and meta-analysis. *Int J Cardiol* 2018;254:230-7. Doi: 10.1016/j.ijcard.2017.10.094.
368. Mehta D., Curwin J., Gomes JA., Fuster V. Sudden death in coronary artery disease: Acute ischemia versus myocardial substrate. *Circulation* 1997;3215-23. Doi: 10.1161/01.CIR.96.9.3215.
369. Crespo C., Linhart M., Acosta J., et al. Optimisation of cardiac resynchronisation therapy device selection guided by cardiac magnetic resonance imaging: Cost-effectiveness analysis. *Eur J Prev Cardiol* 2020;27(6):622-32. Doi: 10.1177/2047487319873149.
370. Huikuri HV., Castellanos A., Myerburg RJ. Sudden Death Due to Cardiac Arrhythmias. *N Engl J Med* 2001;345(20):1473-82. Doi: 10.1056/nejmra000650.
371. Fernández-Armenta J., Penela D., Acosta J., et al. Substrate modification or ventricular tachycardia induction, mapping, and ablation as the first step? A randomized study. *Hear Rhythm* 2016;13(8):1589-95. Doi: 10.1016/j.hrthm.2016.05.013.
372. Andreu D., Fernández-Armenta J., Acosta J., et al. A QRS axis-based algorithm to identify the origin of scar-related ventricular tachycardia in the 17-segment American Heart Association model. *Hear Rhythm* 2018;15(10):1491-7. Doi: 10.1016/j.hrthm.2018.06.013.
373. Berte B., Zeppenfeld K., Tung R. Impact of micro-, mini- And multi-electrode mapping on ventricular substrate characterisation. *Arrhythmia Electrophysiol Rev* 2020;9(3):128-35. Doi: 10.15420/AER.2020.24.
374. Okubo K., Frontera A., Bisceglia C., et al. Grid Mapping Catheter for Ventricular

- Tachycardia Ablation. *Circ Arrhythmia Electrophysiol* 2019;12(9). Doi: 10.1161/CIRCEP.119.007500.
375. Hadjis A., Frontera A., Limite LR., et al. Complete Electroanatomic Imaging of the Diastolic Pathway Is Associated with Improved Freedom from Ventricular Tachycardia Recurrence. *Circ Arrhythmia Electrophysiol* 2020:927-37. Doi: 10.1161/CIRCEP.120.008651.
376. Anter E. Limitations and Pitfalls of Substrate Mapping for Ventricular Tachycardia. *JACC Clin Electrophysiol* 2021:542-60. Doi: 10.1016/j.jacep.2021.02.007.

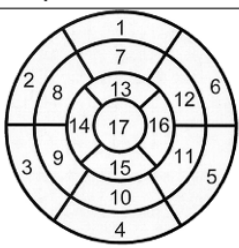
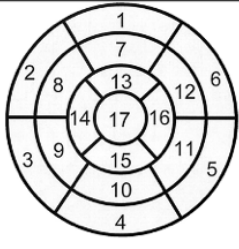
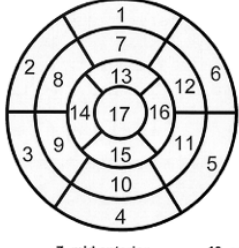




# 10. ANEXOS

## ANEXO I: HOJAS DE RECOGIDA DE DATOS

Recogida de datos para el estudio FOOTPRINT (artículo 1):

<b>Nombre y apellidos:</b>																													
<b>NHC:</b>																													
7 DÍAS	Nº total de canales: ..... Datos por canal:																												
	<table border="1" style="width: 100%; border-collapse: collapse;"> <thead> <tr> <th style="width: 10%;">ID canal</th> <th style="width: 40%;">Distribución</th> <th style="width: 20%;">ID segmento</th> <th style="width: 30%;">Capas</th> </tr> </thead> <tbody> <tr><td>1</td><td>Longit. / Transv. / Diag.</td><td></td><td></td></tr> <tr><td>2</td><td>Longit. / Transv. / Diag.</td><td></td><td></td></tr> <tr><td>3</td><td>Longit. / Transv. / Diag.</td><td></td><td></td></tr> <tr><td>4</td><td>Longit. / Transv. / Diag.</td><td></td><td></td></tr> <tr><td>5</td><td>Longit. / Transv. / Diag.</td><td></td><td></td></tr> <tr><td>6</td><td>Longit. / Transv. / Diag.</td><td></td><td></td></tr> </tbody> </table>	ID canal	Distribución	ID segmento	Capas	1	Longit. / Transv. / Diag.			2	Longit. / Transv. / Diag.			3	Longit. / Transv. / Diag.			4	Longit. / Transv. / Diag.			5	Longit. / Transv. / Diag.			6	Longit. / Transv. / Diag.		
	ID canal	Distribución	ID segmento	Capas																									
	1	Longit. / Transv. / Diag.																											
	2	Longit. / Transv. / Diag.																											
	3	Longit. / Transv. / Diag.																											
4	Longit. / Transv. / Diag.																												
5	Longit. / Transv. / Diag.																												
6	Longit. / Transv. / Diag.																												
<table style="width: 100%;"> <tr> <td style="width: 50%;">VTDVI (mL): .....</td> <td style="width: 50%;">Scar (g): .....</td> </tr> <tr> <td>VTSVI (mL): .....</td> <td>BZ (g): .....</td> </tr> <tr> <td>FEVI (%): .....</td> <td>Core (g): .....</td> </tr> <tr> <td>Notas:</td> <td>BZ mass (g): .....</td> </tr> </table>	VTDVI (mL): .....	Scar (g): .....	VTSVI (mL): .....	BZ (g): .....	FEVI (%): .....	Core (g): .....	Notas:	BZ mass (g): .....																					
VTDVI (mL): .....	Scar (g): .....																												
VTSVI (mL): .....	BZ (g): .....																												
FEVI (%): .....	Core (g): .....																												
Notas:	BZ mass (g): .....																												
<b>Esquema de los canales</b>																													
																													
<table style="width: 100%; font-size: 0.8em;"> <tr> <td>1. basal anterior</td> <td>7. mid anterior</td> <td>13. apical anterior</td> </tr> <tr> <td>2. basal anteroseptal</td> <td>8. mid anteroseptal</td> <td>14. apical septal</td> </tr> <tr> <td>3. basal inferoseptal</td> <td>9. mid inferoseptal</td> <td>15. apical inferior</td> </tr> <tr> <td>4. basal inferior</td> <td>10. mid inferior</td> <td>16. apical lateral</td> </tr> <tr> <td>5. basal inferolateral</td> <td>11. mid inferolateral</td> <td>17. apex</td> </tr> <tr> <td>6. basal anterolateral</td> <td>12. mid anterolateral</td> <td></td> </tr> </table>	1. basal anterior	7. mid anterior	13. apical anterior	2. basal anteroseptal	8. mid anteroseptal	14. apical septal	3. basal inferoseptal	9. mid inferoseptal	15. apical inferior	4. basal inferior	10. mid inferior	16. apical lateral	5. basal inferolateral	11. mid inferolateral	17. apex	6. basal anterolateral	12. mid anterolateral												
1. basal anterior	7. mid anterior	13. apical anterior																											
2. basal anteroseptal	8. mid anteroseptal	14. apical septal																											
3. basal inferoseptal	9. mid inferoseptal	15. apical inferior																											
4. basal inferior	10. mid inferior	16. apical lateral																											
5. basal inferolateral	11. mid inferolateral	17. apex																											
6. basal anterolateral	12. mid anterolateral																												
6 MESES	Nº total de canales: ..... Datos por canal:																												
	<table border="1" style="width: 100%; border-collapse: collapse;"> <thead> <tr> <th style="width: 10%;">ID canal</th> <th style="width: 40%;">Distribución</th> <th style="width: 20%;">ID segmento</th> <th style="width: 30%;">Capas</th> </tr> </thead> <tbody> <tr><td>1</td><td>Longit. / Transv. / Diag.</td><td></td><td></td></tr> <tr><td>2</td><td>Longit. / Transv. / Diag.</td><td></td><td></td></tr> <tr><td>3</td><td>Longit. / Transv. / Diag.</td><td></td><td></td></tr> <tr><td>4</td><td>Longit. / Transv. / Diag.</td><td></td><td></td></tr> <tr><td>5</td><td>Longit. / Transv. / Diag.</td><td></td><td></td></tr> <tr><td>6</td><td>Longit. / Transv. / Diag.</td><td></td><td></td></tr> </tbody> </table>	ID canal	Distribución	ID segmento	Capas	1	Longit. / Transv. / Diag.			2	Longit. / Transv. / Diag.			3	Longit. / Transv. / Diag.			4	Longit. / Transv. / Diag.			5	Longit. / Transv. / Diag.			6	Longit. / Transv. / Diag.		
	ID canal	Distribución	ID segmento	Capas																									
	1	Longit. / Transv. / Diag.																											
	2	Longit. / Transv. / Diag.																											
	3	Longit. / Transv. / Diag.																											
4	Longit. / Transv. / Diag.																												
5	Longit. / Transv. / Diag.																												
6	Longit. / Transv. / Diag.																												
<table style="width: 100%;"> <tr> <td style="width: 50%;">VTDVI (mL): .....</td> <td style="width: 50%;">Scar (g): .....</td> </tr> <tr> <td>VTSVI (mL): .....</td> <td>BZ (g): .....</td> </tr> <tr> <td>FEVI (%): .....</td> <td>Core (g): .....</td> </tr> <tr> <td>Notas:</td> <td>BZ mass (g): .....</td> </tr> </table>	VTDVI (mL): .....	Scar (g): .....	VTSVI (mL): .....	BZ (g): .....	FEVI (%): .....	Core (g): .....	Notas:	BZ mass (g): .....																					
VTDVI (mL): .....	Scar (g): .....																												
VTSVI (mL): .....	BZ (g): .....																												
FEVI (%): .....	Core (g): .....																												
Notas:	BZ mass (g): .....																												
<b>Esquema de los canales</b>																													
																													
<table style="width: 100%; font-size: 0.8em;"> <tr> <td>1. basal anterior</td> <td>7. mid anterior</td> <td>13. apical anterior</td> </tr> <tr> <td>2. basal anteroseptal</td> <td>8. mid anteroseptal</td> <td>14. apical septal</td> </tr> <tr> <td>3. basal inferoseptal</td> <td>9. mid inferoseptal</td> <td>15. apical inferior</td> </tr> <tr> <td>4. basal inferior</td> <td>10. mid inferior</td> <td>16. apical lateral</td> </tr> <tr> <td>5. basal inferolateral</td> <td>11. mid inferolateral</td> <td>17. apex</td> </tr> <tr> <td>6. basal anterolateral</td> <td>12. mid anterolateral</td> <td></td> </tr> </table>	1. basal anterior	7. mid anterior	13. apical anterior	2. basal anteroseptal	8. mid anteroseptal	14. apical septal	3. basal inferoseptal	9. mid inferoseptal	15. apical inferior	4. basal inferior	10. mid inferior	16. apical lateral	5. basal inferolateral	11. mid inferolateral	17. apex	6. basal anterolateral	12. mid anterolateral												
1. basal anterior	7. mid anterior	13. apical anterior																											
2. basal anteroseptal	8. mid anteroseptal	14. apical septal																											
3. basal inferoseptal	9. mid inferoseptal	15. apical inferior																											
4. basal inferior	10. mid inferior	16. apical lateral																											
5. basal inferolateral	11. mid inferolateral	17. apex																											
6. basal anterolateral	12. mid anterolateral																												
4 AÑOS	Nº total de canales: ..... Datos por canal:																												
	<table border="1" style="width: 100%; border-collapse: collapse;"> <thead> <tr> <th style="width: 10%;">ID canal</th> <th style="width: 40%;">Distribución</th> <th style="width: 20%;">ID segmento</th> <th style="width: 30%;">Capas</th> </tr> </thead> <tbody> <tr><td>1</td><td>Longit. / Transv. / Diag.</td><td></td><td></td></tr> <tr><td>2</td><td>Longit. / Transv. / Diag.</td><td></td><td></td></tr> <tr><td>3</td><td>Longit. / Transv. / Diag.</td><td></td><td></td></tr> <tr><td>4</td><td>Longit. / Transv. / Diag.</td><td></td><td></td></tr> <tr><td>5</td><td>Longit. / Transv. / Diag.</td><td></td><td></td></tr> <tr><td>6</td><td>Longit. / Transv. / Diag.</td><td></td><td></td></tr> </tbody> </table>	ID canal	Distribución	ID segmento	Capas	1	Longit. / Transv. / Diag.			2	Longit. / Transv. / Diag.			3	Longit. / Transv. / Diag.			4	Longit. / Transv. / Diag.			5	Longit. / Transv. / Diag.			6	Longit. / Transv. / Diag.		
	ID canal	Distribución	ID segmento	Capas																									
	1	Longit. / Transv. / Diag.																											
	2	Longit. / Transv. / Diag.																											
	3	Longit. / Transv. / Diag.																											
4	Longit. / Transv. / Diag.																												
5	Longit. / Transv. / Diag.																												
6	Longit. / Transv. / Diag.																												
<table style="width: 100%;"> <tr> <td style="width: 50%;">VTDVI (mL): .....</td> <td style="width: 50%;">Scar (g): .....</td> </tr> <tr> <td>VTSVI (mL): .....</td> <td>BZ (g): .....</td> </tr> <tr> <td>FEVI (%): .....</td> <td>Core (g): .....</td> </tr> <tr> <td>Notas:</td> <td>BZ mass (g): .....</td> </tr> </table>	VTDVI (mL): .....	Scar (g): .....	VTSVI (mL): .....	BZ (g): .....	FEVI (%): .....	Core (g): .....	Notas:	BZ mass (g): .....																					
VTDVI (mL): .....	Scar (g): .....																												
VTSVI (mL): .....	BZ (g): .....																												
FEVI (%): .....	Core (g): .....																												
Notas:	BZ mass (g): .....																												
<b>Esquema de los canales</b>																													
																													
<table style="width: 100%; font-size: 0.8em;"> <tr> <td>1. basal anterior</td> <td>7. mid anterior</td> <td>13. apical anterior</td> </tr> <tr> <td>2. basal anteroseptal</td> <td>8. mid anteroseptal</td> <td>14. apical septal</td> </tr> <tr> <td>3. basal inferoseptal</td> <td>9. mid inferoseptal</td> <td>15. apical inferior</td> </tr> <tr> <td>4. basal inferior</td> <td>10. mid inferior</td> <td>16. apical lateral</td> </tr> <tr> <td>5. basal inferolateral</td> <td>11. mid inferolateral</td> <td>17. apex</td> </tr> <tr> <td>6. basal anterolateral</td> <td>12. mid anterolateral</td> <td></td> </tr> </table>	1. basal anterior	7. mid anterior	13. apical anterior	2. basal anteroseptal	8. mid anteroseptal	14. apical septal	3. basal inferoseptal	9. mid inferoseptal	15. apical inferior	4. basal inferior	10. mid inferior	16. apical lateral	5. basal inferolateral	11. mid inferolateral	17. apex	6. basal anterolateral	12. mid anterolateral												
1. basal anterior	7. mid anterior	13. apical anterior																											
2. basal anteroseptal	8. mid anteroseptal	14. apical septal																											
3. basal inferoseptal	9. mid inferoseptal	15. apical inferior																											
4. basal inferior	10. mid inferior	16. apical lateral																											
5. basal inferolateral	11. mid inferolateral	17. apex																											
6. basal anterolateral	12. mid anterolateral																												

DATA COLLECTION SHEET. FOOTPRINT STUDY: Cath lab & Follow-up ECGs

PATIENT ID (Bea): \_\_\_\_\_

DATE OF MYOCARDIAL INFARCTION: ...../...../.....

Site of myocardial infarction (check all that apply):

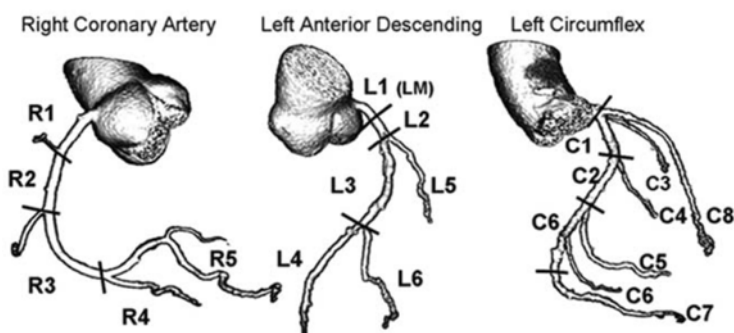
Septal (V1-V2)	Anterior (V3-V4)	Inferior (II, III, aVF)	Lateral (V5-V6, I-aVL)
----------------	------------------	-------------------------	------------------------

Lesions found after catheterization:

Specify segment, % of stenosis, which was the culprit lesion, the revascularization approach, initial and final TIMI:

.....  
 .....  
 .....  
 .....  
 .....  
 .....  
 .....  
 .....  
 .....  
 .....  
 .....  
 .....

Coronary Artery Segmentation Model



Taken from Cerdi RJ, et al. Circ Cardiovasc Imaging 2012;5:587-595.

ECG 1 DATE: ...../...../.....

Rhythm: Sinus Atrial fibrillation Other:.....

Conduction disturbances:

- AV block? Specify: 1<sup>st</sup> 2<sup>nd</sup> Mobitz I (Wenckebach) 2<sup>nd</sup> Mobitz II 3<sup>rd</sup>
- Bundle branch block? Specify: RBBB LBBB LAFB LPFB

Intervals/segments (ms):

PR	QRS	ST	RR	QT	QTc (Bazett)
----	-----	----	----	----	--------------

Wave measurements (mm):

	I	II	III	aVR	aVL	aVF	V1	V2	V3	V4	V5	V6
Q												
R												
S												

Selvester QRS Score (check all that apply):

Complete 54-Criteria, 32-Point QRS Scoring System*			
Maximum Lead Points	Criteria	Points	
I (2)	Q≥30 ms (1)	(1)	V <sub>1</sub> Anterior (2) Any Q (1) Q or S≥1.8 mV (1)
	R/Q ≤1 (1) R≥0.2 mV (1)	(1)	
II (2)	Q≥40 ms (2) Q≥30 ms (1)	(2)	Posterior (4) R/S ≥1 (1) R≥50 ms (2) R≥1.0 mV (2) R≥40 ms (1) R≥0.6 mV (1) Q and S≥0.3 mV (1)
		(1)	
aVL (2)	Q≥30 ms (1) R/Q ≤1 (1)	(1)	V <sub>2</sub> Anterior (1) Any Q (1) R≤10 ms (1) R≤0.1 mV (1) R≤R <sub>V1</sub> mV (1)
		(1)	
aVF (5)	Q≥50 ms (3) Q≥40 ms (2) Q≥30 ms (1)	(3)	Posterior (4) R/S ≥1.5 (1) R≥60 ms (2) R≥2.0 mV (2) R≥50 ms (1) R≥1.5 mV (1) Q and S≥0.4 mV (1)
	R/Q ≤1 (2) R/Q ≥2 (1)	(2)	
		(1)	
		(1)	
V <sub>4</sub> (1)	Any Q (1) R≤20 ms (1) R≤0.2 mV (1)	(1)	V <sub>3</sub> (3) Q≥20 ms (1) R/S ≤0.5 (2) R/Q ≤0.5 (2) R/S ≤1 (1) R/Q ≤1 (1) R≤0.7 mV (1) Notched R (1)
		(1)	
V <sub>5</sub> (3)	Q≥30 ms (1)	(1)	V <sub>4</sub> (3) Q≥30 ms (1) R/S ≤1 (2) R/Q ≤1 (2) R/S ≤2 (1) R/Q ≤2 (1) R≤0.7 mV (1) Notched R (1)
		(1)	
V <sub>6</sub> (3)	Q≥30 ms (1)	(1)	V <sub>5</sub> (3) Q≥30 ms (1) R/S ≤1 (2) R/Q ≤1 (2) R/S ≤3 (1) R/Q ≤3 (1) R≤0.6 mV (1) Notched R (1)
		(1)	

\*When more than one criterion in the brace is met, select the one with the most points. Notched R indicates a notch that begins within the first 40 ms. From Hindman et al.<sup>15</sup>

## Recogida de datos para la ablación de taquicardias ventriculares guiada por RM (artículo 5):

### **Datos Paciente:**

Nombre: Fecha nacimiento:  
Edad:  
NHC: Fecha: N° EEF: Sexo:

### **Datos basales:**

HTA: Sí / No Diabetes: Sí / No Dislipemia: Sí / No Fumador: Sí / No  
/ Ex EPOC: Si/No CKD: Si/No  
Cardiopatía: No / Isquémica / Dilatada / DAVD / DAVI / Hipertrófica / Hipertensiva / ...  
IAM previo: No / Anterior / Inferior / Septal / Lateral / Apical Antigüedad IAM:  
NYHA: I / II / III / IV FA permanente: Sí / No DAI: Previo / Post /  
No  
N° Episodios DAI / TV: N° Terapias (ATP+Choques): N° Choques:  
N° Episodios fuera de zona:  
Medicación:  $\beta$  Bloquers / IECAS-ARA II / Clase I / Sotalol / Amiodarona / Ant-Ca

### **Indicación:**

Indicación: EV-TVNS / TVMS / Síncope+Inducción TV / Terapia DAI / FV  
Tormenta Arrítmica: Sí / No TV incesante: Sí / No

### **Pruebas previas:**

Ecocardiograma: FE(%): DDVE(mm): DSVE(mm):  
Hipocinesia: No / Anterior / Inferior / Septal / Lateral / Apical / Difusa  
KT: Lesiones coronarias: Sí / No N° vasos lesiones: 1 / 2 / 3 N° vasos ReV: 1 / 2 / 3  
RMN: Tipo: 1.5T / 3T Realce Tardío: No / VI / VD Endo / Epi /  
Transmural/Mid  
Localización: No / Anterior / Inferior / Septal / Lateral / Apical  
TAC: Sí / No Holter (%EV):

### **TV Clínica 1:**

ECG 12 derivaciones: Sí / No LCT(ms): Tolerada: Sí / No  
Morfología: BRD / BRI Eje(°): Transición precordiales V.....  
Criterios Epi: Sí / No

### **TV Clínica 2:**

ECG 12 derivaciones: Sí / No LCT(ms): Tolerada: Sí / No  
Morfología: BRD / BRI Eje(°): Transición precordiales V.....  
Criterios Epi: Sí / No (Pseudo Delta / Q en V1-V2 / Q en dI / MDI)

### **Sustrato y approach TV:**

EV-TV Tracto Salida – Tracto Entrada idiopática / Otras idiopáticas / EV por cicatriz  
Sustrato Cardiopatía Isquémica / Sustrato Cardiopatía No Isquémica / Sustrato DAVD

**Datos procedimiento:**

Sustrato:

Mapa CARTO: VD / VI / Ambos

	Loc Scar	Ablación	Pts Mapa	Pts Azules	Pts Naranjas	Pts Verdes	Pts Negros	Pts RF
<b>Endo</b>								
<b>Endo Remap</b>								
<b>Epi</b>								
<b>Epi Remap</b>								

*Loc Scar: No / Anterior / Inferior / Septal / Lateral / Apical Ablación: No / Lineal / Puntual / Mixto*

*Azul: Potencial retrasado; Naranja: doble extra negativo; Verde: doble extra positivo; Negro: entrada de canal*

**Tabla TV observadas en procedimiento (redondear TV clínicas):**

Nº TV	BRD / BRI	LCT (ms)	Eje (°)	Transición Precordiales	Tolerada	Target	Approach de la TV
1							
2							
3							

*BRD / BRI: Morfología taquicardia (bloqueo de Rama Derecha o Izquierda)*

*LCT (ms): Longitud de ciclo de la taquicardia en ms*

*Eje: Grados (de -180° a 180°)*

*Transición precordiales: V1-V6 (V0 = sin transición)*

*Tolerada: TV tolerada hemodinámicamente (Si / No)*

*Target: Intento de ablación de la TV, incluso sin aplicar RF (Si / No)*

*Approach TV: Approach mediante Pacemapping (PM), o mediante mapeo en taquicardia (Act o Act Carto)*

Nº TV	Stop durante RF	Lesión	Origen	Epi	Inducción	Istmo TV	Localización Istmo	Canales
1								
2								
3								

*Stop durante RF: La TV paró mientras se aplicaba RF (Si / No)*

*Lesión: Lesión puntual o Lineal*

Origen: Localización del origen de la taquicardia: TSVD / TEVD / TSVI (Valsalva / Seno Coronario / Infravalvular / Unión mitroaórtica) / TEVI / Scar VD / Scar VI

Inducción: Espontánea-mecánica/Inducción basal/Residual

Localización Istmo: Lugar del mapa de voltaje donde se identifica el istmo (No / Core / BZ / Helathy)

Canales: Identificación canales por: Late potentials (LP) / Voltaje / No

**Materiales:**

Técnica: CARTO / Convencional / NAVX/ Rhythmia Catéter: 4 mm / 4 mm irrigado / 8 mm/3.5 mm irrigado/MiFi

Agilis: Sí / No Guía Epi inicial: Sí / No Fusión: TAC / RMN / RMN + Scar / No

Acceso: Venoso: Sí / No Arterial: Sí / No Epi: Sí / No Transeptal: Sí / No

Estrategia: Endo / Epi / Epi tras mapeo endo / Epi tras ablación endo fallida

Canalización SC: Sí / No posible / No intentado PentaRay: Sí / No Orión: Si/No  
EG patológicos tras RF: Sí / No

**Inducción:**

Inducción Basal: No / Espontánea / Clínica / No clínica / No realizado

Protocolo inducción: Maastrich / Basal Iso: No / Basal / Final / Basal y Final

Protocolo inducción: No / Basal / Final / Basal y Final

**Datos Finales:**

Tiempo (min): RX (min): RX (mGy): RF (Nº): RF (s):

Hora punción femoral: Hora inicio mapeo: Hora fin procedimiento:

TV inducidas: TV target: TV target activación: TV ablacionadas:

TV residuales:

Complicaciones: CVE: Sí / No

Éxito: Sí / No / Parcial

Motivo: Mal tolerada / No induc / Ablación ineficaz / No acceso / Todavía induc/ FV –TP

**EGM Residuales:**

Tipo: [ ] Azul [ ] Negro [ ] Verde

Localización: Anterior/Inferior/Lateral/Septal Endo/Epi

Razón no eliminación EGM:

No se eliminan: Potencias elevadas / Inestabilidad del catéter

Proximidad: Sistema de conducción / Frénico / Coronaria / No accesible



# ANEXO II: APROBACIÓN DE LOS COMITÉS ÉTICOS DE INVESTIGACIÓN CLÍNICA

## Aprobación CEIC para el artículo 1:

### DICTAMEN DEL COMITÉ ÉTICO DE INVESTIGACIÓN CLÍNICA

JOAN ALBERT ARNAIZ GARGALLO, Secretario del **Comité Ético de Investigación Clínica del Hospital Clínic de Barcelona**

Certifica:

Que este Comité ha evaluado la propuesta del promotor, para que se realice el estudio:

DOCUMENTOS CON VERSIONES:

Tipo	Subtipo	Versión
Hoja Información de Paciente	V2_31/08/2016	V2_31/08/2016
Protocolo	V2_31/08/2016	V2_31/08/2016

TÍTULO: Long-term FOllOw-up after an acuTe myocardial infarction to exPloRe the stability of the arrhythmogeNic SubsTrate The FOOTPRINT study.

INVESTIGADOR PRINCIPAL: ANTONIO BERRUEZO SANCHEZ

y considera que, teniendo en cuenta la respuesta a las aclaraciones solicitadas (si las hubiera), y que:

- Se cumplen los requisitos necesarios de idoneidad del protocolo en relación con los objetivos del estudio y están justificados los riesgos y molestias previsibles.
- La capacidad del investigador y los medios disponibles son apropiados para llevar a cabo el estudio.
- Que se han evaluado la compensaciones económicas previstas (cuando las haya) y su posible interferencia con el respeto a los postulados éticos y se consideran adecuadas.
- Que dicho estudio se ajusta a las normas éticas esenciales y criterios deontológicos que rigen en este centro.
- Que dicho estudio cumple con las obligaciones establecidas por la normativa de investigación y confidencialidad que le son aplicables.
- Que dicho estudio se incluye en una de las líneas de investigación biomédica acreditadas en este centro, cumpliendo los requisitos necesarios, y que es viable en todos sus términos.

Este CEIC acepta que dicho estudio sea realizado, debiendo ser comunicado a dicho Comité Ético todo cambio en el protocolo o acontecimiento adverso grave.

y hace constar que:

1º En la reunión celebrada el día 15 de septiembre de 2016, acta 18/2016 se decidió emitir el informe correspondiente al estudio de referencia.

2º El CEIC del Hospital Clínic i Provincial, tanto en su composición como en sus PNTs, cumple con las normas de BPC (CPMP/ICH/135/95)

3º Listado de miembros:

**Presidente:**

- FRANCISCO JAVIER CARNE CLADELLAS (Médico Farmacólogo Clínico, HCB)

HOSPITAL CLÍNIC DE BARCELONA  
Villarroel, 170 - 08036 Barcelona (España)  
Tel. 93 227 54 00 Fax 93 227 54 54  
www.hospitalclinic.org



**Secretario:**

- JOAN ALBERT ARNAIZ GARGALLO (Médico Farmacólogo Clínico, HCB)

**Vocales:**

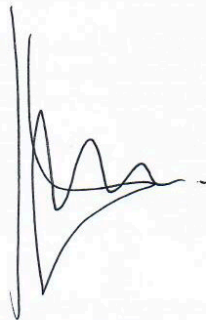
- ITZIAR DE LECUONA (Jurista, Observatorio de Bioética y Derecho, UB)
- MONTSERRAT GONZALEZ CREUS (Trabajadora Social, Servicio de Atención al Usuario, HCB)
- MIRIAM MENDEZ GARCÍA (Abogada, HCB)
- MONTSERRAT NUÑEZ JUÁREZ (Enfermera, HCB)
- JOSE RIOS GUILLERMO (Estadístico. Plataforma de Estadística Médica. IDIBAPS)
- JOSE MIGUEL SOTOCA (Farmacéutico Atención Primaria, CAP Les Corts)
- ANTONI TRILLA GARCIA (Médico Epidemiólogo, HCB - Director UAPS)
- OCTAVI SANCHEZ LOPEZ (Representante de los pacientes)
- MARIA JESÚS BERTRAN LUENGO (Médico Epidemiólogo, HCB)
- MARTA AYMERICH GREGORIO (Médico Hematólogo, HCB)
- GISELA RIU VILADOMS (Farmacéutica Hospitalaria, HCB)

CIF - G-08431173

En el caso de que se evalúe algún proyecto del que un miembro sea investigador/colaborador, este se ausentará de la reunión durante la discusión del proyecto.

Para que conste donde proceda, y a petición del promotor,

Barcelona, a 13 de septiembre de 2016



Mod\_04 (V3 de 29/06/2016)

**CLÍNIC**  
**BARCELONA**  
Hospital Universitari  
COMITÈ ÈTIC  
INVESTIGACIÓ CLÍNICA

Reg. HCB/2016/0621

PR

**D. Joan Albert Barberá Mir**, Adjunto a la Dirección de Investigación del Hospital Clínic de Barcelona,

CERTIFICA:

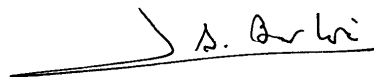
Que el Comité de Investigación del Hospital Clínic, en la sesión celebrada en el día de hoy, ha analizado el proyecto de investigación titulado:

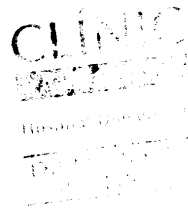
*Role of serum biomarkers of cardiac fibrosis and magnetic resonance imaging to predict adverse cardiac remodeling and ventricular susceptibility.*

cuyo investigador principal es el Dr. **Berruezo Sánchez, Antonio** del Servicio de **Cardiología**

entendiendo que dicho estudio se incluye en una de las líneas de investigación biomédica acreditadas en este centro, cumpliendo los requisitos metodológicos necesarios, y que es viable en todos sus términos, por lo que lo ha considerado adecuado y ha decidido su aprobación.

Lo que firmo en Barcelona, a 25/11/2010





Registro: 2010 / 6148

DICTAMEN DEL COMITÉ ÉTICO DE INVESTIGACIÓN CLÍNICA

NEUS RIBA GARCIA, Secretaria del **Comité Ético de Investigación Clínica del Hospital Clínic de Barcelona**

Certifica:

Que este Comité ha evaluado la propuesta del promotor, para que se realice el estudio:

DOCUMENTOS CON VERSIONES:

Tipo	Subtipo	Versión
Protocolo		v. 1
Hoja Información de Paciente	Subproyecto 1, 2, 3 4 y 5	v. 1

TÍTULO: Caracterización del Sustrato Arritmogénico y Evaluación de su Utilidad en la Predicción de Eventos Arritmicos y Guiado de los Procedimientos de Ablación

INVESTIGADOR PRINCIPAL: ANTONIO BERRUEZO SANCHEZ

y considera que, teniendo en cuenta la respuesta a las aclaraciones solicitadas (si las hubiera), y que:

- El estudio se plantea siguiendo los requisitos de la legislación vigente.
- Se cumplen los requisitos necesarios de idoneidad del protocolo en relación con los objetivos del estudio y están justificados los riesgos y molestias previsibles para el sujeto, teniendo en cuenta los beneficios esperados.
- Son adecuados tanto el procedimiento para obtener el consentimiento informado como la compensación prevista para los sujetos por daños que pudieran derivarse de su participación en el ensayo (si procede).
- Que se han evaluado las compensaciones económicas previstas (cuando las haya) y su posible interferencia con el respeto a los postulados éticos y se consideran adecuadas.
- La capacidad del investigador y sus colaboradores, y las instalaciones y medios disponibles, tal y como ha sido informado, son apropiados para llevar a cabo el estudio.
- Que dicho estudio se incluye en una de las líneas de investigación biomédica acreditadas en este centro, cumpliendo los requisitos necesarios, y que es viable en todos sus términos.

Este CEIC acepta que dicho estudio sea realizado, debiendo ser debiendo ser comunicado a dicho Comité Ético todo cambio en el protocolo o acontecimiento adverso grave.

CIF - G-08431173

y hace constar que:

1º En la reunión celebrada el día 11/06/2015, acta 11/2015 se decidió emitir el informe correspondiente al estudio de referencia.

2º El CEIC del Hospital Clínic i Provincial, tanto en su composición como en sus PNTs, cumple con las normas de BPC (CPMP/ICH/135/95)

3º Listado de miembros:

**Presidente:**

- FRANCISCO JAVIER CARNE CLADELLAS (Médico Farmacólogo Clínico, HCB)

**Vicepresidente:**

- BEGOÑA GOMEZ PEREZ (Farmacéutica Hospitalaria, HCB)

**Secretario:**

- NEUS RIBA GARCIA (Médico Farmacólogo Clínico, HCB)

**Vocales:**

- ITZIAR DE LECUONA (Jurista, Observatorio de Bioética y Derecho, UB)
- MONTSERRAT GONZALEZ CREUS (Trabajadora Social, Servicio de Atención al Usuario, HCB)
- MIRIAM MENDEZ GARCÍA (Abogada, HCB)
- MONTSERRAT NUÑEZ JUÁREZ (Enfermera, HCB)
- JOSE RIOS GUILLERMO (Estadístico, Farmacología Clínica, USEM, UASP, HCB)
- JOSE MIGUEL SOTOCA (Farmacéutico Atención Primaria, CAP Les Corts)
- ANTONI TRILLA GARCIA (Médico Epidemiólogo, HCB - Director UAPS)
- OCTAVI SANCHEZ LOPEZ (Representante de los pacientes)
- MARIA JESÚS BERTRAN LUENGO (Médico Epidemiólogo, HCB)
- MARTA AYMERICH GREGORIO (Médico Hematólogo, HCB)

En el caso de que se evalúe algún proyecto del que un miembro sea investigador/colaborador, este se ausentará de la reunión durante la discusión del proyecto.

Para que conste donde proceda, y a petición del promotor,



Barcelona, a 23 de junio de 2015

Reg. HCB/2014/1114

Mod\_02 (V2 de 22/10/2013)

PS



## ANEXO III: PUBLICACIONES ADICIONALES AL DOCTORADO

### ARTÍCULOS CIENTÍFICOS:

1. Soto-Iglesias D, Acosta J, Penela D, Fernández-Armenta J, Cabrera M, Martínez M, Vassanelli F, Alcaine A, Linhart M, Jáuregui B, Efimova E, Perea RJ, Prat-González S, Ortiz-Pérez JT, Bosch X, Mont L, Cámara O, Berruezo A. Image-Based Criteria to Identify the Presence of Epicardial arrhythmogenic Substrate in Patients with Transmural Myocardial Infarction. **Heart Rhythm 2018**;15:814-821.
2. Berruezo A, Efimova E, Acosta J, Jáuregui B. Isolated, Premature Ventricular Complex-Induced Right Ventricular Dysfunction Mimicking Arrhythmogenic Right Ventricular Cardiomyopathy. **HeartRhythm Case Rep 2018**;4:222-226.
3. Andreu D, Fernández-Armenta J, Acosta J, Penela D, Jáuregui B, Soto-Iglesias D, Syrovnev D, Arbelo E, Tolosana JM, Berruezo A. A QRS Axis-Based Algorithm to Identify the Origin of Scar-Related Ventricular Tachycardia in an American Heart Association 17-Segment Model. **Heart Rhythm 2018**;15:1491-1497.
4. Soto-Iglesias D, Andreu D, Jáuregui B, Linhart M, Mont L, Berruezo A. Mini-electrodes help identifying hidden slow conduction during ventricular tachycardia substrate ablation. **J Electrocardiol 2018**; 51:1011-1013.
5. Korshunov V, Penela D, Linhart M, Acosta J, Martinez M, Soto-Iglesias D, Fernández-Armenta J, Vassanelli F, Cabrera M, Borràs R, Jáuregui B, Ortiz-Pérez JT, Perea RJ, Bosch X, Sanchez-Quintana D, Mont L, Berruezo A. Prediction of premature ventricular complex origin in left vs. right ventricular outflow tract: a novel anatomical imaging approach. **Europace 2019**;21:147-153.

6. Pedrote A, Acosta J, Frutos-López M, Jáuregui-Garrido B, Alarcón F, Arana-Rueda E. Analysis of late reconnections after pulmonary vein isolation: Impact of interlesion contiguity and ablation index. **Pacing Clin Electrophysiol** **2019**;42:678-685.
7. Penela D, Martínez M, Fernández-Armenta J, Aguinaga L, Tercedor L, Ordóñez A, Acosta J, Martí-Almor J, Bisbal F, Rossi L, Borràs R, Linhart M, Soto-Iglesias D, Jáuregui B, Ortiz-Pérez JT, Perea RJ, Bosch X, Mont L, Berruezo A. Influence of myocardial scar on the response to frequent premature ventricular complex ablation. **Heart** **2019**;105:378-383.
8. Berruezo A, Penela D, Jáuregui B, Soto-Iglesias D, Aguinaga L, Ordóñez A, Fernández-Armenta A, Martínez M, Tercedor L, Bisbal F, Acosta J, Martí-Almor J, Aceña M, Anguera I, Rossi L, Linhart M, Borràs R, Doltra A, Sánchez P, Ortiz-Pérez JT, Perea RJ, Prat-González S, Teres C, Bosch X. Mortality and morbidity reduction after frequent premature ventricular complexes ablation in patients with left ventricular systolic dysfunction. **Europace** **2019**;21:1079-1087.
9. Jáuregui B. Biology, Culture and Society, Factors Configuring Health From a Gender Perspective. Has Cardiology Overcome the Challenge? **Rev Esp Cardiol (Engl Ed)** **2019**;72:800-802.
10. Crespo C, Linhart M, Acosta J, Soto-Iglesias D, Martínez M, Jáuregui B, Mira Á, Restovic G, Sagarra J, Auricchio A, Fahn B, Boltyenkov A, Lasalvia L, Sampietro-Colom L, Berruezo A. Optimisation of cardiac resynchronisation therapy device selection guided by cardiac magnetic resonance imaging: Cost-effectiveness analysis. **Eur J Prev Cardiol** **2020**;27:622-632.

11. Linhart M, Doltra A, Acosta J, Borràs R, Jáuregui B, Fernández-Armenta J, Anguera I, Bisbal F, Marí-Almor J, Tolosana JM, Penela D, Soto-Iglesias D, Villuendas R, Perea RJ, Ortiz JT, Bosch X, Auricchio A, Berruezo A. Ventricular arrhythmia risk is associated with myocardial scar but not with response to cardiac resynchronization therapy. **Europace** **2020**;22:1391-1400.
12. Arana-Rueda E, Jáuregui B, Frutos-López M, Acosta J, Sánchez-Brotóns JA, García-Riesco L, Campos-Pareja A, Nieto C, Pedrote A. Long-term survival and implantable cardiac defibrillator therapies according to sex. A propensity-matched study. **J Womens Health (Larchmt)** **2020**. doi: 10.1089/jwh.2020.8475 [Online ahead of print]
13. Alcaine A, Jáuregui B, Soto-Iglesias D, Acosta J, Penela D, Fernández-Armenta J, Linhart M, Andreu D, Mont L, Laguna P, Cámara Ó, Martínez JP, Berruezo A. Automatic Detection of Slow Conducting Channels during Substrate Ablation of Scar-related Ventricular Arrhythmias. **J Interv Cardiol** **2020**;2020:4386841.
14. López Rodríguez E, Jáuregui Garrido B, Ruiz Franco-Baux J, Caballero Gullón L, Guisado Rasco A, Jiménez-Hoyuela García JM. Valor pronóstico de la gammagrafía de perfusión miocárdica en pacientes diabéticos sin lesiones coronarias. **Rev Esp Med Nucl Imagen Mol** **2021**;40:100-106.
15. Acosta J, Soto-Iglesias D, Jáuregui B, Fernández-Armenta J, Penela D, Frutos-López M, Arana-Rueda E, Pedrote A, Mont L, Berruezo A. Long-term Outcomes of Ventricular Tachycardia Substrate Ablation Incorporating Hidden Slow Conduction Analysis. **Heart Rhythm** **2020**;17:1696-1703.



16. Penela D, [Jáuregui B](#), Berruezo A. Intracardiac Versus Transesophageal Echocardiography: If You Don't Compare Them You Don't Have the Answer. **JACC Clin Electrophysiol** **2020**;6:880-881.
17. Fernandez-Armenta J, Soto-Iglesias D, Silva E, Penela D, [Jáuregui B](#), Linhart M, Bisbal F, Acosta J, Fernandez M, Borrás R, Villuendas R, Cano L, Guasch E, Mont L, Berruezo A. Safety and Outcomes of Ventricular Tachycardia Substrate Ablation During Sinus Rhythm: A Prospective Multicenter Registry. **JACC Clin Electrophysiol** **2020**;6:1435-1448.
18. Berruezo A, Penela D, [Jáuregui B](#), Soto-Iglesias D. The role of imaging in catheter ablation of ventricular arrhythmias. **Pacing Clin Electrophysiol** **2021**;44:1115-1125.
19. [Jáuregui B](#), Fernández-Armenta J, Acosta J, Penela D, Terés C, Ordóñez A, Soto-Iglesias D, Silva E, Chauca A, Carreño JM, Scherer C, Pedrote A, Berruezo A. MANual vs. automatIc Local Activation Time Annotation for Guiding Premature Ventricular Complex Ablation Procedures (MANIaC-PVC Study). **Europace** **2021**;23:1285-1294.
20. [Jáuregui B](#), Penela D, Fernández-Armenta J, Acosta J, Terés C, Ordóñez A, Soto-Iglesias D, Silva E, Chauca A, Carreño JM, Scherer C, Falasconi G, Pedrote A, Berruezo A. Impact of a Pre-defined Pacemapping Protocol Use for Ablation of Infrequent Premature Ventricular Complexes: A Prospective, Multicenter Study. **Heart Rhythm** **2021**;S1547-5271(21)00450-1. [Online ahead of print]
21. Penela D, Teres C, Fernández-Armenta J, Aguinaga L, Tercedor L, Soto-Iglesias D, [Jáuregui B](#), Ordóñez A, Acosta J, Bisbal F, Aceña M, Silva E, Chauca A, De Sensi F, Vatasescu R, Sánchez-Millán P, Carballo J, Mont L, Berruezo A. Premature ventricular

- complex site of origin and ablation outcomes in patients with prior myocardial infarction. **Heart Rhythm** **2021**;18:27-33.
22. Teres C, Soto-Iglesias D, Penela D, Jáuregui B, Ordóñez A, Chauca A, Huguet M, Ramírez C, Oller G, Jornet A, Palet J, Santana D, Panaro A, Maldonado G, De León G, Gualis B, Jiménez G, Evangelista A, Carballo J, Berruezo A. Left atrial wall thickness of the pulmonary vein reconnection sites during atrial fibrillation redo procedures. **Pacing Clin Electrophysiol** **2021**;44:824-834.
23. Gandjbakhch E, Berruezo A, Gourraud JB, Sellal JM, Martins R, Sacher F, Pison LA, Pruvot E, Jáuregui B, Frontera A, Kumar S, Wong T, Della Bella P, Maury P. Outcomes After Catheter Ablation of Ventricular Tachycardia Without Implantable Cardioverter-Defibrillator in Arrhythmogenic Right Ventricular Cardiomyopathy. **Europace** **2021**;euab172. [Online ahead of print]
24. Teres C, Soto-Iglesias D, Penela D, Jáuregui B, Ordóñez A, Chauca A, Carreño JM, Scherer C, Huguet M, Ramírez C, Oller G, Palet J, Santana D, Panaro A, Maldonado G, De León G, Jiménez G, Evangelista A, Carballo J, Berruezo A. Personalized Atrial Fibrillation Ablation by Tailoring Ablation Index to the Left Atrial Wall Thickness. The “Ablate By-LAW” Single Center Study. **Europace** **2021**;euab216. [Online ahead of print]
25. Berruezo A, Jáuregui B, Penela D. Towards an Improved and Personalized Risk Stratification of Sudden Cardiac Death in Dilated Non-Ischemic Cardiomyopathy Is the Time for Ejection Fraction Coming to an End? **Eur Heart J Cardiovasc Imaging** **2021**;22:1139-1141.

26. Jáuregui B, Acosta J, Bosch X, Berruezo A. "Echocardiographic response" to sacubitril-valsartan: Diminishing the implantation of defibrillators, but also the incidence of malignant arrhythmias? **Rev Esp Cardiol (Engl Ed) 2021**;S1885-5857(21)00253-X. [Online ahead of print]
27. Falasconi G, Penela D, Soto-Iglesias D, Jáuregui B, Chauca A, San Antonio R, Ordóñez A, Terés C, Carreño JM, Scherer C, Viveros D, Huguet M, Torres J, Vergara P, Maldonado G, Panaro A, Cámara Ó, Berruezo A. A Standardized Stepwise Zero-Fluoroscopy Approach with Transesophageal Echocardiography Guidance for Atrial Fibrillation Ablation. **J Interv Card Electrophysiol 2021**. [Accepted, ahead of publication]

### CAPÍTULOS DE LIBRO:

1. Berruezo A, Fernández-Armenta J, Penela D, Acosta J, Brugada J, Mont L, Jáuregui B. Scar-Related Ventricular Tachycardia Mapping and Ablation Using Contrast-Enhanced Magnetic Resonance Imaging. In: Shenasa M, Hindricks G, Callans DJ, Miller JM, Josephson ME, editors. **Cardiac Mapping. 5<sup>th</sup> Ed.** Hoboken, NJ, USA: Wiley-Blackwell; 2019. p. 1062-1072. ISBN: 978-111-91-5259-0.
2. Berruezo A, Acosta J, Fernández-Armenta J, Jáuregui B. Do We Need Epicardial Ablation in All Patients with Arrhythmogenic Right Ventricular Cardiomyopathy? In: D'Avila A, Marchlinski FE, Aryana A, Reddy VY, editors. **Percutaneous Epicardial Interventions: A Guide for Cardiac Electrophysiologists. 1<sup>st</sup> Ed.** Minneapolis, MN, USA: Cardiotext Publishing; 2020. p. 229-234. ISBN: 978-1-942909-31-6.

3. Jáuregui B, Penela D, Berruezo A. Ischemic Heart Disease. In: Zipes D, Jalife J, Stevenson W, editors. **Cardiac Electrophysiology: From Cell to Bedside. 8<sup>th</sup> Edition**. Philadelphia, PA, USA: Elsevier; 2021. [Pre-Print]
4. Jáuregui B, Acosta J, Penela D, Fernández-Armenta J, San Antonio R, Berruezo A. Taquicardia ventricular en cardiopatía estructural no isquémica. En: Datino Romaniega T, Benito Villabriga B, editores. **Manual de arritmias y electrofisiología cardíaca. 2<sup>a</sup> Edición**. Barcelona, España: Pulso Ediciones SL; 2021. [Pre-Print]

#### OTROS MATERIALES O COLABORACIONES:

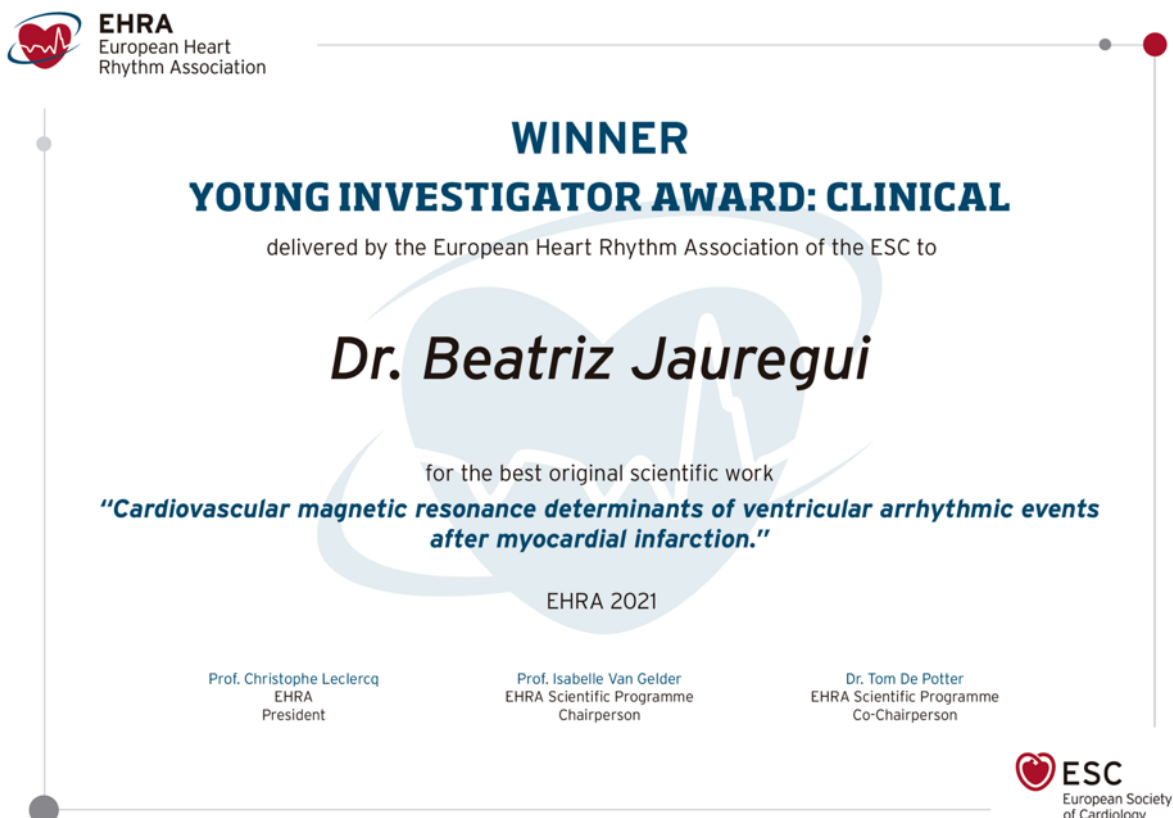
1. Lección del Máster propio online de Arritmología Cardíaca e Intervencionista de la Sociedad Española de Cardiología, Instituto para la Mejora de la Asistencia Sanitaria (IMAS) y la Universidad Rey Juan Carlos (90 créditos ECTS), durante los cursos 2018-2020 y 2020-2022, con el tema "*Arritmias ventriculares en cardiopatías no isquémicas*" (autores: Jáuregui B, Fernández-Armenta J, Acosta J, Penela D, Berruezo A).
2. Profesora colaboradora del Máster Oficial Universitario en Medicina Translacional de la Universitat de Barcelona (60 créditos ECTS), durante los cursos 2017-2018, 2018-2019, 2019-2020, 2020-2021 y 2021-2022, impartiendo la clase "*Diagnostic imaging for cardiac remodeling (tissue remodeling)*" (autores: Jáuregui B).



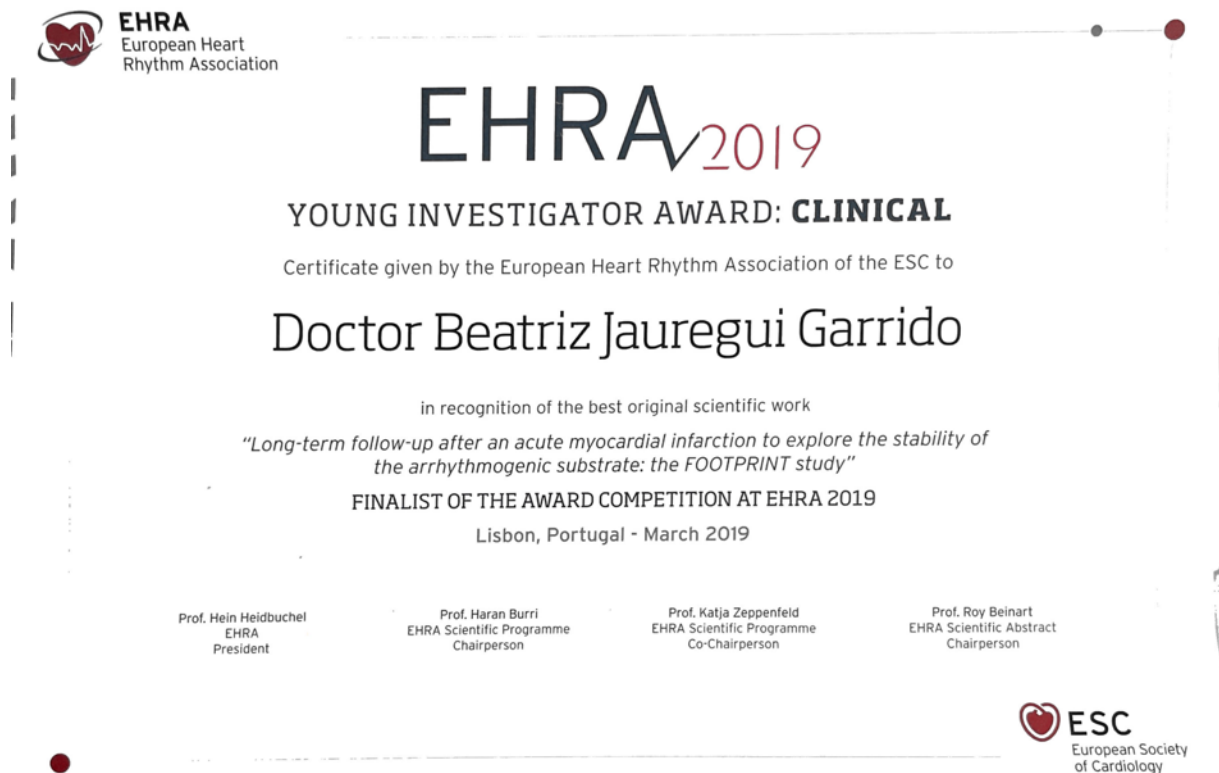
## ANEXO IV: PREMIOS Y BECAS OTORGADOS RELACIONADOS CON LA TESIS

### PREMIOS OTORGADOS

Los resultados del artículo nº 4 de la presente Tesis (*"Cardiovascular Magnetic Resonance Determinants of Ventricular Arrhythmic Events after Myocardial Infarction"*) (354) fueron presentados en el Congreso Europeo de la *European Heart Association* (EHRA) de 2021, recibiendo el premio a mejor comunicación clínica del citado congreso para jóvenes investigadores. Se adjunta el certificado acreditativo:



Por otro lado, el artículo nº 1 (*"Follow-up after Myocardial Infarction to Explore the Stability of Arrhythmogenic Substrate - The FOOTPRINT Study"*) (301) fue finalista de los citados premios, en el Congreso Europeo de la EHRA del año 2019. Se adjunta el certificado acreditativo:



## BECAS OTORGADAS

En relación al objeto de la presente Tesis, el proyecto titulado “**AutoMatic integration of electrocardiogram and cardiac Magnetic Resonance Imaging to guide caTheter-based substrate ablation for Ventricular Arrhythmias - The MERIT-VA Project**” y cuyos resultados se presentan más adelante, fue uno de los 170 proyectos premiados con una beca de 100.000€ de la iniciativa de investigación ATTRACT-EU, recogida dentro del proyecto Horizon 2020 de la Comisión Europea (grant agreement No 777222) (<https://ec.europa.eu/programmes/horizon2020/>) y co-liderada por las siguientes organizaciones: Aalto University, European Organization for Nuclear Research (CERN), European Industrial Research Management Association (EIRMA), European Molecular Biology Laboratory (EMBL), ESADE Business School, European Southern Observatory (ESO), European Synchrotron Radiation Facility (ESRF), European X-Ray Free Electron Laser Facility (European XFEL), Institut Laue-Langevin (ILL).

El proyecto MERIT-VA puede consultarse en la página web de la Organización:

<https://attract-eu.com/showroom/project/automatic-integration-of-ecg-and-cardiac-mri-to-guide-catheter-based-substrate-ablation-for-ventricular-arrhythmias-merit-va-project/> y

ha sido referenciado en: <https://sciencebusiness.net/taking-magnetic-resonance-imaging-new-dimension>

Los resultados del citado proyecto, en formato artículo científico tal y como se envió al Comité Evaluador del ATTRACT, están disponibles para su descarga en <https://attract-eu.com/wp-content/uploads/2019/05/MERIT-VA-Project.pdf>.





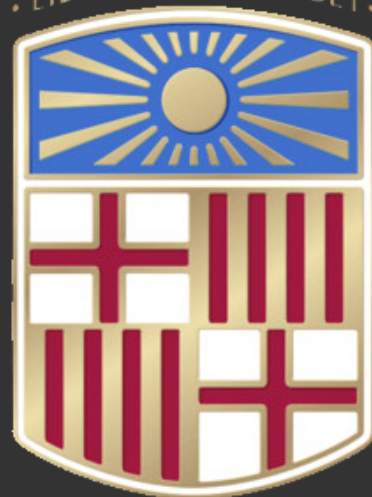
# 11. DECLARACIÓN DE CÓDIGO

## ÉTICO Y BUENAS PRÁCTICAS

Durante la presente Tesis se han seguido las directrices nacionales e internacionales en materia de ética clínica (Código Deontológico, Declaración de Helsinki). Asimismo, se ha respetado la normativa vigente sobre el uso y confidencialidad de los datos (Ley 14/2007 de Investigación Biomédica y Ley Orgánica 3/2018 de Protección de Datos Personales [LOPD] y Garantía de los Derechos Digitales). El tratamiento, la comunicación y la cesión de los datos personales de los participantes se ha ajustado a lo dispuesto por el Reglamento Europeo de Protección de Datos (UE 2016/679). En la sección de anexos se adjuntan copias de las aceptaciones del Comité Ético de Investigación Clínica del Hospital Clínic i Provincial de Barcelona correspondientes a los distintos trabajos de investigación que componen la Tesis. La autora de esta Tesis declara no tener conflictos de interés relacionados con el objeto de la investigación. Las fuentes de financiación correspondientes se detallan al final de cada uno de los trabajos publicados.



• LIBERTAS PERFVNDET •



• OMNIA LVCE •